VIRGO

Final design

Version 0. - June 1995

READ ME FIRST

This document is the draft of the first part of the Final Design of the VIRGO interferometer. By October 1995, it will be completed by an update of the cost evaluation and by detailed planning diagrams. This is essentially an internal document, written by the VIRGO teams, for the VIRGO teams. For the outside world, it is not self explanatory without the previous documents it refers to.

One of the important ideas of the Final Design is to describe a « Reference Solution » for each subsystem. The reference solution is by definition the most satisfying « proven » solution that we have today. The first priority for each « subsystem manager » is to realize his (her) reference solution in due time. In a few cases, when the reference solution still requires a validation, we try to clearly identify the corresponding remaining R&D effort. Exceptionally, with the agreement of the whole collaboration, a reference solution could be changed.

The elaboration of the Final Design document was requested in November 1994 by the Technical Manager of the project, for the main reason that the last general document, the « Final Conceptual Design » (FCD) which had been written in 1992, was not sufficiently detailed to be used as a reference, now that the construction is going to start.

Actually, the FCD is relatively detailed as concerns the « Infrastructure » (site, buildings, vacuum system, ...), and also the « standard » parts of the superattenuators, but it has become obsolete because the VIRGO teams have had time to imagine and to test many improvements in these designs.

As concerns the « detector » (laser, optics, interferometer,...), and the most sophisticated parts of the superattenuators, the FCD was less detailed, containing only general descriptions of the various subsystems. Here also, it has become obsolete : the principles have not changed, but it is now possible to describe precisely the various components which will be built. Then, the « detector » part of the Final Design is much more complete than in 1992. Most of the technical solutions are better proven and more performant, sometimes simpler, than in 1992.

The planning has also seen some evolution since 1992, for different reasons :

- the final approval, and the signature of the French-Italian agreement have been somewhat slower than expected, as well as the site acquisition : then the starting time of the construction has been delayed.
- before the final approval, INFN had asked for a smoother spending schedule. This resulted in a reshuffling of the construction planning. Technically, the new planning will actually be much more satisfying than the previous one : the guiding idea is to try to

compensate a slower spending schedule by a faster and safer commissioning of the interferometer. Instead of putting all the construction effort on the infrastrtucture before we begin the installation of the interferometer, we have decided to progress in parallel : the infrastructure will start with the central buildings, while most of the interferometer is being built in the different laboratories. Two years after the start of the construction (by the end of 1997 if there is no more delay in the site acquisition), the central buildings will be ready to receive the central part of the interferometer (laser, input and detection optics, electronics, data management system,...).

Between 1997 and the end of 1999, we will be able to build the 3 km arms, containing the biggest part of the vacuum system, while we will progressively test and improve all the basic functions of the detector in Cascina. It is important to understand that the so-called « 1997 interferometer » is not a prototype, all its components are final parts of the 1999 interferometer, except for the mirrors which are smaller. The final mirrors will also be built during this period.

In that way, the heavy infrastructure costs are well spread over the 5 years of construction. At the end of 1999, we could finish the installation, and start operating very rapidly, since most of the commissioning will have been done.

This ideal schedule is realistic if there is no more budgetary delays, and if the direction of the project can become strong enough to monitor and to control efficiently the respect of the plannings within each group.

Table of contents

2000- Infrastructure

2100- Infrastructure on site

2500- Mirrors infrastructure

3000- Vacuum

3100- Tube

3200- Baffles

3300- Towers

3400- Pumping system

4000- Interferometer

4100- Lasers and input benches

4200- Detection bench

4300- Mirrors

4400- Alignment

4500- Calibration

4600- Superattenuators

4700- Marionettes

4800- Clamps and wires

4900- Isolation control electronics

5000- Electronics

5100- Global control

5200- Standardized components

5300- Networks

5400- Data acquisition

5500- Data archiving

5600- SIESTA

-2000-

Infrastructure

INFRASTRUCTURE

2100.1. INTRODUCTION

The infrastructure for the VIRGO Project consists of two main parts: the buildings and equipments necessary to the interferometer installation on the Cascina site, which will be described first, and the building in Lyon, for the large mirrors production chain, which will be described in the last paragraph of this section.

The installation of the VIRGO interferometer has to satisfy the following requirements:

- build a detector and an infrastructure frame capable of a 20 year operation time
- keep the performances of the detector at the limits of present technologies
- build the apparatus on a flat, controlled area, as far as possible away from mechanical vibration sources, as roads, trains, etc., within a reasonably short distance from one of the collaborating laboratories
- keep the expenses for the acquisition of the land much lower than the cost of the apparatus itself
- give a minimum perturbation to the geological, biological and economical equilibrium of the surrounding region.

In the next paragraphs the chosen site and its characteristics will be described, together with the infrastructures designed to accept the VIRGO interferometer: the tunnels hiding the long vacuum pipes and the relative assembly halls, the experimental halls, and the control room.

2100.2.- THE SITE

2100.2.1.- Site choice

A very accurate search has been performed in a 100 km radius region around Pisa. Much more distant sites have also been investigated: the INFN National Laboratories at GranSasso and Legnaro and a site in the south of Italy, that was being considered to install large air shower detectors. All morphological, technical and administrative aspects have been investigated, including detailed seismic noise measurements. A site has been selected as very suitable for the installation in the Comune di Cascina (fig. 1); the Mayor assures full collaboration to solve administrative problems in the land acquisition procedure. Outstanding characteristics of this site are the perfect flatness (+/-0.5 m) and the low population density.

To satisfy the requirements listed in the introduction, the site has been selected according to the following rules:

- reduce to a minimum the number of crossed lanes and irrigation channels
- keep the distance of the tube from farm houses above a minimum of 50 m
- keep the distance of the mirrors above a minimum of 500 m from roads and of 200 m from electrical power lines.

The relevance of the noises generated by these sources has been investigated theoretically and experimentally and possible screening methods have been suggested, while not necessary in the chosen situation.

2100.2.2.- Site morphology

The area needed for VIRGO, shown in fig. 2, consists of five laboratory areas, about 40000 m^2 each, connected by two orthogonal land strips 30 m wide and 3 km long. At the crossing point (fig. 3) the "central building" contains, under vacuum inside the towers (vacuum tanks), the pendulum chains, called Super Attenuators (SA), supporting the various optical parts. At the other ends of the pipes, inside the "terminal buildings", the chains supporting the other two mirrors of the interferometer are installed. A fourth hall, at 140 m from the central one, along the West arm, contains the mode-cleaner mirror. At 100 m from the central hall there are the control building and a service building for electricity and thermal plants. On the orthogonal strips, above ground level, there are the tunnels hiding the 3 km vacuum pipes and, at half way, the halls for vacuum pipe assembly.

The vertical profiles of the two arms have been carefully measured and they turn out to be flat within +/- 0.5 m. Only in a 100 m radius zone, around the arm crossing, the ground level is 2 m higher; a clever architectural design uses this characteristics to allow to circulate freely around the central area, despite the presence of the tunnels, and to use more efficiently the central building volume, entering at the first floor.

The plane of the interferometer will be horizontal in the north-south direction, but inclined by 2 m over 3 km, in the east-west direction. Being this slope perfectly tolerable for the apparatus operation, it will not be corrected.

Only a few crossings have to be forseen: a few irrigation channels and one paved road on each arm. The channels are only a few meters wide and do not represent a problem; the small roads will get bridges to allow the crossing of the VIRGO tunnels. Two smaller bridges will be built for unpaved country lanes.

2100.2.3.- Site geology and stability requirements

The site geological survey, performed along the two whole arms, included penetrometric tests, core borings and water table height measurements. The study reached a depth of 50-60 m and, at few locations, 180 m. Undisturbed core samples have been collected at different depths and laboratory analyzed. The complete study is contained in detailed reports, where all the data are collected and possible foundation types are envisaged, to meet the stability requirements.

Main feature of the ground is a surface, 4 m thick, clay layer, with a load capability between 10 and 20 kg/cm^2, followed by a sequence of softer (4 kg/cm^2)and stronger (up to 60 kg/cm^2) clay and sand layers, extending down to a gravel layer situated at a depth variable between 30 m and 60 m. Beyond the 5 m thick gravel layer, there is again clay extending few hundred meter deep.

The stability requirements for a safe VIRGO operation are summarized in what follows.

The foundations of the halls have to guarantee the stability of the Super Attenuators suspension points, located at the top of the vacuum tanks. It is required that the suspension points move at an instantaneous speed lower than 1 mm per day and, in a 20 year period, the overall displacement must stay well within the adjustment range of a few cm in all directions. Tidal effects and thermal dilatation are expected to produce movements up to 0.2 mm with 6, 12, 24 hour periods.

As far as the tunnel is concerned, it is required to have the center of any pipe cross-section allways inside an ideal 2.5 cm radius cylinder. The instantaneous displacement speed of any such centre point must not exceed 0.5 cm per month and its integral must not exceed 1 cm per year. This allows to realign the vacuum pipe not more often than once in a year.

Given the tight requirements, a study of the ground motion expected in the next 20 years has been performed. The study included:

- precision measurements of the ground level up to 20 km away from the site
- collection of historical data on the ground level
- measurements of the water height in existing and on purpose drilled wells

- collection of historical data on the water height
- use of the ground knowledge acquired through the quoted geological measurements
- development of a computer program for the dynamical simulation of the interaction between solid and liquid phases in the ground
- tuning of the simulation program on the available historical data
- computing of the ground level evolution in the next 20 years.

The comfortable result is that, despite an overall subsidence (ground lowering) reaching 15 cm at some point, the differential subsidence will be less than 5 cm. This means that the planarity of the site is expected to be preserved to better than +/-2.5 cm. This could even allow to do not readjust the vacuum tube alignment in the 20 year liftime of the apparatus. It has to be remarked that also the gravel layer suffers of most of the subsidence, due to the underlying deep clay layer.

2100.2.4.- Seismic measurements

Seismic measurements have been performed on the chosen site, showing that it is normal/good from this point of view, the seism intensity being below $10^{-6}/\nu^2$ mHz$^{-1/2}$ in the whole relevant frequency range (0.5 Hz < ν < 3000 Hz).

Ground vibration measurements have also been performed at different distances from ploughing tractors; the result is that, in the VIRGO site ground type, the effect reduces at the natural seism level at about 80 m distance from an operating machine. This does not give any problem for the mirrors, since their suspensions are located at the center of 100 m radius laboratory areas. Also the vibrations induced on the vacuum tube are not expected to be dangerous, even if ploughing tractors could go as close as 15 m to the tube axis; the baffle system designed to stop the diffused light is, in fact, performing well enough to get rid also of this problem. Moreover ploughing and other heavy agricultural works last few days per year and can be brought to coincide with apparatus maintenance periods, when data taking is, anyway, stopped.

2100.3.- BUILDINGS

The executive design is finished for the "central buildings" (central building, control building, mode cleaner building and tunnel, electrical and thermal technical building); for this set of buildings the shown drawings correspond to what will be built in the reality. For the arms of the interferometer (tunnels, teminal buildings, tube assembly buildings), the drawings, when shown, correspond to the preliminary design.

2100.3.1.- The experimental halls

There are four experimental halls; the central building, at the crossing of the two arms, is very large, since it contains the main optical components, suspended to six independent SA chains, inside six large vertical vacuum tanks. Only the bottom part of a seventh tank will be installed, to have the possibility, in the future, to use the dual recycling technique; the installation of such an heavy object would be impossible later. At the far ends of the two arms, two smaller experimental halls contain the end mirrors of the interferometer inside their vertical vacuum tanks. A fourth smaller hall contains the far mirror of the mode cleaner, also suspended in vacuum to a shorter suspension chain. In the central hall, inside appropriate rooms, are installed the lasers and part of the acquisition and control electronics. The four experimental halls cover an area of 26x30, 15x22, 15x22, 8x10 m^2, respectively and have a useful 15 m

height, to allow to lift up the upper parts of the vacuum tanks and make accessible the pendulum chains. (figs. 4, 5, 6)

The halls are equipped with 5 ton cranes; they are controlled in temperature to +/- 2 °C and humidity is kept at 50-60%; the inner volume is kept in overpressure with respect to the outside and supplied only with filtered air, in order to be free of dust.

To avoid mechanical vibrations all equipment containing motors or moving parts (pumps, air conditioning, laser power supplies and cooling, etc.) will be isolated or confined well outside the buildings.

To avoid noises produced by human activity, the control room of the whole interferometer is located in a separate building, 100 m apart from the central one, connected by a bunch of cables to the apparatus.

The foundations of the experimental halls (fig. 4a) consist of large drilled piles resting on the gravel layer, existing at a depth of about 40 m. Such deep piles are necessary to guarantee the requested stability to inclination and not to avoid subsidence lowering. The piles support a strong concrete platform, which is rigidified by the double concrete wall constituting the perimeter wall of the main level (the level containing the axes of the interferometer); on this platform rest the 20 ton vacuum tanks. Under the main level there is a basement level, the "gallery", allowing to access the tanks bottom, where an aperture is located for optical equipment introduction; the gallery structure further contributes to the platform rigidity.

The platform supports also the upper part of the halls, composed by a very stiff and light steel structure enclosed between two walls, made of a metal sheet/thermal insulation sandwitch. The hall structure has been designed in order to be free of high Q-factor mechanical resonances, below 7.5 Hz, since in this frequency range the SA performancies become poor.

Most of the volume of the experimental halls is fully open, only a fraction of it, close to the outer walls, is subdivided in laboratories of standard height.

2100.3.1.1.- The central building

Inside the central building there are laboratories organized in three levels, plus the gallery, in the basement (fig. 4a). Following the description of the site vertical profile (§ 1.2), in the central building the gallery and the first level are underground; the first level is also called "main level" since it contains the plane defined by the interferometer beams, running at 1.1 m above the floor.

At the main level of the central building (fig. 4c) there are seven towers arranged as a cross, with the beam splitter tower at the centre. In the south part of this floor, there are two adjacent clean rooms, class 100000, one where the laser will be installed and the other, containing two cleaner zones (class 100-1000), for optical parts assembly. A staircase and an aperture in the floor allow to bring to the gallery (fig. 4b) clean optical parts, which will be installed, from below, in the towers. To this aim, also the gallery is a clean room, supplied with clean air through the towers. A detailed description of clean rooms and gallery will be given in the tower section.

At the main level there are also: the large valves connecting the towers to the arm tubes, the large primary pumps for the arm tubes and the laboratory to assemble the SA chains. Inside two volumes protruding out of the rectangular shape of the building, there are the clean air generators, an optical and mechanical parts washing chain and the air conditioning machinery.

In the floor, along both sides of the tower cross, there are cable passages for power and service cables. Signal cables, coming out from the towers at 2.5 m height, reach the read out electronics, at the upper floor, on aerial cable trays.

At the large valves location, suitable apertures are available for tower bases and valves installation. The connection between the central building and the tunnels is made through transition rooms containing auxiliary equipments for the large valves and the piping going from the primary pumps to the beam tubes; the room toward the west arm makes the connection also to the mode cleaner tunnel, it is therefore quite large and will be used for storage.

The personnel and truck entrances are located at the upper level (fig. 4d), coincident with the outer ground level. The truck entrance is closed and its removable roof will be opened to access the load with the crane, only after stopping the truck engine and waiting for dust deposition. People coming in through the personnel entrance will either stay in the reception and visiting gallery zone or enter the laboratory zone after changing shoes and dress. The data acquisition

room is located at this level; in this way the signal cables come out of the towers at about the same height of the double floor of this room. Through the double floor comes also the cooling air flow for the electronics racks. On this level there are also: the electronic workshop and the toilets.

The upper and last level of the central building has a surface of about 150 m^2, divided in seven offices.

All the inner surfaces accessible by the crane will be used as storage space for parts of the towers and other equipment.

2100.3.1.2.- The terminal buildings

The terminal buildings (fig. 5) have a structure very similar to the central one, but reduced in surface since they contain only one tower; the height is the same since the terminal towers contain a full size SA chain. Inside there is one inner floor, equiped with a clean room, and a gallery, long enough to allow to adjust the tower longitudinal position by +/-1.5 m.

2100.3.1.3.- The mode cleaner building

The fourth hall (fig. 6) is only 10 m high since it contains a small tower with a three stage SA, the tower position can be adjusted by +/-2.0 m along the mode cleaner beam. Very little assembly space is required, since this hall is located only 140 m apart from the central hall, where the necessary technical facilities are available.

2100.3.2.- The pipe assembly halls

A vacuum pipe assembly hall will be built in the middle of each arm of the interferometer. The covered area will be 16x60 m^2, with an useful height of 8 m. Trucks coming from the pipe factory will be unloaded in the delivery zone and the incoming vacuum pipe elements will be stored in the storage area. The preparation zone is a clean area where the pipe elements will be prepared for installation and mounted on suitable trolleys to be brought in position, along the tunnel. One 6 ton crane will serve the delivery and preparation zones.

2100.3.3.- The control building

This building (fig. 7), located in the central zone, has a surface of 280 m^2 and is two floor high.

At ground floor there are: a 50 people meeting room, the guardian room, the guardian house and a small cafeteria. At first floor there are: the control room of the whole experiment, the computer room and some office space for people in shift. Control and computer room are equiped with a double floor for cable passage and cooling air flowing to the electronics racks.

2100.3.4.- The technical building

The technical building (fig. 8) contains the electrical power station and the climatisation plant for the central buildings. It is situated at the border of the central zone, in order to be easily reached for inspection and fuel supply. The building is divided in two halves, with two floors each. The power half contains: at the upper floor, the connection to the 15 kV power line and the transformers, at the ground floor, the Uninterrupted Power Supply (UPS) and the diesel generator. The climatisation half contains: on one floor, the hot water generator, on the other floor, the chilled water generator; water at the proper temperature, according to the season, is brought via insulated piping to the heat exchanger of the different buildings of the central zone.

2100.4.- TUNNELS

2100.4.1.The interferometer tunnels

The 1.2 m diameter vacuum pipes, containing the beams of the interferometer, will be installed inside a protection structure, the "tunnel", containing also all the cables connecting the central building with the terminal ones. The beam tube axis is at 1.45 m above tunnel floor.

The tunnel has the cross-section shown in figure 9a, with a maximum inner height of 2.8 m and a width of 5.0 m. These dimensions are needed for installation and replacement of the vacuum pipe elements (as described in the relevant section), of the relative pumps and of the tools necessary for baffle installation. The passage for a man has to be easily allowed at any moment, for survey and maintenance purposes.

Taking into account the nature of the ground, as described in the geology section, the tunnel could lay directly on the ground, since the expected subsidence is lower than the maximum tolerable displacement.

The top ground layer, 1-2 m thick, will be rearranged in order to obtain perfectly straight arms and the correct slopes, from the tunnel toward the sides of the land strip; this is necessary to collect water into the lateral drain channels. This could produce local ground disuniformity or compression, demanding for somewhat deeper foundation, resting on undisturbed ground layers.

Hence, every 12 m, there are two piles, 32 cm in diameter and 24 m deep, joined by a single rectangular capital. The tunnel floor and walls are made by a single concrete beam, poured continuously on site, resting on the capitals.

The designed structure does not suffer from resonance problems, due to the great dumping effect of the ground. This avoids vibrations that, transferred to the pipe, could modulate the cavity beams, through the diffused light phenomenon. Residual oscillations of the structure have, anyway, little relevance, since the tube supports rest on the capitals, directly connected to the piles, hence to the ground. The final value of the distance between piles, i. e. between tube supports, will be optimized during the executive design of tube and tunnel, in the coming months.

The tunnel floor will be aligned to better than 1 cm, correcting for earth curvature. The floor will be smooth enough to allow the displacement of pipe elements from the assembly halls to the installation point, using suitable trolleys, guided by rails.

Doors to enter the tunnel are forseen every 300 m, in correspondence of the pumping stations. On the wall opposit to doors there are cable trays for power and control cables and fluids.

The tunnel cover is a light one, made of curved sandwitch plates (metal/insulation/metal) similar to those used for the outer walls of the buildings.

Aerators will be made on tunnels roof, to evacuate the heat produced during vacuum pipe bake-out; exploiting natural convection, without fans, a 1 m^2 aperture every 10 m will be sufficient to evacuate 0.5 kW per metre of pipe.

2100.4.2.- Mode cleaner tunnel

This tunnel (fig. 9b) is forseen to be parallel to the west arm and has a smaller cross-section with respect to that of the interferometer tunnel, since it contains a much smaller vacuum pipe (0.2 m diameter) and , being only 140 m long, does not contain pumps.

2100.5.- TECHNICAL FACILITIES AND SERVICES

2100.5.1.- Fluids

There is one water circuit, for bathrooms and cleaning purposes. Bathrooms with showers will be sufficient for a 20 working persons occupacy, in the central and assembly halls and in the control building; for 10 persons in all other buildings. During construction phase, auxiliary services will be available in trailers.

Cooling water, for laser and vacuum pumps, will be produced locally in the experimental halls and along the tunnels, with closed circuit cooling systems.

Compressed air will be used for vacuum valves actuation and for tool powering; it will be distributed in the experimental and assembly halls and in the tunnels. In principle compressed air for cleaning purposes will not be allowed, to avoid dust propagation. Suitably large air reservoirs will be provided, in order to provide buffers for emergencies and to let the compressors work at long intervals and at controlled times.

A general vacuum cleaner system will be available in each building.

2100.5.2.- Electricity

The electrical power distribution will be achieved with two separate networks: one for installation and normal operation and one for bake-out of the vacuum system.

The normal operation network will be connected to the italian electricity company (ENEL) medium voltage network (15 kV) at the technical building. A distribution back bone will deliver, through five local transformers, 500 kW in the central zone, 50 kW in each of the tube assembly zones and 100 kW in each of the terminal zones. The total installed power is 800 kW and includes: illumination (inner and outer), air conditioning, white rooms, cranes, workshops, vacuum pumps, electronics and computers. Auxiliary power supply are forseen for short and long break-downs. The Uninterrupted Power Supply (UPS) for fast interventions to keep working computers and electronics (150 kW, lasting 15 minutes) and diesel generators (IPS) for long term emergency power supply (250 kW).

The bake-out network is considered to be part of the vacuum tube and will be described in the vacuum system section; the power requirement is 0.2 kW/m, i.e. 0.6 MW at the same time, that will be supplied by diesel generators. The towers require, to be baked-out, only 30 kW each; therefore they will be connected to the general power supply.

2100.5.3.- Control cables

Signals coming from every part of the set-up will converge, along the tunnels, in the central building for local use and/or to be sent to the control building. It is forseen to have a few hundred cables or fiber optics from each arm, demanding for a cross-section of the order of 100-200 cm^2 on the cable trays.

Inside the buildings cables are installed in suitable cable trays, as previously described.

2100.5.4.- Vacuum

The VIRGO vacuum tubes will be evacuated from atmospheric pressure by clean primary pumps. Three groups of dry primary pumps will be installed in a suitable location in the three main experimental halls (fig. 4c, 5). Each group will be used to pump one 3km pipe at a time.

The vertical tanks, the pipe of the mode cleaner and other smaller volumes will be pumped down by smaller local dry primary pumps.

Primary pumps will not need to be mechanically isolated, since they will not be running during data taking.

Pumps (turbomolecular, getter, etc.) needed to reach the final vacuum, below 10^{-8} mbar, will be installed close to their pumping port and will be dedicated, in general, to one single item.

2100.5.5.- Cranes

Five ton cranes will be available in the experimental halls to assemble or disassemble the vacuum tanks and the pendulum chains. Movable rented cranes will be used for the installation of the bases of the tanks, since these pieces have a weight much larger (up to 20 ton) than all other pieces. The operation will be performed once for all, through suitable large aperture available at the large valves locations.

Suitable cranes will be installed in the assembly halls for handling the pipe elements.

2100.5.6.- Access and service roads

The access to the site is good, through already existing paved roads, linked to the Pisa-Firenze motor-way. The most relevant distances are: 15 km from Pisa, 8 km from Cascina, 21 km from INFN laboratory in San Piero a Grado (fig. 1). The Pisa-Firenze railway has a stop in Cascina and an almost dismissed railway runs at about 5 km west of the central zone; it could be useful for tube elements delivery, during the installation.

The VIRGO area will be closed by a fence and surrounded by a drain channel. Controlled access to the VIRGO area will be only through the central zone, even if it could be possible also through the terminal zones. In fact all three zones are within a distance of 0 - 100 m from already existing roads.

A service road, 4 m wide, will allow displacement of cars and trucks along the interferometer; the road will become wider in correspondence of the pumping stations and around the buildings, to allow parking and truck crossing.

2100.6.- SURVEY AND ALIGNMENT

The position of three points, necessary to define the directions and the lengths of the interferometer arms, can be easily determined with "standard" techniques, with a 1 cm error in three coordinates; this is largely sufficient for VIRGO. GPS systems, allowing relative precisions below 1 cm, will be used for all alignment and positioning purposes.

After the first survey, soil movements displacing a pipe section out of axis by more than 2 cm will be considered unacceptable. Global rigid displacements preserving the coplanarity of the apparatus will be neglected. The alignment of the pipe elements needs not to be corrected on-line, since the expected displacements are inside the previously indicated limits; the alignment will be monitored continuously and corrected, if necessary, on a yearly basis.

The distance between the mirrors of each arm has to stay constant within a very small fraction of a micron, given the way of operation of the interferometer. Daily movements, by a fraction of a millimeter, will be corrected by the various feed-back loops at different levels: by the coils-magnets systems on the SA's and by the micrometric tables displacing the suspension points. Slower changes of this distance, of the order of 1 mm in one month, are reasonably expected and will be corrected again with the micrometric tables; their main source can be the inclination of the towers, which could also be easily monitored and corrected, on a long timescale, in the maintenance periods.

2100.7. FIGURE CAPTIONS

1 Geografical location of the site
2 Soil area needed for VIRGO
3 Arrangement of central area on Cascina site
4 Central experimental hall; a - vertical cross-section, b - gallery (second underground), c - main level (first underground), d - ground level
5 Terminal building
6 Mode-cleaner building
7 Control building; a - ground floor, b - first floor
8 Technical building; a - ground floor, b - first floor
9 a - Tunnel cross-section, b - mode cleaner tunnel cross-section

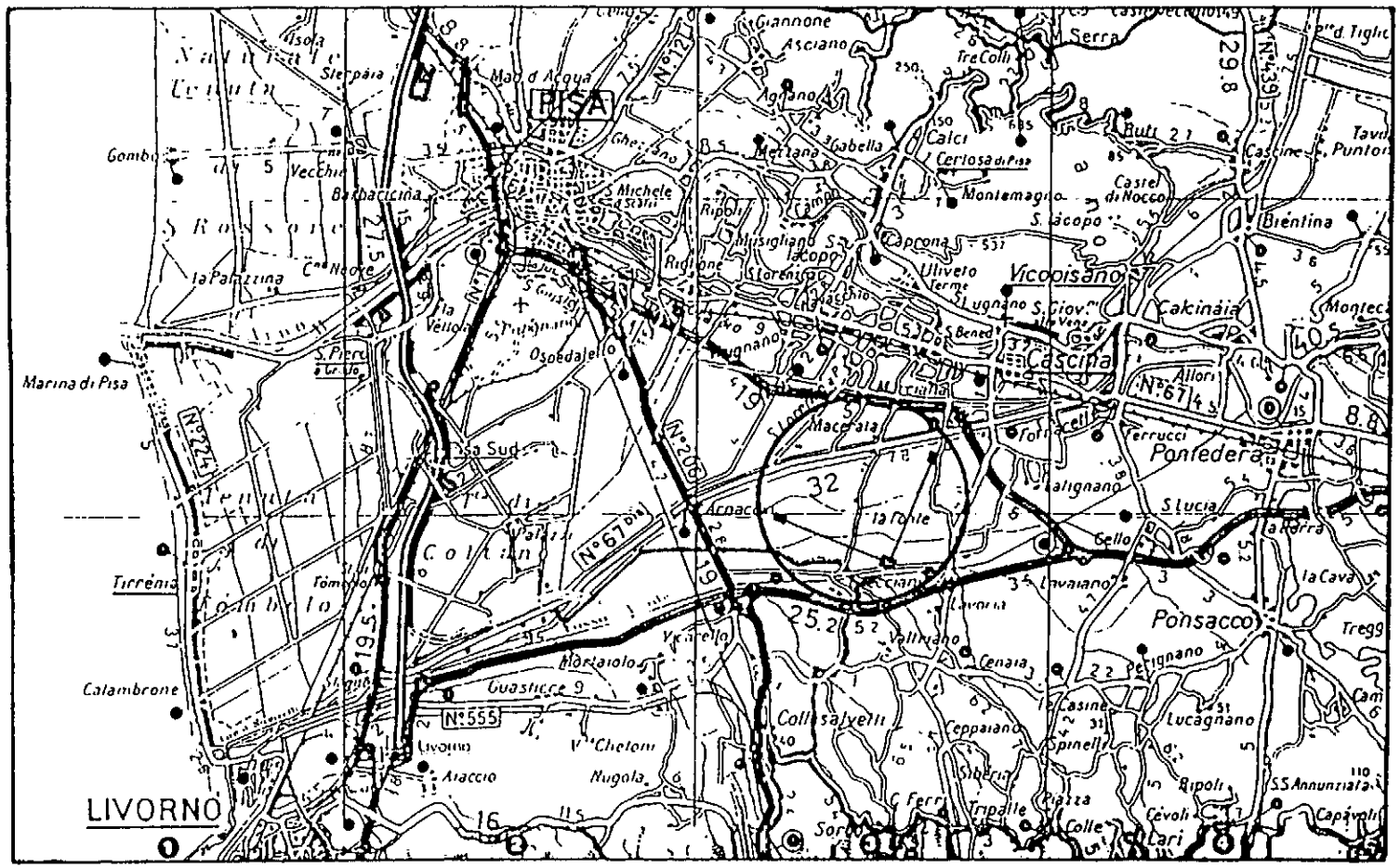
PISA
LIVORNO
Vicopisano
Cascina
Pontedera
Ponsacco
Marina di Pisa
Calambrone
Tirrenia
Colline
Sept. 1993 - De Carolis
2 1 0 4 8 12 16 20 Km

Fig. 1

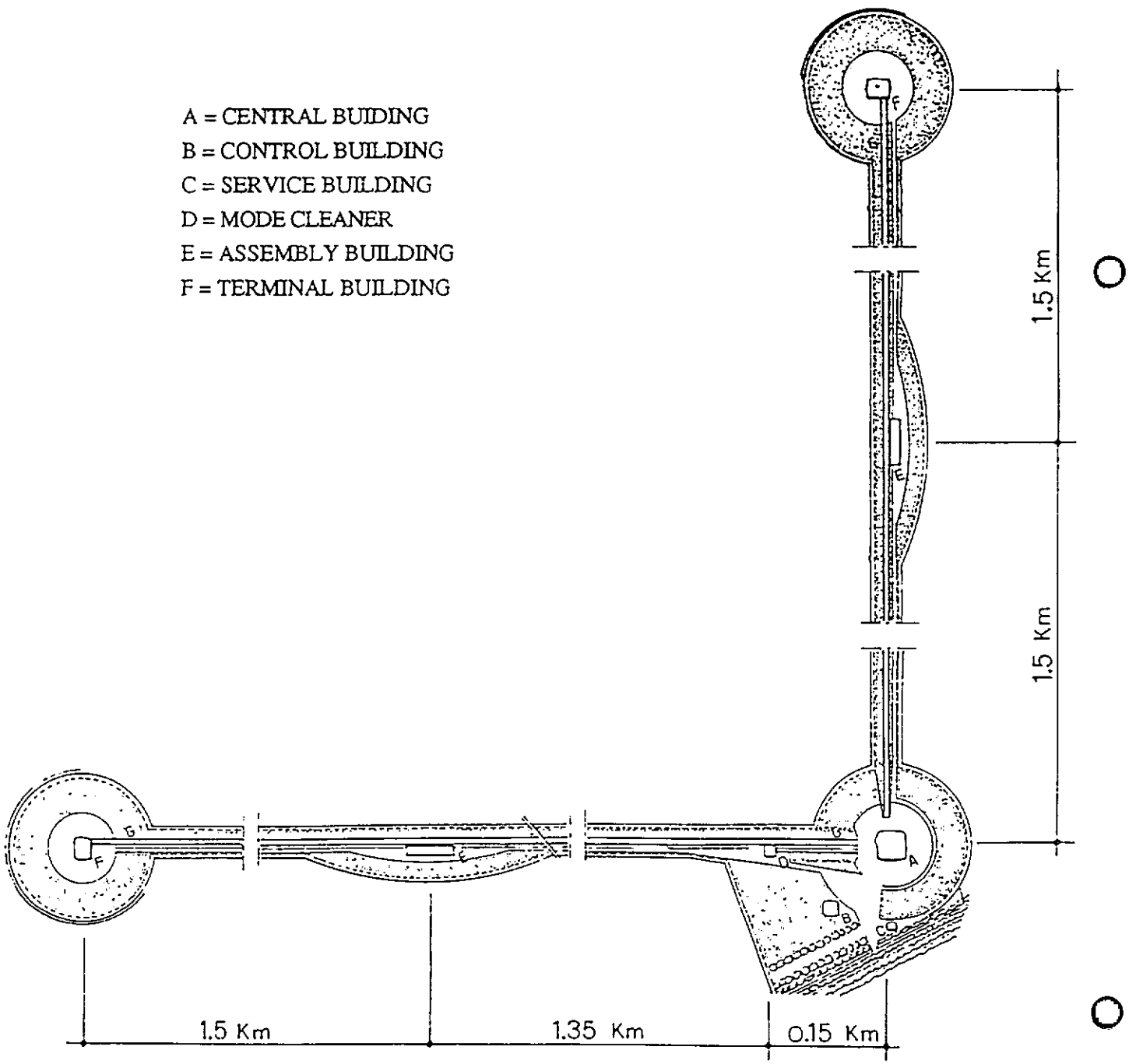
A = CENTRAL BUIDING
B = CONTROL BUILDING
C = SERVICE BUILDING
D = MODE CLEANER
E = ASSEMBLY BUILDING
F = TERMINAL BUILDING
1.5 Km
1.5 Km
1.5 Km
1.35 Km
0.15 Km

Fig. 2

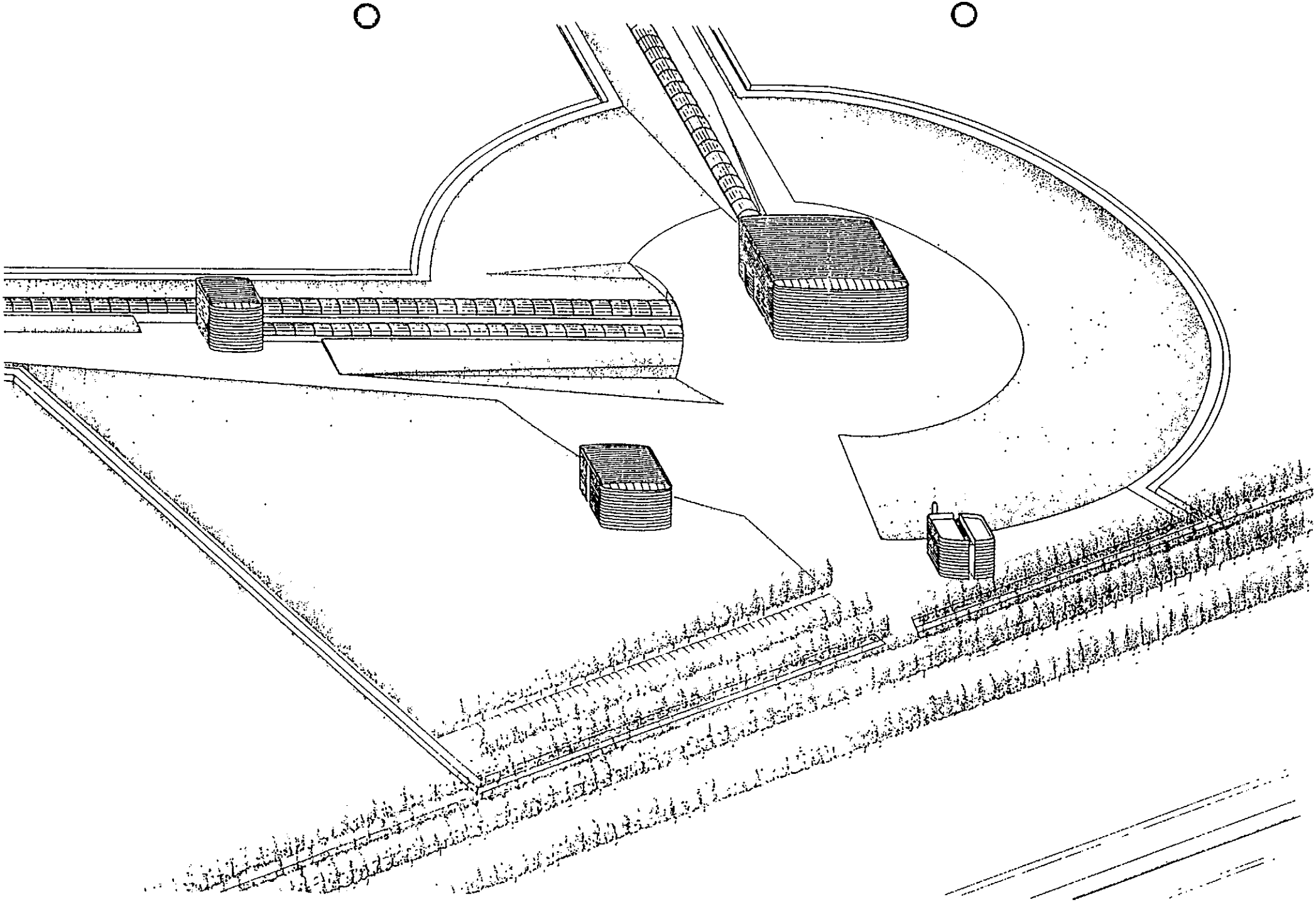

Fig. 3

Fig. 4/a

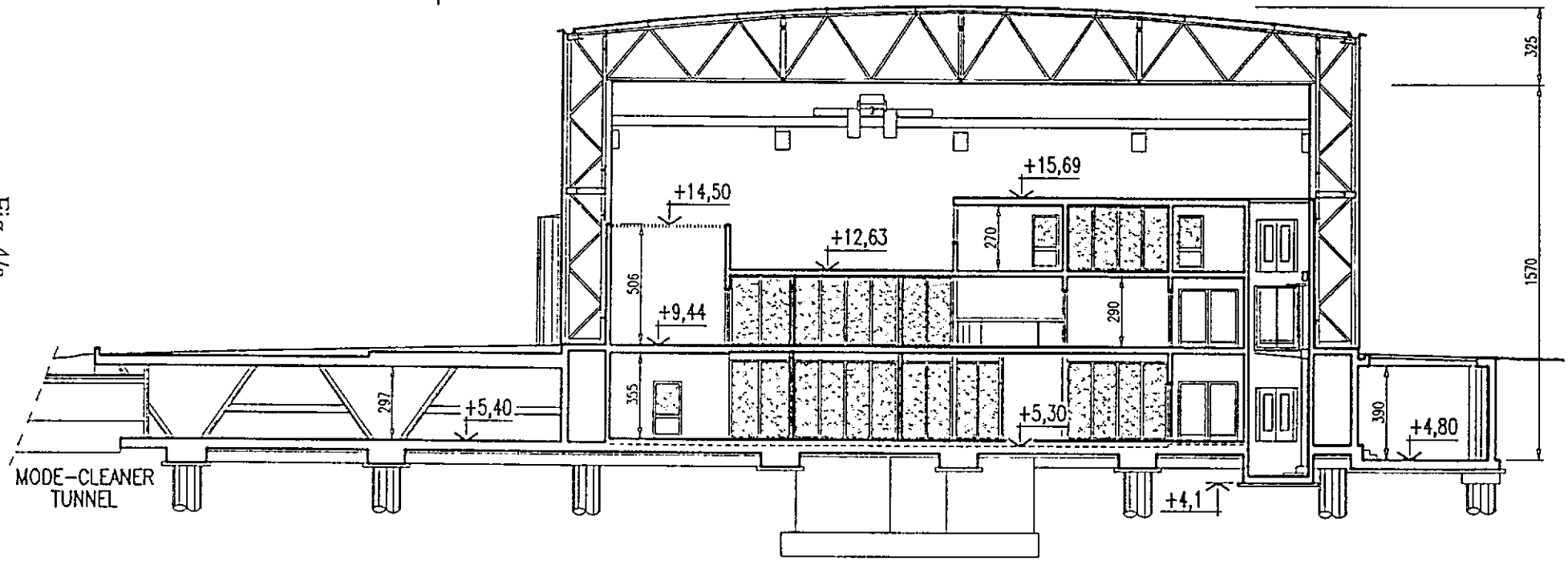

VERTICAL CROSS-SECTION

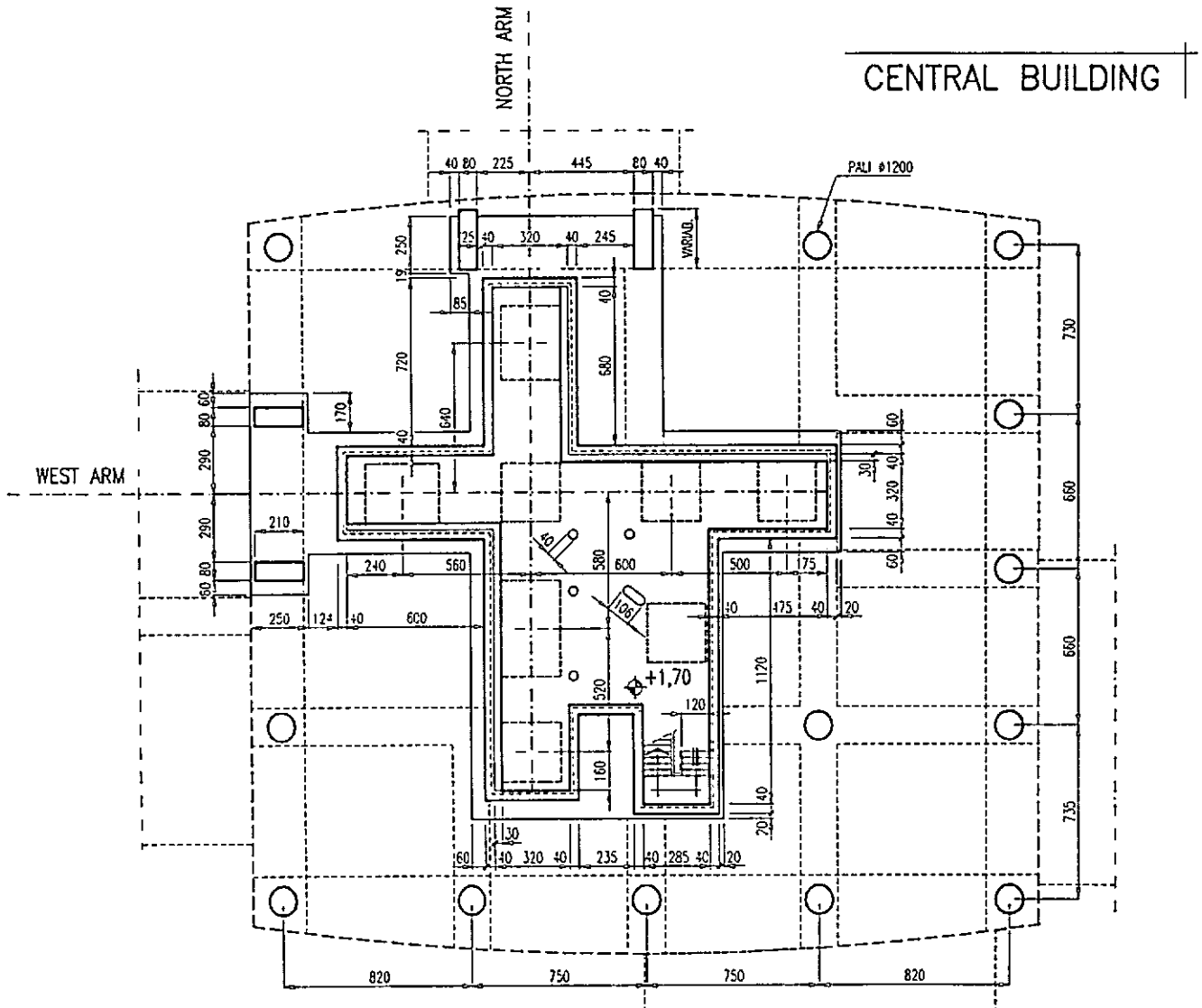

GALLERY (SECOND UNDERGROUND)

Fig. 4/b

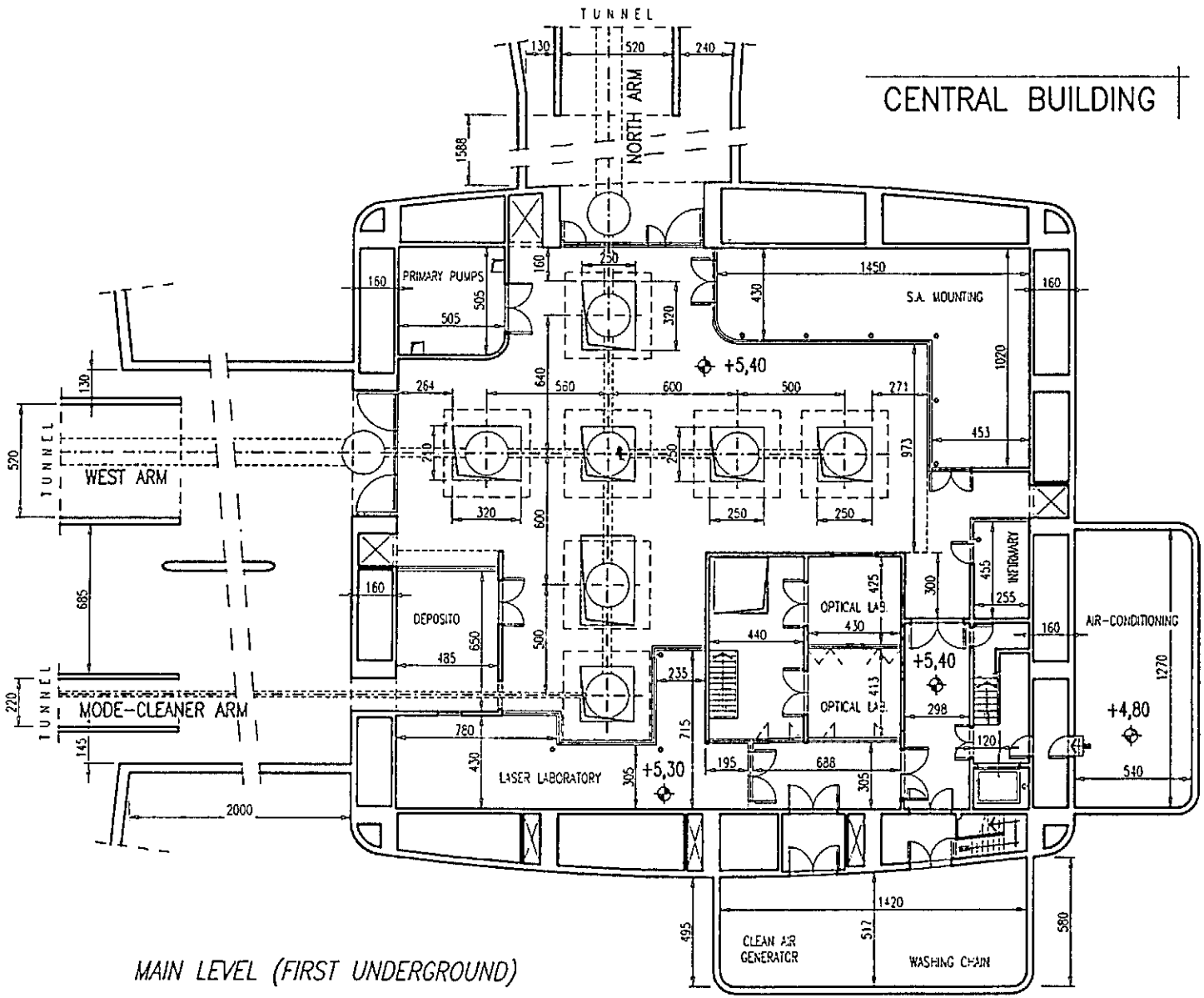
CENTRAL BUILDING
TUNNEL
NORTH ARM
WEST ARM
TUNNEL
MODE-CLEANER ARM
TUNNEL
PRIMARY PUMPS
S.A. MOUNTING
DEPOSITO
LASER LABORATORY
OPTICAL LAB.
OPTICAL LAB.
INFIRMARY
AIR-CONDITIONING
CLEAN AIR GENERATOR
WASHING CHAIN
+5,40
+5,40
+5,30
+4,80
MAIN LEVEL (FIRST UNDERGROUND)

Fig. 4/c

Fig. 4/d

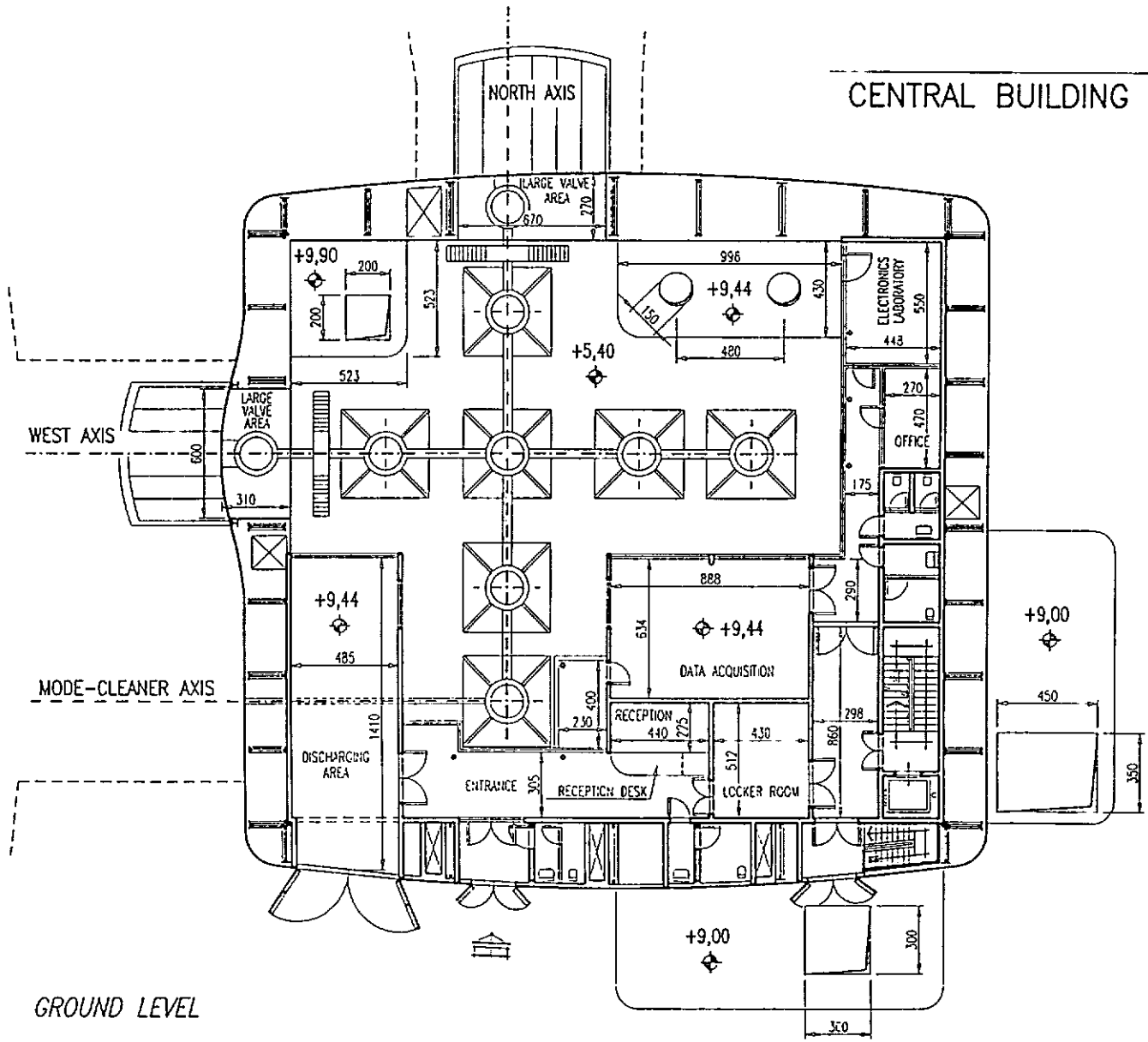
CENTRAL BUILDING
NORTH AXIS
WEST AXIS
MODE-CLEANER AXIS
LARGE VALVE AREA
670
270
+9,90
200
200
523
523
+5,40
996
+9,44
150
480
430
ELECTRONICS LABORATORY
550
443
270
470
OFFICE
175
LARGE VALVE AREA
600
310
+9,44
485
1410
DISCHARGING AREA
888
614
+9,44
DATA ACQUISITION
290
+9,00
450
350
490
230
RECEPTION
440
275
430
512
298
860
ENTRANCE
305
RECEPTION DESK
LOCKER ROOM
+9,00
300
360
GROUND LEVEL

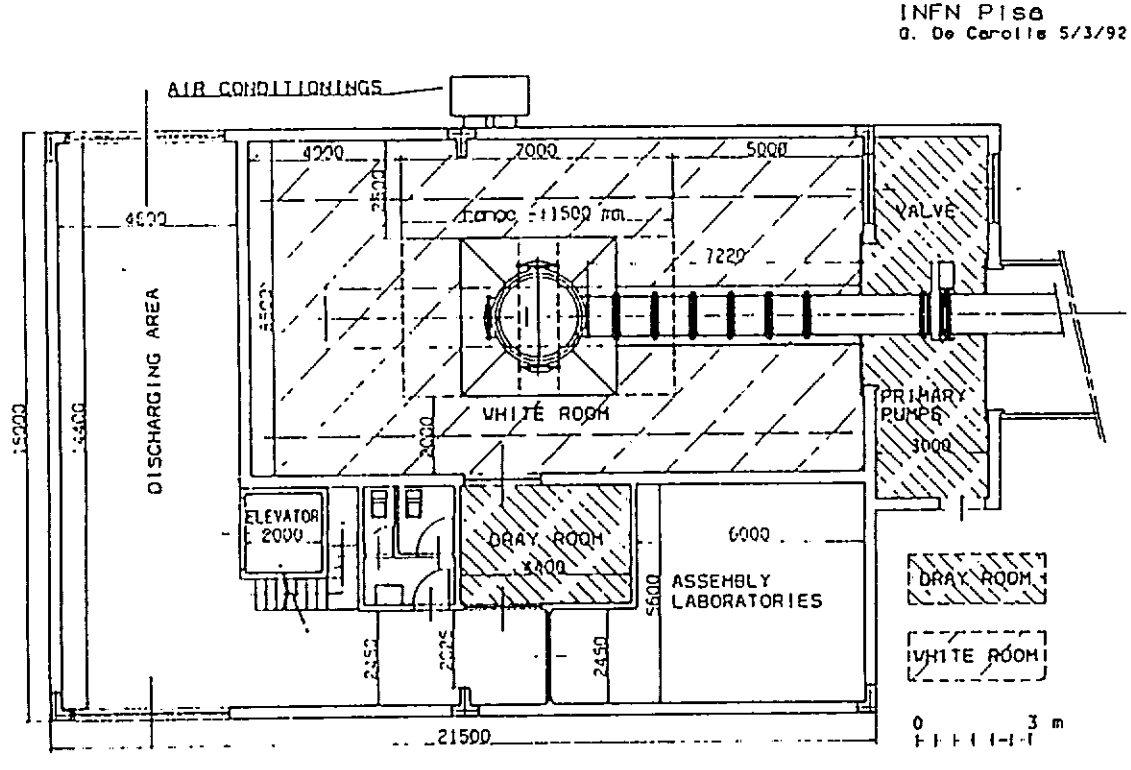
INFN Pisa
G. De Carolis 5/3/92
AIR CONDITIONINGS
DISCHARGING AREA
4000
2000
5000
Tank = 11500 lit.
7220
VALVE
WHITE ROOM
PRIMARY PUMPS
3000
ELEVATOR 2000
DRAY ROOM
3400
6000
ASSEMBLY LABORATORIES
5600
2450
DRAY ROOM
WHITE ROOM
21500
0
3 m

Fig. 5

MODE–CLEANER BUILDING

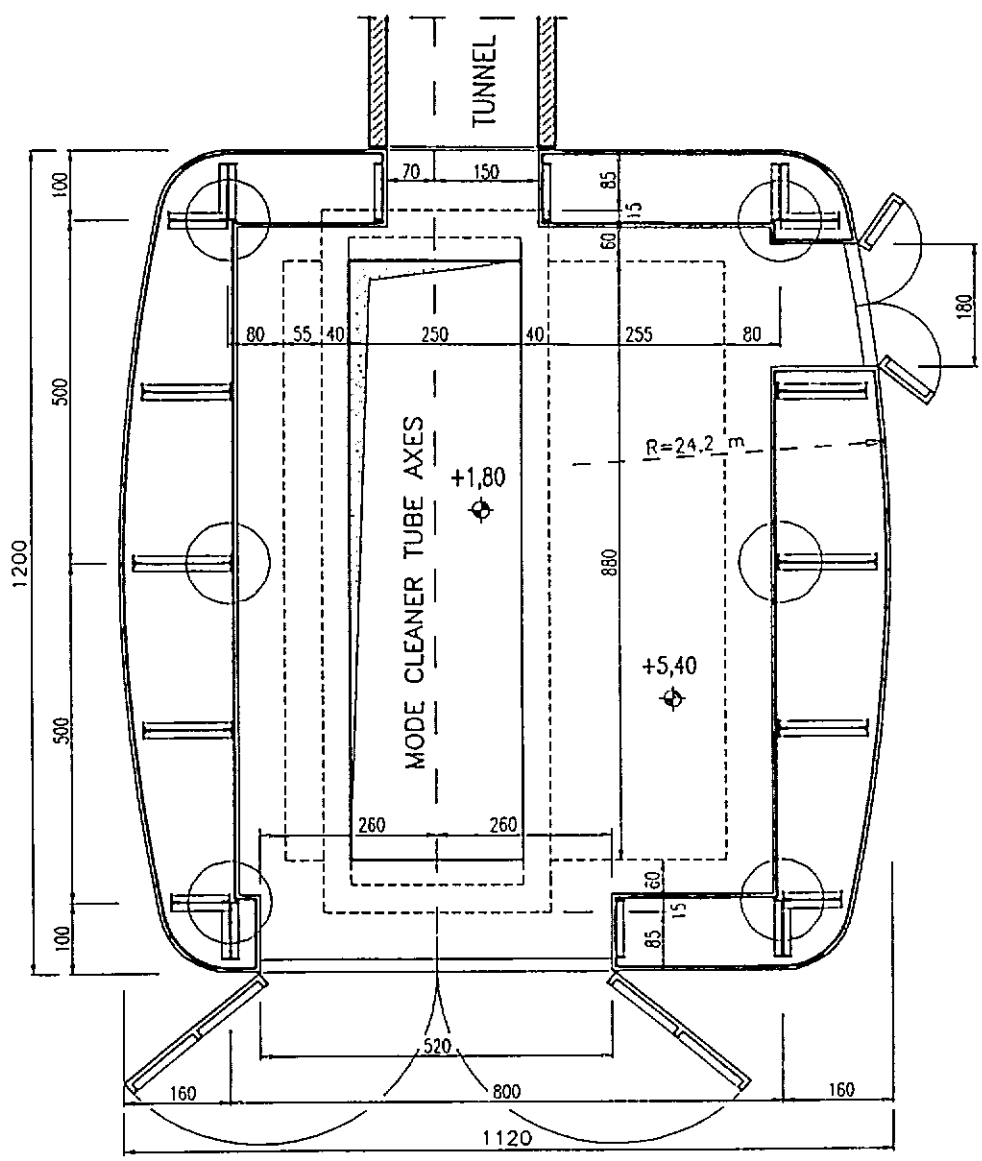

GROUND FLOOR

Fig. 6

Fig. 7

CONTROL BUILDING

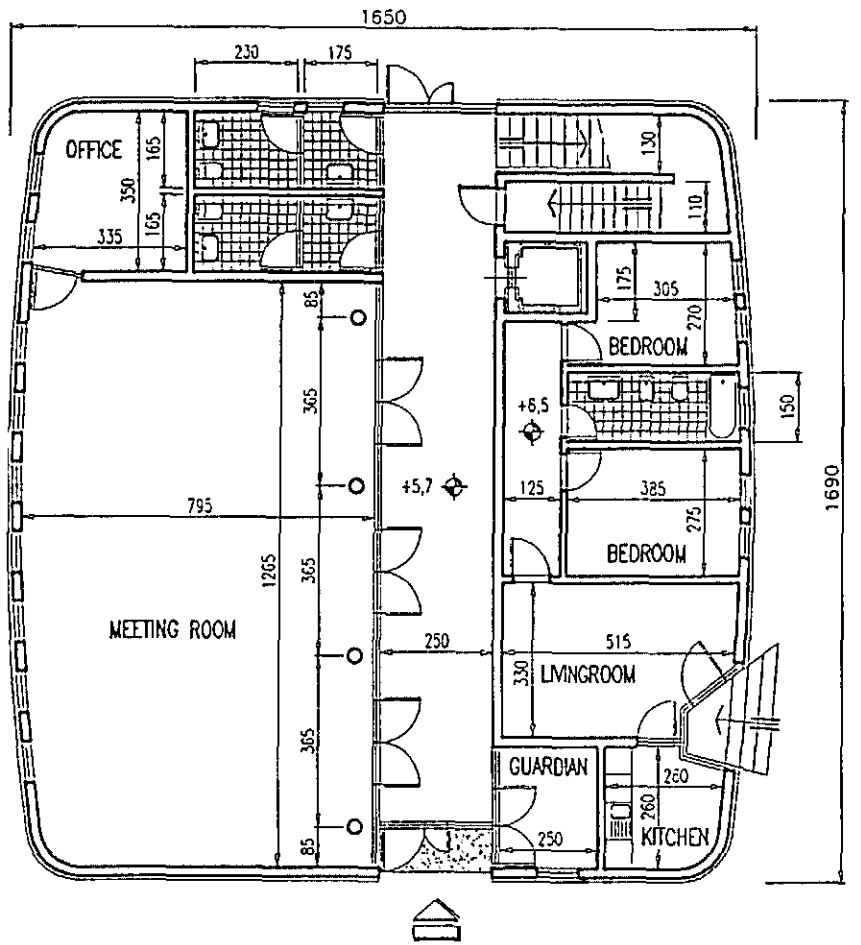

GROUND FLOOR

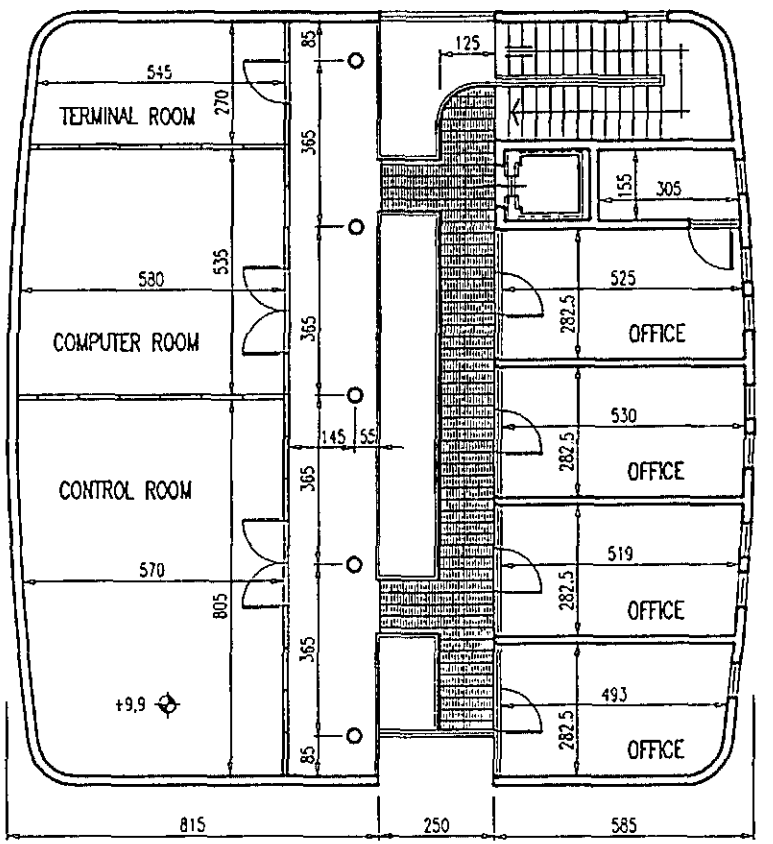

FIRST FLOOR

TECHNICAL BUILDING

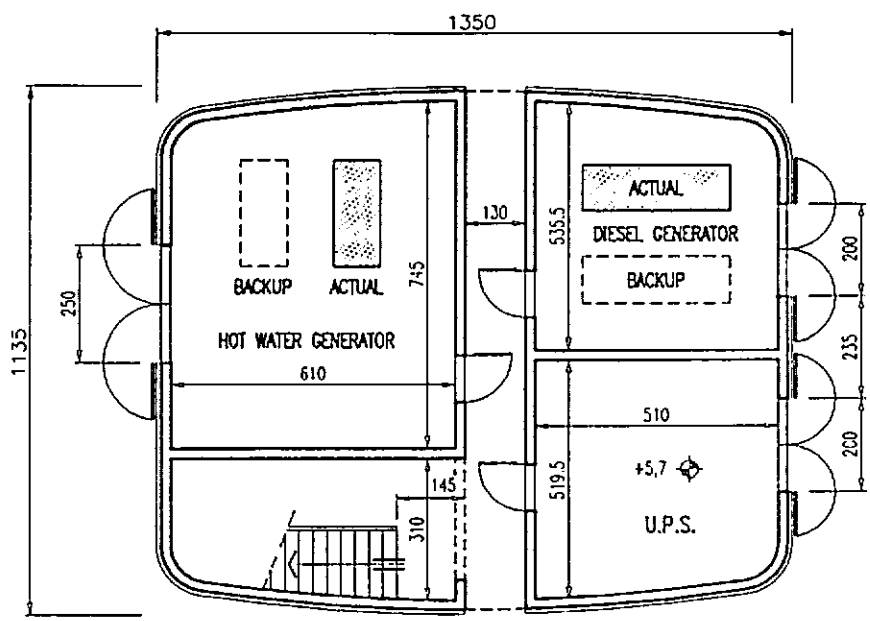

GROUND FLOOR

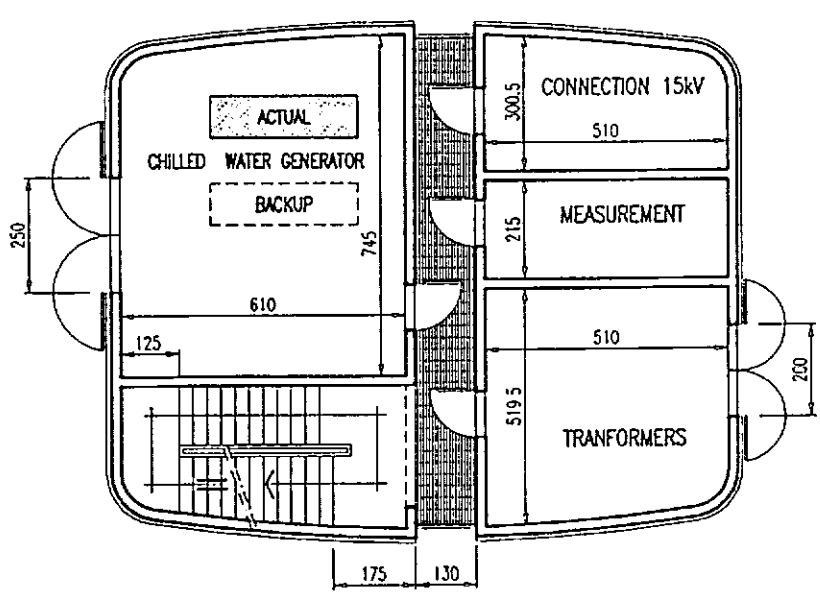

FIRST FLOOR

Fig. 8

LONGITUDINAL SECTION

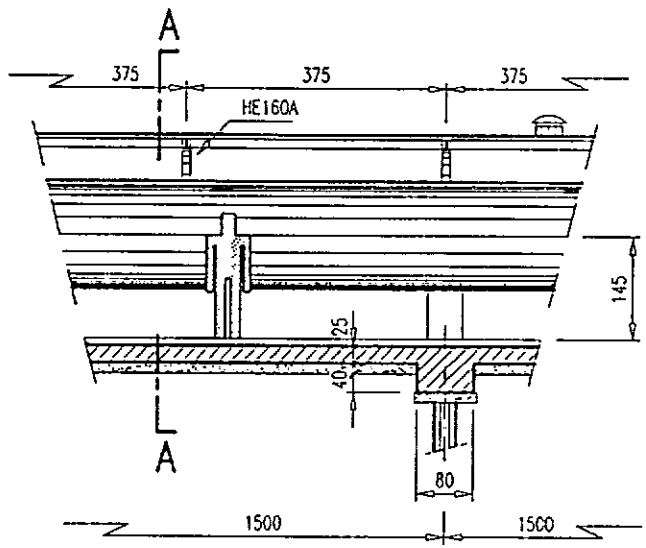

SECTION A–A

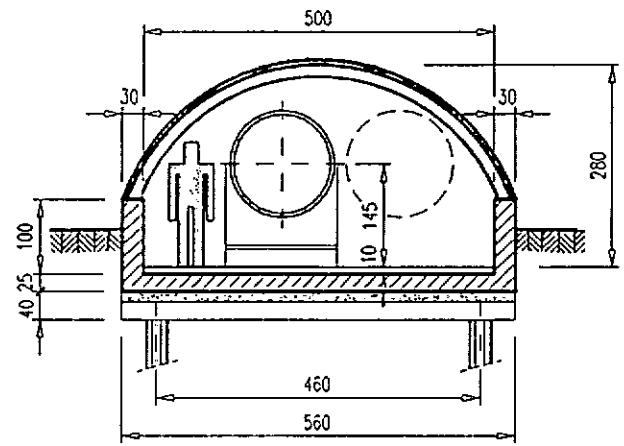

TRANSVERSAL SECTION

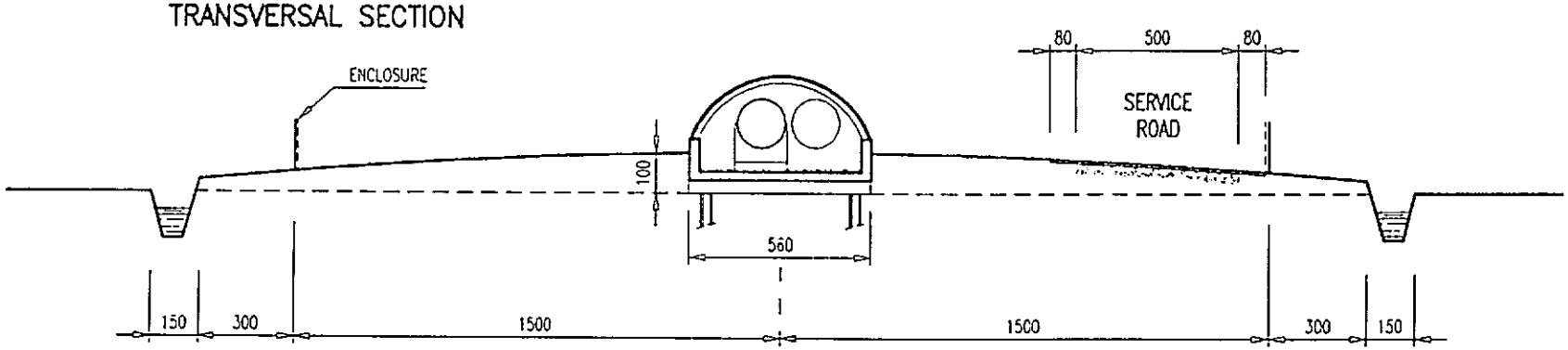

Fig. 9/a

MODE-CLEANER TUNNEL

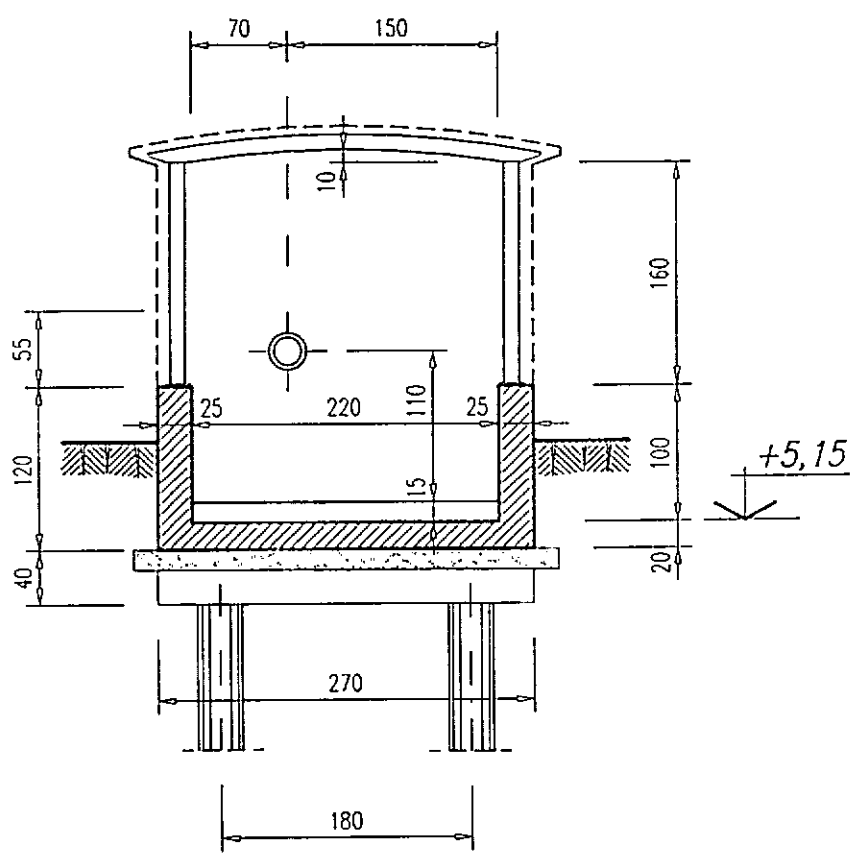

Fig. 9/b

MIRRORS INFRASTRUCTURE

As foreseen in the F.C.D., the elaboration of Virgo mirrors requires a new plant with clean areas facilities.

Technip and Tecair technical reports of February 1994 leads the CNRS to start its own study and on the 11 th of may 1994 the Virgo Council has decided to renew the Lyon Synchrocyclotron building. Then, the Direction des Affaires Immobilières (D.A.I.) and the Service Matériaux Avancés (S.M.A.) have been working to write the building specifications required for the Virgo Mirror Process.

On the 15 th of December 1994, all the people involved in the infrastructure choose the 4 assay offices companies. The 27 th of January 1995, the CNRS gave to this firms the building specifications. They have subjected their studies on the 10 th of February and the definitive choice of the assay office has been done in May 95. After receiving the order, the selected company has 4 months to define and optimize the best design, evaluate and quote all the parts. Before the call for tender, the Virgo Council must accept the proposals, taking into account the technical and budget considerations. Actually, a delay has been added due to the CNRS audit. This time is used to precise and to improve the clean room design.

The delivery is foreseen between 18 and 24 months after the beginning of the construction.

Configuration of the mirror infrastructure

General description

Preliminary work

The mirror process infrastructure must be designed taking in account the synchrocyclotron environmental location.

The nearest motorway induces vibrations and pollution. These two points lead to install the inlet of air at the right place to save air filters. Concerning vibrations, the optical tables isolation system can solve the problem. For the coater, the main problem comes from the cryopumps. Their vibrations will be important and we must chose an appropriate mounting system to minimize them. The vacuum chamber will also be isolated from the building main frame.

In the synchrocyclotron, a special room for radioactive products was used. So, it will be necessary to make a decontamination before starting the work.

There is also an electrical power station in the underground. The electrical transformers will have to be reconfigured or replaced.

The big water pipe coming from a well will have to be moved to avoid a leak risk in the air exhaust zone under the clean areas.

A part of the synchrocyclotron will be affected for S.M.A. and directly funded by IN2P3.

The technical concept of the clean areas is to use a floor for air treatment over the clean rooms and an exhaust under those ones to have a total laminar flow.

The following table gives the class specification, and the corresponding areas according to the Virgo process requirements.

CLASS	SURFACE * (m^2)	PROCESS STEP
1	181	Substrate cleaning, loading and coating. Optical characterizations. Thermal annealing. Shipping.
10 000	42	Laser power supply, ultrasonic bench.
N A	47	Reception, technical local, stock, transport preparation.
N A	248	Offices, sand blasting, working tool.
N A	25	Ultra pure water production.
N A	9	Central vacuum cleaner.

* **The surfaces given here are minimum useful surfaces and do not include locks.**

The building is designed to allow the circulation of persons, working stock, clean parts. Each path is realized to avoid a crossing between clean ways and dirty ones. This leads to build enough locks to maintain the class quality.

On the figure 1 , we can see this concept and the different ways for technical staff, working stock and clean parts.

Special equipments

To elaborate the mirrors, it is necessary to install some special equipments listed below:

- ultra pure water production and heater system to provide adequate water for the substrate cleaning.
- gas lines for vacuum process and dry nitrogen to vent the coater and flow the optical benches.
- centralized vacuum cleaner system for the cleanliness of the laboratories and equipments.

These installations will be in the underground with their different lines. We must optimize their location taking into account the access and the restricted areas of the air treatment.

A special care must be taken for the high power line of the ultra pure water heater. This equipment will need about 400 kW for non continuous operation time. It is difficult to use a thermal exchange unit because the flow of the ultra pure water is not continuous. The water purity is strongly dependent of the storage conditions. This will be done by pressurizing the water tank with nitrogen. To prevent bacteriological growing we will use special UV lamps. The production of ultra pure water is really critical for`` Low quantities ``and non continuous flow.

Large coater facility

This area is the heart of the Virgo mirror process. The large coater needs a place in a central class 1 zone and its installation will need removable walls. Its weight is also a constraint for the floor during delivery and set up.

The coater will be assembled in the level 0 of the building and then moved up at its place. This possibility allows for the construction of the coater and the clean room at the same time on two floors.

-3000-

Vacuum

VACUUM SYSTEM
Introduction

The entire interferometer is put in vacuum in order to suppress several sources of noise, each one of them being strong enough at atmospheric pressure to prevent the observation of gravitational waves. They are :

- the transmission of acoustical noise,
- the damping of the mirror suspension and the corresponding increase of its thermal noise,
- the scattering of light by residual gas molecules,
- the brownian motion of the mirrors,
- the random fluctuations of the refractive index.

This last one is by far the largest one related to vacuum. If one finds satisfactory conditions for it, then all the other ones will be fulfilled. The fluctuations of the number of molecules contained inside the volume of the light beam is the source of variations of the optical path length. These fluctuations may be produced either by the poissonian distribution of the molecules in steady vacuum or by the occurrence of sudden bursts of molecules. In both cases, the effect is proportional to the polarizability of the molecules. In practice one expects the dominant residual gas to be hydrogen which has a low polarizability.
In a steady vacuum, the poissonian fluctuations of the number of molecules within the beam are evaluated as if the ratio of the volume of the tube to the volume of the beam was infinity. The basic correlation time corresponds to the time for evacuating the molecules through the boundaries of the beam (or to the reverse). It is 60 μs for hydrogen and 180 μs for water vapour. This is to be compared to 10 μs for the light transit time between two mirrors and about 500 μs for the light storage time.

1. QUIET VACUUM.

The relationship between the sensitivity of the antenna and the average pressure has been derived in the 1990 Virgo proposal. We would like the gas pressure noise not to be a limiting factor for the antenna sensitivity, that is, at least, one order of magnitude lower than the shot noise level (see fig. 2-15-1).

The target sensitivity of the antenna has been set to be $\tilde{h} = 10^{-23}\,Hz^{-1/2}$. A pressure of hydrogen, in the absence of other gases of $2.\ 10^{-7}$ mbar ($2.\ 10^{-5}$ Pa) would give a corresponding noise level of $\tilde{h} = 10^{-24}\,Hz^{-1/2}$, in agreement with the above requirement. Due to their higher polarizability, a total pressure of $2.\ 10^{-8}$ mbar ($2.\ 10^{-6}$ Pa) for most other gases, in the absence of hydrogen, would give the same noise level.

Having in mind future improvements of the antenna sensitivity by an order of magnitude, the ultimate pressure should be 100 times lower. This could be achieved either by a higher pumping speed or alternatively by a lower outgassing rate, far easier to perform. Virgo proposes from the start to reach the ultimate hydrogen outgassing rate through an air firing treatment of the stainless steel at 400°C.

Furthermore, the residual gas must be free of hydrocarbons, in order to keep the optical surfaces clean. A partial pressure of less than 10^{-14} mbar (10^{-12} Pa) is required if one wants to avoid the cumulative deposition of a single layer of hydrocarbons on the optics in 4 years.
Then, the target for the average partial pressures on the optical path of the Virgo beam are :

	Acceptable value at start (1999)	Ultimate realistic value
H_2	$1.\ 10^{-7}$ mbar ($1.\ 1u^{-5}$ Pa)	$1.\ 10^{-9}$ mbar ($1.\ 10^{-7}$ Pa)
Σ other gases	$1.\ 10^{-8}$ mbar ($1.\ 10^{-6}$ Pa)	$1.\ 10^{-10}$ mbar ($1.\ 10^{-9}$ Pa)
Hydrocarbons	$1.\ 10^{-14}$ mbar ($1.\ 10^{-12}$ Pa)	$1.\ 10^{-14}$ mbar ($1.\ 10^{-14}$ Pa)

2. BURSTS OF MOLECULES.

These phenomena are very difficult to assess, but a first attempt is to describe the various possible sources and then try to develop their consequences on the behaviour of the antenna.

2.1. *The possible sources.*

Mechanical motions of the inner part of the vacuum system is a well known source. It can be produced by vibrations. By far, the most dangerous, from practical experience, is the friction between metallic surfaces (actuation of vacuum valves).

Ion pumps have been found responsible for molecular bursts. This could originate from micro-fragments of titanium being extracted either from the cathode or sometimes from the anode. These objects, which have absorbed many molecules, bounce between the two electrodes and can release molecules bursts at some stage.

At the present time, the only possible policy is to try to observe these effects in laboratory conditions, and to minimize their consequences on the antenna.

2.2. *The burst characteristics.*

2.2.1. - the time dependence

If the emission time is short, then the rise time of the pulse is of the order of D/V_i, where D is the tube diameter and V_i the molecule velocity, it is typically 680 µs for hydrogen. Otherwise, the rise time is longer.

The decay time is of the order of v/S where v is the volume of a 300 m section and S is the pumping speed on the section, that is roughly 100 s for hydrogen.

This asymetry between rise time and decay times gives a possible way of recognizing the signature of a pressure burst.

2.2.2. - the dangerous level

Both the statistical fluctuations of the quiet vacuum and the molecule bursts are the source of optical index variations. In consequence, the dangerous level will be assumed to be equivalent to the statistical fluctuations for a hydrogen pressure of $2\ 10^{-5}$ mbar.

At this pressure, the number of molecules in the beam volume of diameter d, 10 cm, is $1.3\ 10^{19}$ and the variance $3.5\ 10^{9}$. Since one assumes the burst of molecules to fill up the whole cross section of the tube, the relevant number will be a factor $(D/d)^2$ higher that is $3.5\ 10^{11}$. Distributed locally over 1 m length of tube, it would produce a pressure variation of $1.5\ 10^{-11}$ mbar.

Only the antenna is capable of detecting such a small variation.

With the ion pump located at one end of the titanium sublimator (see paragraph "pumping system - unit #3"), the number of molecules reaching the tube would roughly be a factor of 10 smaller, for a fresh layer of titanium.

With the very low outgassing rates and the large pumping speed foreseen for the vacuum system of Virgo, the ion pumps will work in very good conditions and one can expect these events to be rare.

3. SHORT DESCRIPTION OF THE VACUUM SYSTEM.

It consists basically of two tubes, each 3 km long, joined in an L shape and of ten towers disposed as shown in fig. 1. All the vacuum vessels are made in 304 L stainless steel. Each tube and tower can be isolated from the connected elements by large gate valves. The full volume can be divided in two parts: a ultra high vacuum volume and a modest vacuum volume.

3.1. *The tubes.*

Each 3 km tube has a diameter of 1.2 m. It is made of ten 300 m long sections. Every section will be built and tested separately for leaks and for ultimate vacuum after bake out. The sections will remain under vacuum until they are all ready to be connected.

The tubes will be in ultra high vacuum. This will be achieved thanks to air firing of the tube modules, adequate surface cleaning, subsequent 150 °C bake out and finally thanks to a large permanent pumping speed.

3.2. *The diaphragms.*

They are made of special glass and distributed in the tube so as to kill the scattered light as much as possible.

3.3. *The towers.*

Seven of the ten towers [mirror towers] will be built in two parts, the so-called "tower upper part" and "tower bottom part", connected by a small conductance. The bottom part of the mirror towers which contains only clean optics, will be in ultra high vacuum. This will be achieved thanks to air firing of the raw stainless steel, adequate surface cleaning, subsequent 150° C bake out and finally thanks to a large permanent pumping speed.

In contrast, the upper part of the mirror towers which contains the superattenuators and the actuators [large outgassing rates] and the three other towers consisting of single blocks, will require a modest vacuum i.e. a pressure around 10^{-4} Pa.

3.4. *The pumping system.*

The pumping system has been designed to allow for a high running efficiency of the antenna.

The tubes and the towers will be evacuated by dry pumps in order to avoid the air pollution in the environment ; the two parts of the mirror towers will be evacuated by the same dry pump.

At a later stage and during the bake out period an intermediate pumping will be used on the high vacuum volumes, and in the end the permanent pumping will be achieved with the help of large Ti sublimation pumps and small ion pumps.

Turbo pumps will be used for the intermediate and permanent pumping of the modest vacuum volumes.

The vacuum monitoring is done by measuring boxes.

All the pumps and the instrumentation boxes are connected to the large vacuum chambers through gate valves.

4. R & D PROGRESS IN THE RECENT PERIOD.

Three years ago VIRGO launched two parallel programs at Calambrone and at Orsay in order to study large scale prototypes of the vacuum tube. These were called respectively the Strengthened Reinforced Tube (SRT) and the Corrugated Tube (CT) prototypes. Both groups aimed at ultimate low hydrogen outgassing rates through either a prolongated air firing at 400 C° or a 950 °C vacuum firing. In the recent period, their results were analyzed in the light of the theory of hydrogen diffusion and solubility in the stainless steel matrix. The latter, besides the temperature dependance of the mechanism, was examined in connection with the existing hydrogen pressure arising either through water vapor dissociation during the elaboration of the alloy or from the natural hydrogen content in air.

One can summarize the results as follows.

Both kinds of prototypes experienced industrial fabrication and surface cleaning. After bake out for about a week at 150 °C, they presented similar outgassing rates for hydrogen, the dominant gas species, namely 2 to 3 10^{-12} mbar l cm^{-2} s^{-1}. The 48 m long Calambrone prototype was then air fired at 380 °C for 100 hours maintaining a constant inner gas flow in order to eliminate the contamination by the hydrogen being released in the inner part of the tube. Subsequently an outgassing rate around 5 10^{-15} mbar l cm^{-2} s^{-1} was obtained after a standard bake out and pumping as described above.

At Orsay a second prototype made of stainless steel sheets, 950 °C vacuum fired for 2 hours, gave an outgassing rate of 2,5 10^{-14} mbar l cm^{-2} s^{-1}. The difference with the rate obtained on the Calambrone tube was attributed to the weld contamination by traces of water vapor dissociated by the argon arc discharge. In order to test this hypothesis, the first Orsay prototype was split into three elements. Each of these was air fired at 400 °C for 38 hours (or similar conditions), respecting the necessary precaution to evacuate the hydrogen released from the metal. After reconstituting the prototype and a standard bake out and pumping, an ultimate outgassing rate of hydrogen of 1,5 10^{-15} mbar l $cm^{-2}cm^{-2}$ s^{-1} was obtained. The improvement factor is sensibly in agreement with the reduction of the length of the welds, when comparing the second and the third test.

For an industrial construction of the tubes, VIRGO took a conservative value of 5 10^{-14} mbar l cm^{-2} s^{-1} for the hydrogen outgassing rate. This is more than an order of magnitude larger than the ultimate rate achieved. It is still compatible with a process involving a 400 °C air firing of the metal sheets which would exclude the treatment of the welds.

Other developments were made on bake out (heating tapes and Impedance Heating System), on thermal insulation, on pumping aspects (dry pumping for evacuation, permanent pumping with titanium sublimators, cryogenic pumping for the tower upper parts) and finally on instrumentation.

Hydrocarbon contamination after a normal cycle of bake out and pumping using a TMP and a mechanical forepump separated by a zeolite trap, was found to be close to the level required by VIRGO.

All these efforts confirmed the feasibility of vacuum performances far better than the ones presently needed for VIRGO, thus allowing for increased performances in other field limiting the antenna sensitivy.

Concerning the tube, a choice had to be made between the CT and the SRT solutions, although both could meet the final requirements of Virgo. Based on financial considerations the SRT solution was selected. It however incorporates some of the CT ideas, concerning essentially lips and welding and nibbling robots.

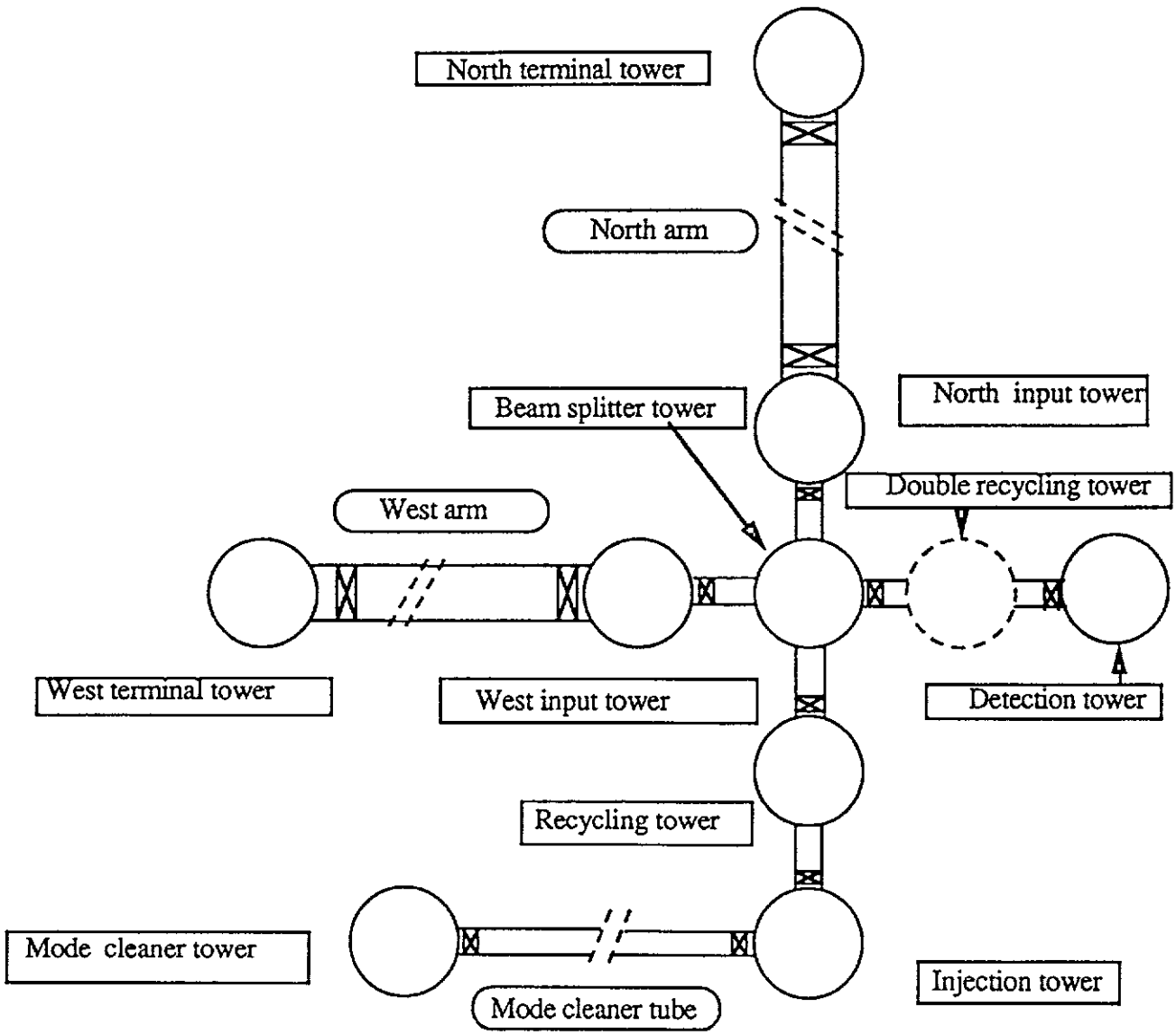
North terminal tower
North arm
Beam splitter tower
North input tower
Double recycling tower
West arm
West terminal tower
West input tower
Detection tower
Recycling tower
Mode cleaner tower
Mode cleaner tube
Injection tower

Figure A

TUBE

3100.1. GENERAL SPECIFICATIONS

The general sketch of the antenna, limited to tubes and towers is presented in Fig.A
The main parameters of the two 3km long vacuum tubes are summarized below:

Inner diameter	1200 mm
External pressure	1 bar
Length of each arm	3000 m
Residual pressure	10^{-9}mbar for H2
	10^{-14} mbar for hydrocarbons
	10^{-10}mbar for other gas species
Outgassing rate	5.10^{-14} mbar l/s cm^2 for H_2
Temperature of reference	20°C
Temperature range	-20°c, +150°C (250°C occasionnaly)
Working temperature range	-5°C, +40°C
Lifetime	20 years
Viton valves at ends of arms	1200mm
Bake-out temperature	150°C (maximum power 150 W/m)
Distance between pumping groups	300 m
Distance between floor and tube axis	1450mm

Straightness: the tube axis has to be contained within a 50mm diameter
Presence of baffles in the tube
No elastomere gaskets for the permanent seals
Minimum amplification of the seismic noise for any frequency

3100.2. CHOICE OF THE MODE OF CONSTRUCTION

Given the huge dimension and the relative simplicity of the required chamber geometry, the VIRGO group has investigated the typical industrial requirements for pipes and has tried to adopt its mechanical construction with a few changes to meet the severe vacuum parameters of VIRGO.
The VIRGO pipe, even if submitted to vacuum and not to internal pressure, is certainly, from a technical point of view, fully within the field of application of pressure codes, such as ASME VIII div.1 and 2, which represent the state of the art of tested techniques of industrial usage. On this line, structural calculations were performed for a plain tube, 5mm thick and reinforced with rings (doc 559C0201, 1994). Such a rigid section, together with an expansion joint and with flexible and fixed supports could represent a module. Along this line, the VIRGO group designed and realized a full-dimension prototype, (except for the length), to check both the fabrication procedures as well as the efficiency of material treatments to reach the internal pressure required by VIRGO. Particular care was devoted to finding a type of weld to join together the modules on site.
Special attention was put on cost and savings in general i.e. the adoption of bellows working in plastic regime and standard supports, as used in industrial applications.
On the basis of the promising results of the prototype, where an outgassing-rate below $5x10^{-15}$ mbar l/s cm ^{2} was obtained after a 400°C air- firing, followed by a standard 150° bake-out. The technical specification VV000 including several annexes, for the first 300m of vacuum tube, applicable to the manufacturing of the two, 3km long tubes of VIRGO was writen.
Details will be summarized in the following pages concerning the construction and the on-site assembly.

3100.3.CONSTRUCTION OF A 25 m LONG BASIC ELEMENT

3100.3.1.Description

1.1 Components
A 25 m long basic module, shown in Fig. 1 is made of :
- a long plain tube with stiffening rings
- a short section containing the bellow

It is terminated with lips to be automatically welded to the next module on the site.
The length of 25 m has been chosen to limit the number of welds to be performed in the tunnel during the assembly and also the number of deliveries, however considering special transport above a length of 12 meters. Nevertheless, the final length could be reduced without any major drawbacks if a cost analysis, enlarged to the infrastructures and to the whole project, would point out the opportunity.
1.2 Realization
Following a cal for tender, the managing laboratory chooses a factory, which will manufacture the tubes; purchase the bellows and supports, perform the assemblies and all the operations up to the delivery on site of the modules already equipped with thermal insulation of the rigid part. The laboratory can order directly the stainless steel.

3100.3.2.Description of the components

3100.3.2.1.Tubes

3100.3.2.1.1.Raw material

The raw material is 304 L stainless steel, in cold rolled 5mm thick sheets with surface roughness 2 B (<1μm) obtained without any further treatment. It is a standard product for which there will be a detailed specification with acceptance tests for the chemical composition, the mechanical properties, the amount of inclusions and a quality control program (Annex VV003).

3100.3.2.1.2.Fabrication

The tube element, about 24m long, 1200mm inner diameter, is built starting from sheets, properly calendered and welded to form ferrule, plasma butt-welded together. Each ferrule is equipped with stiffening rings, properly machined and welded to strengthen the structure. The two end pieces are machined to reduce the thickness from 5 to 2mm to match respectively the bellow or the lip joint.

3100.3.2.2.Bellow section.

The bellow section, about 1meter long, is shown in Fig.2.
The end piece of the previous tube element is TIG butt-welded to the bellow. This is followed by a short ferrule welded to a lip. A stiffening ring is welded into the short ferrule. The next tube element starts by a lip and another stiffening ring. After welding the two lips, the two rings are rigidly connected so as to avoid any stress on the lips.
The bellows have to fulfil general specifications concerning external pressure, residual internal pressure, outgassing rate, lifetime. Following Annex VV004, technical specifications are here reported:

- Internal diameter = 1200 mm
- Thickness = 2 mm
- Material = A240-304 L
- Reference temperature = 20 °C
- Axial compression = 55 mm (150°C)
  = 100 mm (250 °C)
- Axial extension = 10 mm
  (20 mm once at assembly)
- Lateral displacement (+ -) < 2 mm
- Permanent load : exter. pressure 1 bar, inter.pressure 10^{-9} mb
- Vacuum control : Q =10^{-9} mbar l s^{-1}
- Life (year) = 20
- Cycles number =10 due to bake-out
  at 150 °C (optional 250 °C) for a time of a week per cycle.
- Convolutions number =5-10 in accordance
  with standard criteria ANSI B-31-3, E.J.M.A. 93.

3100.3.2.3.Supports

For each 25m long module, a central fixed support carries out weight, lateral thrusts and axial forces due to the bellow deformations. One sliding support, at each end, carries out weights and permits longitudinal displacements due to thermal effects (Fig.4). Their function will appear more evident in the chapter dedicated to 300m sections.

All the supports (Figs.3,4) are divided in two parts, one on top of the other. The top one, rigidly fixed to dedicated stiffening rings of the tube, is designed to allow the transportation of the module and wil be finally bolted to the bottom - stand by means of rubber blocks. These isolate electrically the tube from the ground and are part of the sliding supports, thus allowing for the thermal expansion.

3100.3.3.Cleaning

3100.3.3.1.Cleaning condition.

The essential aim of the cleaning process, here summarized from the annex VV001, is to obtain an ultra-high vacuum in the range of 10^{-9}mbar, hydrogen equivalent, all along the tubes.

A stainless-steel workshop must be available for manufacturing all the components, but in addition, a few steps wil have to be performed in a clean area (Annex VV005) where temperature and environmental cleaning is under control. Adequate flooring, proper illumination and specific entrance-exit controls are mandatory.

3100.3.3.2.Cleaning treatments of vacuum exposed surfaces

3100.3.3.2.1.Degreasing

The degreasing procedure is divided in two phases in order to remove traces of hydrocarbons. The first one foresees organic solvents like acetone, benzol and ethyl alcohol, the second one alkaline phosphates detergents in a warm solution (app.60°C). For the final modules, the solution can be projected onto the pieces by means of a high pressure jet. However a water film has to be kept on the surface till the final rincing in order to avoid alcaline deposit.

3100.3.3.2.2.Rinsing

After degreasing, all the pieces are rinsed first with ordinary tap water and then with a demineralized water jet.

3100.3.3.2.3.Drying and preserving

At this point, the components must be dried with dry hot air, free of dust and oil for the final vacuum test and then protected with plastic bags.

3100.3.4.Vacuum Control

3100.3.4.1.Operating mode

As mentioned before, each 25m long module is terminated with lips for the connection of adjacent modules on the site. Vacuum seals are provided still at the factory by coupling these lip-joints with provisional covers and viton gaskets for the vacuum test which is performed in the clean area by the factory in the presence of qualified VIRGO specialists (Annex VV002).

3100.3.4.2.Acceptance criterion

The components meet the following standard:

a) localized leaks < 1×10^{-10} mbar l/s

b) total leak per component, 5×10^{-10} mbar l/s

3100.3.4.3.Vacuum inspection system

The whole system is supplied by the manufacturer and consists of:

- a pumping group containing an oil-free turbo molecular pump
- an helium leak detector with sensitivity in the range 10^{-5} -10^{-11} mbarl/s
- calibrated Helium leaks in the range of 10^{-8} mbar l/s

3100.3.5.Thermal insulation

Following the leak test the module is vented with dry air up with a light over-pressure, while at the factory, the rigid part of the module (about 24m) is equipped with insulating material for the future bake-out operations. Two overlapping rock-wool layers, fixed with wires and covered with an aluminium sheet provide a high uniformity temperature distribution. With a thickness of 15 cm for the thermal insulation, the power per unit length is 150W/m for a bake-out temperature of 150°C. Fig. 3 and 4 show that the addition of this insulation increases the tube diameter up to 1500mm without compromising the module transportation.

3100.3.6.Packing and shipment

Packing is the last operation in the factory. Each module, still completely isolated and slightly over-pressurised, has to be cleaned externally before being protected by means of plastic bags for the shipment.

3100.3.7.Special modules

According to the strategy of the assembly, which is analysed in the next chapter, each 3 km long tube consists of ten sections. Each section, 300m long, consists of 12 modules, but the first and the twelfth are slightly different in comparison to the standard ones and are called initial and terminal. The initial doesn't have a bellow component. The terminal one has three ports equipped with CF flanges for pumping and instrumentation, temporarily sealed off with blind counter flanges during tests and shipment. The main difference, however, is in their fixed supports which are designed to endure the stress due to atmospheric pressure during the vacuum test of each 300 meters section foreseen in the assembly plan (Fig.5).

3100.4.ASSEMBLY

3100.4.1.Reception

Two tunnels wil house the vacuum tubes of the interferometer. In the middle of each tunnel a service area of 60m long x10m wide will be placed alongside the tunnel to receive the modules from the factory. The hall will be equipped with a crane, a 200 KW power source and distribution of water, compressed air and a clean air source. It will be divided into two parts, A and B, separated by a plastic tent in order to complete the final operation on the modules before the assembly phase preventing risks of hydrocarbon and dust contamination. Part A is dedicated to the reception of the modules to the installation of removable insulation jackets on the bellow portions and to air firing; part B a sort of clean area is dedicated to the storage and finally to the introduction of all the components into the tunnel through a large gate.

3100.4.2.Air-Firing

Air-firing is a process, well experimented on the prototype, to deplete the initial atomic hydrogen concentration, ultimately responsible for the outgassing rate, of the stainless-steel walls of the modules. Practically, each module has to be brought up to 400°C for 5 days with a slight inner air flux.

Heating is achieved via Joule effect in the electrical resistance of the tube walls, providing DC current through the tube by means of a mobile group composed of adiesel generator, avoltage transformer and an AC/DC converter.

The operation will be performed in part A of the hall on four modules temporarily connected in series with copper clamps attached to the stiffening rings of the supports.

As soon as the modules are received, they will be freed from the viton gaskets in a continuous clean air flux and protected by a tent. The power consumption reaches now 1.5 KW /m with the above thermal insulation (Annex VV006).

3100.4.3.Installation of the Sections

3100.4.3.1.Strategy

The modules, after firing, are moved and stored in part B of the hall before being taken into the tunnel one by one. This part of the service area, not yet completely designed, could overlap the tunnel. The crane operating there can directly load the modules on suitable trolleys for their transportation and assembly in the tunnel. Given the dimension of the tunnel in comparison to the modules, the trolleys, conveniently guided, can be used also for the replacement of a faulty module when the tube is already assembled.

As far as the guiding is concerned, a solution could be to use 3 tramway-like rails embedded in the floor all along the whole length of the tunnel (Fig.6).

Fig.7 shows a schematic view of the module assembly in the tunnel. At the same time, four modules are air-fired in service area A, while in part B other modules are prepared and stored.

3100.4.3.2. Alignment

As mentioned before, the tube axis has to be contained within a 50mm diameter. This tolerance must take into account:

a) the defectt of the tube construction
b) the imperfections of the implementation
c) the long term evolution of the tunnel

One fifth of the tolerance will be given to points a and b.
On the top part rigidly fixed to the module, a fiducial mark indicates precisely a fixed distance from the central axis of the tube. During the assembly, the modules are positioned refering these marks to a reference system represented by two straight lines, one on the floor and the other on the walls of the tunnel, materialized by visible marks every 50m. The reference system and the two straight lines can be supplied by the optical alignment group taking into account their special equipment and, more important, their absolute reference system.
Future contacts with them to exchange ideas and information, will give us the possibility of finalizing an operative procedure to assemble the tube respecting the required tolerance.

3100.4.3.3. Welding with protective tent

The assembly of the first section, starts with the initial module and continues with the 10 standard modules up to the terminal one. Each one of them puts in place by the trolley matching the top part of the support with the respective bottom one, which is immediately fixed to the ground. Some adjustments, performed with the help of the same trolley, are necessary to align the module into the correct position before bolting together the two parts of the supports. When two adjacent modules are in position, the lip welding is performed by means of the welding robot.
Each operation with a risk of contamination such as dismounting, end covers, counter-flanges and the same lip welding itself, is implemented under a movable air-fluxed protective tent.

3100.4.3.4. Baffle Installation

Some baffles have to be placed in the tube to prevent the laser light from being scattered on the tube walls. Each module will be equipped with baffles after having been lip-welded to the previous one in the tunnel. A proper device can do the job.

3100.4.4. Processing of the Sections

3100.4.4.1. Vacuum test and leak search

During the assembly each 300 meters section is prepared for the vacuum test. The first end-cover of the initial and the last one of the terminal module are vacuum-tight mounted, the counter-flanges of the terminal module are replaced by gate valves, followed by the proper pumping systems. The insulation jacket around the lip-welds joints is removed and finally the evacuation and the search for leaks can take place. Leaks can be repaired only by delaying the next bake-out operation.

3100.4.4.2. Bake-out

The initial and terminal modules have special current connections (Figs. 5,8). Heating is achieved via Joule effect in the electrical resistance of the tube walls, providing DC current from the electrical installation. The power per unit length is now 150W/m. However, a return conductor must be provided in the tunnel. (Annex VV006)
Once the bake-out is over, the residual pressure for hydrogen at room temperature has to reach the required value of 10^{-9} mbar in order for the section to be accepted.

3100.4.5.Connecting of the Sections

The assembly of a tube proceeds with the sections separately receive tested as described in **4** . When all the ten sections are vacuum-accepted, the final assembly can be done, after a proper venting and removing the provisional covers from the initial and terminal modules. Each section presents one lip joint at both ends and is connected to the adjacent section by inserting a bellow type B (Fig.2B), conveniently compressed, and operating at both sides the automatic welds with the robot.
Fig.9 shows a schematic view of the section and of the 3km long tube. At the both ends of the tube, two gate valves are installed which complete the final assembly.

3100.5.- THE MODE CLEANER TUBE

The mode cleaner tube, the mode cleaner tower and the input optics tower constitute a special chamber isolated from the Virgo tubes and mirror towers by a window. The function of this system is roughly the same as the one of the large Virgo vacuum system, i.e. to reduce the sources of noise which are :

- the acoustical waves,
- the thermal gradients on the optical path,
- the motion of dusts.

The vacuum contributes also to keep the optics clean.

The specifications for the mode cleaner system are by far less stringent than those of the Virgo vacuum system and a nominal pressure of 10^{-6} mbar is sufficiently low to ensure a safe pressure range for running the pumps. This figure is less than those imposed by scientific needs. It is required that the mode cleaner tube could be dismantled near the input optics tower.

The mode cleaner tube, 20 cm in diameter, 144 ± 2 m long is made of 24 modules 6 m long each, 4 bellows and 2 valves. All these components are made of stainless steel and are equipped with KF flanges using viton gaskets (the flanges are designed to be able to accommodate soft metal gaskets as aluminium or indium). The pumping module is located in the central building. The valves are directly connected to the towers. The bellows are close to the valves and the pumping module.

DRAWINGS - FIGURES

Fig.1 Standard module (VTSM 100X)

Fig.2 Bellow section: a) Type A (VTBM1001); b) Type B (VTBM2001)

Fig.3 Fixed support (VTFS1001)

Fig.4 Sliding support (VTSS1001)

Fig.5 Initial module (VTIM1001)

Fig.6 Cross-section of tunnel

Fig.7 Assembly

Fig.8 Electric connection (VTEC1001)

Fig.9 An Arm (3km long tube) and a standard section

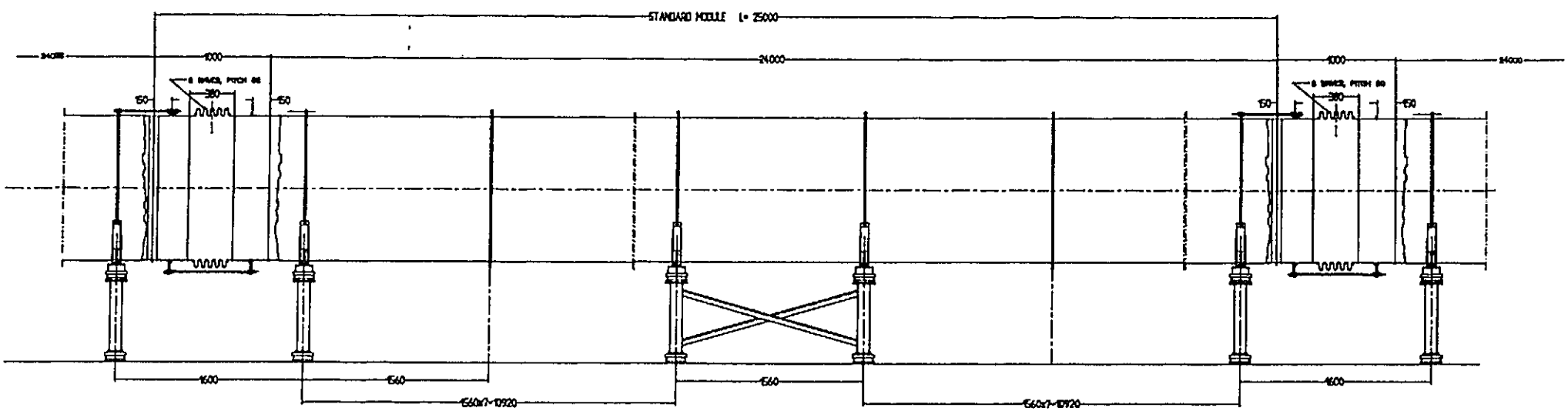

Fig.1 STANDARD MODULE (VTSM100X)

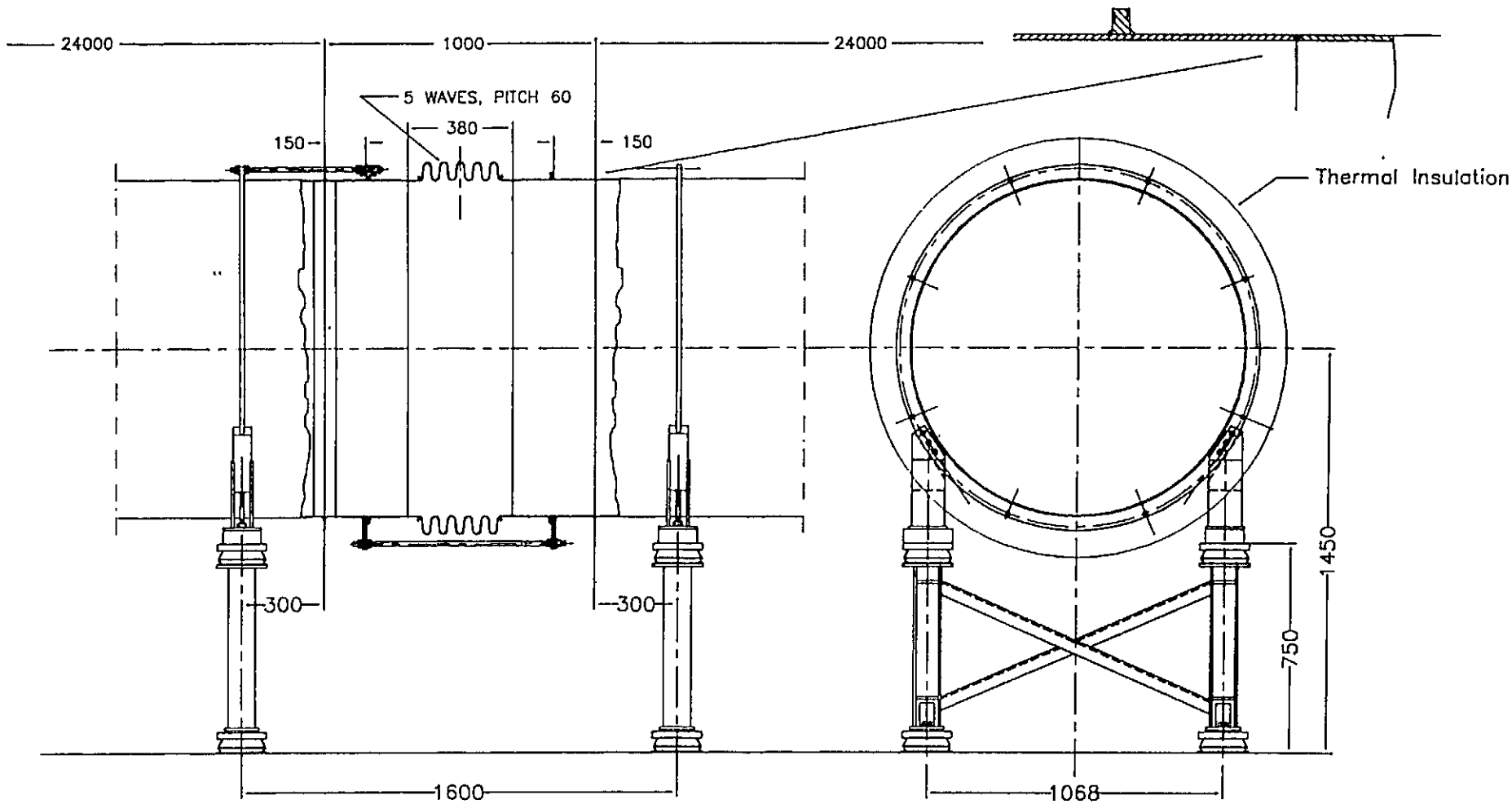

Fig.2 BELLOW SECTION
a) Type A (VTBM1001)

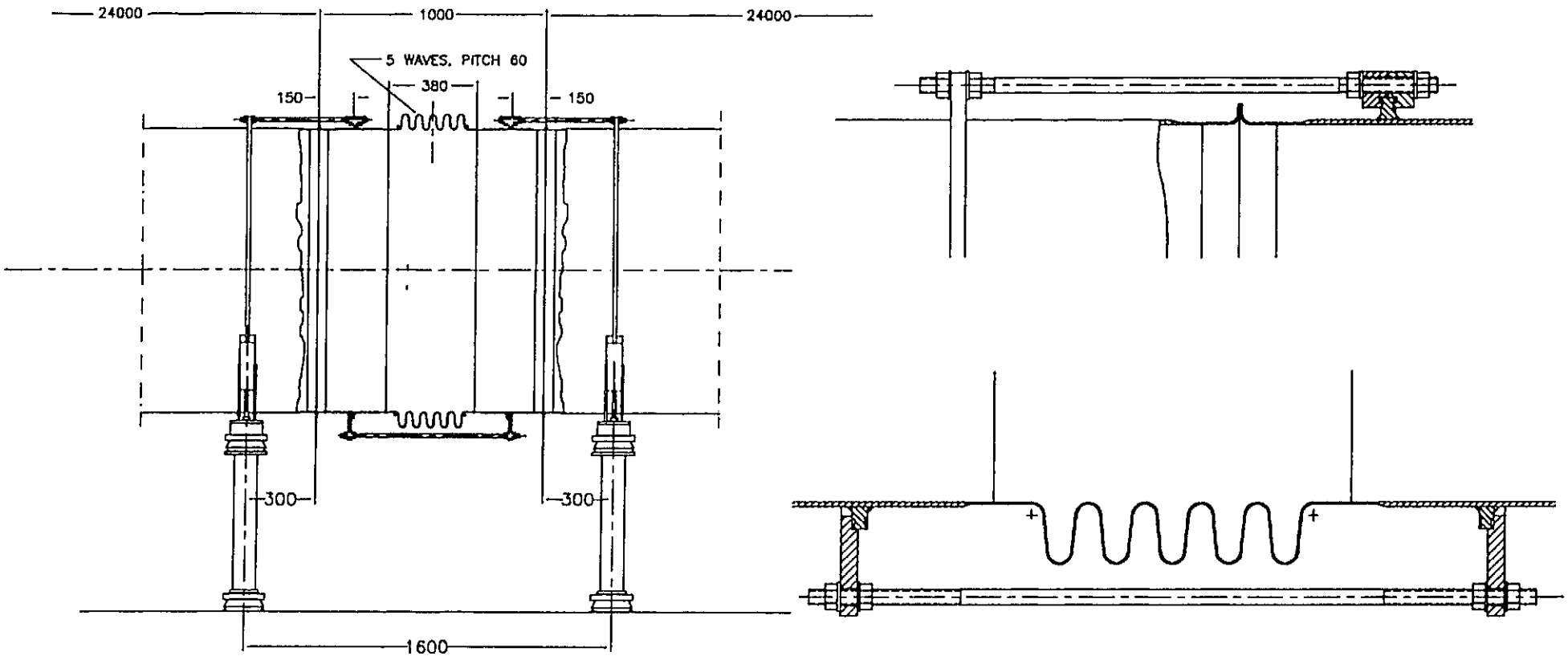

Fig.2 BELLOW SECTION
b) Type B (VTBM2001)

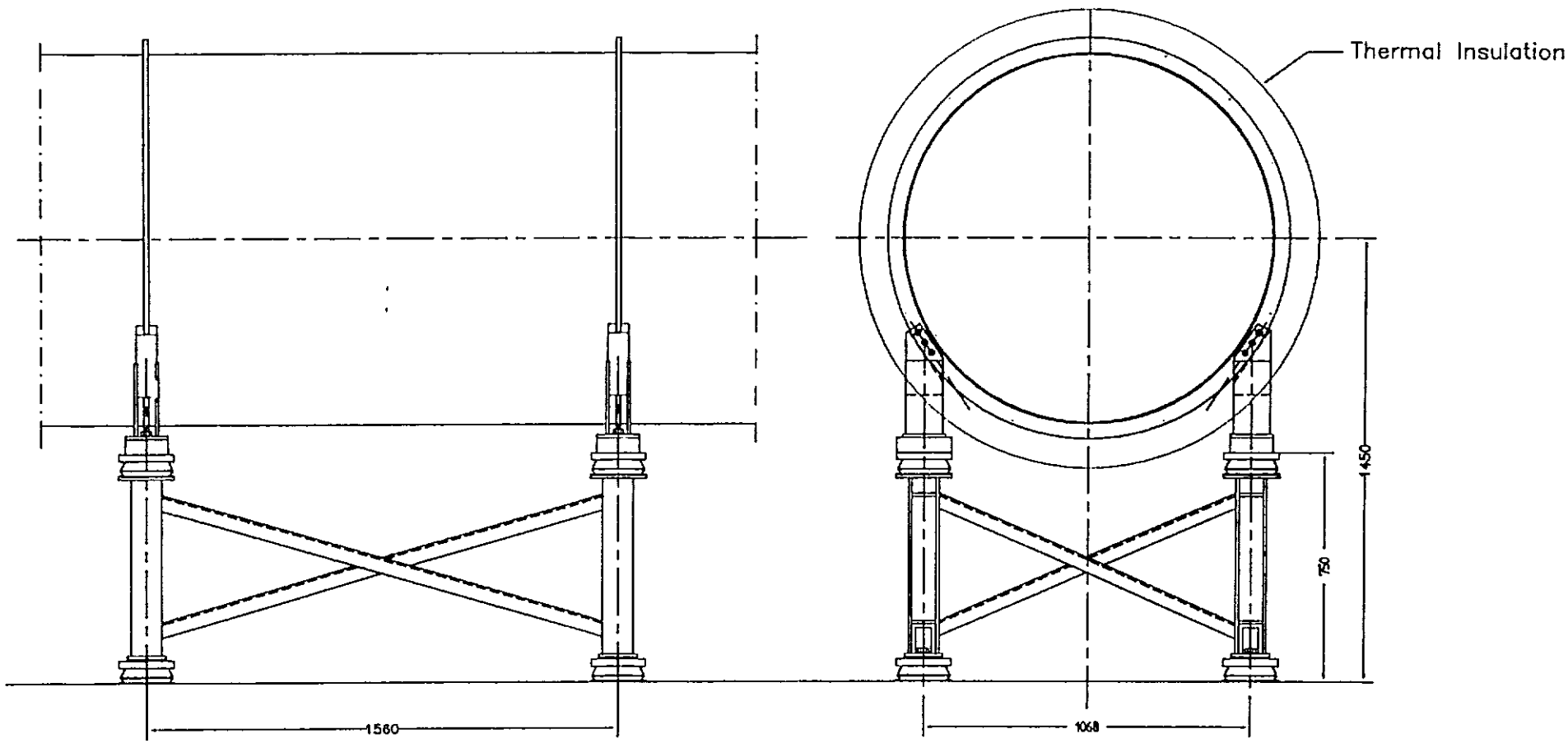

Fig.3 FIXED SUPPORT (VTFS1001)

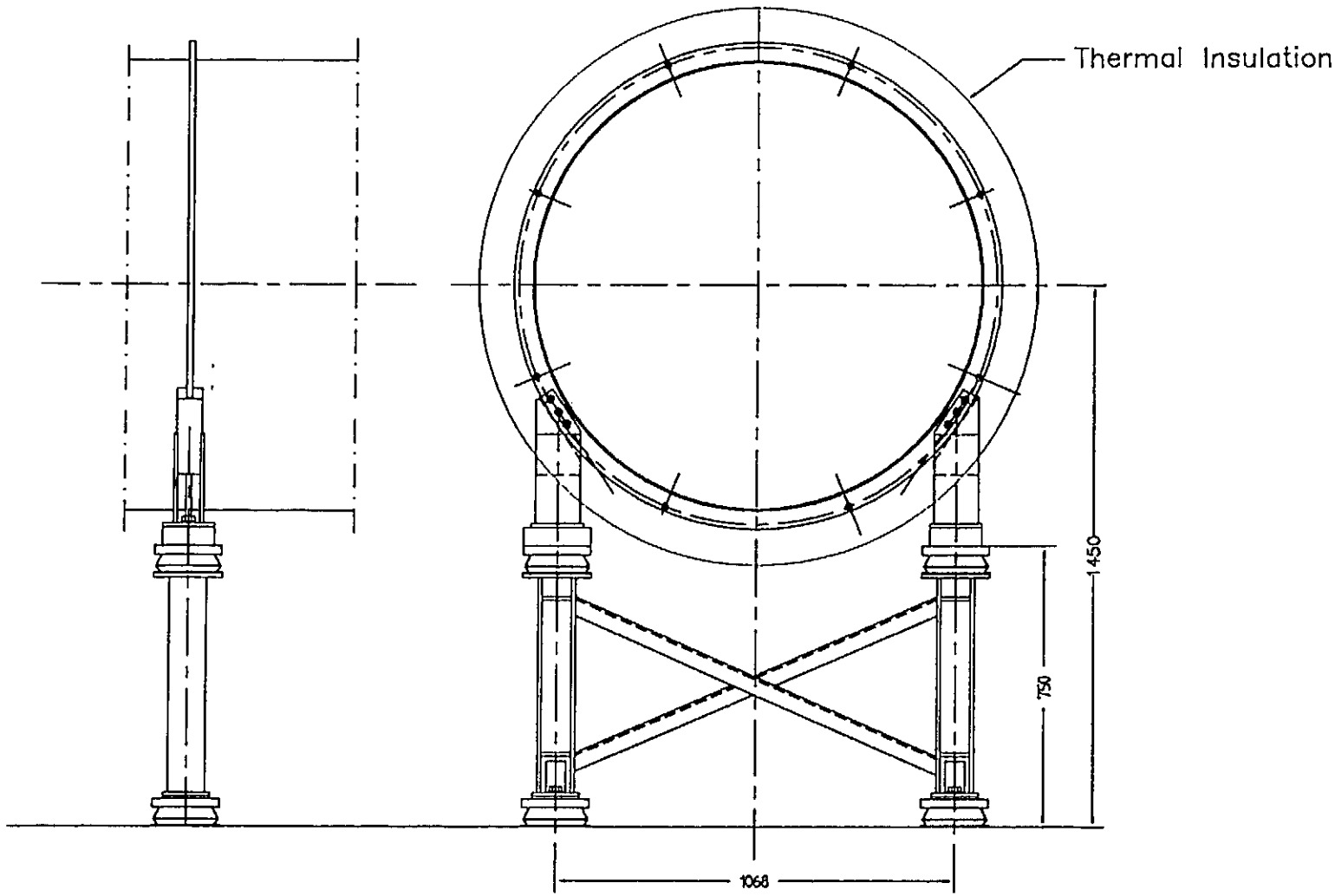

Fig.4 SLIDING SUPPORT (VTSS1001)

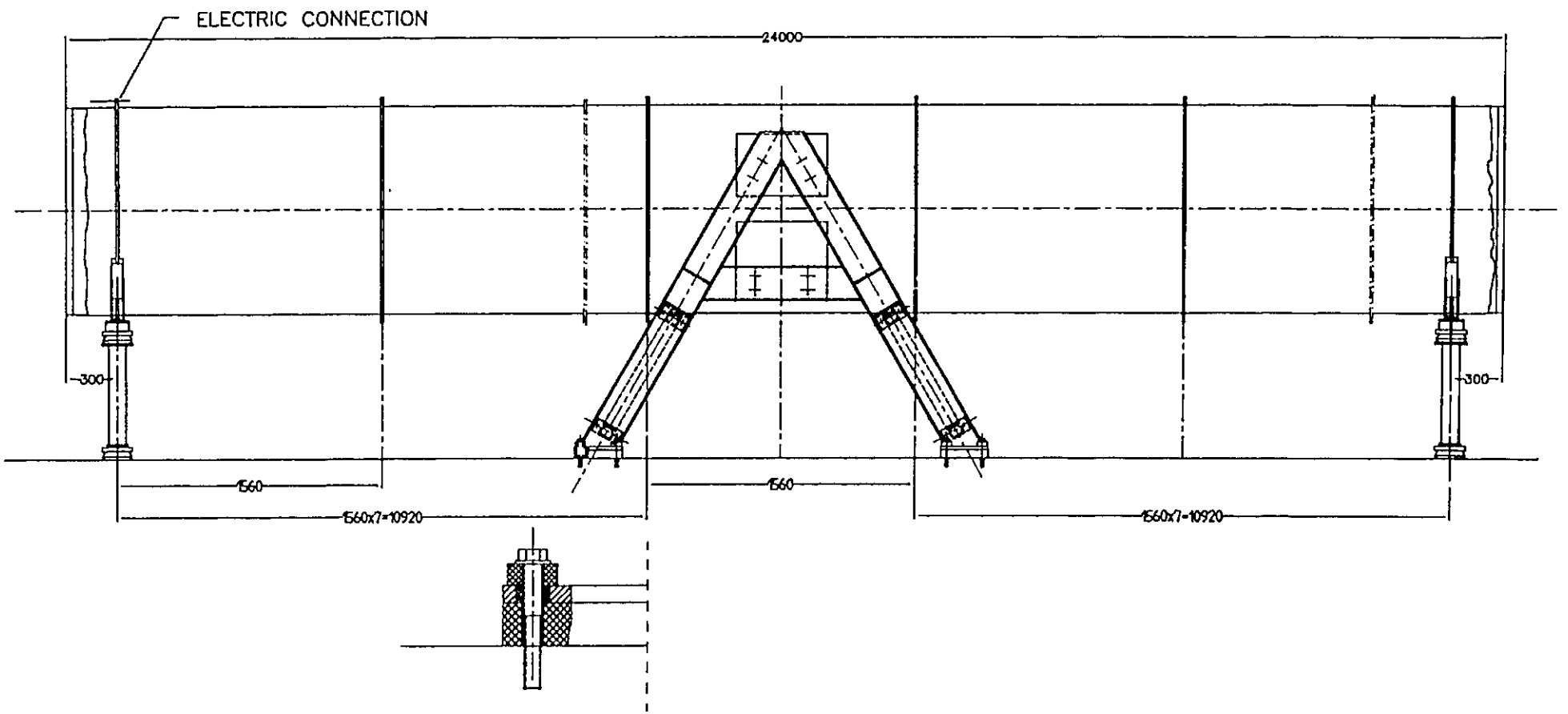

Fig.5 INITIAL MODULE (VTIM1001)

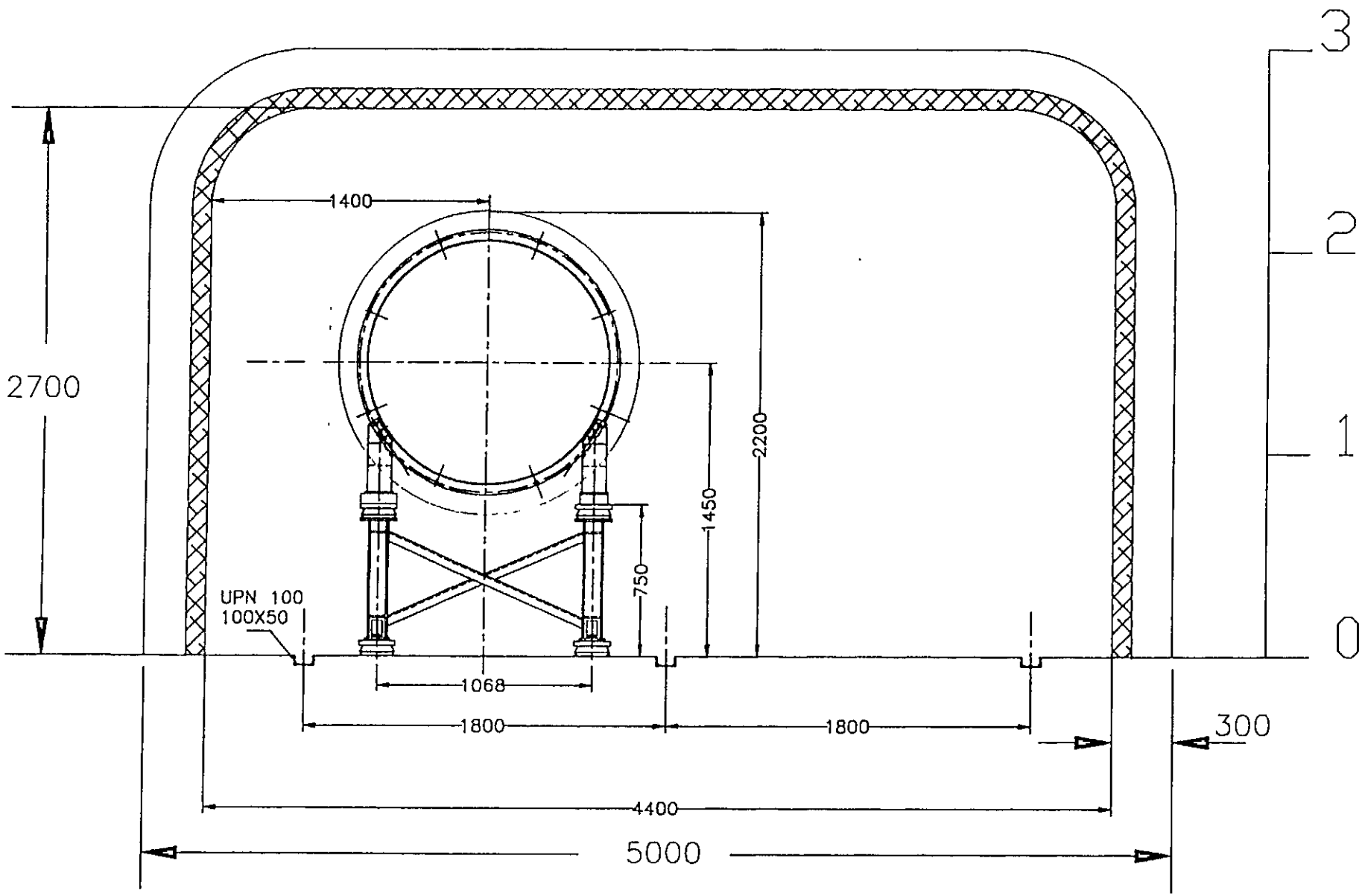

Fig.6 CROSS SECTION OF TUNNEL

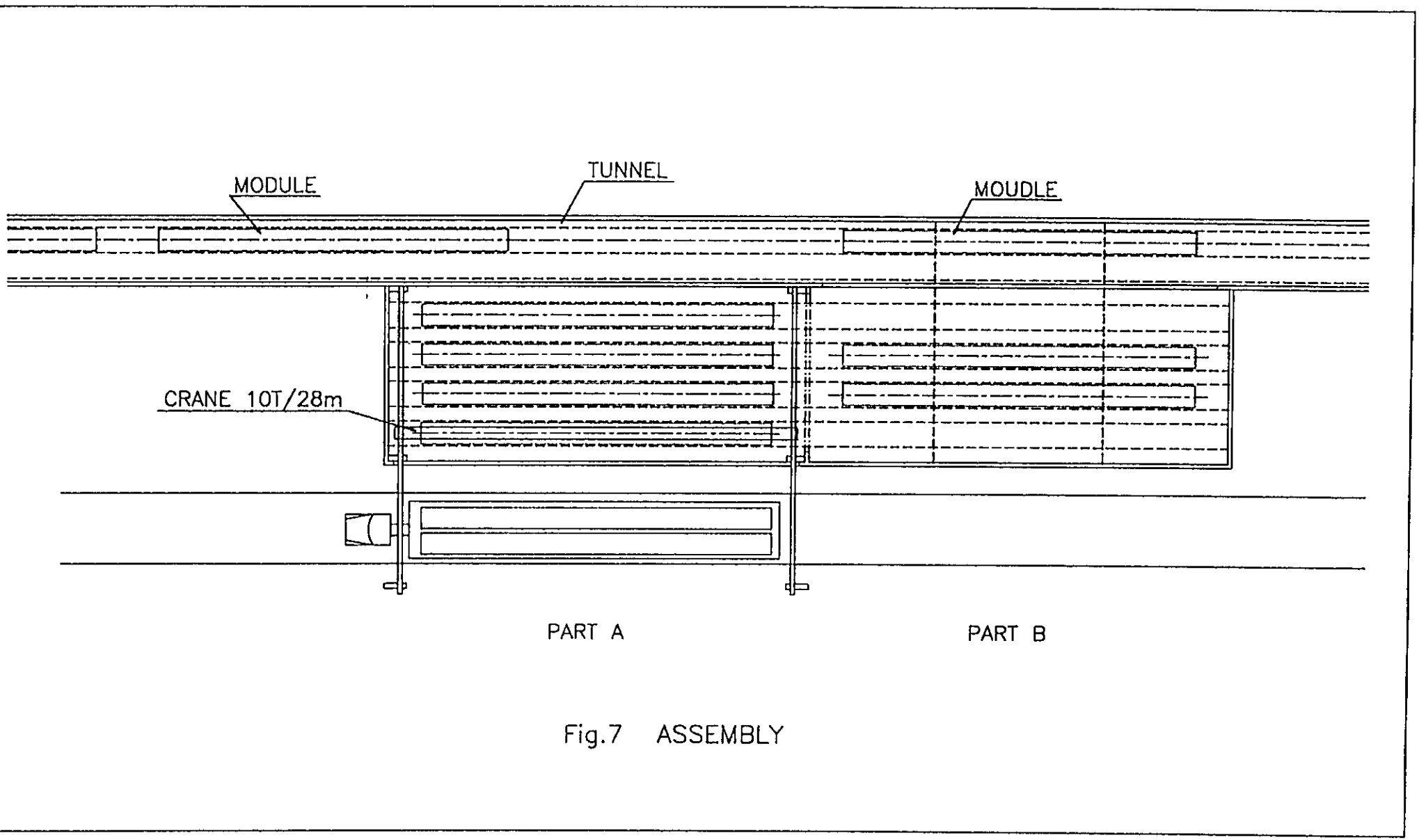

Fig.7 ASSEMBLY

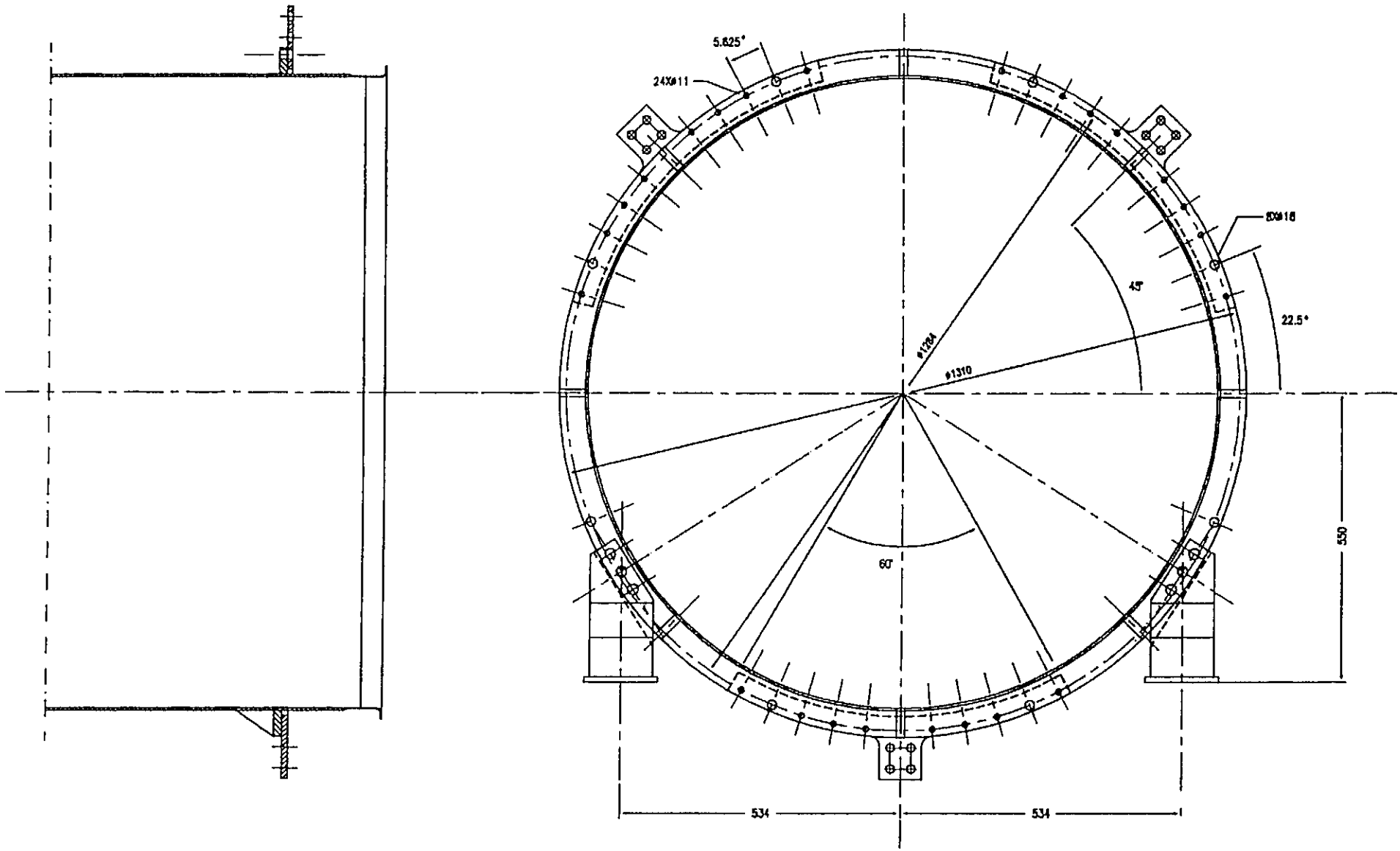

Fig.8 ELECTRIC CONNECTION (VTEC1001)

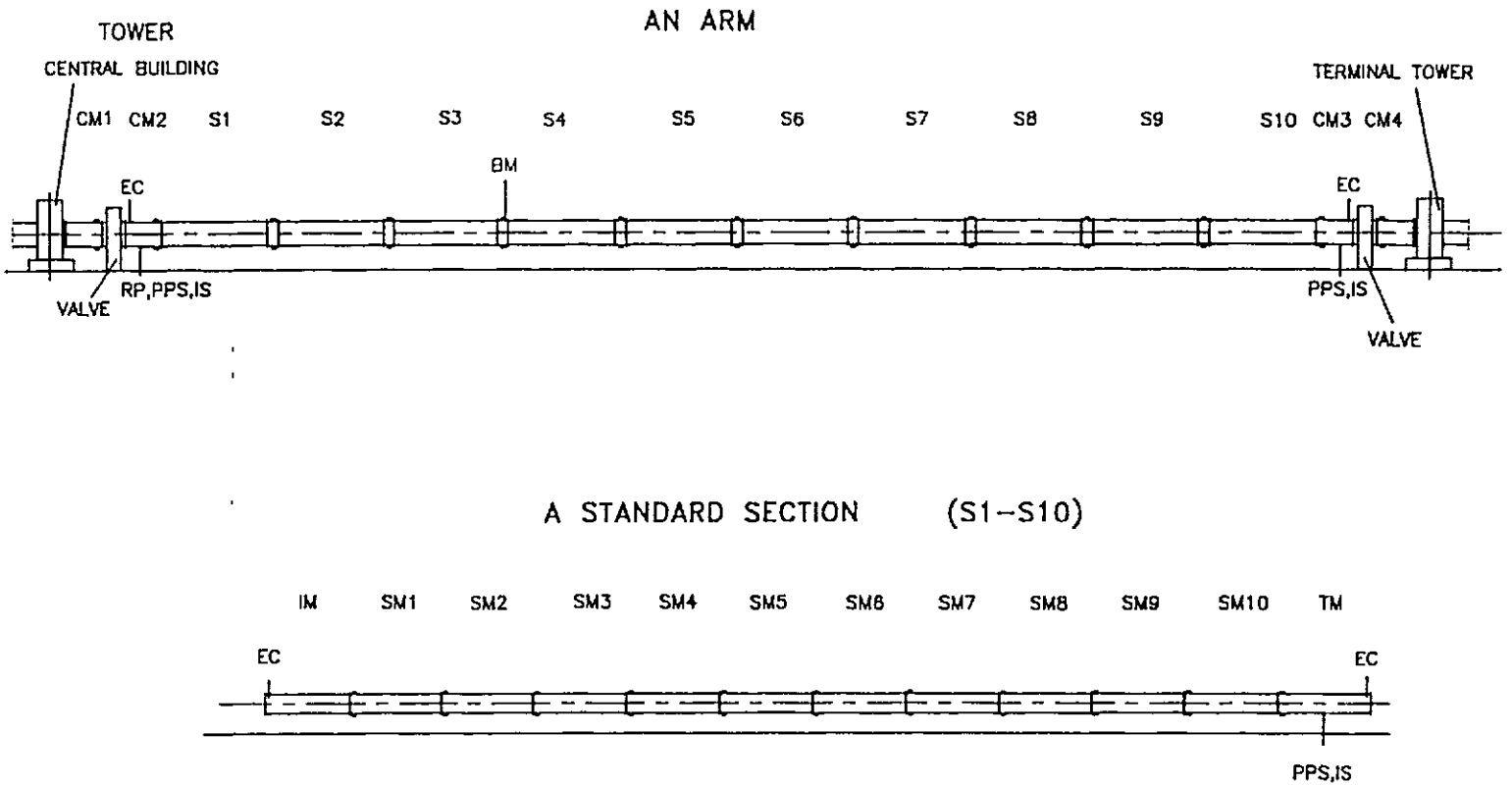

Fig.9 AN ARM (3km long tube) and A STANDARD SECTION

CM1–CM4--Connection module, 7m long, with bellow. S1–S10--Standard section, 299m long.
BM--Bellow between sections, 1m long. IM--Initial module of a section.
SM1–SM10--Standard module, 25m long, with bellow. TM--Terminal module of a section.
EC--Electric connection for bake out. RP--Rough pumping. PPS--Permanent pumping station.
IS--Instrumentation station.

BAFFLES

3200.1.- Introduction

The light scattered by diffusion off the mirrors of Virgo may be an important source of background, due to the possible recombination of scattered photons with the main beam : if these photons have been scattered by vibrating obstacles, after their eventual recombination they may simulate an event. This effect has first been studied by Marvina Cobal by mean of a simulation program, with the result that inserting steel baffles did not solve the problem. Then a new philosophy has been proposed (Virgo notes (1)), consisting of absorbing the scattered light in glass baffles before a 1st interaction with the pipe, at a level such that the probability for any photon to get out of the baffle is smaller than what is required for keeping the noise much smaller than the sensitivity of the experiment (namely ≤ 10 % of the thermal noise). The whole solid angle corresponding to the vacuum pipe is covered with such baffles, so that no photon can interact with the tube, and the geometry and surface state of the tube are irrelevant to the problem.

The problem of scattered light and its solution will first be exposed for the long arm cavities (A), then for the central area (B).

3200.2.- Scattered light in the long cavities

A complete computation of the noise due to scattered light has been done for all the possible effects (reflexion, diffusion, diffraction) and summarized in a Virgo note (2)).

The level of extinction necessary to fulfil the mentionned conditions of noise ($h < 10^{-25}\ m\ \sqrt{Hz}$) has been computed to be ~ 10^{-6} (see (1)), for what concerns reflexion and scattering. This number has been the main specification for the baffle design. The other specification, the free aperture, has been increased after the FCD : in order to preserve future and to be able to house 2 or 3 interferometers later on, we have tried to design the baffles such that a free aperture of 1 meter is left.

3200.2.1.- Principle of the baffle

The idea is to absorb the photons as much as possible, while mastering the trajectories after an interaction with the baffle ; the material is absorbing black glass (transmission < 10^{-7} pour $\lambda = 1\ \mu$) with a non diffusing surface. The geometry is shown in fig 1 :

A glass cone (45°) inserted in a glass cylinder allows the incoming photons to be reflected 3 times if they come from the left (on the figure), and more than 5 times if they come from the right. The reflectivity R of the glass surface has to be such that $(R)^3 \leq 10^{-6}$ which gives $R \leq 10^{-2}$. Geometrically, the baffle is oriented as shown in fig 1 for the 1st half of the tube (near the input mirror), and symmetrically with respect to a vertical plane $\perp$ to the tube axis in the middle of the tube, for the end part of the tube.

3200.2.2.- Position of the baffles - Number of baffles

The whole solid angle must be covered : each baffle must be placed at the end of the shadow on the tube of the preceeding baffle, with of course a little recovering (Fig.2).

The law for the z position is very simple :

$$z_n = z_1 \, \alpha \left(\frac{r}{r-h} \right)^{n-1}$$

α is the coefficient for recovering.

All this geometry is symmetrical with respect to the middle of the tube.

There is no need to decide the exact position of the baffles right now ; α will depend on the details of the design when completely finalized.

If we want to house only one interferometer, the total number of baffles is about 80 per arm and about 100 for 2 interferometers.

3200.2.3.- Detailed design of a baffle

3200.2.4.

3200.2.4.1.- glass

The glass must have the following properties :

- Transmission $< 10^{-7}$ for $\lambda \sim 1\,\mu$
- Diffusion very small ($\int$ diffused light $\leq 10^{-5}$)
- Reflectivity ~ some 10^{-3} bettween 0° and 45°.

The last point necessitates an anti-reflective coating, which will be detailed in the next pages.

The only existing glass fulfilling the 2 first points is welding protective glass, which has been found only in 2 firms : Schott Desag (Germany) and Corning-Sicover (France).

The required transmission can be obtained for a 3 mm thickness and the available dimensions would allow the make the 2 final components of the baffle (cone and cylinder) in one piece each if it is possible to shape them.

The raw material has nearly no diffusion, and the diffusion measured after coating is also very small ($< 10^{-5}$).

3200.2.4.2.- coating

The idea of coating the finished baffle by vacuum evaporation is not realistic because of the price.

Another solution has been found : the dip coating process, developed both by Desag and by a collaboration CEA- REOSC in Paris. The process consists in dipping the glass in a solution of metaloxide and to obtain a thin layer deposited on the surface, the thickness of which is mastered by the speed of extracting the glass from the solution. Then a protective layer of siliconoxide is deposited by the same process.

- At Desag the coating must be done on flat glass plates, which have to be shaped afterwards.
- At CEA- REOSC it may be possible to deposit the layer on already shaped pieces, but some R+D is still needed, in particular to determine whether it is possible to deposit layers in a non vertical position.

The Desag coating has been optimized to provide a reflectivity R between 10^{-3} and $5.7\ 10^{-3}$, for incident angles θ between 0 and 45° and for the worst polarization state. This is still true for glass plates after the bending they will be submitted to after coating for getting the required shape. So we consider that their R + D on coating is finished.

So presently with the Desag coating the cylinder parts, always reached by the photons around 0°, have a reflectivity of ~ 10^{-3}. Even with an uncoated cone (R ~ 4.10^{-2}), the overall reflectivity of the baffle is $1.6\ 10^{-6}$, which is probably O.K.

3200.2.4.3.- shaping

Desag has already realized parts of the cylinder (6 pieces altogether) by bending coated glass in a specially shaped moulder. They are unable to realize a one piece cone.

Two French firms (MVR and Gobba) have succeeded in making a one piece cone of the right dimensions with the black glass, by heating a flat piece of glass resting on a coneshaped moulder in an oven with a careful control of the temperature.

3200.2.4.4. machining

Some of the glass components have to be machined on some of their edges.

3200.2.4.5.- assembly

Provided we find a correct glue, the six pieces of the cylinder have to be assembled with glue (fig.3). The envisaged glue has a tolerable outgassing rate (see below).

The glass pieces must have a precise geometry, which is the case for the pieces already provided by Desag.

Once the complete cylinder is assembled, the cylinder and the cone have to be glued together.

Presently this assembling has been realized at Orsay on a scale 1 aluminium mock-up, the rigidity of the whole is good.

A full size glass prototype is being realized and should be ready before next summer.

3200.2.4.6.- outgassing

The outgassing rates of the coated glass and of the glue have been measured. The results are presented in table 1, together with the areas of the different materials. In the next to last column the outgassing fluxes are given.

The conclusion is that compared to the tube itself the outgassing of the baffles is very small (table 1).

3200.2.5.- Further requirements

3200.2.5.1.- baffle edges

The noise due to reflexion on the cone internal edge has been computed (1) : in order to be of the same order of magnitude as the other components of the noise, the radius of curvature of the ridge has to be less than 0.2 mm, which is technically feasible.

3200.2.5.2.- Diffraction effects

The noise introduced by diffraction on the baffle edges can be very small, provided that coherence effects due to a perfect radial geometry are broken : the conclusion is that the beam must slightly displaced off the tube axis, and that the baffle should be slightly tilted with respect to the vertical plane, which will be done naturally by the construction imperfections.

3200.2.6.- Overall noise

With the foreseen characteristics of the baffles, the overall noise in the long arm cavities lies between 10^{-24} and 10^{-25} m/$\sqrt{\text{Hz}}$ at 10 Hz, the uncertainty being due to all the assumptions which had to be made in order to compute analytically the noise. This evaluation has been checked by means of a Monte Carlo program propagating the photons, done in Pisa.

3200.3.- Scattered light and baffles in the Central Area

Due to the number of optical components in the central area, it is impossible to compute analytically the noise due to scattered light.

A Monte Carlo has been especially developed in Pisa, following the photons impiging of the different optical components in all their interactions with all the obstacles
(tower body, link tubes between towers etc).

The results are exposed in a Virgo note(3).

For the construction of the interferometer, the constraints following from this study are :

- The diameter of the link tubes should be at least equal to 40 cm.
- In the 3 main towers : beam splitter, west and north input mirrors, the Ø 1000 windows seeing the beam should be covered by Ø 1200 coated glass circles with a centered Ø 200 hole (fig.4).
- In addition, in case a Ø 250 valve is used in the middle of the links, a Ø 400 coated glass circle, with a Ø 250 centered hole, should be inserted on each side of the valve.

Under these conditions, the noise in the central area is also between 10^{-24} and 10^{-25} m/$\sqrt{Hz}$ at 10 Hz and 100 Hz.

DRAWINGS - FIGURES - REFERENCES

References :

1. A solution for removing the scattered light, V. Brisson, Virgo note 92/1.

Feasibility of glass baffles, V. Brisson, Virgo note 92/2.

2. Scattered light evaluation, and calculation of the induced phase noise,

J.Y Vinet, V. Brisson, S. Braccini, Virgo note.

3. Scattered light evaluation in the central area, S. Braccini, V. Brisson,

J.Y. Vinet, Virgo note.

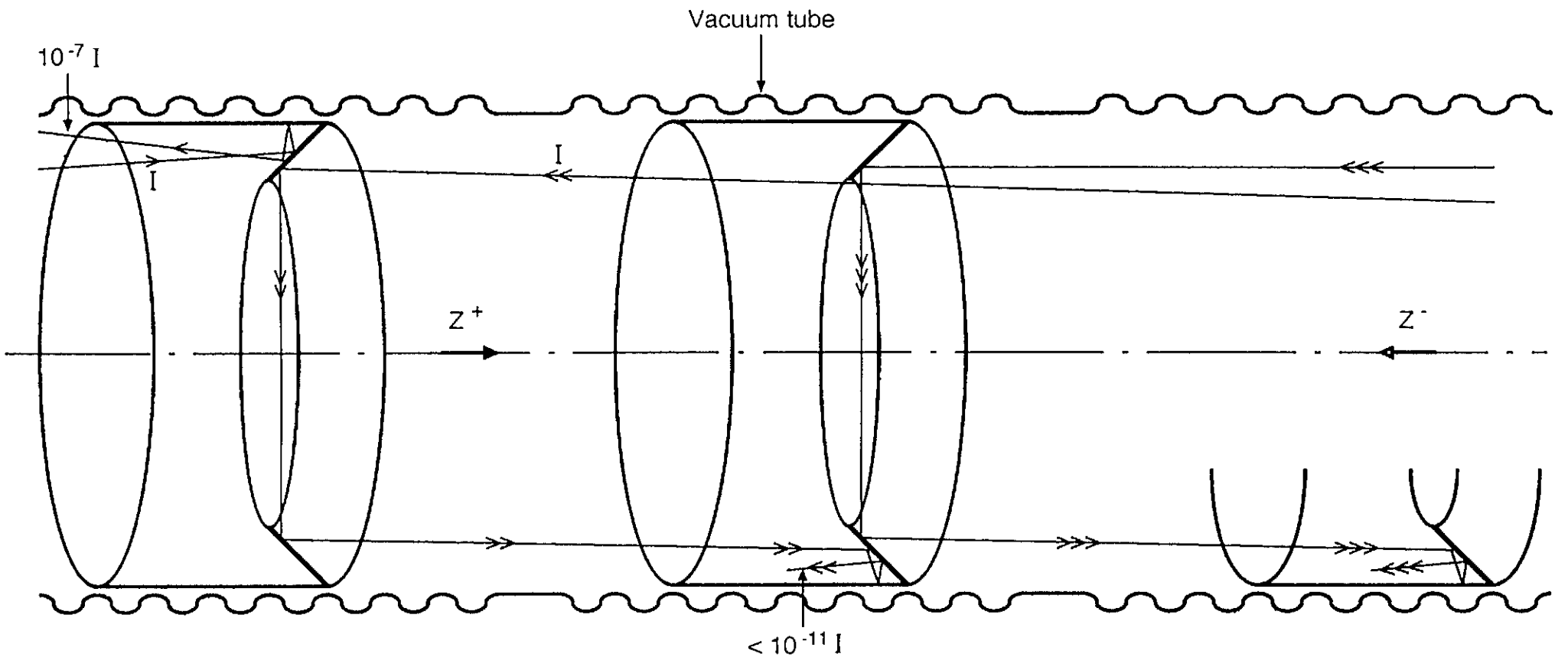

Fig. 1 Geometry of the baffles

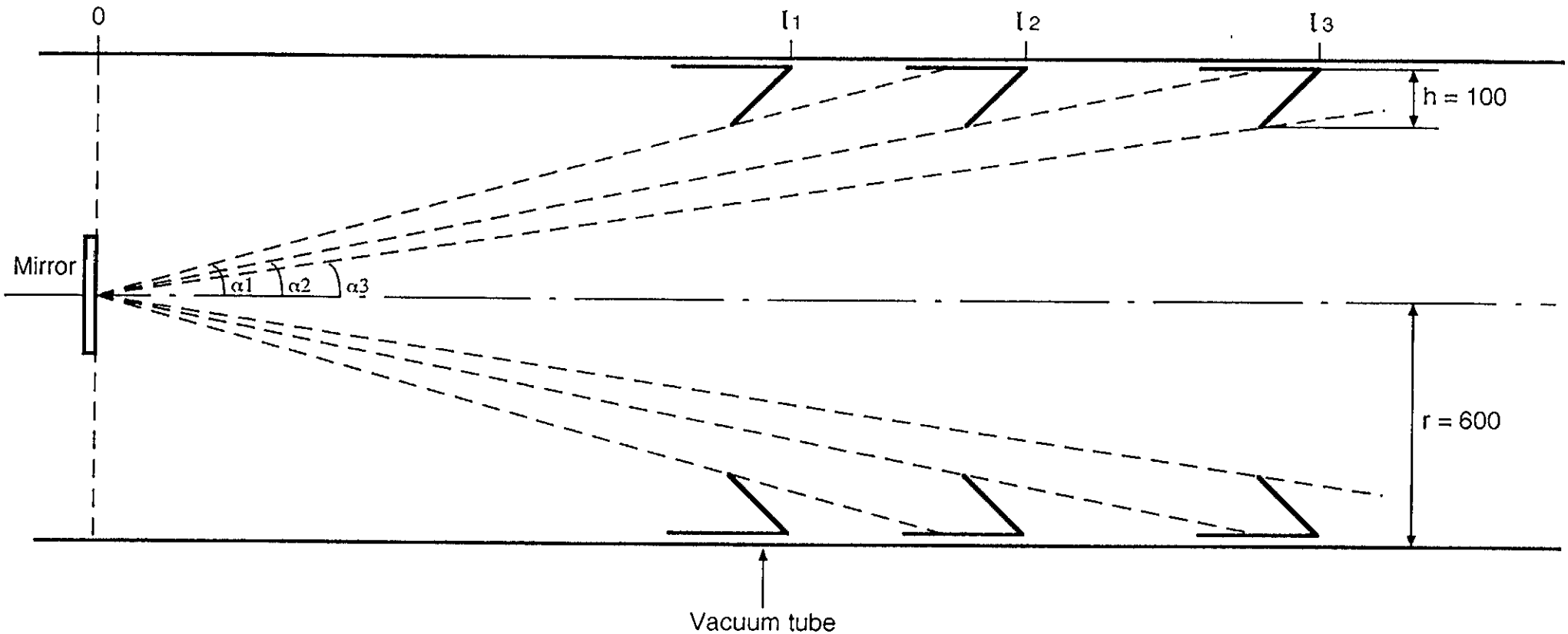

Fig. 2 Position of the baffles : $l_n = l_1 \left(\frac{r}{r-h} \right)^{n-1}$

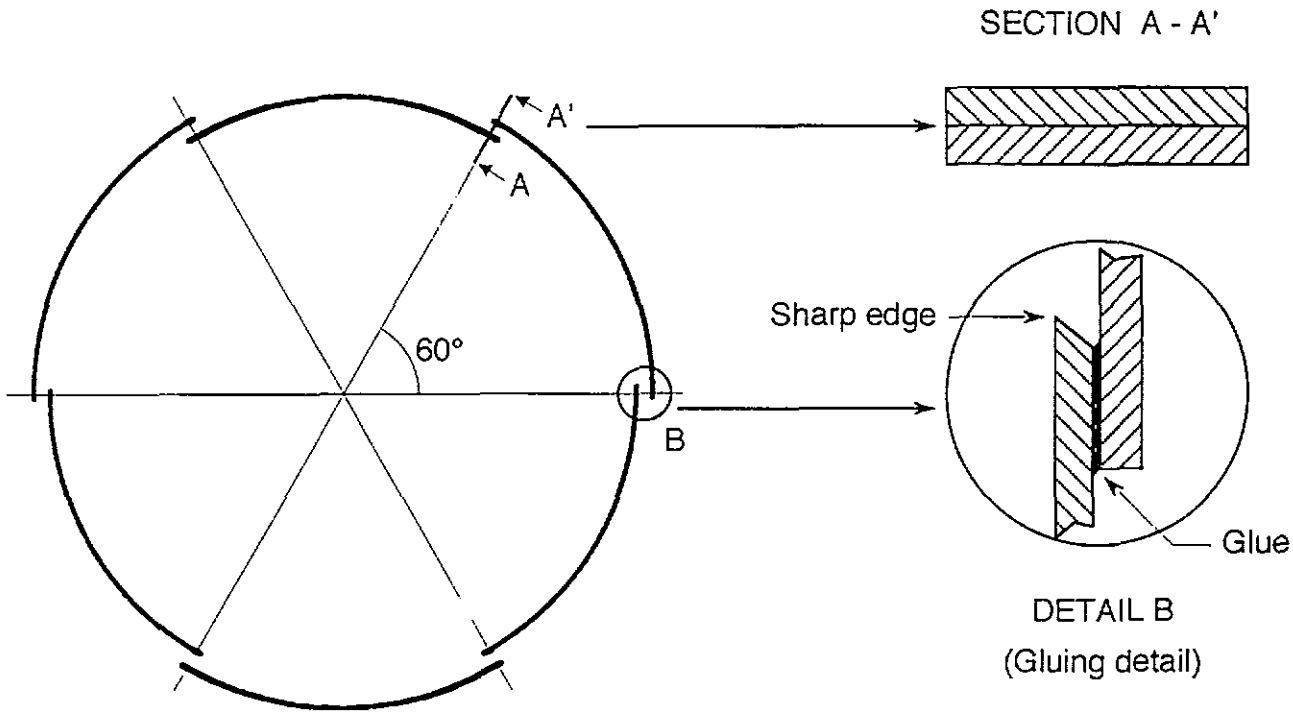

Fig. 3 Cylinder

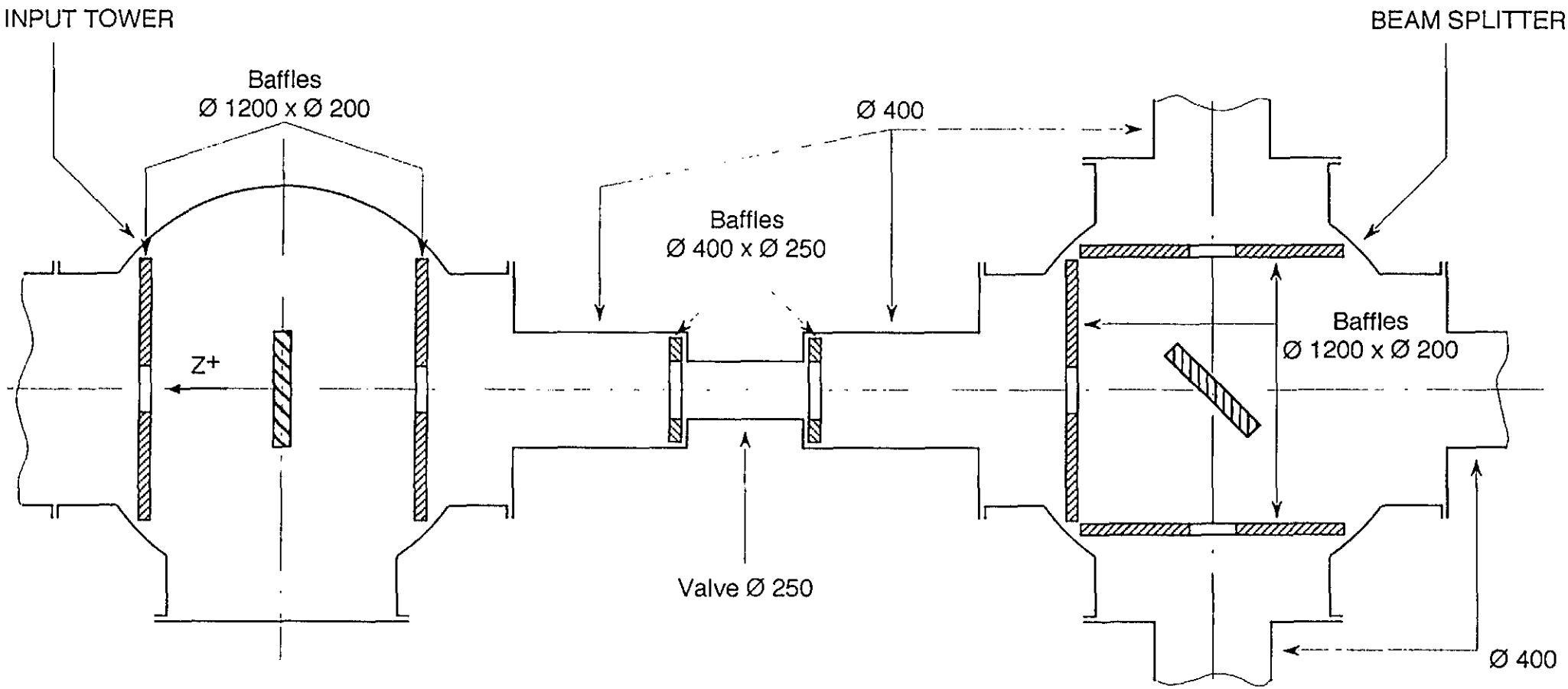

Fig. 4 Baffles in the central area

OUTGASSING RATES

	TOTAL AREA PER ARM (cm^2)	OUTGASSING RATE ($mbar \cdot l \cdot s^{-1} \cdot cm^{-2}$)	OUTGASSING FLOW ($mbar \cdot l \cdot s^{-1}$)	GAS
TUBE	$12 \cdot 10^7$	$5 \cdot 10^{-14}$	$6 \cdot 10^{-6}$	H_2
BAFFLES (100 per arm)	$33 \cdot 10^5$	$3 \cdot 10^{-13}$	$1 \cdot 10^{-6}$	H_2
GLUE	$33 \cdot 10^2$	$\sim 10^{-12}$	$\sim 3 \cdot 10^{-9}$	Others

Table 1

TOWERS

The final design of the tower clean air supply and of the optics protection depends on the tests which are now in progress on the lower tower prototype at Annecy.

The air firing of the lower tower stainless steel is still under discussion.

The design of the links is now in its final phase.

3300.1. General description.

The VIRGO interferometer is decoupled from environmental noise being suspended in ultra high vacuum. The suspension of its components uncouples them from seismic noise and the ultra high vacuum provides the uncoupling from acoustic and light propagation noise.

Multistage suspensions are implemented in towers [fig. 1] of various heights, depending on the locally requested seismic noise decoupling. They hang on an inner structure built inside the tower vacuum tank. Their payload is an optical component coupled to positioning and protection devices.

The lower tower which houses the payload is the assembly node of the interferometer vacuum tank. It allows for the connection of its various arms, provides optical access for the component alignment and allows for the human access needed by the payload installation.

Seven towers are interlinked in the central building, three towers are linked at a distance from this central building. On **figure 2**, towers are named according to their payload functionality: injection and detection, beam splitter, north / west input , power and signal recycling in the central building, north / west end and mode-cleaner in dedicated buildings

Towers and links are assembled in the central building in a clean environment, as usual UHV components. The setting up of the optics requires human action in a white environment to be created in the lower towers. This is realized by implementing an underground gallery allowing for a dedicated clean tower access.

3300.2. Technical needs

3300.2.1. Metrology.

- The respective locations of the towers in the central building are determined by the details of the selected locking scheme. Provision has been made to allow for an asymmetry of 160 cm between the two arms, allowing the displacement of the two input towers within +/- 40cm. The power recycling tower can also be translated within +60 and -100cm. The beam height is fixed at 1100mm relative to the building ground???

3300.2.2. Decoupling from environmental noise

3300.2.2.1.- seismic noise

One of the most remarkable and unique feature of VIRGO will be its high sensitivity for gravitational waves in a frequency band starting as low as 10 Hz. This feature is achieved with the multi-stage filters, so called superattenuators. They reduce the seismic noise on the interferometer test mass in all the six degrees of freedom. As a consequence, the mechanical structure supporting the filter should have a resonance frequency above 15 Hz, i.e. well inside the frequency band which is damped by the superattenuators.

3300.2.2.2.- outgassing

The total outgassing of the towers must be low enough to be compatible with the vacuum requirements of the long tubes, since the conductance between the towers and the tubes is generally very high.
The requirements are less stringent in the injection and detection benches and in the Mode Cleaner tube and tank where these partial pressures have to be 10^{-6} mbar.

3300.2.2.3.-light scattering.

The light scattered by the mirrors of VIRGO may be an important source of background, due to possible recombination of scattered photons with the main beam. In addition to the baffles foressen inside the long tubes, it may be necessary to add some baffles inside some of the towers in the central building.

3300.2.2.4.- acoustic noise.

The vacuum specifications established for the stability of the index of refraction along the optical path provide the necessary decoupling with the acoustic environmental noise.

3300.2.3.Implementation of UHV and optical components.

The above mentioned residual partial pressures determine the cleanness to be achieved on the components to be set up to form the vacuum tank. All these components have thus to be cleaned at factory according to field proven cleaning procedures. The specified water partial pressure requires a 150ºC in situ tank baking.

The specifications on the Fabry Perot optics aim to limit diffusion losses at the ppm level for clean optics. To keep such a performance, one has to limit the losses due to dust deposits at a smaller or comparable level. This consideration situates the obscurancy factor (i.e. the ratio to the active surface, of the surface covered by dust particles) at the ppm level for a mirror set in operation.

3300.2.4.Implementation of the suspensions.

The number of filtering stages of a suspension depends on the requested decoupling from seismic noise . Once in place, a suspension can be moved as a whole with a system of motors operating in vacuum. These motors determine the angle around the vertical (± 15º) and the x, y, z positions of the component. The z motor moves the suspension vertically from rest to working positions. The y,z motor have a range of ± 4,5.mm.

A complete suspension may weight more than a ton. Its control requests many services which have to be passed from vacuum to atmosphere: 2 hydraulic feedthroughs are requested for the adjustment of the stiffness of a filter, 268 electric feedthroughs are requested for the control of its various components.

As the outgassing of all these elements may be important, it is necessary to isolate the suspension compartment with a separating roof in order to preserve the high quality vacuum in the light propagation compartment. A small 0,3l/sec (for water vapor) conductance, fit in the separating roof, allows for the feedthrough of the suspension wire .

Given the size of the filters, they cannot be assembled in a white environment. They are assembled in a dedicated clean area as usual UHV components, and transported as a whole by crane above their corresponding lower tower.

3300.2.5.-Implementation of the payloads.

The payload is the system hanging on the suspension, below the above mentioned separating roof. It involves a marionetta, an optical component , a reference mass and, if necessary a protection device.

The marionetta is controlled through the separating roof. The acting force is generated by the current circulating through coils fixed to the suspension and surrounding magnets fixed to the marionetta. They control the rotation of the optical component around the two axis perpendicular to the beam and its position along the beam. Coils and magnets are located on either side of the separating roof. A motor allows for the balancing of the marionetta: 6 wires, to be passed through the conductance hole, are necessary for its control.

The optical components are either a mirror, an injection or a detection bench. Their characteristics are listed on **table I**. The characteristics of the 1997 components are adapted to the final components with adhoc interfaces.

A reference mass is implemented for the control of the longitudinal position of all mirrors. It is hanged to the marionetta. The longitudinal correction is produced by either magnetic or electrostatic forces acting between reference mass and mirror. The necessary power is feed with 8 wires running down the suspension and passing the separating roof through the conductance hole.

The protection device shields the optical component against dust which could be deposited during its installation. For the time being, the simplest protection is made with a the reference mass properly shaped.

The position of an optical component is measured using the deflection of a laser beam on its surface for several incidences. To that purpose, one makes provision of optical ports to install laser beams and position detectors .

The global operation of the interferometer is tested with an independent calibration set up which requires the implementation of dedicated optical ports.

3300.2.6.Implementation of the pumping system.

The above mentioned vacuum compartments are evacuated with tower pumping systems described in.the chapter "Pumping system".

3300.2.7.Flexibilities and testing facilities.

For setting up and maintenance any tower has to be accessible independently of the pressure status of its neighbouring towers.

To easy the implementation of new ideas which would require modifications on the lower tower tanks it has been decided to realize each lower tower with large lateral DN1000 mm covers: any such cover can thus be replaced with another one compatible with the new requirements.

3300.3.Technical choices

3300.3.1.Tank raw material.

The vacuum specifications defined above and the size of the vacuum chamber favour stainless steel for the choice of the chamber raw material . The 300 series of austenitic steels is

the most frequently used in vacuum and cryogenic work because it is corrosion resistant, easy to work and non magnetic. The US 304L or ISO Z2CN18-10 variety has been chosen.

3300.3.2.Tower pumping.

For the pumping strategy, each tower is taken as an independent vacuum vessel. Sectioning valves are implemented on the links in between two towers in order to isolate the different towers. Tower roughing is achieved via the upper compartment put in communication with the lower compartment for that operation. UHV vacuum is performed with turbomolecular pumps attached to each compartment. Towers with a single compartment like injection, detection and mode cleaner have only an upper pumping station.

The lower compartment pumping station is implemented on a lateral window as indicated in **table I.**

Turbomolecular pumping is stopped when beam is on. A permanent, vibration free, Ti sublimation and ion pumping system takes over. These systems are installed on the links.

3300.3.3.Tank cleanness.

The tank inner surface is produced to limit outgassing rate and dust adhesion forces. A very low RA ($\leq 1.6\mu$) is thus realized by abrasion and electropolishing.

Cleanness specifications impose to fear hydrocarbons (vacuum) and dust particles (optics) . Hydrocarbons are removed by standard cleaning procedures. Fighting dust requires clear cuts in building conception and construction planning's: dedicated dust free areas have to be realized and well defined clean assembly sequences have to be granted.

The vacuum tank components are handled in the central building which has to meet a pollution level compatible with such an operation. As many different installations go on in this building, the vacuum tank assembly can only take place in granted periods during which oil vapour or dust producing activities are prohibited.

Optics is manipulated in a qualified environment accessed via airlocks. As a consequence, the 7 towers erected in the central building are deserved by a dedicated underground gallery feed with clean air. A cleaning facility and a classified assembly laboratory are build in line with it. Each tower is fed with filtered air to preserve the optics cleanness during installation. The air flow is such that the generated over-pressure preserves the tank cleanness during its access from gallery or during connection of any accessory at the hall level.

The air feeding is done at the top of the lower tower via a Ø250 mm port.

3300.3.4.Tower mechanical structure.

The vacuum specifications require the construction of a tank with 15mm wall thickness fit with metallic sealing in its UHV (baked) compartment.

Taken as a linear tube of finite length (12m), diameter (2m) and thickness (1cm), the tower fundamental frequency is at 15 Hz. If this tube is rigidified every 2 meters with stiffening ribs, one computes a collapse factor of 9.

A more elaborate tower modelling within the framework of the SYSTUS code produced distributions of static deformations and stresses under various loading conditions (tank under its proper weight at normal temperature, tank under vacuum at normal temperature, tank under vacuum at 150ºC). The model taken for baking assumes a uniform heating between protection plate and top of square pedestal. An additional oven is used to heat the lower cover.

The details of the lower tower geometry have been optimized to rise the fundamental frequency at 16Hz (figure 3. A collapse factor of 12.8 during baking under vacuum

Results of the modelling have been verified on the lower tower prototype.

3300.3.5. Tower anchoring.

Any tower has to be accessed or baked independently of the pressure status of its neighbouring towers. A tower is thus screwed to ground to stand pressure differences and free with respect to ground to allow for baking.

In our configuration, end towers stand the highest pressure difference. Their situation is taken as a reference for computations.

Input and end towers stand 11310 DaN induced by the beam tube vacuum. They are screwed to ground and bear on metallic plates anchored on the beam tube side. So they can be unscrewed for baking. When the tube is under vacuum, an input tower expands thus towards the beamsplitter tower. When it is at atmospheric pressure, i.e. the 1997 situation, the metallic plate is removed to allow for dilatations towards the tube, bearing on spacing rods inserted between input and beamsplitter tower pedestals.

Other towers are also unscrewed for baking. Towers sandwiched between two neighbours at a different pressure are balanced with spacing rods introduced between processed and evacuated towers.

3300.3.6. Inner structure.

Once the inner structure supports the resting attenuator chain it is submitted every meter to a 600mm*150kg torque. An U shaped beam of 300mm width and 100mm wings stands these forces with deformations in the .5 mm range.

A detailed modelling with the SYSTUS code produced the distributions of z deformations, strains and buckling. Loaded with the filter, the structure collapse factor is above 100. In the absence of loading, its fundamental mode is at 4.02 Hz.

3300.4. The technical description

The vacuum tank set up in the central building is assembled with 7 towers linked with 400mm diameter tubing. The towers located in the Mode Cleaner and in the End buildings are assembled along the same principles. All the parts described below are cleaned at factory according to our specifications. Cleaning quality is checked by a residual gas analysis. Parts are transported to the site with specific protections.

3300.4.1. Vacuum tank.

The basic structure shown on **figure 2** is reproduced for each tower. Depending on their functionalities, towers have the specificities shown on **table I** and **II.** A tower has two compartments: an upper one for the implementation of its suspension, a lower one for the implementation of its payload. A separating roof, fit with a hole for the feedthrough of the suspension wire, is implemented in the lower tower. The suspension rests on an inner structure fit with a technical ring supporting the hydraulic and electric feedthroughs of the suspension services.

3300.4.1.1.Lower tower.

The lower tower shown on **figures 4, 5** is a cylindrical tank (2 m in diameter, 15 mm in thickness , 2.74 m in height) with four lateral DN 1000 windows and two axial DN 2000 apertures. Its lateral windows allow for the connection to other towers or for the implementation of alignment / pumping devices. Its lower aperture is dedicated to the payload introduction. Its upper aperture is the interface with the upper tower and its suspension. The separating roof divides the lower tower into two communicating vacuum vessels.

The lower vessel which contains the payload aligned on the beam. It can be evacuated at 10^{-8} mbar. At atmospheric pressure, it is a white room supplied via 8 ports by a clean air feed pipe. It is 1515mm high. The two vessels are assembled on an inner flange 1650 mm in diameter and 40mm in thickness. This flange supports the movable separating roof.

The upper vessel contains the separating roof. It is evacuated at 10^{-6} mbar. It is 905mm high. The square flange surrounding the vessel (2400x2400x60mm) is shaped to fix the fundamental frequency of the lower tower (figure 4).

Optical ports are detailed on figure 6: 8 DN 160 CF optical ports are available on the lower vessel for alignment purpose. On the upper vessel, there are 4 DN 300 to fix the mechanisms, 1 DN 250 CF for the feedthrough of services and 1 DN 200 CF for the upper tower pumping. The DN 250CF dedicated to services is used for wires which don't have to be uncoupled from seismic noise like those of the device measuring the suspension wire position in the conductance hole. Flanges in diameter ≥ 300mm are forged and receive either metallic or "viton" seals.

A clean air feed pipe surrounds the lower vessel: it supplies the lower vessel via 8 Ø100mm ports. The pipe itself is connected to the clean air supply via a ø 250mm port.

The cylindrical tank is welded to a very massive 4 m x 4 m square pedestal . It rests on 4 or 6 massive sockets (400x400x100) used for its ground anchorage with 16 screws 24mm in diameter. The pedestal, the tank and the upper square flange are bound with 4 vertical stiffening ribs. A 20mm thick plate is welded around the tank above the air feed pipe: it is a protection for the pipe and a floor for the installation of the mechanisms.

The assembled lower tower, with its 4 lateral DN 1000 covers and its cupola, weights about 16540 kg.

3300.4.1.2.Lateral windows and lower cover.

The lateral DN 1000 windows allow for the tower linking. Towers interlinked in the central building are connected through 12 lateral flanges produced with a central DN 400 CF. The 4 towers connected to the 3km long tube are linked with flanges produced with an outer DN 1200. The 2 mode cleaner tube interface flanges have a central DN 250 /400CF.

To simplify the tower linking, the tower pumping is installed on the available lateral windows. This cannot be done for the beamsplitter tower. 8 lateral DN 1000 flanges are thus produced with 2 DN 200 CF for pumping purpose.

The 5 DN 1000 end windows which close the beam lines as well as the 9 remaining unemployed lateral windows are ready to be equipped??

The lower cover has a diameter of 2 m. It is 180mm high and weights 1000 kg. It is stiffened with four welded horizontal ribs. It has two apertures. The one with 450mm in diameter allows for the tower access, the central one is devoted to the introduction of the payload.

Cover details are specified on **table II**.

3300.4.1.3.Technical ring, standard rings and cupola.

According to the tower height, a different amount of standard rings and a cupola are fit around the inner structure to define the vacuum tank of the suspension. All the rings are 2000mm in diameter and have forged flanges to receive either metallic or "viton" seals.

The technical ring is fit with three ports, 250mm in diameter, at 120° from each other. It is 500mm high.

Standard rings are 1967mm high . The upper ring has a special 100mm high upper flange for its linking with the inner structure.

The cupola rests on the upper ring. It is 1300mm high and weights 1000 kg. It can also be used to close a lower tower .

A complete tower with its technical ring, 3 rings and a cupola is 10441mm in height and 22990kg in weight.

3300.4.1.4.Lower tower baking.

Baking at 150°C is achieved with a hard, modular, dismountable oven structure. [**figure 12**]

The lower tower oven is build with four corner modules, enclosing the lower tower. Doors provide the apertures for the links. On the pumping system side, on the cupola, and below the pedestal the isolation is done with properly fit mattresses. The tower basis is isolated from ground.

Circulating air is heated on 20 KW resistors and distributed between the tower and the oven structure.

The lower cover, accessed from the gallery, is heated for its own with a 3kw module.

3300.4.2.Inner part : separating roof, structure and mechanisms

3300.4.2.1.Separating roof.

The differential vacuum separating roof [figure 7] is made with a central hole to be fit with the conductance and with 4 circular holes to be fit with cylindrical glass casings. These casings separate the marionetta permanent magnets from their command coils, they are attached to arms fixed to the last suspension stage [**figure 8**]

The 2l/sec conductance is a small, easy to change, piece fixed to the separating roof. The glass casings allow for the vertical translation of the suspension from rest to work positions.

Once under vacuum, the separating roof can be lifted and translated continuously in x and y directions with mechanisms [**figure** 7].Lifting is essential to achieve smooth translations. It increases the conductance between the two tower compartments and allows thus the lower tower roughing through the upper compartment. This feature is essential for a clean lower tower roughing. Translations allow for the centering of the suspension wire inside the conductance and of the marionetta command coils in their glass casings. It can be either manual or remote controlled. Its range is +/- 25mm in both directions. Commands are outside the tank, at atmospheric pressure. The wire position with respect to the conductance hole is measured with a shadowmeter looking at the shadow of the enlightened suspension wire on a row of photodiodes.

Injection , detection , signal recycling towers, as well as the mode cleaner tower don't have a differential vacuum. Their separating roof is thus simpler.

3300.4.2.2.Inner structure.

The inner structure [fig 9] supports the multistage attenuator chain. It is composed with three vertical U shaped pillars, 300mm wide with 110mm wings, about 6m in height. They are welded at 120° to upper and lower rings. It is mounted with a pillar in the beam direction.

The motors which move the attenuator chain as a whole are fit on the top of the structure. Sockets, mounted on the pillars provide a rest position for the different filters.

The filters are fit on the inner structure in a dedicated assembly area where the suspension is set up. Once ready, the filters are blocked in their rest position and the suspension is transported as a whole towards its lower tower.

The structure is then screwed on the upper square flange of the lower tower on one side, and on the upper ring flange on the other side.

Services as cables, pipes run in the U shape from the top of the structure to the the technical ring. The suspension stays at rest to receive its payload. An upper motor sets then the system in operation.

3300.4.3.Links.

This part concerns the tubing connecting the towers erected in the central building. The connection between two towers has to account for :

- dilatations generated by baking at 150ºC: 6mm. for a 3m tube.
- misalignment between towers: +/- 5mm
- mechanical tolerances on DN1000 flanges: +/- 5mm in beam direction and +/- 5mm perpendicular to the beam.
- mechanical tolerances on the links : +/- 5mm in the beam direction,
- implementation of sectioning valves, permanent or tower (beamsplitter) pumping systems,

Their characteristics are listed on **table III.**

A link is thus build up with a long bellow, a Ø400 valve and two cm long straight sections. The bellow allows for longitudinal displacements of ± 40 mm and lateral displacements of ± 15mm. End flanges are freely rotating to allow an assembly with upright valves. Such an ensemble [**fig 10, 11**] is mounted on a dedicated supporting structure designed for an easy transport and fitting in. Once in place, the supporting structure is allowed to move according to dilatations.

The outgassing of the equipments set up in the injection and detection towers may prevent the achievement of the expected UHV performances. To assert the 1997 interferometer, these towers will be linked across optical ports as shown on **figure 13.**

There are thus eight different links in the central building. Their characteristics are listed on **table II.** Light scattering calculations fix the link diameter at 400mm with Ø250mm sectioning valves in the middle of a link.

Each link is associated to a couple of spacing rods which fix the distance between a baked tower and an evacuated neighbouring tower .

3300.4.4.Lower tower / gallery linkage.

This linkage is airtight to allow a small over-pressure in the tower access gallery in order to preserve its cleanness with respect to the hall. It stands high temperature and during baking at 150ºC. It is realized with a stainless steel sheeting shape. It is screwed to the lower tower and glides along the gallery roof during dilatations.[**figure 17**]

3300.5.The component assembly.

The cleanness required for vacuum component assembly and for optics installation requires adhoc facilities at the earliest stage of the assembly operation. A first condition is to establish a clear cut between normal, clean (vacuum) and white (optics) installations. The policy is to start the vacuum tank assembly only when a clean environment can be granted in the hall and to start optics installation only when the complete vacuum tank, has been fully tested, baked and delivered. At that time, clean areas have to be processed and ready for operation.

3300.5.1.Hall infrastructures.

Areas dedicated to optics handling are fed with controlled air. Dust deposit per unit area and time depends on filtering installations, flow rate, temperature and hygrometry of supplied air. It depends also on the vertical/horizontal position of the sample. Our specifications are based on the working hypothesis that the assembly in the optics laboratory may take several days and that the in situ fixation on the suspension may last a few hours. According to experimental data, the requested obscurancy specification is achieved with air filtered at 99.9997% DOP (less than 10^{-5}particles <.3μ) flowing laminar in the assembly laboratory and at a turbulent rate of 20 volumes/h in the tank. The assembly laboratory is a CLASS 100 *laminar* clean room. The tank is a CLASS 10 *turbulent* clean room. Conditioning the controlled air flow below 55% hygrometry at a stable temperature, minimizes the particulate adhesion forces and ensures cleanness reproducibility.

The cleaning facility is a dishwasher operating in air controlled environment with purified and pressurised liquids (DI water and isopropyl alcohol). It has to accommodate devices like marionettas, reference mass, or any other piece to be used in qualified environment.

The access gallery is not really a classified area. The access to the tank under process is confined with a polyan tent. A local, low flow of clean air creates a buffer volume acting as a protection for the tank.

The layout of pumping and clean air piping in the central building is shown on **figure 16.**

The power installed to operate the lower tower prototype is detailed on **table IV.**

Calories produced by the oven cooling down have to be evacuated from the hall.

3300.5.2.Lower tower installation and linking.

Once on the experimental site, the lower towers are submitted to a vacuum test in order to certify their integrity after transportation. They are put in place with rolling sockets and aligned with respect to 3 markers located on their upper flange. They are thermally isolated from ground and tightly linked with the gallery .

On a reserved area, to be shared with the suspension assembly, links are assembled on a rolling support . After a vacuum test a link is moved as a whole by crane and lowered near its final place where it is fit in with its rolling support.

Once linked and equipped with the tower pumping, the lower vacuum chamber is evacuated and baked.

3300.5.3.Separating roof and suspension installation.

After this first vacuum test, one proceeds to the roof installation. The associated mechanisms are mounted and put in operation. A scaffolding resting on the 20mm thick square flange is mandatory for this operation .

The suspension installation follows. It is moved as a whole with its inner structure. On top of the lower tower, a smooth guiding is mandatory to fit precisely the marionetta coil holder into their glass casings.**[figure 19]**

Rings are piled up. A functionality test precedes the cupola installation. A new stair of scaffolding is necessary to access the top of the suspension and its related cabling.

After a thorough vacuum and baking test , the lower tower is fed with controlled air and accessed from the gallery for cleaning.

3300.5.4.Payload installation.

The payload is set-up and tested in the assembly laboratory.[**figure 21**]. Its weight is detailed on **table V**. A special conditioning is necessary for its transportation to the lower tower. This conditioning is dust tight, easy to clean and easy to remove. It stabilizes the payload components during transportation.[**figure 20**]

To limit the payload pollution during its setting up in the assembly lab, one starts its assembly by hanging the marionetta to a movable arm and follows with reference mass, mirror and protections. All these components are handled with a dedicated clean elevator chariot. The set up is balanced before its preparation for transportation. The movable crane is designed to install the payload on the gallery chariot.

This chariot lowers and moves the payload at the vertical of its tower. There it elevates it for introduction. The final approach is smoothly controlled with a positioning table.

Dedicated clean tools, cupboards and small rolling tables have to be available in the assembly laboratory and near the tank access.

3300.5.5.Tower pumping system implementation.

The implementation of the prototype lover tower pumping system and clean air feed pipe is shown on **figure 14.**

List of tables:

List of figures:

Table I : The towers specificities

Towers	Injection	Mode cleaner	power recycling	Beam splitter	input north	input west	output north	Output west	signal recycling	detection
tower displacement		+/-200cm	60/-100cm		+/-40cm	+/-40cm				
suspensions number of filters height	3	≤2	7	7	7	7	7	7	0	3
rings number	1	1	3	3	3	3	3	3	0	1
services hydraulic electric										
separating roof conductance mechanism wire position readout	yes no no	yes no no	yes yes manual yes	yes yes manual yes	yes yes manual yes	yes yes manual yes	yes yes remote yes	yes yes remote yes	no	yes
optical component weight dimensions mm			750 g Ø120x30	≥ 3.5 kg Ø230x≥50	21.2 kg Ø350 x100	21.2 kg Ø350 x100	21 to 42 kg Ø350 x200	21 to 42 kg Ø350 x200		
reference mass weight dimensions				yes	yes	yes	yes	yes		
marionetta weight dimensions										
special features	pumping port on the upper tank only	pumping port on the upper tank only		no lower tower pumping access						pumping port on the upper tank only
mirror protection										
clean air supply										
oven			inorth	iwest	inorth	iwest	onorth	owest		

Table II: Tower specificities, ports and covers

Table III Links characteristics

	Link nominal length	Standard tube length	Pumping port	adjusting tube	Fixed flange	optical window	Support type
Detection / Signal recycling	2000 Ø400	650			4	1	Short
Injection / Power recycling	2000 Ø400	650		-600 +1000	4	1	Short
Beamsplitter / Power recycling	3000 Ø400	1800	Perm.	+600 -1000	2		Long
Beamsplitter / Input north	3400 Ø400	1800	Perm.	+/-400	4		Short
Beamsplitter / Signal recycling	3000 Ø400	1800	Perm.+ B.S. pump		2		Long
Beamsplitter / Input west	2600 Ø400	1000		+/-400	4		Short
Input north / Beam tube	Ø1200		Perm.	+/-400			
Input west / Beam tube	Ø1200		Perm.	+/-400			

Towers	Injection	Mode cleaner	power recycling	Beam splitter	input north	input west	output north	Output west	signal recycling	detection
lateral windows										
north	link	pumping	link	link	tube	free	end	free	pumping	pumping
south	end		link	link	link	pumping	tube	pumping	free	
east		DN 200	free	link	pumping	link	pumping	tube	link	end
west	DN 200	end	pumping	link	free	tube	free	end	link	link
lower cover										
payload access		yes	yes	yes	yes	yes	yes	yes	yes	
human access	yes	yes	yes	yes	yes	yes	yes	yes	yes	yes
service port										
alignment										
optical ports										
calibration optical ports										
vacuum tanks										
upper	10-6 mbar	10-6 mbar	10-6mbar	10-6mbar	10-6mbar	10-6 mbar	10-6mbar	10-6 mbar		10-6 mbar
lower	10-6 mbar	10-6 mbar	10-8 mbar baking	10-8 mbar baking	10-8 mbar baking	10-8mbar baking	10-8 mbar baking	10-8 mbar baking	10-8 mbar baking	10-6 mbar

Table IV: Lower tower power and fluid request

Power consummations:

Rough pumping, ADP31	1.8 KW
Turbo pumping ATP1500	1.5 KW
Leak detector	0.8 KW
Clean air generator (3000m^3)	10 KW
Baking without tower	20 KW
Counters and gauges	2 KW
Crate for slow control	0.5 KW

Water:

Rough pumping	120 l/h
Turbo pumping	20 l/h
Cold water closed loop	to be defined

Compressed air:

Tank of 20 l at 7 bars

Power requested in the gallery, for one tower:

Lower cover baking	3 KW
Instrumentation, hoovers,	2 KW
Elevator	4 KW

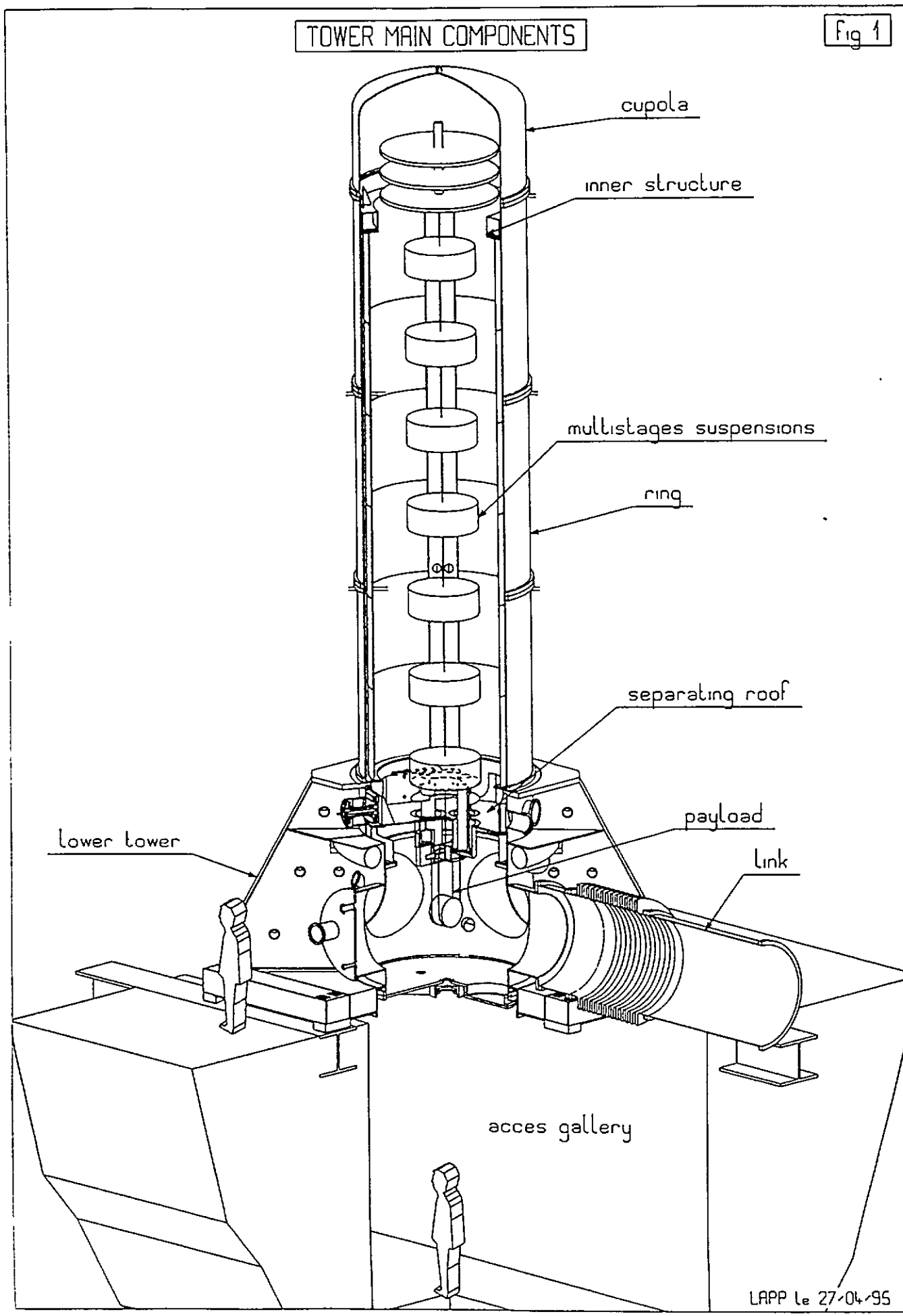
TOWER MAIN COMPONENTS
Fig 1
cupola
inner structure
multistages suspensions
ring
separating roof
payload
link
lower tower
acces gallery
LAPP le 27-04-95

LAYOUT OF VIRGO

Fig 2

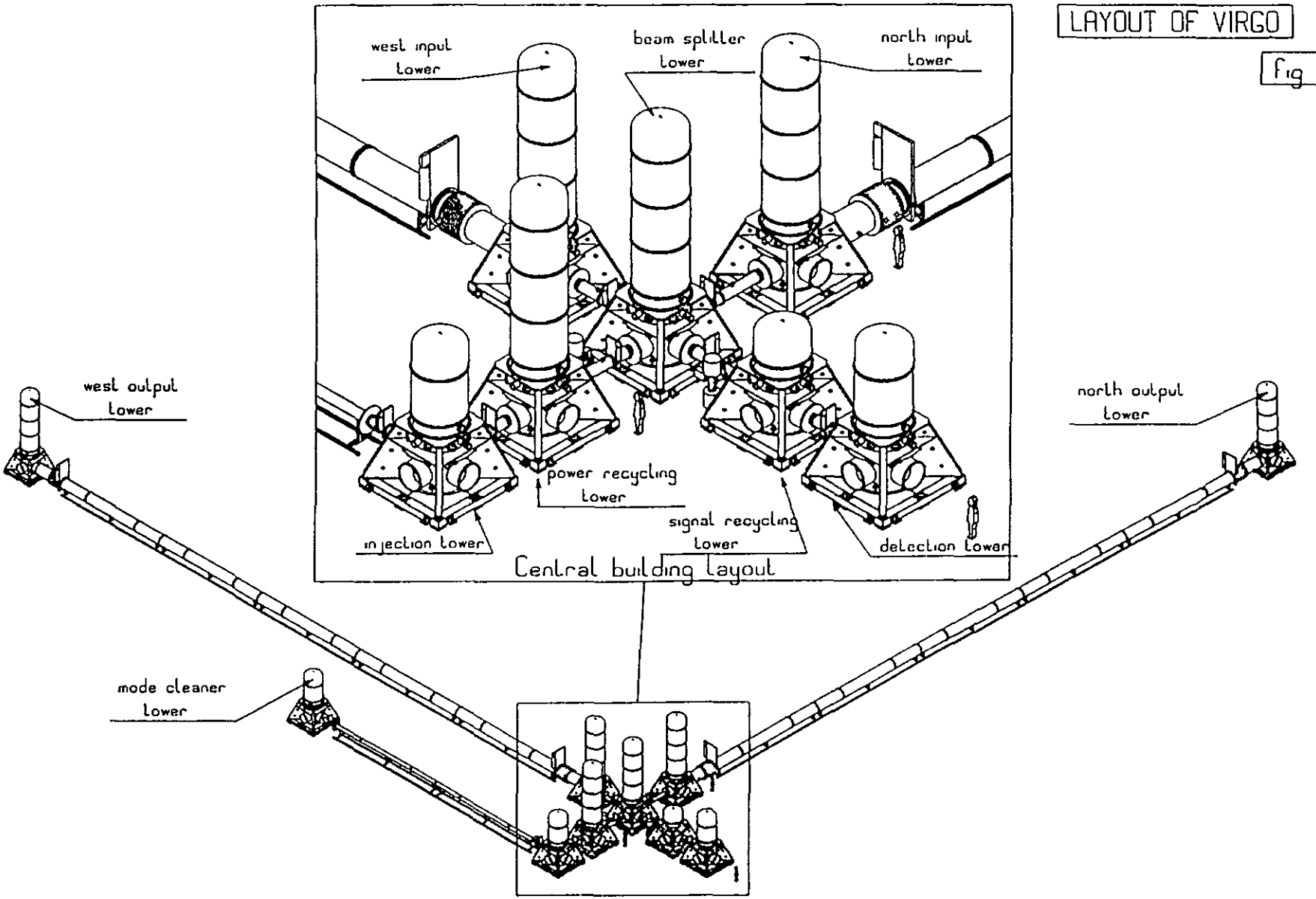

LAPP le 26/04/95

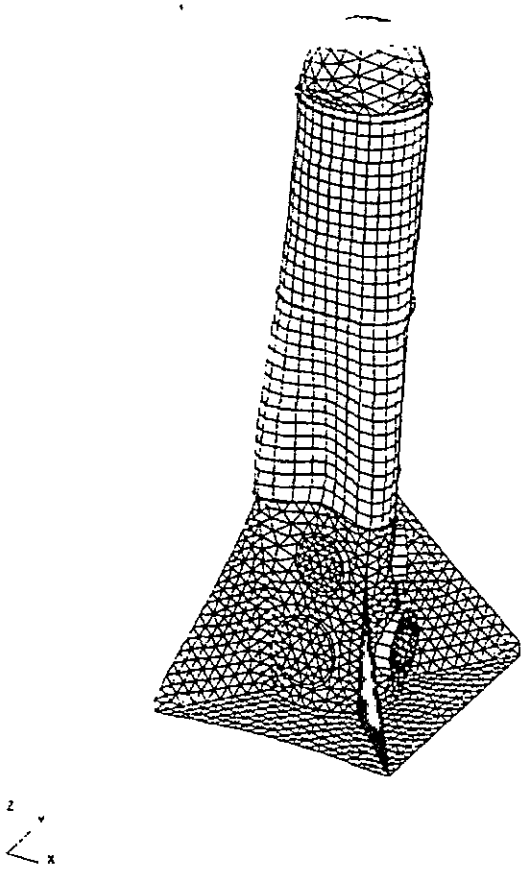

MODE NO 1 FREQUENCE = 14 978

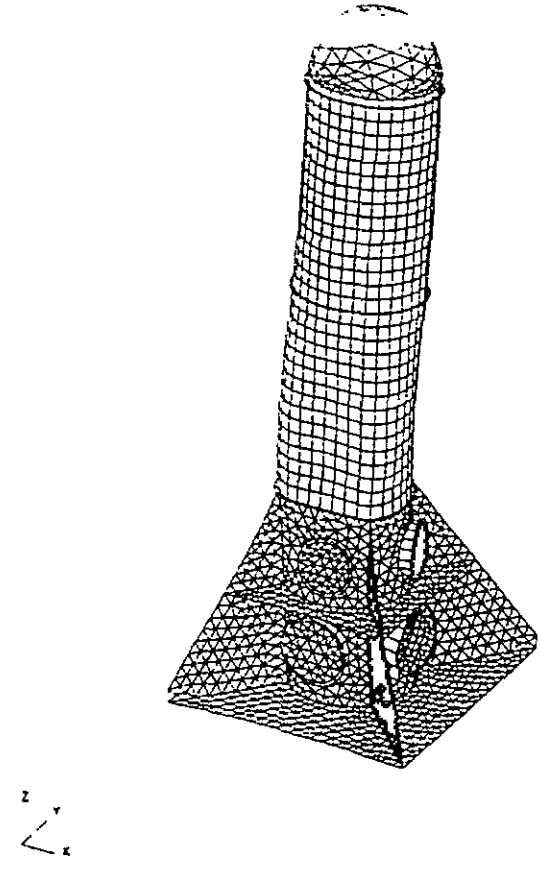

MODE NO. 1 FREQUENCE = 21.891

TOUR PHI 2M

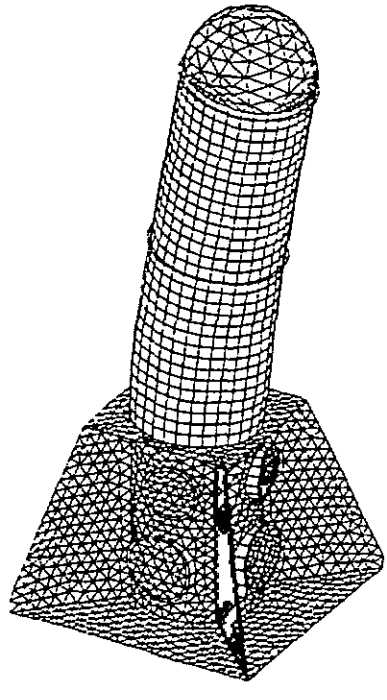

MODE NO 1 FREQUENCE = 27 248

Tower fundamental vibration frequency as a function of its structure.

Fig 4

LOWER TOWER 3D

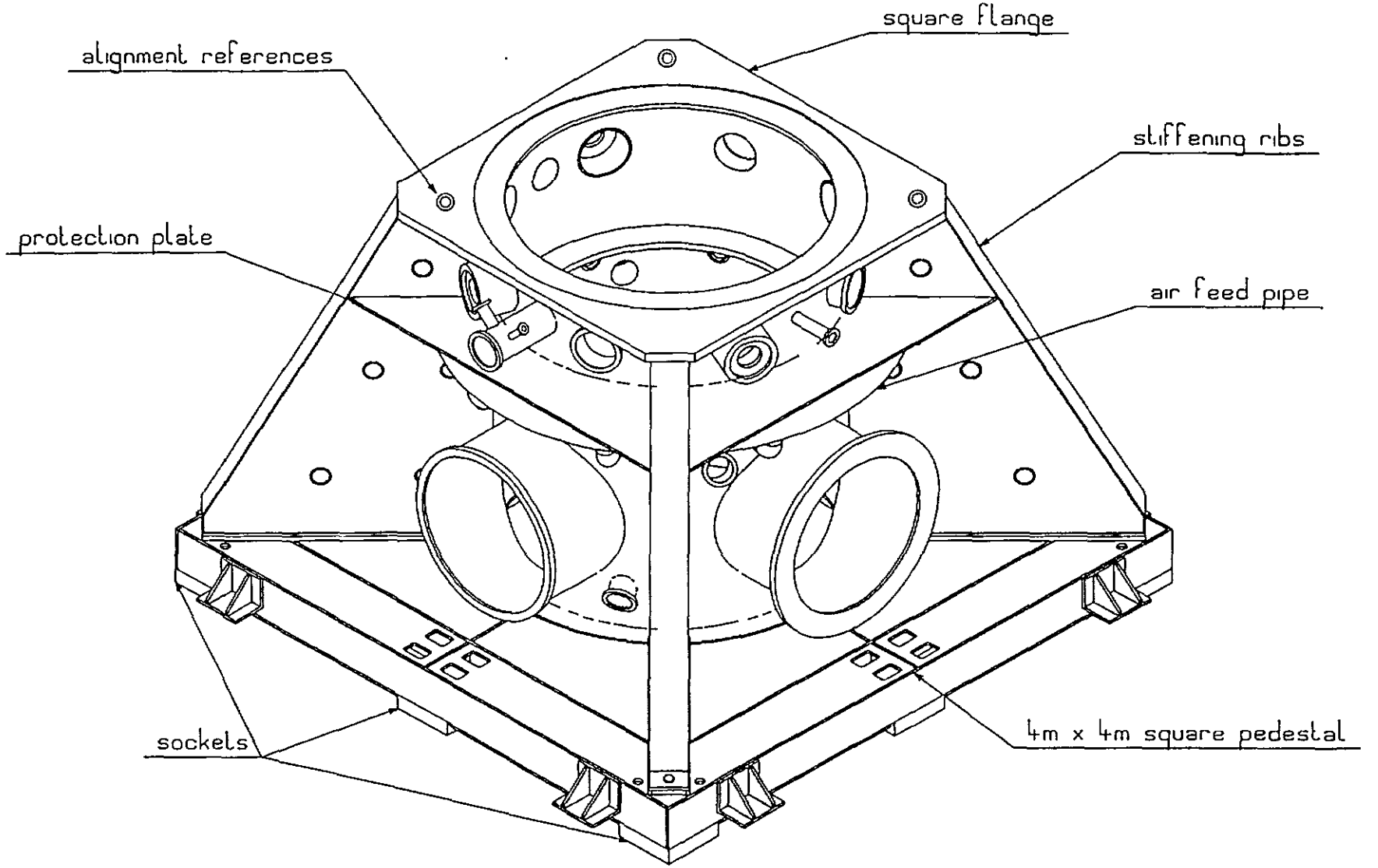

LAPP the 03/05/95

Fig 5

LOWER TOWER GEOMETRY

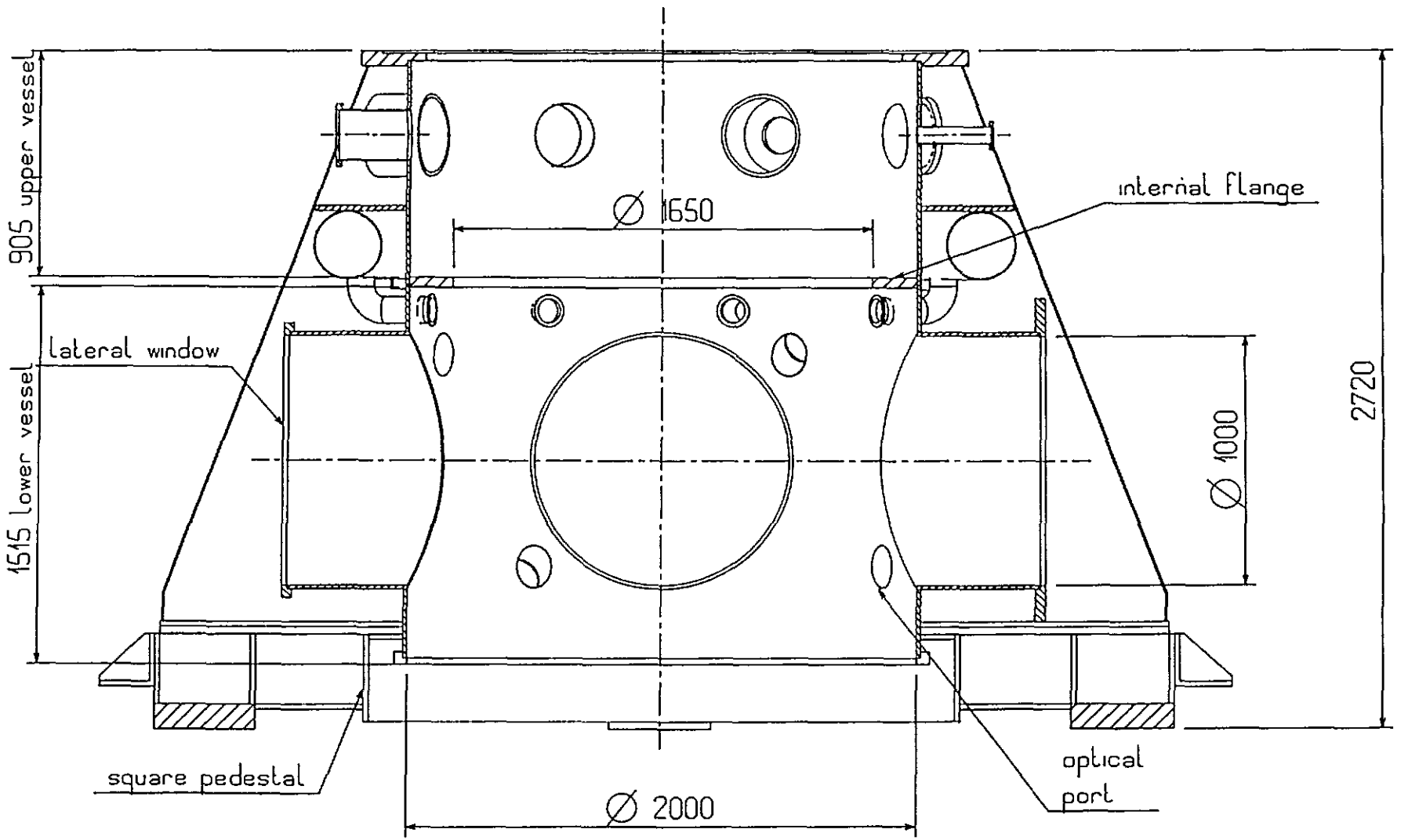

LAPP the 03/05/95

Fig 6

LOWER TOWER OPTICAL PORTS

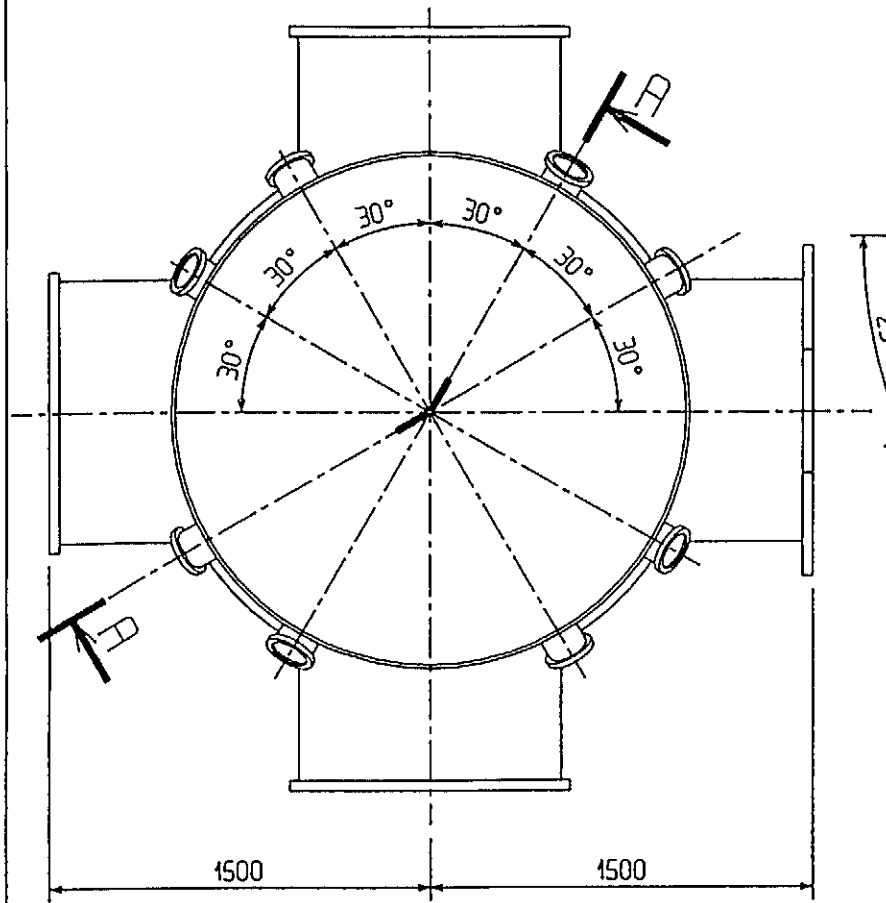

COUPE AA

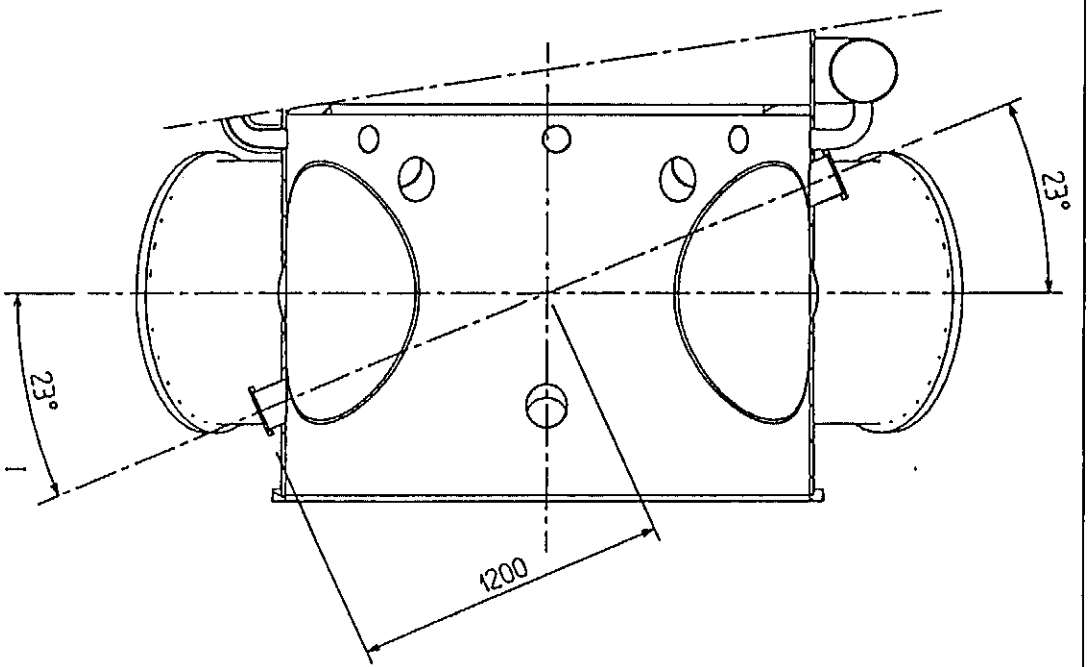

LAPP the 10/05/95

THE SEPARATING ROOF WITH ASSOCIATED MECHANISMS

Fig 7

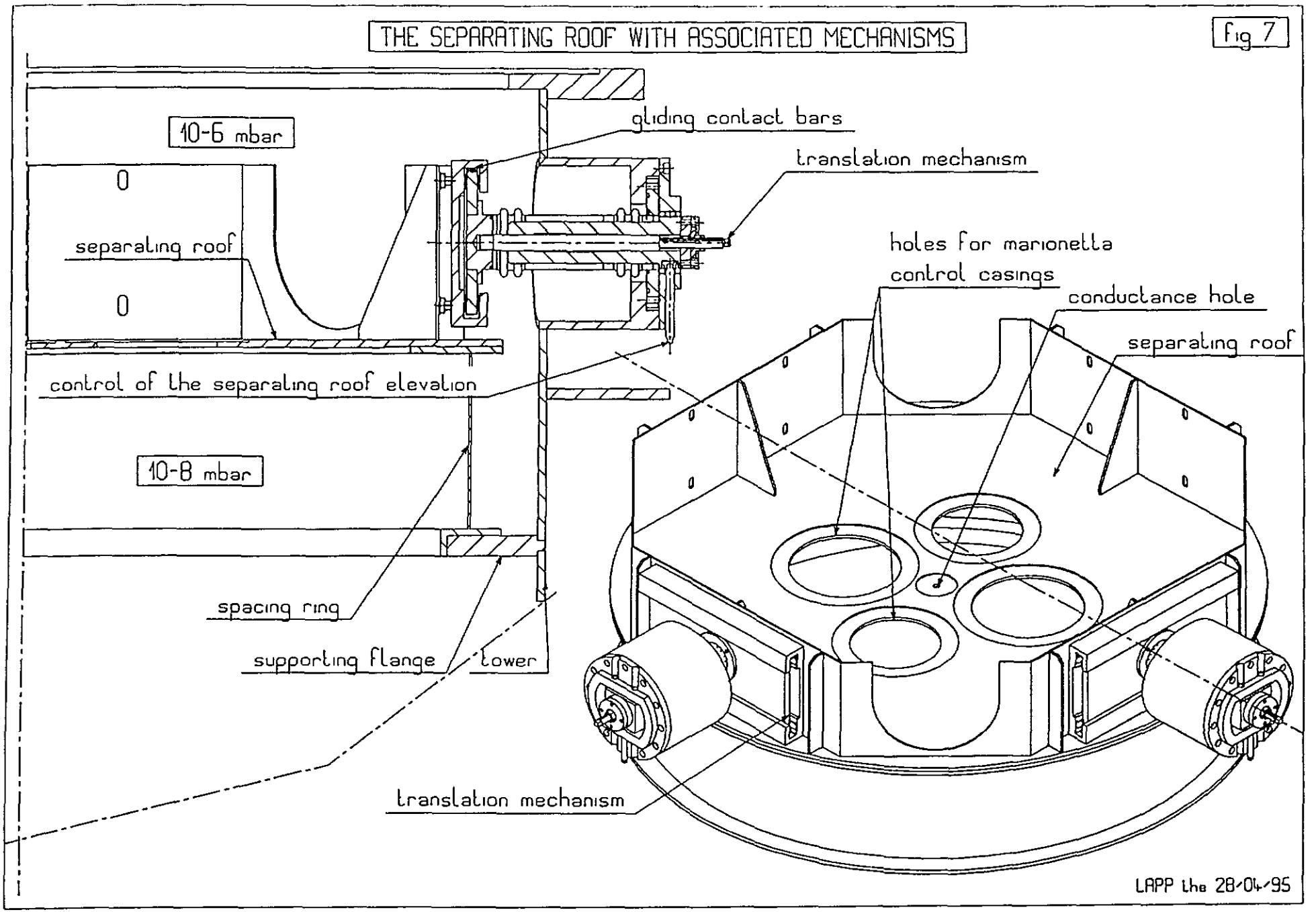

LAPP the 28/04/95

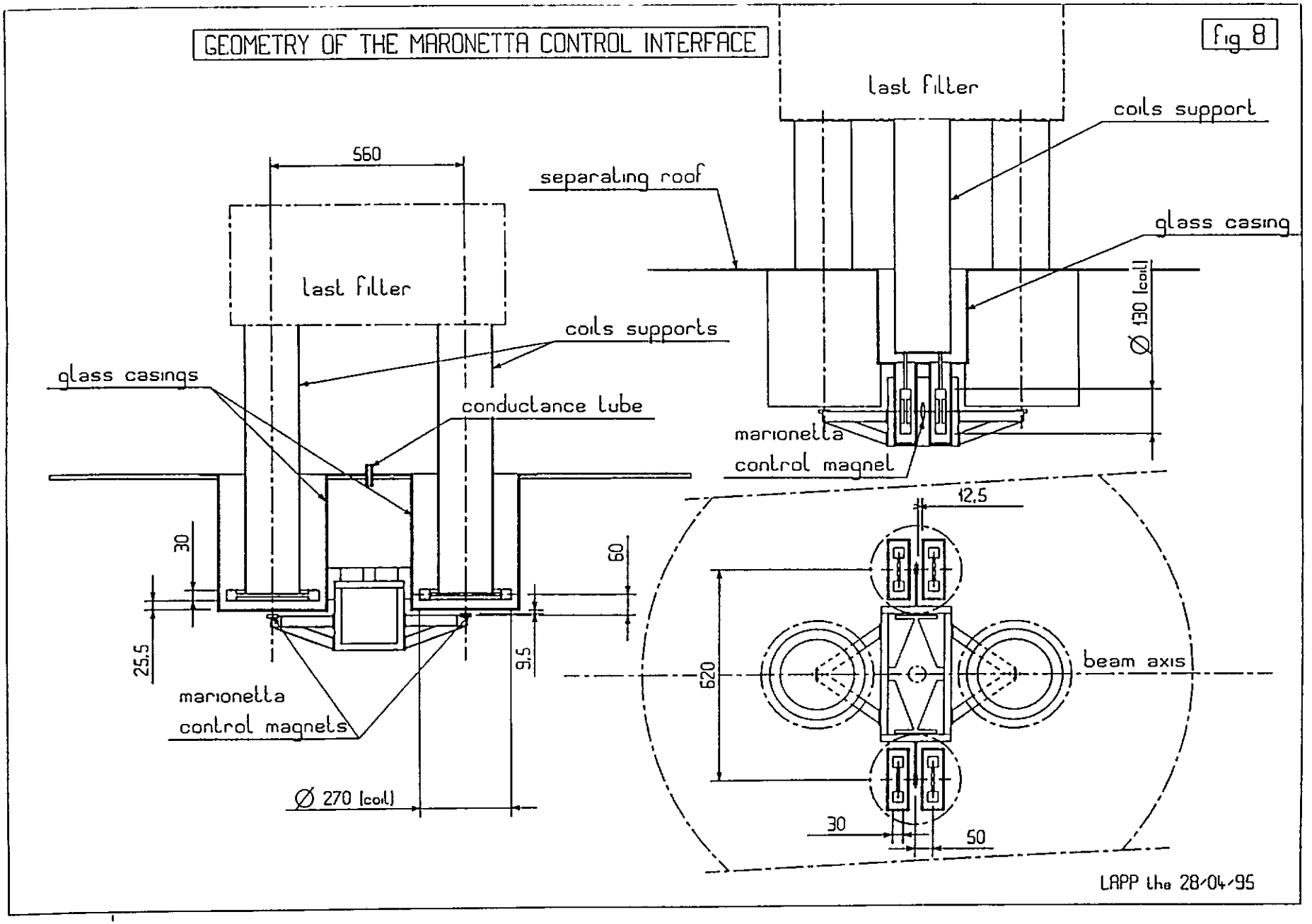
GEOMETRY OF THE MARONETTA CONTROL INTERFACE
fig 8
last filter
coils support
separating roof
glass casing
Ø 130 (coil)
560
last filter
coils supports
glass casings
conductance tube
marionetta
control magnet
12,5
30
60
25,5
9,5
620
beam axis
marionetta
control magnets
Ø 270 (coil)
30
50
LAPP the 28/04/95

THE PROTOTYPE INNER STRUCTURE

fig 9

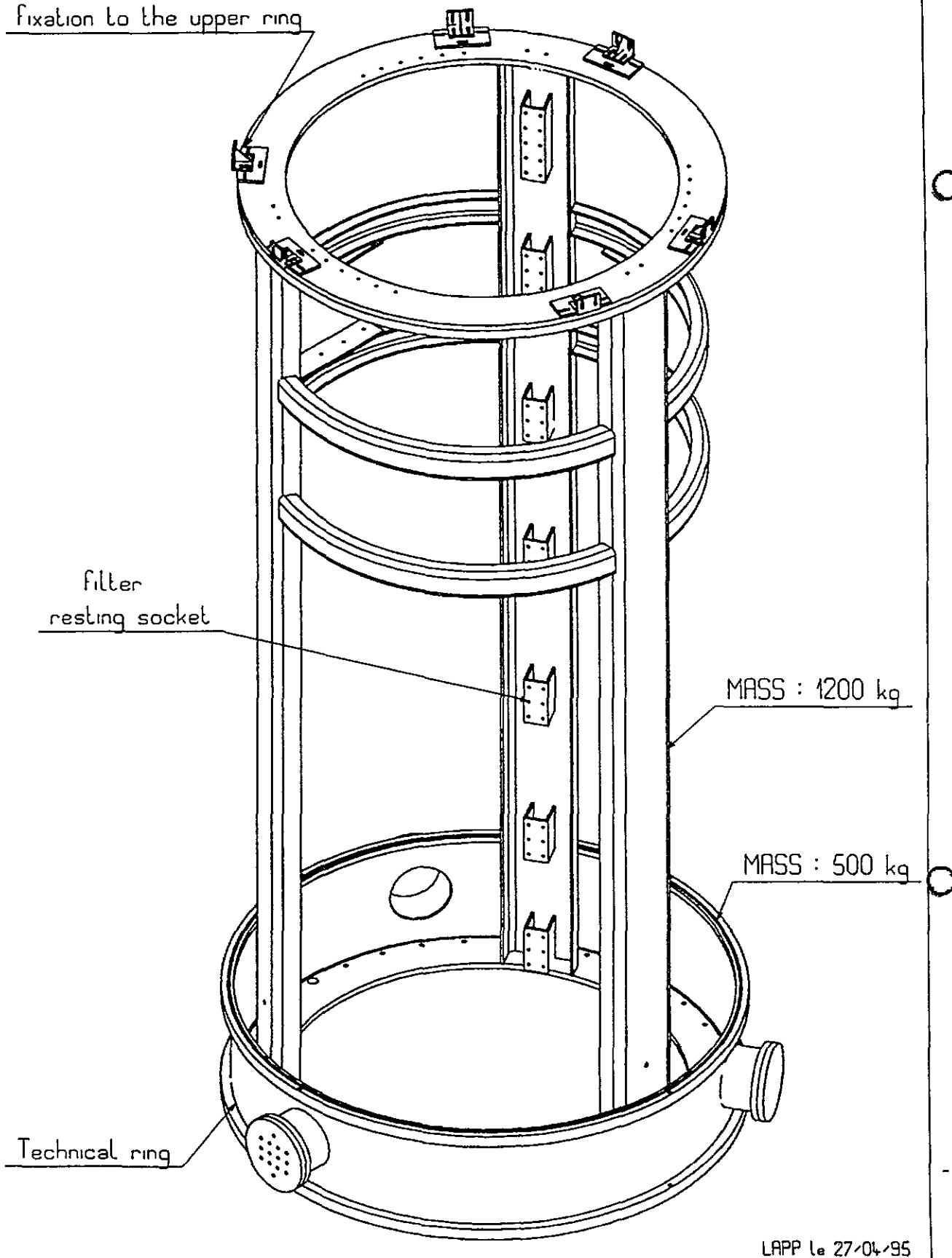

LAPP le 27/04/95

THE UPPER TOWER RING ASSEMBLY

Fig 10

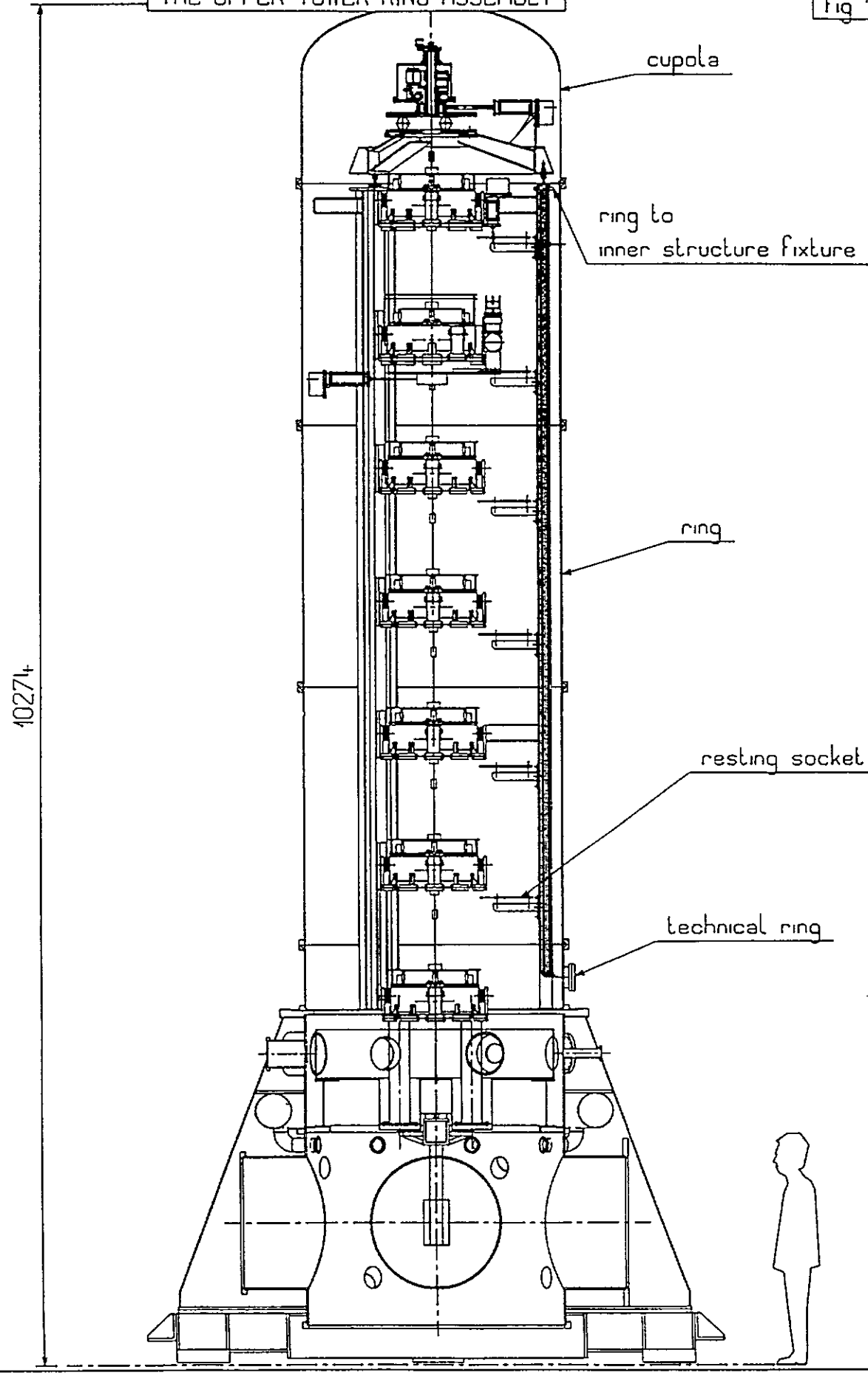

A TYPICAL LINK

Fig 12

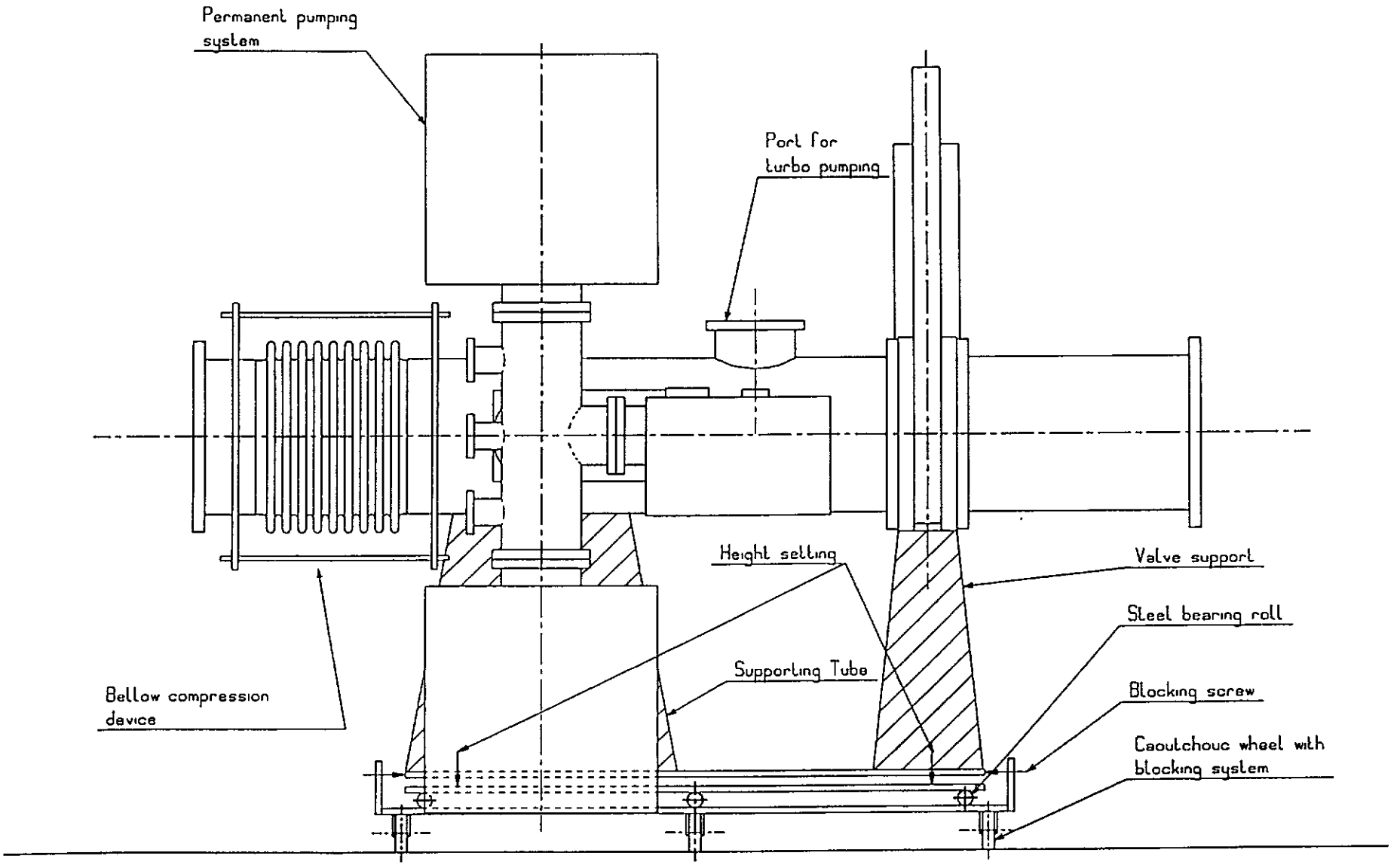

l.a.p.p. le 17/05/95

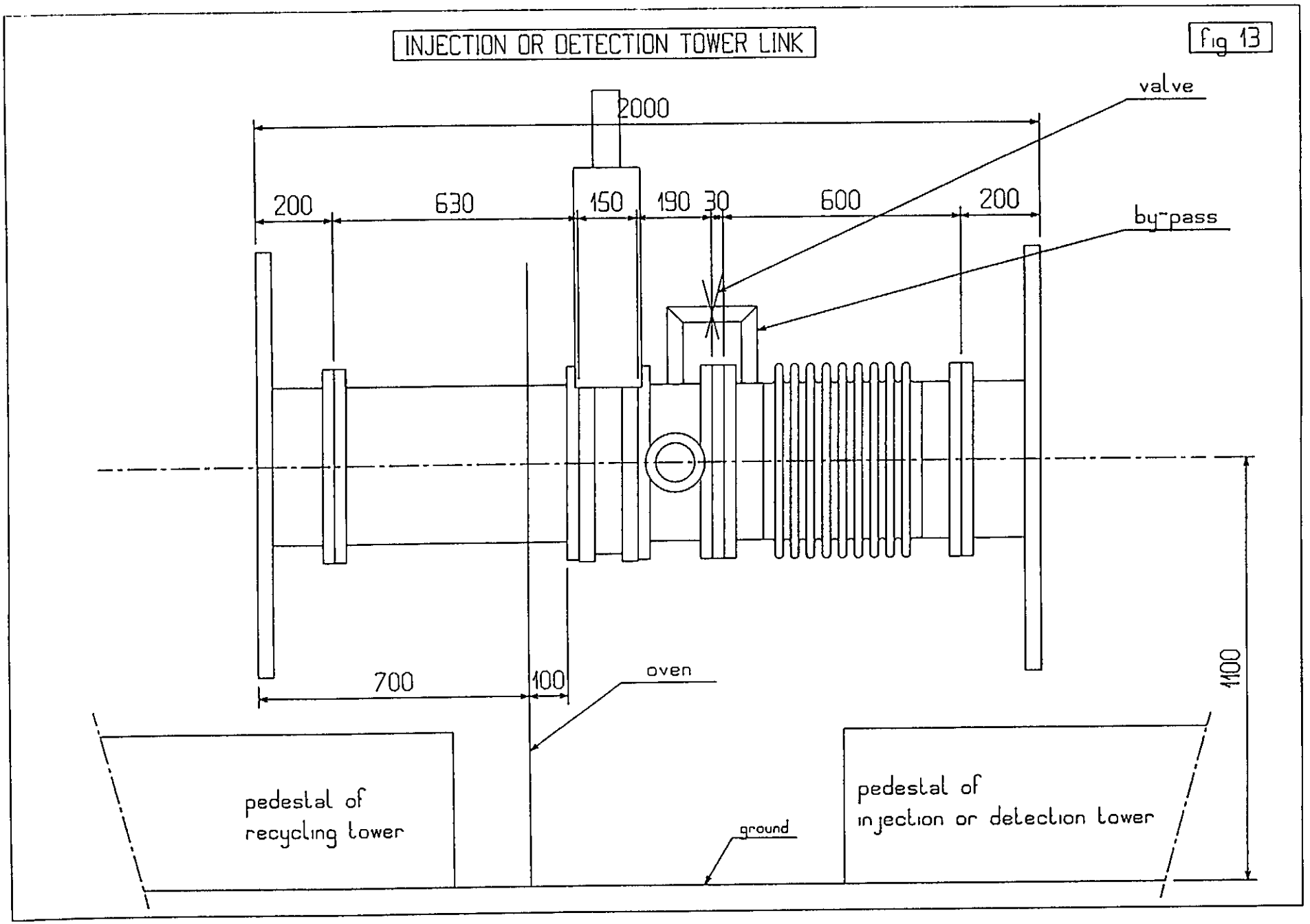
INJECTION OR DETECTION TOWER LINK
Fig 13
valve
2000
200
630
150
190
30
600
200
by-pass
700
100
oven
1100
pedestal of
recycling tower
ground
pedestal of
injection or detection tower

IMPLEMENTATION OF THE PROTOTYPE PUMPING SYSTEM

Fig 14

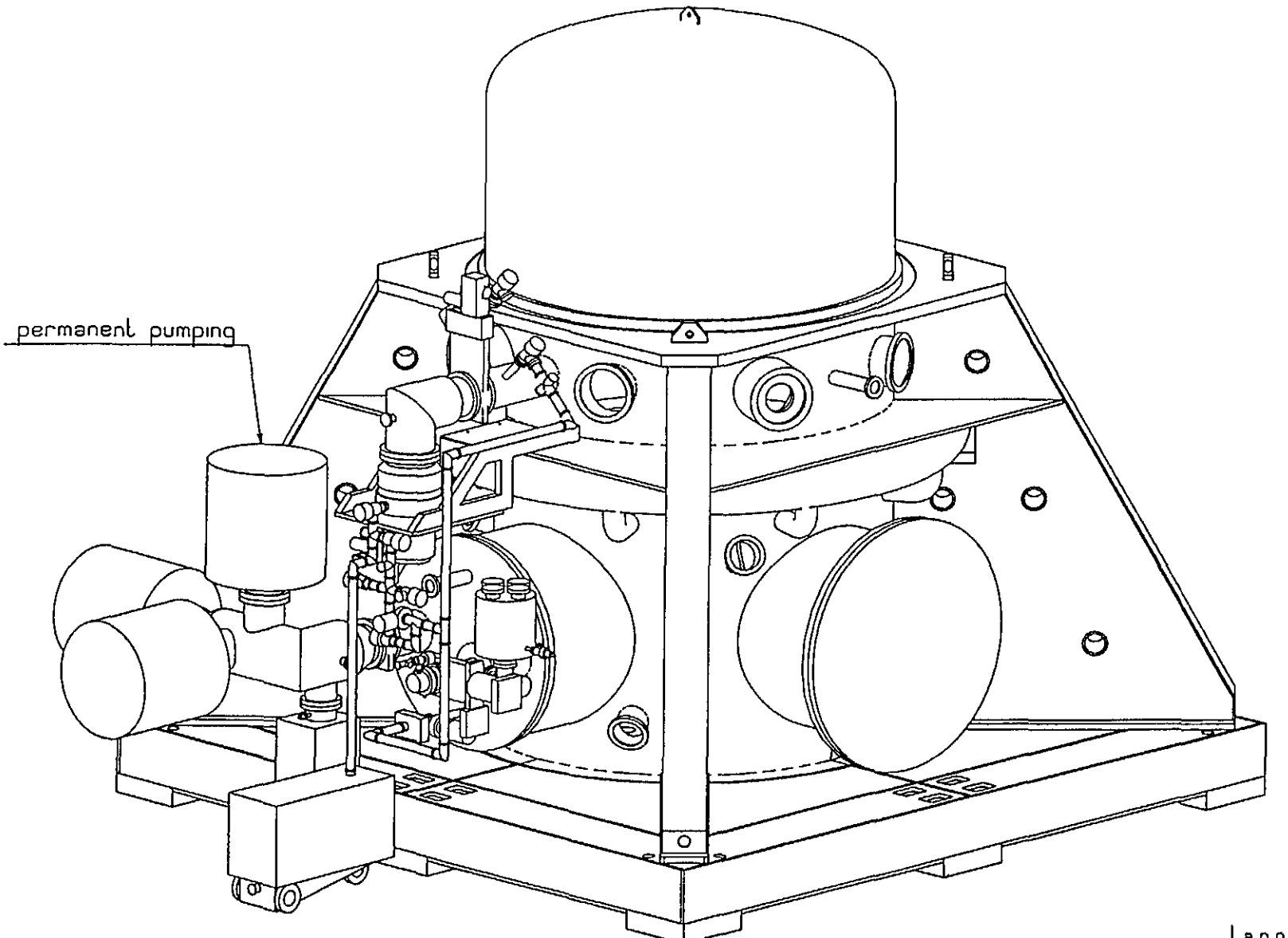

l.a.p.p. le 17-05-95

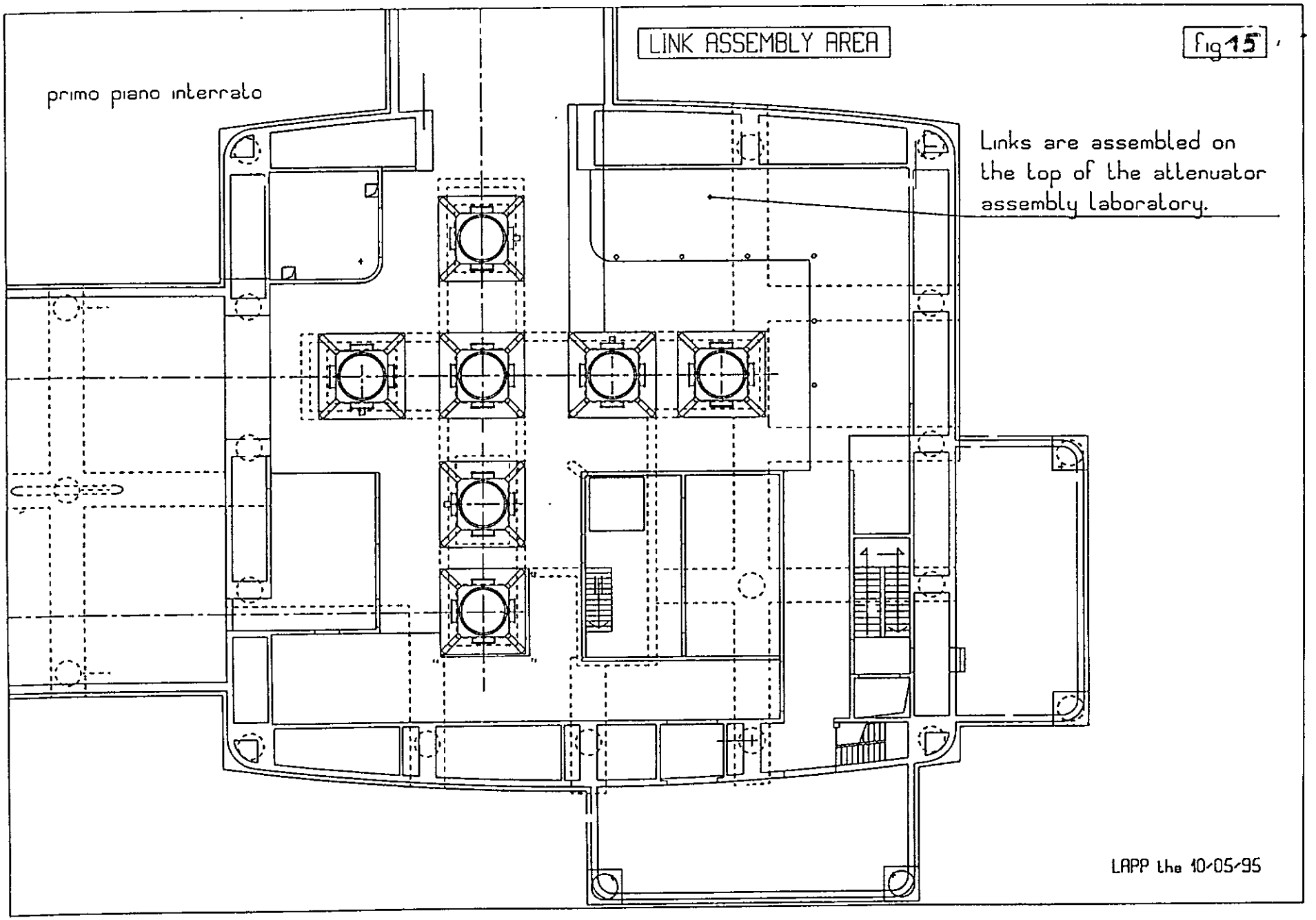
LINK ASSEMBLY AREA
fig 15
primo piano interrato
Links are assembled on the top of the attenuator assembly laboratory.
LAPP the 10-05-95

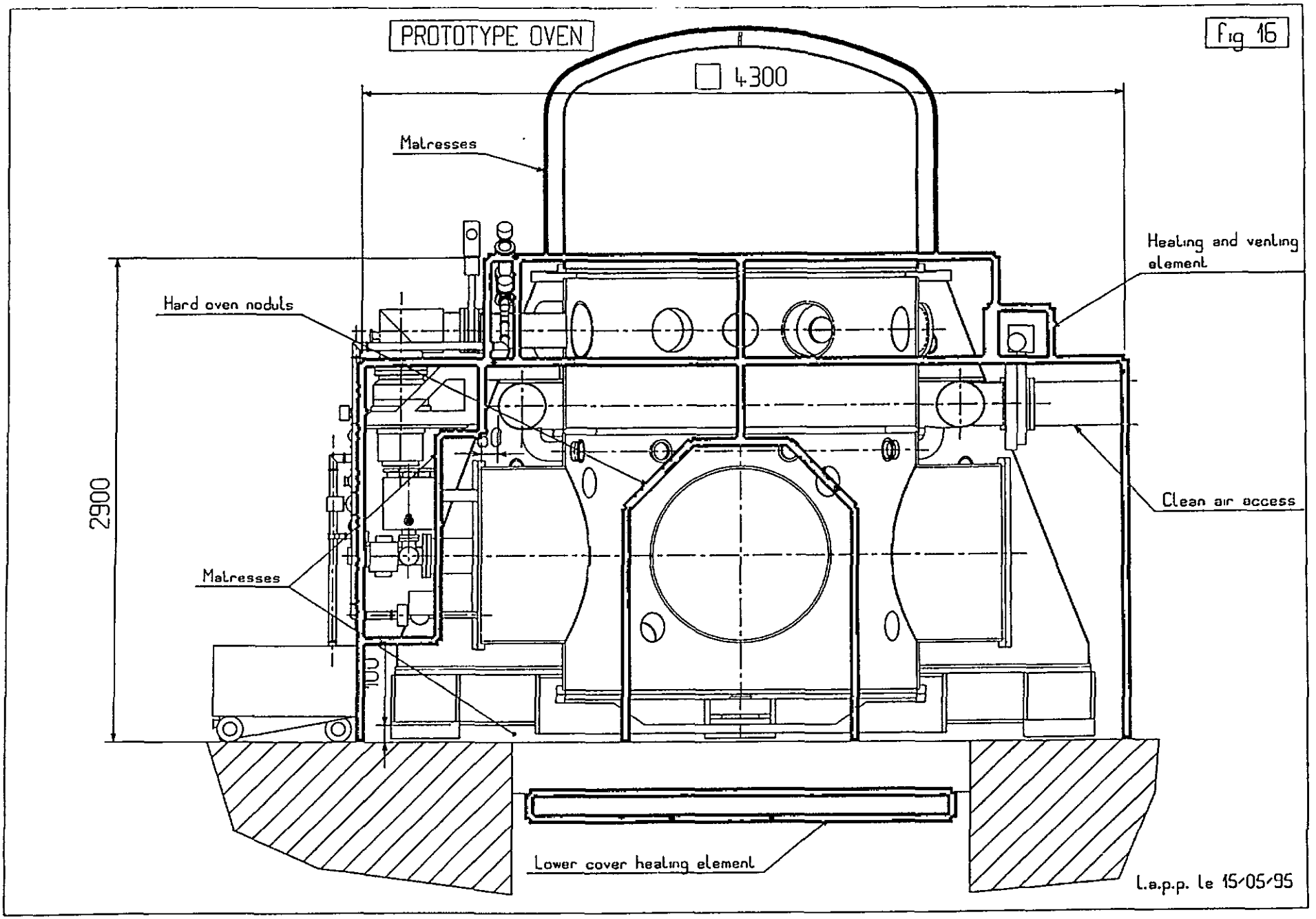
PROTOTYPE OVEN
Fig 16
4300
2900
Matresses
Hard oven noduls
Heating and venting element
Clean air access
Matresses
100
Lower cover heating element
l.e.p.p. le 15/05/95

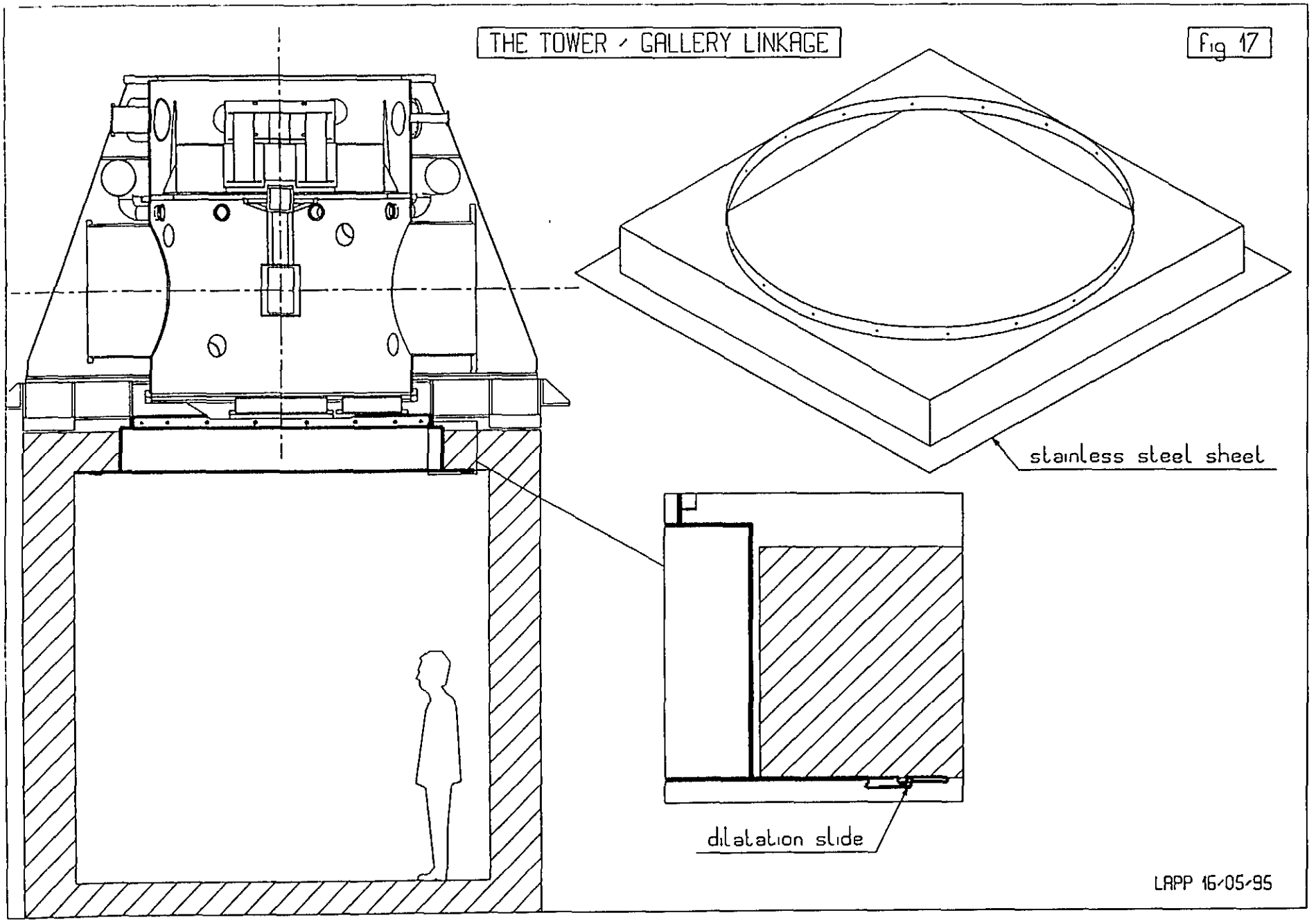
THE TOWER - GALLERY LINKAGE
Fig 17
stainless steel sheet
dilatation slide
LAPP 16/05/95

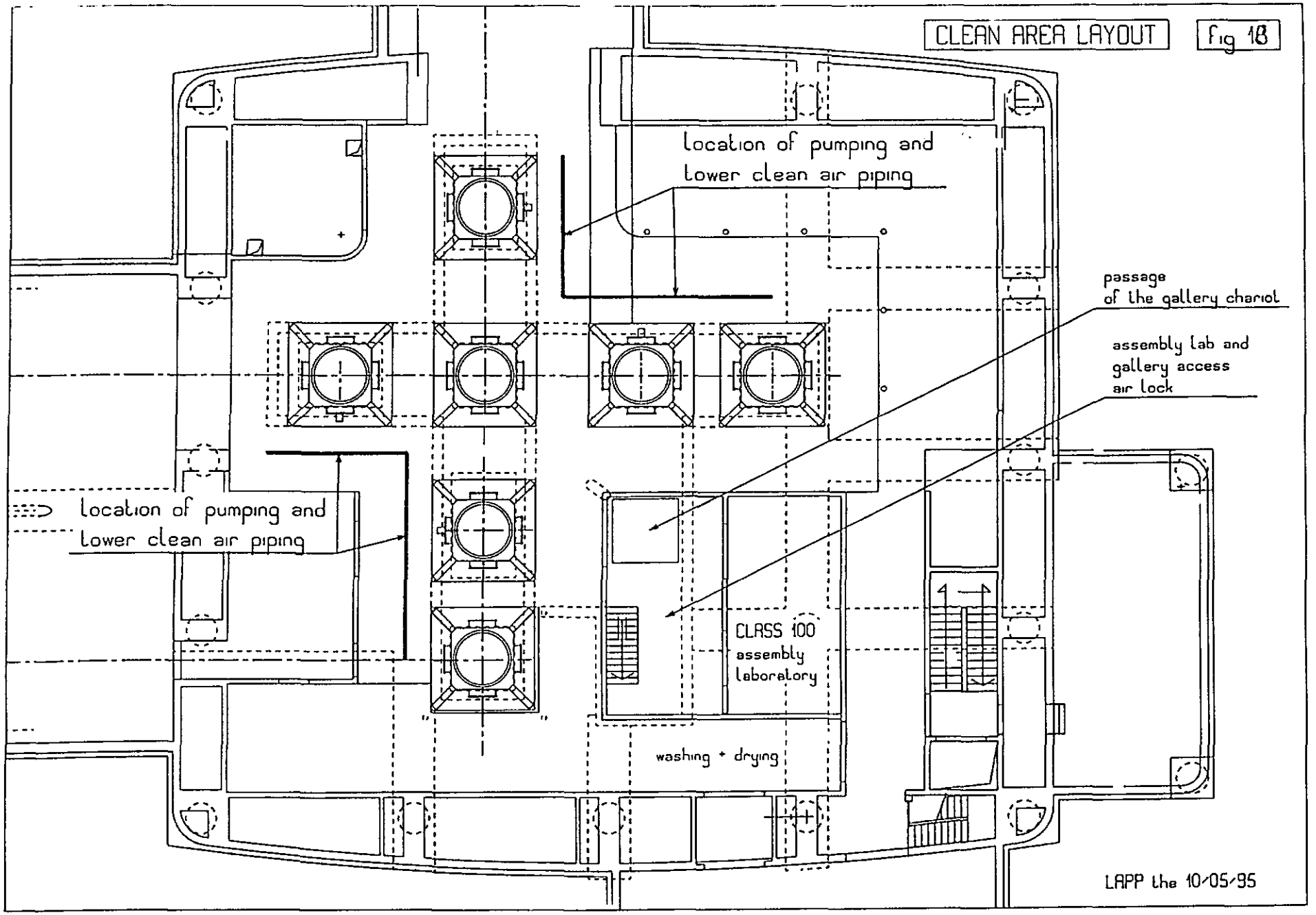
CLEAN AREA LAYOUT
Fig 18
location of pumping and
lower clean air piping
passage
of the gallery chariot
assembly lab and
gallery access
air lock
location of pumping and
lower clean air piping
CLASS 100
assembly
laboratory
washing + drying
LAPP the 10/05/95

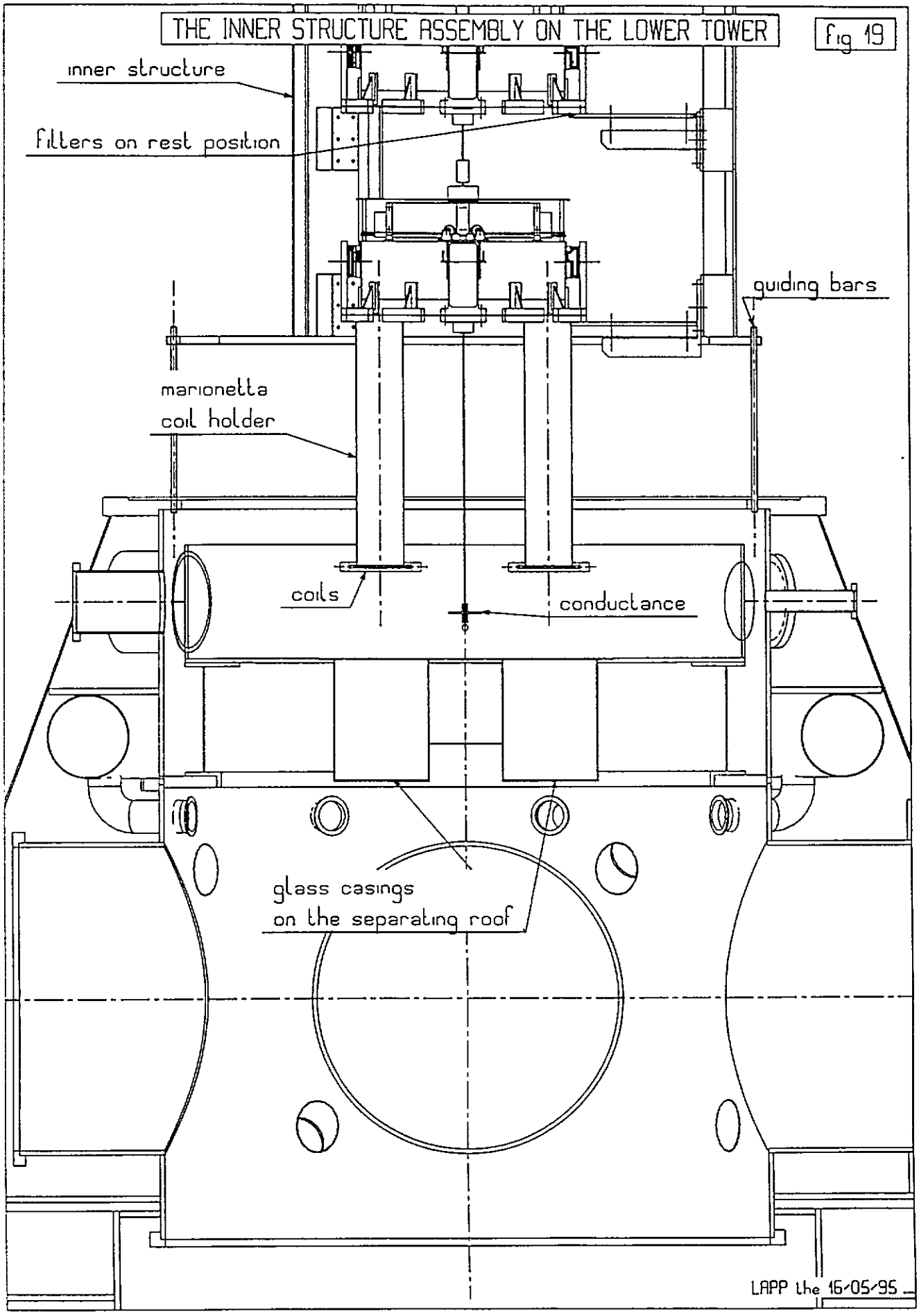
THE INNER STRUCTURE ASSEMBLY ON THE LOWER TOWER
Fig 19
inner structure
filters on rest position
guiding bars
marionetta
coil holder
coils
conductance
glass casings
on the separating roof
LAPP the 16-05-95

Fig 20

PAYLOAD TRANSPORTATION BOX

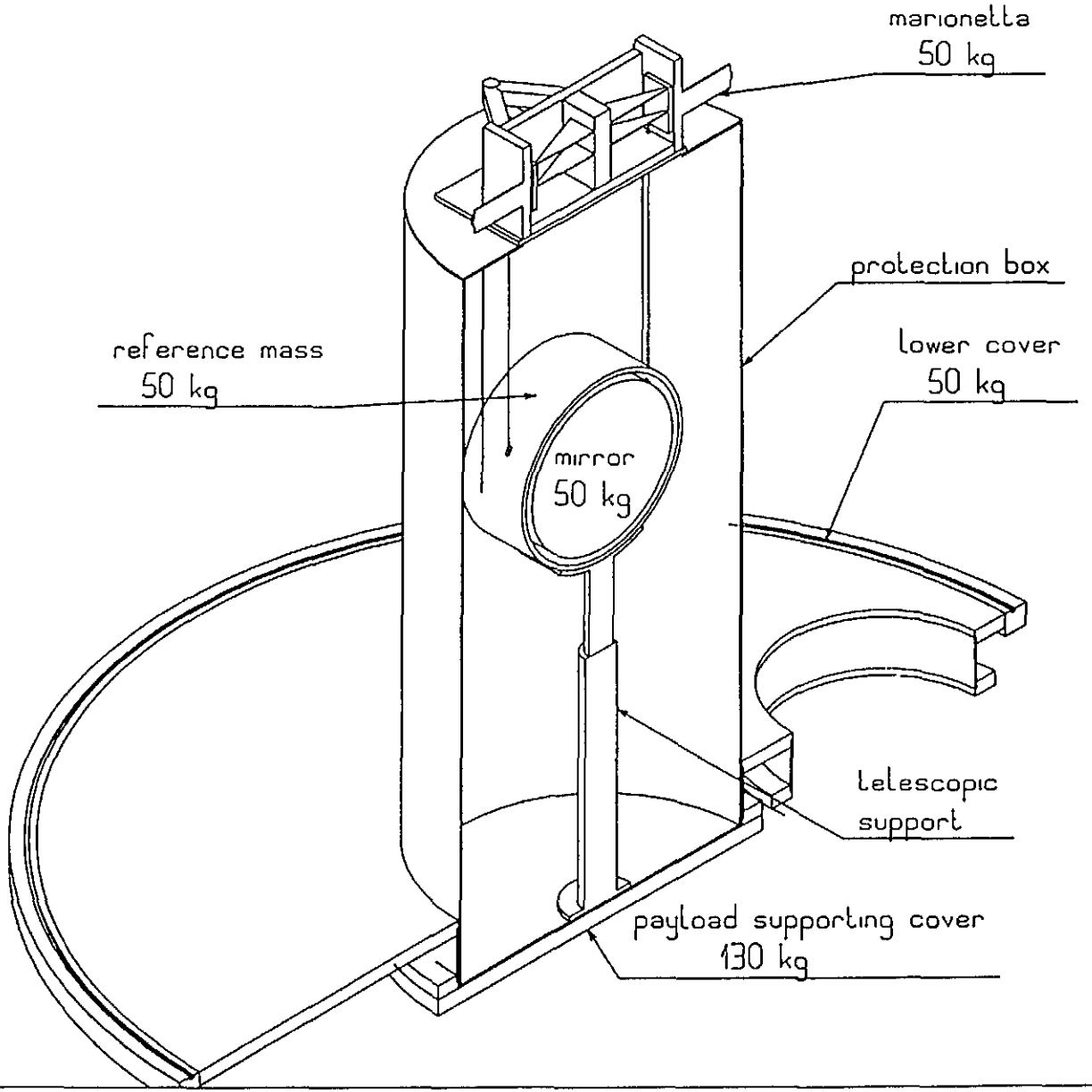

LAPP le 27/04/95

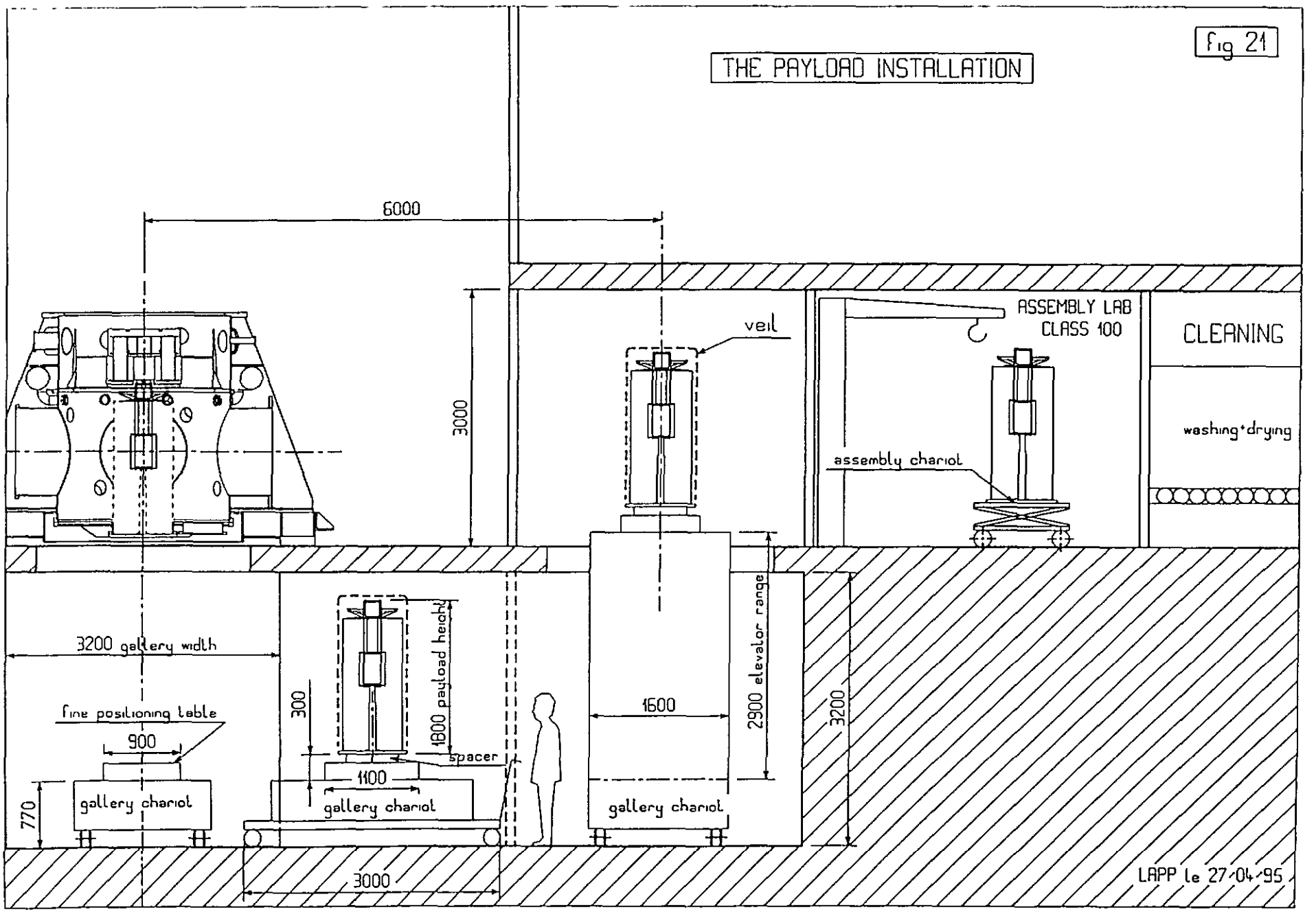
Fig 21
THE PAYLOAD INSTALLATION
6000
3000
veil
ASSEMBLY LAB
CLASS 100
CLEANING
washing+drying
assembly chariot
3200 gallery width
fine positioning table
900
770
gallery chariot
300
1800 payload height
spacer
1100
gallery chariot
1600
2900 elevator range
3200
gallery chariot
3000
LAPP le 27-04-95

PUMPING SYSTEM

3400.1.GENERAL SPECIFICATIONS AND STRATEGY

3400.1.1.SPECIFICATIONS

3400.1.1.1.Gas Pressure

As already said in the introduction, the target for the average partial pressure in the Virgo ultra vacuum system are :

	Acceptable value at start (1999)	Ultimate realistic value
H_2	1. 10^{-7} mbar (1. 10^{-5} Pa)	1. 10^{-9} mbar (1. 10^{-7} Pa)
Σ other gases	1. 10^{-8} mbar (1. 10^{-6} Pa)	1. 10^{-10} mbar (1. 10^{-9} Pa)
Hydrocarbons	1. 10^{-14} mbar (1. 10^{-12} Pa)	1. 10^{-14} mbar (1. 10^{-12} Pa)

3400.1.1.2.Operation Constraints

- Possibility of intervention on a tube or on a tower without interfering with the other items.

- Maximum temperature in the tunnel : 40°C

- Minimum temperature in the tunnel : - 5°C

- Running time of the installation : 20 years.

3400.1.1.3.Environmental Constraints

- No polluting smokes rejected outside.

3400.1.1.4.Cleanliness

The problem of pollution by dusts is critical.

3400.1.2.MAIN SOURCES OF GASES IN THE UPPER PART OF THE SYSTEM

3400.1.2.1. Outgassing of single items

	Area (cm^2)	Outgassing rate ($mbar.l.s^{-1}.cm^{-2}$)	Outgassing flux ($mbar.l.s^{-1}$)	gas
Tube	$1.2\ 10^8$	$5\ 10^{-14}$	$6\ 10^{-6}$	H_2
Baffles	$3.3\ 10^6$	$3\ 10^{-13}$	$1\ 10^{-6}$	H_2
Tower (lower part) empty system (*)	$4\ 10^5$	$5\ 10^{-14}$	$2\ 10^{-8}$	H_2
Tower (upper part)(**)			$3\ 10^{-7}$ $1\ 10^{-7}$	Other H_2
Valve Ø = 1200 (body))	$1.5\ 10^5$	$2\ 10^{-12}$	$3\ 10^{-7}$	H_2
Viton gasket (Ø = 1200)	$120*\pi*1.6*\pi = 1.9\ 10^3$	$2\ 10^{-10}$	$3.8\ 10^{-7}$	Other
Valve Ø = 200 (body)	$1.5\ 10^4$	$2\ 10^{-12}$	$3\ 10^{-8}$	H_2
Viton gasket Ø = 200	$20*\pi*1*\pi = 200$	$2\ 10^{-10}$	$4\ 10^{-8}$	Other
Valve Ø = 63 (Body)	$5\ 10^3$	$2\ 10^{-12}$	10^{-8}	H_2
Viton gasket Ø = 63	70	$2\ 10^{-10}$	$1.4\ 10^{-8}$	Other

From the tests on the prototypes, values lower than $5\ 10^{-15}$ $mbar.l.s^{-1}.cm^{-2}$ were obtained for the outgassing rate of stainless steel. With a safety factor of at least 10, the figure of $5\ 10^{-14}$ $mbar.l.s^{-1}.cm^{-2}$ is taken as basis for the vacuum calculations.

(*) This implies that all the stainless steel components of the lower parts have been vacuum fired at 950°C.

(**) The conductance between the two parts of a tower is made of a cylinder 1 cm in diameter, 50 cm long. Its value is 0.9 $l.s^{-1}$ for hydrogen, 0.3 $l.s^{-1}$ for water vapor, 0.24 $l.s^{-1}$ for nitrogen and less than 0.2 $l.s^{-1}$ for hydrocarbons. The pressure in the upper part is supposed to be 10^{-6} mbar and the residual gases to be water vapor for 90 % and hydrogen for 10 %.

The problem of the hydrocarbon outgassing of the various components contained in the upper part of the towers is of utmost importance. Presently, it is considered from the point of view of minimizing the outgassing of the specific components. Ways to reduce its impact on the mirrors part are also investigated.

3400.1.2.2. Total flux per arm

Item	number	total flux H_2 (mbar.l.s^{-1})	total flux (other gas) (mbar.l.s^{-1})
Tube	1	6 10^{-6}	--
Baffles		1 10^{-6}	--
Tower (lower part) empty system	3	.06 10^{-6}	--
Tower (upper part)	3	.3 10^{-6}	1 10^{-6}
Valves Ø = 1200 (bodies)	2	.6 10^{-6}	--
Viton gaskets Ø = 1200	2	--	.76 10^{-6}
Valves Ø = 200 (bodies)	4 per tower 22 per tube = 34	1.02 10^{-6}	--
Viton gaskets Ø = 200	2 per tower, 11 per tube = 17	--	.68 10^{-6}
Valves Ø = 63 (bodies)	4 per tower 12 per tube = 24	.24 10^{-6}	--
Viton gaskets Ø = 63	2 per tower 12 per tube = 18	--	.25 10^{-6}
Total		≈ 9 10^{-6}	2.7 10^{-6}

3400.1.2.3. Comments

The outgassing rate is composed of 9 10^{-6} mbar.l.s^{-1} for hydrogen and 2.7 10^{-6} mbar.l.s^{-1} for other gas species, mainly H_2O. Viton and upper part towers account respectively for 2/3 and 1/3 of this last figure. For hydrogen, the gate valves contribute to 20 % of the total.

3400.1.2.3.1. For hydrogen :

With a total pumping speed for the Ti sublimators of 42 000 l.s^{-1} (11 units), the pressure will be about 2 10^{-10} mbar (4 10^{-10} with the so-called "saturated" Ti layers). This has to be corrected for a form factor due to the tube conductance (≈ 1.5 for hydrogen and 300 m section). So **the hydrogen pressure should, at all time, be less than 6 10^{-10} mbar.**

3400.1.2.3.2. For other species :

With a total pumping speed of 2200 l.s^{-1} (11 units), the ion pumps should provide for a limit of 1.3 10^{-9} mbar.

For water vapour, the pumping speed of the wall has to be considered. One monolayer over the inner surface of the tube would have a capacity of 4.5 10^3 mbar.l. An outgassing flux of 4.7 10^{-6} mbar.l.s^{-1} for water vapor would take 30 years to saturate a monolayer. One might expect water vapour molecules to be concentrated close to the towers. Even a factor of 10 would lead to a 3 year time duration. In conclusion, **the 1.3 10^{-9} mbar figure above will be strongly reduced in practice.**

3400.1.3.STRATEGY FOR PUMPING

In order to increase the running efficiency of the antenna a few main choices were decided 'a priori':

- gate valves must separate the different large vacuum chambers, tubes and towers, to enable one to vent each large volume for interventions without spoiling the vacuum of the others.
- gate valves must separate the pumping sets and the instrumentation boxes from the large vacuum chambers to allow for interventions.
- the gate valves that are normally open will have viton gaskets for reliability reasons and for saving on the cost. The ones that are normally closed will have vice versa metal gaskets for avoiding permeation;
- all the operations for the control-command of the vacuum system, including safety and data acquisition are computerised.

Moreover the pumping system must satisfy other requirements of the antenna, namely :

- No mechanical vibration for the permanent pumping;
- No molecular bursts either;
- No hydrocarbon contamination.

The solution, described below, is a conservative solution designed according to the "golden rules" of the vacuum technology.

In order to arrive to the solution described below, the criteria for optimising the permanent pumping were used in the following order :

(1) pumping speed
(2) pressure stability
(3) absence of pollution
(4) absence of mechanical vibrations
(5) flexibility for future R&D
(6) pumping capacity
(7) easy maintenance
(8) cost.

3400.2.PUMPING SYSTEM

The whole pumping, tubes and towers, is achieved with the help of modular units of 6 different types.

3400.2.1.TUBE

3400.2.1.1.Rough pumping of the tubes : unit #1

Each tube requires a pumping speed of about 150 m^3h^{-1} in order to reach 10^{-2} mbar in less than ten days. For the rough pumping, regular spacing of the pumps along the tube is of no importance. A single unit, "Pumping Unit #1", located in the central building, will be used to pump down each long tube, one after the other.

The main specification concerns the absence of pollution, neither internal nor external. Internal pollution refers to hydrocarbons. Consequently the rough pumps will be achieved by "dry pumps" used in conjunction with a roots group in order to obtain a pumping speed of about 150 m^3h^{-1} . Typically Alcatel ADS 315 or a Leybold system [Allex+VSU250] will meet these requirements.

3400.2.1.1.1.Description

Nb	Items
2	All metal valve CF 100
1	150 m^3h^{-1} roots group with its venting valve (*)
7	Pirani gauge with its controller (3 gauges on each tube, one on the tube)
2	Differential manometer (1 per tube for venting)

(*) All the venting valves, even those on the mechanical pumps, are provided with two filters in series, 1µm and 0.1 µm, in order to trap dusts. This applies also to all the other units

3400.2.1.2.Intermediate pumping of the tubes : unit #2

In order to avoid large pressure gradients during bake out, a 300 m spacing between pumping stations is chosen. Altogether, there will be **11 stations per tube**, including one at both ends.

3400.2.1.2.1.Description

Nb	Items
1	All metal valve CF200
1	Viton valve KF40 between the TMP and the fore pump
1	1000 $l.s^{-1}$ TMP ceramic bearing model with a CF 200 flange, an integrated venting valve, an air cooling system and its controller
1	30 $m^3.h^{-1}$ mechanical pump, a trap and a venting valve
1	Penning gauge with its controller
1	Pirani gauge with its controller

3400.2.1.3.Permanent pumping of the tubes : unit #3

3400.2.1.3.1.Description

Nb	Items
1	Pumping chamber
1	Viton valve CF200
2	Ti sublimator (h=600, Ø=600, 1.6 m^2, 48000l/s) with the control unit
1	Ion pump, noble diode 240l/s with its power unit
1	Instrumentation chamber
1	Viton valve CF63 for the instrumentation chamber
1	Penning gauge with its controller
1	RGA with its electronics
2	All metal valve CF40 for the rough pumping of the chambers

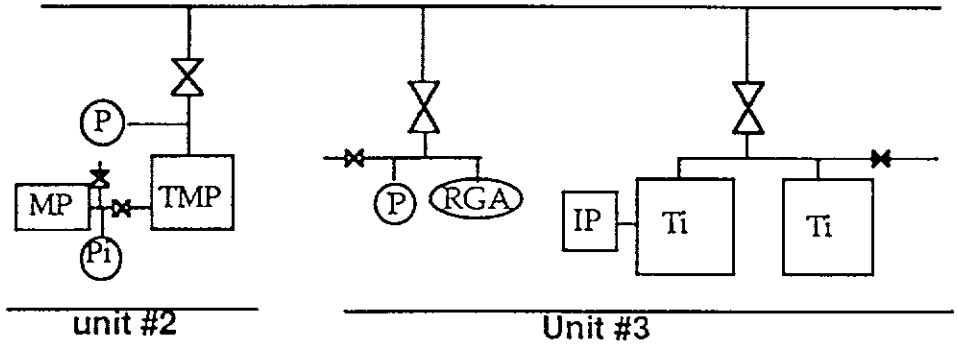

Synopsis of the intermediate and permanent pumping of the tube (unit #2 and 3)

3400.2.1.3.2.Expected performances

3400.2.1.3.2.1.Pumping speed

During the bake out, the effective pumping speed of unit #3 on the tube will be 900 l/s for N_2 and H_2O. For a maximum outgassing rate of 10^{-8} mbar.l.s^{-1}.cm^{-2} for H_2O, the maximum pressure at 150 m from the unit would be 3.10^{-5} mbar, a limit for molecular gas flow.
During the permanent pumping phase, the effective pumping speed on the tube will be 3800 l/s for H_2 and 200 l/s for rare gases.
With the above conditions (see § on Main sources of gas), one fresh sublimation per year will be sufficient.

3400.2.1.3.2.2.Pressure stability

The ion pump is the only source of molecule bursts in the unit. There are many evidences that micro-objects are expelled from ion pumps. In order to minimize this effect, the ion pump is shielded from the tube by placing it after one of the Ti sublimator.

3400.2.1.3.2.3.Absence of pollution

The correct use of the TMP, together with a trap and a mechanical pump, for a limited period of time during bake out will not endanger the optics of Virgo.
Titanium migration, if any, during a sublimation will be avoided by closing the gate valves. The absence of Ti dusts or peeling was demonstrated for typical layers, 0.1 µm thick. This figure would correspond to a 20 year pumping without venting.

3400.2.1.3.2.4. Absence of mechanical vibrations

During the permanent pumping phase, the system does not generate internal vibrations.

3400.2.1.3.2.5.Flexibility

The gate valves insure a maximum flexibility in all respects.

3400.2.1.3.2.6.Pumping capacity

With one 15 g Ti ball per sublimator, the lifetime of the permanent pumping is insured for hundreds of years !

3400.2.1.3.2.7.Easy maintenance

This will be achieved with the help of the gate valves.

3400.2.2.MIRROR TOWERS

3400.2.2.1.Rough pumping of the mirror towers : unit #4

The design of the mirror towers was recently modified, opening a large conductance between the two parts of the tower during the rough pumping and the venting. Consequently the pumping of the towers was simplified in respect to the present pumping station built for the first tower.
Several non turbulent cycles of pumping and venting between atmospheric pressure and 1 mbar are required in order to eliminate dusts. Such a time consuming process requires one rough pump unit per tower.

3400.2.2.1.1.Description

Nb	Items
1	All metal valve CF40
1	30 $m^3.h^{-1}$ dry pump and its venting valve
2	Pirani gauge with its controller
1	Differential manometer for venting

3400.2.2.2.Permanent pumping of the mirror tower upper parts : unit #5

The upper part of the tower is connected to the lower part through a conductance of about 0.3 l/s for water vapor. It contains many electronic components, mechanical devices and the associated wiring, the outgassing flow of which is not completely known.

A pressure of 10^{-6} mbar is required in order to have a gas flux towards the lower part as small as $0.3.10^{-6}$ mbar.l.s^{-1}. One assumes at the moment an outgassing rate of 10^{-3} mbar.l.s^{-1}. A TMP of effective speed 1000 l/s is therefore sufficient. If a larger pumping speed turned out to be necessary, one should have recourse to a cryo-pump.
For reliability reasons (MTBF larger than 10 years), a magnetic bearing TMP is chosen. The dry pump of unit #4 is also used as the fore pump of unit #5.

3400.2.2.2.1.Description

Nb	Items
1	1500 l/s TMP magnetic bearing model with a CF250 flange, an integrated venting valve, an air cooling system and the controller
1	Viton valve CF250
1	Penning gauge with its controller
1	Viton valve KF40 between the TMP and the fore pump
1	Instrumentation chamber
1	Viton CF63 valve for the instrumentation chamber
1	Viton CF40 valve for venting the instrumentation chamber
1	Pirani gauge with its controller
1	BA gauge with its controller
1	RGA head

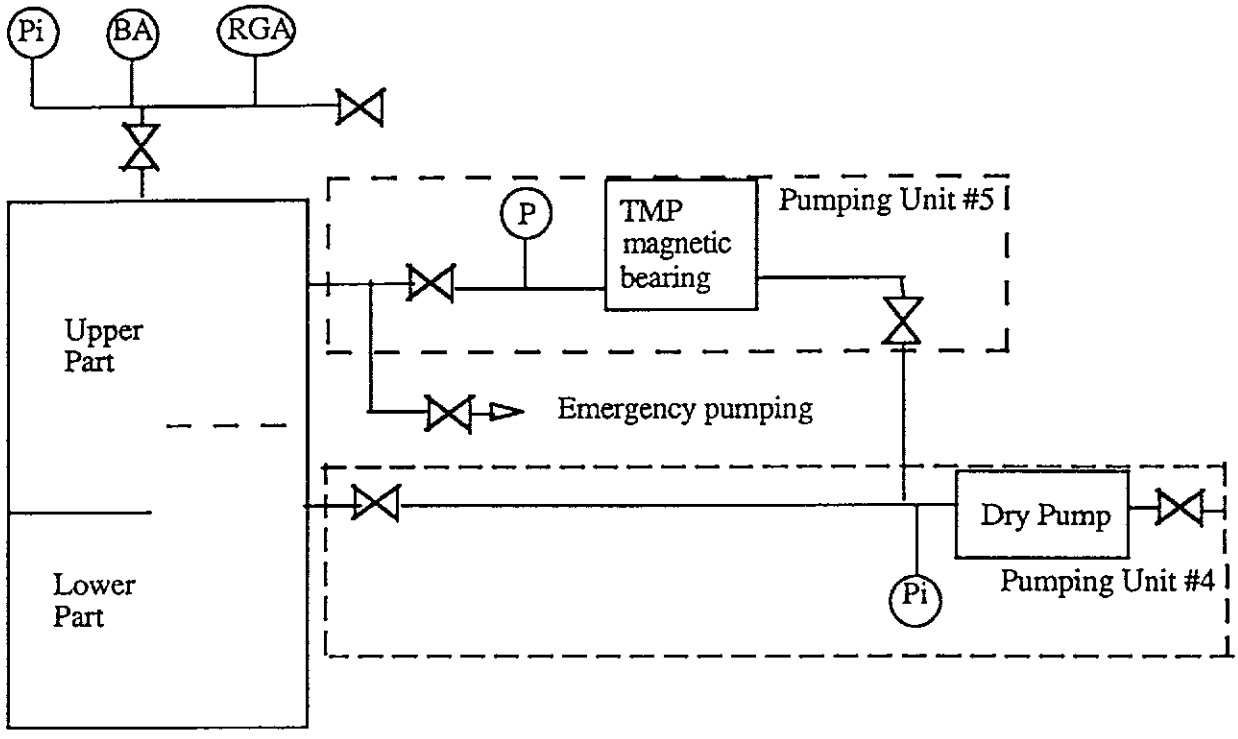

Synopsis of the pumping of a mirror tower (unit #4 and 5)

3400.2.2.3. Emergency pumping of the mirror tower upper parts : unit #6

In case of emergency (failure of the TMP or of the fore pump), unit #5 must be switched off. It is mandatory to be able to immediately switch on a temporary unit of smaller pumping speed. This consists of a 250 $l.s^{-1}$ hybrid TMP model, a Penning and a Pirani gauge, connected to the tower by and a CF 100 gate valve. For the fore pumping an ordinary mechanical pump, equipped with a trap will be used.

3400.2.2.3.1. Description

Nb	Items
1	All metal valve CF100
1	Viton valve KF16 between the TMP and the fore pump
1	250 l/s TMP hybrid model, an integrated venting valve, an air cooling system and the controller
1	10 $m^3.h^{-1}$ mechanical pump, a trap and a venting valve
1	Penning gauge with its controller
1	Pirani gauge with its controller

3400.2.2.4. Intermediate pumping of the mirror tower lower parts : unit #6

The intermediate pumping system is identical to the one used for the emergency pumping of the upper part (unit#6). The pumping speed is well adapted to the bake out of a 40 m^2 chamber.

3400.2.2.5.Permanent pumping of the mirror tower lower parts : unit #3

This permanent pumping unit is identical to the one used on the tubes, with an implemented instrumentation.

3400.2.2.5.1.Description

Nb	Items
1	Instrumentation chamber
1	Viton valve CF63 for the instrumentation chamber
1	All metal valve KF40 for venting the instrumentation chamber
1	BA gauge with its controller
1	Penning gauge with its controller
1	RGA with its electronics

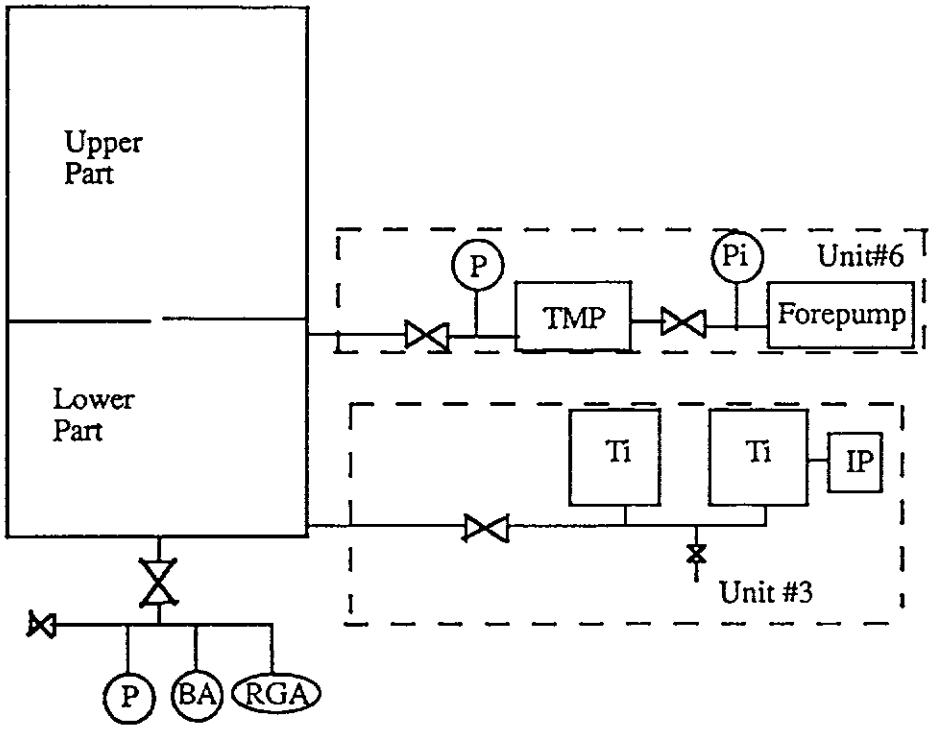

Synopsis of the pumping of a mirror tower (unit #3 and 6)

3400.2.3.OTHER TOWERS AND MODE CLEANER TUBE

3400.2.3.1.Rough pumping of other towers and Mode cleaner tube: unit #4

The rough pumping is identical to the one used on the mirror tower.

3400.2.3.2.Permanent pumping of other towers : unit #5

The permanent pumping is identical to the one used on the mirror tower upper parts.

3400.2.3.3.Intermediate pumping of the mode cleaner tube : unit #6

The intermediate pumping is identical to the one used on the mirror tower lower parts.

3400.2.3.4.Permanent pumping of the mode cleaner tube

The permanent pumping of the mode cleaner tube will be achieve by the permanent pumping units of the two connected towers.

3400.2.4.SUMMARY OF THE PUMPING SYSTEM

			unit	# 1	# 2	# 3	# 4	# 5	# 6
Tubes		Rough pumping	unit #1	1					
		Intermediate pumping	unit #2		22				
		Permanent pumping	unit #3			22			
Mirror Towers		Rough pumping	unit #4				7		
	Upper part	Permanent pumping	unit #5					7	
		Emergency pumping	unit #6						7
	Lower part	Intermediate pumping	unit #6						7
		Permanent pumping	unit #3			7			
Other towers		Rough pumping	unit #4				3		
		Permanent pumping	unit #5					3	
Mode cleaner tube		Rough pumping	unit #4				1		
		Intermediate pumping	unit #6						1
			TOTAL	1	22	29	11	10	15

3400.3.OPERATION

3400.3.1.Search for leaks

A leak flow large enough to increase the partial pressure of gases different from hydrogen by a factor of two on one of the instrumentation stations along the tube do not perturb seriously the Virgo data taking. The gas flow of this leak will be of the order of the outgassing for gases other tahn hydrogen of a tube section, i.e. of the viton gaskets of the valves of a section $1\ 10^{-7}$ mbar l/s. Let us assume this leak as the typical one we are interested to detect and to localize.
The Argon partial pressure profile along the tube, measured by the RGA of the eleven instrumentation station, will allow us (see Figure) to detect the presence of a leak and to identify its position with an accuracy or the order of 200 - 300 m; this means that the helium leak search will be reduced to 8 -12 lip welds that are the only points not tested before installation.

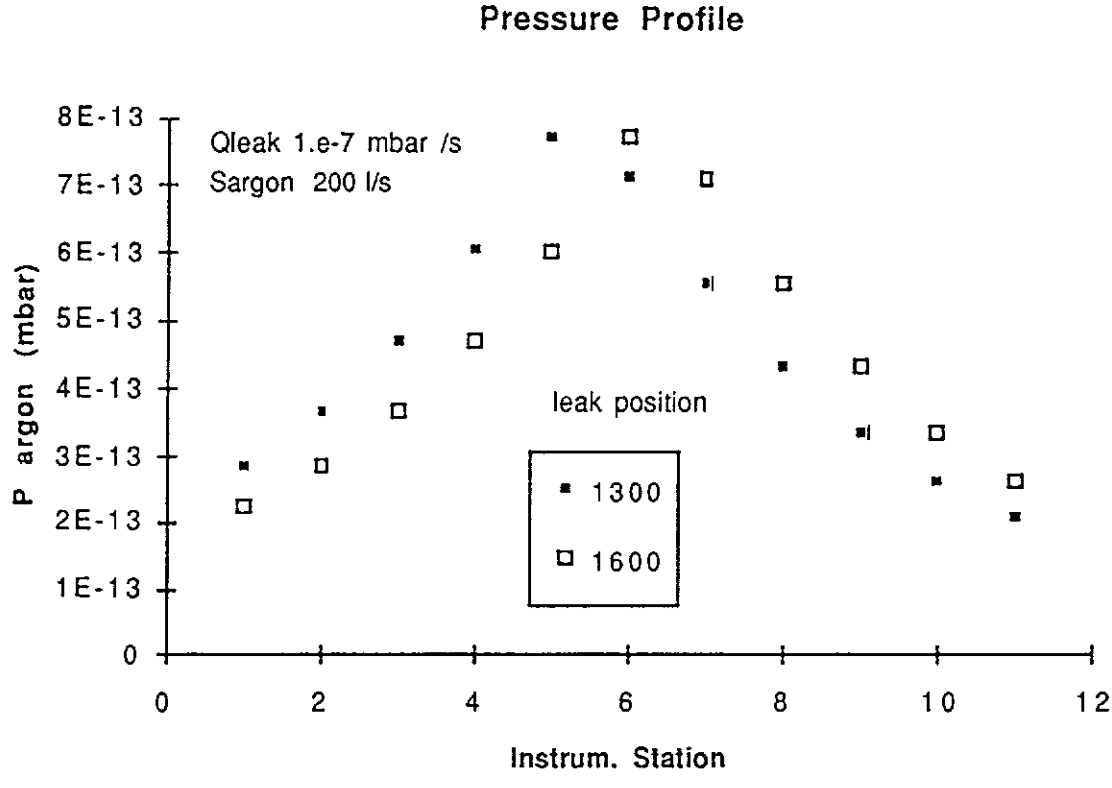

3400.3.2.*Venting of the tube*

The venting of the tube will be done using a clean and dry gas produced at both ends of each arms. The system will allow to produce a small over pressure to guaranty a out coming flow of air on both sides when the tube will be open. Each one of the three installations needed, in the central building and at the far ends of the two arms, will provide a gas flow of 100 m^3/h. The alternative of using filtered and dried air or N_2 produced by LN_2 evaporation has still not been completely evaluated. A technical and economical estimate is foreseen in a near future.

3400.3.3.Running efficiency of the installation

The possibility to take data continuously for very long time is one of the relevant performances we hope to realize for the VIRGO detector. The pumping system has been specifically designed to require a very reduced maintenance and to guaranty the working conditions also when some of the pumping units is forced to stop by some fault.
In the high vacuum volume (tubes and mirror towers lower part) the permanent pumping is done by Ti sublimation pumps and ion pumps. A fresh Ti sublimation will be done once per year and can be done without perturbing the data taking. A permanent pumping station on the tubes or on the terminal towers can be switched off without perturbing the data taking; a small perturbation will be vice versa produced if the permanent pumping station on the beam splitter tower or on the recycling towers is switched off.
The permanent pumping on the "bad vacuum" volumes, mirror towers upper part, injection, detection and mode cleaner towers is done by magnetic bearing turbo pumps and dry pumps; these will require some maintenance twice per year. Anyway the presence of the emergency pumping groups will allow to reduce the perturbation on the data taking during the maintenance or in case of faults of the dry or turbo pumps.
The time needed for venting and evacuating again a tube or a tower is also of interest. The estimated times are reported in the following table.

Operation	Tube hours	Mirror towers hours	Other towers hours
Venting	24	12	10
Evacuating			
Rough pumping	260	15	11
Bake-out	170	72	
Total	454	99	21

-4000-

Interferometre

The interferometer (optics)

The interferometer is the sensitive part of VIRGO, the equivalent of a detector in a high energy physics experiment. It consists in a laser system, the input bench, which contains optics and optronics for adapting the laser beam to the interferometer, the large interferometer (mirrors and suspensions), the detection bench, which also contains optics and optronics for monitoring, cleaning and detecting the main interference signal, and all the ancillary equipment (secondary detectors for the locking and alignment servosystems, local control stations), and the calibration device(s).

The suspensions are described in the next chapter.

The main caracteristics of the optical system are the following :

- The laser system consists in a high power Nd:YAG ring laser at 1.06μm, injection-locked from a monolithic 1 Watt laser. It is actively stabilized, in frequency and in amplitude. The beam is phase modulated, to allow for a shot-noise limited detection, and filtered by transmission through a resonant (mode-cleaner) cavity. The power will be about 25W.
- The large interferometer is a Michelson interferometer, with 3 km long arms. Each arm contains a Fabry-Perot cavity of length L≈ 3 km. The light power is increased through the use of a standard recycling technique. The nominal values are a finesse of 50 for the Fabry-Perot's, and a recycling coefficient of 50 (corresponding to a finesse of 150 for the recycling cavity).
- These performances are obtained through the realization of very low loss mirrors, having typical surface qualities of λ/100, whose fabrication and tests are performed by the VIRGO teams.
- The main interference beam, which carries the gravitational signals, is filtered with an output mode-cleaner, and detected with an a multiple InGaAs detector of high quantum efficiency.
- All the secondary beams leaking through, or reflected by, the interferometer, are split onto two quadrant detectors and one InGaAs detector. This provides redundant information for the alignment and locking servosystem.
- We use a set of computerized CCD cameras looking inside each tower, in order to monitor the preliminary (nonlinear) alignment and to measure precisely the position of each mirror relative to its own tower and to the laser beam
- The calibration will be done by applying time-dependent forces on the mirrors, in two different ways : a magnetic force onto a set of magnets glued to the mirrors, and laser induced radiation pressure.

The 1997 interferometer

By the end of 1997 (or about two years after the site acquisition), it will become possible to install a short interferometer in the central building. We call it the 1997 interferometer. It will differ from VIRGO only by the absence of the far mirrors of the 3 km Fabry-Perot's, by a lower laser power (10W), and by the choice of the radius of curvatures and of the reflectivities of the other mirrors. The interferometer geometry will be simpler than in VIRGO, and the mirrors will be of smaller diameter. Except for that, it will provide a complete, full size, test of all the critical parts of VIRGO (suspensions, laser, benches, data management, control and alignment systems, mirror quality, data management, ...).

The presence of this test bench will accelerate the commissioning of VIRGO after the end of the construction, since everything, except the final large mirrors, and the locking and alignment of the long Fabry-Perot's will have been tested.

Lasers and Input Benches

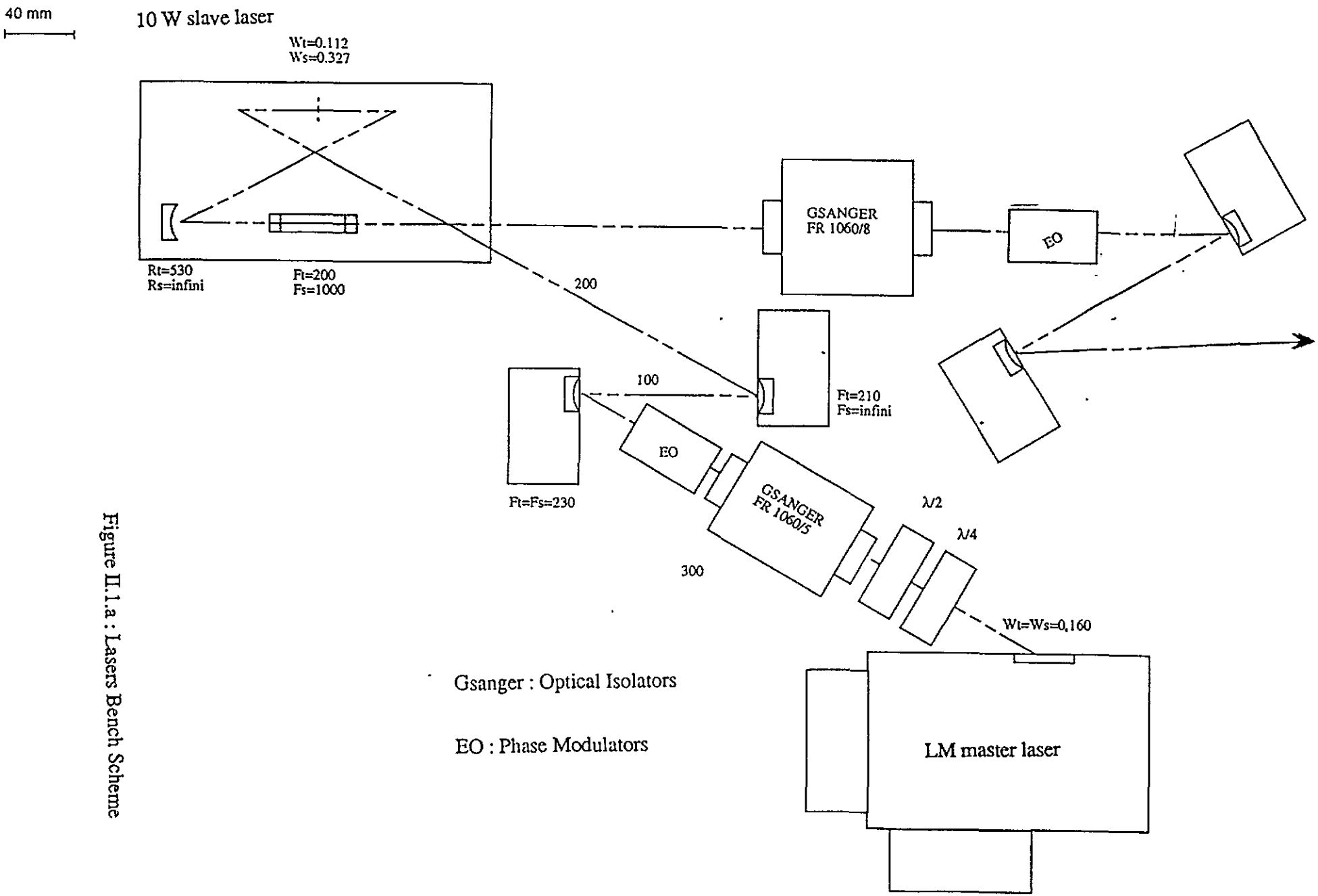

Figure II.1.a : Lasers Bench Scheme

4100.1. Functions of Lasers and Input Optics

The Lasers and Input Optics Subsystem is designed to produce the input light of the interferometer, with the stabilisations required for the expected sensitivity of Virgo as well as the beam geometry matched to that of the cavity arms. The light will be generated by high power Nd:YAG lasers pumped by laser diodes, injection-locked by prestabilized low power diode-pumped Nd:YAG lasers. It must also be stable in amplitude and geometry.

The Input Optics sitting under vacuum on the suspended Input Bench serve to filter the beam, to stabilize its position and yield the necessary movements to align the beam to the axis of the interferometer. The Input Bench supports also the Reference Cavity on which the laser frequency is prestabilized before getting into the Mode Cleaner. The Mode Cleaner is a three-mirror cavity used in transmission, in a ring shaped configuration, and has its two input-output plane mirrors forming a corner-cube and sitting on the Input Bench, while the far curved mirror is suspended alone about 150 m away on an axis perpendicular to that of the corner-cube.

The main components of the benches are described in the following two chapters, giving the optical characteristics as well as the mechanical characteristics. The last chapter presents the alignements strategy and the readout and local controls of the two benches.

4100.2.The Lasers Bench

4100.2.1.General description of the Bench

The laser bench (LB) sitting on a table, contains the laser system delivering to the Input bench the necessary power, which is phase modulated and adapted to match in size the beam required on the IB. It also contains the optical isolation system to avoid feedback into the high power laser, from the cavities formed by the whole interferometer. The optical scheme of the LB is sketched in the **Figure II.1.a**, followed by the technical description of each system.

The optical blocks one can find on the LB are the following :

- Injection Locked lasers
- Phase Modulation for the frontal modulation of the interferometer
- Prestabilisation of the master laser : the error signal extracted from the reference cavity is fed back to the pzt of the master laser and its thermal control as well as to an outside phase corrector (which can be the same crystal EO2 as the one used for the frontal modulation).
- Optical Faraday isolation
- Matching optics to the reference cavity, which sit on the Input Bench, under vacuum, to prevent excess phase noise .
- Reference photodetectors picking up light behind high reflectivity mirrors for all the local controls of the laser.

4100.2.2.The Master Laser :

It is a commercial Nd:YAG diode-pumped laser (from Laser Zentrum Hannover) built in the technology of monolithic piece (MISER), single frequency operating and delivering more than 700 mW. The monolithic technology makes the laser intrinsically stable and the use of two laser diodes for pumping the Nd:YAG is an guarantee of continous operation (a broken laser diode can be replaced while the other keeps operating).

The power is adequate for injection locking of a high power laser of a few tens of Watts. The cavity is formed by the crystal itself and the frequency tuning of the laser is done in the low frequency range by a thermal control of the crystal while the fast part (up to 30 kHz) iz done by a pzt bonded on the crystal (first resonance frequency around 50kHz, sensitivity $\geq$ 4MHz/Volt)

The laser beam is elliptically polarized, there is a need of a quarter-wave plate and a half wave plate to match its polarization to the one of the phase modulator and the high power laser. The delivered beam is slightly asymmetric, so the matching optics between the lasers have to take it into account.

4100.2.3.The Frequency Prestabilisation:

4100.2.3.1.Requirement on Prestabilisation:

The specification for the frequency stabilisation at the input of the interferometer is calculated from the strain sensitivity expected for Virgo (**Figure II.3.1.a**). We report here the curve (**Figure II.3.1.b**) giving the requirements of the laser beam at the level of the beamsplitter and at the level of the prestabilisation on the reference cavity. The low-pass corner frequency is around 500 Hz for the Mode Cleaner and 5 Hz for the recycling cavity. The details of the calculations can be found in the Virgo note PJT 94-036.

4100.2.3.2.The Pound-Drever-Hall Technique:

A standard technique for locking the frequency of a laser to the resonance frequency of a cavity is the so-called Pound-Drever-Hall technique, which consists in phase modulating the laser at a high (RF) frequency, and demodulating the reflected beam.This is represented on the **Figure II.3.2 a**. The first advantage of this technique is to phase modulate the beam at a frequency where the laser noise is shot noise limited ; for the Nd:YAG laser this is usually the case above 7-8 MHz; the second advantage of this technique is that the error signal is not delayed by the time constant due to the storage time of the high finesse cavity.

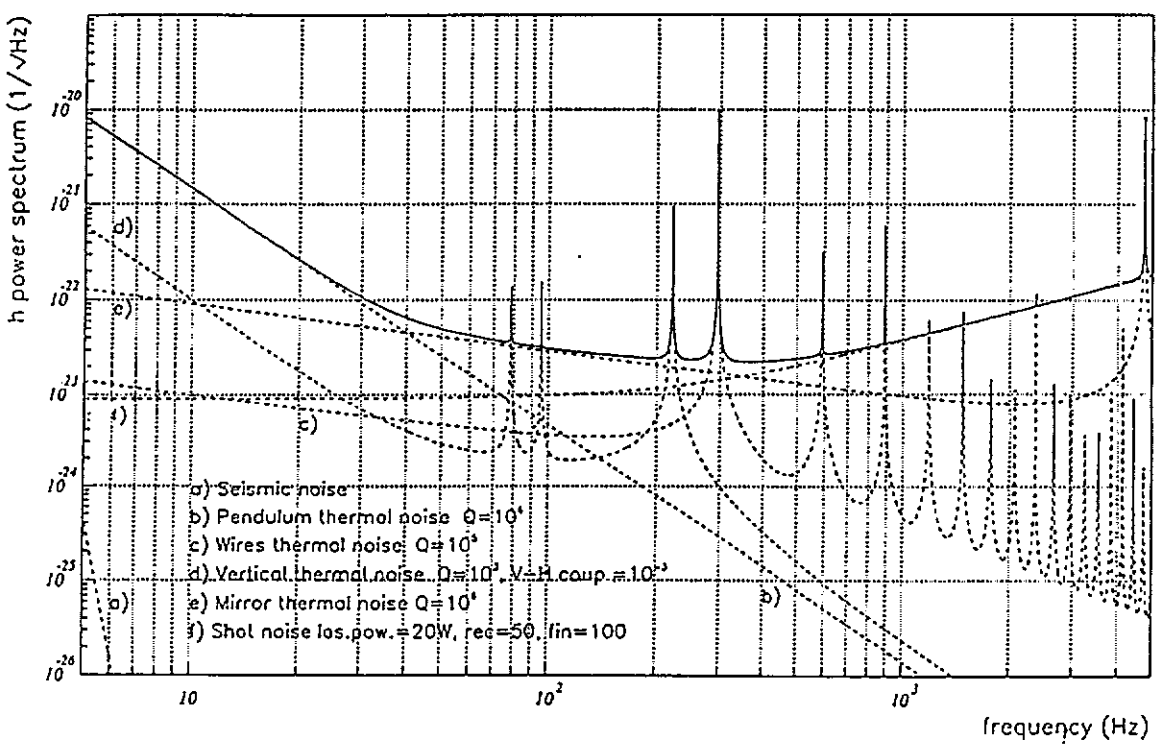

Figure II.3.1.a: Equivalent strain sensitivity of Virgo for 1 kW of light incident on the Michelson.

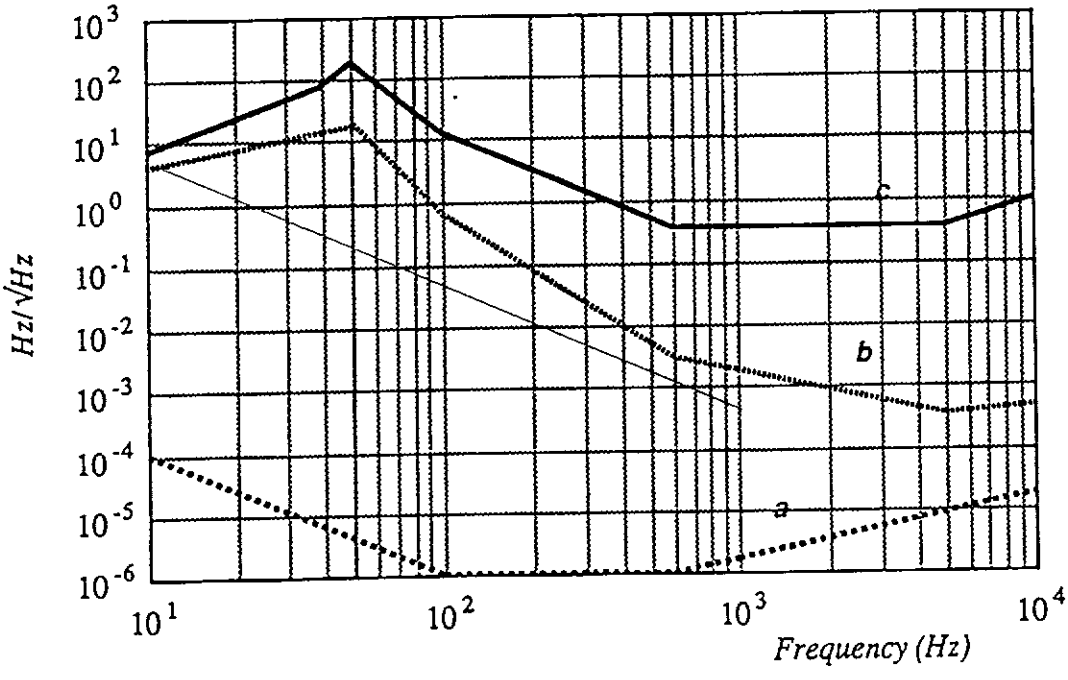

Figure II.3.1.b: Laser Frequency Fluctuations (Hz/√Hz).
curve a: final request
curve b: at the input of the Mode Cleaner
curve c: at the input of the recycling cavity.

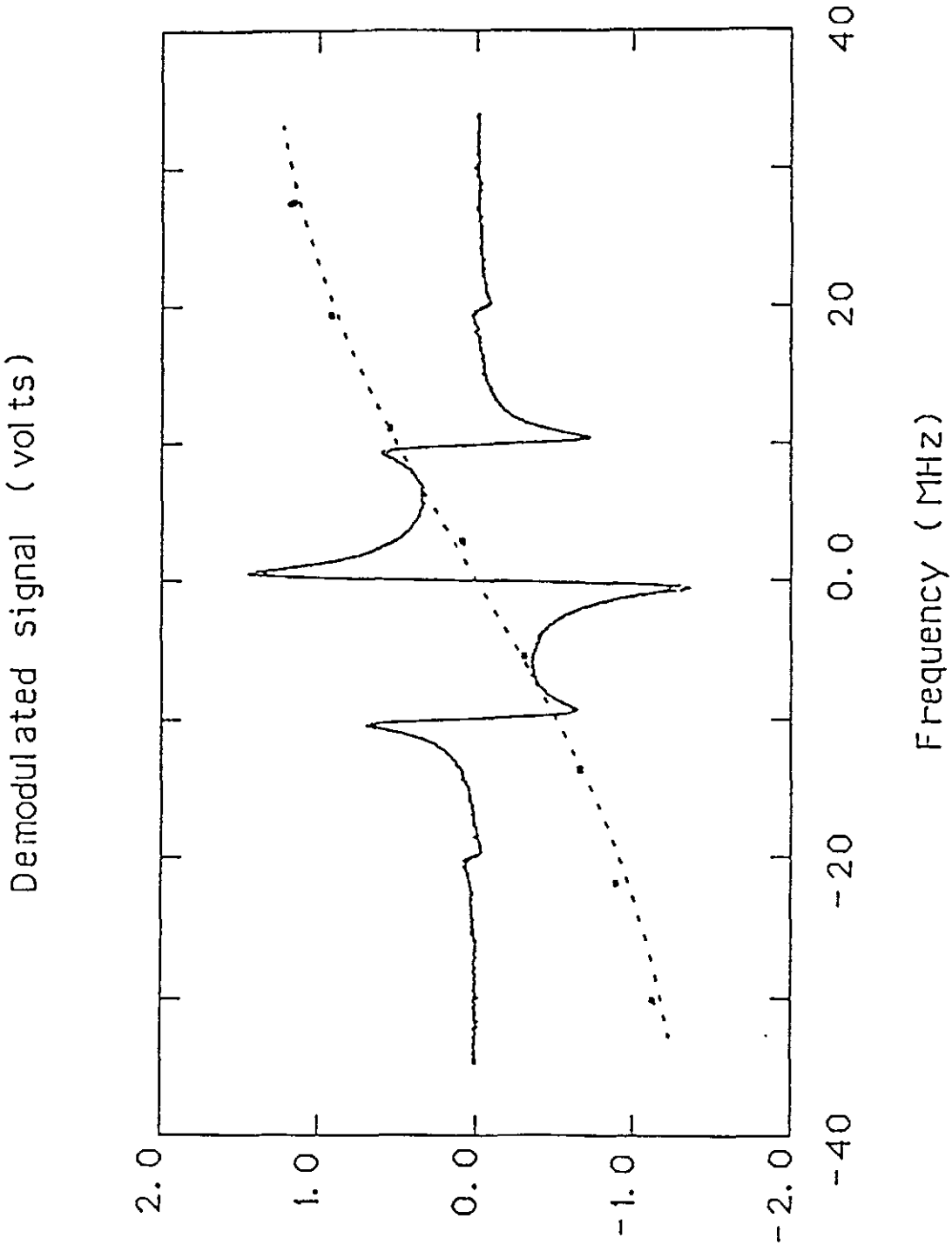

Figure II.3.2.a: Pound-Drever-Hall error signal.This error signal has an odd dependance vs the frequency and is not null inside the range $2W$, which is extending the dynamic range of the correction. Curve *a*: calculated signal fitted with the experimental points ; curve *b* is a magnification of curve *a* in the central zone.

4100.2.3.3. Reference Cavity Design:

The reasons of the choice of the shape, the material and the size of the Reference Cavity have been described in a note (PJT 93-009), we give only the drawing of the shape (**Figure II.3.3.a**) and the calculated first mechanical resonances obtained from a finite element calculation. This "Rugby-ball shape" provides resonance frequencies as high as 10 kHz and is relatively simple to machine and to support.

The optical cavity is a three-mirror ring cavity with a measured finesse of 35 000 and a contrast in reflection of 0.6. The length of the cavity is 300 mm and the curvature of the end mirror is 500 mm giving a beam waist between the two input mirrors of 285 microns.

The material used for the spacer is ULE (Ultra Low Expansion, vitro-ceramic with an expansion coefficient of 3×10^{-9} C^{-1} at 20°C) manufactured by Corning, and the mirrors were polished and coated by REO (Boulder, USA), who also rtealized the optical contacting of the mirrors to the spacer. There is no observable power standing problem on the mirrors of the cavity, tests have been performed with 300 kW/cm^2 of stored light (60-70 mW incident). The usual power used for the prestabilization will be 10 mW incident, meaning about 50 kW/cm^2 in normal operation.

In order to keep the intrinsic stability of the cavity and avoid acoustical perturbations and dust contaminations of the mirrors, the cavity was put inside a vacuum housing, evacuated by a smal ion pump. To keep the mechanical resonance of the ULE (previous measurements have given Q of 200 000 but not under vacuum) the cavity sits on three small rods which size have been calculated in order to filter the residual seismic noise above 25 Hz (**Figure II.3.3.b**).

4100.2.3.4.The Servo-Loop Transfer Function:

As it has been explained in the note PJT93-009, the prestabilization loop is a three-stage loop, the goal being to have a large unity gain frequency and a very high gain at low frequency where the laser has the largest technological noise.

The servo-loop diagram is represented on the **Figure II.3.4.a**, with the three transducers used for the correction ; the fastest one being an external Electro-Optic phase-modulator which allows to have a unity gain bandwith of the order of 1.5 MHz with a transfer function of $1/f$ slope. A corner frequency at 32 kHz has been chosen then to switch the slope to a $1/f^4$ at low frequencies, and for long term drifts an additional integration (global slope of $1/f^5$ below 0.07 Hz) is used to complete the long term locking.

The modulation index required for the prestabilization has a quite flat optimum vs the signal to noise ratio, in the current tests it was around m= 0.3. This modulation impinging sidebands on the beam is produced by the Electro-Optic EO1 sitting on the Laser Bench between the Master Laser and the Slave Laser. We give below (II.6.2) the characteristics of EO1 and the voltage applied to produce the modulation.

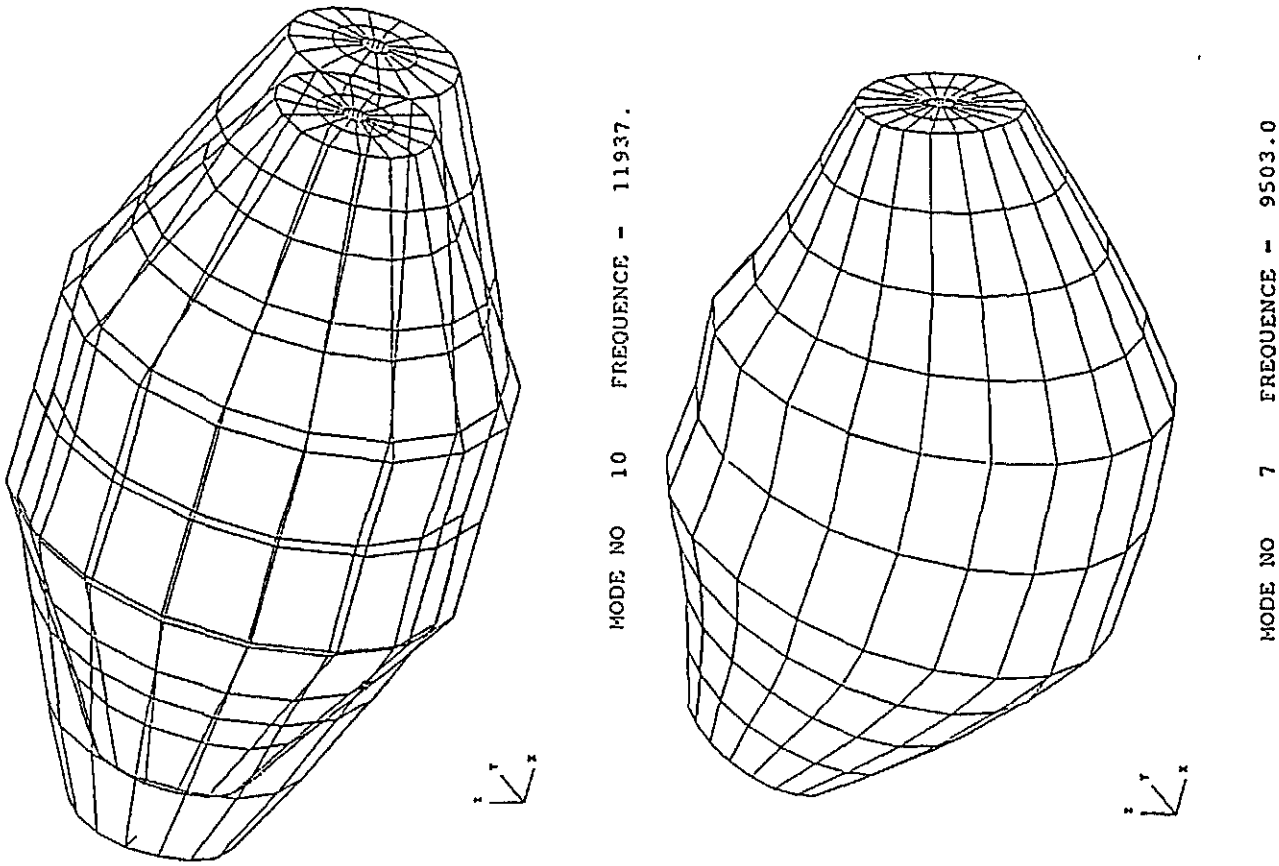

Figure II.3.3.a: Reference Cavity shape and first mechanical resonances calculated by a finite element analysis.

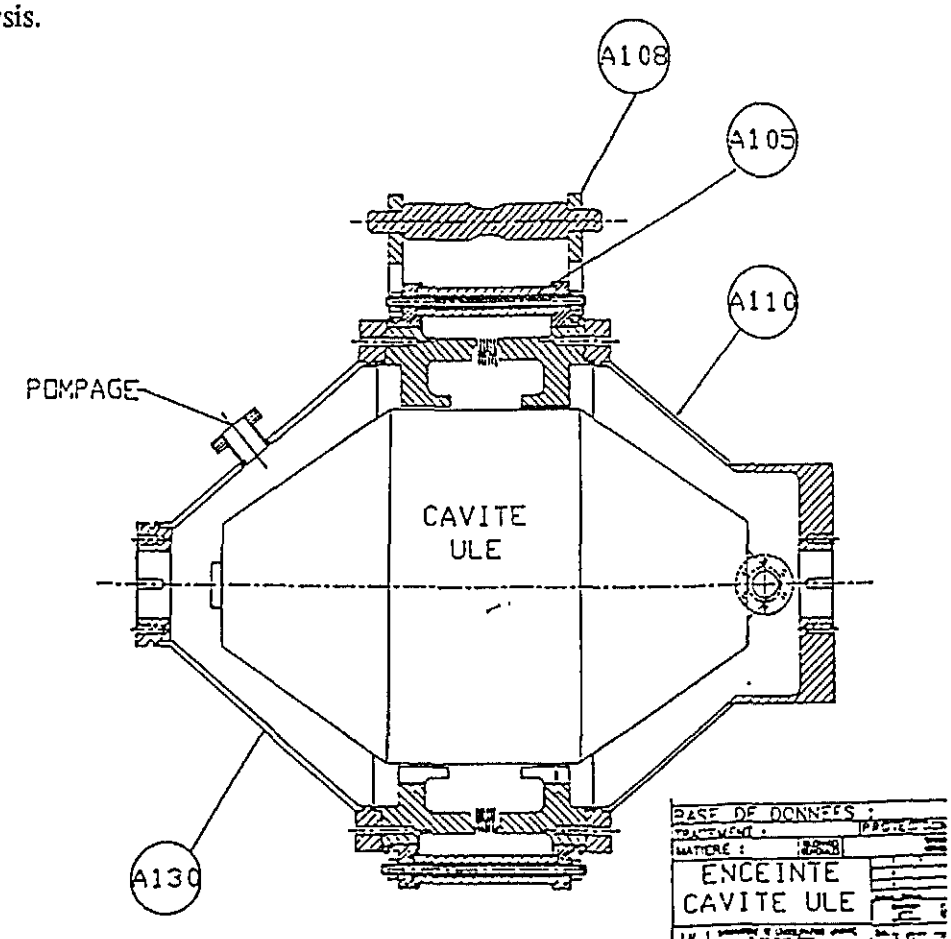

Figure II.3.3.b: Reference Cavity and its vacuum housing

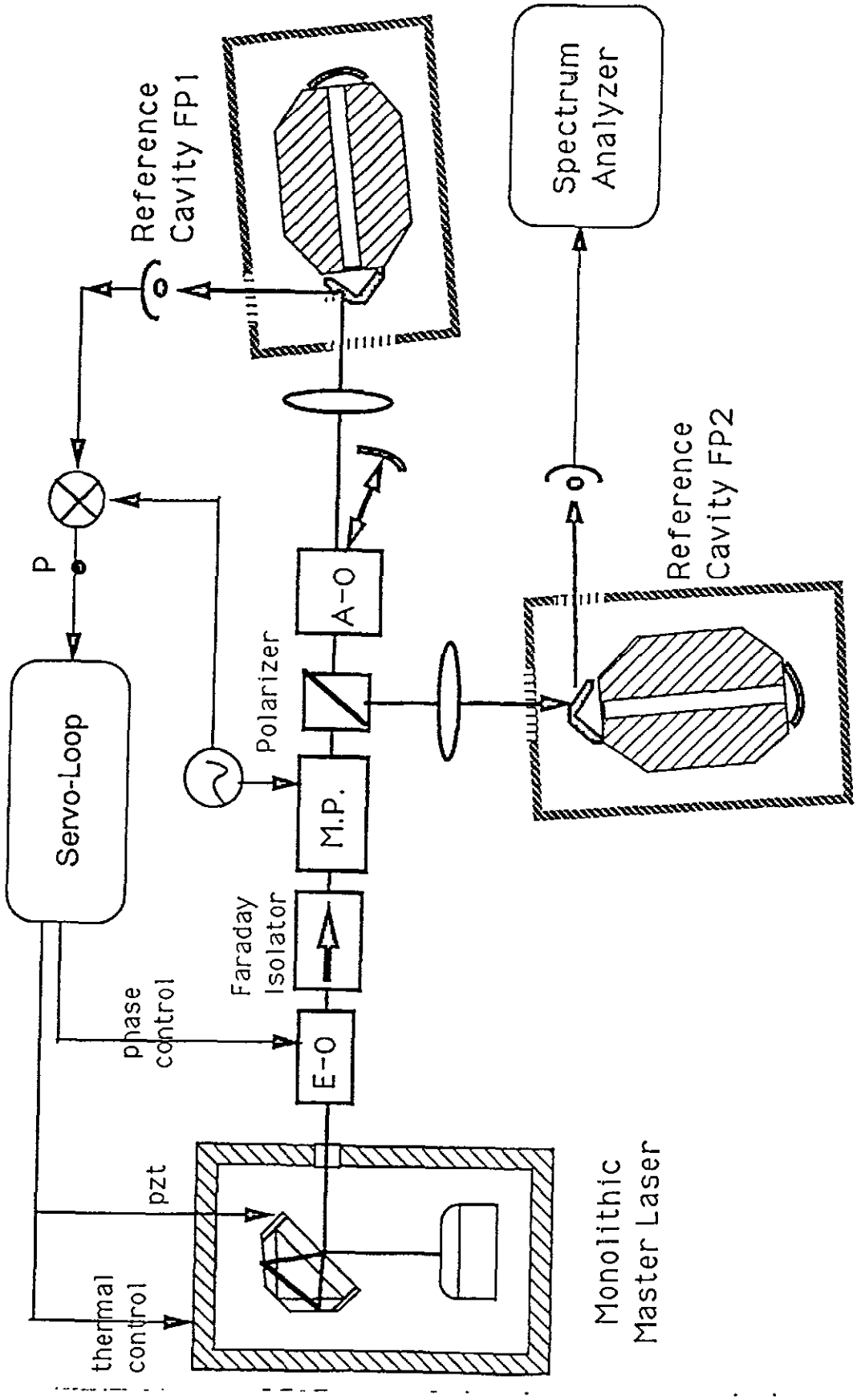

Figure II.3.5.a: Optical Scheme of the Reference Cavity noise measurements : An Acousto-Optic serves to shift the frequency of the laser to match the *FP2* resonance, while it is locked to the length of the *FP1* by a three-stage servo-loop using A pound-Drever-Hall technique with sidebands created by the phase modulator *MP*

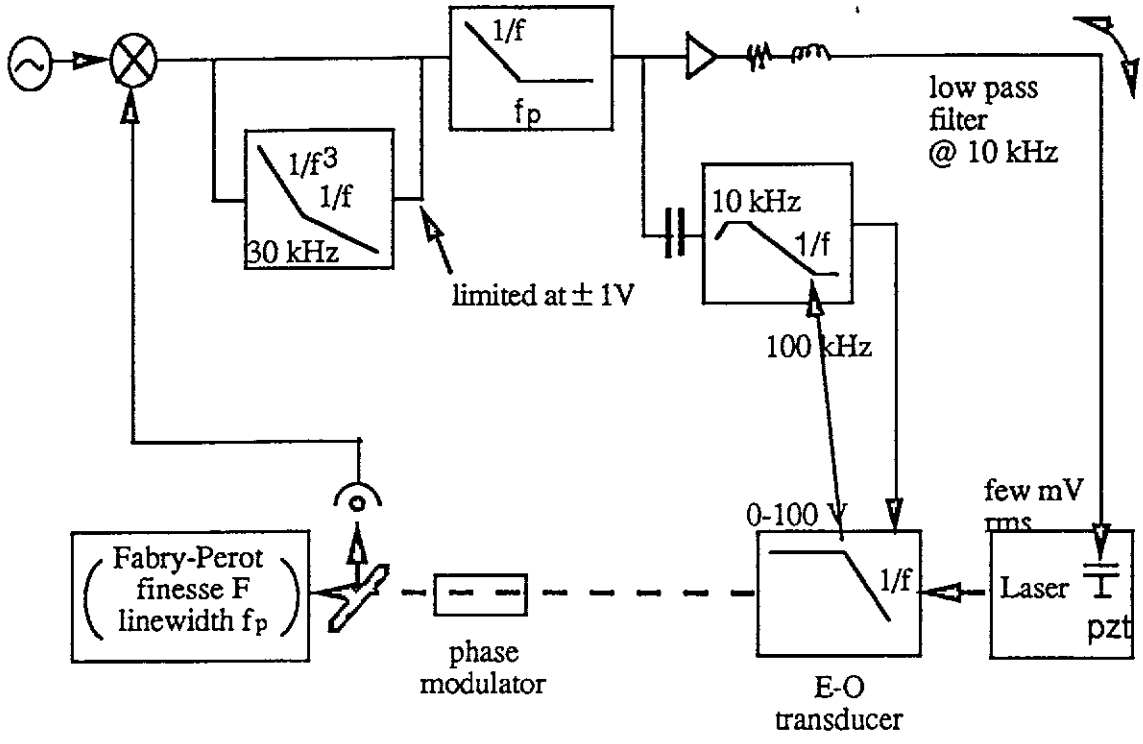

Figure II.3.4.a : Servo-loop diagram of the prestabilization

4100.2.3.5. Frequency Prestabilisation Measurements:

To be able to measure the intrinsic noise of the Reference Cavity (RC), we have carried out experiments at Orsay at the end of 1994 where a Master Laser is locked to one RC and the residual frequency noise is monitored by a second identical RC, used as a freqsuency discriminant. The **Figure II.3.5.a** shows the optical scheme and the details are described in the NTS-25 note. The **Figure II.3.5.b** shows the linear spectral density of the Reference Cavity noise. If we compare it to the Virgo requirement, one can see that these cavities are good enough for Virgo and even for the 97 where the requirements are slightly different [Virgo note PJT94-036].

The fast transients perturbations are taken care of by an automatic relock of the servo which works as follows: when the laser unlocks, the switches open the $1/f^4$ function leaving only the $1/f$ part. A ramp acting on the laser pzt starts to sweep the laser frequency and as soon as a signal proportional to the transmission of the cavity is detected at a level higher than a given threshold, the ramp is suspended and the $1/f^4$ function is switched on again.
The combination of the very fast and high dynamic range servoloop and of this automatic relocking system provides an excellent reliability : running completely unattended, the laser does not unlock more than once per week, and relocks within a few seconds.

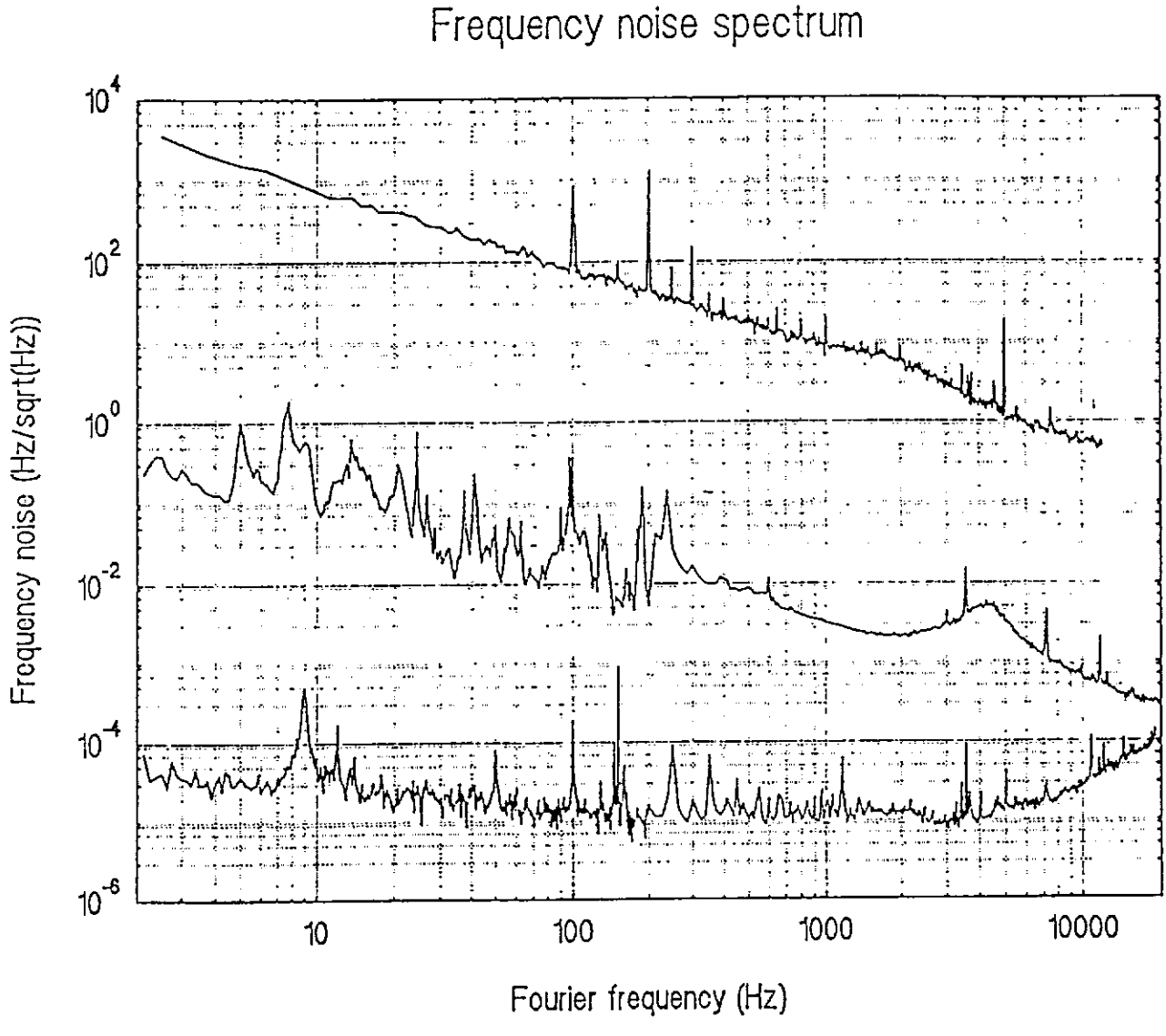

Figure II.3.5.b: Linear Spectral density of the RC noise vs the frequency.
lower curve : error signal obtained with laser locked on Reference Cavity n°1;
middle curve : sum of noises of the two RC;
upper curve : Free-running laser noise

4100.2.4.The Slave Laser:

4100.2.4.1.Requirements on Laser Power:

The accuracy of the phase measurement at the output of the interferometer is limited by statistical fluctuations or shot noise in the detection. This noise varying proportionally with the Fourier frequency F, one can see that it becomes dominant only above 500 Hz, and below that, the other sources of noise are of various thermal origins. The **Figure II.3.1.a** in the previous paragraph gives the strain equivalent sensitivity of Virgo for 1 KW of light incident on the beamsplitter. The requirement of a 1 kW laser with the level of stability needed is very stringent, because no such laser does exist today, but thanks to the use of recycling cavity in Virgo which allows us to expect a recycling gain of the order of 50, the remaining incident laser power is now 20 W. It has become possible to realize such a laser since high power laser diodes are now available for pumping solid-state lasers. We had anticipated that in 1987, and had started working with Nd:YAG lasers.

We will develop the laser in two steps: for the Virgo 97 interferometer a 10W laser will be used and its reliability tested in comparison with the rest of the interferometer while we will be developing a 20 W laser for the full size 1999 Virgo.

4100.2.4.2.The 97 High Power Laser:

A prototype of the high power laser has been studied in Orsay in terms of feasibility, optimization of pumping efficiency and control of the injection locking. This study is summarized in the PJT93-005 note. An extrapolation of this study to a 10 W laser is the subject of a contract with the BMI company who will construct the laser, pumped by fibercoupled laser diodes. These diodes are a good solution for the maintenance of the laser : though the coupling of the 808 nm light from the diodes arrays to the YAG crystal through optical fibers bundles decrease slightly the efficiency, in counterpart it relieves engineering difficulties because of the physical separation between the diode arrays and the active YAG material and it allows replacement of a deficient laser diode without stopping the laser, thus avoiding to stop all the servo-loops involved in the lockings of the interferometer.

The specifications of the slave laser are given below:

- Diode pumped Nd:YAG laser
- Emission wavelength: 1064 nm
- CW operation in single mode TEMoo with linear polarization
- Unidirectional output power: 10 Watt +/- 5%
- Reliability (limited by the laser diode lifetime): 5 000 to 10 000 hrs

A schematic lay-out is given on **Figure II.4.2.a**. The slab Nd:YAG crystal is transversely pumped on one side by 10 fibers optic bundles emitting 10 watts each. Transverse rectangular pumping has been chosen mainly because of its demonstrated ability for minimizing the stress-induced birefringence. The thickness and the zig-zag path are optimized for maximizing the gain through the filling factor and the absorption efficiency.

The two pumped faces normal to the zig-zag plane are conductively homogeneously cooled. The external incidence angle of the infrared light on the YAG crystal is the Brewster angle for polarization selection. The laser beam encounters 12 total internal reflections.

The 10 fibers optic bundles are separated by about 3 mm along the rod lens in order to flatten the pumping distribution in the plane of the zig-zag path. The thickness of this pumped volume is 1.5 mm. This value is a reasonable compromise between realistic maximum mode waist and minimum homogeneous pump waist. Taking into account the experimental thermal

focal length of the slab, the mode waist will be adjusted to half this value with a proper choice of the curvature of the cavity mirrors.

An X-shaped ring cavity is used to avoid feedback of the light into the master laser during the injection-locking process. The oscillation in one direction will be performed automatically by the injection of the external light and one of the cavity mirrors can be cylindrical for the astigmatism compensation of the beam. The polarization state is selected by the Brewster angle of the slab.

Mechanical and thermal stability are ensured by a Zerodur plate where will be clamped all the mirror mounts. The residual thermal expansion of the zerodur is negligible compared to that of the slab itself (for a 5cm slab and a cavity of 50 cm long, the frequency shift due to the slab is 450 MHz/°C). That's why it is necessary to control in long term the temperature of the slab with a precision better than 1°C corresponding to the available dynamics of the pzt transducer. A thermoelectric Peltier element is mounted around the slab cooler for this purpose. The temperature stabilization of the laser bench itself is then required to only a few degrees. In order to avoid mechanical vibrations, the cooling of the laser head will be done by radiators.

We have also decided to keep the cavity length as short as possible (under 500 mm) in order to get a large locking range and a good stability of the whole.

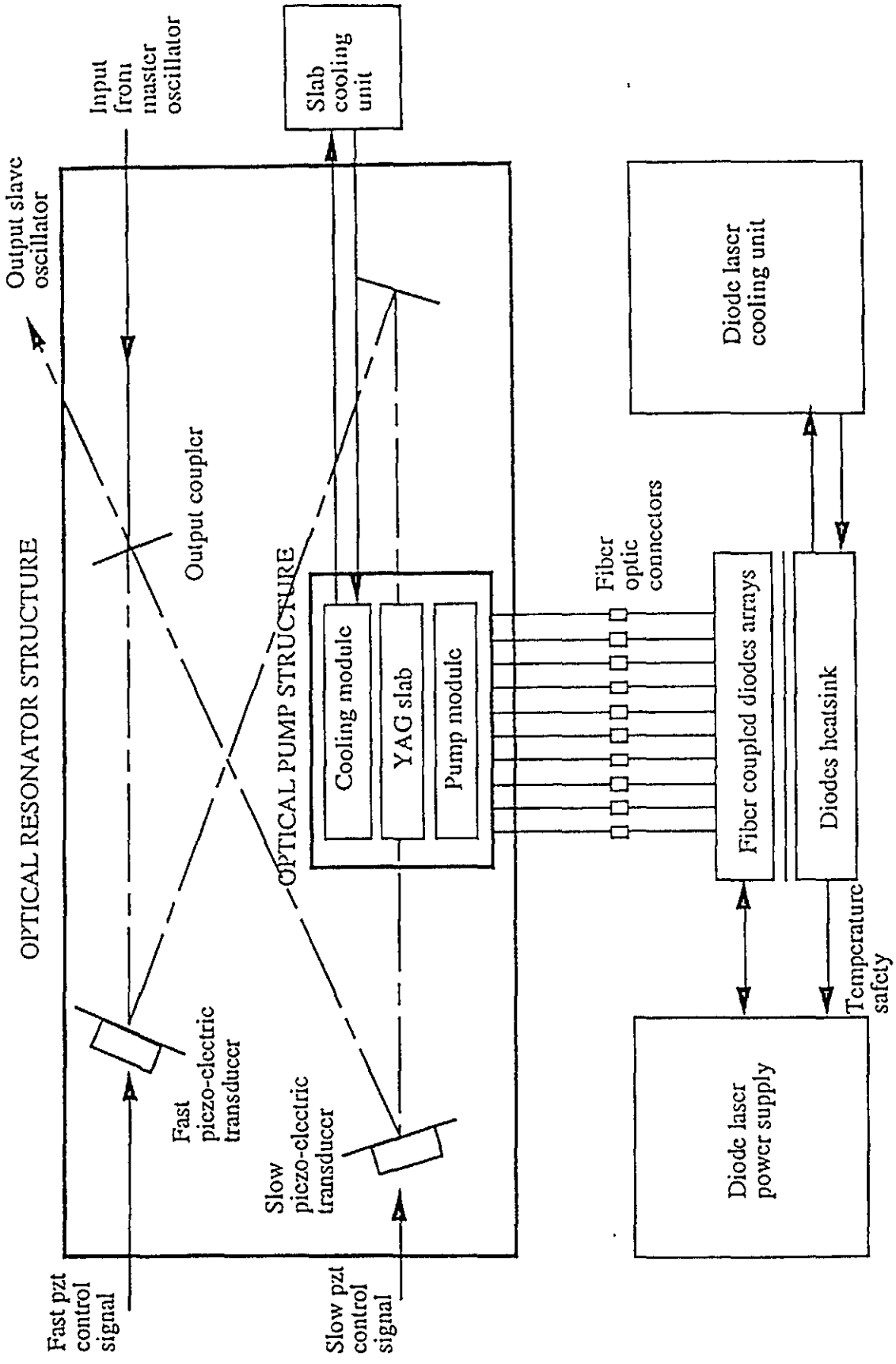

Figure II.4.2: Schematic of the high power laser delivering 10 W and pumped by 10 fiber-coupled laser diodes.

4100.2.4.3. The pzt-mirror mounted transducers

The transducers used to achieve frequency correction in the slave laser are piezoelectric actuators supporting cavity mirrors. The expected noise to be corrected is usually a few hundred kHz at low frequencies due mainly to acoustic and mechanical perturbations. Even for a solid state laser the noise frequency range reaches easily 20kHz. Moreover in the long term range (below 1 Hz) there are drifts due mainly to temperature fluctuations of the environment. If one assumes a temperature stabilization of the laser crystal better than 1°C then useful dynamic for the slow pzt is 1GHz at low frequency (below 1Hz). Above 20 kHz, the fluctations are smaller and we can estimate them to be around a few hundred Hz, which gives the dynamic range required for the fast pzt.

High level transients may occasionally unlock the servo-loop, but the automatic locking system can close the loop in less than a second as for the prestabilization scheme.

The pzt's are mounted with the flat mirrors of the slave cavity, the slow one supports a mirror of f 7.75 mm x 4 mm and can work up to 10-15 kHz with a dynamic of 6GHz; the fast one supports a f 5 mm x 1 mm mirror and can work up to 150 kHz.

4100.2.5.Injection Locking:

4100.2.5.1.Optical Implementation:

A scheme of the injection locking is given in **Figure II.5.1.a** where one can recognize a phase modulator EO1 and a Pound-Drever-Hall scheme used to maintain the slave laser in the injection locking range (which will be in the order of 1 MHz), the transducers used for the locking being the two pzt of the slave cavity and we have obtained in our tests a unity gain bandwidth of 100 kHz. The modulation frequency needed for this servo-loop has to be larger than 1-2 MHz which is the estimated half-linewidth of the slave laser. The behaviour of the injection locking loop completed by the Pound-Drever servo can be qualitatively explained as followed, the details of the process can be found in the note NTS xxxxx . If dn_1, dn_0 , dn_2 are respectiveley the frequency fluctuations of the slave cavity, the master laser and the injected laser, the injection locking process sets a relation between them and the injection locking range G (which is chosen to be of the order fo 1 MHz) by :

$$\delta\nu_2 = \frac{\Gamma}{\Gamma+f}\delta\nu_0 + \frac{f}{\Gamma+f}\delta\nu_1$$

we can see that the fluctuations of the slave cavity are filtered out at first order with a cut-off frequency of G and the fluctuations of the master laser are transmitted to the slave cavity up to the same frequency. The Pound-Drever loop then increases the gain at low frequencies by adding an extra $1/f$ slope between 10 kHz to 100 kHz and a slope of $1/f^4$ below 10 kHz.

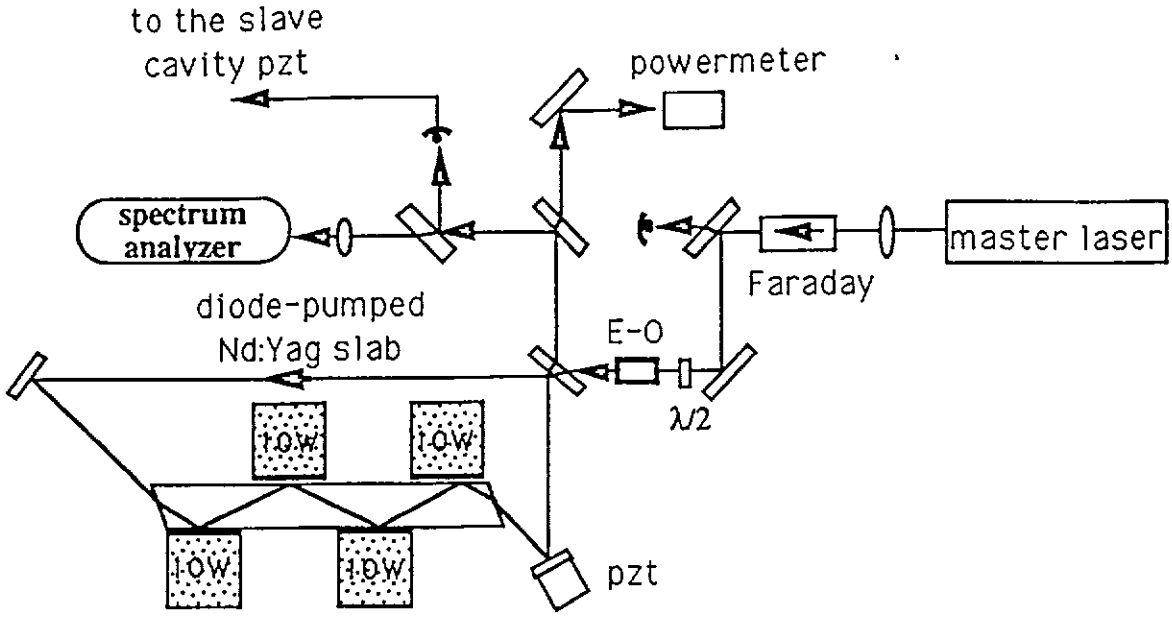

Figure II.5.1.a: Injection Locking optical scheme

A Faraday isolator (specified below) is used to prevent feedback into the Master Laser in case of unlock of the injection and oscillation of the counterunning wave.

The matching between the two lasers serves to optimize the overlapping between TEM_{00} mode of the master laser and TEM_{00} mode of the slave cavity. Matching is therefore dependent on final lasers to be used and the use of two curved mirrors (M1 and M2 on the Figure) provides 4 degrees of freedom to set 4 variables (2 waist sizes in the two horizontal and vertical planes, and 2 waist longitudinal positions).

Let's examine the cases of misalignments and mismatchs between the two lasers: assume k, the ratio of master power coupled in the TEM_{00} mode of the slave cavity divided by the power of the master laser (k =1 in case of perfect matching)

On the sizes of the beams one can tolerate a mismatch 20% on the sizes of the waists because it leads to a coupling coefficient of k = 96% meaning a reduction of the locking range of only 2%.

On the longitudinal positions of the waists, a coupling of 96% also means a longitudinal shift between waists of $\frac{z_R}{2}$, $z_R = \frac{\pi w^2}{\lambda}$ being the Rayleigh range, which is quite tolerant.

A lateral shift Δ of both lasers axis leads to a coefficient $\kappa = exp\left(-\left(\frac{\Delta}{w}\right)^2\right)$.= 0.96 for $w/\Delta = 5$.

In the same way, we can calculate the effect of an angular misalignment q between the two axis of the lasers: the coupling coefficient can be calculated: $\kappa = exp\left(-\left(\frac{\theta \pi w}{\lambda}\right)^2\right)$; $k = 0.96$ for $\theta w = 7 \times 10^{-8}$ m.rd (for standard laser beam, θ is of the order of 100 to 200 mrd, which can be done easily with the standard positioner).

All these estimations allows us to quantify the angular long term stabilty of the mirrors and their mounts. Moreover to avoid that the angular instability is converted into a lateral shift on the output coupler of the slave cavity one needs the distance dl between the mirror M2 and the slave laser to be smaller than $2\Delta/\theta$ and the distance $dl + d$ between the mirror M1 and the slave laser, to be smaller than $4\Delta/\theta$.

4100.2.5.2. Mixed servo-loops for injection locking and prestabilization

We can adopt the same scheme as the prestabilization of a master laser described above, and compensate the frequency fluctuations of the slave laser by tuning the master frequency and by an external phase correction on the high power laser beam. In this scheme, the master laser itself acts as a frequency transducer below the corner frequency of 32 kHz (see above).

With the presence of injection locking and the injection servo-loop of 100 kHz unity gain bandwidth, the slave laser reproduces in the ratio 1, the behaviour of the master laser. So the feedback of the prestabilization to the master laser below 32 kHz is reproduced exactly in the slave laser.

Above 32 kHz and up to 1 MHz, the correction is ensured by the external phase corrector, and if this phase corrector EO2 is placed on the beam of the slave laser, we run into the same servo-loop charateristics as the ones of the prestabilization test of the master alone.

Since the results on stability of the Reference Cavity shows that we can arrive down to VIRGO specifications, they are kept for the slave laser if we can check that the injection process does not introduce more noise in the slave laser than the free-running master laser itself.

The **Figure II.5.2.a** gives the residual frequency noise between master laser and injected oscillation. One can see that the residual frequency noise between the master and the slave laser is small compared to the noise of the free-running master laser.

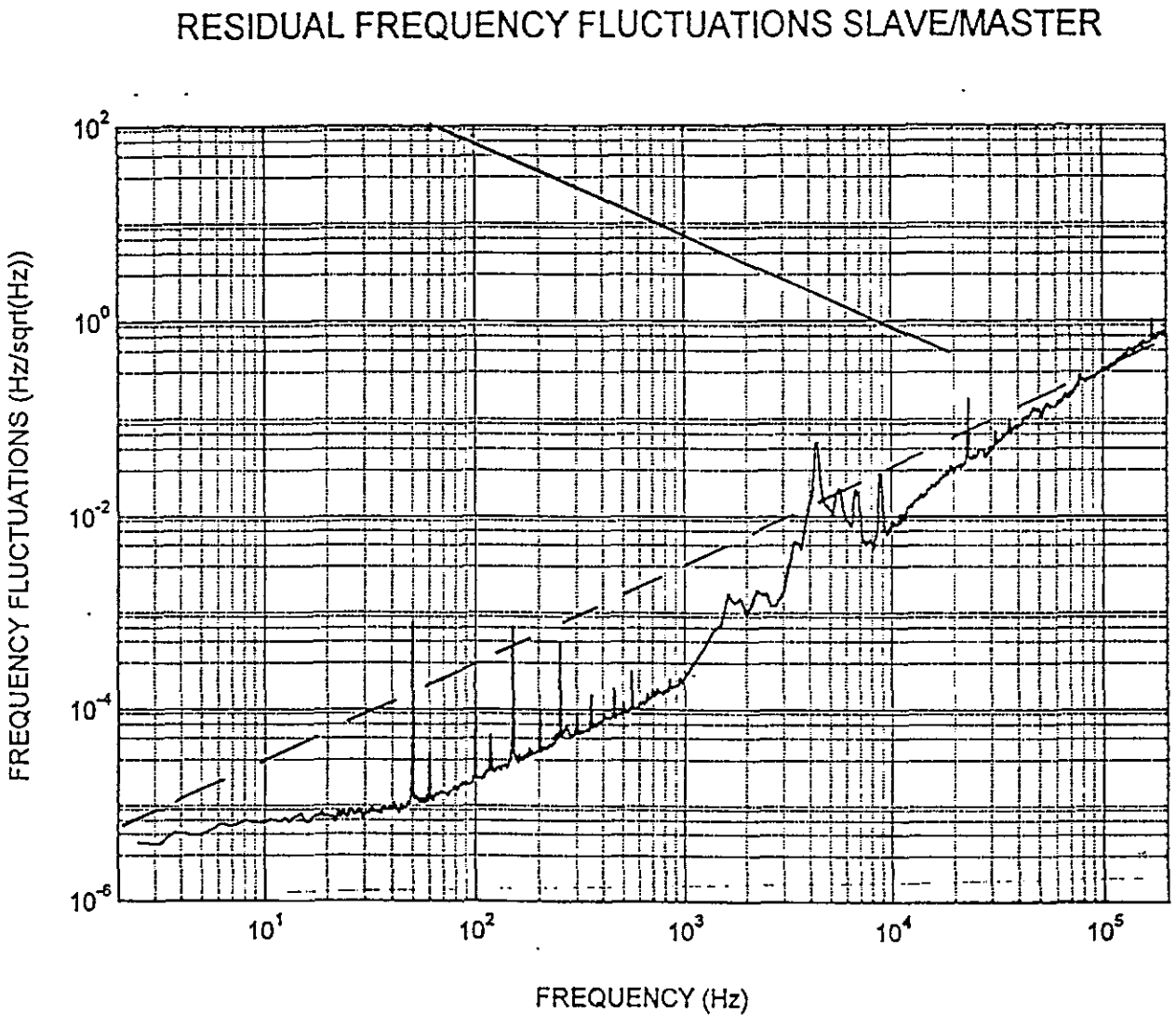

Figure II.5.2.a : Residual frequency noise of the slave laser when injection locked by the master laser with the Pound-Drever servo-loop having a unity gain bandwidth of 100 kHz.

4100.2.6.The Optical Components:

In this paragraph there are two kinds of components: the passive ones which are the mirrors used for beam deflection, the waveplates, and the optical isolator comprising a Faraday crystal and polarizers. The active components are the phase modulators or electro-optics used to generate sidebands on the beam. For all them the goal to be reached is minimum insertion loss and maximum transmission. As far as possible the refracting components will be used at Brewster angle.

4100.2.6.1.The Passive Components:

First we have deflecting mirrors HR at 45°, the only loss is due to some needed transmission of 50 to 100 ppm in order to used that fraction of light for the monitoring of the laser power, the laser beam quality, etc...

A quarterwave plate and a halfwave plate are needed behind the master laser to recover the right linear polarization for the injection locking of the slave laser. Their loss are only due to the non-perfect AR coatings on both sides (loss per AR around 2-3 $x10^{-4}$). Besides that, their power standing is beyond the requirement as they can stand 2 MW/cm^4 in CW operation.

The optical isolation needed for the Faraday can be set as follow: a good rule of thumb sets an admissible feedback power smaller than one thousandth of the output power. That means a 40db isolation for a 10 watts slave laser and a 1watt master laser. With an aperture of 5mm , a 94% transmission, and a $750W/cm^2$ threshold (against the $245W/cm^2$ needed for the present one watt master laser), crystals of l/10 distorsion over the full aperture are commercially available. Let's notice that part of the transmission is due to non-perfect polarizers mounted with the standard Faraday.

4100.2.6.2.The Active Components:

In the near-infrared range the most efficient phase modulators are the Lithium Niobate or Lithium Tantalate Xtals, as their sensitivities are 20 times better than the classical KDP or ADP, and they have the advantage to have no hygroscopic properties. The modulation index produced is typically 0.2 /Volt. for a xtal of 5 x 5 x 70 mm^3.

Used obviously in transmission their insertion loss is not negligible and can become a critical parameter. On the Laser Bench, we foresee to use only two EO's, grouping on each Xtal as many functions as possible:

- EO1 is used to put sidebands for the injection locking servo and the same sidebands are used for the prestabilization. It is positioned between the master and the slave laser.
-EO2 is used as phase correction for the prestabilization and to generate sidebands for the modulation-detection of the interferometer main signal. It is positioned on the main laser beam immediately at the output of the slave laser, and on the Laser Bench.

4100.2.7.The matching optics of the Lasers Bench

Their goal is to match the beam delivered by the slave laser to the Reference Cavity (RC) positioned on the Input Bench. It will image the waist of the slave laser which is of the order of 0.6 mm to the waist of the RC which is 0.286 mm, a few meters away. The only requirement that we have to meet is that this telescope is a two-or three-mirrors telescope serving in the same time as auto-beam positioners for the auto-alignment of the beam to the RC.
Two mirrors will be carrying 4 pzt transducers allowing to perform the remote alignment on the 4 degrees of freedom.

4100.2.8.Mechanical Stability of the Lasers Bench:

The constraints on the mechanical stability of the Laser Bench have their origin on the jitter of the beam delivered to the Input Bench. Two causes of fluctuations are possible : mechanical vibrations of optical mounts and vibrations of the table itself. The low frequency noise of the bench is minimized with a good seismic isolation (cut-off frequency around 1 Hz) while the thermal drifts of the components can be taken care of by the piezo-mounted mirrors of the laser bench telescope so they can be corrected in the low frequency range (below 1 kHz).

4100.2.8.1.Beam fluctuations requirements

The lateral or angular jitter of the beam can couple to imperfections in the interferometer and result in a phase difference at the output interference pattern. The imperfections are of many kinds: mismatching of the recombined output wavefronts in their tilts or in their curvatures, waist mismatchings between the two arms, originating from residual misalignements of beamsplitter and/or test-mass themselves.

For each coupling the calculations have been done [P.Hello, FCD] or or Calloni [meeting Lapp 1/95]. We summarize here the results, and we specify the noise in term of linear spectral density.

1) The coupling of the laser jitter $\alpha(t)$ in rd.Hz$^{-1/2}$, with the interferometer misalignements $\Delta\xi$ (in rd) gives a phase jitter:

$$\delta\phi(t) = \frac{2\pi}{\lambda}\,\frac{1-\sqrt{R_{rec}}}{1+\sqrt{R_{rec}}}\,\Delta x\,.\,\alpha(t) = 1.23\ 10^{5}\ \Delta x\,.\,\alpha(t)$$

with a recycling mirror of $R_{rec} = 0.92$ (cf Interferometer Ref sol.note PJT 94-024). We can transform this jitter into noise densities and express that we want this induced phase noise to be smaller than the Virgo sensitivity: $\tilde{\delta\phi}_{misalign}(F) < \tilde{\delta\Phi}_{Virgo}(F)$

This sets a limit to the product of misalignment by laser jitter :

$$\tilde{\alpha}(F)\,.\,\Delta x < \frac{\tilde{\delta\Phi}_{Virgo}(F)}{1.23\ 10^{5}}$$

This laser jitter does not encounter any filtering by the recycling cavity as the jittering causes coupling to higher order modes which are not resonant with the 3 kms arms. Considering the fact that the rotation control of the end test-mass is limited by the resolution of the readout system which will probably be around 10^{-9} rd, this brings a residual misalignment of: $\Delta x = 3\ \text{km}\,.\,10^{-9} = 3\ 10^{-6}$ m , therefore we can set now a limit to the jitter of the input beam delivered by the Input Bench:

$$\tilde{\alpha}(F) < \frac{\tilde{\delta\Phi}_{Virgo}(F)}{0.37}$$

and represented versus the frequency in the **Figure II.8.1.a.**

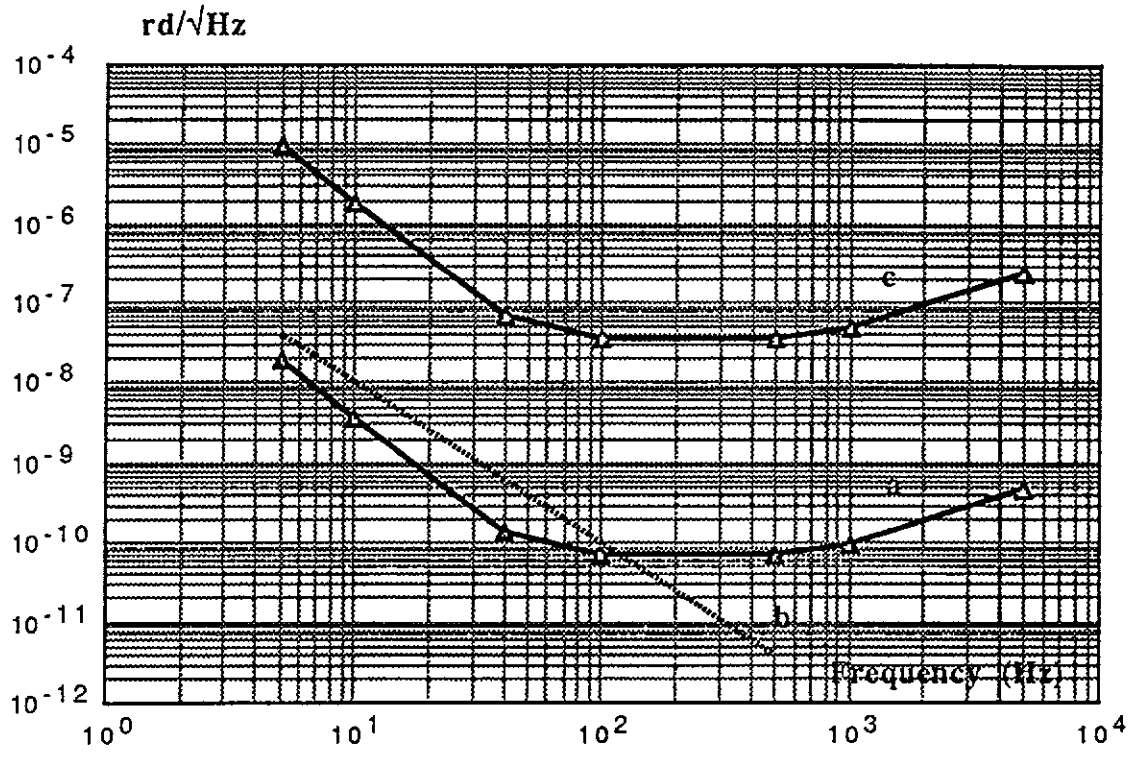

Figure II.8.1.a : Curve *a*: Residual jitter of laser beam required at the exit of the Input Bench coupled with an Interferometer misalignment of 10^{-9} rd (3mm over 3 km).
Curve *b*: Effect of the seimic noise on the Input Bench in terms of tilt .
Curve *c*: Residual jitter of laser beam required at the entrance of the Input Bench if the spatial filtering of the MC is 2×10^{-3}.

One can see on the figure that the highest requirement for the laser beam is a few times 10-8 rd/√Hz around 100 Hz, which is easily obtained for output laser beam. Furthermore we have also measured the effect of acoustic noise and air pressure on the beam jittering and we have found that their effect is completely negligible even in a normal lab environment.

4100.3.INPUT BENCH

4100.3.1.General description:

The Input Bench (IB) is a suspended system working under vacuum and on it we can find, besides all the matching optics for the MC (TMC) or the interferometer (TIB), the 2 input-output mirrors of the MC, the ULE reference cavity for the prestabilization (RC), the fast transducer for the phase-lock of the laser to the interferometer arms (PZT), and the photodetector serving to stabilize the laser in amplitude and inserted after the passive filtering of the MC. The Figure III.1.a shows the optical scheme, the technical parts are described afterwards.

The technical choice has been to use only reflective optics on the Input bench in order to avoid beam distorsions and parasitic reflexions encountered in refractive optics. For instance the different matching optics will be formed only with curved mirrors.

4100.3.2.Mechanical Stability of the bench:

The mechanical fluctuations of the bench and its components are translated in terms of phase fluctuations at the input of the itf. These phase noise has to be compared to the requirements of the laser phase noise given in the **Figure II.3.1.b.** Knowing that any path length fluctuation $\delta\tilde{l}\,f$ is equivalent to a laser frequency fluctuation $\delta\tilde{\nu}(f)$ as:

$$\delta\tilde{\nu}(f)=\frac{2\pi}{\lambda}f\ \delta\tilde{l}(f)$$

let's examine the noise encountered by each component sitting on the bench.

4100.3.2.1.Seismic noise of the Reference Cavity and the Mode Cleaner

For the usual seismic noise on $10^{-6}/f^2$ m/$\sqrt{}$Hz, we get the curve *a* of the **Figure III.2.1.a** which is well below the requirement (curve *c*). So as far as the RC is concerned, the seismic isolation of the bench will prevent excitation of the small rods supporting the cavity.

For the Mode Cleaner, any length fluctuation is enhanced by a factor which is equal to the number of roundtrips of the beam multiplied by the low pass transfer fucntion of the MC. With a finesse of 1 000 and a cut-off frequency of 500 Hz, the seismic noise usual $10^{-6}/f^2$ m/$\sqrt{}$Hz induced flutuation is given by the curve *b* of the same Figure. One can see that there is a need of seismic isolation for the MC, and then with a three-stage super attenuator, we can reach our goal.

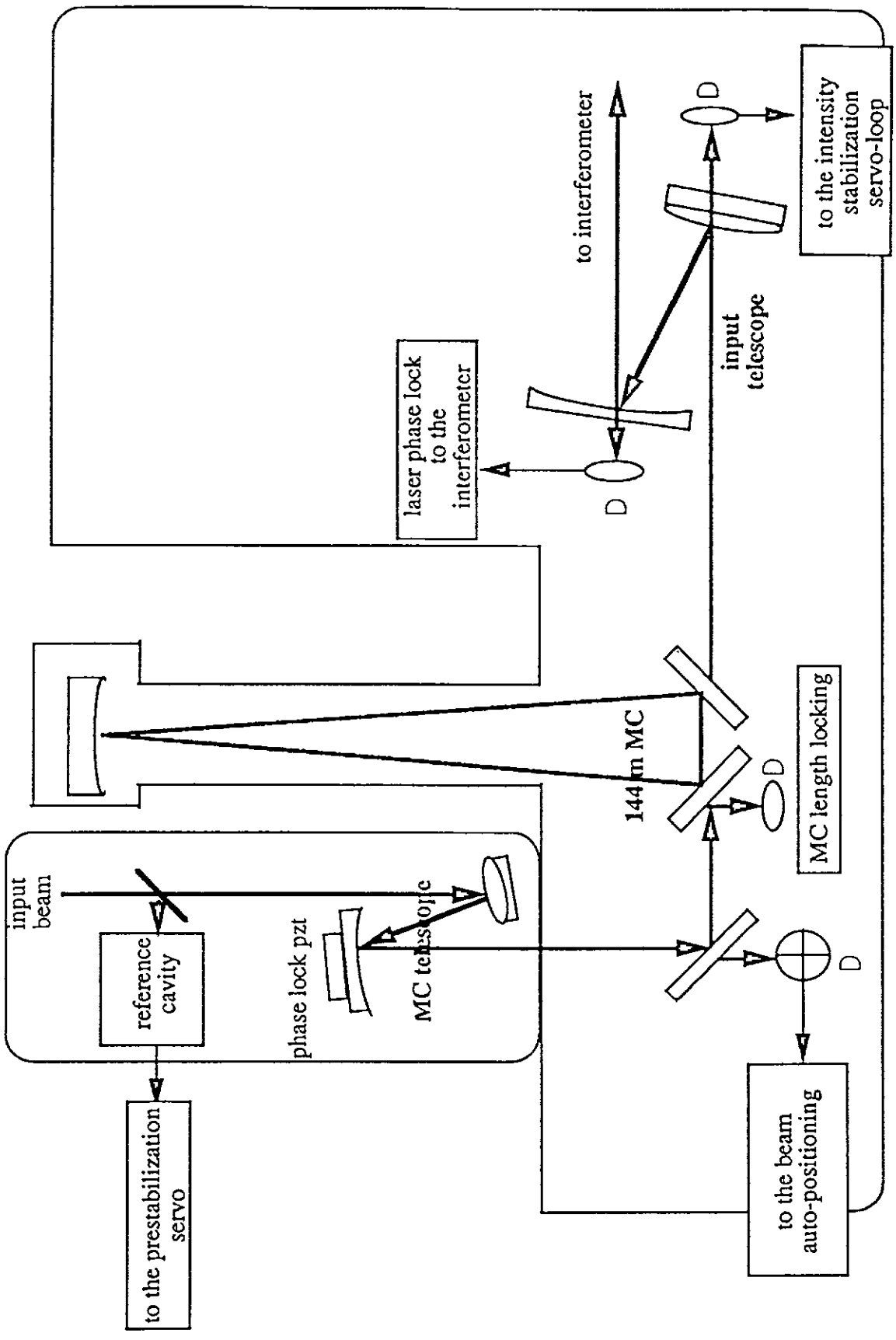

Figure III.1.a. : Schematic of the Input Bench

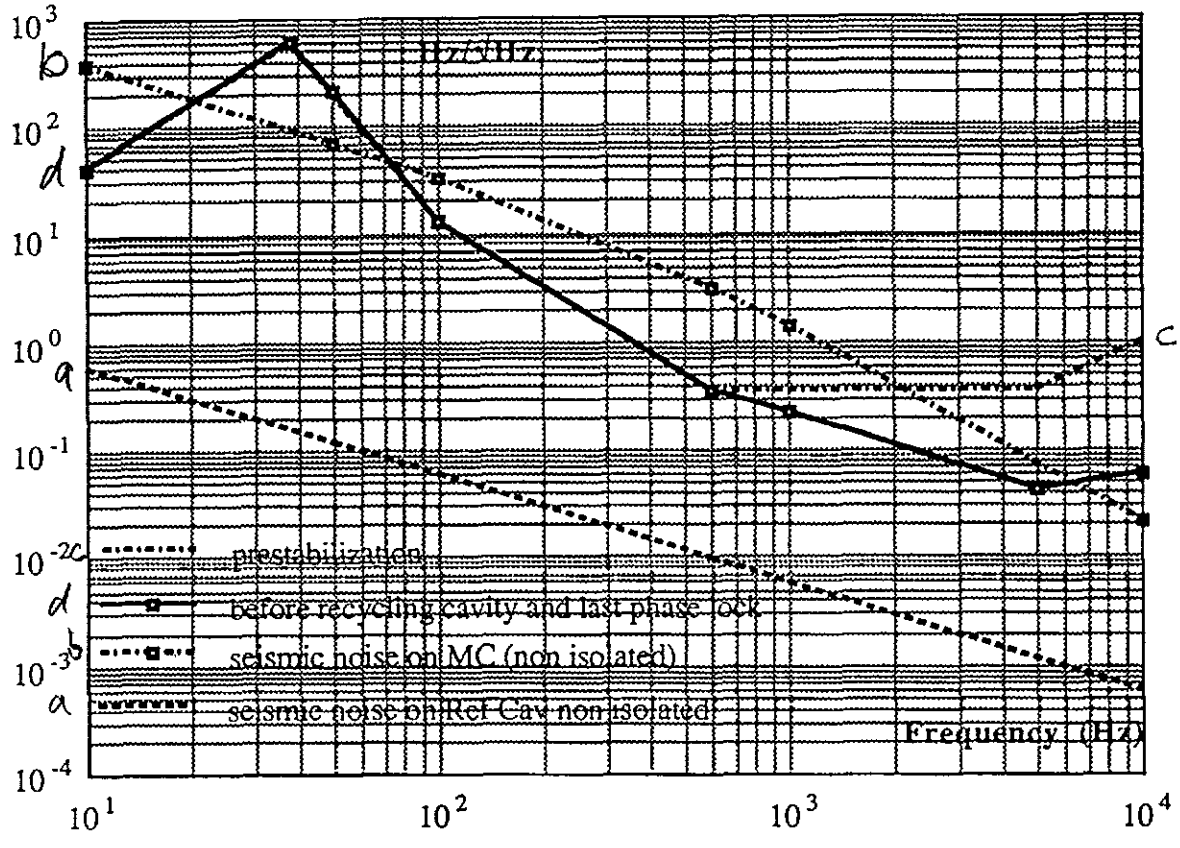

Figure III.2.1.a : Seismic noise effect on the Reference cavity (curve *a*) , on the Mode Cleaner (curve *b*), translated in terms of laser frequency noise and compared to the requirement for the prestabilization (curve *c*), and for the laser noise at the input of the interferometer (curve *d*).

4100.3.2.2. The Seismic and Thermal Noises of the Input Bench :

The first effect for the requirement stability of the Input Bench is coming from the beam fluctuation. The beam jitter in angle induced by the seismic noise is plotted on the Figure (II.8.1.a) above ; one can see that a seismic insulation of 3 stages the Super attenuator will be enough for the Input Bench in the case when the individual components sitting on the Bench have no other noise sources. Of course it is not allowed to reintroduce any seismic noise through coils attached to the ground to control the position of the Bench or the Mode Cleaner. We have now to worry about the mechanical stability of each component on the Input bench and the way it influences the jitter of the output beam.

Let's list the possible sources of noise inducing beam jitter of the laser at the exit of the Input Bench. The first ones are those due the thermal noise of the Bench in its whole, the second ones are due to the thermal noise of the components (mirror mounts etc...) including the thermal noise of the Mode Cleaner, and finally those due to the residual jitter of the laser itself. Let's put orders of magnitude on all this.

The laser jitter exiting form the bench can be also due to the thermal noises induced by the bench itself or by the mechanical supports of the components of the bench (like the input telescope) and finally by the thermal noise of the IMC.

Estimates of these different noises have been made some time ago [Virgo note PJT94-

025]. We summarize here the sources of noise and the results.

1) Thermal noise of the bench suspension: let's Q_{sus} be the quality factor of the suspension, with a resonance frequency F_0 of 1 Hz, then the global thermal motion of the bench above the resonance is:

$$\delta\tilde{x}_{sus}(F) = \sqrt{\frac{4\,kT\,F_0}{8\,\pi^3 M\,Q_{sus}\,F^4}} = \frac{8 \times 10^{-13}}{\sqrt{Q_{sus}}\,F^2} \quad m/\sqrt{Hz}$$

which is negligible even with a critically dapmped pendulum ($Q_{sus} = 1$).

2) Bench internal deformations: they are caused by seismic noise, temperature fluctuations and internal thermal noise. To limit the influence of the first one which is difficult to evaluate precisely, the solution is to limit the Q factors of the bench resonances. Temperature fluctuations will be responsible of long term misalignments and mismatch of the laser beam, but they will be likely compensated by the the tuning possibility that we will provide to correct the Interferometer thermal effects that are larger than in the bench.

3) Thermal noise of the optical mounting: assuming an internal damping, the rotation fluctuations of a single mechanical resonator is given by:

$$\tilde{\delta\theta} = \sqrt{\frac{2\,kT\,\omega_0^2}{I\,Q\,\omega}}\;\frac{1}{(\omega - \omega_0)^2 + \frac{i\,\omega_0^2}{Q}}$$

where I is the inertia momentum, $I = M.d^2$ and depending on the number of reflections of the beam on this kind of mount, we can deduce the beam jitter easily. The curves below show the beam jitter for Q = 1 000, two resonance frequencies of 100 Hz and 1 kHz and 10 cm large mirror mounts of different sizes. We didn't forget that the deflection is twice the rotation angle of the mirror.

The **Figure III.2.2.a** gives the above estimated noises translated in term of laser phase noise at the output of the bench and compared to the Virgo requirement for the laser. xxx

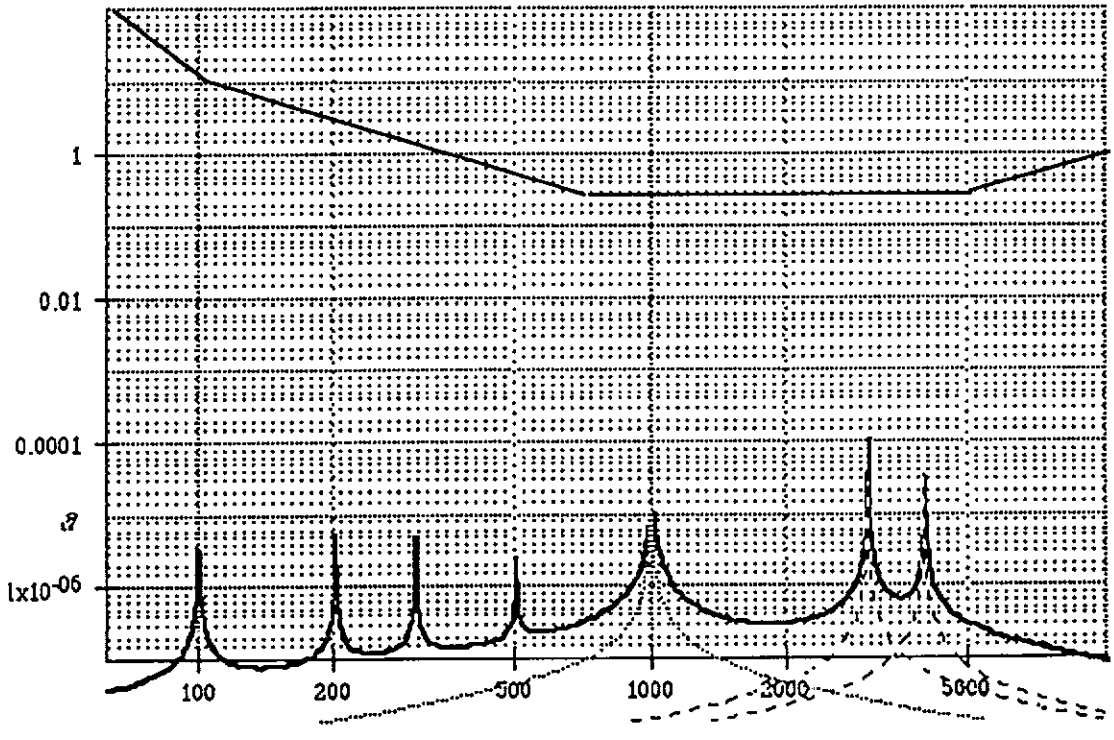

Figure III.2.2.a.: Equivalent laser phase fluctuations vs frequency induced by the IB thermal noise (4 resonances between 100 and 400 Hz with mass M=100 kg and Q=1 000) and its components (assuming 3 components have resonances at 1 kHz, 3 components with resonances at 3 kHz and 2 components at 4kHz, M=0.5 kg each at Q=1 000). The upper curve is the Virgo requirement on the laser noise before the MC.

4100.3.2.3. Structure of the Bench:

The bench will be realized with a material having a good damping factor, and after measurements of Q made with a large of samples, we have kept two possible candidates which are two alloys of Mg, Zr. One of them is easily manufactured in any mechanical shop while the other should be preformed at the factory. Outgassing measurements wil guide us in the choice of the material

4100.3.3. Input Mode Cleaner (MC):

4100.3.3.1. Optical Specifications:

The MC is a three-mirror cavity formed by two input plane mirrors positioned on a "corner-cube" sitting on the Input Bench, served as input-output mirrors and one end curved mirror suspended inside the MC tower at 144 m away. The length of this MC has been chosen in such a way that it is a multiple of the recycling cavity length [Virgo note PJT94-007]. To avoid degeneracy of the high-order modes with the fundamental ones, the curvature of the end mirror has been chosen to be 181 m giving a Rayleigh range of 73 m and a beam waist between the plane mirrors of 4.9 mm.

As the free spectral range is 1.06 MHz , in order to hav a low pass filter of around 500 Hz for the laser noises, the finesse of the MC has been chosen to be around 1 000 meaning a HR reflectivity end mirror and the two plane mirrors of reflectivity 0.997 for "s" polarization. The **table III.3.1.a** summarizes the optical parameters of the MC.

Length	**144m**
beam waist near input mirrors	**4.9 mm**
Rayleigh parameter	**73m**
End mirror curvature	**181m**
beam at end mirror	**11 mm**
R_{ar}	0.997

Table III.3.1.a : Optical parameters of the Mode Cleaner

4100.3.3.2. Filtering effect of the MC

If the incident beam has a lateral jitter $a(t)$ and an angular jitter $\alpha(t)$, the idea of the Input Mode Cleaner (IMC) is to reduce them so the ouput beam of the IMC has the following jitters $a'(t)$ and $\alpha'(t)$ [Virgo note 93-004]:

$$a'(t) = w_0 \frac{t_{10}}{t_{00}} \left(\frac{a}{w_0} \cos \psi_{10} + \frac{\alpha}{\theta_0} \sin \psi_{10} \right)$$

$$\alpha'(t) = \theta_0 \frac{t_{10}}{t_{00}} \left(-\frac{a}{w_0} \sin \psi_{10} + \frac{\alpha}{\theta_0} \cos \psi_{10} \right)$$

where ψ_{10} is the phase shift encountered by the first transverse mode inside the cavity. In the case of a three-mirror IMC the phase shift is expressed as:

$$\psi_{10} = tg^{-1} \left(\frac{\sin \varphi^a_{10} + R \sin(2\varphi_{10})}{\cos \varphi^a_{10} - R \sin(2\varphi_{10})} \right)$$

where: $\varphi_{10} = \varphi_{00} - 2\, tg^{-1} \left(\frac{d_{MC}}{z_R} \right) = \frac{\omega d_{MC}}{c} + \cos^{-1} \left(1 - \frac{L_{MC}}{R} \right)$

and $$\varphi^a_{10} = \frac{\omega a}{c} + tg^{-1} \left(\frac{a}{z_R} \right)$$

a , L_{MC} , d_{MC} being respectively the distances between the two plane mirrors, the length and the roundtrip length of the MC; $d_{MC} = 2L_{MC} + a$.

For the case of the Virgo MC, the ratio of the transmission between the first mode and the fundamental one is 2×10^{-3}, therefore the typical orders of magnitude for the filtering are:

$$a' = 2 \times 10^{-3}\ a + 10^{-10}\ \alpha \approx 2 \times 10^{-3}\ a$$

$$\alpha' = 2.5 \times 10^{-7}\ a + 2 \times 10^{-3}\ \alpha \approx 2 \times 10^{-3}\ \alpha$$

with this attenuation , the beam jitters of the laser at the input of the IMC are represented in the Figure II.8.1.a, curve c. As these orders of magnitude are typically the ones measured with current lasers, we are really at the limit if there is some extra acoustic noise in the room: a measurement on site of the acoustic effect on the jitters of the beam should be performed and we may have to add some acoustic protection.

4100.3.3.3. Thermal noises of the MC

If it is rigidly connected to the bench, the corner-cube of the mode cleaner will add its thermal noise to that of the bench and the resulting noise is plotted on the **Figure III.3.3.a** in comparison with the laser requirement at the output of the mode cleaner. One can see now that the thermal noise of the corner-cube can be critical if it has a high Q factor and if its first resonance is in the detection range. There is a need to design carefully the shape of that corner-cube.

In the **Figure III.3.3.b** , we plotted the same curve by adding now an extra seismic isolation between the corner-cube and the bench with a cut-off frequency of 150 Hz. One can see that the things can get better in the medium frequency range.

The thermal noise of the mode cleaner suspension (mainly for the far mirror) can be calculated in the same way, and even with the enhancement factor due to the roundtrips, this effect is negligible and we do not have to worry about it.

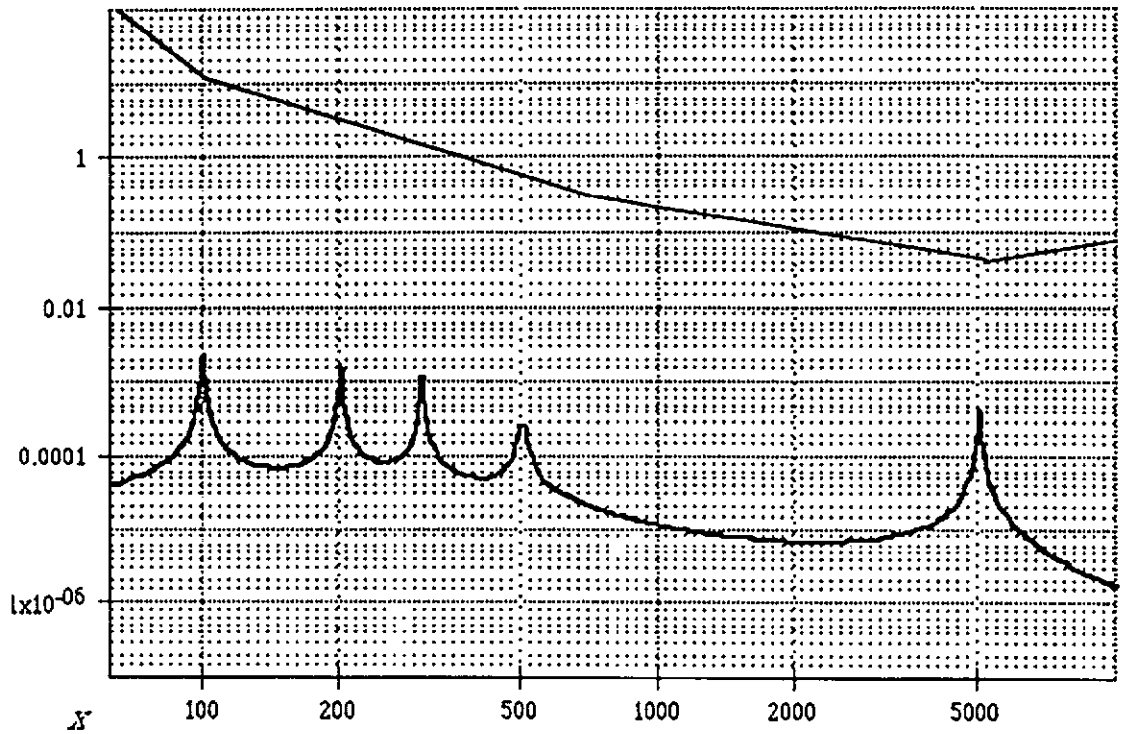

Figure III.3.3.a : Equivalent frequency fluctuation induced by corner-cube MC thermal noise of mass M=1 kg, Q=100, resonance at 5kHz and by the IB (4resonances between 100 and 400 Hz. The upper curve is the Virgo requirement on the laser noise after the MC.

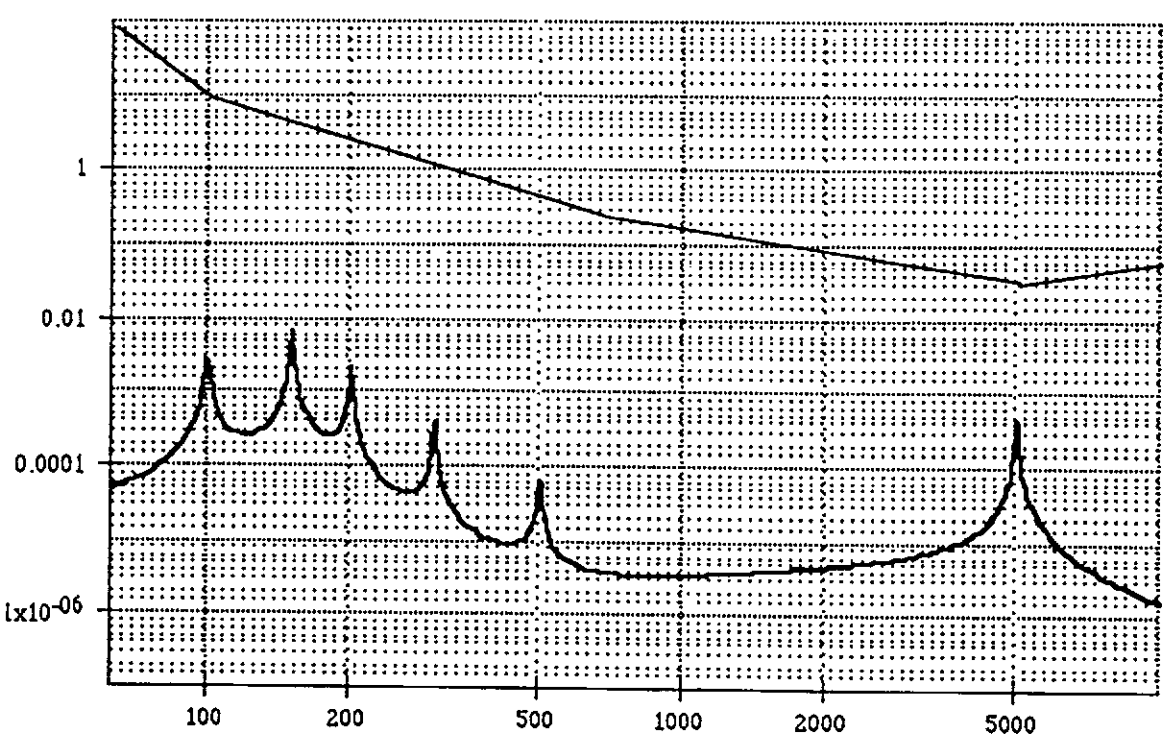

Figure III.3.3.b : same curve as III.3.3.a , except the presence of an extra isolation between the corner-cube and the IB acting as a lowpass filter at 150 Hz.

4100.3.3.4. Mechanical structure of the MC:

Calculations with a finite element analysis program are performed to find the best shape and dimensions of that corner cube carrying the two plane mirrors. The goal is to get the first mechanical resonance of it at the highest possible frequency ie near the limit of the detection range of Virgo. This corner-cube is made out Silica and the two mirrors will be optically contacted on it at forming an angle of almost 90°. It will be sitting on small rods designed to act as a low pass filter of around 100 Hz.

As far as the end mirror is concerned it is a simple cylindrical mirror and the calculation of resonances is easier.

4100.3.3.5. MC Matching Optics:

The matching optics for the MC have a factor of 4 to 5 in magnitude as they transform a laser beam of the order of 1 mm into a waist of 4.9 mm in a distance fitting the size of the bench. The design of this telescope takes into account the aberrations due to off-axis curved mirrors as well as possible implementation problems. One possible solution for a low loss telescope is sketched on the **Figure III.3.5.a** with a minimum length of about 800 mm. The loss encountered here and calculated with our beam propagation model, is smaller than 10^{-3}.

4100.3.4.Matching Optics of the Main Beam:

4100.3.4.1. Design of the telescope

The waist of the beam entering the interferometer (matched to the FP cavities) should be located at the input beam of the FP with a size of about 20 mm. The recycling mirror is a thick converging lens [minutes of Interferometer meeting 12/4/95] and the size of the beam at the level of the Input bench is of the order of 6.8 mm. That gives a magnification of 1.4 for the telescope. This telescope is also a two off-axis concave and convex mirrors. The design is less critical for this telescope in terms of power losses, so its minimum length can be as small as 400 mm.

The summary of the cavities is in the table III.4.a below: the laser beam originated from the slave laser, must be adapted first to the reference cavity RC by the LB telescope, then to the mode cleaner MC by the MCT, and finally to the Virgo interferometer FP. The data of the cavities and the corresponding beam parameters are listed in the following table:

Cavity /beam data	Slave laser	RC	MC	FP
shape		Δ	Δ	-
length L		300 mm	144 m	3000 m
mirror radius R		500 mm	180 m	3450 m
waist $2w_0$		580 µm	9.9 mm	39.6 mm
Rayleigh length $2\Lambda_R$		440 mm	147 m	2300 m
beam angle 2φ		2.4 mrad	140 µrad	34 µrad
finesse F		50000	1000	50

MC

Table III.4.a : Data of the different cavities

4100.3.4.1.1.

4100.3.4.2. Tuning of the telescope

The telescope is in an afocal position in order to keep enough sensitivity to adjust the size and position of the waist inside the itf in case of thermal problems which could cause thermal lensing in the FP cavities. The two mirrors are positioned on two pzt-motors each, for tilt and rotation and one translation stage for fine adjustement of the distance.

4100.3.5. Power stabilisation

4100.3.5.1. Requirements:

The relative amplitude noise of the laser must be below the shot noise limit at the photodetector. Assuming a contrast defect in the interferometer of $1\text{-}C$, the amplitude fluctuations must fulfill:

$$\frac{\delta\tilde{P}}{P} < \frac{\delta\tilde{P}_{SN}}{P} = \sqrt{\frac{h\nu}{\eta P\,(1\text{-}C)}} = 4.2 \times 10^{-10}\ /\sqrt{\text{Hz}}$$

where the laser power incident on the interferometer is 1 kW and the contrast defect is 10^{-3}. This requirement is extremely stringent for any laser, especially in the low frequency range, where there are many causes of technical noise. This brings us to the main reason why the detection should be done at a frequency where the laser is shot noise limited ie above a few MHz for most lasers including the Nd:YAG lasers. Even at RF frequency, one has to check that the laser can fulfill this requirement.

Another cause of amplitude noise is due to the finite open loop gain of the mirror position servo system yielding a residual offset from the dark fringe. This residual offset has been estimated to be $dL_{offset} = 10^{-11}$ m [ref xxx] and corresponds to a dephasing of:

$$\delta\Phi_{offset} = \frac{2\pi\,\delta L_{offset}}{\lambda}\,\mathcal{F} = 3 \times 10^{-5}\ \text{rd}$$

for a finesse $\mathcal{F}$ of 50 in the arms of the interferometer. So the requirement in amplitude noise in the detection range between 10Hz and 10 kHz is given by:

$$\frac{\delta\tilde{P}}{P} < \frac{\delta\tilde{\Phi}_{Virgo}}{\delta\tilde{\Phi}_{offset}}$$

The curve **a** of the **Figure III.5.1.a** gives the level of amplitude stability requirement following the level of strain sensitivity expected for Virgo. We can see that the lowest level required is $\delta P/P \approx 10^{-8}\ /\sqrt{\text{Hz}}$ at a frequency @ 500 Hz. This corresponds to the shot-noise level for a power of a few mW.

The beam impinging on a mirror causes a displacement induced by radiation pressure:

$$\delta\tilde{L} = \frac{\delta\tilde{P}}{M\,\omega^2\,c}$$

which is transformed into an equivalent strain sensitivity when there is an asymmetry a between the arms:

$$\tilde{h}_N = \frac{\alpha\ \delta\tilde{L}}{L_{arm}}$$

where L_{arm} is the length of 3 km. This strain noise must be small compared to the Virgo sensitivity

, and we can deduce the level of amplitude stability required:

$$\frac{\delta\tilde{P}}{P} < \tilde{h}(F)\,\frac{M\,c\,(2\pi F)^2\,L_{arm}}{P\,\alpha}$$

with an intracavity laser power of 15 kW, an asymmetrey of 10^{-3}, test mass of 30 kg, we get:

$$\frac{\delta\tilde{P}}{P} < 7.10^{13}\,F^2.\,\tilde{h}(F)$$

the curve **b** of the **Figure III.5.1.a** shows the stability required. We can see that it is more stringent at low frequency @ 20 Hz than the noise mentioned above; the overall level of amplitude stability is the minimum of the 2 curves at each point.

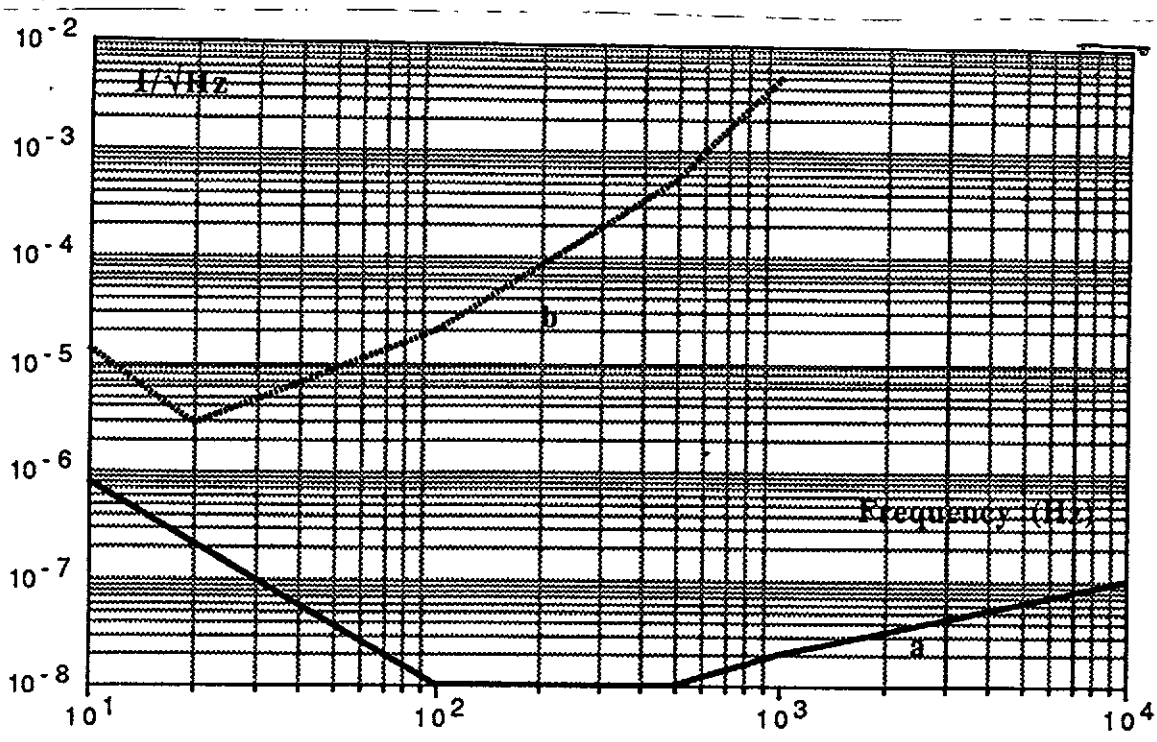

Figure III.5.1.a : Requirement on relative amplitude stability, curve *a*: due to residual error in mass position, curve *b*: due to radiation pressure on test-mass.

4100.3.5.2. Expected Results from the Injection Locking

The injection locking technique acts as a low pass filter for the frequency fluctuations of the slave laser with a cut-off frequency of the order of 1 MHz, meaning that injection locking is a good way to suppress the relaxation oscillation of the slave laser which is usually around 100 kHz. But any noise of the master laser around that frequency can excite it again. We can base our estimates today on the measurements we have performed on the relative intensity noise of the slave prototype laser. The **Figure III.5.2.a** shows the relative intensity noise of the slave laser vs frequency. Clearly, it is necessary to actively stabilize the laser power.

4100.3.5.3. Transfer Function of the Servo-Loop:

The intensity stabilization of the laser will use a photodiode sitting on the Input Bench hit by a small fraction of the main beam transmitted by the Mode Cleaner (to take advantage of its low-pass filtering) through the transmission of one of the telescope mirrors. The requested power is a few tens of mW.

The feedback will be done on the laser diode current directly instead of the laser beam. The electronics will split the feedback into two parts : the slow path will be provided by the "monitor" input available on the commercial power supplies; the fast path will be a fast voltage controlled current source, to be designed.

A rough integration of *dP/P* over the frequency band showed that a peak correction current of several amps will be required for the fast path.

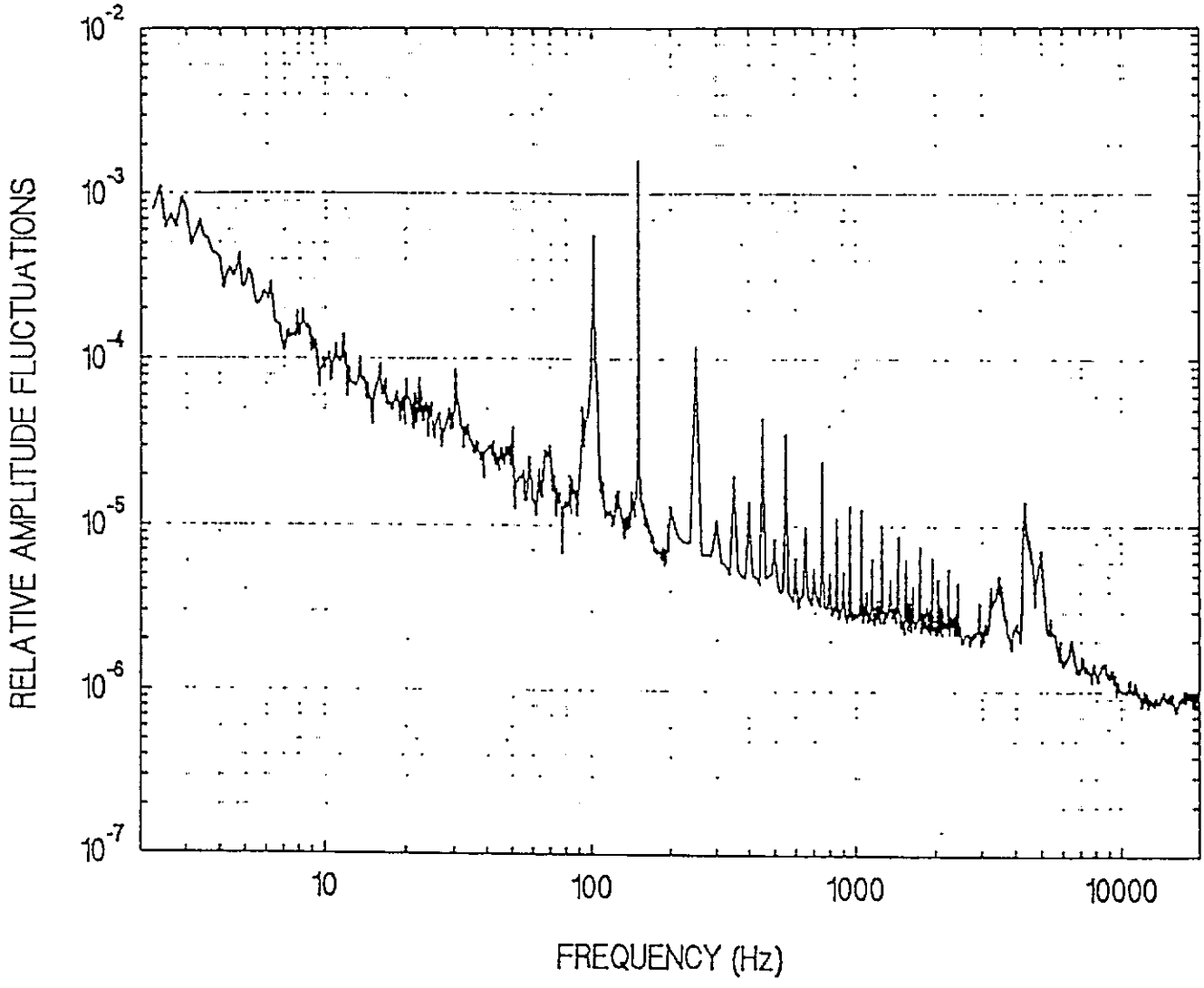

Figure III.5.2.a : Relative amplitude stability dP/P vs frequency of the slave laser when it is injection-locked.

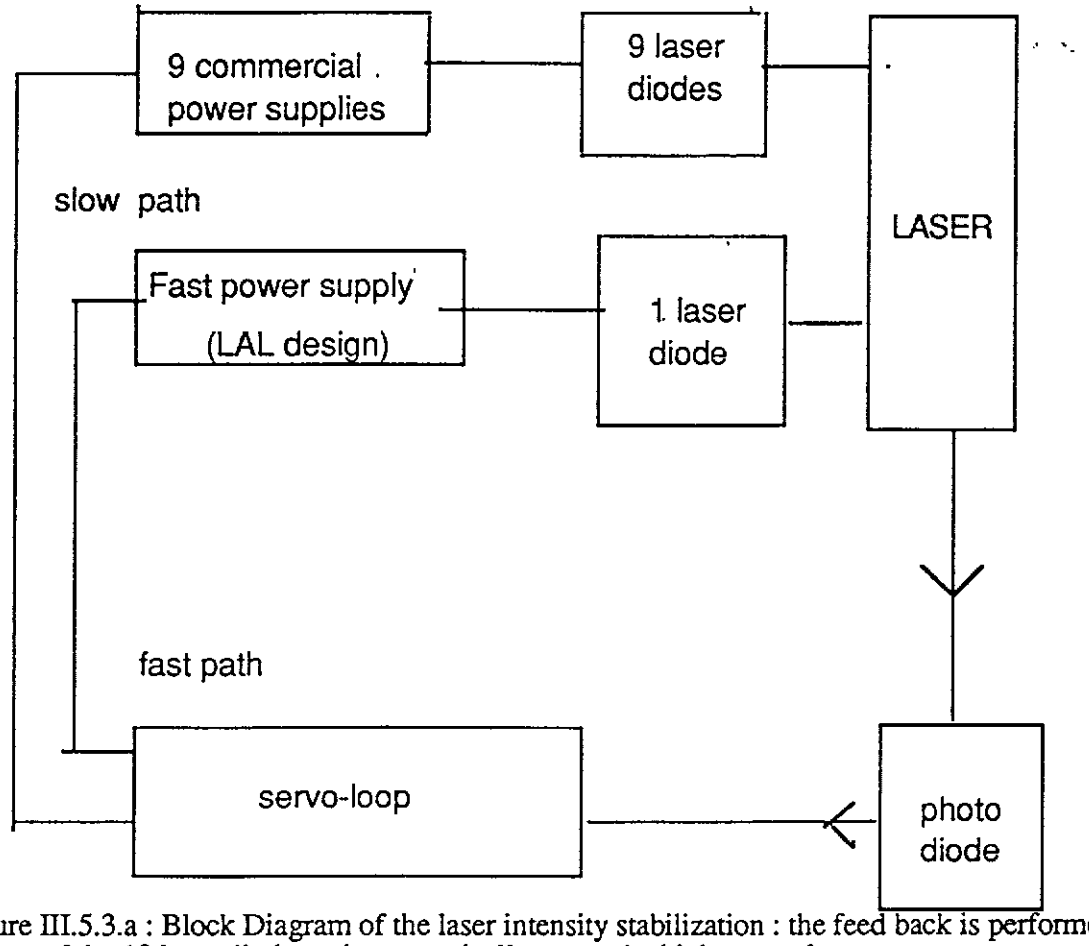

Figure III.5.3.a : Block Diagram of the laser intensity stabilization : the feed back is performed on one of the 10 laser diodes using to optically pump the high power laser.

4100.4. Alignments and Local Controls of the benches

4100.4.1. Laser Control:

It controls the diodes power supply, the laser power and some prestabilisations. The diodes power supply control will be in a VME crate connected to the slow monitoring network. The functions required by this control are:
-turn the laser on or off (diodes supply on or off).
-monitor parameters as diodes state, diodes and Yag temperature, global current.
-prestabilise the laser power acting on the global current in the diodes.
-keep the Yag in monomode operation.
~~-maintain a fixed temperature in the reference FP cavity.~~
-It can also monitor the status of the analog servo loops.

The laser power and frequency prestabilisations are done by analog servo loops which are autonomous, but which can also exchange informations via the VME system with a high level task.
The laser power and the phase noise of the laser relative to the 3km cavity are sampled in ADC's located in VME crate and sent to the data acquisition through the vertical bus, at the same rate as the dark fringe signal.

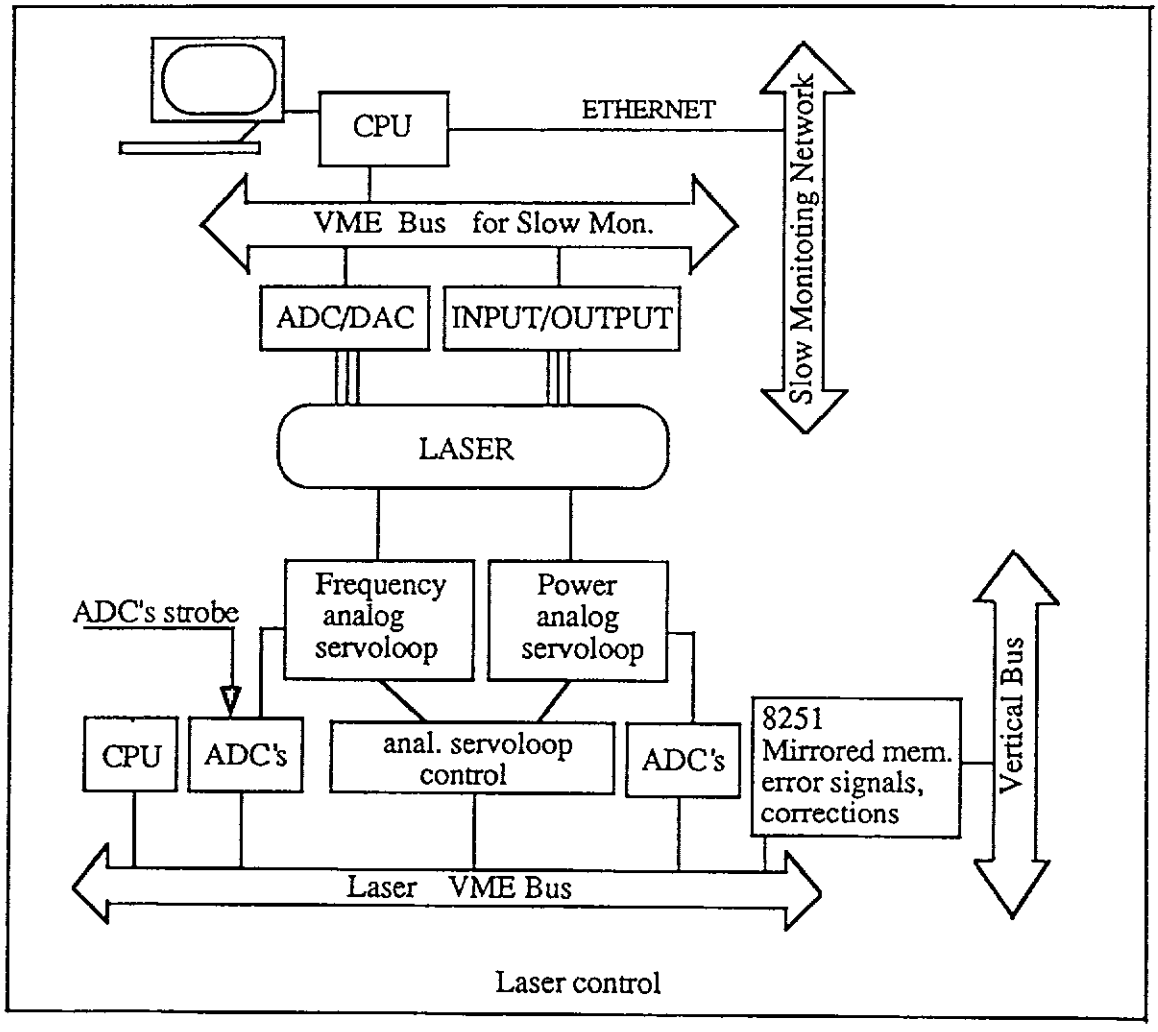

Laser control

4100.4.2.Alignment Strategy between the Benches

The incident laser beam is mode matched to and kept aligned on the reference cavity. This is equivalent to saying that its orientation is fixed with respect to the entrance bench, provided that the RC is fixed itself in a stable way. The subsequent mode matching for the mode cleaner is done by a telescope, which, at the same time, serves for (automatic) aligning of the beam with respect to the MC, and possibly for fast phase corrections for improving the laser frequency stability. The mode ceaner mirrors themselves are controlled only locally, and steered only during the phase of initial alignment. A final telescope matches the beam exiting from the MC to the interferometer. Its mirrors can be steered, too, for automatic alignment of the beam to the ifo. Their distances can be controlled in order to choose the waist position.

4100.4.3.Alignment of Reference Cavity:

This is the first cavity encountered by the laser beam incident on the entrance bench. The beam matching for the reference cavity can be done outside the IB vacuum tower, which facilitates the specifiactions for the components to be used. Small changes of the distance telescope-IB (e.g. due to drifts or pendular movements) are not very critical, considering the Rayleigh length of 500mm of the RC.

The telescope mirrors will be equipped with tilt actuators in order to keep the beam aligned on the RC. The necessary error signal will be obtained by using the information contained in the beam reflected off the RC (automatic alignment with the Ward technique). Thus the RC itself is used as a reference for the incident beam orientation.

4100.4.4.Optical Memories:

The task of the local control is to measure and, if necessary, correct the position and orientation of a suspended mass (in this case, the entrance bench) with respect to a local reference system. As opposed to the global control (control of the mass relative to other suspended masses), it will work also during the prealignment phase, when the mode cleaner is not yet resonant. The local control is necessary for:

- *the prealignment*:: The local control allows reading and correcting the mass position in order to achieve the right orientation for the MC resonance.
- *the optical memory:* The mass position is continuously monitored (or stored once after the first alignment is finished) and, in case of a fault (out-of-lock condition...), the last position can be read from memory and restored manually or by computer, thus avoiding a completely new alignment starting from zero.
- *damping of the pendular motions:* The pendulum Q should be reduced to quite close to unity in order to avoid excessive mass movements, which disturb the prealignment and cause fluctuations of the beam position/angle after the mode cleaner, the latter even while global control (longitudinal locking/autoalignment) is working.

In the case of the EB, the local control system can be active even after alignment (during normal operation); it then receives the positioning commands from the global control (locking and autoalignment systems) instead of from a local reference system or the operator.

4100.4.4.1. Determining the mass positions with a CCD camera

The reading of the mass position/orientation will be done with a CCD camera, read out by computer (Annecy camera [VIRGO note PJT92-032]). The scheme is shown in the **Figure IV.4.1.a.** The mass itself carries two colour marks. If the mass moves in x or y direction, or turns around the z axis, then the images af the marks on the camera move accordingly, which gives informations on these 3 degrees of freedom. For the other 3 variables, two lasers and an auxiliary miror are arranged in such a way as to create two light spots on the camera. The beam of laser 1 is folded, so its spot on the camera does not change with z. It thus gives a precise information on q_x and q_y. For measuring z, laser 2 is used. The angular dependence of ists spot position on the camera surface must be corrected using the informations obtained with laser 1.

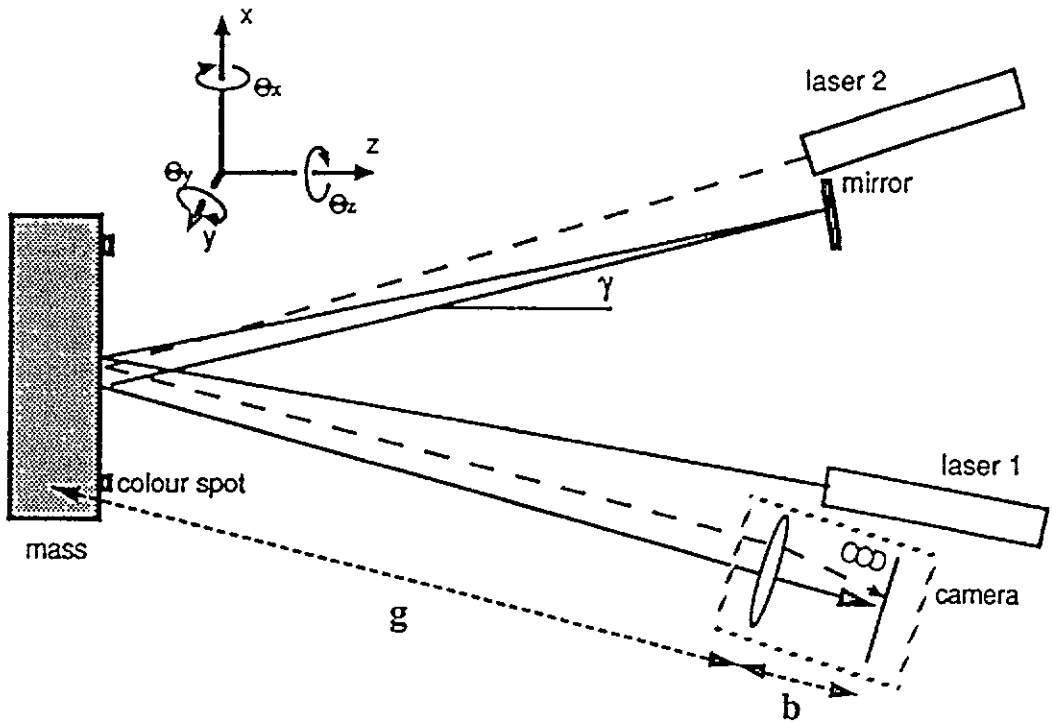

Figure IV.4.1.a: Optical scheme for determining the mass position with a camera, similar to the one proposed by Annecy. The spot generated by laser 1 serves for determining θ_x, θ_y; the image of the two points on the CCD gives x,y and θ_z; laser 2 gives informations on z.

4100.4.4.2. Calculating mass positions using 4 reference marks

According to the scheme explained above, the position and orientation of a suspended mass will be measured by observing two laser beams and the images of two color marks on the mass. During the phase of initial alignment, however, it may happen that the mass is strongly disaligned, such that the laser beams will not hit the CCD at all. In this case, one can use 4 instead of 2 color marks, and no lasers. Appropriate combination of the position of the 4 images on the CCD allows to determine the 6 degrees of freedom of the mass, although the precision is less than in the previous case.

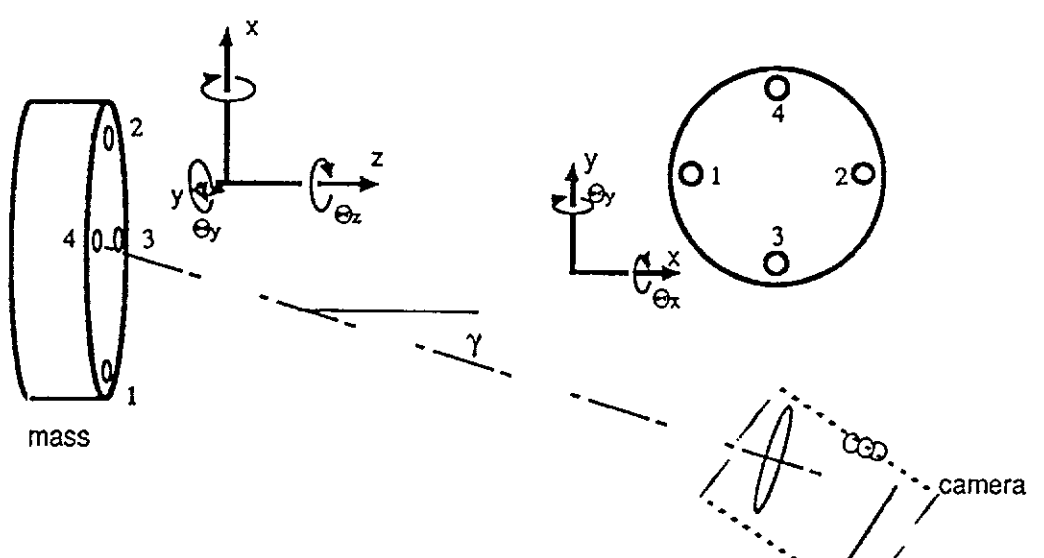

Fig. IV.4.2.a : Camera scheme for determining the mass position without lasers, seen from above.

Since we want to switch between the two modes of measurement according to the state of alignment and the desired precision, the optical configuration here must be the same as for the previous scheme; the lasers are not used, hence not drawn. For measuring z, the perspectivic change in the distance between the images of mark 3 and 4 is used, which leads to a smaller precision for this variable. The uncertainty in z will be partially transferred to the measurement of x due to the angle g under which the mass is regarded.

4100.4.5.Alignment of the MC:

If the MC telescope's optical components are mounted on actuators, then it can also be used to align the beam onto the MC. That means that the end mass (curved mirror) of the MC is controlled only locally, and residual drifts of it and the two plane MC mirrors on the EB are compensated for by tilts and translations of the beam coming from the RC.

The distance of the telescope mirrors must possibly be controlled actively, since the output waist position could be very sensitive to it (see output telescope); but this depends on the design details. The actuator responsible for the longitudinal mirror movement can also be used to phase modulate the beam for correcting residual laser frequency fluctuations (the error signal for this comes from the L_1+L_2 signal on D_2). In order to achieve the required speed, the actuator must act on the first mirror of the telescope, which can be small because it sees the small beam coming from the RC. The change of telescope geometry due to the phase corrections is not significant.

All three telescopes will serve at the same time as beam alignment devices, i.e. their mirrors are equipped with actuators such as to control the x and y displacement and the x and y direction of the outgoing beam (4 degrees of freedom, e.g. 2 mirrors with 2 actuators each). It may also be necessary to change the waist position and diameter, which would require two more degrees of freedom. Fast phase corrections will be done before the MC, probably using the first mirror of the MC telescope.

4100.4.6.Auto-Alignment of Cavities:

4100.4.6.1. Auto-alignment technique

As it was said above, the telesopes will be used for aligning the beams on the cavities. In order to do so, error signals are required, giving informations about the misalignments of the respective cavities. For the output telescope, these error signals will come from a global interferometer alignment system, which is treated elsewhere. Thus it is necessary to derive error signals for automatic alignment of entrance bench and mode cleaner; this requires a technique for obtaining informations about the type and size of the disalignment between a beam and a resonant cavity. This can be achieved using a differential phase sensing technique, which was proposed and experimentally demonstrated by the Glasgow gravitational wave group. The technique is an extension of the Pound-Drever modulation scheme for locking the length of a cavity to the frequency of a laser. In both cases, the incident laser beam is phase modulated at a high frequency (e.g. around 10 MHz), and the light reflected from the cavity is observed with a photodiode; the information contained in the photocurrent is extracted by demodulating with the modulation frequency. In the first case a simple photodiode is used, while the second one needs two quadrant photodiodes, one in the near field, and the other one in the far field (with a lens).

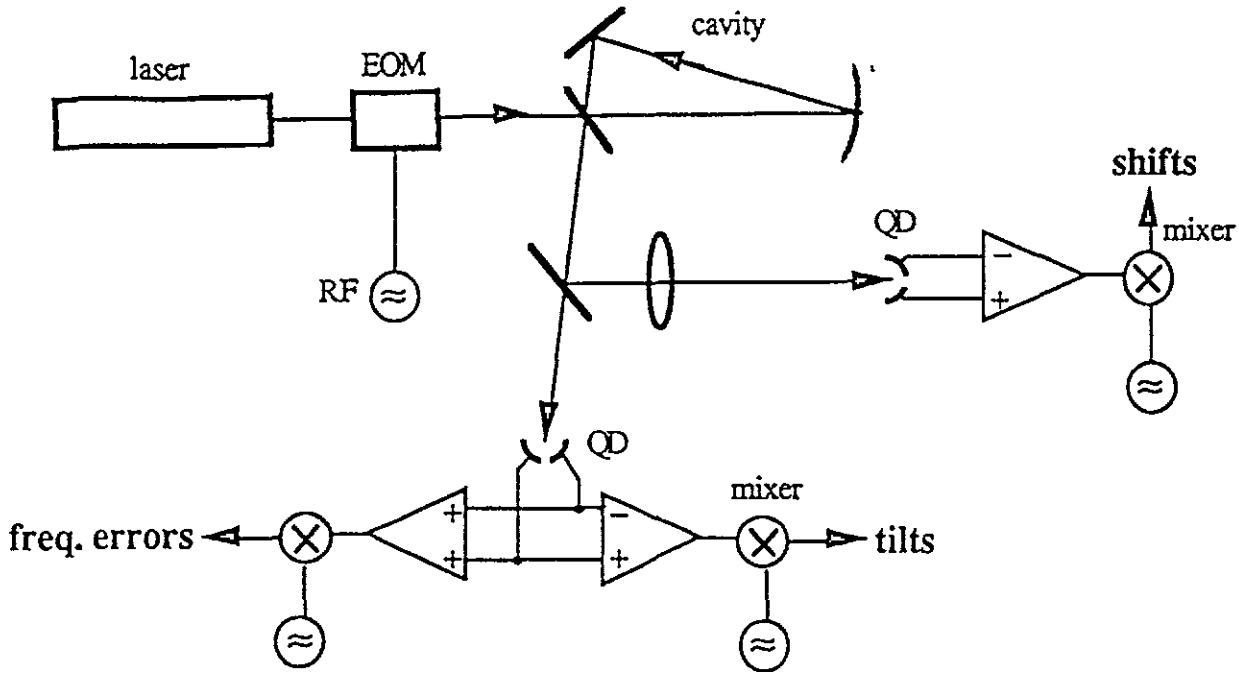

Figure IV.6.1.a :Typical setup for measuring the alignment (and frequency) errors of a laser with respect to a cavity. (EOM=electro-optical modulator; QD=quadrant photodiode; RF=radio frequency generator).

The principle of this technique can be understood as follows (for simplicity, only one lateral dimension is considered). In the case of simple frequency locking, the light reflected directly at the cavity entrance mirror (including the modulation sidebands) interferes with the light having entered the cavity and being transmitted back through the cavity entrance mirror (indirect reflection, containing only the carrier); the demodulated signal contains an information about the frequency error, coming from the dephasing between the two interfering components, which depends on the detuning. In the case of a misalignment, the beam incident on the cavity can be decomposed with respect to the cavity reference system in terms of the Hermite-Gaussian cavity eigenmodes U_n. Especially, an only slightly misaligned (mismatched) beam can be represented as a simple superposition of low-order modes:

beam error	*eigenmode decomposition (phase)*
lateral misalignment (shift)	U_0 & U_1 (0°)
angular misalignment (tilt)	U_0 & U_1(90°)
waist size mismatch	U_0 & U_2 (0°)
waist position mismatch	U_0 & U_2(90°)

In general, the U_n will have different resonant frequencies, so only the U_0 will enter the cavity and resonate; the other modes are reflected off the entrance mirror. So the direct reflection off the cavity entrance mirror (R_1) contains the original U_0 and $U_{1/2}$ contributions, including the modulation sidebands, whereas the part transmitted back through the cavity entrance mirror (the "indirect reflection", R_2) contains only the U_0 part. The total reflected beam will thus consist of two beams: the unaltered (misaligned) incident beam plus a fundamental beam U_0 aligned with the cavity axis. The beat of both gives:

1) the beat of the fundamental part (U_0) of R_1 with R_2 gives the information about the frequency error between laser and cavity

2) the beat of the first order contribution U_1 of R_1 ("misaligned part") with R_2 gives a two-lobed beat signal, which can be detected with a symmetrically split photodiode (for both lateral dimensions: quadrant photodiode) to yield information about the misalignment. Acoording to the type of misalignment (lateral shift or tilt, which determines the relative phase between U_0 and U_1), the beat note occurs in the near field or in the far field of the reflected light.

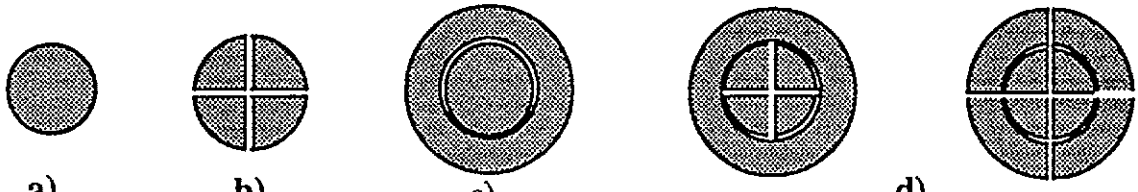

Photodiode types for a) frequency locking (Pound-Drever technique); b) automatic alignment c) automatic beam matching; d) alignment and matching

Thus, in order to obtain the required informations, 3 photodiodes are necessary:

1) a quadrant diode looking at the light reflected from the cavity for obtaining informations about the beam tilts

2) a quadrant diode in the focus of a lens collecting the light reflected from the cavity for obtaining informations about the lateral beam shifts

3) an ordinary photodiode for obtaining informations about the frequency deviation of the laser (this can be replaced by the sum of the 4 quadrants of photodiode 1).

In order to keep track of a mode mismatch between the laser beam and the cavity resonant mode (error of diameter or position of the beam waist), the information carried by the second-order modes can be recovered using annularly split photodiodes; those could be combined with the quadrant diodes, giving five- or eight-segment elements.

4100.4.7.Input bench control:

It controls the aligment of the laser in the input bench (Automatic Beam Positioner) by moving mirrors acting on piezo electric actuators and reading the beam positions by mean of a quadrant diode.
It keeps the mode cleaner locked by running servo loops exchanging data with the end mirror mode cleaner control through optical links. The beam position is obtained by calculations made from the image of CCD cameras. Correction signals are applied to coils acting on the marionettes.

Monitoring signals are sent to the data acquisition through the vertical bus at the same rate as the dark fringe signal

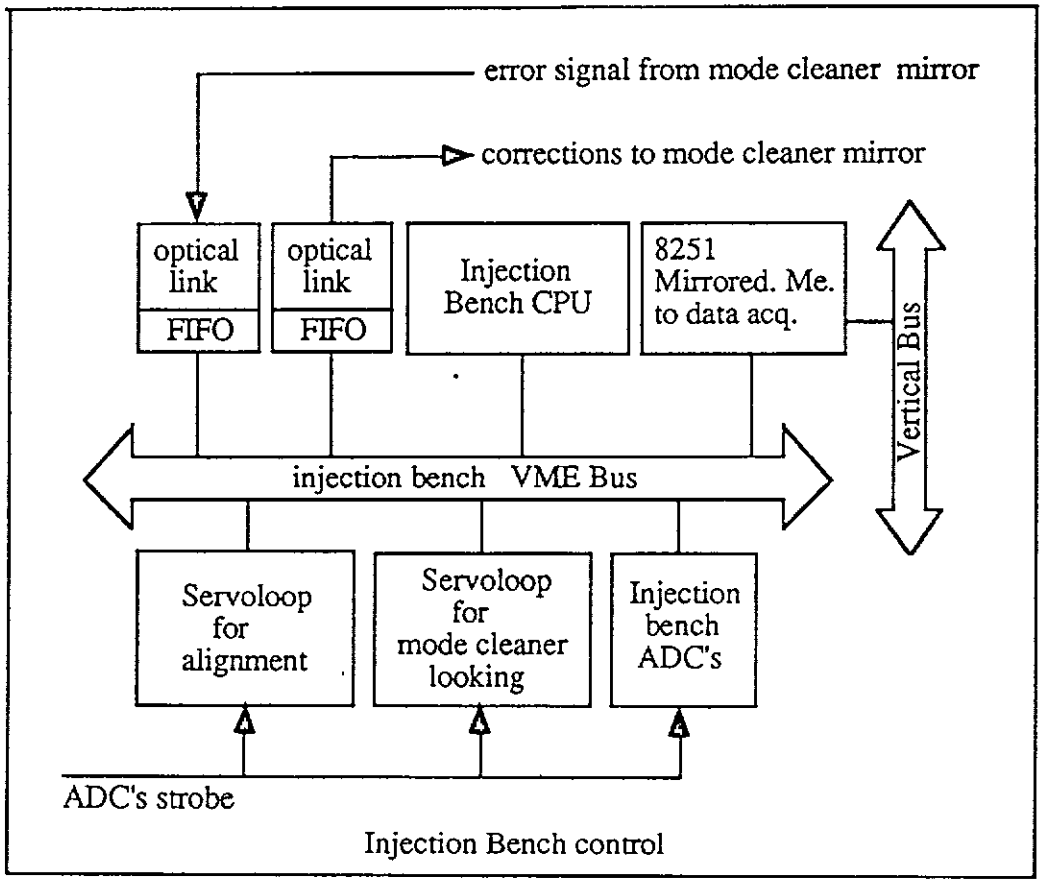

Detection Bench

4200.1. Introduction

In this chapter the main characteristics of the detection bench are presented. By detection bench we consider all the items located inside or directly around the detection tower and related to the signal detection. As much as possible, all the beams communicating with the "outside world", getting out or entering the detection tower are organized in such a way that they are grouped to pass through the same (1m diameter) window. A detailed investigation, leading to an optimized set of parameters, has been performed and can be found in the VIRGO note NTS95-010. These calculations and the method used will not be developped in this chapter, we will here only give the main corresponding results when needed. The main hypothesis are the VIRGO "reference solution" that is a frontal modulation scheme for the interferometer, with a modulation frequency of 6.27MHz and an asymetry of the recycling cavity of 0.8m

4200.2.Role of the Detection Bench

Two beams are comming from the beamsplitter towards the detection bench, the "dark fringe beam" and the small fraction of the beam coming from the North arm which is reflected by the beamsplitter. The tasks devoted to the detection bench are twofold:

- the detection of the gravitational wave signal which is carried by the "dark fringe"
- the measurement of the various signals needed to control the interferometer locking.

4200.2.1.The "dark fringe" detection requirements

The beams coming from the West and North VIRGO arms recombine on the beamsplitter to produce the so-called "dark fringe" beam which we shall call beam A. This beam, which carries the gravitational wave signal, must have the best properties in order to maximise the signal to noise ratio, the corresponding requirements have been studied in a dedicated VIRGO note[1]. In the frame of the reference solution which is discussed here, we take as working hypothesis the following conditions:

- A frontal modulation scheme is used
- The modulation frequency used is 6.27MHz
- The recycling cavity has an asymmetry Dl=0.8m

On figII-1 is shown the evolution of the SNR, as a function of the contrast defect, for several values of the mean power reflection of the large cavities.

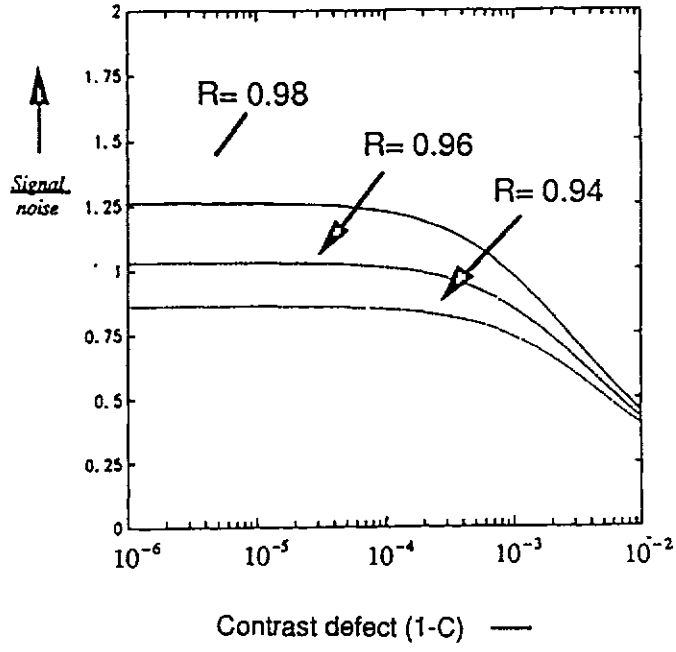

Difloss= 0

R= mean power reflection coefficient of large cavities

Fig II-1

In order to improve the effective contrast, we will use a Fabry-Perot mode-cleaner which will allow only the TEM_{00} mode to reach the detectors. As a working example, if we assume 10ppm losses as a mean value for the large cavities mirrors, the optimised values are:

Recycling mirror power transmission factor = 0.0203

Modulation index = 0.292

Mode-cleaner finesse = 96

Under these conditions, using the optimised values found, the beam power at DC, at modulation frequency for $h=2.10^{-23}$ and at twice the modulation frequency are:

$$P(0) = 0.722W$$

$$|P(\Omega)| = 0.84\ 10^{-9}W$$

$$|P(2\Omega)| = 0.669W$$

$$\frac{Signal}{noise} = 1.53$$

This gives a constraint on the specifications of the detector. The "cleaning effect" of the detection bench mode-cleaner is shown on figII-2. It shows how important it is to use a mode-cleaner on the detection bench in order to remove the parasitic modes. This effect remains important even with mirrors having very small losses.

Another important point is that the SNR increases like the square root of the detector quantum efficiency, this implies the use of diodes with the highest value for this parameter.

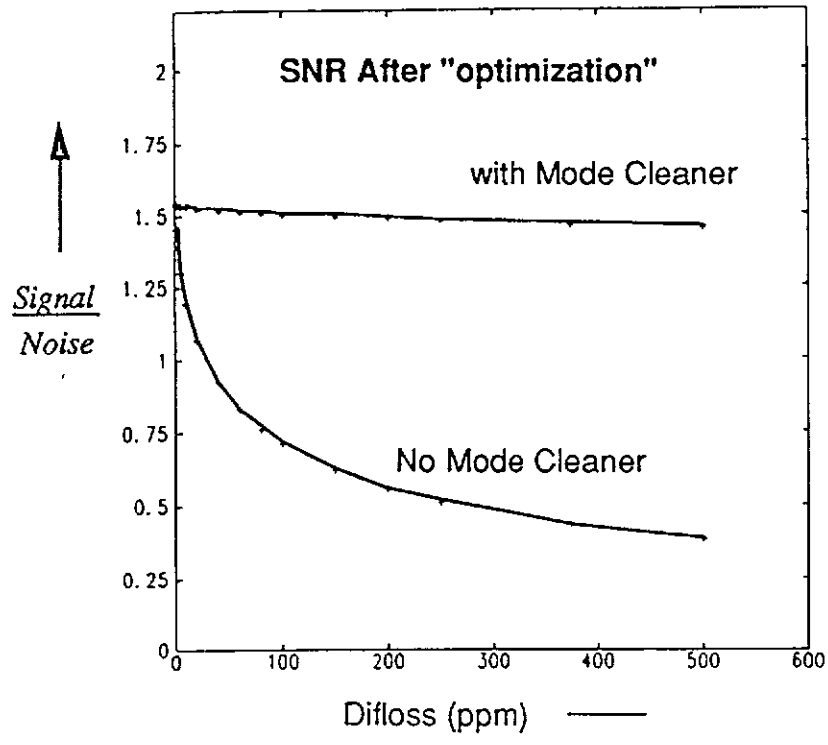

Fig II-2

4200.2.2.The reflected beam detection requirements

The beam reflected from the North arm cavity, on the anti-reflection coated face of the beamsplitter, will have a power of about 100mW, we shall call it the B beam. This beam is mainly used for locking, alignment and monitoring purposes. The mode content of this beam is essentially TEM_{00} and the required detection performances are not particularly stringent.

4200.3.Implantation

The general implantation of the detection bench is shown in figIII-1, beams A and B enter the detection bench with a waist of about 2cm, a separation of the axis in the horizontal plane of 7mm, and an angle of 3.6 mrad between them (see figIII-1). The optical properties of the telescope are explained in the next chapter. The two beams are separated at the focal point of a first large diameter lens of focal length 1m using a small plane mirror. An enlarged view of the separation region is shown in figIII-2.

DETECTION BENCH IMPLANTATION

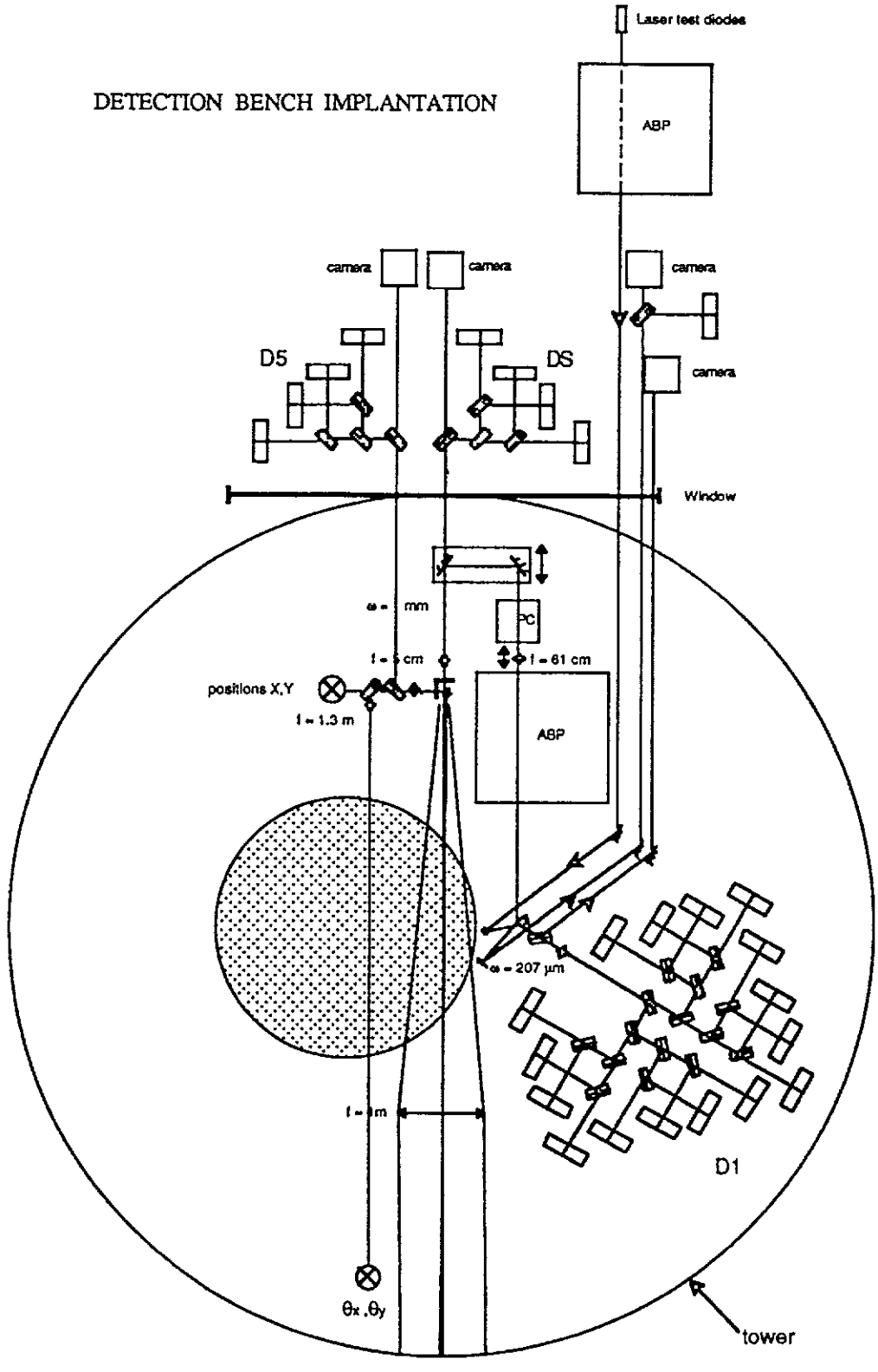

Δx = 7mm
Ω = 3.6 mrad
ω = 2 cm

Fig III-1

4200.3.1.The B beam line

The B beam is deflected by 90^0, an adjustable diaphragm is placed on both A and B beams, along their respective beam line, 2cm after the separation mirror. At level of the separating mirror, the beam radius is 400μm and at the focal point their waist size is 17μm.

Following the B beam line, after the diaphragm, a lens of focal length 5cm adjusts the beam before two beam-splitters, the reflectivities of which remain to be dzetermined. These splitters are used to deflect the B beam outside the tower, towards the detector D5 which is used in the interferometer locking system and towards a camera devoted to the beam shape analysis. Through these splitters the beam reaches directly a quadrant photodiode and via a lens of focal length 1.3m another quadrant photodiode. These two sensors are used in the alignment respectively in transverse directions and angles of the detector bench table.

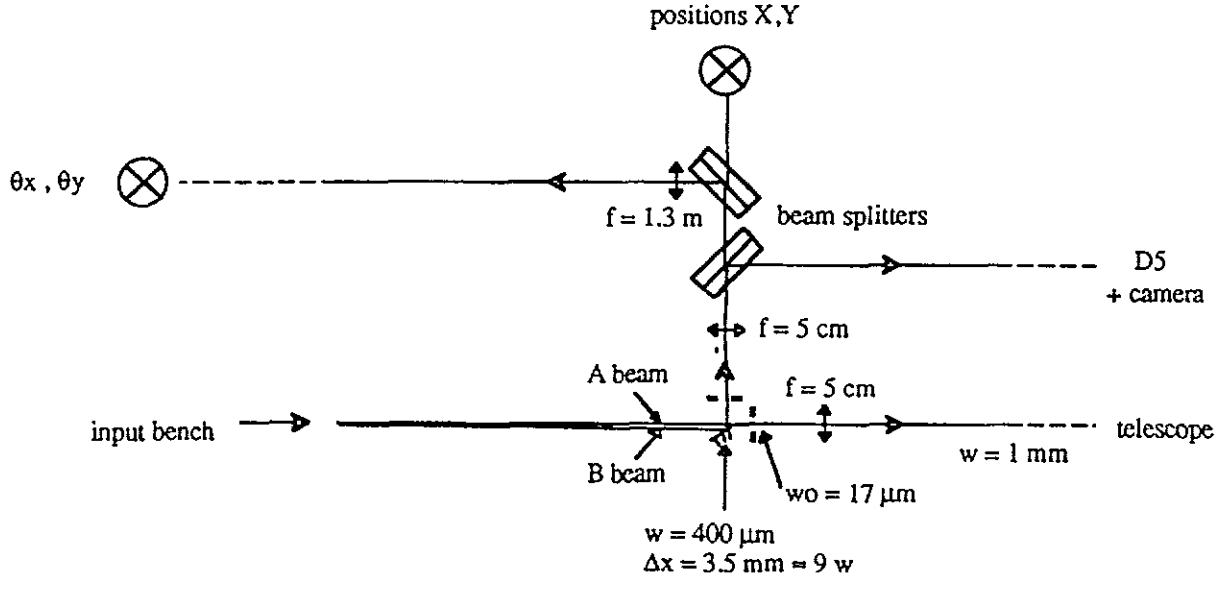

Fig III-2

4200.3.2.The A beam line

The A beam (see figIII-1), unaffected by the separation mirror, is adjusted by a lens (f=5cm) before being "U-turned" by a system of two mirrors deflecting the beam by 90^0 each. These two deflecting mirrors are installed on a movable table which allows to change the optical length in order to adjust the beam waist at the mode-cleaner level. As shown on figIII-1, a fraction of the A beam is directed outside the detection tower to allow a control of the beam status both by a camera and a detector DS (the S stands for start because this detector will be mainly used at the adjustment stage when starting the interferometer). Following the U-turn is placed a Pockel's cell, which is optional and will be used if needed

to lock the mode-cleaner (this locking operation still needs some R&D). An Automatic Beam Positioner (ABP)[2] is then used to adjust both in angle and in transverse position the beam at the mode-cleaner level.

4200.3.3.The Mode-cleaner Region

On figIII-3, an enlarged view of the mode-cleaner region is shown. The mode-cleaner itself is described in sectionVIII, the A beam enters the mode-cleaner, from the top on figIII-3, its TEM00 part is directed towards the detector D1 after a size adjustment, to fit the diodes' diameter, performed by a lens. A small fraction of this "cleaned beam" is directed outside the tower for controls with a camera and a photodiode detector.

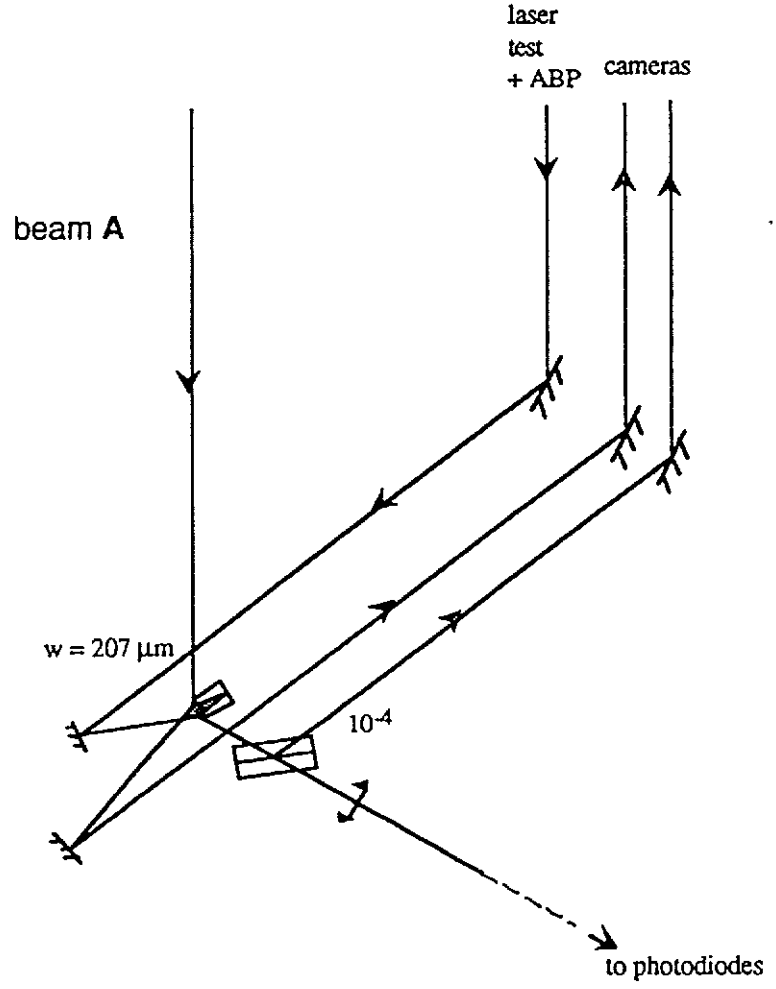

Fig III-3

The non TEM_{00} part of the A beam is reflected by the mode-cleaner and directed outside the tower towards a camera for suitable controls.

A laser beam, adjustable with an ABP in positions and angles from outside the tower, is directed on the output face of the mode-cleaner in order to be reflected along the filtered A beam. This laser line allows to test the response of the photodiodes D1, even when the interferometer is not working.

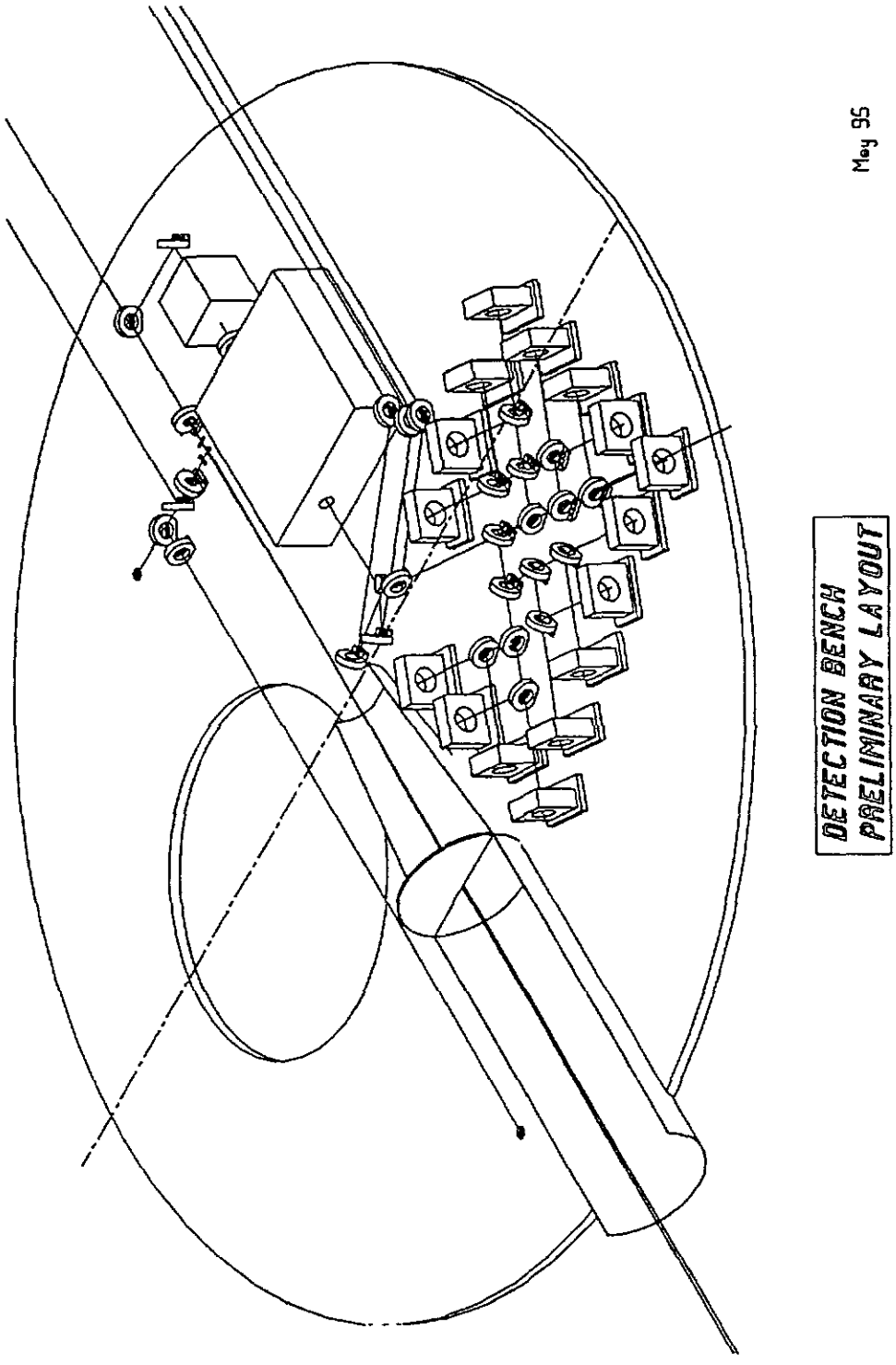

FigIII-4

On figIII-4 is shown a preliminary version of the implantation of the items described above, clearly this figure is only an illustration. Some detailed implantation studies have still to be done before reaching the accuracy needed for the construction.

4200.4. The Telescope

4200.4.1. Introduction

The two output beams from the interferometer, must be adjusted both in size and position at the detection bench level. In this section we describe the telescope which will fulfil the above mentioned requirements. The interferometer will be installed starting with its central region. Before the final large cavities are installed, there will be some time during which the central part will be operated as a small interferometer (the 1997 interferometer). This strategy will save time allowing to tune all the delicate items belonging to this central part. Here we describe the telescope foreseen at the final stage. The intermediate situation, which corresponds to a different beams geometry, will be adjusted to the final solution by the adjunction of a temporary optical system allowing to mimic the final beams properties.

4200.4.2. Requirements

The main beam in the interferometer is gaussian TEM_{00} with its minimum waist of 1.984cm. We take the position of this waist at the recycling mirror. Then, from the beamsplitter, two beams are directed towards the detection bench:

- The "dark fringe" beam, let us calle it the "A beam"
- The reflected beam from the beamsplitter, that is the beam reflected by the North arm cavity, which we call the "B beam".

On figIV-1, taken from J.-Y. Vinet and A. Marraud[3], is sketched this output beams configuration, one should note the off-axis position and the angles with respect to the main axis of beams A and B. The angle between beam A and B is 3.6mrad because of the 1mrad wedge-shaped beamsplitter. These beams, when reaching the detection bench, are nearly superimposed, there is therefore a need for a separation of the two beams. A further strong constraint, concerning beam A, is that it must match the detection bench mode-cleaner geometry which demands a minimum waist of 207μm[1].

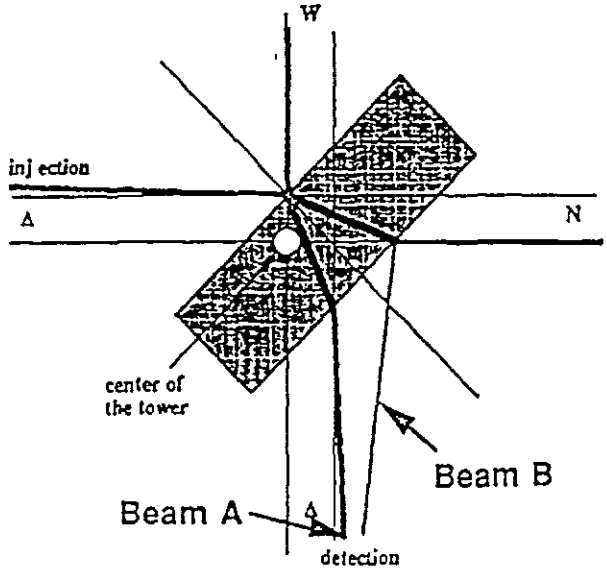

Fig-IV-1

4200.4.2.1. Beam A telescope

On figIV-2 the telescope scheme is shown, the corresponding numerical values are listed in tableIV-1

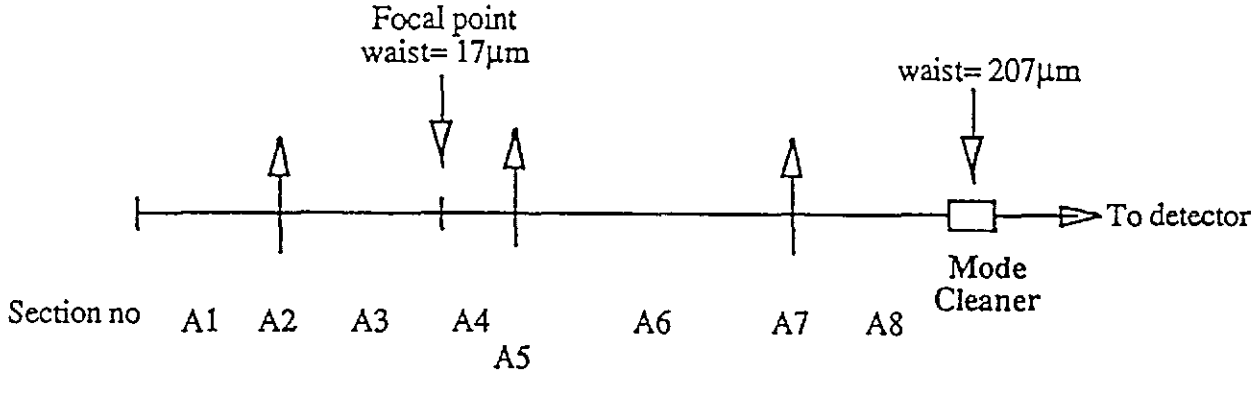

Fig. IV.2

The waist of beams A and B is assumed to be at the recycling mirror, that is, at the output port, located 5m before the detection tower centre which we take as reference abscissa. On figIV-2, this waist is at the beginning of section A1. The lens A2, of focal length 1m, is used to separate beams A and B, the diameter of this lens is taken as 230mm, the same as the beam splitter[4] because of the beams sizes. At the level of this lens the axis of beams A and B are separated by only 1.54mm, therefore we do not need to enlarge the lens size to ensure the free passage of the two beams through the same lens. At the focal point of lens A2, the beam waist is 17μm and the spots of beams A and B are separated by 3.6mm, the separation of these two beams will be simply done by inserting a plane mirror (not shown on figIV-2) slightly before this focal point, to deflect beam B out of the physical path of beam A. At the end of straight section A4 is located the lens A5 of focal length 50mm, the length of section A6, will be adjustable in order to allow the fine tuning of the beam geometry at the mode-cleaner level (see below). Finally a lens of focal length 0.61m, with a tunable position along the beam axis, is the last ingredient of this telescope which allows the beam A to match both in size and position the waist of the mode-cleaner. In figIV-3 are shown the beam waists around the end of section A3 and at the mode-cleaner level (end of section A8). From the VIRGO signal detection point of view, only the A beam quality is critical, both concerning the beam wave front deformation and the losses. Below we describe only the beam A telescope main components; the parts concerning the B beam, which contains only conventional mirrors and lenses, as well as the detailed implantation on the detection bench, are to be found in the global detection bench description.

Section Number	Type of section	Length (m)(*) or Focal length (m)	Diameter of lens (m)	Beam waist at end of Section (m)
A1	straight	4.54 (F)		$19.84\ 10^{-3}$
A2	lens	1. (F)	0.23	
A3	straight	1. (F)		$0.017\ 10^{-3}$
A4	straight	0.0503 (F)		$0.998\ 10^{-3}$
A5	lens	0.05 (F)	.025	
A6	straight	0.6097 (A)		$0.9455\ 10^{-3}$
A7	lens	0.61 (F)	0.025	
A8	straight	0.5638 (A)		$0.207\ 10^{-3}$

(*) F=fixed value, A= adjustable value. See text for details on beam adjustments. First section is at 6m from beamsplitter.

Table IV-1

4200.4.3.Power losses in beam A

With this beam telescope configuration, the beam remains (within a few mrad) collinear with the optical axis of the lenses, the deformation of the wave front is then minimised. The losses in the TEM_{00} mode corresponding to the deformations induced by the most sensitive lens, which is A5, have been evaluated to be $1.2\ 10^{-4}$. We then expect negligible losses from the lenses aberrations. The other losses expected from this telescope, will come from the absorption in the lenses material and from the non-perfect anti-reflection coatings of the optical elements. Carefully optimising these two parameters, the losses are expected to remain at the level of a few hundred ppm per optical element.

4200.4.4.Tuning of beam A

The non-TEM_{00} light coming from the interferometer and reaching the detectors will contribute to a decrease in sensitivity, it must therefore be rejected as much as possible. A first obvious way is to shield the detection bench from spurious light by allowing only the light coming along the A and B beam path to enter the detection tower. This will be done by a tube placed around the beams up to near the end of section A3 where is placed the separation flat mirror. A simple diaphragm cannot filter in an efficient way a Gaussian beam[5], but, as shown in the J.Y. Vinet note[6], one can make use of a combination of lens and diaphragm to filter out part of the unwanted modes. This will be done placing at the focal point of lens A2 a diaphragm (this diaphragm must be removable and adjustable in order to allow the alignment of the system).

Fig IV-3

The delicate point in this beam adjustment is the matching with the mode-cleaner beam geometry, this matching consists in a 6 variables adjustment:

- The minimum waist size
- The minimum waist longitudinal position which must be located on the symmetry axis of the mode-cleaner
- The two angular directions of the beam axis
- The two transverse positions of the beam axis

The minimum waist size and position, at the mode-cleaner level, is almost linearly dependent of the length of section A6 and of the longitudinal position of lens A7. This is displayed on figIV-4. These length and position will then be made remotely tunable.

The adjustment of the two angular directions and two transverse positions will be performed by an Automatic Beam Positioner[2] not shown on figIV-2. This device has been developed by the LAL team as a part of the VIRGO beam injection system.

Beam tuning at Mode Cleaner level

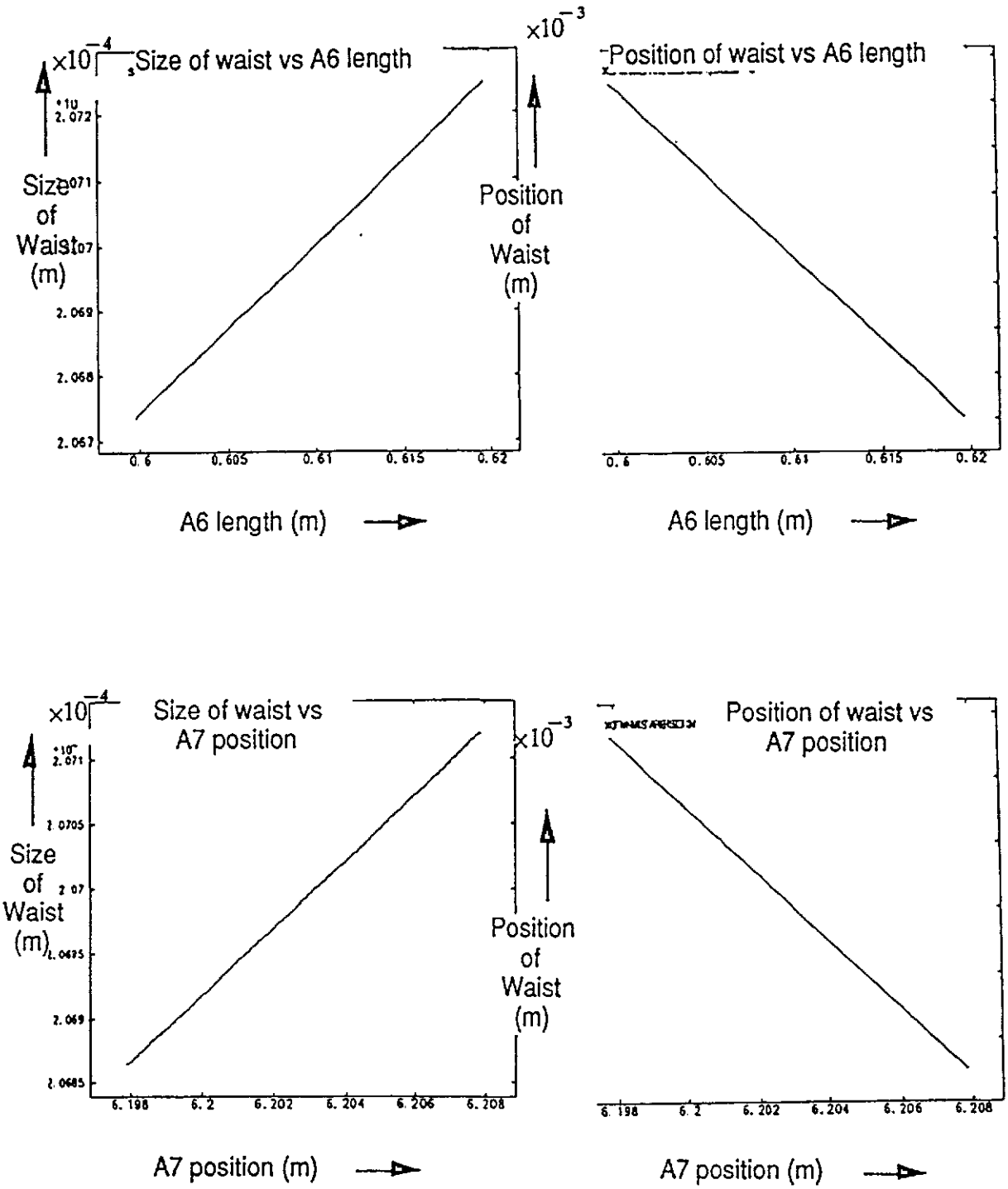

Fig-IV-4

4200.5.The position sensors

4200.5.1.Requirements

The main alignment constraint comes from the fact that the A beam must match the resonant beam of the mode-cleaner cavity. The demanded corresponding precisions have been estimated by a calculation of the mismatch corresponding to losses in the TEM00 mode and the corresponding induced signal. The obtained values at the mode-cleaner are:

- transverse displacement: $\sigma_x = 2\ 10^{-6}$ m
- angular displacement: $\sigma_\theta = 1.63\ 10^{-5}$ rd

4200.5.2.Sensors performance

These transverse and angular displacement of the A beam with respect to the mode-cleaner, correspond to a displacement of the bench table with respect to the beam A at the level of the detection tower entrance. Therefore a suitable continuously controlled displacement of the table will adjust the position and angle matching between beam A and mode-cleaner. We plan to use a redundant system, the ABP allows to tune this matching at the beginning and the table displacement will then follow the matching.

The position and angle displacements will be measured by the two quadrant photodiodes which measure the B beam position on the bench (see section III). The idea here is to use the fact that the beams A and B are related to each other because they come both from the beamsplitter, then a measurement on the B beam gives the position of the detection table with respect to the A beam. The use of the B beam to perform the position measurement is guided by two remarks: 1) its almost pure TEM_{00} content gives it a better defined geometrical shape, 2) the removal of some power from it does not affect the SNR (this is not the case for the A beam).

Taking into account of the optical matrices transfer of the bench, we can transform the needed precision at the mode-cleaner level to the precision required at the level of the quadrant photodiodes, the results are:

- for the transverse displacement diode: $\sigma_x = 0.4\ \mu m$
- for the angular displacement diode: $\sigma_x = 1.6\ \mu m$

4200.6.The detectors

As discussed in section II, the light power to be detected, after the mode-cleaner, that is on detector D1, amounts to about 0.72W in DC mode and to 0.67W at 12.5 MHz (that is the double of the modulation frequency). The detection must be performed with high quantum efficiency detectors working at high current and at MHz frequencies.

4200.6.1.The photodiodes

The above mentioned requirements do not correspond to commercial diodes. Instead of developing a new type of diode, we have investigated the working conditions of commercially available diodes under our conditions. This work, in its first phase has been published[7] and some further investigations have been pursued[8]. The main results can be summarised as follow:

- Photodiodes of the InGaAs type have a suitable quantum efficiency (higher than 85%)

- provided a careful attention is taken concerning the light density on the photosensitive part of the diode, it is possible to work far away the quoted limits given by the firms producing these diodes. A total power of 100mW on a photodiode of 3mm diameter can be detected with full efficiency up to 10MHz.

Our conclusion is that, provided we do not overexpose the diodes, this type of diode can be chosen. We have chosen the Hamamatsu producer because this firm proposes to perform a special coating on the diodes in order to guarantee a quantum efficiency of 95%.

4200.6.2.The detector arrangement

The maximum allowed power on a diode is a limitation which can be solved by splitting the total power to be detected into beams of less than 100mW. The solution we adopt is sketched on figVI-1. The beam is splitted into 16 equally intense beams using conventional 50% beam splitters.

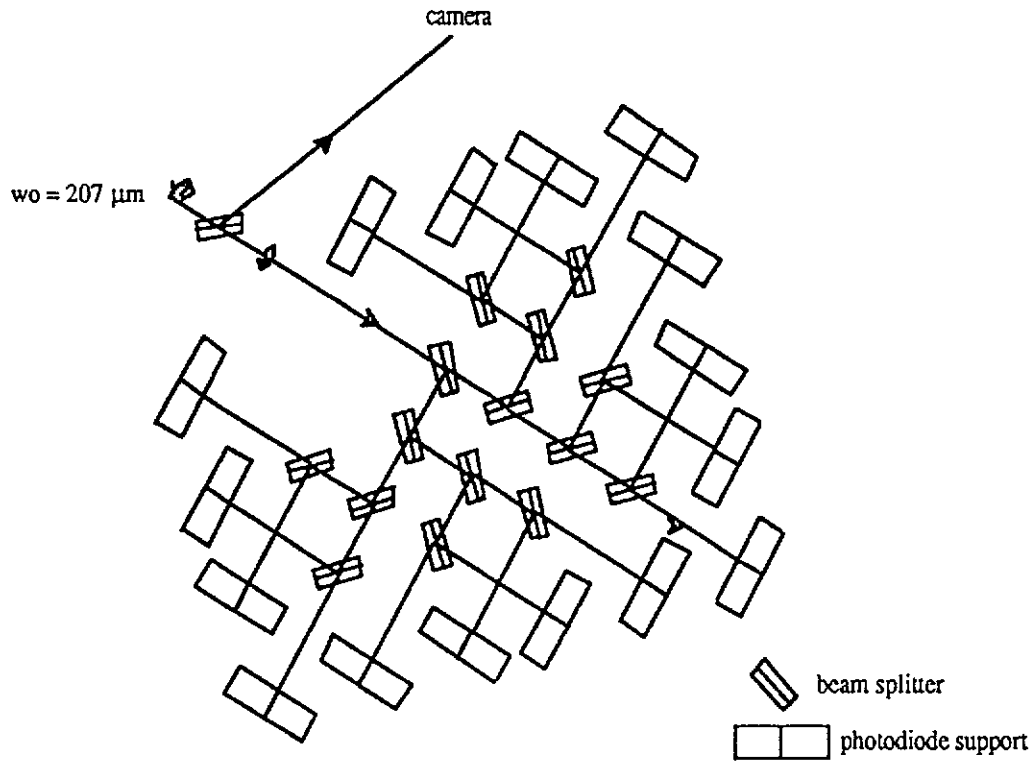

Fig VI-1

They are then directed towards 16 photodiodes. The mechanical arrangement is organised in such a way that, from the incident beam on the first splitter, the distance is equal to reach anyone of the 16 diodes. This peculiar geometry allows to have the same beam diameter on all the diodes, using only one adjusting lens placed before the detector (see figVI-1).

4200.7.The electronics

4200.7.1.Introduction

In this section we describe the analog electronics and cabling which will be implemented in order to transform the photodiodes current into a suitable signal ready to be digitised. The modulation frequency, envisaged in this reference solution, is 6.27MHz. It might be increased to 12 or 18MHz, note that a change of frequency implies some hardware work on this system and therefore is an important operation which cannot be envisaged without some preparation.

4200.7.2.Generalities

The interferometer's beams to be detected are used either for the signal detection or for the interferometer locking. The general principle is to organise the beams geometry in order not to exceed 100mW of light peak power per diode. Taking into account a "radiant sensitivity" of 0.8A/W, this implies a current of about 80mA per diode channel, the number of channels will then depend upon the beam power. Here we concentrate on the electronics associated to a single diode.

For example, the "dark fringe beam" will contain the following total power distribution[1]:

$$P(DC) = 0.7W$$
$$P(\Omega) = 0.8\ nW$$
$$P(2\Omega) = 0.67\ W$$

where P(DC) is the total DC power, $P(\Omega)$ is the power at modulation frequency, the value given here corresponds to a pure gravitational wave signal of $h = 2\ 10^{-23}$, $P(2\Omega)$ is the power at a frequency double of the modulation. Both the DC and double frequency signals will be used to monitor the system. The DC current will give a coarse response status of each diode, its main advantage is its presence even when the modulator does not operate, it also allows to check the relative optical positioning of the diodes independently of the phase difference introduced by each photodetector. The $P(2\Omega)$ signal monitoring will give a check about an eventual drift of the phase of the high frequency signal. Such a drift is a symptom of ill-functioning of the photodetectors, very important to monitor because of the delicate working point we use for these diodes[7],[8], here also only a coarse measurement is needed.

From ref 4:
the optical power in the Hz range is about 8 orders of magnitudes larger than the power above 10Hz
This amplitude difference is related to the locking scheme

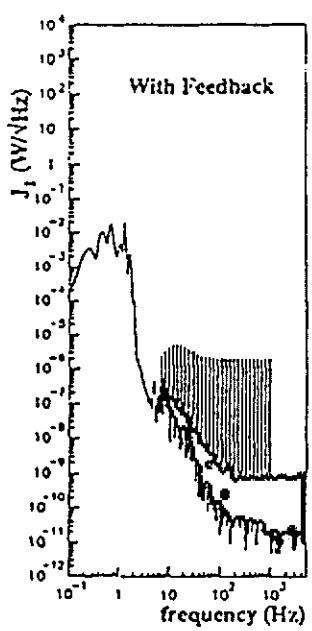

Fig VII-1

Concerning the signal at modulation frequency, the situation is more complicated. As can be seen on figVII-1, which is taken from ref9, the dynamical excursion of this signal is large, once demodulated. At low frequency it is dominated by the contribution from the locking system and its feedback. Above 10Hz, where we expect the gravitational wave to appear, one must be able to reach the shot-noise level, about 8 orders of magnitude lower. These demands impose severe constraints on the electronics. Moreover, since we use a frontal modulation scheme, on some channels, one should demodulate the signal in phase and in quadrature with respect to the initial modulation frequency. The consequences of these constraints and the solutions foreseen are described below.

4200.7.3.Design of a detection channel

4200.7.3.1.Dynamic range

For each photodiode, the peak current is 80 mA and the average current 40 mA. This induces a shot noise current of 10 $pA.Hz^{-1/2}$. The detection must be limited by the shot noise, so the current dynamic range is about 10^9 $Hz^{1/2}$
which is a rather high value for the detection electronics.

4200.7.3.2.2Ω component filtering

The 2Ω component can be filtered and attenuated relative to the Ω component. This residual 2Ω signal is sufficient to ensure the function of diodes' monitoring described above. To achieve this filtering, we use a short-circuited cable tuned to the modulation frequency ($L=l_{mod}/4$) so that , at Ω, the cable presents an infinite impedance, and, at 2Ω, a short circuit. Experiments have shown that such a system can reduce the 2Ω component by a factor of at least 100 (40 dB).

4200.7.3.3.Demodulation

The signal at Ω must be synchronously demodulated in order to recover the information used for locking and signal measurement. The input signal of the demodulator (mixer) must be a voltage. A 50 Ω resistor is used to transform the current supplied by the photodiode into a voltage. This voltage must be amplified to bring the signal at the maximum value required by the mixer.

4200.7.3.4. Filtering and ADCs

Because of the high dynamic range of the signal : about 7 orders of magnitude (fig VII-1), a single ADC will not be able to perform the digitisation. Two ADCs will be used : one below 10 Hz and another above 10 Hz with appropriate filtering and scaling amplification. A schematic diagram of the whole detection channel is given on figVII-2.

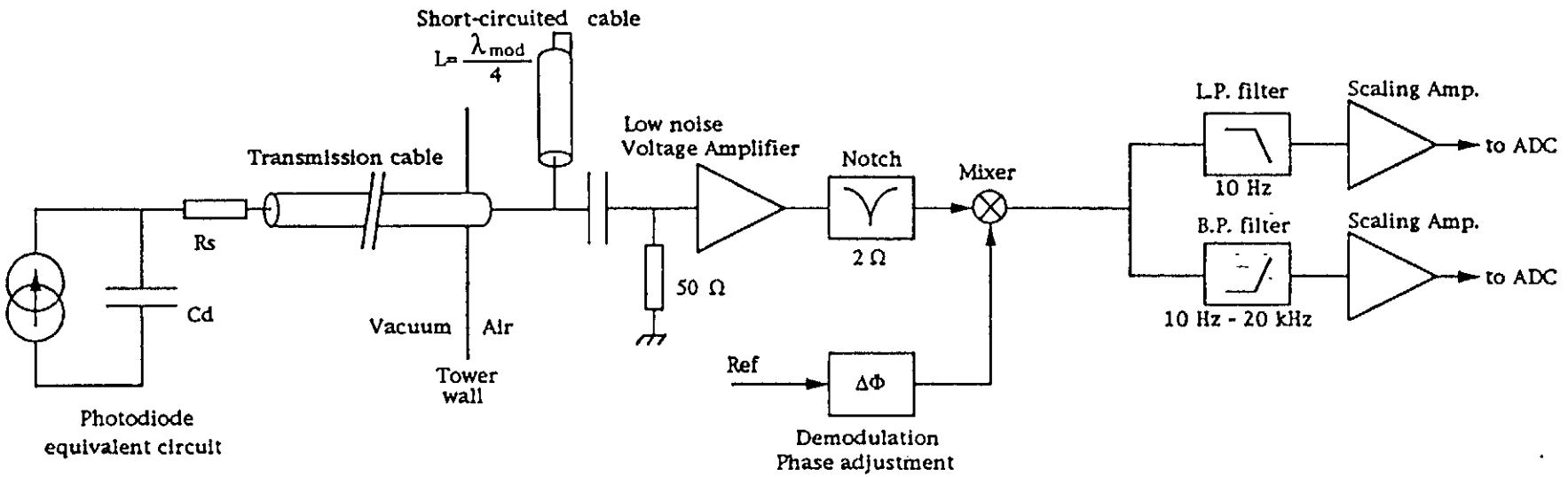

Fig.VI-2 Schematic diagram of a detection channel

4200.7.3.5.Noise Considerations

The electronics components should not add noise in order to keep the shot noise limited detection. The voltage induced by the shot noise across the 50W resistor (figVII-2) is about 5 $nV.Hz^{-1/2}$. Measurements have shown that the input equivalent noise of the electronics is 1.6 $nV.Hz^{-1/2}$[8].

4200.7.3.6.Frequency response

The equivalent circuit of the photodiode is a parallel capacitor and a serial resistor (figVII-2). The frequency limitation of the system is made by the photodiode itself. However, the detection channel can be used even at a frequency higher than the photodiode cut-off frequency. The signal and shot noise will be reduced by the same amount, so the signal to noise ratio will not be affected, provided the shot noise remain above the electronic noise.

4200.7.4.Implementation

4200.7.4.1.Bias Voltage

The reverse bias voltage is driven by an external DAC. The DC current and the applied bias voltage are measured by two dedicated circuits, the output ports of these circuits are connected to a multiplexing system which allows a channel by channel visualisation of current and voltage and to direct these informations towards the acquisition system ADC's. The bias voltage to the diode is ensured via a triaxial cable connected between the voltage supply and the end of the signal cable coming from the diode (see figVII-2 and figVII-3), as explained before, this cable which is located outside the tower, has a length equal to one fourth of the modulation wavelength.

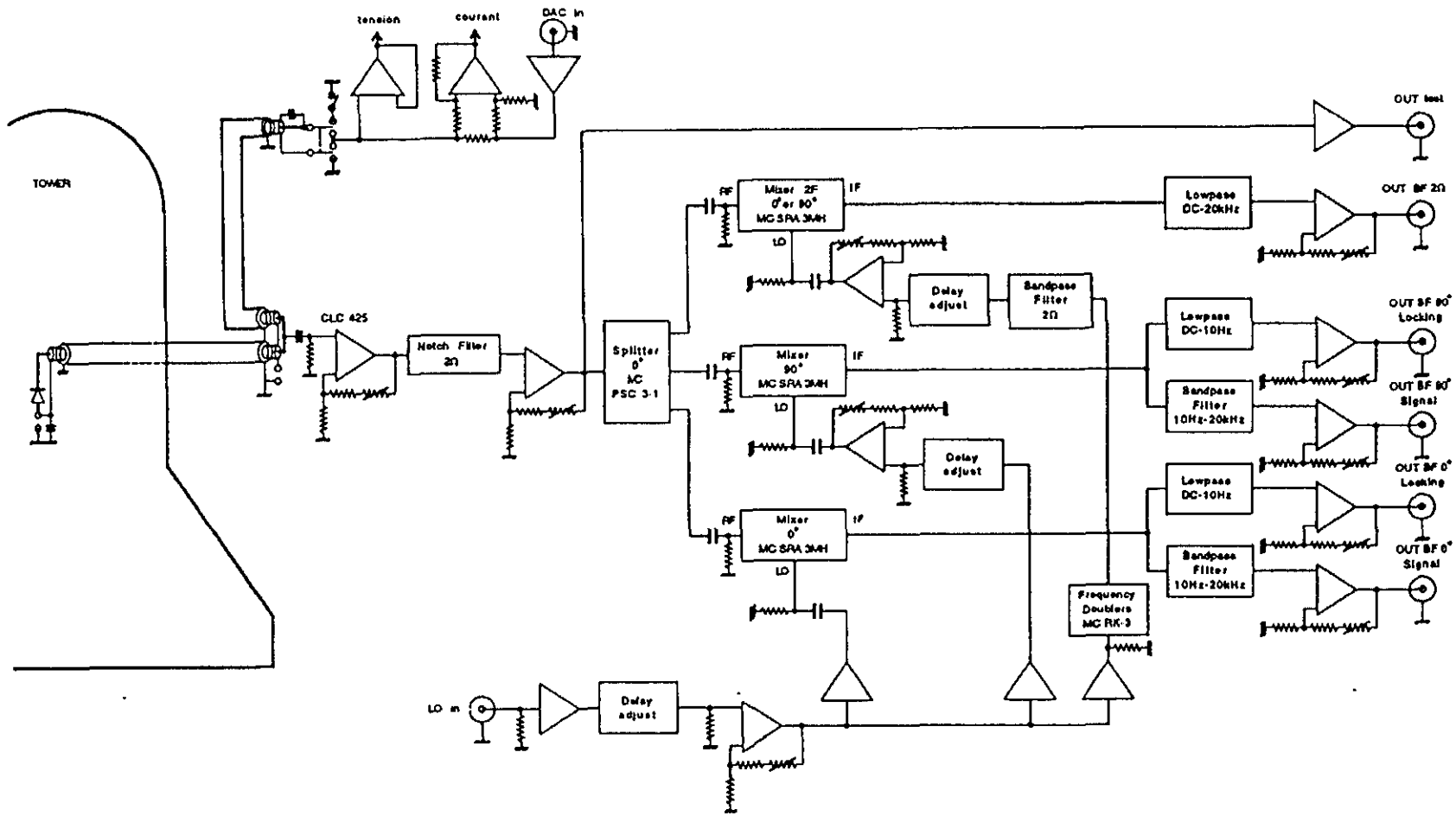

Fig VII-3. Schematic implantation of a detection channel

4200.7.4.2. Amplification

The operational amplifier used is the CLC425 circuit, which has the following characteristics:

- noise voltage = 1.05 nV.Hz
- gain bandwidth product =1.7 GHz
- offset = 100 μV
- gain = 10 to 1000
- dynamical range = 182.5 db.$Hz^{1/2}$

the gain of this amplifier is limited by the dynamical range of the signal used by the locking. Behind this first amplifier, is placed a notch filter at 2Ω with an attenuation between 60 and 80dB. A second amplifier allows the amplitude adjustment of the signals before the RF input port of the demodulators, via a 3-ways splitter with 0^0 phase shift. A test output is foreseen in order to allow a visualisation of the signal between the second amplifier and the splitter.

4200.7.4.3. Demodulators

Behind the splitter, are installed 3 demodulators, mini circuits SRA3MH:

- LO input = 13 dBm
- RF input = 9 dBm
- dynamics > 170 dB.

On the local oscillator, a tunable delay (10ns±50ps), allow to compensate for the delay dispersion, due to the electronics, on each electronics channel. On the first demodulator, the signals on the RF and LO input port are in phase within ±50ps. On the second demodulator, the signals on the RF and LO input ports are set in quadrature using an adjustable delay (40ns±50ps) on the LO signal. The third demodulator is used for the 2Ω signal, the mini circuit RK-3 is used to double the local oscillator frequency, the output signal from this circuit is filtered by a band-pass filter at 2Ω. The signals at the RF and LO input are adjusted in phase using a variable delay (80ns±50ps) on the LO signal.

4200.7.4.4. Filtering and output levels

The output signal, from the 2Ω demodulator, is filtered in a low pass filter (DC to 20kHz) and then directed towards the ADCs after suitable amplification. As shown on figVII-2 and figVII-3, both the in-phase and in-quadrature demodulated signals are filtered by a low pass filter (DC to 10 Hz) and by a band pass filter (10Hz to 20 kHz) before a suitable amplification is performed to match the ADC range needed. It should be noted that the in-phase and in-quadrature demodulation is needed only on some channels, it will be implemented only when necessary.

4200.7.4.5. Implantation

All the electronics (described above for one channel), is implanted on a VME printed circuit board.

4200.8. The mode-cleaner

The status of the detection bench mode-cleaner is at the prototype level. Some R&D are needed before one can ensure a safe and well understood device. The envisaged solution which, as a theoretical object, fulfils our requirements[1] consists in a monolithic triangular shaped fused silica Fabry-Perot. On figVIII-1 the principle is sketched: the dark fringe beam (A beam) enters the cavity with an incident angle of 70^0 , after filtering the TEM_{00} content of the beam exits symmetrically towards the detectors D1.

The optical half length of the cavity is taken to be 4cm and the radius of curvature of the spherical end mirror is 0.44m. These choices together with a cavity Finesse between 100 and 200 (the best value is to be defined when the mirrors losses will be measured), correspond to the optimised values found to maximise signal/noise[1]. The method we will use in order to lock this cavity on the TEM00 mode is still under investigation, it will be the main object of the R&D work which remain to be done concerning this apparatus.

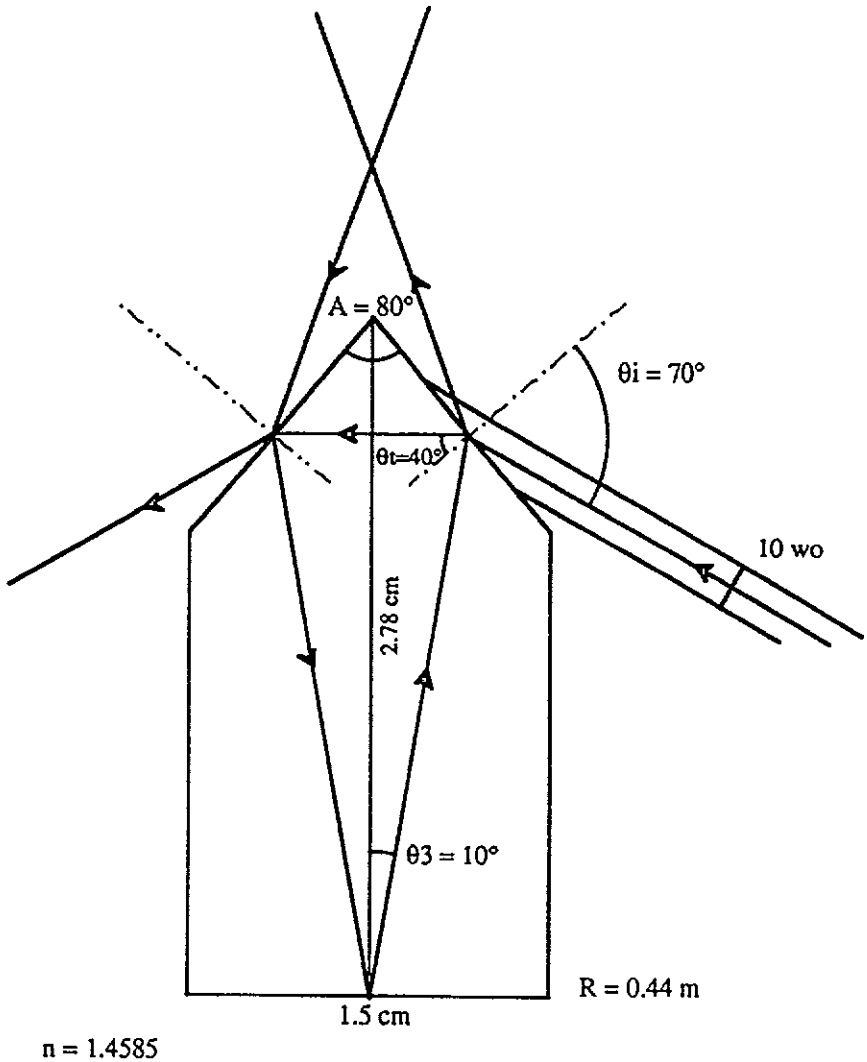

Fig VIII-1

4200.9. References:

1) A. Dominjon, R. Flaminio, R. Hermel, M. Yvert., Annecy-LAPP team
Detection bench parameters optimisation, a first step
VIRGO Note NTS95-010

2) An Automatic Beam Positioner (ABP) has been designed and constructed by the Orsay group. Contact: C.N. Man, LAL
See also: Contrôle numérique de l'ABP
H. Heitmann (LAL) VIRGO note 18/08/1994

3) J.-Y. Vinet, A. Marraud
Prism Splitter. VIRGO Note PJT 94-016

4) C. Nary Man Definition of the VIRGO interferometer Mirrors
VIRGO Note PJT94-024

5) A. Dominjon, M. Yvert Mode cleaning with diaphragms
VIRGO Note NTS95-007

6) J.-Y. Vinet Spatial filtering by holes and lenses
VIRGO Note NTS95-012
see also NEWPORT Catalogue , Spatial filters, page A18

7) Photodiodes selection for the VIRGO detector, the first step
B. Caron; A. Dominjon; R. Flaminio;R. Hermel; J.C. Lacotte; F. Marion; L. Massonnet;
R. Morand; B. Mours; D. Verkindt; M. Yvert
LAPP-EXP-94-12 Presented by A. Dominjon at the
6th Pisa meeting on advanced detectors:
Frontier Detectors for Frontier Physics 22-28 may 1994 La Biodola Isola d'Elba
to appear in NIM
And VIRGO note PJT94-014

8) A. Dominjon, R. Hermel, J.C. Lacotte,L. Massonnet, M. Yvert, Annecy-LAPP Team Detection diodes, the second step VIRGO note NTS95-009

9) B. Bourdas, B. Caron, F. Marion
Study of two control strategies for the locking in the case of frontal modulation
VIRGO note NTS95-006

LARGE MIRRORS

4300.1.General Description

4300.1.1.Introduction

The technology required for the Virgo optical components coatings, whose specifications are very severe, is the one used in the gyrolaser applications: the reactive Dual Ion Beam Sputtering (D.I.B.S.). The deposition technique leads to dense (near bulk density) and very stable films (no columnar microstructure).

4300.1.1.1.Deposition process

In the D.I.B.S. process, we use a broad-beam Kaufman ion source or equivalent which generates a spatially well defined , monoenergetic (between 700 and 1300 eV) and positive ion beam to sputter the material (Target) we want to deposit.

This beam (argon ions or noble gas ions) is neutralized by the electron injection : this can be achieved by a hot tungsten filament or others electron sources such as a plasma bridge neutralizer or a hollow cathode. The neutralization has two purposes : at first, it prevents the substrate and the target from discharge because we are using dielectric materials; secondly, it prevents beam spread by repulsion between ions.

The planar sputtered target (Silicon dioxide, Tantalum, Tantalum pentoxide) is tilted so that the ions coming from the source are incident at an angle of approximately 60° to maximize the sputtering yield of the target.

The purity of this target is a crucial point and it should be as high as possible to prevent the layers from contaminations.

The sputtering ion beam has an elliptical cross-section to minimize the ellipticity of the beam footprint of the tilted target.

A second ion source, directed to the substrate, is used to control the stoechiometry of the growing film with oxygen ions. This source is equipped with an appropriate grid to permit the generation of low energy ions (50-100 eV).

Another important point in the D.I.B.S. process is the size of the coater where the base pressure ranges from 10^{-7} to 10^{-8} Torr : the box coater has to be large to prevent contaminations from interactions between ions and the walls. Thus, the size should be well adapted to the diameter of the substrate we have to coat. Moreover, the chamber geometry must be design to avoid gas phase interactions for a given working pressure (between 1 to 4 10^{-4} Torr); so, the atoms sputtered from the target reach the substrate with a very low probability of energy losses.

4300.1.1.2. Process justification

A comparative study (Electron gun evaporation, Ion assisted deposition, R.F. diode deposition) has been done and it has shown that only the D.I.B.S. process is able to obtain very low losses.

The losses are due to absorption and scattering : the absorption can be reduced at a value ranges from 5 to 15 ppm for all the techniques but the scattering remains high (100 - 300 ppm) for these techniques except for the D.I.B.S. (5 - 50 ppm). This latter point is the key of our choice.

By decreasing the losses, higher reflectance values are achievable.

Moreover, the layers realized with the D.I.B.S. technique have special properties: due to a very low porosity, we can mention for example a high thermal stability, scratch and flux resistance.

As the deposition speed is low (a few Å/s), it is easier to monitor the thickness homogeneity, to control the growing structure and the layer composition. Nevertheless, to be able to obtain low loss samples, the environment around the deposition chamber must be very clean to keep the dust particles to a minimum : the elaboration, the characterization, the transportation and the mounting of the Virgo components has to be done in clean conditions, typically in class 10 or better.

4300.1.2. State of the art with regard to the Virgo F.C.D. specifications

Until now, we have undertook a R&D study to improve all the performances of our coatings. Moreover, the ESPCI group develops tools to allow us to optimize the coatings fabrication to reach the required goals.

To be able to do that, some equipments have been built or developed to characterize :

* the scattering (CASI scatterometer @1064 nm from TMA) and the transmission value; with this system, mappings are possible. To do accurate and sensitive measurements, a clean environment (class 1) has been required.

* the absorption (photothermal absorption measurement system @1064 nm)

* the cleanliness (particle counter); this point can also be evaluated with a scattering measurement. The two methods are totally complementary and very sensitive.

4300.1.2.1.The scattering level

We have reached @1064 nm a scattering level close to 1 ppm on 1 inch diameter which is an average value on the entire surface of the sample. That means all the eventual point defects are included; consequently, this is a very realistic value.

This improvement (about 20 times) is due to several factors.

The first one is the use of new micropolished silica substrates from PMS which have neither scratches nor digs (the RMS microroughness is lower than 0.4 Å).

The second factor of improvement is linked to a new cleaning technique which guarantees a very low particles contamination level. But, to preserve the cleanliness, all the sample manipulations must be done under class 10 or better environment : this is a crucial point.

4300.1.2.2. The absorption level

At ESPCI, the optimization of the "Mirage" detection using a quasi collinear geometry of the pump and the probe beam has led to a sensitivity better than 10 ppb which is good enough to probe absorption losses in the ppm range. This level of sensitivity does not need to be improved in the near future.

The real mirror absorption level @1064 nm is now 1 ppm on 1 inch diameter. To reach this low value, an improvement of the deposition process has been done to reduce the more we can the layer contaminations which controls the absorption level. To converge and find the best solution, some S.I.M.S. (Second Ion Mass Spectrometry) and E.D.S. (Energy Dispersive X-ray Spectrometry). analyses have been done.

4300.1.2.3.Total losses and birefringence measurements

The total losses measurement is more "classical", nevertheless the ESPCI group had a specific approach in order to take advantage of the specificity of their YAG laser (average power 1W, 200 ns pulses at 2 kHz highly multimode).

The sensitivity reached is 1 ppm which is enough for the large mirrors of Virgo.

he reproducibility is rather good, the main problem was the residual absorption of the gas (air, N_2) between the two mirrors; it has been overcome by evacuation of the optical path.

Secondly, using a modulated birefringence added to the static one, the ESPCI group has reached a sensitivity of 10^{-5} rad, large enough to test the Virgo parts which will be crossed by the light.

4300.1.2.4.

4300.1.2.5.Centering, Mirrors and antireflective coatings performances

A multidielectric mirror only reflects the light on a small domain of wavelength (typically 200-250 nm) with a high efficiency; the middle of this band corresponds to the centering wavelength which must be 1064 nm in our case.

The centering of the coating at the good wavelength (1064 nm) is another important point we have studied; it controls the optical performances of the coating and, particularly, the transmission loss of the mirrors.

A new centering method has been developed which allows us to guarantee now a difference between the experimental centering and the desired centering less than 5 nm. Thus, the transmission variation is quite negligible.

Thanks to very low absorption and scattering losses, high reflectance values can be achieved (R>99.995%) and, for antireflective coating, we can also have good optical efficiency (T#99.9945%)if we monitor precisely each monolayer. The Virgo F.C.D. specifications are reached on 1 or 2 inches diameter.

4300.1.2.6.The thickness uniformity

The coating homogeneity is critical for the wavefront preservation in the interferometer. This point is evaluated with a ZYGO Mark IV xp (λ = 633 nm) which is now in Lyon. This system has been tested preliminarily at ESPCI. It has been demonstrated that the reproducibility of the measurement is 4 nm if great care is taken in the positioning of the optical piece. Moreover, the reference mirror was found to be better than 10 nm over 50 mm.

This interferometer allows us to measure low spatial frequencies (<< a few mm^{-1}).

A simulation program has been developed to optimize the thickness distribution of the coatings by changing the sample holder and the target angles. Moreover, a new sample holder, which has a planetary motion, has been built.

This leads to an homogeneity on monolayers between 3.10^{-3} and 8.10^{-3} on 2 inches; on 80 mm diameter mirrors, a uniformity of $\lambda/40$ (λ = 633 nm) peak to valley on 25mm and $\lambda/10$ peak to valley on 70mm has been reached (note : this value has not been obtained with the best angle conditions).

Moreover, with the ZYGO Mark IV, we are trying to evaluate the mechanical stress of our coatings which has an important role on the wavefront shape.

Other systems have been developed at ESPCI to explore other spatial frequencies domains.

At first, a system based on slopes measurements has been built (medium range spatial frequencies

~1 mm^{-1}). The required sensitivity for all the terms of the surface deformation whose order are larger than 2 (curvature) has been reached.

Secondly, for high spatial frequencies (<< 1 mm^{-1}), a polarizing microscope interferometer

(λ=0.67 μm) of picometric sensitivity (in the range of 10^2-10^3 mm^{-1}) provides informations which can be compared to the results of the scatterometer but with a more local approach.

4300.1.3.The wavefront improvement

The wavefront preservation is a priority at the moment because the Virgo specifications on the maximum wavefront deformation are not satisfied. A simple planetary motion is not enough.

That is why a small robot, piloted with a computer, is under construction and it will be evaluated and tested during the first semester of 1995 in the present coater.

An other advantage of this system is that the distance between the substrate and the target will be greater : this will be a more favourable case to homogenize in a better way the layer thickness.

Probably, this system alone will not be sufficient to reach the goal : the use of masks between the substrate and the target gives good homogeneity results; but to reach the Virgo specifications, a planarization method should also be used to make the final correction (a few hundred angströms).

The principle of this method is to add locally on the SiO_2 last layer of the multilayer stack a small amount of SiO_2 , where it is necessary, to obtain a surface as plane as possible. To have an idea of the wavefront topography before this corrective coating, an interferometric measurement is used.

Two solutions are studied to realize the corrective treatment :

* on the one hand, a correction pixel by pixel through a hole can be done.

* on the other hand, a grid with variable density of holes on its surface can also be used.

The advantage of the second solution is that it takes less time to realize the corrective coating.

To validate the principle of this method, we checked that the absorption and the scattering losses are not locally deteriorated by the deposition of a small amount of SiO_2 on the last layer. It has to be pointed out that the correction must come after the thermal treatment of the sample : indeed, it stabilizes the optical performances and relaxes the constraints which modifies the wavefront.

The same principle will be used for the large mirrors in the future large coater.

4300.2.Specifications and constraints on the substrates and the coatings

4300.2.1.interferometer

It has been decided to build a small interferometer in 1997 to begin to test all the sub-systems of Virgo : the interferometer is a simple Michelson formed by the recycling mirror M_R and the input mirrors M_E.

Different solutions concerning the size and the shape of the optical components have been studied; the chosen solution is the one with small substrates of 2 inches (except for the beam splitter) instead of large substrates. Thus, the components can be made in the present D.I.B.S. coater in Lyon.

The specifications of the 1997 interferometer components are summarized in the table 1 below. The substrate quality must be the same to the one we are using at the moment. The losses (absorption + scattering) should be in the range of 1 ppm.

The coating of the curved substrate (input mirror) is in fact not a technical problem. The problem is the feasibility for the polisher to obtain a substrate with the desired curvature R and with a good accuracy (the accuracy on the radius of curvature is ± 2-3%). In fact, there is a safety margin because what is important is the ratio R/L where L is the length of the cavity.

Consequently, if there is a small difference between the two input mirrors curvatures, the length of each cavity can be adjusted for the interferometer to work well.

Moreover, in parallel with pure metrology, the ESPCI group will collaborate with the Orsay group in order to develop the simulation programs for Virgo 97, get the theoretical limit of this interferometer and define the optimized specifications of the optics. This program will also allow the Virgo teams to validate and to improve the SIESTA global simulation code developed by the Annecy group.

The ESPCI group will mainly focus its attention to the influence of the wavefront defects at various spatial frequencies.

Table 1 : Virgo 1997 optical components specifications

Component	M_R	M_{E1} , M_{E2}	B.S.
Material	SUPRASIL 312	SUPRASIL 312	SUPRASIL 311
Diameter (mm)	50	50	230
Thickness (mm)	15 - 20	15 - 20	55
Shape Face 1	Flat	Concave R = 83 to 102 m	Flat
Shape Face 2	Flat	Flat	Flat
Angle between the faces	Wedge 0.3 mrad +/- 15"		Wedge 1 mrad +/- 15"
Incident angle	0°	0°	45°
Coating diameter (mm)	40	40	50
Coating Face 1 (S polarization)	A.R. $R<10^{-3}$	H.R. R>99.99 % T > 10 ppm	T = R = 50% +/- 0.5 %
Coating Face 2 (S polarization)	R = 98.5 to 99.5 %	A.R. $R<10^{-3}$	A.R. $R<10^{-3}$
Surface Deformation Face 1 coated Pick to valley (nm)		10 nm on Ø=10 mm 35 nm on Ø=40 mm	10 nm on Ø=10 mm 35 nm on Ø=50 mm
Surface Deformation Face 2 coated Pick to valley (nm)	10 nm on Ø=10 mm 35 nm on Ø=40 mm		
Substrate Surface Deformation	10 nm on Ø=40 mm		<10 nm on Ø=200 mm (PMS data)

4300.2.2.The 1999 Virgo interferometer

In April 1995, the shape of the recycling mirror M_R has been adopted : it will be a plane-convex mirror

The specifications for the other components are listed below (Table 2).

Table 2 : Virgo 1999 optical components specifications

Component	M_{X1} , M_{X2}	M_{E1} , M_{E2}	M_R	B.S.
Material	ULE or other	SUPRASIL 312	SUPRASIL 312	SUPRASIL 311
Diameter (mm)	350	350	120	230
Thickness (mm)	200	100	30	55
Shape Face 1	Concave R = 3450 ± 100 m	Flat	Convex 4-5 m	Flat
Shape Face 2	Flat	Flat	Flat	Flat
Angle between the faces				Wedge 1 mrad +/- 15"
Incident angle	0°	0°	0°	45°
Coating diameter (mm)	280	100	100	200
Coating Face 1 (S polarization)	H.R. R>99.995 % T > 10 ppm	A.R. $R<10^{-3}$	A.R. $R<10^{-3}$	T = R = 50% +/- 0.5 %
Coating Face 2 (S polarization)	A.R.	R # 88 %	R # 92 %	A.R. $R<10^{-3}$
Surface Deformation Face 1 coated Pick to valley	10 nm on Ø=110 mm and 35 nm on Ø=280 mm			10 nm on Ø=60 mm and 35 nm on Ø=200 mm
Surface Deformation Face 2 coated Pick to valley		10 nm on Ø=40 mm and 35 nm Ø=100 mm	10 nm on Ø=40 mm and 35 nm on Ø=100 mm	
Substrate Surface Deformation				<10 nm on Ø=200 mm (PMS data)

The ESPCI group will be in charge of testing the quality of the large optical pieces which are passed through by the light beam and which will be used in the final antenna. The main test will be : homogeneity of the refractive index, local defects, birefringence, absorption losses for the silica substrates.

Direct contact with European and American glass companies will continue during the various phases of the project in order to get state of the art materials.

To be able to realize such large samples, new facilities have to be built in Lyon.

At first, a new plant must be built with all the clean areas class 1 needed for the process.

Secondly, a new large coater (a cube of 2.5-3 m) must be conceived to be able to coat such large samples. The cleanliness of the large substrates before deposit is also a crucial point; so, a new large wet cleaning machine is needed.

At last, a new metrology, a handling and packaging method have to be developed for the large components.

Concerning the metrology, the major task of the ESPCI group is to build the corresponding equipment to be installed in Lyon with a scale matching the Virgo mirrors. If most of the difficulties have been overcome, there is still work on the wavefront control which will be coupled to the large coater where the corrective coating will take place and which will take advantage of the handling and moving systems of the coater.

4300.3.Description of the "Large mirrors "sub-system

4300.3.1.Introduction

At the moment of the Final Design conception, there are several points which are still not well defined and frozen, for example concerning the large coater and the corrective coating.

Some strategies are in balance because we have not enough data to make a satisfying choice. We hope, in the next months, to be able to solve all the problems mentioned.

Nevertheless, this paragraph will contain a detail presentation of what should be done to realize the Virgo large mirrors.

4300.3.2.The Virgo optical components

4300.3.2.1.The substrates

As it is mentioned in the Virgo 1999 specifications, the nature of the bulk material of all the optical components has been chosen:

- SUPRASIL 311 form Heraeus for the beamsplitter
- SUPRASIL 312 from Heraeus for the input mirrors and the recycling mirror
- ULE from Corning or other for the end mirrors.

An other American company (OHARA) produces a glass similar to the ULE; but, nevertheless, it has a thermal stability three times worse.

The beamsplitter has already been purchased because it will be used in the Virgo 1997 interferometer. The polishing made by Research Electro-Optics (R.E.O.) will be achieved in the middle of 1995.

Except for the beamsplitter, the choice of the polisher has not yet been done. A list of the manufacturers capable of doing micropolished substrates can be performed : the French companies REOSC and SAGEM, R.E.O., PERKIN-ELMER, ITEK OPTICAL from the Litton group, ZEISS.

Because the polishing quality has a strong influence on the scattering level, we have fixed very strict specifications on the polished surfaces :

* RMS roughness : 0.3 +/- 0.1 Å (measured with the "Micromap" system)
* Pick to valley : 5 +/- 1 Å on the coating diameter
* Surface deformation : < 10 nm

As we know, R.E.O. is able to guarantee such performances.

Moreover, as the final shape of the mirrors is not at the moment frozen, we are not in a hurry to make a choice. Nevertheless, in 1996, the bulk material will be purchased.

The ESPCI group is in charge of the large polished substrates control to see if the specifications and the requirements are respected : homogeneity of the refractive index, birefringence, absorption losses of the silica but also control of the microroughness and the flatness.

To avoid problems of manipulation by too many people, it will be easier and safer to do these controls in Lyon, near the large coater and the cleaning station, because all the infrastructure (essentially the white rooms) will be in place.

4300.3.2.2.The coatings

After having checked that the substrates have the good specifications, we have to prepare them for the coatings.

l Because of their weight, new tools have to be developed to handle them the right way. To do so, we will get informations from people who are used to manipulate large telescope components (REOSC, MATRA, SESO).

l Concerning the cleaning, a prototype of a wet cleaning station is under test. A lot of technical problems have occurred leading to a waste of time; thus, we are still waiting to perform some tests to validate the process. Nevertheless, we have learned a lot and it will be easy to avoid these problems for the future large cleaning system which is the only way to clean big substrates.

The cleaning station needs ultra pure water which is heated during one part of the process. A special care should be taken for a high power line of the ultra pure water heater; indeed, this equipment will need about 400 kW for a very short time.

l The optical performances of each Virgo component is summarised in the table 2. The losses (Absorption + Scattering) should be in the range of 1 ppm.

These losses will be measured on test samples which will be put on several places of the large sample holder. By putting all the mappings together, we can make a good estimation of the scattering losses for example. A reflection and transmission measurement will also be performed.

Concerning the corrective treatment to restore the wavefront, it will be described in the next paragraph.

l Before shipping the coated components, they will be cleaned an other time and packaged in a box that will conserve the cleanliness of the sample during the transportation. We have already realized some metallic boxes which gave good results.

4300.3.3. The coater : Technical description

a) The shape of the coater has not yet been frozen : it can be a cylinder or a parallelepiped

(2.5 - 3 m). The first solution is the best to reduce the weight of the system : it can be decreased by a factor of 30 %.

Nevertheless, we are used to work with parallelepipedic coaters and we have a great skill on this kind of systems; moreover, it is easier to install all the coater parts in such a vacuum chamber.

b) At the moment, we are using an ion source with filaments; it can not be the same in the future coater because of the short filament lifetime (≈ 30 hours). Indeed, in the large coater, the process will last at least one hundred hours.

The solution of this problem is to use a Radio-Frequency (R.F.) ion source. But our main interrogation is to know if this source is able to work hundreds of hours without any drop out. Thanks to R.E.O. informations, we know that the Oxford source does not work well during a long time.

Moreover, people from Ion Tech told us that they solved that by putting a third grid on their source to protect the two active grids; we would like, before making a choice, to verify this information.

There is an other alternative to the R.F. source: this is the Hollow Cathode. It has been demonstrated (R.E.O.) that the couple Hollow Cathode (to sputter) and the Plasma Bridge Neutralizer (to neutralize the beam) is working well during very long runs. The drawback of the Hollow Cathode is that the spare parts are very expensive and that they must be changed very often.

We will choose the right solution as soon as possible.

Nevertheless, the source size will be quite small (about 20 cm) because larger sources (40-50 cm) are not enough reliable and also because they are only used for etching. These sources will be water cooled.

At the moment, we are developing a new coating simulation program : a real coating in the future large coater can be simulated; thus, we will see if the deposition speed with one source is not too small. Otherwise, two sources will be eventually used in parallel to obtain process times which are acceptable.

Concerning the targets, their size should be the double of the source size (about 40 cm).

In our small coater, high purity targets are used (99.99 %); it should be the same quality for the larger ones. We have to check if the target manufacturer can provide high purity materials, whatever the size we will choose, to minimize the layers contamination.

In the coater, the target movement will be an axial rotation.

d) The primary vacuum (up to 10^{-2} Torr) will be achieved in 30 minutes with two oil free groups (roots + dry pump); the base pressure (about 10^{-7} Torr) will be obtained in 4 hours with two cryopumps. These calculations have been done for a 2.5 meters cubic chamber.

The chamber walls are electropolished; the coater will also have double walls to make the cleaning of the system easier.

At last, to suppress water vapour in the chamber, a « Polycold » will be used in vacuum.

e) To control the process in-situ, we will only use a quartz balance which is a very reliable system. In our present chamber, we are using only one quartz. Probably, in the future coater, several quartz will be used to increase the accuracy of the control.

f) The coater will be piloted with a real time system using C or C++ language; the connections between the computer and the coater will be cables or fibers. The software will be home-made or bought from a company ; it will depend on who will build the coater.

There are two solutions :

☒ The coater will be entirely built by a manufacturer with our specifications; the problem of this solution is that the collaboration with the manufacturer will be close to zero. Moreover, it will be difficult to follow in detail the construction of the machine because there are only foreign manufacturers. Thus, we may have some unpleasant surprises when it will be delivered.

* A consortium will be in charge to develop and build the coater. The advantage of this solution is that we know very well the people in the consortium (they have a great skill in vacuum systems) and, also, that they are located near Lyon; thus, we will be in direct contact everyday. Moreover, the integration of the coater in the Virgo plant in Lyon can be done as soon as the main work is finished : the coater can be mounted in the basement of the building in parallel with the final installation of the rooms (white rooms for example) on the ground floor. As soon as everything is finished, the coater will be put in the class 1 white room with an elevator. Time will be saved with this solution.

g) On one door of the coater will be placed the robot which will support the silica substrates. It will have an "intelligent" robotic motion. The final scheme of this system will depend on the result that we will get with the small robot which is under test in air at the moment; it will be mounted on the small coater, to be tested in vacuum, during the second semester of 1995. Thus, we hope to validate the corrective coating method.

The door with the robot will be used as a vertical optical table.

The procedure that will be used to achieve to the wavefront specifications is the following :

- The multilayer coating will be realized and will be stopped at the right moment before the end.

- Then, the sample will be annealed before making the wavefront metrology (indeed, the major part of the layer stress will be relaxed).

- Then a small correction will be done to planarize the surface by adding a very thin SiO2 layer. At this moment of the deposition, it will not be necessary to anneal again the sample; we have already checked that that the losses are not locally deteriorated.

To realize the corrective treatment, two solutions will be studied on our small robot :

* A correction pixel by pixel through a silica hole can be done; the drawback of this solution is the time needed to perform the correction.

* A silica grid with a variable density of holes on its surface can be used. This solution will save time and avoid process hazards. Nevertheless, for each deposit, a new grid should be designed.

4300.4.Mirrors metrology

The VIRGO optical parts must exhibit charateristics at the frontier of the possibilities of nowadays technology in order to keep the signal to noise ratio at its best level.

Our role is to :

- Offer to the IPNL team the tools which will allow them to optimize the coatings fabrication and to reach the requiral goals for the conective coating.

- Check the quality of the final optical parts and to model the influence of residual defects on the behaviour of VIRGO 97 or of the final antenna.

4300.4.1.Results already obtained at ESPCI

4300.4.1.1. Absorption losses

The optimisation of the "Mirage" detection using a quasi collinear geometry of the pump and the probe beam has led us to a sensitivity better than 10ppb which is large enough to probe absorption losses in the ppm range (typ 0,8) and their homogeneity (typ 15%).

This level of sensitivity has not need to be improved in a near future.

4300.4.1.2. Total losses

This measurement is more "classical" wa had a specific approach in order to take advantage of the specificity of our YAG laser already used in the absorption losses (≈av. power 1W, 200 ns pulses at 2KHz highly multimode).

The sensitivity that we have reached is 1ppm which is enough for the large mirrors of VIRGO.

The reproducibility is rather good, our main problem was the residual absorption of the gaz (air, N2) between the two mirrors.

4300.4.1.3. Birefringence Bench

Using a modulated birefringence added to the static one we havec reached a sensibility of 10^{-5} rd large enough to test the parts of VIRGO which will be crossed by the light. A map of the final beamspliter substrate birefringence will be done in sept. 95.

4300.4.1.4. Substrate point defects

In order to map point defects (bubbles) inside the substrates, we will build between june and september 95 a bench dedicated to this measurement and provide a map of the final beamsplitter point defects.

4300.4.2. Surface examination

4300.4.2.1. Low spatial frequencies (<< a few mm^{-1})

A commercial Fizeau interferometer (¬=0,63 µm, Zygo Mark IV) has been tested with optical pieces smaller than 10 cm in diameter.

Whe have demonstrated that the reproducibility of the measurement is 4nm if great case is taken in the positionning of the optical pieces. Moreover the reference mirror flatness was found to be better than 10nm peak to valley over 50mm.

This setup, nom in Lyon, will be used for the optimisation of the fabrication process (anealing and wavefront conection).

The field of wiew beeing divided in 250x250 pixels the higher spatial frequency for a 12 cm excimination field will be ≈ $1mm^{-1}$.

In this range a higher accuracy will be needed than the 10nm which are close to the limit of such interferometers.

4300.4.2.2. Medium range spatial frequencies (≈$1mm^{-1}$)

The sensibility has been increased for these higher spatial frequencies by building a system based on slopes measurements.

The differential system that we have built has reach the required sensibility for all the terms of the surface deformation whose order are larger than 2 (curvature).

4300.4.2.3. High spatial frequencies (<< $1mm^{-1}$)

The polarizing microscope interferometer of picometric sensitivity (in the range of 10^2-10^3 mm^{-1}) provides informations which can be compared to the results of the scatterometer ar IPNL but with a more local up to how the wave length used in this system is 0.67 µm. A twin microscope will be build in september 1995 that will work at 1.064 µm.

4300.4.3. Metrology group program

The results that we have described have demonstrated that we have reached in the research phase many of the goals imposed by VIRGO metrology.

On major task will be now to build the corresponding equipment to be installed in IPNL with a scale matching the VIRGO mirrors (VIRGO 97 mirrors will be tested in Paris because of their smaller size).

If most of the difficulties has been overcome we still have to work on the wavefront control which will be coupled to the large coater and which will take advantage of the handling and moving systems of the coater.

Even if the low spatial frequencies deformation have to be examine by a commercial system (≈10nm) the slope based system had to be implemented because he will exhibit a much higher sensitivity in the high frequency range.

Alignment of the VIRGO interferometer

4400.1.Position monitoring

During the interferometer normal operation, the six degree of freedom coordinates defining the position of each optical element (both mirrors and benches) will be monitored continuously and recorded with a sampling time much lower than for the G.W. data. If the locking point of the interferometer is lost, these data will be necessary to move back the optical elements to positions where the linear alignment procedure can be restarted. This requirement gives the constraints on the sensitivity of the monitoring apparatus that should be used:

$\theta_x = 10^{-7}$ rad	$x = 10^{-4}$ m
$\theta_y = 10^{-7}$ rad	$y = 10^{-4}$ m
$\theta_z = 10^{-4}$ rad	$z = 10^{-6}$ m

where z is the optical axis of one arm of the interferometer. Moreover, the monitoring apparatus will be in place permanently. Thus, the stability of the system over a long time of observation is crucial.
Concerning the measurement bandwidth, we can accept an integration time in the range of 0.1 - 1 s.

A scheme for such a monitoring, operating in principle with only one camera, has been proposed and tested on a table top experiment by C. Drezen and H. Heitmann [1]. This method can be implemented in the VME based imaging system, developed at LAPP [2], by means of which the commercial CCD camera EG&G-Reticon M9256 has been interfaced and calibrated. In [1] it is noticed that, in order to achieve a first alignment of the mirror, a camera with lens which monitors the position of four coloured spots is sufficient. However, the best resolution on θ_x,θ_y and z, can be reached using two laser beams (one direct and one folded) and a camera without a lens. Thus, we propose a solution which, for each optical element to be monitored, implies the use of

a) two cameras, one with and the second one without lens;
b) two laser beams;
c) one lamp;
d) an auxiliary mirror;
e) four point markers on the mirror surface out of the coated zone.

The overall measurement scheme we propose is shown in fig. 1. These components will be placed in front of the two windows of each

tower forming an angle of 30 degrees with the optical axis of the mirror on the tower's horizontal section. These windows (fig. 2) are located on the tower side that permits to look at the coated surface of the optical element and will be completely dedicated to this purpose. The use of other windows is precluded by the use of a reference mass (see Section about Marionette and Reference Mass).

In the case of the beam splitter we plan to look still to the coated side of the element using the two windows at 15 degrees. The layout of the cameras used to monitor the positions of the six mirrors of VIRGO is in fig. 3 where also the positions of the camera used for the non linear alignment are shown. Each measuring system (lasers and cameras) will be attached to the structure of the towers by supports which will comply to the following specifications:

- the supports must not have mechanical resonances at frequencies lower than 100 Hz;
- their design should insure the possibility to remove the elements from the towers before outgassing;
- the positioning of each element should be reproducible within 0.1 mm, in order to facilitate re-calibration of the measuring apparatus after every assembly.

Care will be taken to isolate all measuring apparatus from the acoustic noise in the environment and from the fluctuations of air refraction index which could limit their sensitivity.

Bibliography

1 - H. Heitmann, *Virgo Notes*, 21.4.1994, 11.8.1994, 9.1.1995.
2 - A. Bazan et Al., *Astroparticle Phys.* **2**, 229 (1994).

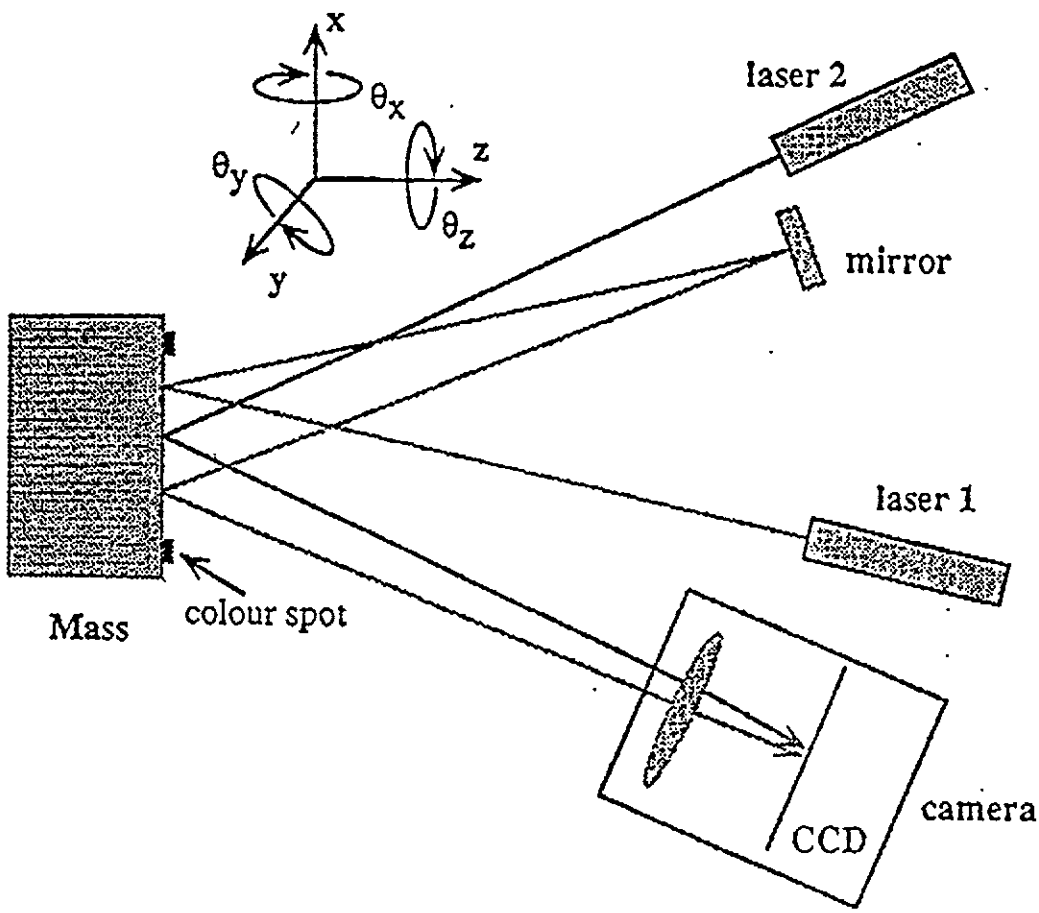

Fig. 1: scheme proposed in [1] for determining the mass position. Laser 1 gives θ_X, θ_Y. The image on the camera gives x,y,θ_Z and a rough value for z. Laser 2 measures z more precisely.

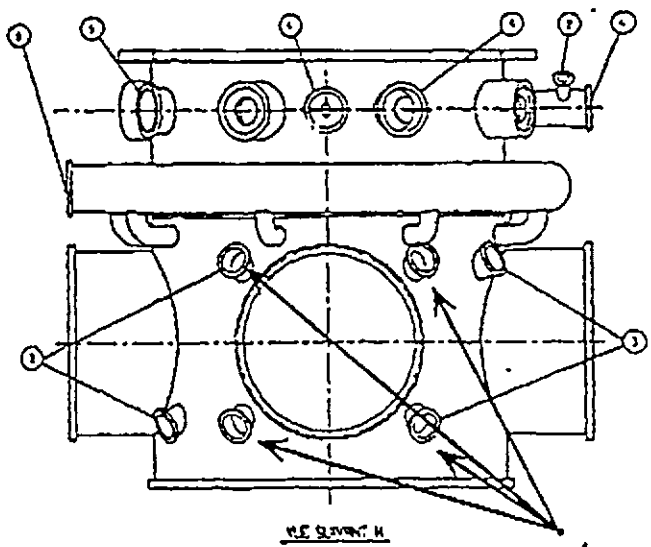

Fig. 2: optical window layout. Particular extracted from the constructive designs of the tower. Four windows on the tower side looking at mirror face will be used for non-linear alignment as well as for optical memory purposes.

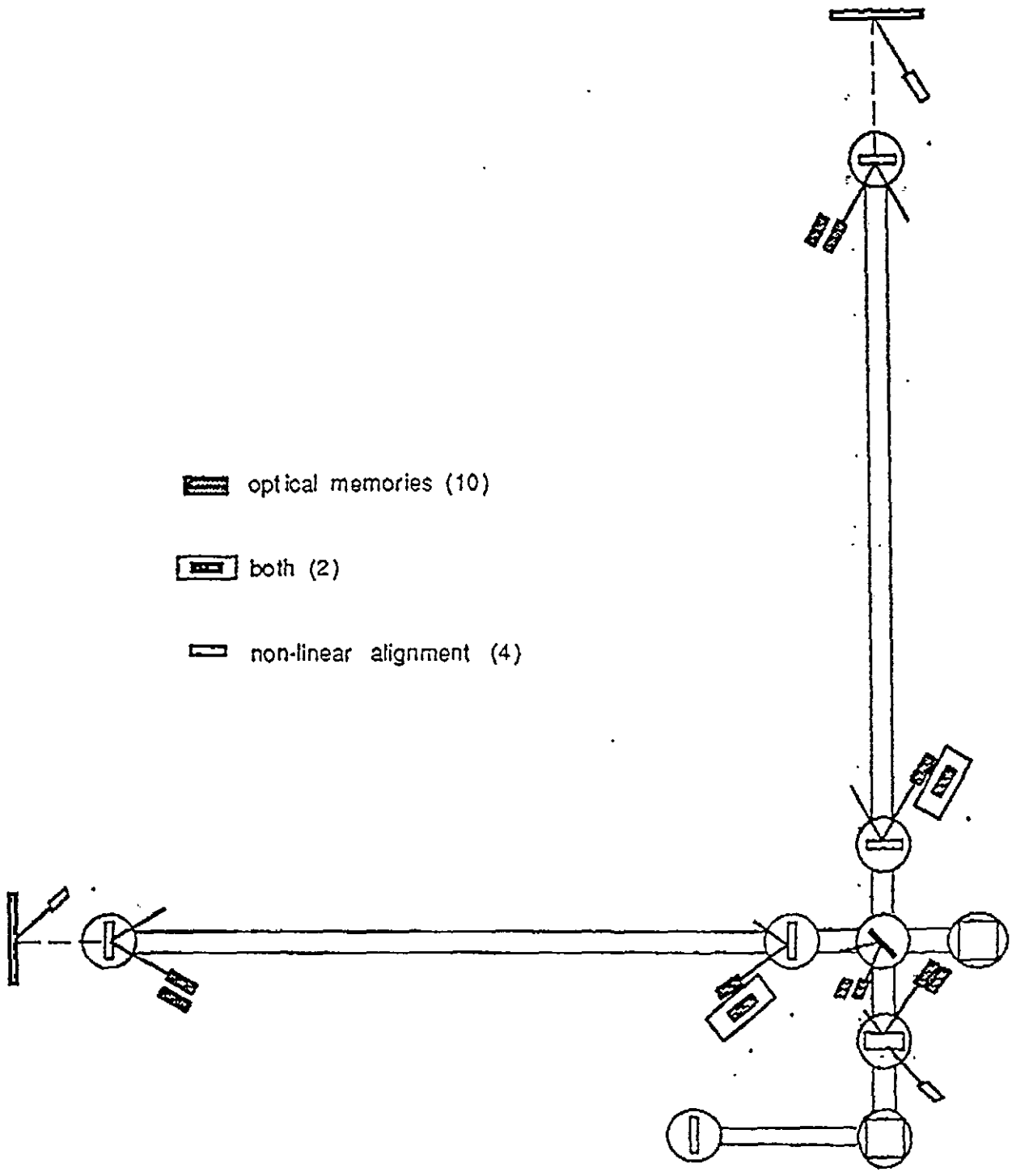

Fig. 3: layout of the 16 CCD cameras.

1 Geometric Considerations

In ref.[1] we showed that the optical length of a FP-cavity depends on the deviation angles $\theta_{1,2}$ of the two terminal mirrors $M_{1,2}$ from the conditions of perfect alignment. This can be seen in a greater detail by considering both the finite size of the mirrors and the positions of their rotation centers. Let us consider fig.(1)

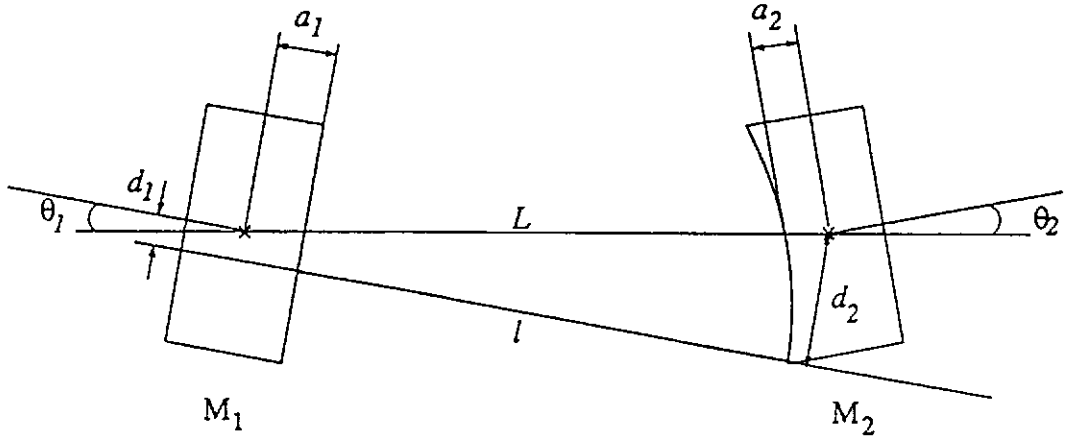

Figure 1

where:

$\theta_{1,2}$ are the mirror deviation angles;

$a_{1,2}$ are the mirror half thicknesses;

L is the separation between the two centers of masses;

l is the actual length of the cavity;

R is the curvature radius of the mirror M_2 (3450 m);

$l_0 = L - a_1 - a_2$ is the optical length in condition of perfect alignment(2988 m).

With simple geometrical considerations one can show that the actual length of the cavity can be written in the following way

$$l(t) = l_0 + (R + a_2)[1 - \cos(\theta_1 - \theta_2)] - L(1 - \cos\theta_1). \tag{1.1}$$

By taking a series expansion up to second order in $\theta_{1,2}$, this equation reproduces the expression given by eq.(1) of ref.[2].

$$l(t) \approx l_0 + \alpha\theta_1^2 + \beta\theta_2^2 + \gamma\theta_1\theta_2, \tag{1.2}$$

where

$$\alpha = \frac{1}{2}(R + a_2 - L), \quad \beta = \frac{1}{2}(R + a_2), \quad \gamma = -2\beta \tag{1.3}$$

2 Sensitivity Requirements

Terrestrial gravitational wave detectors will monitor $l(t)$ only at frequencies above a few tens of hertz, whereas the alignment errors $\theta_{1,2}$ are dominated by static (*offsets*) or slowly varying components (below 10 Hz). Faster angle fluctuations, at frequencies within the observation band, are considerably smaller.

Let us suppose that the angular fluctuations of the two terminal mirrors can be specialized in the time and frequency domain, in the following form

$$\begin{aligned} \theta_k(t) &= \theta_k^{(0)}(t) + \eta_k(t) + \varepsilon_k(t) \\ \bar{\theta}_k(f) &= \theta_k^{(0)}\delta(f) + \bar{\eta}_k(f) + \bar{\varepsilon}_k(f) \end{aligned} \qquad (k = 1,2) \tag{2.1}$$

where $\theta_k^{(0)}$ are the static angular offsets and

$$\begin{aligned} &\bar{\eta}_k(f) \neq 0, \qquad 0 < f \leq \omega \\ &\bar{\varepsilon}_k(f) \neq 0, \qquad f > \omega \end{aligned} \qquad \omega \approx 10\ Hz, \tag{2.2}$$

$$\int_{-\omega}^{\omega} |\,\bar{\eta}_k(f)\,|^2\, df >> \int_{-\infty}^{+\infty} |\,\bar{\varepsilon}_k(f)\,|^2\, df\,, \tag{2.3}$$

i.e. the low-frequency component carries substantially more spectral power than the high-frequency component. The Fourier transform of eq.(1.2) follows from the convolution theorem

$$\mathcal{F}(f \oslash g) = \mathcal{F}(f) \cdot \mathcal{F}(g), \tag{2.4}$$

and is given by

$$\bar{l}(f) = l_0\,\delta(f) + \alpha\,(\bar{\theta}_1 \otimes \bar{\theta}_1) + \beta\,(\bar{\theta}_2 \otimes \bar{\theta}_2) + \gamma\,(\bar{\theta}_1 \otimes \bar{\theta}_2)\,. \tag{2.5}$$

After some algebra, eq.(2.5) can be reduced to the form

$$\begin{aligned} \bar{l}(f) = \sum_{k=1}^{2} \Big[\bar{d}_k^{(0)}\,(\bar{\varepsilon}_k + \bar{\eta}_k) + \bar{d}_k \otimes \bar{\varepsilon}_k(f)\Big] + \alpha\Big[(\bar{\varepsilon}_1 \otimes \bar{\varepsilon}_1) + (\bar{\eta}_1 \otimes \bar{\eta}_1)\Big] \\ + \beta\Big[(\bar{\varepsilon}_2 \otimes \bar{\varepsilon}_2) + (\bar{\eta}_2 \otimes \bar{\eta}_2)\Big] + \gamma\Big[(\bar{\varepsilon}_1 \otimes \bar{\varepsilon}_2) + (\bar{\eta}_1 \otimes \bar{\eta}_2)\Big] \end{aligned} \tag{2.6}$$

where:

$$\bar{d}_1^{(0)} = 2(\alpha\theta_1^{(0)} - \beta\theta_2^{(0)}), \qquad \bar{d}_2^{(0)} = 2\beta(\theta_2^{(0)} - \theta_1^{(0)}) \tag{2.7}$$

and no assumption has been made. However, since the angular fluctuations can be considered as purely stochastic processes, the correlation functions of the last three terms of eq.(2.6) can be neglected and this expression simplifies into

$$\bar{l}(f) = \sum_{k=1}^{2} \Big\{\bar{d}_k^{(0)}\bar{\eta}_k(f) + \bar{\varepsilon}_k(f) \otimes [\bar{d}_k(f) + \bar{d}_k^{(0)}\delta(f)]\Big\}\,. \tag{2.8}$$

The two quantities $\bar{d}_{1,2}(f)$ are the moment arms separating the perturbed optical axis from each mirror's center of rotations and are given by

$$\bar{d}_1(f) = 2(\alpha\bar{\eta}_1 - \beta\bar{\eta}_2), \qquad \bar{d}_2(f) = 2\beta(\bar{\eta}_2 - \bar{\eta}_1) \tag{2.9}$$

Two specific cases can be considered:

a. The alignment errors are determined only by static and/or slowly varying angular displacements (below 10 Hz) due to long-term thermal drift and seismic vibrations combined with the low-pass filtering action of the suspensions. In this case $\bar{\varepsilon}_{1,2} \approx 0$ and eq. (2.8) becomes

$$\bar{l}(f) = \sum_{k=1}^{2} \bar{d}_k^{(0)} \bar{\eta}_k(f) \tag{2.10}$$

b. In the general case where $\bar{\varepsilon}_{1,2}(f) \neq 0$, the high frequency components of $l(f)$ will be coupled to the effect of the low-frequency noise. This can be seen as follows. Let us put

$$\bar{A}_k(f) = \bar{d}_1^{(0)}\delta(f) + \bar{d}_k(f) \qquad (k = 1,2) \tag{2.11}$$

and let us take the square of eq.(2.8) for $f >> 10\ Hz$ ($\bar{\eta}_{1,2} = 0$). The expressions of the two diagonal terms become ($k = 1,2$)

$$\begin{aligned}[\bar{\varepsilon}_k \otimes \bar{A}_k(f)]^2 &= \int_{-\infty}^{+\infty} \bar{\varepsilon}_k(f')\,\bar{A}_k(f-f')\,df' \int_{-\infty}^{+\infty} \bar{\varepsilon}_k(g')\,\bar{A}_k(f-g')dg' \\ &= \int_{-\infty}^{+\infty} \bar{\varepsilon}_k(f')\,\bar{\varepsilon}(f'+x)\,dx \int_{-\infty}^{+\infty} \bar{A}_k(f-f')\,\bar{A}_k(f-f'-x)\,df'\end{aligned}$$

where $x = g' - f'$. In absence of any correlations among the values of $A(f)$ calculated at different frequencies, one has

$$\begin{aligned}\int_{-\infty}^{+\infty} \bar{A}_k(f-f')\,\bar{A}_k(f-f'-x)\,df' &= \Delta f\ <\bar{A}_k^2>\ \delta(x) \\ &= \Delta f\,(\bar{d}_k^{(0)^2} + \sigma_{d_k}^2)\,\delta(x)\end{aligned} \tag{2.12}$$

For the same reason, the two non-diagonal terms vanish and the expression of $l^2(f)$ reduces to

$$\frac{\bar{l}^2(f)}{\Delta f} = \sum_{k=1}^{2} \bar{\varepsilon}_k^2(f)\,(\bar{d}_k^{(0)^2} + \sigma_{d_k}^2) \tag{2.13}$$

where the contributions of the two mirrors can be assumed to be approximately equal. This expression can be compared with eq.(14) of ref.[2] and it's worthwhile to notice that the $\bar{d}_k$ *RMS*-values entering the latter, appears to be multiplied by an extra factor 2, which, apparently, is unjustifiable.

The first case shows that, at least in principle, the offset contributions appearing in eqs.(2.9) can be trimmed down to zero by applying a periodic torque to the mirror and by monitoring the correspondent variations of the optical length of the cavity. Moreover, measurements performed on the superattenuators and estimates of the thermal noise indicate that:

- the low frequency angular noise is dominated by the suspension noise, that is concentrated in the region below 1 Hz and has a total RMS- value of about $2.5 \cdot 10^{-5}$ rad;
- the high frequency (> 10 Hz) component of the spectrum is dominated by the thermal noise that is estimated to be $2 \cdot 10^{-17}$ $rad/\sqrt{Hz}$ at 10 Hz and $3 \cdot 10^{-20}$ $rad/\sqrt{Hz}$ at 100 Hz.

The RMS-value of the angular noise at low frequency would cause

$$d_1^{RMS} = 9\ cm \qquad\qquad d_2^{RMS} = 12\ cm$$

in each direction. Following (2.13), this would give a limit of $h = 1.4\ 10^{-21}/\sqrt{Hz}$ at 10 Hz. For the sensitivity limits of

$$\begin{array}{l} h < 10^{-22}/\sqrt{Hz} \quad \text{at } 10\ Hz \\ h < 10^{-23}/\sqrt{Hz} \quad \text{at } 100\ Hz \end{array} \tag{2.14}$$

the 10 Hz region is the most demanding and the d_i^{RMS} come out to be 1.5 cm. To achieve this, the RMS-values of the low-frequency angular noise must be reduced down to 10^{-6} rad.

3 The Fabry-Perot Alignment

The methods of D.Z.Anderson and H.Ward [3, 4] have been originally suggested for the alignment of one single Fabry-Perot (FP) and no attempt has ever been made to extend this procedure to the case of a complete Michelson Interferometer (MI). In both these methods the beam is frequency modulated and, in the Anderson scheme, the modulation equals the frequency difference between the TEM_{00} and TEM_{10} modes ($\Omega/2\pi = 19.1\ KHz$). The alignment information is related to the detection of the TEM_{10} components, in phase or in quadrature, with the main TEM_{00}. All these details have been widely discussed elsewhere [1, 3, 4].

In the case of a single FP, the knowledge of a tilt and/or displacement of the optical axis, is sufficient to identify the mirror that caused it. But this is not true for a complete MI, where a misalignment signal measured behind one FP, will not be sufficient to single out the mirror(s) that caused it. In order to disentangle the information, more measurements are needed. In ref.[1] we initiated to consider the complete Michelson Interferometer where the beam splitter and the recycling mirror remained perfectly aligned. With the Anderson method and under some simplifying assumptions, we reached the following conclusions :

a. the left/right or up/down asymmetries, measured behind the terminal mirrors of one of the two FP's, yields direct informations of the tilt of the FP-cavity axis, but its displacement appears always in a linear combination with the displacement of the other FP-cavity;

b. this cross-talk between the two arms couples the two displacements only. Neither angle/angle nor angle/displacement couplings are predicted;

c. the coupling effect for the displacements is very close to one;

d. with a maximum power of 10 mW impinging on the quadrant photodiodes, the limits imposed by the shot-noise would be :

$$\begin{aligned} \frac{\alpha}{\theta_\infty} &= 9.9 \cdot 10^{-7}/\sqrt{Hz} \\ \frac{a}{w_0} &= 3 \cdot 10^{-8}/\sqrt{Hz} \end{aligned} \tag{3.1}$$

where α and a refer to the optical axis of the FP-cavities.

4 Alignment of the Full Interferometer with the Anderson Method

In order to obtain a better approximation, we removed two of the limitations that affected the results of ref.[1], *i.e.*:

1. the recycling mirror was kept "fixed" in a perfectly aligned condition;

2. the FP-reflectivities for the resonant (β) and non-resonant (γ) frequencies

$$\beta = \frac{|\, R_1 - R_2 \,|}{1 - R_1 R_2} \qquad \gamma = \frac{R_1 + R_2}{1 + R_1 R_2} \tag{4.1}$$

were both assumed to be equal to 1 ($T_2 = 0$).

With the values

$$\begin{aligned} R_1^2 &= 0.882 \quad T_1^2 = 0.118 \\ R_2^2 &= 0.9999 \quad T_2^2 = 10^{-4} \end{aligned} \tag{4.2}$$

taken from ref.[5], one has instead:

$$\beta = 0.99841, \qquad \gamma = 0.999997 \tag{4.3}$$

and even if tiny, this difference can play a significant role. By limiting ourselves to consider only the horizontal plane. we have to measure the 2-displacements ($a_{1,2}$) and the 2-angles ($\alpha_{1,2}$) of the FP-cavity axes and the angle of the recycling mirror (θ_0): in total five unknown quantities. Three quadrant photodiode will be sufficient to disentangle the problem: two located right behind the two terminal mirrors, and a third on the injection bench, to measure the component reflected back from the recycling mirror (see fig.(2)). However a further fourth photodiode can be used to measure the component reflected from

the uncoated part of the beam splitter: this is not necessary but can add an important extra piece of information.

Given a complete set of mirror misalignments, the equilibrium condition among the three electric fields impinging upon the recycling mirror, imposes the following relation :

$$\vec{E}_3 = T_0\vec{E}_1 + i\,R_0\vec{E}_2 \tag{4.4}$$

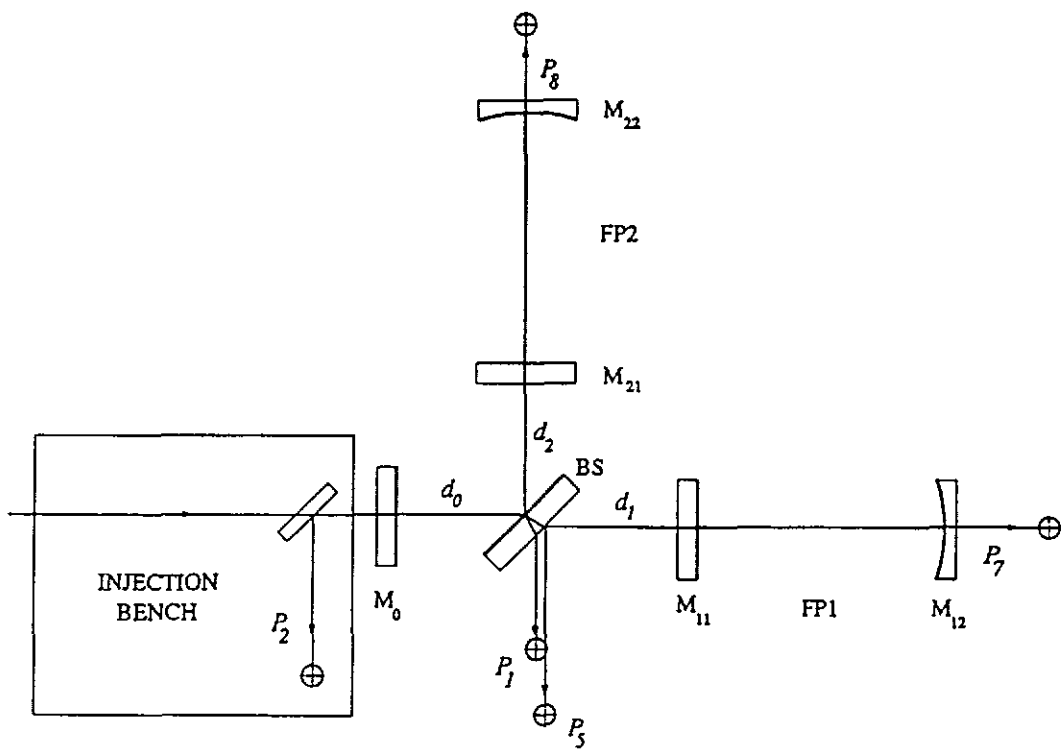

Figure 2

where:

$\vec{E}_1$ is the external incident beam;

$\vec{E}_2$ is the beam impinging on the recycling mirror after a complete round trip in the interferometer;

$\vec{E}_3$ is the beam leaving the recycling mirror for the tour of the interferometer;

R_0 and T_0 are the amplitude reflectivity and transmittivity of the recycling mirror, respectively.

According to ref.[5], the reflectivity and transmittivity of the recycling mirror will be assumed to be:

$$R_0^2 = 0.92, \qquad T_0^2 = 0.08 \tag{4.5}$$

After some tedious algebra, eq.(4.4) drives to the misalignment signals expressed in terms of the misalignments specified for each mirror.
The left/right power components transmitted behind the two terminal mirrors are (+ =left, − =right):

$$P_{7,8}^{L,R} = \frac{P_{inc}T_0^2T_2^2F}{4(1-\beta R_0)^2}\Big[J_0^2 \pm \sqrt{\frac{2}{\pi}}\frac{J_0J_1}{1+\gamma R_0}\Big(A_{7,8}\cos\Omega t + B_{7,8}\sin\Omega t\Big) + O(\alpha_{h,k}^2, a_{h,k}^2, a_{h,k}\alpha_{h,k})\Big] \tag{4.6}$$

where P_{inc} is the incident power laser and

$$\begin{aligned} A_{7,8} &= [(\beta-\gamma)R_0 - 2]\,a_{1,2} - (\beta+\gamma)R_0\,a_{2,1} \\ B_{7,8} &= [2-(\gamma+\beta)R_0]\,\alpha_{1,2} + (\beta-\gamma)R_0\,\alpha_{2,1} + 4\gamma R_0\,\theta_0 \\ F &= \frac{T_1^2}{(1-R_1R_2)^2} \end{aligned} \tag{4.7}$$

By neglecting the higher order terms, the left/right asymmetry, which is free from systematic errors, is given by:

$$\Sigma_t^{FP_{1,2}} = \frac{\text{left -right}}{\text{left + right}} = \sqrt{\frac{8}{\pi}}\frac{J_1}{J_0}\frac{1}{1+\gamma R_0}\Big(A_{7,8}\cos\Omega t + B_{7,8}\sin\Omega t\Big) \tag{4.8}$$

The component reflected from the recycling mirror (P_2) and its asymmetry are:

$$P_2^{L,R} = \frac{P_{inc}}{2(1-\beta R_0)^2}\Big[(\beta-R_0)^2J_0^2 \pm \sqrt{\frac{2}{\pi}}\frac{J_0J_1T_0^2(\beta+\gamma)}{(1+\gamma R_0)^2}\Big(A_2\cos\Omega t + B_2\sin\Omega t\Big) + O(\alpha_{h,k}^2, a_{h,k}^2, a_{h,k}\alpha_{h,k})\Big] \tag{4.9}$$

$$\Sigma_r^{Rec} = \sqrt{\frac{2}{\pi}}\frac{J_1}{J_0}\frac{T_0^2(\beta+\gamma)}{(\beta-R_0)^2(1+\gamma R_0)^2}\Big(A_2\cos\Omega t + B_2\sin\Omega t\Big) \tag{4.10}$$

where:

$$\begin{aligned} A_2 &= (R_0-\beta)(1+\gamma R_0)(a_1+a_2) \\ B_2 &= \Big[(R_0+\beta)(1+\gamma R_0) - 2(\gamma+\beta R_0^2)\Big](\alpha_1+\alpha_2) \\ &\quad +4R_0[\gamma\beta - 2 + R_0(2\beta-\gamma)]\theta_0 \end{aligned} \tag{4.11}$$

The component reflected by the uncoated face of the beam splitter (P_5), and its asymmetry are:

$$P_5^{L,R} = \frac{P_{inc}T_0^2}{4(1-\beta R_0)^2}\Big[\beta^2J_0^2 \pm \sqrt{\frac{2}{\pi}}\frac{(\gamma+\beta)J_0J_1}{1+\gamma R_0}(A_5\cos\Omega t + B_5\sin\Omega t) + O(\alpha_{h,k}^2, a_{h,k}^2, a_{h,k}\alpha_{h,k})\Big] \tag{4.12}$$

$$\Sigma_r^{FP_1} = \sqrt{\frac{2}{\pi}}\frac{J_1}{J_0}\frac{\beta+\gamma}{3^2(1+\gamma R_0)}\left(A_5\cos\Omega t + B_5\sin\Omega t\right) \tag{4.13}$$

where:

$$A_5 = \beta\left[(\beta R_0 - 2)a_1 - \beta R_0 a_2\right] \tag{4.14}$$

$$\begin{aligned} B_5 = {} & \Big\{\alpha_1[2\beta - 2\gamma(1-\beta R_0)(2+\gamma R_0) - \beta^2 R_0(1+\gamma R_0)] \\ & +\alpha_2 R_0[\beta^2(1+\gamma R_0) + 2\gamma^2(1-\beta R_0) - 2\beta\gamma] + 4\beta\gamma R_0\theta_0\Big\}\Big/(1+\gamma R_0) \end{aligned} \tag{4.15}$$

Finally, the beam going toward the fringe detector P_1 has not been considered because, under these approximations, it contains informations on the misalignments only at the second order level.

In all these expressions, displacements and angles are always measured in units of beam waist ($w_0 = 1.98\cdot 10^{-2} m$) and angular divergency ($\theta_\infty = 1.7\cdot 10^{-5} rad$). Moreover, for the sake of simplicity, we have assumed that:

- the propagation phases in the recycling cavity are the same for all the beams,
- the beams are either on-resonance or perfectly off-resonance in the FP's,
- only the resonant beams are transmitted by the FP's.

(4.16)

With these approximations, a first numerical evaluation is reported in table I. With the values $J_1^2 = 10^{-2}, \Omega/2\pi = 19.1\ KHz$, the table shows the contributions that every angular misalignment gives to the in phase/in quadrature components of the asymmetries.

Beam		θ_0	θ_{11}	θ_{12}	θ_{21}	θ_{22}
$\Sigma_t^{FP_1}$	sin	$1.58\cdot 10^{-3}$	$3.45\cdot 10^{-5}$	0	$-6.33\cdot 10^{-7}$	0
	cos	0	$3.187\cdot 10^{-4}$	$-2.444\cdot 10^{-3}$	$3.052\cdot 10^{-4}$	$-2.34\cdot 10^{-3}$
$\Sigma_t^{FP_2}$	sin	$1.58\cdot 10^{-3}$	$-6.33\cdot 10^{-7}$	0	$3.45\cdot 10^{-5}$	0
	cos	0	$3.052\cdot 10^{-4}$	$-2.34\cdot 10^{-3}$	$3.187\cdot 10^{-4}$	$-2.444\cdot 10^{-3}$
Σ_r^{Rec}	sin	$-3.71\cdot 10^{-3}$	$-3.95\cdot 10^{-5}$	0	$-3.95\cdot 10^{-5}$	0
	cos	0	$6.352\cdot 10^{-4}$	$-4.87\cdot 10^{-3}$	$6.352\cdot 10^{-4}$	$-4.87\cdot 10^{-5}$
$\Sigma_r^{FP_1}$	sin	$1.61\cdot 10^{-3}$	$-5.33\cdot 10^{-5}$	0	$1.65\cdot 10^{-5}$	0
	cos	0	$3.327\cdot 10^{-4}$	$-2.551\cdot 10^{-3}$	$3.052\cdot 10^{-4}$	$-2.34\cdot 10^{-3}$

Table I

All the coefficients of table I, as well as in table II and III, have been calculated for $\theta_i = 10^{-2}$.

The θ_i variables expressed in units of the beam angular divergency, have the following meaning:

- θ_0 is a tilt of the recycling mirror (M_0),
- $\theta_{11,12}$ are tilts of the ($M_{11,12}$) mirrors that produce a displacement a_1 and a tilt α_1 of the FP_1 cavity axis, according to $[a_0 = w_0/\theta_\infty = 1.16 \cdot 10^3\ m/rad]$

$$a_1 = \frac{l_0 - R}{a_0}\theta_{11} + \frac{R}{a_0}\theta_{12}, \qquad \alpha_1 = \theta_{11} \tag{4.17}$$

- $\theta_{21,22}$ are tilts of the ($M_{21\,22}$) mirrors that produce a displacement a_2 and a tilt α_2 of the FP_2 cavity axis, according to

$$a_2 = \frac{l_0 - R}{a_0}\theta_{21} + \frac{R}{a_0}\theta_{22}, \qquad \alpha_2 = \theta_{21} \tag{4.18}$$

Some immediate comments to these results are:

- θ_0 induces only sin-components (angles)
- $\theta_{12,22}$ induce only cos-components (displacements)
- $\theta_{11,21}$ induce both sin and cos-components but to a much smaller extent

Moreover:

- θ_0 acts on P_7 in the same way as θ_0 acts on P_8
- θ_{11} acts on P_8 in the same way as θ_{21} acts on P_7
- θ_{12} acts on P_8 in the same way as θ_{22} acts on P_7
- θ_{11} acts on P_2 in the same way as θ_{21} acts on P_2
- θ_{12} acts on P_2 in the same way as θ_{22} acts on P_2

as it must be expected from the symmetry of the problem: the two FP's are specularly located with respect to the plane of the beam splitter.

5 Achievable Accuracies

The expressions (4.6, 4.9, 4.12) for the power detected by the quadrant photodiode, are always of the kind

$$P^{L,R} = P_0 \pm P' \sin(\Omega t + \varphi) \tag{5.1}$$

where

$$P^L + P^R = 2P_0 = P_{Tot} \tag{5.2}$$

$$< P^L > = < P^R > = P_0 \tag{5.3}$$

The asymmetries of eqs (4.8, 4.10, 4.13) are defined in terms of the quantities (5.1)

$$\Sigma = \frac{P^R - P^L}{P^L + P^R} = \frac{P'}{P_0} sin(\Omega t + \varphi), \tag{5.4}$$

and the corresponding errors

$$(\Delta\Sigma)^2 = \frac{4}{(P^L + P^R)^4} \left[(P^R)^2 (\Delta P^L)^2 + (P^L)^2 (\Delta P^R)^2 \right]. \tag{5.5}$$

will be calculated on the ground that both P^L and P^R are only affected by the shot-noise associated to their mean value ($= P_0$).Therefore assuming a quantum efficiency $= 1$, the shot-noise errors $\Delta P^{L,R}$ are given by

$$\Delta P^{L,R} = \frac{4.3 \cdot 10^{-10}}{\sqrt{P_0}} \, W/\sqrt{Hz}, \tag{5.6}$$

and eq.(5.5) becomes

$$\Delta\Sigma = 4.3 \cdot 10^{-10} \sqrt{\frac{1 + \Sigma^2}{P_{Tot}}}. \tag{5.7}$$

Finally, since it is always $|\Sigma| \ll 1$ and assuming that the maximum power tolerated on the photodiodes is 10 mW, the minimum asymmetry that can be appreciated is

$$\Delta\Sigma = 4.3 \cdot 10^{-9}. \tag{5.8}$$

As shown in table I, there are eight available signals of the five independent variables $\theta_0, \theta_{11}, \theta_{12}, \theta_{21}, \theta_{22}$, so there are several possible systems of five equations that can be solved to deduce the values of the angles. Not all the possible choices are equivalent; actually not all the signals are independent. For example, the $\Sigma_r^{Rec}(cos)$ equation is proportional to the sum of $\Sigma_t^{FP_1}(cos)$ and $\Sigma_t^{FP_2}(cos)$ equations.

It can be seen that a good choice (others choices are equivalent) is the system made of equations $\Sigma_t^{FP_1}(sin)$, $\Sigma_r^{Rec}(sin)$, $\Sigma_r^{Rec}(cos)$, $\Sigma_r^{FP_1}(sin)$, $\Sigma_r^{FP_1}(cos)$. Taking into account the shot-noise limitation, given by eq.(5.8), one can reconstruct all the angular misalignments with the accuracies shown in the first column of table IV.

The same calculation can be repeated by removing the approximations (4.16) used to construct table I and introducing the arm-length difference of 0.8 m requested by the longitudinal locking scheme [6] ($d_0 = 6.0\ m, d_1 = 5.6\ m, d_2 = 6.4\ m$). The results are reported in table II and do not show any significant variation. Again, the detector signals have been omitted because they are extremely small. The symmetry properties are substantially maintained and the values of the σ's, reported in the second column of table IV, remain almost the same.

Beam		θ_0	θ_{11}	θ_{12}	θ_{21}	θ_{22}
$\Sigma_t^{FP_1}$	sin	$1.483 \cdot 10^{-3}$	$-3.728 \cdot 10^{-5}$	$5.662 \cdot 10^{-4}$	$-7.161 \cdot 10^{-5}$	$5.627 \cdot 10^{-4}$
	cos	$3.809 \cdot 10^{-4}$	$2.900 \cdot 10^{-4}$	$-2.304 \cdot 10^{-3}$	$2.785 \cdot 10^{-4}$	$-2.201 \cdot 10^{-3}$
$\Sigma_t^{FP_2}$	sin	$1.483 \cdot 10^{-3}$	$-7.170 \cdot 10^{-5}$	$5.634 \cdot 10^{-4}$	$-3.739 \cdot 10^{-5}$	$5.670 \cdot 10^{-4}$
	cos	$3.814 \cdot 10^{-4}$	$2.785 \cdot 10^{-4}$	$-2.201 \cdot 10^{-3}$	$2.900 \cdot 10^{-4}$	$-2.304 \cdot 10^{-3}$
Σ_r^{Rec}	sin	$-3.910 \cdot 10^{-3}$	$-1.839 \cdot 10^{-4}$	$1.144 \cdot 10^{-3}$	$-1.830 \cdot 10^{-4}$	$1.137 \cdot 10^{-3}$
	cos	$7.796 \cdot 10^{-4}$	$5.774 \cdot 10^{-4}$	$-4.575 \cdot 10^{-3}$	$5.775 \cdot 10^{-4}$	$-4.575 \cdot 10^{-3}$
$\Sigma_r^{FP_1}$	sin	$1.517 \cdot 10^{-3}$	$-1.240 \cdot 10^{-4}$	$5.591 \cdot 10^{-4}$	$-5.471 \cdot 10^{-5}$	$5.636 \cdot 10^{-4}$
	cos	$3.842 \cdot 10^{-4}$	$3.048 \cdot 10^{-4}$	$-2.408 \cdot 10^{-3}$	$2.764 \cdot 10^{-4}$	$-2.201 \cdot 10^{-3}$

Table II

So far the modulation frequency has been always kept at the value of 19.1 KHz, but nothing forbids to add to this frequency an integer number n of $c/2L$ of the Fabry-Perot (50.166 KHz). In particular with $n = 125$, the modulation frequency is 6.2898 MHz, which is very close to the optimal value for the longitudinal locking of 6.29032 MHz. Indeed, with the recycling cavity only 9 mm longer, the frequency for the logitudinal locking will coincide with the one for the alignment.

Beam		θ_0	θ_{11}	θ_{12}	θ_{21}	θ_{22}
$\Sigma_t^{FP_1}$	sin	$-3.973 \cdot 10^{-4}$	$-6.998 \cdot 10^{-5}$	$2.290 \cdot 10^{-3}$	$4.559 \cdot 10^{-4}$	$-2.128 \cdot 10^{-3}$
	cos	$-4.624 \cdot 10^{-4}$	$9.882 \cdot 10^{-4}$	$7.604 \cdot 10^{-5}$	$-5.181 \cdot 10^{-4}$	$-4.915 \cdot 10^{-5}$
$\Sigma_t^{FP_2}$	sin	$-4.425 \cdot 10^{-4}$	$5.079 \cdot 10^{-4}$	$-2.111 \cdot 10^{-3}$	$-7.482 \cdot 10^{-5}$	$2.275 \cdot 10^{-3}$
	cos	$-4.179 \cdot 10^{-4}$	$-4.671 \cdot 10^{-4}$	$-2.731 \cdot 10^{-4}$	$8.943 \cdot 10^{-4}$	$2.799 \cdot 10^{-4}$
Σ_r^{Rec}	sin	$-1.959 \cdot 10^{-2}$	$1.201 \cdot 10^{-2}$	$1.162 \cdot 10^{-3}$	$7.106 \cdot 10^{-3}$	$1.454 \cdot 10^{-3}$
	cos	$4.473 \cdot 10^{-2}$	$-2.206 \cdot 10^{-2}$	$1.511 \cdot 10^{-3}$	$-2.409 \cdot 10^{-2}$	$1.233 \cdot 10^{-3}$
$\Sigma_r^{FP_1}$	sin	$-2.125 \cdot 10^{-2}$	$1.111 \cdot 10^{-2}$	$-5.108 \cdot 10^{-3}$	$1.084 \cdot 10^{-2}$	$3.665 \cdot 10^{-3}$
	cos	$-1.098 \cdot 10^{-2}$	$8.155 \cdot 10^{-3}$	$6.455 \cdot 10^{-4}$	$2.937 \cdot 10^{-3}$	$5.338 \cdot 10^{-4}$
Σ^{Det}	sin	$-5.021 \cdot 10^{-3}$	$1.333 \cdot 10^{-3}$	$2.063 \cdot 10^{-2}$	$3.438 \cdot 10^{-3}$	$-1.778 \cdot 10^{-2}$
	cos	$1.959 \cdot 10^{-3}$	$2.131 \cdot 10^{-3}$	$-3.282 \cdot 10^{-2}$	$-3.824 \cdot 10^{-3}$	$3.044 \cdot 10^{-2}$

Table III

Therefore with the values :

$$\Omega/2\pi = 6.289840\ MHz$$
$$d_0 = 6.009\ m, \qquad d_1 = 5.6\ m, \qquad d_2 = 6.4\ m \tag{5.9}$$

one obtain the results shown in table III.

Since now the side bands resonate in the recycling cavity, it is not surprising that these results are sensibly better than those reported in tables I,II. Furthermore, it is worthwhile noticing that at this high frequency value, also the detector (P_1) starts exhibiting sizeable signals. However its contribution has not been included in the results of table IV, which summarizes the accuracy levels that are achievable in the 3 cases we have examined.

On the experimental side the use of one single high frequency modulation is highly desirable: the results obtained indicate that this possibility is not out of reach.

	19.1 KHz with (4.16)	19.1 KHz	6.289 MHz with (5.9)
$\sigma(\theta_0/\theta_\infty)$	$3.0 \cdot 10^{-8}$	$3.0 \cdot 10^{-8}$	$3.2 \cdot 10^{-7}$
$\sigma(\theta_{11}/\theta_\infty)$	$7.0 \cdot 10^{-7}$	$6.0 \cdot 10^{-7}$	$3.0 \cdot 10^{-7}$
$\sigma(\theta_{12}/\theta_\infty)$	$3.6 \cdot 10^{-7}$	$2.5 \cdot 10^{-7}$	$1.25 \cdot 10^{-7}$
$\sigma(\theta_{21}/\theta_\infty)$	$2.4 \cdot 10^{-6}$	$2.0 \cdot 10^{-6}$	$3.0 \cdot 10^{-7}$
$\sigma(\theta_{22}/\theta_\infty)$	$4.8 \cdot 10^{-7}$	$4.0 \cdot 10^{-7}$	$1.25 \cdot 10^{-7}$

Table IV

From table IV, we see that the shot-noise limits the reconstruction of the angles of the FP mirrors at most to $4 \cdot 10^{-11} rad/\sqrt{Hz}$, leading to a RMS-value which is much smaller than the value of $10^{-6} rad$ required in section 2.

6 Conclusions

We have demonstrated that in the Anderson scheme, the alignment problem is overdetermined with the five indicated quadrant photodiodes. Moreover this amount of information can be substantially doubled by adding an extra photodiode on each beam. As a matter of fact one could take advantage of the different dephasing effect that the $TEM_{00} - TEM_{01}$ modes undergo in their spatial evolution. This means that measurements of the $TEM_{00} - TEM_{01}$ mixtures at two different dephasing values (typically 0^0 and 90^0) yield two independent informations. This requires only to locate the two photodiodes at a known distances between them, or to use a telescope of lenses.

An accurate analysis of this extra possibility is presently under study. For the time being we strongly recommend the presence of two quadrant photodiodes per beam line (10 total) in the final VIRGO experimental setup.

References

[1] D.Babusci , H.Fang, G.Giordano, G.Matone, V.Sannibale, *LNF-94/027(IR), Virgo note* PJT 94-017 (1994)

[2] S.Kawamura and M.E.Zucker,*Appl. Opt.*, 33 (1994),3912

[3] D.Z.Anderson, *Appl. Opt.*, 23 (1984), 2944 and N.M.Sampas and D.Z.Anderson, *Appl. Opt.* 29 (1990), 394

[4] E. Morrison, B.J. Meers, D.J. Robertson and H. Ward, *Appl. Opt.* 33 (1994), 5041

[5] C.N.Man *Virgo note* PJT 94-024 (1994)

[6] R. Flaminio and H. Heitmann *Virgo note* PJT 93-021 (1993)

Calibration

4500.1. Introduction

The purpose of the calibration of an aparatusis to provide the parameters needed to convert the measured data to a physical quantity which is in our case the metric perturbation **h** induced by a gravitational wave. The first obvious way to do it is to use our detailed knowledge of the various component of the the interferometer (laser power, conversion factors for the photodetectors, interferometer transfer function,...). This process rely on a precise determination of detector calibration constant and on detailed deconvolution which, taking into account the locking system of the interferometer, is a non-trivial operation. Therefore, to gain confidence in our data we will use an independent system to calibrate the interferometer. By calibration, we mean the injection of a signal of known amplitude and phase, which mimics, as well as possible, the effect of a gravitational wave by moving one mirror and the study of the corresponding signal in our recorded data.

The calibration will be used for at least two different goals. The first one is a general study of the Virgo sensitivity. In this mode we should be able to apply periodic or non periodic signal with an amplitude and a frequency which could be changed by few order of magnitude in order to study the full bandwidth of Virgo. The other mode of operation is a permanent monitoring of the Virgo interferometer. In this case, we will apply a periodic signal of a well known amplitude and very stable frequency. In this mode, we will check the stability of the interferometer control system and of the data acquisition system.

This calibration signal should produce a mirror displacement of well known amplitude and time dependance. This means we should know the force applied on the mirror, the mechanical transfer function and the locking transfer function if a feedback is applied on this mirror. To avoid the third condition we will try to move a mirror on which no feedback forces are applied. It is also important to remember that the principle of the calibration is to have a system as independent as possible from the Virgo control system. This means that we will look for an independent actuator. Of course, the calibration signal should not induce additional noise like seismic noise or electromagnetic noise. At least three different way of pushing the mirror could be foreseen:

a) Forces using the locking actuators
b) The radiation pressure from an additional laser beam
c) The gravitational force from a moving rotor

These three possible solutions will now be described.

4500.2. Calibration using the locking actuators

The Locking system could be used to apply an additional force to move the mirror and study the observed signal. This will be done but this is not the real calibration of the experiment.

A possible way to do calibration is to add a calibration signal at the analog input of the locking actuators (coils which control the mirrors). This calibration signal will be provided by an external signal generator. The only device to build is the signal generator which will be a VME CPU driving a DAC to provide the coils analog input. The DAC will be triggered by an stable clock independent of the Virgo timing system. This will be an independent GPS receiver or a Loran C receiver. The use of a digital signal generator will allow us to produce almost any kind of gravitational waveform. There will be one signal generator in the central building and one in one of the end mirror building.

The main drawback of this system is its sharing of the actuator with the standard control system. Any gain uncertainty, non linearity or more important, any unexpected time delay of the actuator will be a problem.

4500.3. Calibration using a laser

The principle of this method is to move the mirror by the pressure of radiation of a light source with a modulated power. The system will be split in two part: the calibration signal generator which will the same as the one previously described and the light source. This method is similar to the previous one except that the actuator: the light, is independent of the control system. Like the previous method it will be able to produce any kind of waveform very easily. The implantation is presented by figure 4500.1 We will equip the input cavity mirror in order to use the system with the Virgo 97 interferometer. Let's now review the light parameters.

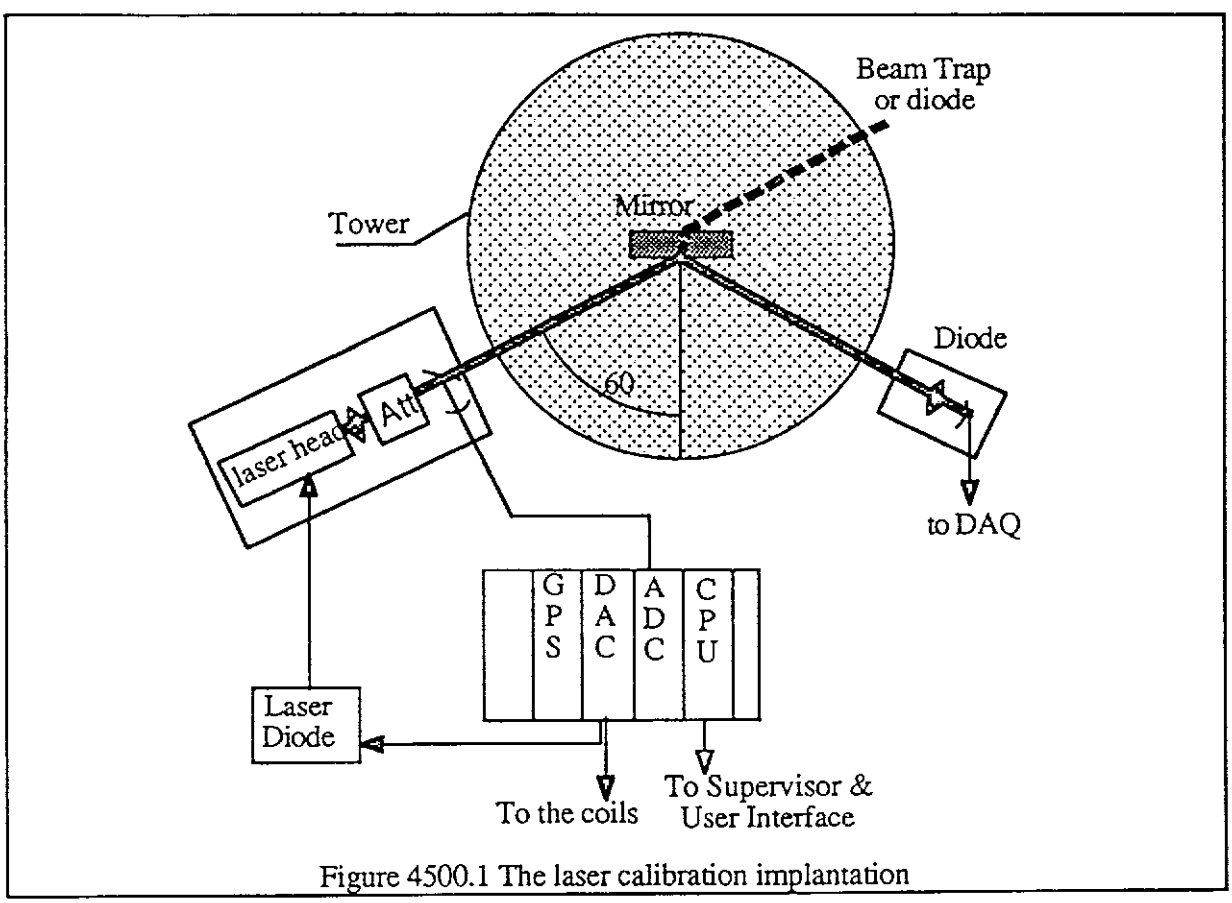

Figure 4500.1 The laser calibration implantation

4500.3.1. Light wavelength

Given our mirror coating, the choice of the wavelength is connected with the choice of the angle on incidence. As figure 4500.2 shows it, when the angle of incidence increases, the area with large reflectivity is shifted to smaller wavelength (0° is for normal incidence). The easier solution for the mechanical point of view is to use angle of incidence of 30° or 60°. In order to avoid any confusion with the main laser beam we will use a wavelength of 810 nm for the calibration laser and therefore we will use the 60° optical port.

4500.3.2.Light power

If we take a light source of power $P = P_0\cos(\omega t)$ perfectly reflected by a mirror, the force applied is:

$$F(t) = P\cos(\alpha) / c$$

Where α is the angle of incidence. Above the pendular fundamental suspension frequency of the mirror of mass M, the mirror motion is:

$$x(t) = F(t) / M\omega^2$$

As an example, if we want a displacement of $x = 10^{-17}$m, at 100Hz,with M=40kg, the needed light power is: P = 100 mW.

To get a better determination of the needed power, we compute the needed power to produce a displacement equal to the noise for one second of integration. The results is presented by the figure 4500.3 assuming a mass of 40 Kg and a angle of incidence of 60°. One can see that a light of 1 Watt is enough to convert most of the frequency range. This correspond to a typical laser diode. It is also interesting to notice that a 1 W laser would provide a large signal in the 10-100 Hz where we could have problem to reach our design sensitivity in the beginning of the Virgo running.

This low power compared to the main beam power (about 10 KW in the cavity) shows that no thermal problem on the mirror surface are expected especially if we use a beam size of several mm. This low power combined with the fact that the calibration light has a different wavelength and is not frequency modulated remove any concern about diffused light going into the main beam.

4500.4. Calibration using turning masses

As it was proposed in the VIRGO FCD this method consists in using the Newtonian forces applied on the mirrors when a nearby mass is moving. Experience coming from bar detector (the Roma Team) has shown that is a working method, but its implementation is fairly complicated. It has not the flexibility of the two other systems in order to produce complicate waveform. It require a detailed knowledge of the rotor and mirror shape as well as the effect on the marionetta. Such a system needs more studies before its implementation could be decided.

Interferometer Suspensions

4600 Suspension requirements

The test masses used in VIRGO have to be sufficiently decoupled from environmental perturbations so that gravitational waves are not masked by local effects. The suspensions for the VIRGO mirrors are designed to deal with the two main sources of noise in position while ensuring reliable operation of an interferometer using suspended mirrors. The resulting requirements are shortly described and the working principles of the suspensions briefly outlined below.

The first source of noise is the motion of the ground itself, the seismic noise. On the site of Cascina it is well described by a position noise spectrum [1]:

$$\tilde{x}(\nu) = \frac{10^{-6}}{\nu^2}\ \mathrm{m}/\sqrt{\mathrm{Hz}} \tag{1}$$

for frequencies above a few Hz. Attenuation for this noise to the required level is achieved by a cascade of mechanical filters. These are essentially harmonic oscillators with a low resonant frequency. A damping mechanism is necessary to limit the oscillation amplitude at resonance to keep the interferometer on its working point.

The other relevant source of noise is the thermal bath the mirrors are in equilibrium with. For any mechanical degree of freedom an amount of energy kT is stored between kinetic and potential energy, resulting in what is commonly called thermal noise. Although the amount of energy stored can be reduced only by working at low temperature, it is possible to confine most of the resulting motion in a range of frequencies where VIRGO would in any case not be sensitive.

There are on the suspension system severe constraints that must be met in order to ensure a reliable operation of the apparatus. The mirror position should be controlled over a suitable range of

Table 1: Position noise requirements for the optical elements, without safety factor.

Device	Residual motion along beam		
	at 10 Hz	at 100 Hz	RMS
	$m/\sqrt{Hz}$		$\lambda = 10^{-6}$ m
Fabry-Pérot Mirrors	$3 \cdot 10^{-18}$	10^{-19}	$6 \cdot 10^{-6}\lambda$
Beam Splitter	10^{-16}	$3 \cdot 10^{-18}$	$2 \cdot 10^{-4}\lambda$
Recycling Mirror	10^{-14}	$3 \cdot 10^{-16}$	$2 \cdot 10^{-3}\lambda$
Mode Cleaner End Mirror	TBD	TBD	TBD
Input bench	TBD	TBD	TBD
Detection bench	TBD	TBD	TBD

frequencies to keep the interferometer on its working point. This requires a huge dynamic range: while the mirror motions due to the signal are of the order of 10^{-18} m there can be at low frequencies motions of the order of the mm due to daily ground displacements. These would not only take the interferometer away from the ideal detection conditions but let it pass through several fringes during data taking with severe consequences on operation efficiency. The solution adopted consists in applying only the "fast" corrections to the mirrors and the slower ones at some point in the attenuation system. The mechanical filters attenuate the high frequency components which would fall within the VIRGO sensitivity range while transmitting the required low frequency motion. Large offsets to the nominal position are applied at the suspension point of the filter cascade.

The last important requirement for the suspension system is that it has to be compatible with the vacuum level required by the experiment. This gives constraints to the overall outgassing rate and on the presence of hydrocarbons that can deteriorate the mirror coatings.

4600.1 Functionality and payload

The various elements of the interferometer are all suspended by means of a superattenuator. However the requests on position noise depend on the specific function of each optical element and are part of the interferometer design (see chapter on interferometer optics). They are summarized in table 1, where *no safety factor is included.* While the requirements within the VIRGO sensitivity in frequency are fulfilled by the suspensions, the low frequency displacements must be corrected by an active feed-back system.

The weight to be carried varies in a significant way from element to element. Optical requirements and thermal noise considerations lead to different mirrors in the Fabry-Pérot interferometers. The far mirrors can be massive to reduce thermal noise while the near mirrors are the result of a compromise between light transmission and thermal noise.

The injection and detection benches carry relatively complex optical systems under feed-back control. The displacement requirements come from possible Doppler shifts. The same can be said for the mode-cleaner end mirror.

Position and orientation of all elements have to be controlled as part of the overall interferometer locking scheme. The position noise introduced by the actuators has to be below the nominal VIRGO sensitivity. The requirements on suspensions are summarized in table 2.

Table 2: Requirements for the suspensions.

Suspension	Payload kg	Size cm	RMS position residuals transverse m	RMS position residuals angular rad
FP near	21	35		10^{-7}
FP remote	43	35		10^{-7}
Beam Splitter	6.4	23		10^{-7}
Recycling Mirror	0.750	12		10^{-7}
Mode Cleaner End Mirror	0.750	12		10^{-7}
Input bench	300	180		10^{-3}
Detection bench	300	180		10^{-3}

4600.2 Seismic attenuation

The solution adopted for the VIRGO suspensions is a sophisticated mechanical structure, called Superattenuator, able to filter the seismic noise down to frequencies of a few Hertz (fig. 4).

The suspension consists in a cascade of massive pendula 1 m each connected one to the other. The working principle relies on the fact that for frequencies above the resonances of the system each stage can be seen as a filter attenuating a signal by a factor

$$A(\omega) \propto \frac{\omega_0^2}{\omega^2}$$

as is well known from the behaviour of a forced harmonic oscillator. In this way the use of pendulum properties results in an attenuation of the position noise from the suspension point to the swinging mass.

It turns out that due to uncontrollable couplings between the pendular and other degrees of freedom it is necessary to attenuate also rotations and the motion in the vertical direction. Rotational degrees of freedom are taken care of with high moments of inertia and short lever arms for torque application. This is achieved by having the connections at the filter level very close one to the other. The resulting resonance frequencies are of the order of 1 Hz.

In the vertical direction a similar result is achieved by suspending the next element of the chain through springs. However the resonant frequency of the system is be high if the Superattenuator is to be sustained with an acceptable elongation. To reach also in this case a low resonant frequency these springs are "softened" [2] around the working position by means of a force increasing locally with displacement. If W is the weight to be supported and k_s is the spring constant the equilibrium position x_0 is given by

$$k_s x_o = W.$$

Considering this addtional force an effective spring constant $k_{eff} = -\mathrm{d}F/\mathrm{d}x$ is obtained:

$$F(x) \cong W - k_s(x_0 + \Delta x) + k_a \Delta x$$

or

$$k_{eff} = k_s - k_a.$$

The solution adopted for the seismic filters uses magnets in a repulsive configuration that move transversally to their magnetic field.

The attenuation of the seismic noise has been studied experimentally[3]. The computed transfer functions along the horizontal and vertical direction for the present superattenuator design are shown in fig. 1. This result doesn't take into account further attenuation that can be achieved using the system designed to damp normal mode oscillations.

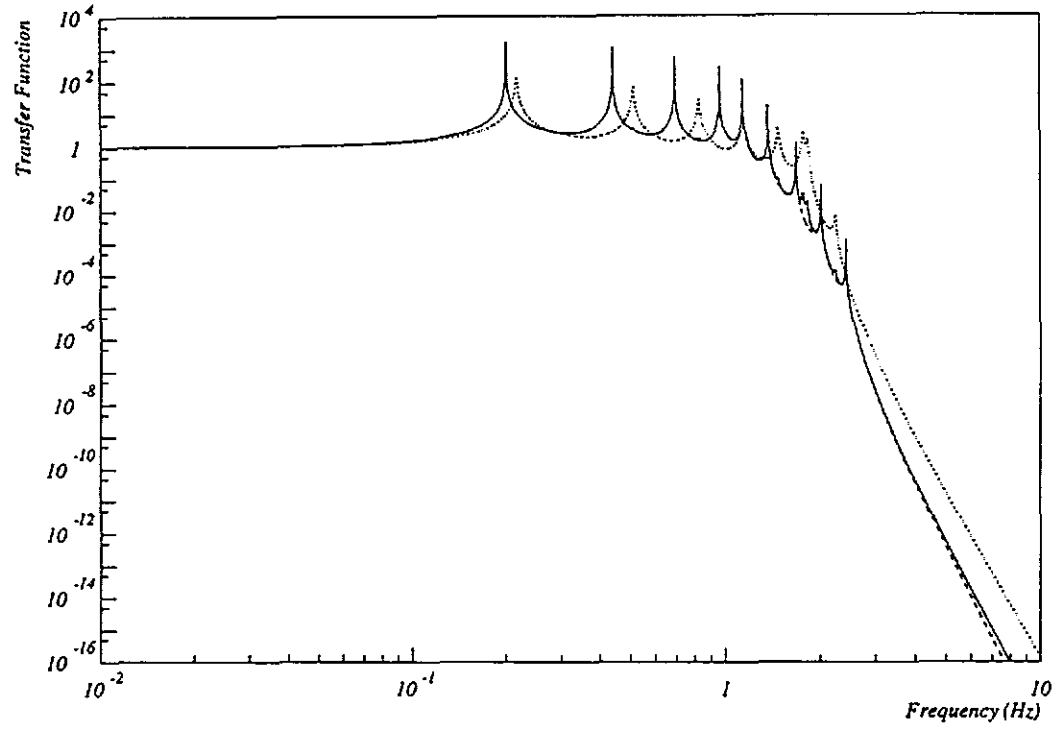

Figure 1: Superattenuator transfer functions from the suspension point to the mirror. The dashed and dotted lines refer to the horizontal and the vertical direction respectively. The continuous line refers to the combined effect of the horizontal and vertical TF (vertical to horizontal coupling of 10^{-2}).

4600.3 Normal modes damping

Once suspended to the Super-Attenuator the mirrors will oscillate at low frequency ($\approx$ 0.3 Hz) with an amplitude of a few tens of μm. This oscillation is maintained by the seismic noise injected at the suspension point and its amplitude is determined by the quality factors associated to the normal modes of the suspension. In order to keep the interferometer optical cavities at resonance this residual motion has to be reduced by several orders of magnitude.

Since a single system would need too high a dynamic range the reduction of the oscillation amplitude is achieved by two control systems in cascade:

1. A local feedback system damps the oscillations using sensors that measure the displacement of the suspension with respect to some reference frame (damping system).

2. A global feedback system preserve the resonance conditions using the interferometer error signals and acting directly on the mirrors (locking).

Such systems have to be effective at the normal mode frequencies while not introducing additional position noise on the test masses in the Virgo sensitivity band. While the locking system has the necessary sensitivity to act on the last stage directly, the damping system, much less sensitive, acts on the second stage of the suspension. In this way any noise introduced by the damping feedback system is filtered by the following stages.

The reference configuration uses 6 position sensors fixed to the supporting structure to provide a measurement of the filter linear and angular coordinates. By applying a feedback force proportional to the velocity one performs a "viscous" damping reducing the quality factor of the normal modes.

In the reasonable hypothesis that the residual rms displacement of the mirror is mostly due to the lowest frequency normal mode (where all the SA stages are moving like a single pendulum) it is simple to evaluate the effect of a viscous damping system. For a pendulum having f_0 as resonant frequency and Q as quality factor one has

$$x_{RMS} = \tilde{x}_s(f_0)\sqrt{\frac{\pi f_0 Q}{2}}, Q = 60 \tag{2}$$

where $x_s(\nu)$ is the seismic noise spectral density.

Assuming $\tilde{x}_s(\nu) = \frac{10^{-6}}{\nu^2}\,\mathrm{m}/\sqrt{\mathrm{Hz}}$ (eq.1), a quality factor of 60 and a resonant frequency of 0.23 Hz (the values measured on the first SA prototype), the rms displacement of the mirror is about 80 μm, which would give difficulties in locking the interferometer. By achieving a Q of 0.5 the residual rms displacement becomes

$$x_{RMS} = 8\,\mu\mathrm{m}, Q = 0.5. \tag{3}$$

This quantity is low enough to make the interferometer work (assuming that the locking system is able to cope with mirror displacements up to 10 μm). A residual displacement $x_{RMS} = 3.4\,\mu$m has been achieved [4] in the suspension prototype developed in the last years in Pisa.

The viscous force applied on the second stage of the SA is not sufficient to reduce the displacement under a few micron. The measurement of the displacement is performed with respect to a grounded noisy structure: by increasing the gain loop of this cooling system, the second stage shall be locked to the grounded structure, short-circuiting the first two stages of the SA. Moreover when forces are applied to the second stage to damp it, vibrations are induced in the structure supporting the actuators and also the sensors. These vibrations can generate oscillations in the feedback system, thus limiting the bandwidth of the damping system and so the resulting gain.

It is foreseen to further reduce the rms displacement below 1 μm by performing a measurement not referred to a noisy structure but to an inertial frame by means of acceleration sensors. Six such devices are installed on the second stage (three of them sensitive to the horizontal acceleration and the other three sensitive to the vertical acceleration) and produce a signal from which the motion of the SA with respect to a local Lorentz frame is derived. These signals can be used to apply appropriate forces through the usual six magnet-coils pairs. In this way not only the resonant motion can be damped but a higher reduction of the low frequency level of the displacement can be achieved. In this case the lowest displacement of the mirror that can be obtained is limited only by the electronic noise of the acceleration sensors. Table 3 summarizes what should be expected for the test mass rms position.

A first version of the inertial damping system has been studied in Pisa and damping has been achieved for three degrees of freedom [5].

Table 3: Residual test mass displacements.

	RMS Mirror Displacement
Without any control system	80 μm
With a viscous damping system	8 μm
With an inertial damping	< 0.2 μm

4600.4 Vacuum compatibility

Refractive index variations due to pressure fluctuations are a source of noise in the optical length measurement. The residual H_2 pressure to be achieved in Virgo is of 10^{-8} mbar and the elements under vacuum have to be compatible with the pumping rate of the installed system (see the chapter on the vacuum pumping system). In addition the partial pressure for hydrocarbons has to be less than 10^{-13} mbar so that the reflective coatings do not loose their properties. To achieve this the suspension towers are divided into an upper and a lower part separated by a conductance pipe for the supporting wire. The conductance is 1 l/s for water. In this configuration the components in the upper tower part should have an overall outgassing rate compatible with a residual pressure of 10^{-6} mbar at a pumping speed of 500-1000 liters/s. In addition the outgassing rate for hydrocarbons should be less than 10^{-10} mbar liters/s assuming 1 l/sec conductance from upper to lower part of the tower also for hydrocarbons.

4600.5 Suspension overview

A complete suspension chain consists, from top to bottom, of the following elements: a movable suspension point, a chain of several seismic filters and a marionetta suspending the mirror.

The micrometric table determines the position of the suspension point relative to the supporting structure. The settings for this device are determined from the alignment error signals and the low frequency component of the locking error signals. Then there is a chain of seven seismic filters, that perform a mechanical attenuation in all six degrees of freedom of a rigid body. The second of these filters is equipped with accelerometers and shadowmeters to damp the normal mode oscillations of the structure. A damping force is applied to this filter through coils that move following the micrometric table motion. Each filter has its own height control so that the spring softening device stays on the right position. According to the requirements for the reference configuration two kind of suspension chains are used, a complete one with seven filters and a short one with only three filters (table 4).

There are additional variations at the level of the last suspension stage, the marionetta, to take care of the differences between mirrors. For the short suspensions positioning of the load is achieved with coils fixed on ground, while for the interferometer mirrors this is done from the last filter in the chain and from a reference mass suspended, liek the mirror, to the marionetta itself.

4610 Micrometric tables

The motion at frequencies below the first resonance frequency of the superattenuator have to be achieved by moving the suspension point. The micrometric table lays at the top of the metal support

Table 4: Suspension structure. The height is from the floor to the suspension point and doesn't include therefore the tower cover.

Suspension	Mar. wgt kg	Position control	Filters	Height m	Total wgt kg
FP near	80	Mar.+Ref.Mass	7	10.430	1037
FP remote	80	Mar.+Ref.Mass	7	10.430	1058
Beam Splitter	80	Mar.+Ref.Mass	7	10.430	1021
Recycling Mirror	80	Mar.+Ref.Mass	7	10.430	1021
Mode Cleaner End Mirror	60	Mar.	3	6.436	TBD
Input bench	TBD	Coils on ground	3	6.436	TBD
Detection bench	TBD	Coils on ground	3	6.436	TBD

Table 5: Micrometric table actuator specifications.

Movement	Range	Force	Step	Speed	Encoder reproducibility
Horizontal	± 4.5 cm	1120 N	0.027 μm	100 μm/1′	10 μm
Vertical	± 3 cm	11000 N	0.031 μm	100 μm/1′	10 μm
Rotation	± 15 °	2000 N m	0.5 μrad	2 mrad/1′	2 μrad

structure of the towers. It defines the average position of the whole SA at the level of a few μm, while carrying the whole weight (11000 N).

The requirement for smooth motion with a large load over a large range leads to a system rolling in elastic regime. Hyperstaticity, as a source of problems for a device that cannot be lubricated, has been avoided. A system of three C6 steel spheres allows two planes to translate and rotate one with respect to the other. The spheres are 89 mm in diameter and are of hardness 60 HRC. The planes are chromed or nickeled to enhance surface resistance. Sphere pressure results in a 1 mm diameter spot with a depth of 1.5 μm on hardened steel. Horizontal motion is obtained with stepping motors working under vacuum that push and pull the plane supporting the suspension point. Two counteracting stepping motors allow rotations around the pendulum axis. Finally a mechanism raises and lower the superattenuator by means of a screw. A drawing of the micrometric table is shown in in fig. 5.

All these motions are remotely controlled but an offset can be applied at the assembly time to the position around the vertical axis. All stepping motors have an absolute position readout to allow for reliable operation when the tower is closed. The specifications for the table motion are indicated in table 5. The local control of the table is performed through a VME interface to the stepping motors. The conditions under which the table moves during data taking are currently under study.

The table is in vacuum and should stand baking cycles at a temperature of 80 °C. The actuators have been redesigned using ultra-high-vacuum compatible components (fig. 6). The availability of motors with a low out-gassing rate and with inorganic lubrication allows operation without contaminating the optics. This will be checked by dedicated tests using sample motors.

The vertical lift (fig. 7 has also been redesigned with vacuum compatible components. This results in the total suppression of pressurised vessels inside the vacuum towers.

4610.1 Cables and controls

Power to the motors has to be brought using vacuum friendly cables. Table 6provides a list of cables needed.

Table 6: Leads to drive one micrometric table and coil holder.

Item	Leads	Length	Remarks
Motor power and monitor	66	10 m	unscreened
Encoders (LVDT) drive	2	10 m	screened
Encoders (LVDT) readout	4	10 m	screened

4610.2 Acceptance tests

In order to qualify the table for final mounting the following points need to be checked.

- Functionality
- Movement within specifications using the prescribed loads
- Behaviour under heating
- Outgassing test

It is estimated that each table test lasts two weeks and requires one engineer half time and a technician full time. The total time for nine tables is 18 weeks, once the test is properly set up.

4620 Seismic filters

Seismic isolation is achieved using a chain of seven mechanical filters in cascade. Each mechanical filter is formed by a massive pendulum consisting of a full metal spring suspended to the previous stage by a 1 m long piano wire.

The elastic elements forming the spring are metal cantilevers made of high quality steel (C70). As it is shown in fig. 8 the cantilevers have a triangular shape and they are pre-bent in order to be straight and horizontal when properly loaded. The triangular shape allows a uniform stress along the loaded cantilever and so reduce the maximum stress. After being cut, bent and annealed at 900 °C, the cantilevers tensile strength is about 160 kg/mm^2 and the elastic limit is about 130 kg/mm^2. Bending curvature and dimensions are such that in a loaded cantilever the internal stress is always kept below 2/3 of the elastic limit. As it is shown in fig. 9 all cantilevers are 3.5 mm thick and 385.5 mm long; the cantilever width changes according with the load it has to support (tab. 7). Once properly loaded, the cantilever vertical resonance is around 1.5 Hz and all cantilever flexural modes of resonance are above 100 Hz. The quality factor of the first flexural mode can be efficiently reduced to a few units by attaching a low Q oscillator to the centre of the cantilever. All cantilevers are protected from rust formation with a thin layer of nickel.

The geometry of a single mechanical spring using metal cantilevers is shown in fig. 9. A cylindrical structure, properly stiffened with ribs, is suspended through a wire attached near the overall centre of mass and supports up to twelve cantilevers. By varying the number of cantilevers and

their dimensions (see tab. 7) it is possible to adapt each spring to the load it has to carry. The tip of each cantilever is connected through two piano wires (0.8 mm in diameter) to the moving part of the spring, that is the central column. This part moves freely in the vertical direction and it is kept on axis through four centring wires (1.2 mm in diameter) on the top of the cylinder and four more wires on the bottom. The central column supports the load through a wire also attached near the spring centre of mass. The distance between the attach points of the two wires is about 5 mm in order to keep the rocking frequency of the spring below 1 Hz. The mass of each stage and the load it has to carry are shown in tab. 7.

Table 7: Seismic filters parameters.

Filter	Mass	Load	Cantilevers	Fixed Cantilevers			Adjustable Cantilevers		
					width	load		width	load
n	(kg)	(kg)	tot. n	n	(mm)	(kg)	n	(mm)	(kg)
1	142	957	12	8	180	93	4	120	53
2	164	793	12	9	180	70	3	120	53
3	135	658	12	8	120	56	4	120	53
4	132	527	10	6	120	52	4	120	53
5	128	399	8	4	120	47	4	120	53
6	116	283	6	4	120	44	2	120	53
7	112	171	4	2	70	32	2	120	53

The hook and nut suspension of the attenuators has been replaced by a symmetric double "nail head" wire obtained by centre-less grinding of a larger diameter piano wire (see fig. 10). The nail head is then mounted inside a screw head by means of a split cup washer. The resulting rotatable wire headings are then simply screwed in two tapped bridges attached to the upper and lower suspension points of the lower and higher attenuators. The advantages of this solution are:

- It is a fully rotationally symmetric system and angular attenuator reorientation can be easily achieved. In particular there is no privileged "rocking" axis, as in the case of the bent wire.
- The wire is left free at a distance which is almost a factor of two shorter than in the older version. The lower and higher suspension points of each attenuators are then closer to each other resulting in a lower swinging frequency.
- Mounting and dismounting of a wire from an attenuator is simpler without need of any half length wire connection.
- While in breaking tests of the hook and nut tests the breaking has happened at the hooking point with a shear break (incidentally hinting to an asymmetric stress and an asymmetric oscillation mechanism) in breaking tests of the "nail head" wire the wire has broken in a random position far from the hooking point and with a clean bottleneck break.

Preliminary tests of the whole hook and split cup have shown that mounting and dismounting is easy also after elongation tests.

A magnetic "anti-spring" is set up on the top of the spring (see fig. 2); it consists of several magnetic rods (up to six) mounted on the top of the cylindrical structure in front of as many rods fixed

to the central column. Each magnetic rod is made of a layer of 7 magnets ($6 \times 2 \times 1.5$ cm^3) producing a magnetic field of about 0.36 Tesla. The magnetic rods are in a repulsive arrangement in order to have an "anti-spring" effect. By varying the number of rods and their relative distance the anti-spring strength can be adapted to the number of cantilever used on each stage. This system allows to decrease the total stiffness of the spring by about a factor of 10 taking the vertical resonance of a single loaded stage from about 1.5 Hz down to about 0.5 Hz. This condition guarantees that all vertical resonances of the suspension are kept below 3 Hz.

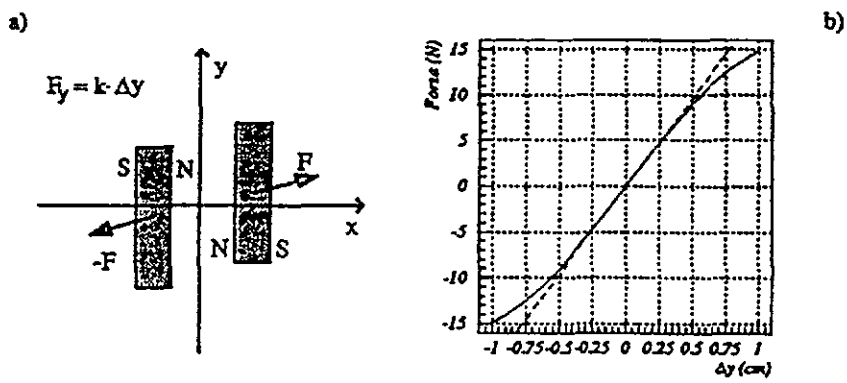

Figure 2: a) The antisprings configuration; b) The force as function of displacement (arbitrary scales).

In order to adjust the spring length and to keep the magnetic rods one in front of the other, the angular positions of some of the cantilevers can be varied. The number of adjustable cantilevers on each stage depends on the total number of cantilever used on that stage (see tab. 7). As shown in fig. 9 these cantilevers are mounted on supports adjustable by varying the length of a bellow. The bellows are filled with water and are connected through a small copper tube (0.7 mm internal diameter and 1.1 mm external diameter) to an external reservoir (fig. 11). A piston driven by a motor allows to vary the volume of the reservoir in order to add or to extract water from the bellow and, consequently, to adjust the inclination of the cantilever. The vertical position of the spring is read through a LVDT (linear variable differential transformer) and this error signal, after having been filtered, is fed back to the motor. The response time of the feedback system is about 3 minutes and is mainly determined by the thin tube response time. The feedback precision is of a few μm. The variation of the vertical position of the spring when the feedback is off is expected to be around 100 μm/ ℃ . This should allow to turn the feedback system off during data taking in VIRGO. To maintain the bellow internal pressure below 1.5 Atm all adjustable cantilevers are 120 mm in width and carry only 53 kg.

As already said the cantilevers internal mode of resonance is damped by attaching a small low Q oscillator to the centre of all cantilever. A similar system use a 2.7 kg mass suspended on three rubber spring to damp a resonance of the central column around 60-80 Hz. The exact frequency of resonance may depend on the precise structure of each stage and a fine adjustment of the absorber will be necessary. The bellows also may produce spurious resonances around 20-30 Hz; these resonances are usually damped once the bellows are filled with water. Finally a small low Q oscillator attached to the middle of the wires connecting one stage with the following one may be used, if necessary, to damp the wire resonance.

4620.1 Test specifications

The filters are suspended with their nominal load, which varies depending on the height in the super-attenuator chain. Transfer functions are measured and resonances identified. Vertically the height compensation parts is tested with a simple feedback loop. Finally the single filter has to be heat and vacuum qualified.

A dedicated setup is being assembled in Pisa, to be able to bake one filter while testing the next one. It is expected that two filters are tuned each week. This implies that 26 weeks are needed to produce all fiftyone filters with two technicians full time. One engineer half time, at least at the beginning, should also be foreseen for this phase.

4630 Damping filter

The second filter of the suspension is equipped with a control system able to damp the normal modes of the suspension. This consists in sensors providing the error measurements and actuators giving the necessary correction forces. This system works on the 6 degrees of freedom of the filter.

The first set of sensors consists in 6 Linear Variable Differential Transformers (LVDT) providing a position measurement referred to the tower internal structure. These sensors follow a 120 ° symmetry around the vertical axis. Translational and rotational coordinates are obtained by forming linear combinations of these measurements. Following the same symmetry a second set of sensors equips the filter. These are linear and rotational accelerometers providing measurements referred to an inertial frame.

The correction forces are applied on the filter following the same 120 ° symmetry of the sensors. More precisely each force is parallel to the measurement axis of the corresponding sensor and is applied within a few centimeters from it. This is achieved by permanent magnets fixed to the filter and coaxial to the LVDT and magnetic coils providing the necessary field gradient. These coils are fixed on a frame which is able to follow the motion of the suspension point.

To implement the three-fold symmetry the second filter is equipped with three mobile springs for height control. This results in a slightly different disposition of the hydraulic system around the filter. The LVDT and the accelerometers characteristics are in more detail in the section on suspension control.

The implementation of the damping stage in a fully working

1. a modified filter with a 120° symmetry to hold the three pairs of accelerometers
2. the linear and angular accelerometers
3. the transducers applying the feedback force
4. a mobile structure to allow the transducers to allow for the motion of the suspension point

Figures 13 and 14 show the linear and the angular accelerometers. Fig. 12 shows a top view of the second filter of the suspension. The three-fold symmetry of the accelerometers is apparent. The actuators for the coil holder are also visible.

4640 Vertical compensation

The length of each pendulum needs to be controlled to ensure that the vertical position of the mirror remains constant. Movement should be smooth not to introduce any noise through vertical-

horizontal couplings. The adopted solution makes use of an hydraulic circuit for each filter which adjusts the equilibrium position of a few springs of the filter. Pressure is brought to each filter by means of thin SL304 stainless steel pipes with an inner diameter of 0.7 mm and a wall 0.2 mm thick. By having each pipe making wide loops from one filter to the other the stiffness of the superattenuator is not increased significantly. Such a thin pipe attenuates rapidly any sound wave generated at one extremity introducing a negligible noise at each stage (fig. 3).

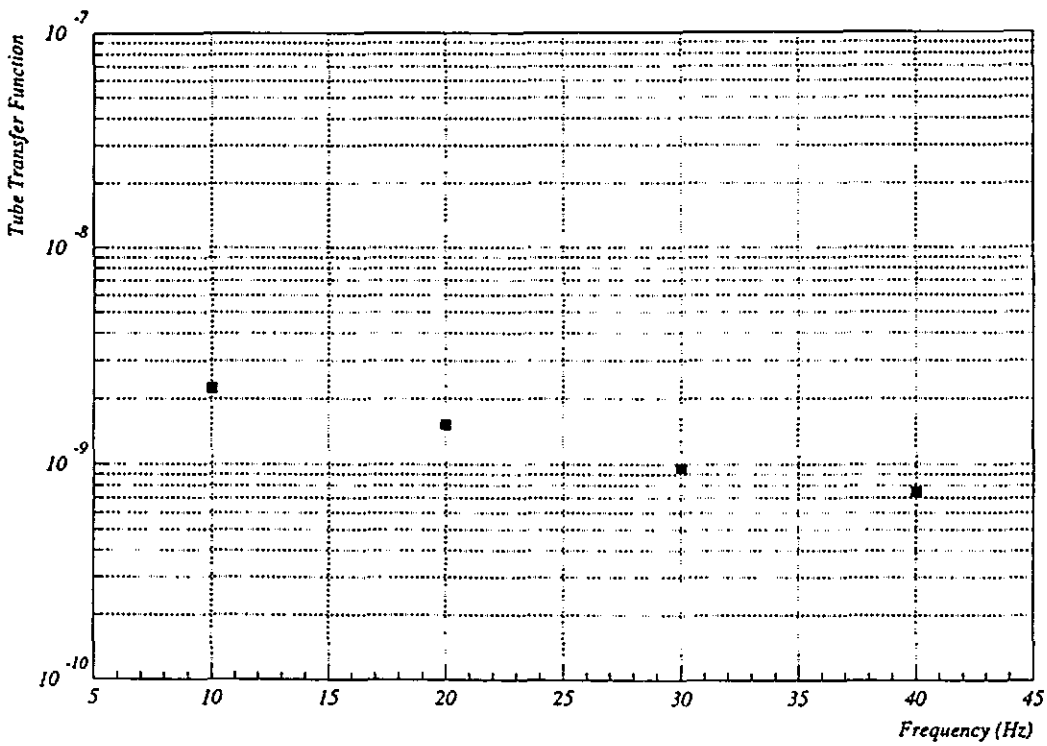

Figure 3: Upper limit for sound transmission by a pipe filled with water 10 m long and with an inner diameter of 0.7 mm.

Vertical position sensing is performed through a differential transformer mounted on the seismic filter and its cross. Height control is performed by acting on a bellow outside the vacuum tower. The following table provides a list of cables needed.

Table 8: Leads for filter height control.

Item	Leads	Length	Remarks
Transformer driver	2	17 m	screened
Transformer sensors	7	17 m	screened
Total for 7 filters	63		

The height of each filter is kept constant by the local control system using the position sensor

on each filter. The feedback is performed by the local processing unit that drives the motor of each filter through a VME interface.

References

[1] *Virgo Final Conceptual Design*, The Virgo Collaboration, 1992.

[2] S. Braccini *et al.*, Rev. Sci. Instrum. **64** 310 (1993).

[3] *Low Frequency Behaviour of the Pisa Seismic Noise Super-Attenuator for Gravitational Wave Detection*, R. Del Fabbro *et al.*, Phys. Lett. A **133**, 471 (1989).

[4] *First Results on the Electronic Cooling of the Pisa Seismic Noise Super-Attenuator for Gravitational Wave Detection*, C. Bradaschia *et al.*, Phys. Lett. A **137**, 329 (1989).

[5] *La Sospensione degli Specchi ed il Controllo di un Interferometro per la Rivelazione di Onde Gravitazionali*, R. Flaminio, Tesi di Dottorato, Pisa, 1995.

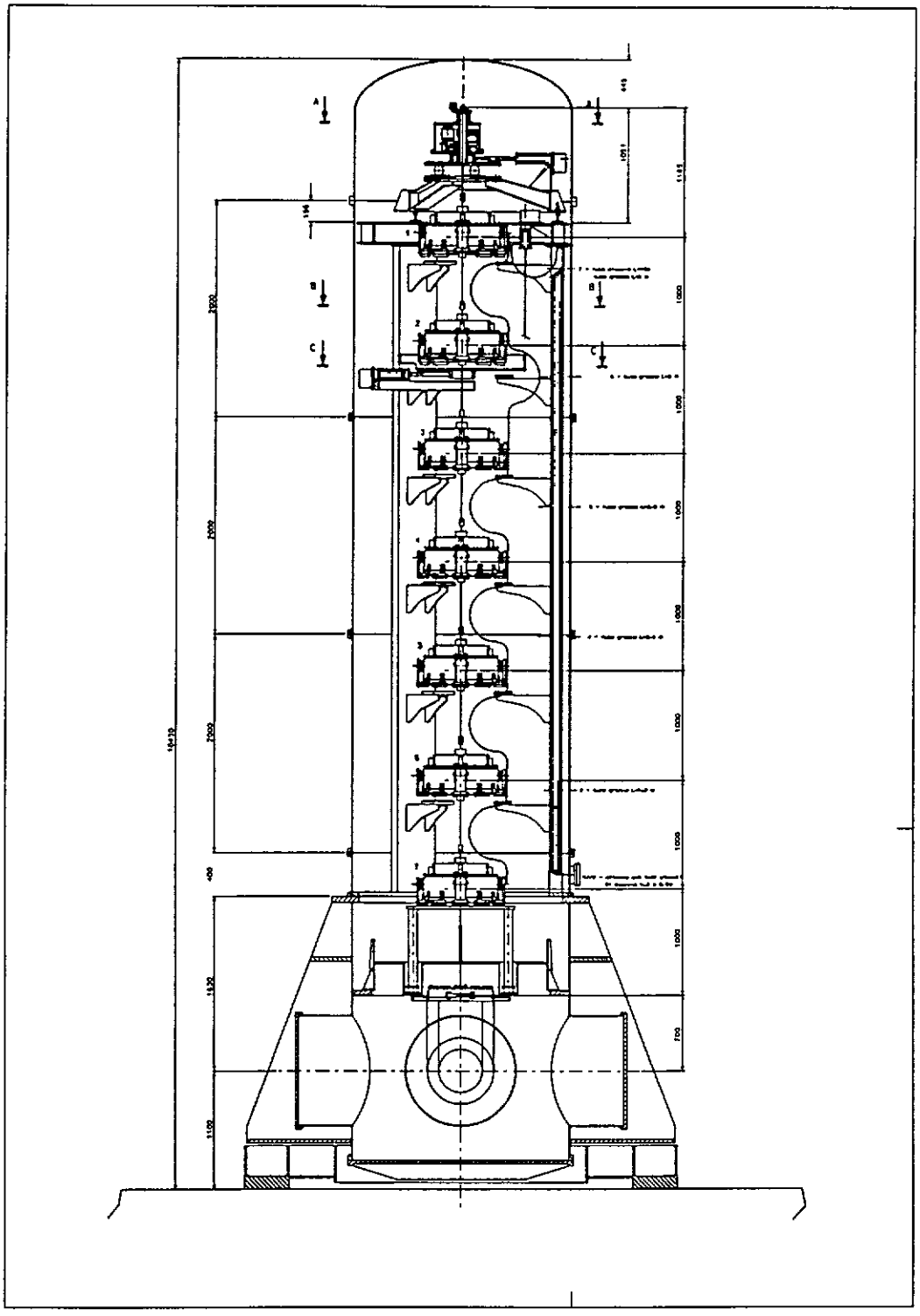

Figure 4: The VIRGO mirror suspension.

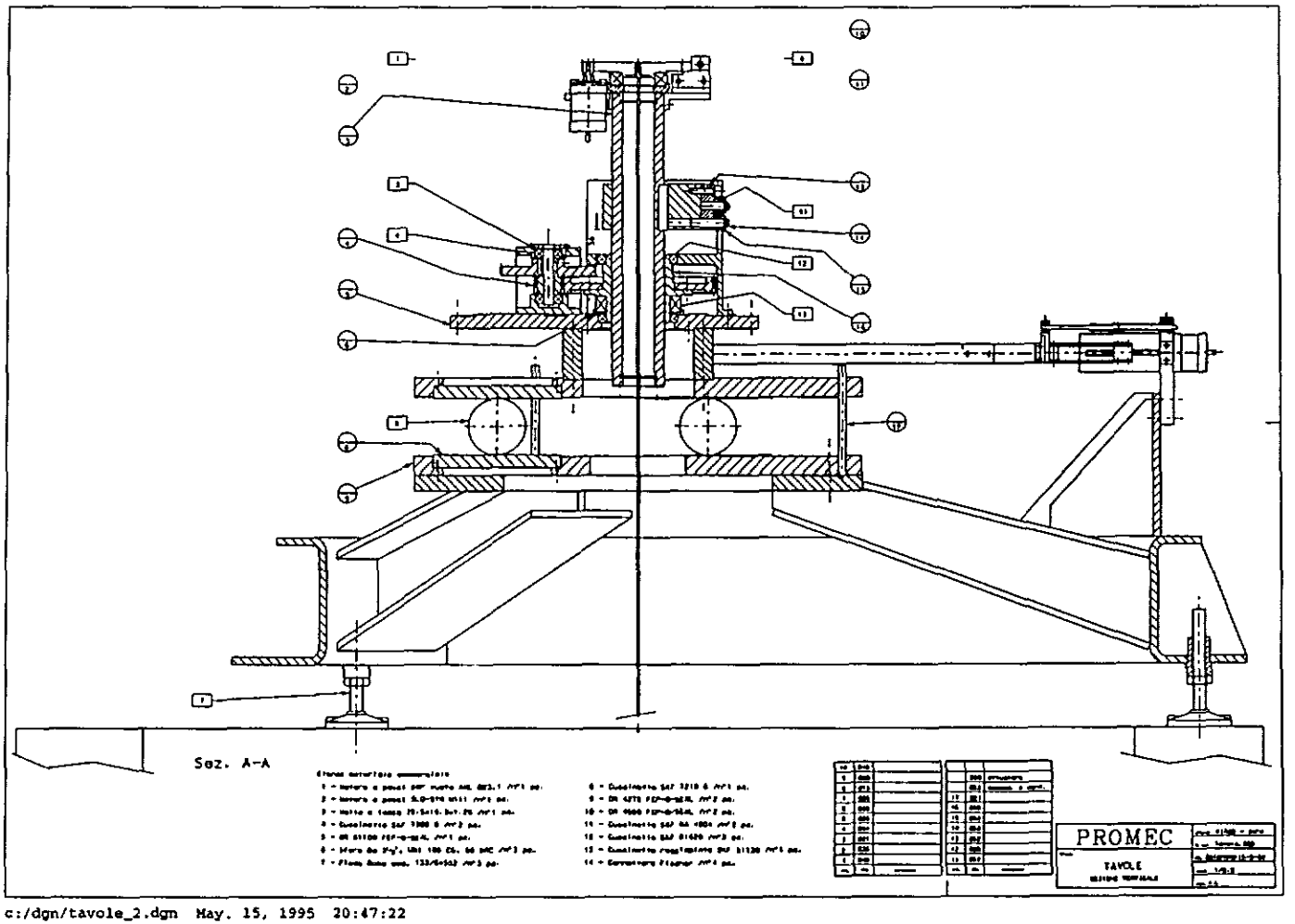

Figure 5: The micrometric table: side view.

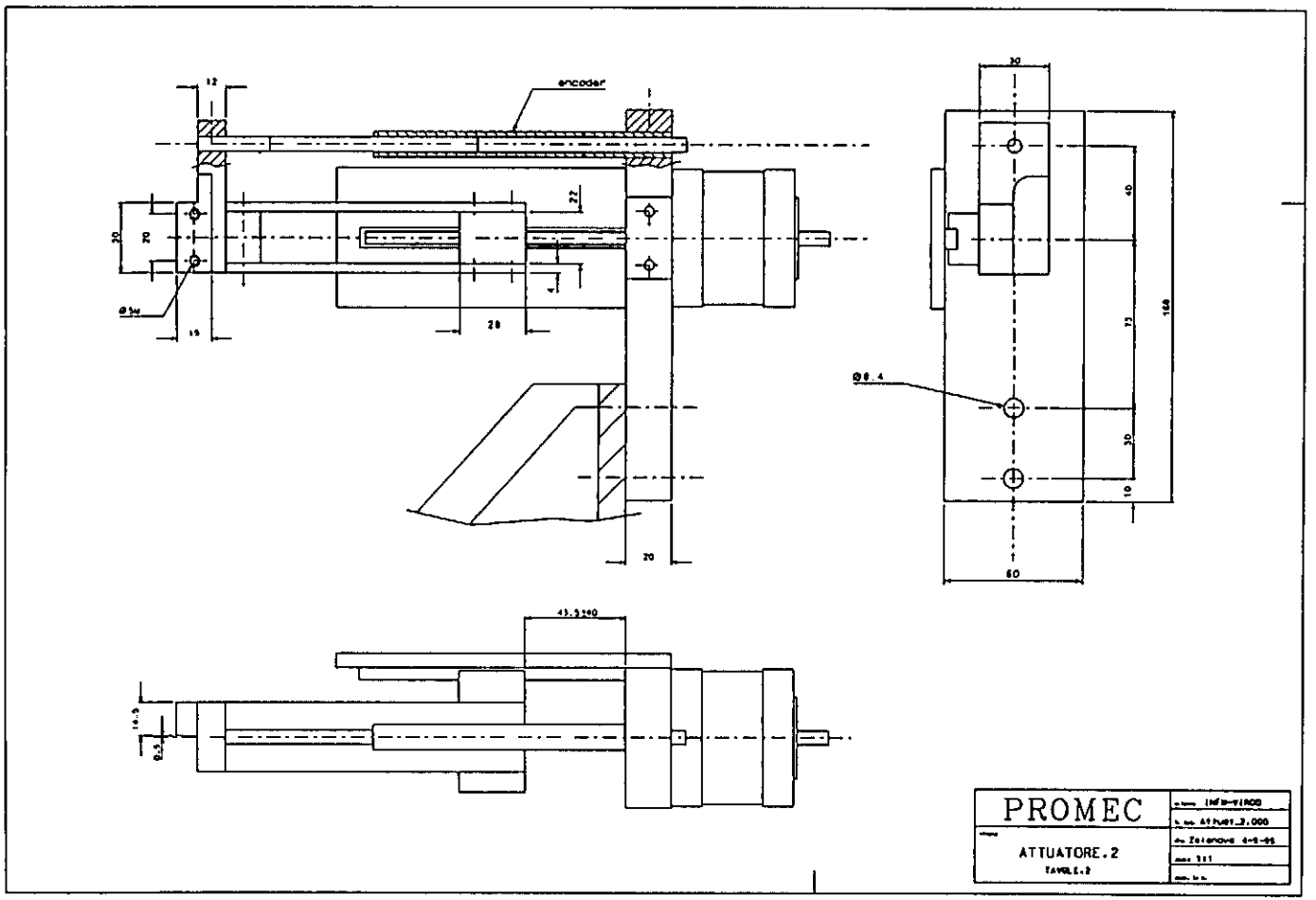

Figure 6: The micrometric table actuator.

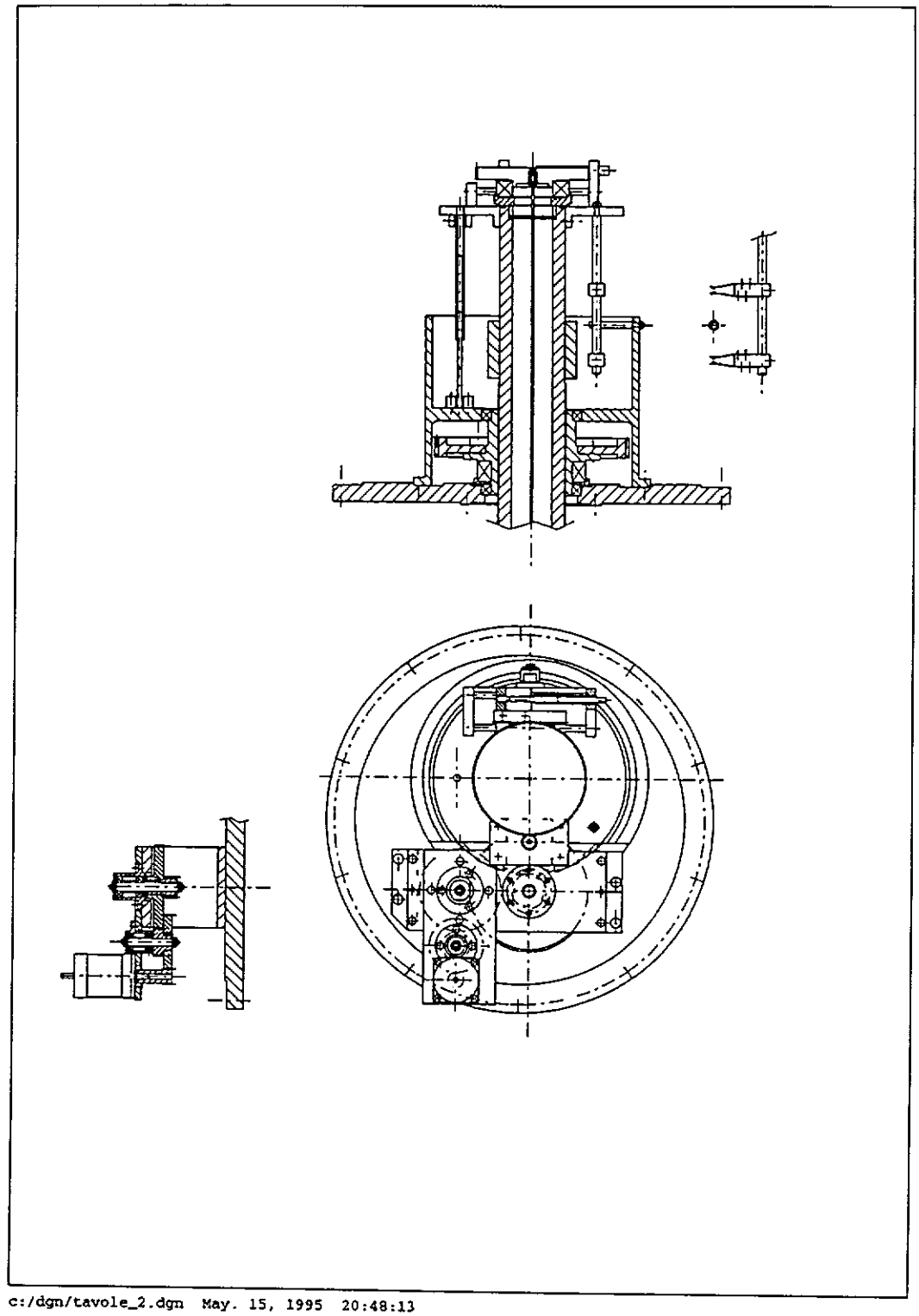

Figure 7: The micrometric table lift.

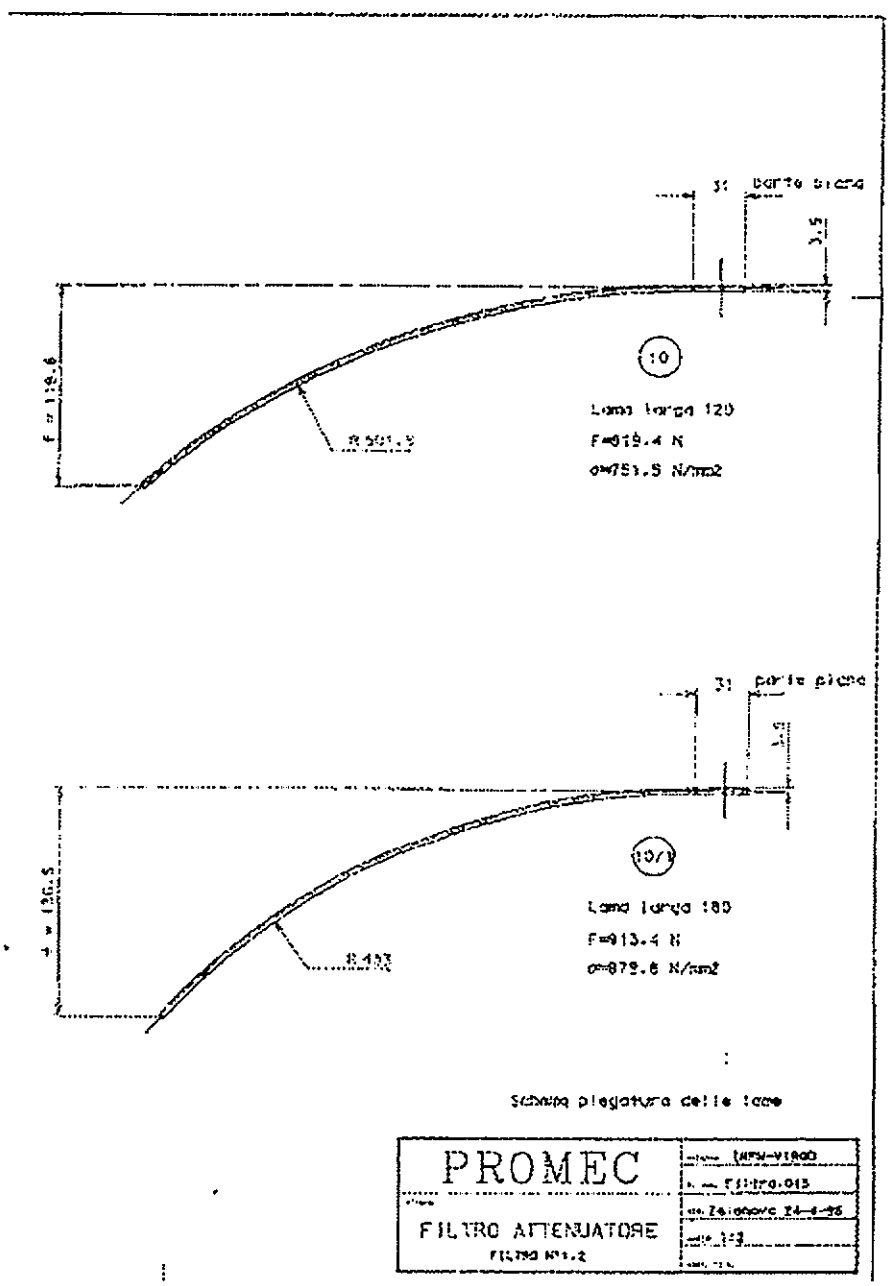

Figure 8: The springs for the seismic filter.

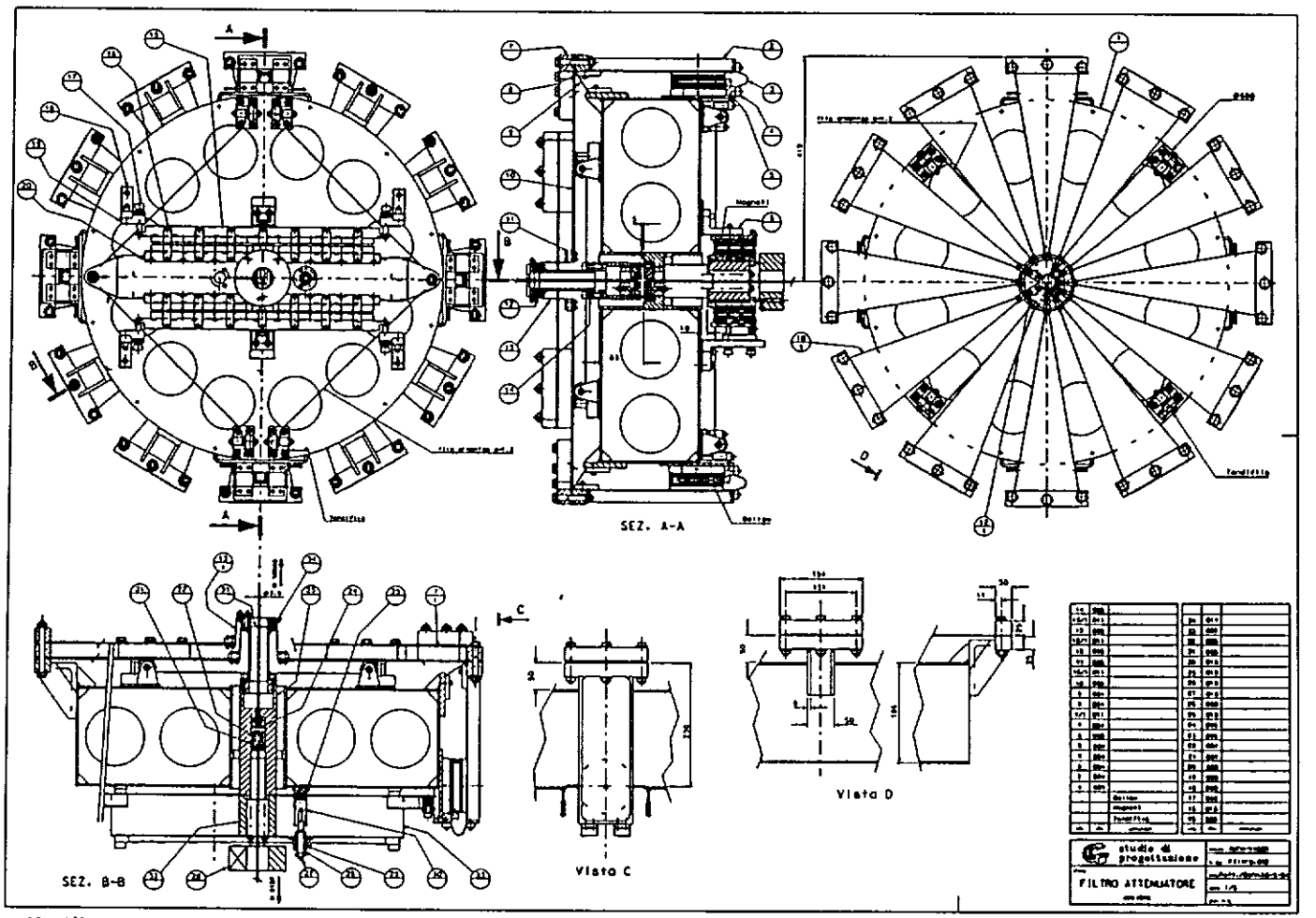

Figure 9: The seismic filter.

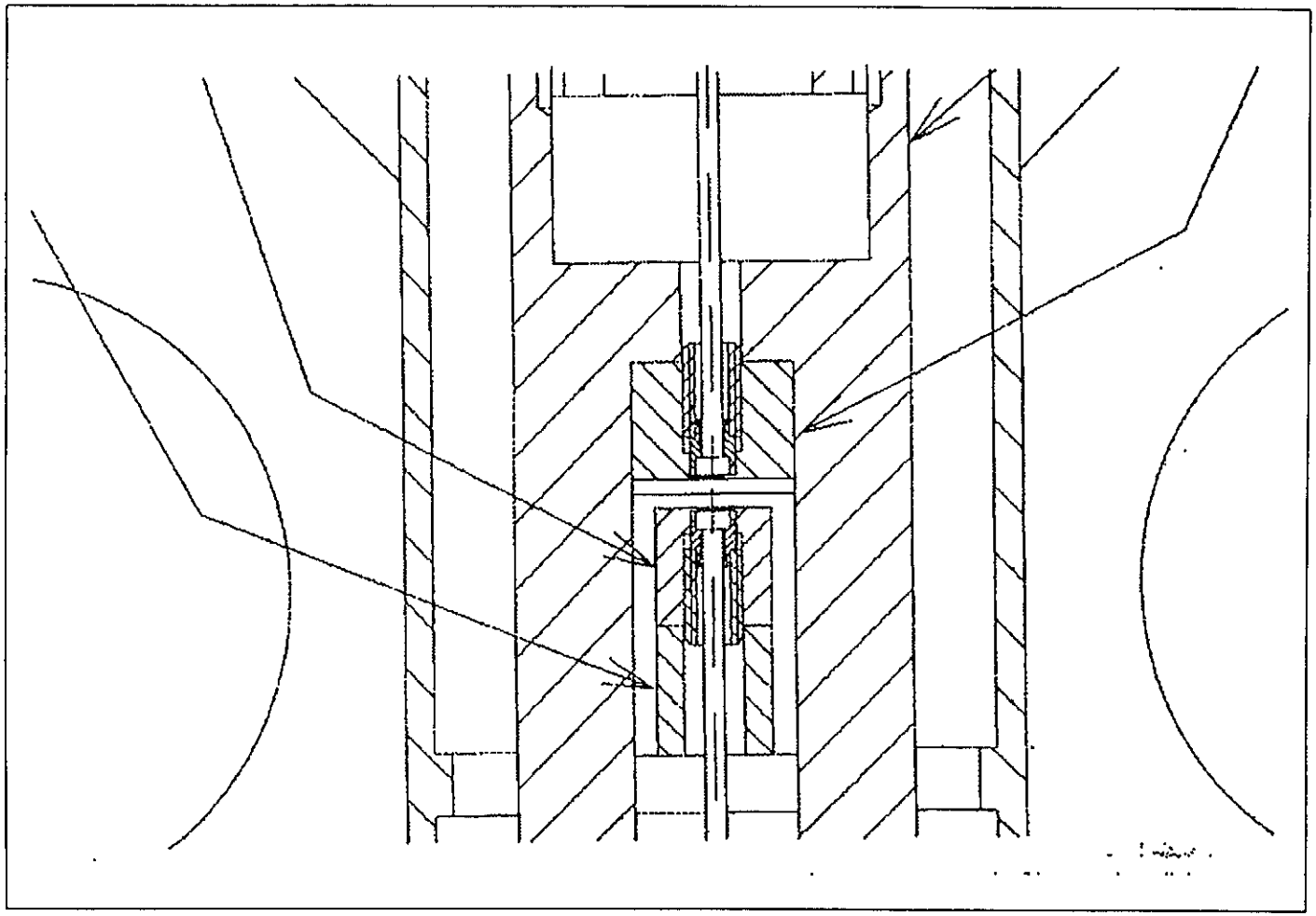

Figure 10: The nail-head hook for the filters.

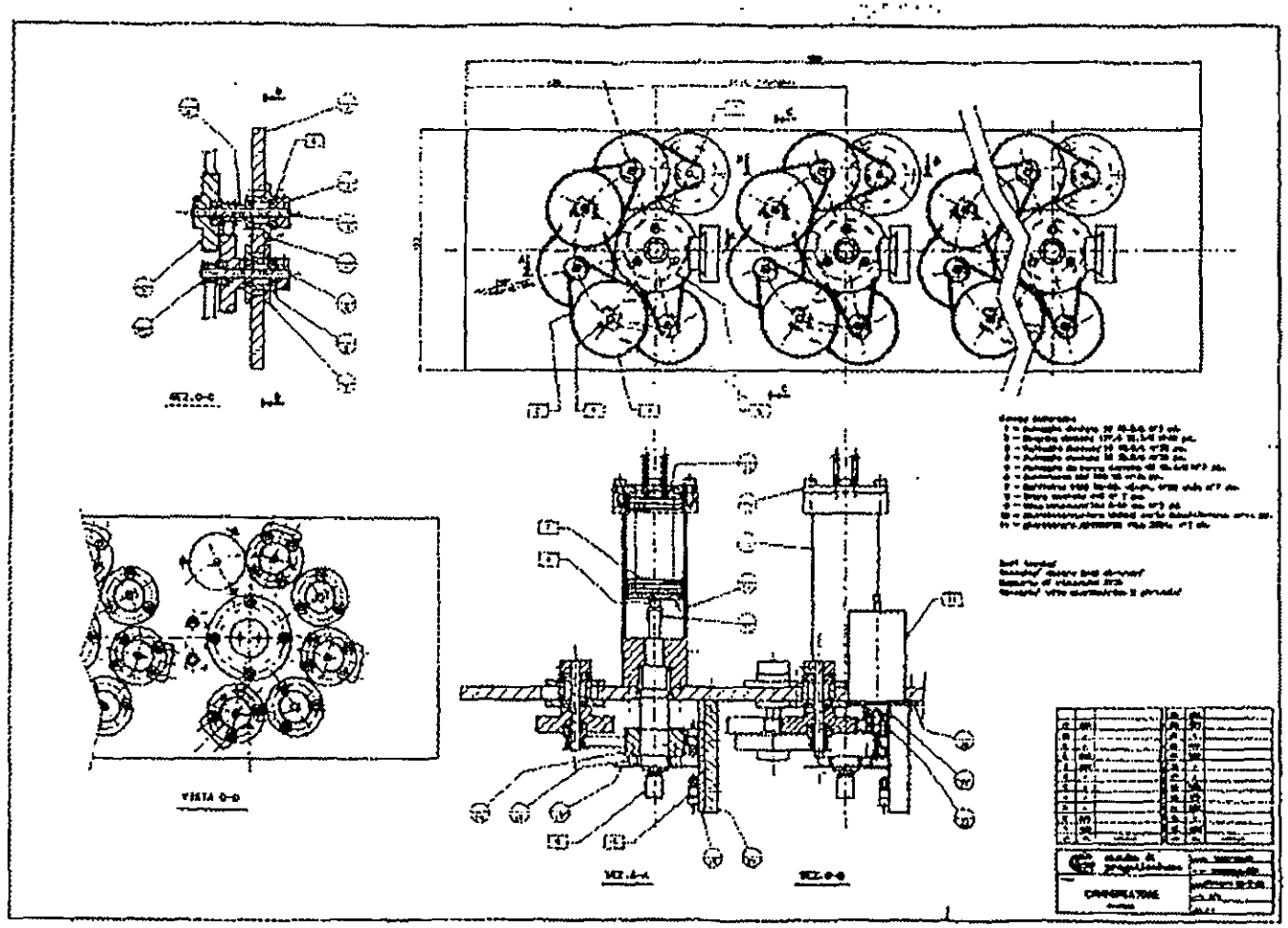

Figure 11: The height compensation system.

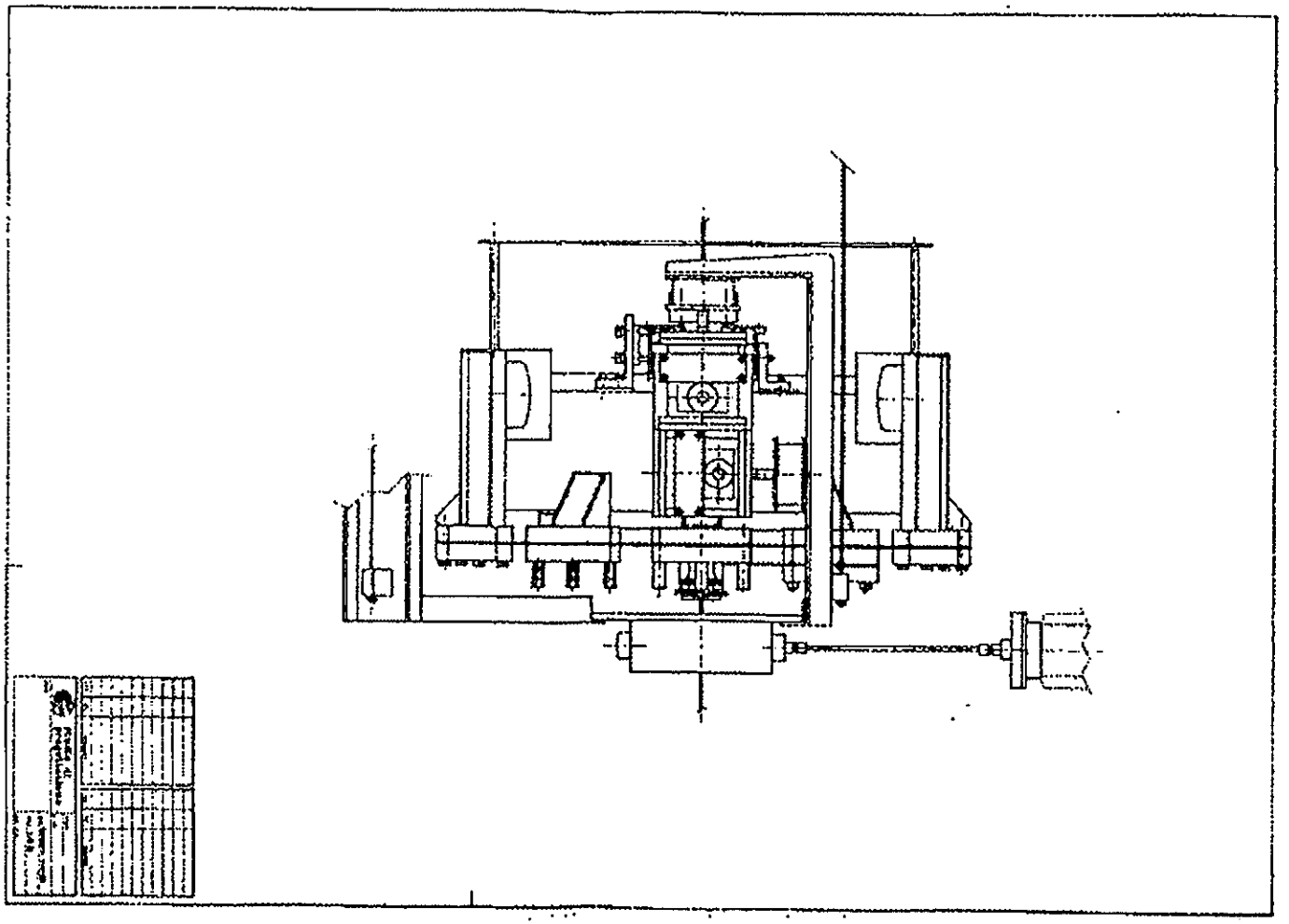

Figure 12: The second stage of the suspension.

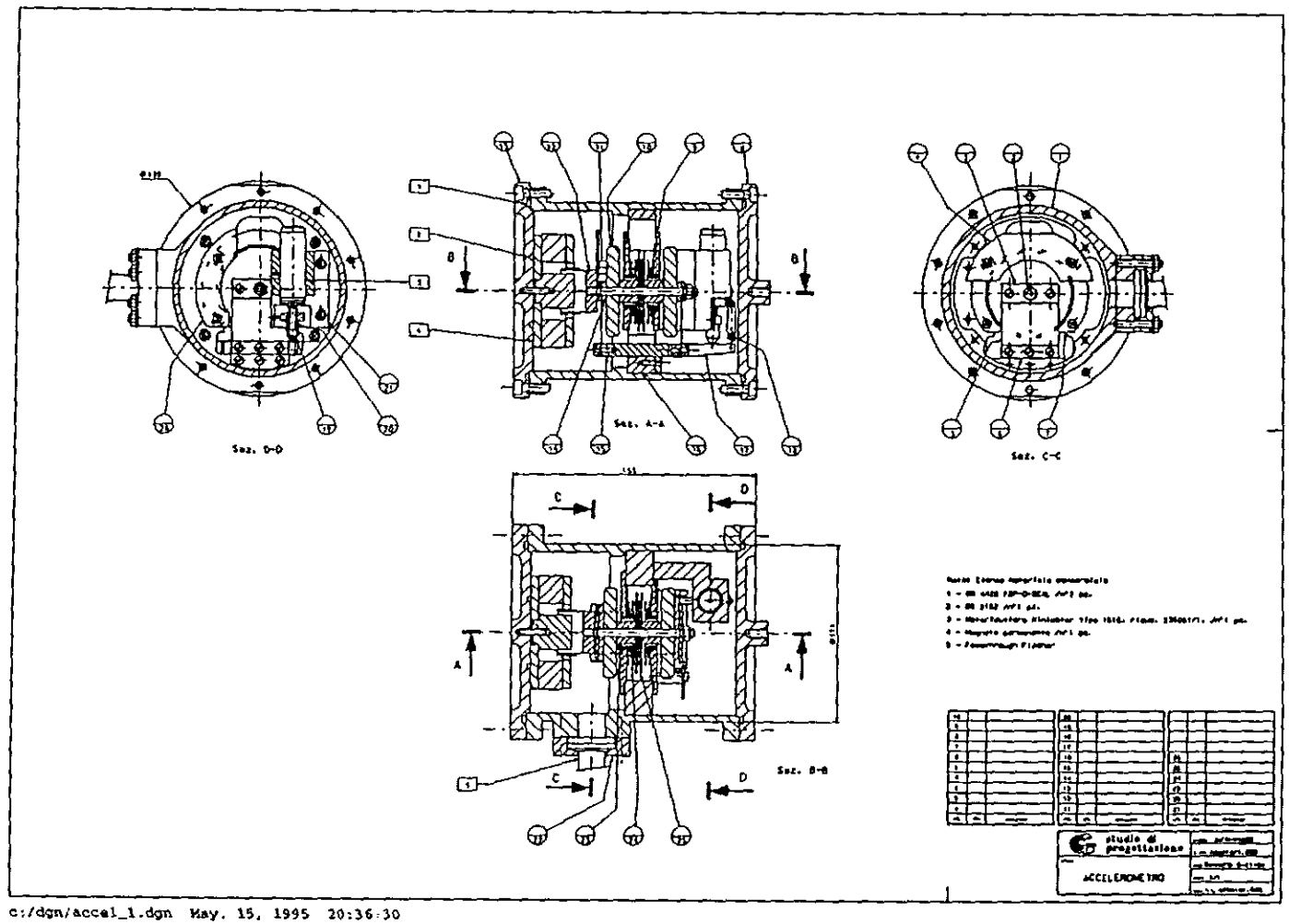

Figure 13: The linear accelerometer.

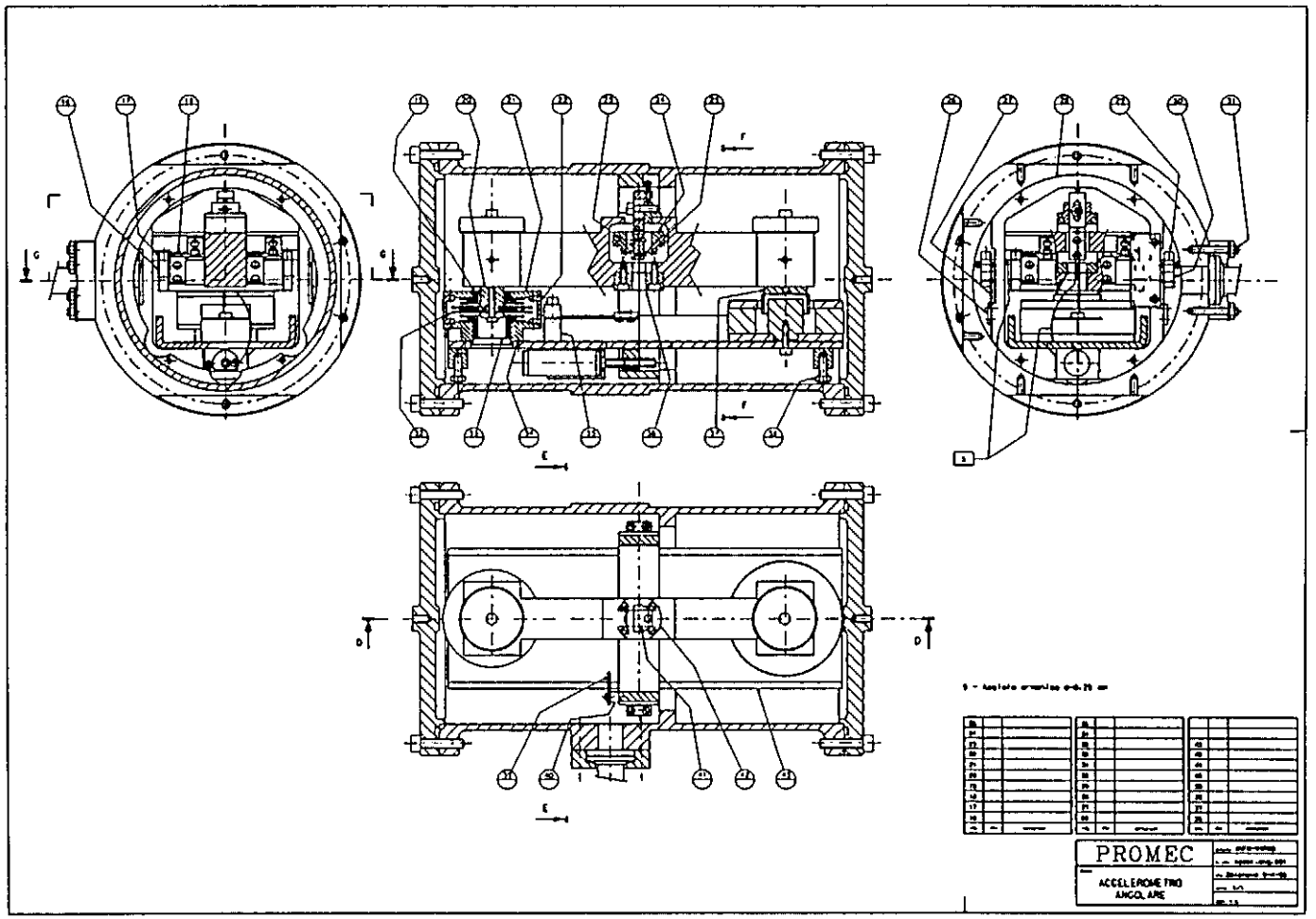

Figure 14: The angular accelerometer.

Last Stage of Interferometer Suspensions

4700 The last stage of the interferometer suspension

4700.1 Overview

The Superattenuator ends with two elements which are located in the cleaner vacuum region: the *marionetta* and the optical component (fig. 3).

The marionetta has the purpose of steering and aligning the optical component in the interferometer. In fact, it is necessary to apply to the test masses displacements of the order of the laser wavelength ($\approx 1\mu$m). Moreover, the remnant seismic noise below Hz must be compensated.

The marionetta allows a fine control on three degrees of freedom out of six: the test mass rotations around the horizontal and vertical axes and the displacement along the mirror axis.

The marionetta itself is used to apply large *dc* corrections to the mirror longitudinal or angular position by electromagnetic actuators consisting of coils and magnets. Such coils are mounted on supports anchored from the last stage of the superattenuator. Smaller *ac* corrections are applied by similar electromagnetic actuators directly to the test mass. To avoid coupling to seismic noise, these coils are mounted on a mass (*reference mass*) suspended to the marionetta as well. A small motor under the marionetta moves a small mass to provide the balancing.

The plate which separates the upper and lower vacuum regions supports cylindrical glass baffles to position the coils as close as possible to the magnets mounted on the marionetta. The marionetta support wire, the motor wires and the wiring to lower coils pass through a small diameter tube (1 l/s conductance).

The mirrors are supported in such a way that the mechanical Q factor is high and rotations around the vertical and horizontal axis crossing the center of mass are possible. A couple of thin wires with 70 cm free length are attached to the marionetta and sustain the mirror as a cradle.

The vertical resonance of the mirror–wire system turns out to be around 10 Hz: the thermal noise associated with this resonance may overcome the pendulum thermal noise for vertical–horizontal

couplings of the order of 10^{-2}, thus deteriorating the overall interferometer sensitivity. The adopted solution is the use of low stiffness metal blades to sustain wires. In this way the mirror–marionetta vertical resonance is shifted around 2 Hz and the vertical thermal noise contribution decreases below the pendulum contribution even for couplings of the order of 10^{-2}.

4700.2 The marionetta

The marionetta is attached to the last stage of the superattenuator through a 1 m length wire. The wire is clamped at the marionetta center of mass to minimize the momentum producing rotations. The suspension wire is shaped with a nail–head at both the attachment points.

The marionetta provides a rotation angular range of ± 2 mrad and a pointing accuracy of $< 1\mu$ rad.

Identical marionettas for all optical elements are foreseen with the constraint that the overall mass of the system marionetta+test mass+reference mass is close to one SA stage mass ($\sim$ 160 Kg). The marionetta is shown in fig. 4.

The material is AISI 304 stainless steel for UHV compatibility and the overall mass is 80 Kg. The wires can be attached both to the marionetta itself or to triangular C70 steel blades. The blades are low stiffness and low mass springs which allow high rigidity in all directions but the vertical one. The blades are annealed and prebent to be horizontal when loaded with the test mass. Two solutions are foreseen: a pair of blades rigidly connected on each side or a single blade per side. The blades are shown in fig. 5.

Various configurations have been experimentally tested on a marionetta prototype and are described in detail in [1]. The comparison of the vertical tranfer functions of the system marionetta+test mass with and without blades shows that with the use of blades the vertical resonance frequency of the system test mass+wires is shifted from 10 Hz to 2 Hz (fig. 1) and the attenuation is more favourable. The resonance peak at 150 Hz is due to the first flexural mode of the blades and is of no concern. The comparison of the horizontal transfer functions (fig. 2) shows that there are no relevant resonances up to the first violin mode of the wires ($\sim$ 200 Hz) besides the one due to the rocking motion of the test mass about an horizontal axis at a few Hz. This effect can be reduced as well be a proper configuration of blades.

Is is found that the configuration without blades can meet the VIRGO requirements in principle. The blade configuration however allows to decrease the contribution of vertical motions of the SA to the thermal noise by one order of magnitude. Even in the pesimistic assumption that the vertical–horizontal coupling is of the order of 10^{-2}, this contribution is well below the contribution from the pendulum mode.

4701 The marionetta steering coils

As discussed above, the marionetta is steered by magnet–coil systems to allow for tilting control and longitudinal traslations along the direction of the laser beam. The coils are outside the cleaner vacuum and are fixed to supports rigidly connected to the last module of the SA (fig. 3). The magnets are mounted on the marionetta and this results in a relatively large distance from the coils. The steering system of the marionetta is shown in fig. 6.

The control of tilt angle is realized by one single coil on each side of the marionetta. Being the marionetta suspended close to the center of mass, the restoring force for tilting is mainly due to the wire stiffness against bending. The magnet is at distance $z = \frac{R}{2}$ from the coil center, where R

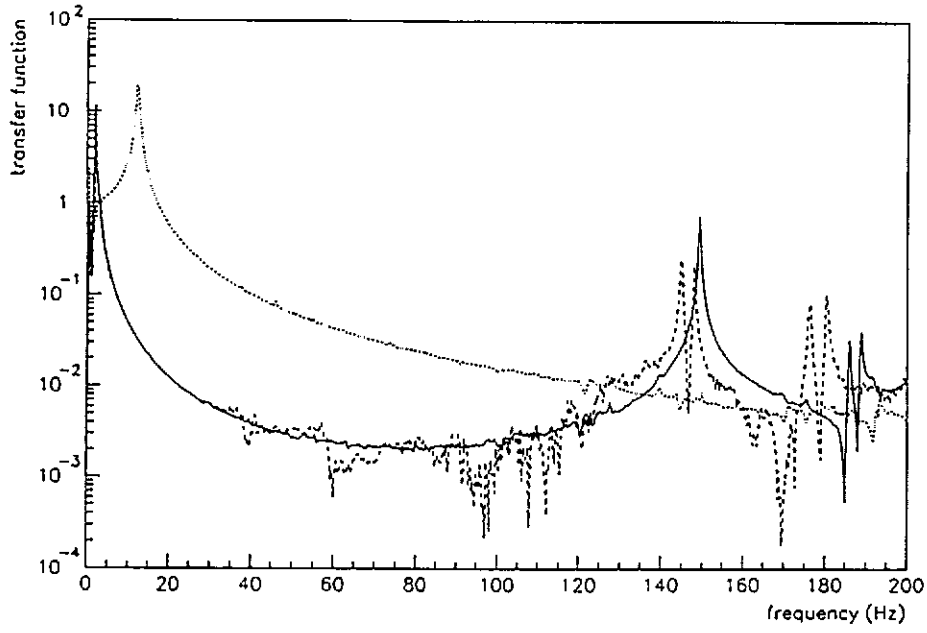

Figure 1: Vertical transfer function for the blade marionetta with blades rigidly connected (solid line) and with the blades blocked (dashed line)

is the coil radius, to have zero force gradient. In this way, the force is not sensitive to transverse misalignments and sensitive only to second order to longitudinal displacements. Since the distance from the magnet to the coil center is 6 cm, the coils have 12 cm average radius. We have choosen 900 turns per coil and one permanent magnet per coil, with 1 T surface magnetic field, 1 cm diameter and 4 mm thickness. Such coils provide a coupling 9×10^{-3} N/A.

The control of longitudinal displacement of the marionetta and test mass is achieved by a pair of identical radius actuator coils (Maxwell pair) at distance $\sqrt{3}R$ and with opposite currents: the magnets are placed equidistantly from each coil on the common axis. The axial force is constant on a relatively large range; moreover, this configuration is insensitive to transverse misalignments as well. We have choosen coils with 6 cm average radius and 900 turns and five permanent magnets for each coil pair. Such coils provide a coupling of 0.25 N/A.

The coil supports are made of ceramic material to have UHV compatibility and make the contributions of Foucault currents negligible. The wires of coil winding are described in detail in the section about wiring and cabling.

The current in the coils must be mantained proportional to the required force, thus the coils must be feeded with a constant current driver.

The baffle which separates the upper from lower chamber is attached to the vacuum housing and thus is subjected to seismic motion. This motion could couple in principle to the marionetta coils/magnets by means of eddy currents in the fields of marionetta controls. It can be shown that this coupling is negligible.

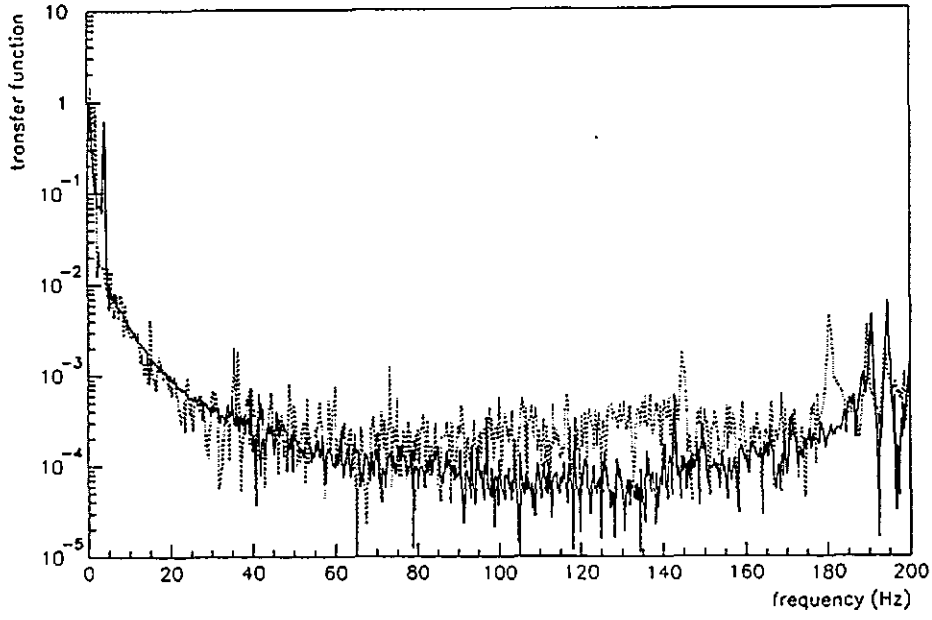

Figure 2: Horizontal transfer function for the blade marionetta with blades rigidly connected (solid line) and with the blades blocked (dashed line)

4701.1 The reference mass

As discussed above, the small ac corrections to the test mass position and the feedback signals from the control are applied directly on the test mass from four coils on a reference mass suspended to the marionetta, thus seismically isolated. The reference mass has the same mass and centre of mass of the test mass to have a system as symmetrical as possible (Fig. 7).

The reference mass is made of a dielectric material to strongly reduce the contribution of Foucault currents. The shape of the reference mass is choosen in such a way to achieve a partial mirror protection from dust.

4701.2 The mirror steering coils

The mirror steering coils mounted on the reference mass face four small permanent magnets mounted on the rear side of the mirror at 90^0. This configuration minimizes the interaction with stray magnetic fields. The coils should have the smallest possible coupling coefficient to reduce the effect of the thermal noise current in the coils and to reduce the coupling of the reference mass pendulum noise to the test mass, just using as much froce is necessary to control the test mass. As above, the coils are driven with a constant current driver.

4701.3 Electrical connections

The overall amount of wiring needed for the marionetta and mirror coils and for the marionetta motor is summarized in Table 1. The electrical connection of the upper coils are of no concern and have the same constraints as the SA cabling. The narrow conductance tube allows the passage of the

item	leads	length(m)	notes
marionetta motor	6	130	screened
marionetta steering coils	12	240	coaxial
mirror steering coils	8	170	coaxial

Table 1: The last stage wiring summary.

marionetta suspension wire and of the wires for the mirror steering coils and the motor. The small diameter imposes a careful mounting to avoid touching the walls and coupling to seismic noise.

4702 The full scale prototype of the last stage

A full scale prototype of the marionetta and test mass has been set up in Pisa to study the thermal noise effects in the same conditions as the final suspension. When better solutions about clamps and materials will be available, the suspension will be upgraded.

4702.1 Last stage assembling

4702.1.1 Overview

The assembling of the last stage is the assembling of the system marionetta+ test mass+ reference mass in the bottom part of the towers. To this purpose, special installation and cleanliness procedures have been devised.

4702.2 Mechanical and vacuum acceptance tests

The marionetta is equilibrated and the mechanical transfer functions measured. Then it is cleaned and the test mass and reference mass assembled. The optical payload is prepared in a class 100 laboratory in a dust tight but not air tight box ($\sim$ 100 Kg).

4702.3 On site assembly

The montage hall is qualified for UHV assembly. The lower part of the tank must be qualified clean and is flushed during access with 1000 m^3/h of air filterd at 99.9997% DOP. The box protecting the optical payload is removed once the system is evacuated.

References

[1] S. Braccini et al, Phys. Lett. A **199**,307 (1995).

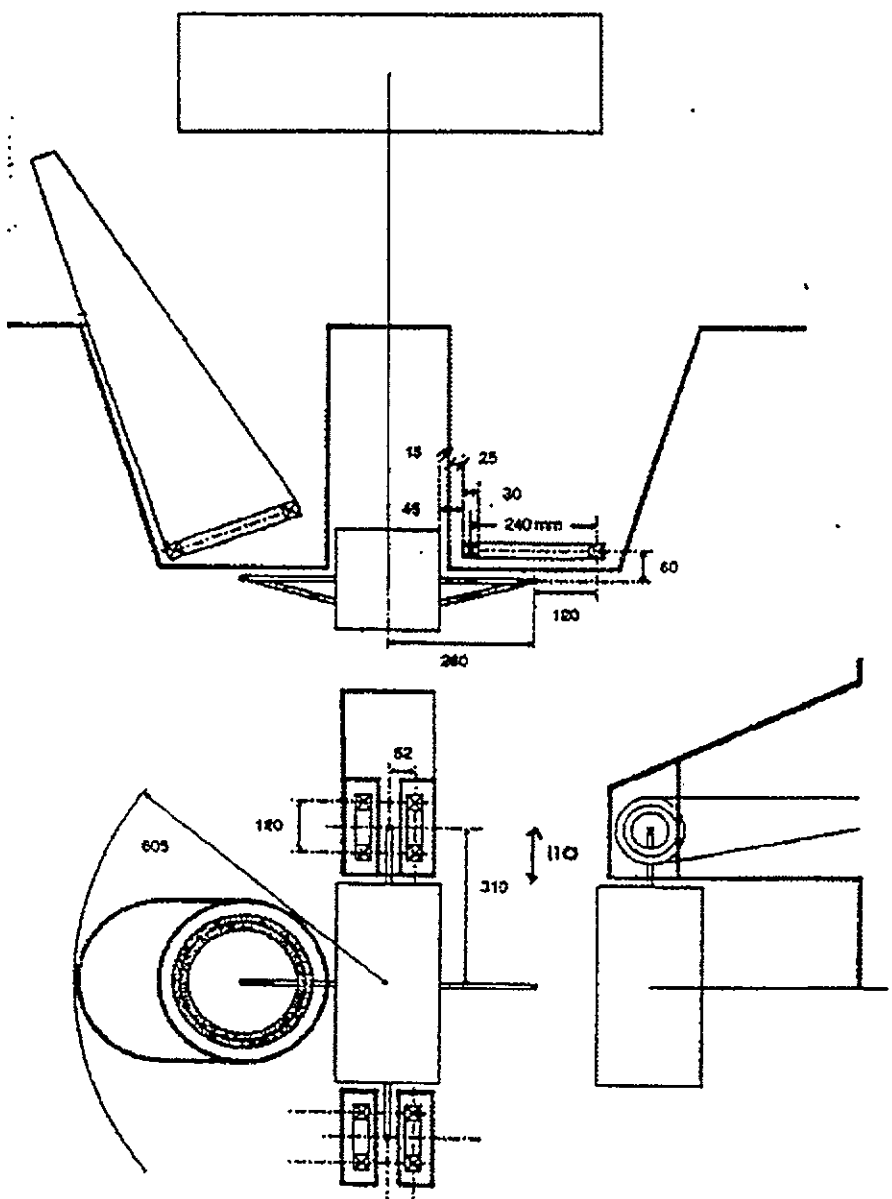

Figure 3: The last stages of the suspension.

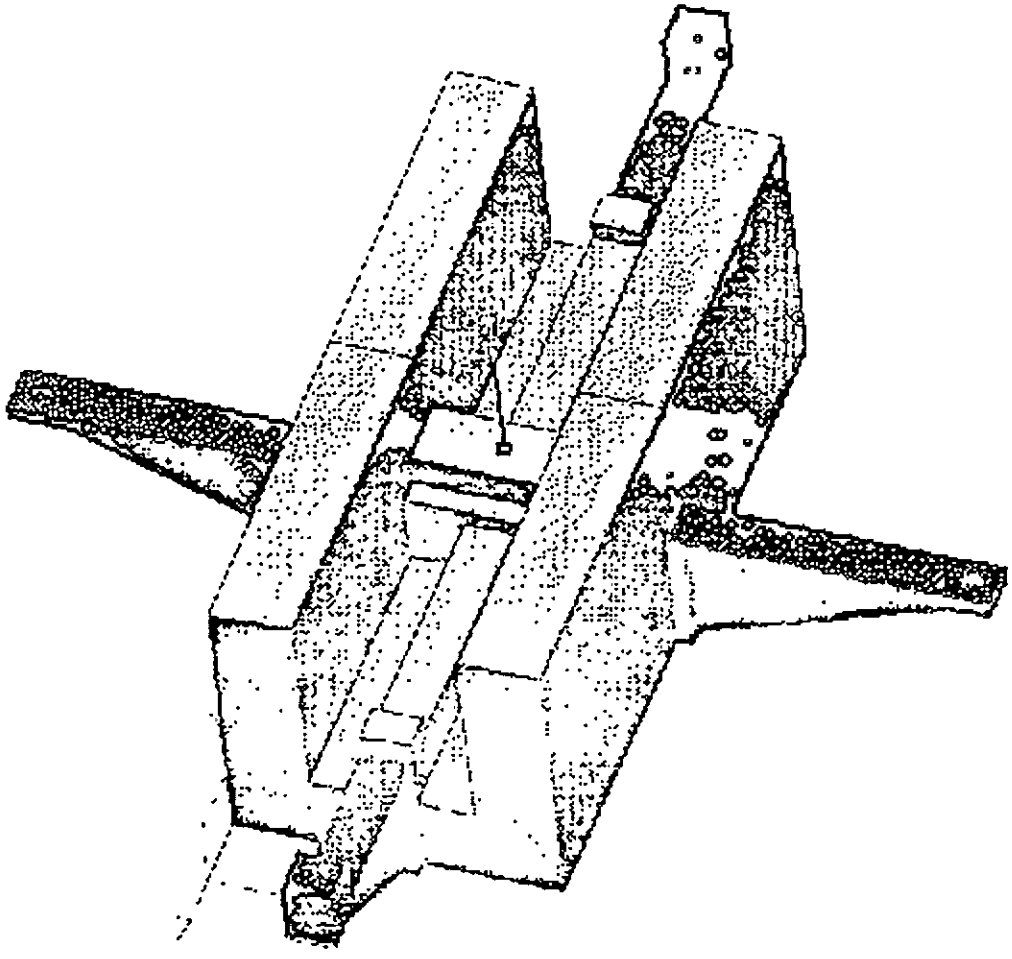

Figure 4: The marionetta.

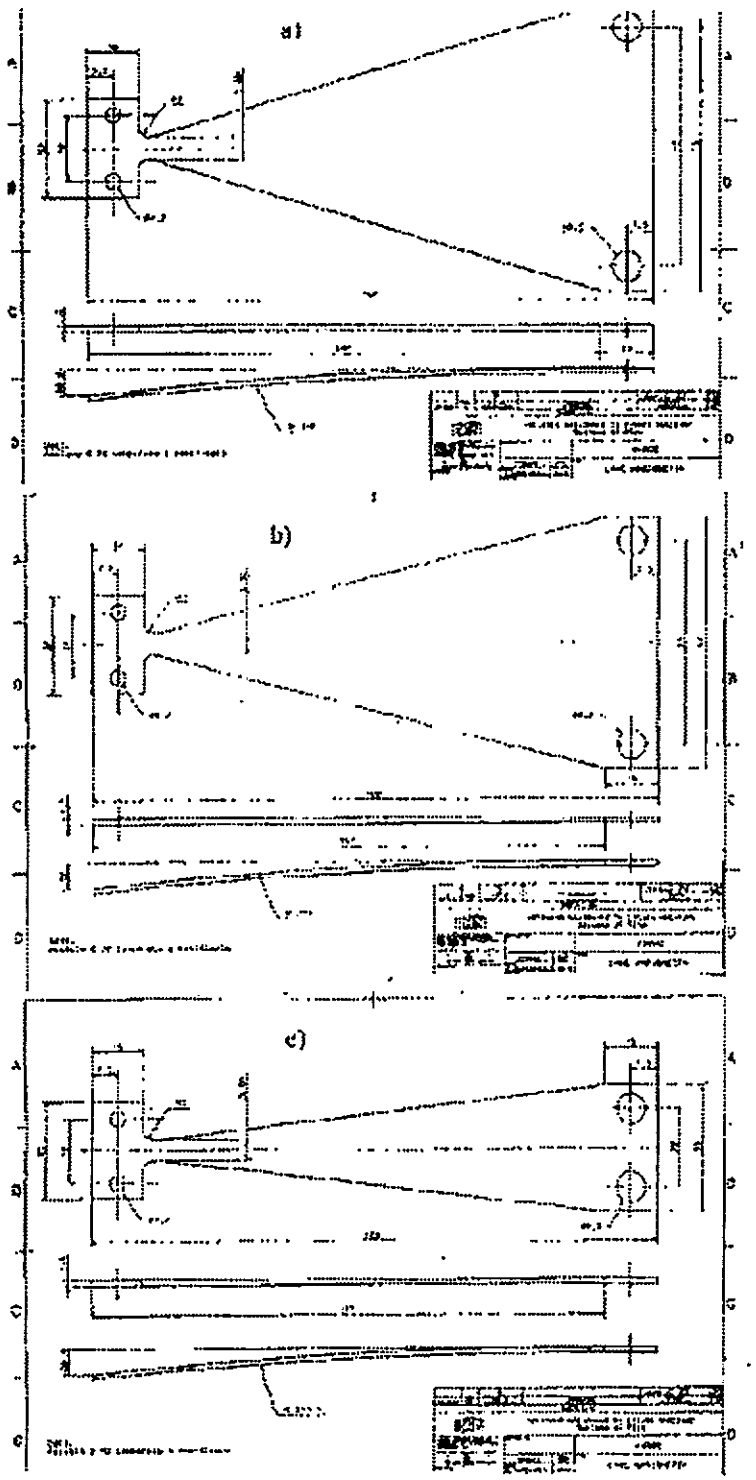

Figure 5: The marionetta blades: one blade per side for the far mirror (a); two blades per side for the far mirror/one blade per side for the near mirror (b); two blades per side for the near mirror (c).

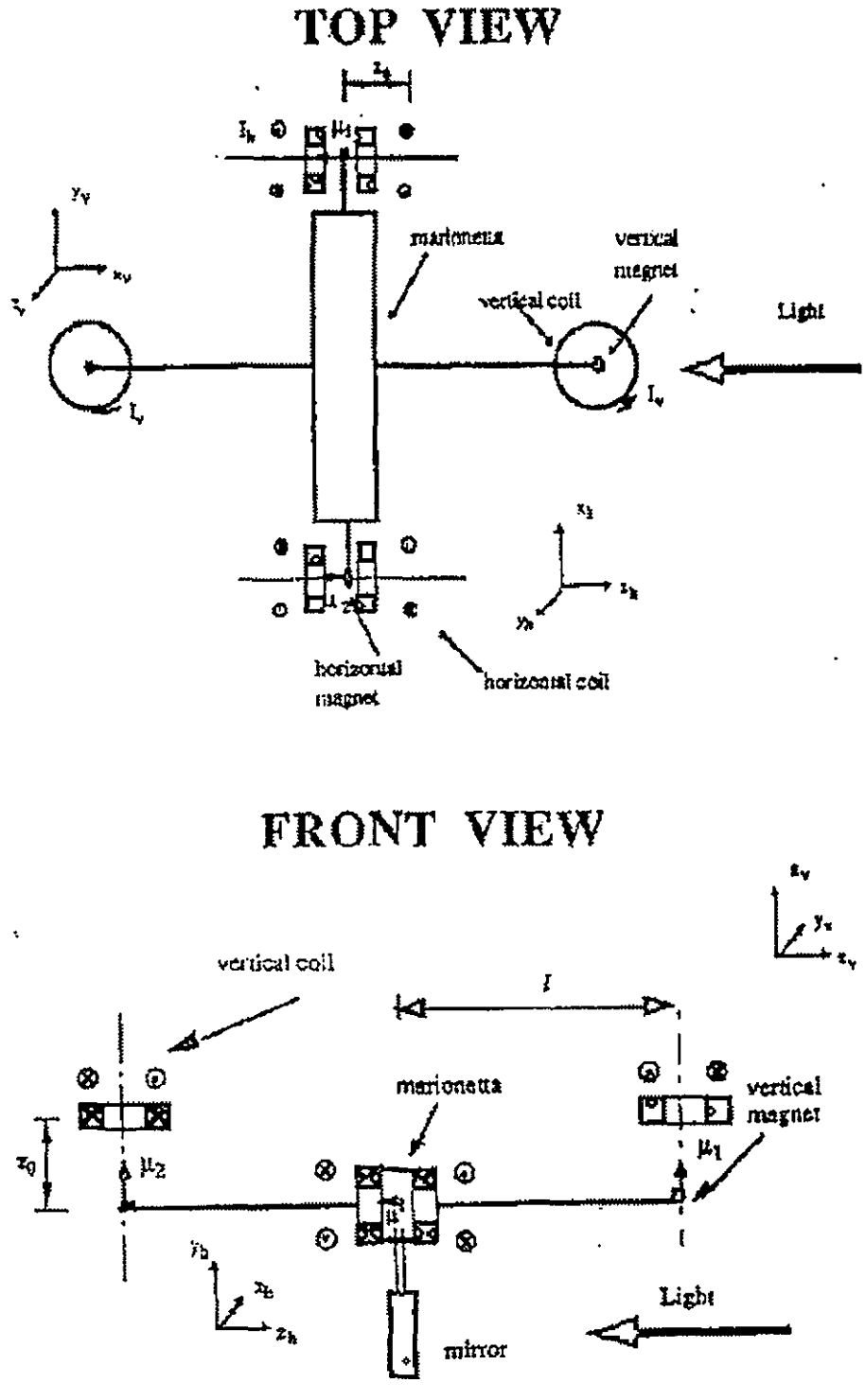

Figure 6: Detail of the arrangement of the marionetta steering coils: top view (a) and side view (b).

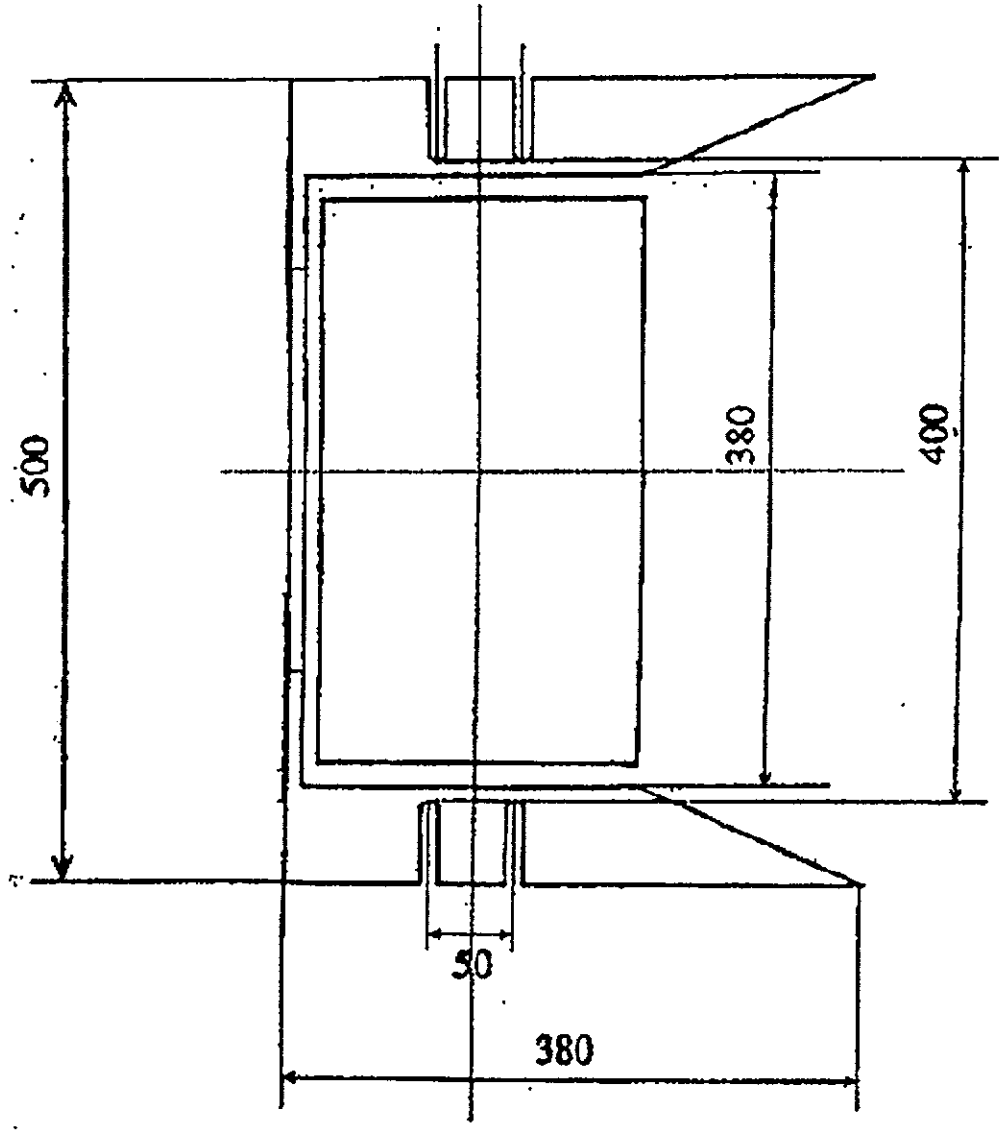

Figure 7: The reference mass (cross section).

Thermal Noise

4800 Thermal noise effects

4800.1 Introduction

Thermal noise produces fluctuations in the position of the suspended elements (test masses and optics) of the interferometer which will limit the sensitivity of VIRGO in the spectral region between 10 Hz and few hundred Hz [1]. It has been suggested that the whole suspension structure (super attenuator) can be treated as a multi-stage pendulum. Due to the action of thermal noise, the position of each element in the pendulum chain will fluctuate in time. This is particularly true for the position of the optical components (mirror, beam splitter or suspended bench) located at the last stage of the chain. Such fluctuations produce a displacement which is directly measured in the gravitational wave signal and sets a lower limit to the antenna sensitivity.

Experimental and theoretical work published since the early fifties recognized that the spectral properties of thermal fluctuations are strictly related to the dissipative properties of the monitored observable. This result led to the formulation of the so called Fluctuation-Dissipation theorem (FDT) [2]. The dissipation of energy by the system can be described in terms of the imaginary part of the response function which, due to FDT, is related to the spectral density of the equilibrium fluctuations.

If we call $x(t)$ a physical observable which quantifies the response of a system to an applied external force $f(t)$, the response function $H(\omega)$ (called "generalized susceptibility" in the physics literature) is a complex quantity defined by:

$$X(\omega) = H(\omega)F(\omega) \tag{1}$$

with $H(\omega) = H'(\omega) + iH''(\omega) = |H(\omega)|e^{i\phi(\omega)}$. Here, capital letters denote the Fourier transform of the corresponding time dependent quantities. The FDT sets a relation between the power spectral density of $x(t)$, $< x(\omega)^2 >$, and $H''(\omega)$, i.e.

$$< x(\omega)^2 >= -4\ kT\ \frac{H''(\omega)}{\omega} \tag{2}$$

for the r.m.s. value $\sqrt{< x^2 >}$, using the Kramers-Kroenig relations[2], we have:

$$< x^2 >= \frac{1}{\pi}\int_0^\infty < x(\omega)^2 > d\omega = kT\ H'(0) \tag{3}$$

In the following, we discuss and evaluate the thermal noise effects of various pendulum motions which are relevant to the VIRGO sensitivity curves.

4800.2 Pendulum mode

The one-dimensional longitudinal motion of a simple pendulum (see figure 1) can be described by the equation of motion for the center of mass position $x = L\ sin(\theta)$, in the small oscillation approximation, as:

$$mL\ddot{x} = -mgx \tag{4}$$

The role played by the presence of real wires on the pendulum dynamics can be taken into account

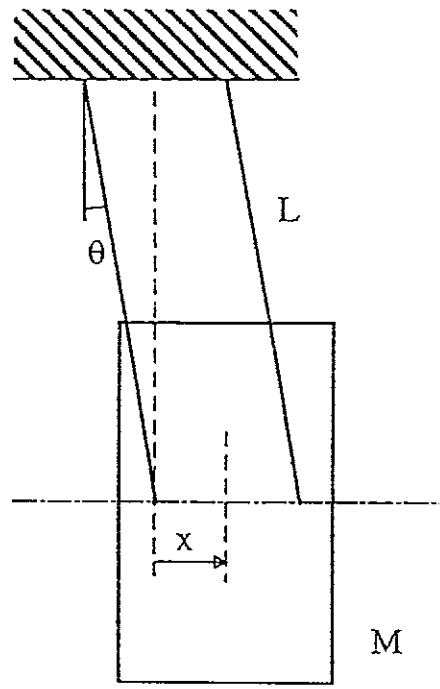

Figure 1: Simple pendulum

by introducing a force-like term (actually the moment of the force):

$$-\int_{-\infty}^{t} \tau(t-s)\ \theta(s)ds \tag{5}$$

on the r.h.s. of the equation of motion:

$$mL\ddot{x} = -mgx - n\int_{-\infty}^{t} \tau(t-s)\,\frac{x(s)}{L}\,ds + L\,F_{ext} \tag{6}$$

where F_{ext} denotes the external force term applied to the center of mass of the pendulum and n is the number of wires employed. The force term in eq. (5) accounts for both the restoring action exerted by the wires, due to the bending, and the dissipative action arising during such bending, as can be easily verified by computing the response function $H(\omega)$:

$$H(\omega) = \frac{X(\omega)}{F_{ext}(\omega)} = \frac{1}{\frac{mg}{L} - m\omega^2 + n\frac{T(\omega)}{L}} \tag{7}$$

The real part of $T(\omega)$, T_R, represents the elastic restoring force from the bent wires, while the imaginary part, T_I, accounts for the dissipative action coming from the bending. The loss angle $\phi(\omega)$:

$$tg(\phi) = \left|\frac{T_I(\omega)}{T_R(\omega)}\right| \tag{8}$$

quantifies the fraction of the elastic energy dissipated per cycle, at resonance. It is important to point out that ϕ is related to the intrinsic properties of the wire material and is independent of the geometry of the wires. Typical values for ϕ, for low dissipation materials, range from 10^{-6} to 10^{-3}, almost independent of frequency, in the low frequency region [3, 4]. In this case:

$$tg(\phi(\omega)) \approx \phi(\omega) \tag{9}$$

The response function written in terms of the loss angle is:

$$H(\omega) = \frac{1}{m\omega_w^2}\,\frac{1}{\left(\frac{\omega_p}{\omega_w}\right)^2 - \left(\frac{\omega}{\omega_w}\right)^2 + i\phi} \tag{10}$$

where we introduced the pendulum resonance frequency due to the wire contribution alone (i.e. in the absence of gravity):

$$\omega_w^2 = n\,\frac{T_R}{mL} \tag{11}$$

and the effective resonance frequency (wires + gravity):

$$\omega_p^2 = \frac{g}{L} + n\,\frac{T_R}{mL} = \omega_g^2 + \omega_w^2 \tag{12}$$

To obtain the power spectral density (see (2)), we compute the imaginary part $H''(\omega)$:

$$H''(\omega) = -m\omega_w^2\phi(\omega)\mid H(\omega)\mid^2 \tag{13}$$

and from (2) we finally obtain:

$$\begin{aligned} < x(\omega)^2 > &= 4m\,kT\,\frac{\omega_w^2}{\omega}\,\phi(\omega)\mid H(\omega)\mid^2 \qquad (14)\\ &= \left(\frac{4k_BT}{m}\right)\frac{\phi(\omega)}{\omega}\,\frac{\omega_w^2}{(\omega_p^2-\omega^2)^2 + \phi^2(\omega)\omega_w^4} \end{aligned}$$

For $\omega \gg \omega_p$, the noise is.

$$\sqrt{< x(\omega)^2 >} \propto \sqrt{\frac{\phi(\omega)}{\omega^5}} \tag{15}$$

For a frequency independent loss angle ϕ, the thermal noise decays asymptotically as $\omega^{-5/2}$.

4800.2.1 Expected thermal noise level

To obtain a quantitative estimate of the thermal noise level affecting the Virgo sensitivity, we should introduce numerical values for the loss angle ϕ and the elastic angular frequency ω_w. We consider the case of a cylindrical mirror (see figure 4) with $R = 0.175\,\mathrm{m}$, $2l = 0.10\,\mathrm{m}$, $b = 0.05\,\mathrm{m}$ and mass $m = 25$ Kg (fused quartz mirror).

The angular frequency ω_w was estimated analytically for piano wires with length $L = 0.7\,\mathrm{m}$ and radius $r = 2.5^{-4}$ m. ω_w is of the order of $\omega_p/21$, in agreement with the numerical estimate. The value of ϕ has been set equal to a conservative value of 10^{-3}.

With these estimates and a resonant frequency $\nu_p = \omega_p/2\pi = 0.6\,Hz$, we obtain a quality factor $Q \approx 4\,10^5$ and

$$\begin{aligned}\sqrt{< x(\omega)^2 >} &\approx 10^{-9}\mathrm{m}/\sqrt{\mathrm{Hz}} \;\; \nu = \nu_0 \\ &\approx 10^{-18}\mathrm{m}/\sqrt{\mathrm{Hz}} \;\; \nu = 10\ \mathrm{Hz} \\ &\approx 10^{-20}\mathrm{m}/\sqrt{\mathrm{Hz}} \;\; \nu = 100\ \mathrm{Hz}\end{aligned} \tag{16}$$

The r.m.s. value is

$$\sqrt{< x^2 >} \approx 3\,10^{-12}\mathrm{m} \tag{17}$$

Estimates of the usual parameter $\tilde{h}$ are easily obtained through the relation

$$\tilde{h} = 2\sqrt{< x(\omega)^2 >}/L,$$

where L is the interferometer arm length. In figure 2, we plot the thermal noise power spectrum in terms of the strain, $\tilde{h}$, for the above pendulum.

4800.3 Rotational mode

Let us consider the rotational mode of a suspended cylindrical mirror (see figure 3 and figure 4). If we call z the height of the mirror center of mass and θ the rotation angle, we can easily write the Lagrangian function L as:

$$\mathrm{L} = \frac{1}{2}m\dot{z}^2 + \frac{1}{2}I\dot{\theta}^2 - mgz \tag{18}$$

where I is the mirror moment of inertia around z axes. If we consider the wire length L as fixed, the motion can be described in terms of a single variable, the rotation angle θ.

$$I\ddot{\theta} = -mg\frac{B^2}{L}\theta \tag{19}$$

where $z = B^2\theta^2/2L$, $B^2 = (R^2 + b^2)$.

The role played by the presence of real wires can be taken into account by introducing the momentum of the force-like term as for the pendulum mode case:

$$I\ddot{\theta} = -mg\frac{B^2}{L}\theta - nB\int_{-\infty}^{t}\tau(t-s)\theta(s)ds - M_{ext}(t) \tag{20}$$

where $M_{ext}(t)$ is the momentum of the external force. The M_{ext}-θ response function resembles eq (7):

$$H(\omega) = \frac{\Theta(\omega)}{M_{ext}(\omega)} = \frac{1}{mg\frac{B^2}{L} - I\omega^2 + nBT(\omega)} \tag{21}$$

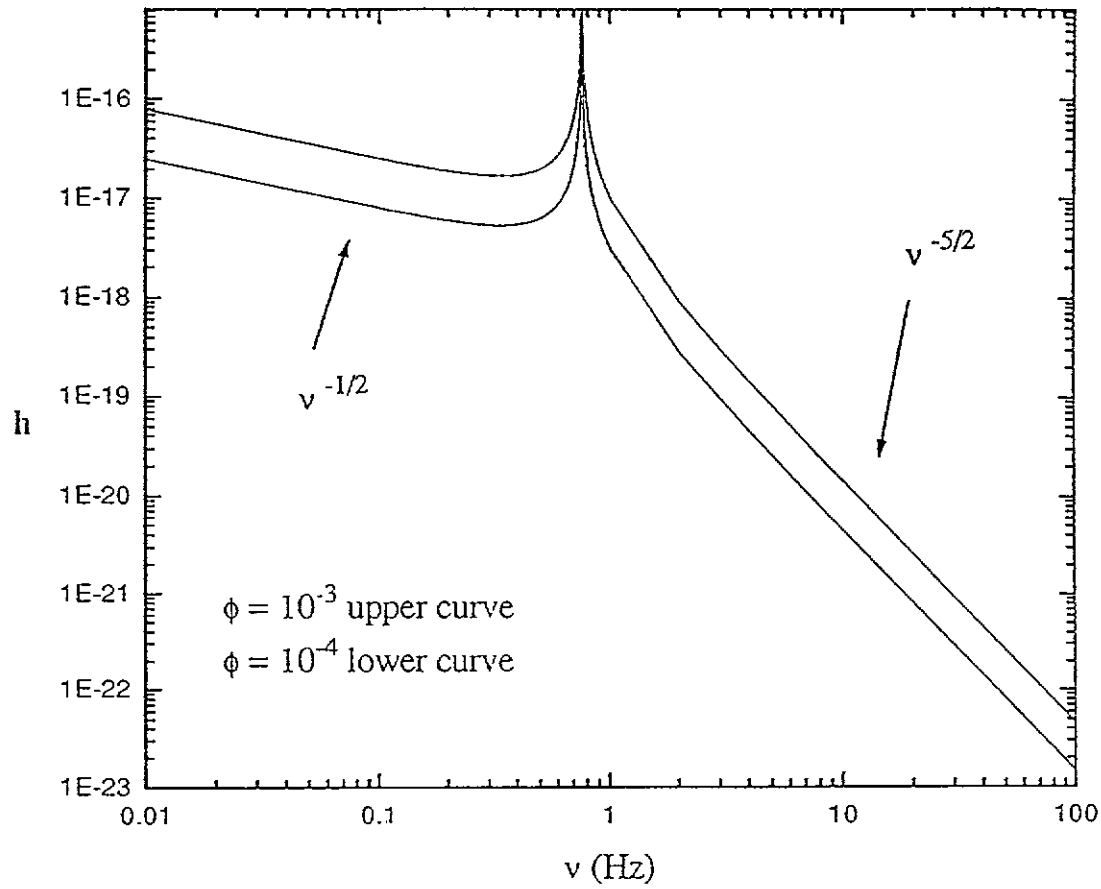

Figure 2: Displacement thermal noise for a pendulum with two different losses for the wire material.

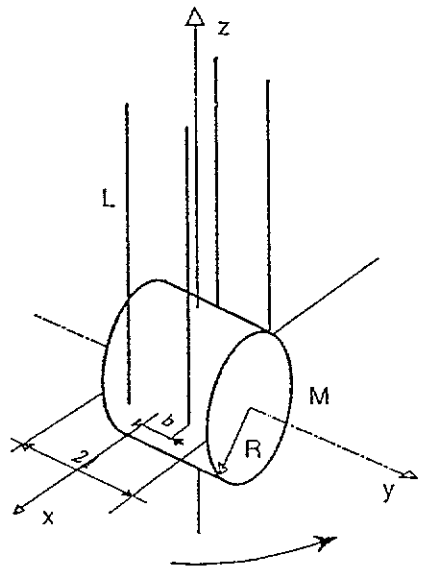

Figure 3: Rotational mode of a suspended cylindrical mirror

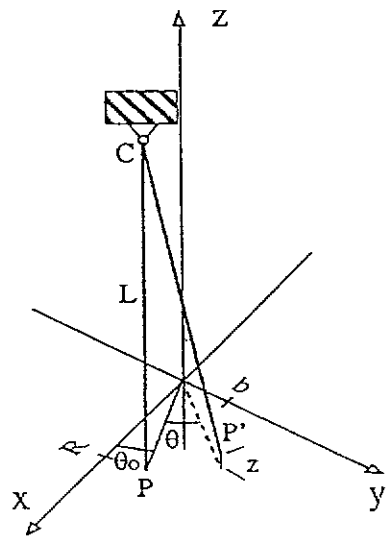

Figure 4: Rotational mode coordinates of a suspended cylindrical mirror

The loss angle $\phi(\omega)$ is the same, too:

$$tg(\phi) \approx \phi(\omega) = \left| \frac{T_I(\omega)}{T_R(\omega)} \right| \tag{22}$$

We can introduce the rotational resonance angular frequency due to the wire elastic contribution as:

$$\omega_{w\theta}^2 = n \frac{T_R B}{I} \tag{23}$$

and the effective resonance angular frequency (wires + gravity):

$$\omega_\theta^2 = \frac{mgB^2}{IL} + \omega_{w\theta}^2 = \omega_{g\theta}^2 + \omega_{w\theta}^2 \tag{24}$$

The response function (21) becomes:

$$H(\omega) = \frac{1}{I\omega_{w\theta}^2} \frac{1}{\left(\frac{\omega_\theta}{\omega_{w\theta}}\right)^2 - \left(\frac{\omega}{\omega_{w\theta}}\right)^2 + i\phi} \tag{25}$$

with quality factor:

$$Q_\theta = \frac{1}{\phi(\omega_\theta)} \frac{\omega_\theta^2}{\omega_{w\theta}^2} \tag{26}$$

As previously stated, the power spectral density of the angular fluctuations (see (2)) is obtained from the imaginary part of the response function (21) through the fluctuation-dissipation theorem:

$$< \Theta(\omega)^2 >= 4I\ kT\ \frac{\omega_{w\theta}^2}{\omega}\ \phi(\omega)\, H(\omega)^2 \tag{27}$$

which has the same form of the longitudinal displacement pendulum mode spectral density $< x(\omega)^2 >$ of eq. (15) with the inertial constant represented here by the moment of inertia I.

4800.3.1 Expected thermal noise level

To obtain a quantitative estimate of the thermal noise level affecting the angular position of the suspended mirrors in the Virgo interferometer, we retain the loss angle ϕ numerical estimate introduced already.

We have $B = 0.18$m, $I = m((2l)^2/12 + R^2/4) = 0.21$ m^{2}Kg. To estimate the value for the rotational angular frequency $\omega_{w\theta}$, the following relation holds:

$$\frac{\omega_{w\theta}}{\omega_{g\theta}} = \frac{\omega_w}{\omega_g} \sqrt{\frac{L}{B}} \tag{28}$$

We obtain $\omega_{w\theta} \approx 1/10\ \omega_{g\theta}$.

Numerical estimates of the spectral density of rotational fluctuations, based on these results give

$$\begin{aligned} \sqrt{< \theta(\omega)^2 >} &\approx 6\ 10^{-9}\ rad/\sqrt{Hz}\ \ \nu = \nu_0\ (about\ 1\ Hz) \\ &\approx 10^{-16}\ rad/\sqrt{Hz}\ \ \nu = 10\ Hz \\ &\approx 10^{-19}\ rad/\sqrt{Hz}\ \ \nu = 100\ Hz \end{aligned} \tag{29}$$

The r.m.s. value of the angle θ is

$$\sqrt{< \theta^2 >} \approx 2\ 10^{-11}\ rad \tag{30}$$

4800.4 Tilt mode

Let us consider now the tilt mode of a suspended cylindrical mirror (see figure 5). Let $\alpha(t) = tg^{-1}(z/b)$ denote the instantaneous tilt angle of the cylinder principal axes with respect to the horizontal equilibrium direction (x axes) with z vertical displacement of the wire-mirror junctions. In this case, the restoring force comes entirely from the four wires.

We can easily write the equation of motion for the variable α, in the small oscillation approximation as:

$$I\ddot{\alpha} = -4\frac{b^2}{L}\int_{-\infty}^{t} k(t-s)\alpha(s)ds - M_{ext}(t) \tag{31}$$

where $M_{ext}(t)$, as usual, is the moment of the external force and $k(t-s)$ is the memory kernel for the response of the stretched wires. The M_{ext}-α response function is:

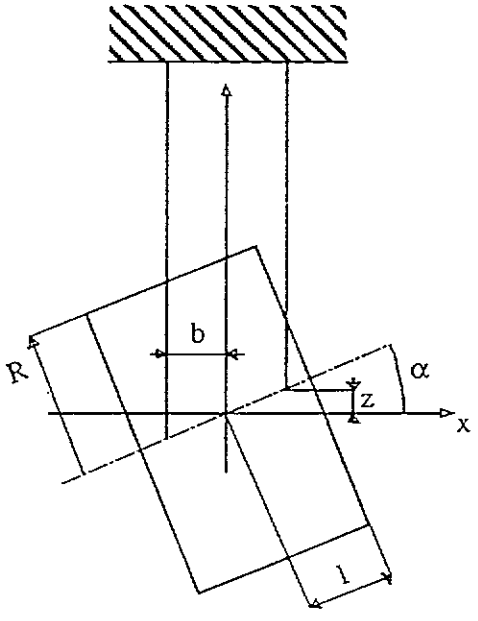

Figure 5: Tilt mode of a suspended cylindrical mirror

$$H(\omega) = \frac{\alpha(\omega)}{M_{ext}(\omega)} = \frac{1}{K(\omega)\frac{4b^2}{L} - I\omega^2} \tag{32}$$

with $K(\omega) = K_R(\omega) + iK_I(\omega)$ the Fourier transform of $k(t)$. As usual, the real part of $K(\omega)$, K_R, represents the elastic restoring force from the stretched wires, while the imaginary part K_I accounts for the energy dissipation

The corresponding loss angle $\tilde{\phi}(\omega)$ is by definition.

$$tg(\tilde{\phi}) \approx \tilde{\phi}(\omega) = \left|\frac{K_I(\omega)}{K_R(\omega)}\right| \tag{33}$$

while the tilting resonance angular frequency is due solely to the wire elastic constant

$$\omega_{w\alpha}^2 = K_R(\omega)\,\frac{4b^2}{IL} \tag{34}$$

The response function becomes:

$$H(\omega) = \frac{1}{I\omega_{w\alpha}^2} \frac{1}{1 - \left(\frac{\omega}{\omega_{w\alpha}}\right)^2 + i\tilde{\phi}} \tag{35}$$

The quality factor for the tilting mode is just $Q_\alpha = 1/\tilde{\phi}$.

The power spectral density of the angular fluctuations (see (2)) is:

$$< \alpha(\omega)^2 >= 2I\ kT\ \frac{\omega_{w\alpha}^2}{\omega}\ \tilde{\phi}(\omega)\ |\ H(\omega)\ |^2 \tag{36}$$

4800.4.1 Expected thermal noise level

A quantitative estimate of the thermal noise level affecting the angular position of the suspended mirrors in the Virgo interferometer was obtained under the assumption $\tilde{\phi} \approx \phi$.

The restoring force constant K_R of the stretched wires, in the limit of small displacements, can be expressed as $K_R = SE$ where S is the wires cross-sectional area and E is the Young's modulus ($E = 205.8\ 10^9 N/\mathrm{m}^2$ for the case of piano wires).

Using this result and eq. (37), we compute the resonant angular frequency $\nu_{w\alpha} = \omega_{w\alpha}/2\pi$ as a linear function of the wire radius r:

$$\nu_{w\alpha} = \frac{r}{2\pi}\sqrt{\pi E \frac{4b^2}{IL}} \tag{37}$$

In particular for $r = 1.4\ 10^{-4} m$ we have $\nu_{w\alpha} \simeq 5.1\ Hz$. This frequency value can be lowered by introducing suspension blades between the marionetta and the wires (see below). In the following, we ignore the presence of such blades.

Numerical estimates of the tilt fluctuations give

$$\begin{aligned} \sqrt{< \alpha^2 >} &\approx 10^{-11}\ rad/\sqrt{Hz}\ \ \nu = \nu_0 \\ &\approx 10^{-14}\ rad/\sqrt{Hz}\ \ \nu = 10\ Hz \\ &\approx 10^{-17}\ rad/\sqrt{Hz}\ \ \nu = 100\ Hz \end{aligned} \tag{38}$$

The r.m.s. of the tilt angle is

$$\sqrt{< \alpha^2 >} \approx 5\ 10^{-12}\ rad\ (\sqrt{< \alpha^2 >} \propto 1/r) \tag{39}$$

4800.5 Violin modes

The pendulum wires that support the test mass mirror have transverse mechanical resonances or violin modes with frequencies given by

$$f_n = \frac{n}{2L}\sqrt{\frac{\tau}{\rho\pi r^2}}\left(1 + \frac{2}{L}\sqrt{\frac{EI}{\tau}}\right) \tag{40}$$

where n is mode number, L is the wire length, $\tau = Mg/4$ is the tension, ρ is the wire density, E is the Young's Modulus, r is the radius of the wire and $I = \frac{\pi r^4}{4}$ is the bending moment of the wire. The violin mode quality factors are given by

$$Q_n = \frac{L}{2\phi}\sqrt{\frac{\tau}{EI}}\left(1 + \frac{(n\phi)^2}{2L}\sqrt{\frac{EI}{\tau}}\right) \tag{41}$$

where ϕ is the inherent loss of the wire material and is independent of the geometry of the wire. By neglecting the restoring force of the wire ($\frac{2}{L}\sqrt{\frac{EI}{\tau}} \ll 1$), the above equations simplify to

$$f_n = \frac{n}{2L}\sqrt{\frac{\tau}{\rho\pi r^2}} \tag{42}$$

and

$$Q_n = \frac{L}{2\phi}\sqrt{\frac{\tau}{EI}} \tag{43}$$

The thermal noise power spectrum from these modes can then be calculated (see for example Saulson [4]).

$$\begin{aligned} < x(\omega)^2 > &= 4 \times 4k_BT \times \frac{2\rho r^2 L}{\pi M^2} \sum_{n=1}^{\infty} \frac{\phi_n \omega_n^2}{\omega[(\omega_n^2 - \omega^2)^2 + \phi_n^2 \omega_n^4]} \\ &= 4 \times 4k_BT \times \frac{2\rho r^2 L}{\pi M^2} \sum_{n=1}^{\infty} \frac{\phi_n}{\omega \omega_n^2}, \ \omega \ll \omega_n \end{aligned} \tag{44}$$

There is an explicit factor of 4 included since there will be contributions from each of the four wires attached to the mirror.

Using the following values for piano wire ($\rho = 7.9\ g/cm^3$, $r = 140\ \mu m$, $L = 0.70\ m$, $M = 21\ kg$ and $E = 2.1 \times 10^{11}\ N/m^2$) gives

$$f_n = n \times 233\ Hz \tag{45}$$

and

$$\phi_n \approx 3 \times 10^{-6} \tag{46}$$

The thermal noise from the first mode will be

$$\begin{aligned} \sqrt{< x(\omega)^2 >} &= 1 \times 10^{-15} \mathrm{m}/\sqrt{\mathrm{Hz}} \ \nu = \mathrm{f_1} \\ &= 2 \times 10^{-20} \mathrm{m}/\sqrt{\mathrm{Hz}} \ \nu = 10\ \mathrm{Hz} \end{aligned} \tag{47}$$

The thermal noise at the violin mode resonant frequency will be seen quite clearly. Since there are many of these resonances, they will appear as a family of sharp peaks that decrease in amplitude as $\omega^{-\frac{3}{2}}$. The off resonance noise contribution of these modes to the gravity wave detection band between 10 Hz and 100 Hz should not be a significant problem.

4800.6 Thermal noise due to the reference mass

The reference mass is a pendulum similar to the mirror that is used to control the position and orientation of the mirror. This will be done by attaching magnets to the mirror and coils to the reference mass. Since the mirror is coupled to the reference mass by this actuator, the mirror will be affected both by the pendulum thermal noise of the reference mass and by the thermal noise of the actuator. The magnets are positioned in the coil in such a way that the force produced by the coil is almost independent of the magnet position. This means that the coupling of the reference mass to the mirror will be a second order effect. The electronic noise in the control circuit, including the shot noise of any steady DC currents needed for the absolute positioning of the mirror, should be filtered so that it does not affect the mirror in the gravity wave detection band. This noise source will not be discussed here.

The coupled mirror–reference mass system can be seen in 6. The magnet–coil actuator can be modelled as a circuit with an inductance, a resistance and a capacity, as seen in figure 7. The equation of motion for the coupled mirror–reference mass system is

$$\begin{aligned} M\ddot{y} &= -\frac{Mg}{l}\left(1+i\frac{1}{q}\right)y - f \\ m\ddot{x} &= -\frac{mg}{l}\left(1+i\frac{1}{Q}\right)x - f + F \end{aligned} \tag{48}$$

The pendulum losses are assumed to be frequency independent. The force term, f, comes from the magnet–coil actuator and has the form

$$f(z,I) \approx [\alpha_0(z_0) + \alpha_1(z_0)(z-z_0)]I \tag{49}$$

Where $z = x - y$ and z_0 is the equilibrium position. I is the coil driving current. By assuming the magnet strength is $0.25\ A \cdot m^2$ and the coils have 1000 turns with an average radius $a = 6\ cm$, the current to force conversion coefficients are: $\alpha_0(a/2) = 0.15\ N/A$ and $\alpha_1(a/2) = 0\ N/A \cdot m$. Using values of $M = 40\ kg$, $m = 21\ kg$, $Q = 4 \cdot 10^5$, $q = 10^2, l = 0.70\ m$, $L = 10^{-3}\ H$ and $R = 10^5\ \Omega$ we can estimate the expected pendulum thermal noise level for the test mass. By using the linear approximation to the equation of motion and the FD theorem we obtained:

$$\begin{aligned} \sqrt{< x(\omega)^2 >} &= 5.4 \times 10^{-18}\mathrm{m}/\sqrt{\mathrm{Hz}}\ \ \nu = 10\ \mathrm{Hz} \\ &= 2 \times 10^{-20}\mathrm{m}/\sqrt{\mathrm{Hz}}\ \ \nu = 100\ \mathrm{Hz} \end{aligned} \tag{50}$$

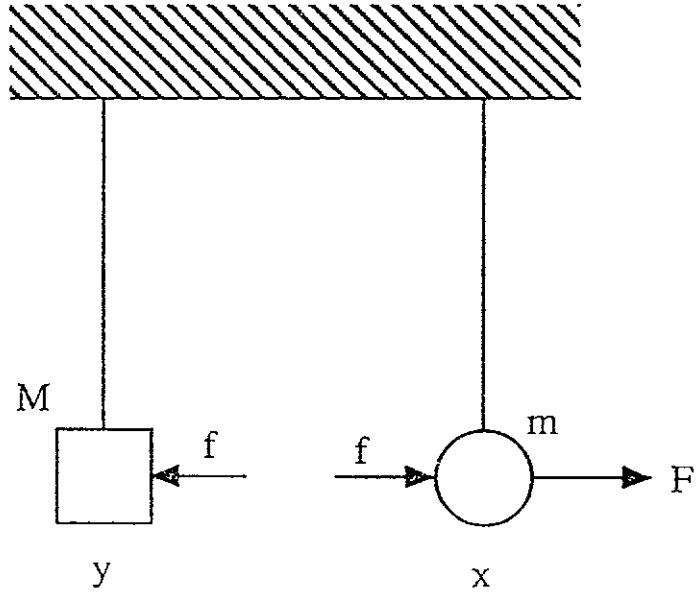

Figure 6: Model of coupled mirror–reference mass system.

The equations of motion used above (49) implicitly include the damping of the pendulum mirror, the reference mass and the coil drive circuit. The losses of the pendulum mirror have already been

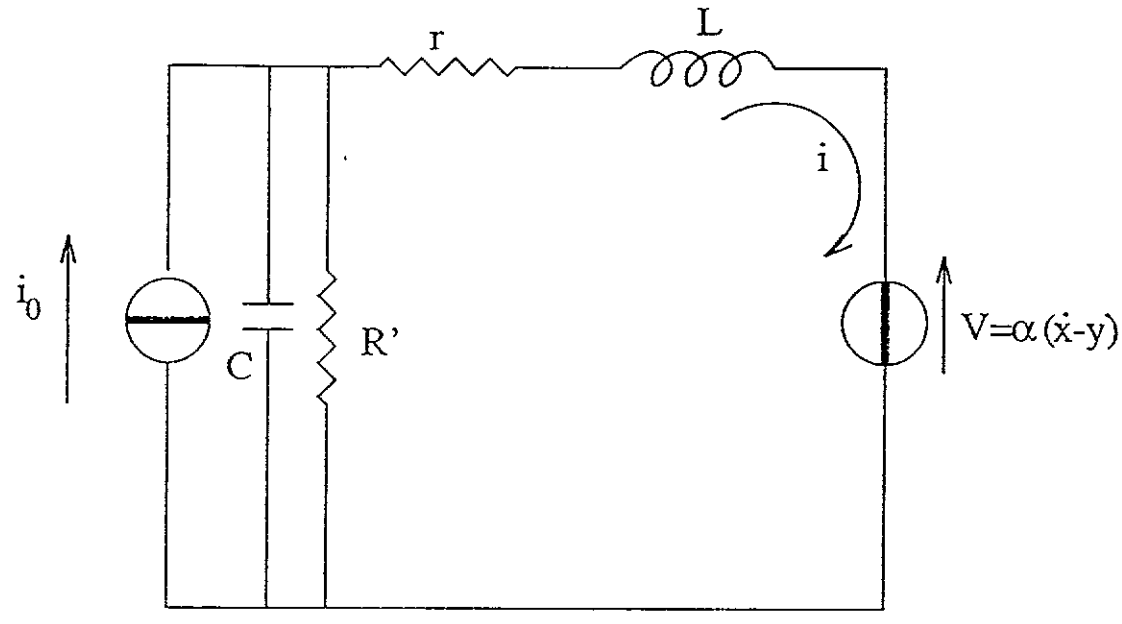

Figure 7: Model of electrical circuit for coil and magnet actuator.

discussed in section 4800.2. The other dissipative elements are the pendulum losses of the reference mass and the internal resistance of the current drive circuit. The pendulum losses of the reference mass can be made small by using the same design techniques as in the mirror suspension.

The internal resistance of the current drive circuit produces a thermal noise current that drives the magnets on the mirror. The thermal noise current for a resistance R is

$$i = \sqrt{\frac{4k_BT}{R}} \tag{51}$$

In order to reduce the effect of the current thermal noise on the displacement noise of the mirror, the internal resistance of the current drive circuit must be made as high as possible. In conclusion, for the set of parameter values considered above, the reference mass does not introduce relevant thermal noise on the test mass.

4800.7 Thermal noise from internal normal modes of the mirror

The end mirror of the gravitational wave detector is a cylinder of fused quartz with many mechanical modes. Since the interferometer measures the position of the mirror surface, normal modes that change the position or shape of the mirror surface can produce displacement signals that are indistinguishable from those of a gravity wave. Although fused quartz can be a very low loss material, there will still be some thermal excitation of the normal modes. In general, the thermal noise displacement spectrum can be expressed using the usual formula (see equation 15)

$$< x(\omega)^2 > = 4k_BT \times \sum_{n=1}^{\infty} \frac{\phi_i\omega_i^2}{M_i\omega[(\omega_i^2 - \omega^2)^2 + \phi_i^2\omega_i^4]} \tag{52}$$

In the above formula, it is common to replace the mass of ther mirror with an effective mass, M_i, for each mode (see for example Bondu [5]). The beam spot on the mirror samples the surface in a manner that is weighted by the beam intensity profile.

$$x = \int_{surface} u(r,\varphi)\, P(r,\varphi)\, r\, dr\, d\varphi \tag{53}$$

$P(r,\varphi)$ is the light power density

$$P(r,\varphi) = \frac{2}{\pi\omega_0^2} \exp\left(-2\frac{D^2}{\omega_0^2}\right) \tag{54}$$

where ω_0 is the beam waist and $D = \sqrt{r^2 + d^2 - 2\,r\,d\,\cos(\varphi - \varphi_1)}$ is a measure of the distance between the mirror centre and the centre of the beam. It is clear that if the beam is centred on the mirror, any mode that produces an anti-symmetric shape about the centre of the mirror will not contribute any thermal noise signal. Also, a bigger beam will contribute a smaller thermal noise signal for circumferential modes with many nodes since the beam a bigger beam samples more of the average mirror displacement.A proper calculation shows that a certain number of modes must be included for a given beam waist and mirror size before the total thermal noise reaches an asymptotic value.

The frequencies of the internal mirror modes usually start in the range of a few kHz so that the low frequency tail of the noise spectrum is of interest in the gravity wave detection band.

$$< x(\omega)^2 >= \frac{4k_BT}{\omega} \times \sum_{n=1}^{\infty} \frac{\phi_i}{M_i\omega_i^2} \tag{55}$$

For a certain aspect ratio, the quantity $\omega_i a/c$ where a is the radius of the mirror and c is the speed of sound is constant for a particular normal mode. Since $M \propto a^3$, then $\omega_i^2 \propto M^{-2/3}$ and the thermal noise will scale as

$$\sqrt{< x(\omega)^2 >} \propto M^{-1/6} \tag{56}$$

Increasing the mass of the mirror then does not substantially change the off resonance thermal noise.

The inherent internal loss of fused quartz should be at least 10^{-6} and independent of frequency. Any procedure that affects the mirror can increase this loss. This includes the actual polishing and coating of the mirror, the manner in which the mirror is hung by the suspension wires and the attachment to the mirror of any additional objects such as magnets. Since some of these steps are unavoidable, their affect on the loss of fused quartz must be understood.

The final parameters that determine the thermal noise from internal modes of the mirror which include the beam waist and the mirror mass and aspect ratio are a compromise between reducing the thermal noise and building a practical optical system. In the calculation by Bondu [5], the total thermal noise from all the mirrors is

$$\sqrt{< x(\omega)^2 >} \approx 5 \times 10^{-19} m/\sqrt{Hz} \times \sqrt{\left(\frac{10Hz}{f}\right)\left(\frac{\phi(\omega)}{10^{-6}}\right)} \tag{57}$$

At $10\,Hz$, this is comparable to the pendulum thermal noise. The internal thermal noise from the mirrors is an important problem that needs further study for a future gravity wave detector with increased sensitivity.

4810 Clamps and wires

4810.1 Overview

The test mass or end mirror of the gravity wave interferometer is a monolithic piece of fused quartz that is suspended as a pendulum. The mirror characteristics are described in the chapter 4200. The design of this pendulum must allow the position of the mirror to be controlled with high accuracy. The mechanical losses of the pendulum must also be small so that the resultant displacement thermal noise is not large. The final design must take into account the actual suspension of the mirror, the type of material that suspends the mirror and the manner in which these pieces are fastened.

The Virgo mirrors will be suspended from the Marionetta by two wires forming each a single loop around the mirror lower surface. This avoids the use of any fixed mechanical contact on the mirror which might reduce the mirror quality factor by post-production machining. With this solution, the true contact points between the wires and the mirror surface will be limited to a short part of the wire touching the mirror itself. The rest of the wire will not play an important role from the point of view of wire-mirror friction.

The use of two wires allows the tilt of the mirror about the horizontal axis perpendicular to the optic axis to be controlled by the suspension point of the pendulum—hence, the term marionetta. One drawback of this scheme is that it raises the frequency of the tilt motion about this axis. This can couple vertical motion into horizontal motion and add noise to the gravity wave signal. The use of blades to lower the vertical spring constant of the suspension helps to reduce this effect.

According to equation 15, we must increase the quality factor

$$Q \equiv \frac{1}{\phi(\omega_0)} \tag{58}$$

to reduce the thermal noise effect The experimentally measured loss angle $\phi_{exp}(\omega)$ can be expressed as the sum of three different contributions:

1. the effective pendulum loss angle $\phi_p(\omega)$
2. the energy loss ϕ_{clamp} due to a *stick-and-slip* process between the suspension wire and the clamp
3. the residual gas damping ϕ_{gas}.

Hence, the measured Q can be expressed as

$$Q_{exp} \equiv \frac{1}{\phi_{exp}} = \frac{1}{\phi_p(\omega_0) + \phi_{clamp} + \phi_{gas}} \tag{59}$$

A maximization of Q_{exp} requires the minimization of the three different contributions.

The gas contribution is the easiest to evaluate. In the case of low pressure, it is possible to evaluate an upper limit for the experimentally measured pendulum Q [4]:

$$Q_{exp} < Q_{gas} \simeq \frac{D\rho\omega_0}{p}\sqrt{\frac{K_B T}{M}} \tag{60}$$

where D is a characteristic length of the pendulum, ρ is the density of the oscillator mass, ω_0 is the oscillation frequency, M is the molecular mass of the residual gas and p is the gas pressure in the vacuum chamber.

For the vacuum pressure forseen in the Virgo setup ($\simeq 10^{-6} Pa$), the residual gas contribution to the quality factor Q is negligeable ($Q_{gas} \simeq 10^{11}$) and the main process limiting the Q of pendulum will be given by $\phi_p(\omega_0)$ and ϕ_{clamp}.

4810.2 Wires

The suspension wires are an important consideration in the final design since they play a crucial role in determining the thermal noise performance of the pendulum. The contribution of the loss angle $\phi_p(\omega)$ to the effective pendulum Q_{exp} is given by

$$\phi_p(\omega) = \phi_\omega(\omega)\frac{1}{2L}\sqrt{\frac{EI}{Mg}} \equiv \phi_\omega(\omega)K \tag{61}$$

where ϕ_ω is the loss that characterizes the material and is independent of the geometry of the pendulum suspension wire, L is the length of the pendulum wire, E is the Young's modulus, I is the moment of inertia of the wire cross section and K describes the dependence of the loss on the pendulum geometry. Since the mass of the mirror is fixed from other design considerations, the only parameters to be optimized are the wire type ($\phi_\omega(\omega)$, E) and thickness ($I = \frac{\pi r^4}{4}$).

It is clear that a thin wire with a low loss is the best choice. The diameter of the wire can only be made as thin as the material strength allows. It is important to find a good compromise between mirror safety, high wire violin frequencies and ϕ_p minimization. If we call B the material yield strength (breaking mass / wire cross section) and M the mirror mass, the wire radius is given by

$$r = \sqrt{\frac{M}{4\pi kB}}. \tag{62}$$

were k is the safety factor in the wire tickness choice; kB represent the maximum breacking-safe load for the suspension wire.

The lower violin frequency is given by

$$f_1 \approx \frac{1}{2L}\sqrt{\frac{Mg}{4\pi\rho r^2}} = \frac{1}{2L}\sqrt{\frac{kBg}{\rho}}. \tag{63}$$

From figure 8 we can evaluate the right safety factor k for piano wire; this picture shows the wire violin frequency and wire radius for a given k factor in three different mirror weight configurations. Selecting $k = 0.5$ (50% of the yield strength) we have $f_1 \approx 233Hz$ and $r_{42Kg} \approx 200\mu m$, $r_{21Kg} \approx 140\mu m$. For a short comparative summary, refer to table 1. We report two different quartz entries because surface damage, which occurs very frequently in quartz wires, can decrease the yield strength by a factor of 100 or 1000.

The choice of a material with a high yield strength also raises the quality factors for the violin modes; in fact equation 41 shows that the quality factors for the violin modes Q_n are proportional to the square root of the yield strength. This reduces the thermal noise of the violin modes in the gravity wave signal band.

The choice of wire material, from the point of view of the inherent loss, is a bit more difficult.If the wire is carefully prepared in a way that eliminates imperfections such as impurities and structural irregularities, the inherent loss in the material itself can be bound by using thermo-elastic damping as a lower limit. Since it is an effect due to well understood thermodynamic properties, it can be calculated exactly. The result shows that fused quartz has the lowest loss. The strength of fused quartz (with surface damage), on the other hand, is much less than that of other materials and the overall thermal noise performance of such a suspension is not significantly better. In fact, by examining the $10Hz$ column in table 2, we can see that the ϕ_p of piano wire and actual quartz (with surface damage) are of the same order of magnitude. Furthermore, the thermal noise spectral displacement amplitude

Table 1: *Wire diameters for different load conditions*

Material	$B\ (\frac{Kg}{mm^2})$	$d = 2r\ (mm)$	
		$M_{mirror} = 21Kg$	$M_{mirror} = 42Kg$
piano wire	180	0.28	0.40
quartz (theoretical)	1000	0.12	0.16
quartz (surface damage)	10	1.2	1.6

Table 2: *Loss angle for different wire configurations and oscillation frequencies*

Wire	$\phi_{thermoelastic}$		ϕ_p	
	$1Hz$	$10Hz$	$1Hz$	$10Hz$
piano wire $d = 0.28mm$	4×10^{-5}	4×10^{-4}	2×10^{-8}	2×10^{-7}
piano wire $d = 0.4mm$	8×10^{-5}	8×10^{-4}	4×10^{-8}	4×10^{-7}
quartz (th.) $d = 0.12mm$	3×10^{-8}	3×10^{-7}	1×10^{-12}	1×10^{-11}
quartz (th.) $d = 0.16mm$	5×10^{-8}	5×10^{-7}	3×10^{-12}	3×10^{-11}
quartz (s.d.) $d = 1.2mm$	3×10^{-6}	3×10^{-5}	1×10^{-8}	1×10^{-7}
quartz (s.d.) $d = 1.6mm$	5×10^{-6}	5×10^{-5}	3×10^{-8}	3×10^{-7}

(see equation 15 depends on the square root of ϕ_p. Thus, since piano wire is an easy material to find and to handle, it has been chosen as reference solution (two piano wire loops, with lenght 1.95 m and diameter $d = 0.28\ mmm$ and $d = 0.40\ mmm$, for the light and heavy mirror, respectively); howewer, several studies are in progress to verify some interesting alternatives.

4810.3 Marionetta-wire clamps

To minimize the clamp energy loss, it is very important to decrease the *stick-and-slip* friction between the suspension wire and the clamp itself. The easiest way to reach this goal is to increase the squeezing pressure exerted by the clamp on the suspension wire.

From several tests performed by the Perugia group and reported in figure 9, it is clear that by increasing the clamping pressure, we obtain an increment of the pendulum Q_{exp} and, consequently, a decrement of the energy loss ϕ_{exp}. In figure 9, the Q_{exp} and the ϕ_{exp} of a small pendulum prototype, made by a $0.4mm$ diameter piano wire with a length ranging between $200mm$ and $300mm$ and with a mass of $762g$ attached to the lower end of the wire, is plotted versus the squeezing torque applied to a group of four screws on the clamping head of the pendulum. By increasing the torque, we increase the clamping pressure. The different curves shown in figure 9 refer to different clamp materials. Aluminium, stainless steel and tool steel have been tested. There seem to be no evident differences between the behaviour of the different materials tested. Tool steel has been chosen to build the part of the clamp where the suspension wire touchs the clamp surface. This avoids surface damage to the clamp after several squeezing and dismounting procedures.

Any mass attached to the blades on the marionetta must be kept small so that the internal normal modes of the blade are at a high frequencies outside of the gravity wave detection band. For this reason, the rest of the clamp will be made of aluminium.

A drawing of the suspension wire clamp is shown in figure 11.

4810.4 Future developments

A high pressure locking of the suspension wire is the easiest way to reduce the *stick-and-slip* process inside the clamp, but not the most efficient. We are investigating the possibility of producing a new generation of "monolithic" suspensions where the wire and the clamp are realized in a single piece, without the use of any mechanical connection or soldering procedure. In fact, by constructing a wire with a large cylindrical head, it is possible to lock the suspension to the support frame in a very rigid manner that almost completely removes any clamp loss. This has been tested in Perugia with a small "monolithic" prototype made by a short ($80mm$) steel strip linked to two big cylindrical heads. The "monolithic" prototype Q behaviour has been compared with a strip pendulum with the "usual" clamp and thus, the usual clamp energy dissipation. The suspension strip also has been squeezed by using small cylinders inside the clamp to localize the pressure to the contact lines between the strip and the small cylinders themselves. This configuration decreases the effect of the *stick-and-slip* process inside the clamp. The obtained results show a much lower ϕ_{exp} for the "monolithic" pendulum at all the squeezing torques tested ($\phi_{monolithic} \approx 3 \times 10^{-4}$,$\phi_{strip} \approx 1.5 \times 10^{-3}$). The technological problem that must be solved in order to use this "monolithic" pendulum as the Virgo suspension geometry is to find a technique to construct "monolithic" wires instead of strips with a length of $700mm$ or more.

A promising enhancement of the "monolithic" solution is to use amorphus quartz to construct the suspension wire and heads. In this case, it is possible to build long wires and to fuse them directly to the heads. The problem with this process is the intrinsic fragility of the quartz wire and its stability over long time periods. A small prototype realized in Perugia showed a $\phi_{exp} \approx 6 \times 10^{-6}$.

References

[1] *Thermal noise effects in a mechanical pendulum*, C. Cagnoli, L. Gammaitoni, F. Marchesoni and M. Punturo, Virgo note PJT94-032 (1994); F. Marchesoni, G. Cagnoli and L. Gammaitoni, Phys. Lett. A 187, 359 (1994)

[2] R. Kubo, M. Toda and N. Hashitsume, Statistical Physics II (Springer, Berlin, 1985); L.D. Landau, E.M. Lifshitz, Statistical Physics (Mir, Moscow, 1976); A.S. Nowick and B.S. Berry, Anelastic Relaxation in Crystalline Solids (Academic Press, New York, 1972)

[3] T.J. Quinn, S.C. Speake and L.M. Brown, Phil. Mag. 65 261 (1992)

[4] P.R. Saulson, Phys. Rev. D 42, 2437 (1990)

[5] *Thermal noise of Mirrors*, F Bondu, Virgo note PJT94-034 (1994)

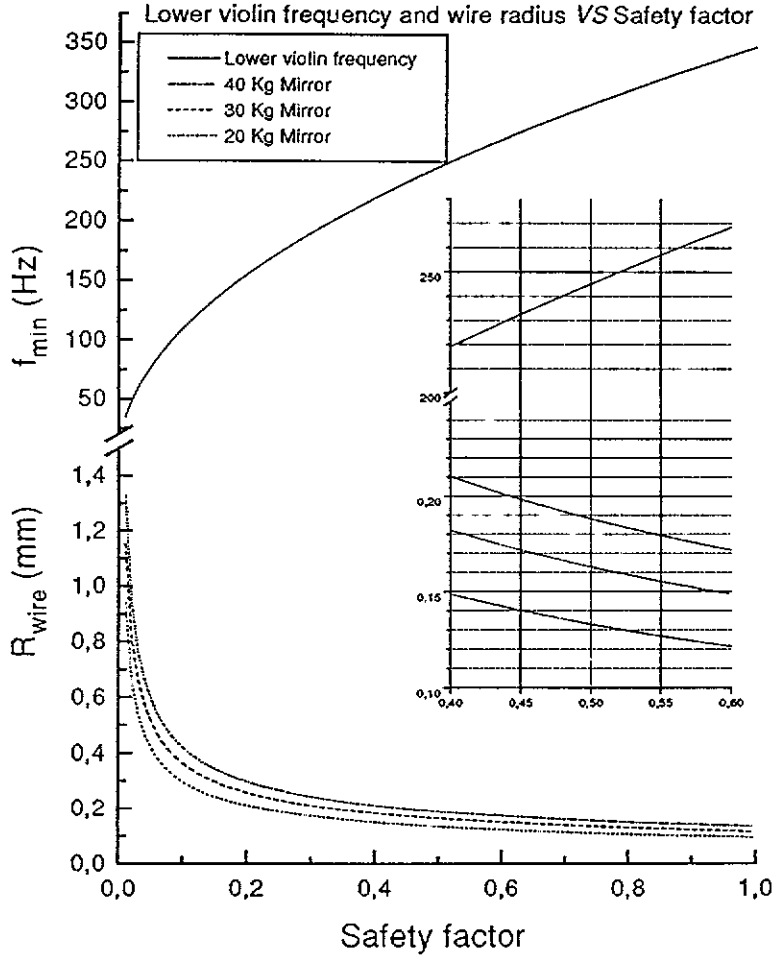

Figure 8: Lower violin frequency and wire radius versus the safety factor for piano wire ($B = 180\frac{kg}{mm^2}$).

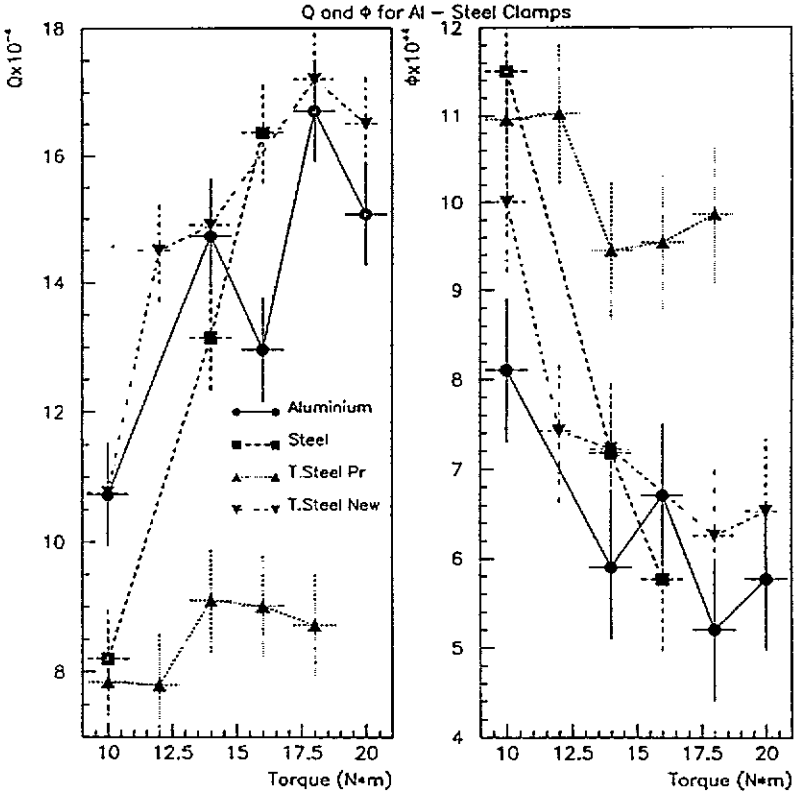

Figure 9: Small pendulum prototype: piano wire suspension with clamps made of different materials.

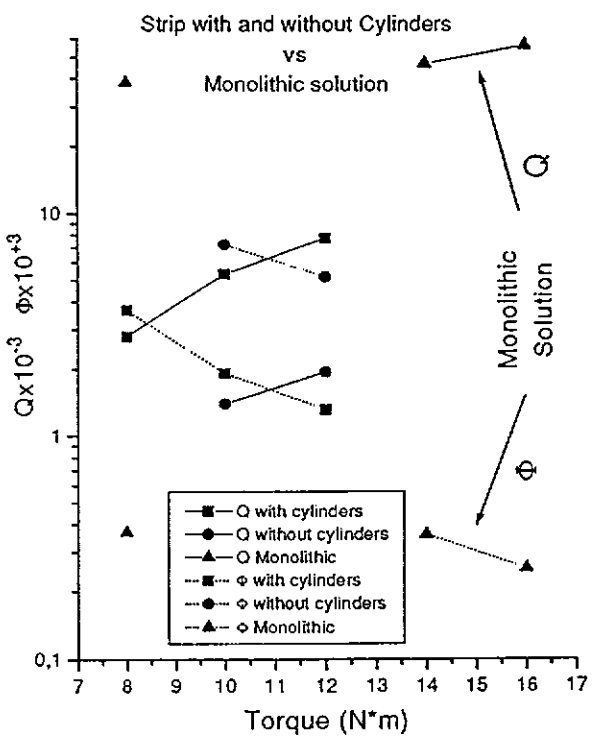

Figure 10: Future developments: Monolithic prototype

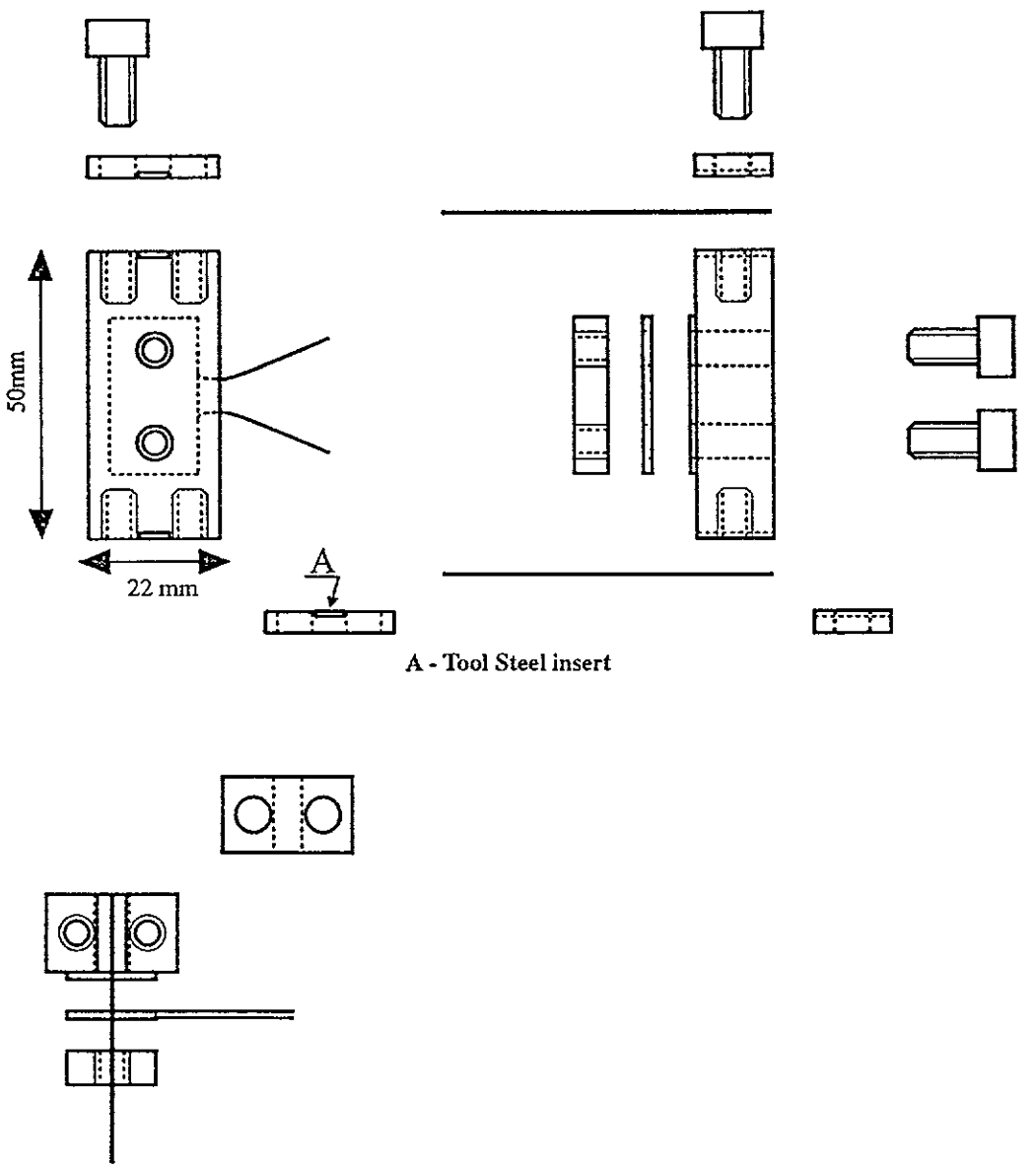

Figure 11: Suspension wire clamp design

Local Electronics

4900 Local electronics

Around each tower a system controls the main operating parameters of the mirror suspension like the position of the various components. It also implements the damping of the suspension normal modes. In addition the control system has to implement the strategy for correcting the mirroro position according to the errors provided by the locking system. This requires the measurement of various transfer functions involved.

This section describes the essential components of the control system. The implementation of the local control system is done in the framework described in chapter 5000 (Electronics and Software).

4910 Normal modes control

4910.1 Accelerometers

The accelerometer developed [1] in our laboratories is a "force balance" sensor. A solid structure supports an inverted pendulum. A force proportional to the relative displacement between the pendulum and the supporting structure is applied to the pendulum in order to keep the suspended mass always in his rest position. This force is proportional to the acceleration of the supporting structure

(fig. 1). Table 1 summarizes the accelerometer characteristics while fig. 3 and fig. 4 show the actual devices for linear and angular measurements respectively.

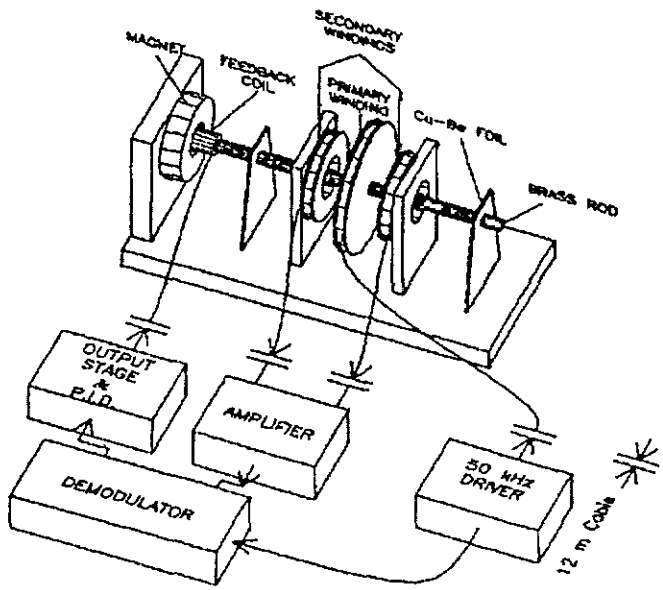

Figure 1: Linear accelerometer structure.

Table 1: Main accelerometer characteristics

Bandwidth (Frequency Response)	dc to 400 Hz
Sensitivity	300V/g
Noise Spectra Referred to Ground Acceleration	$5.3 \cdot 10^{-10}\,\mathrm{m\,sec^{-2}}/\sqrt{\mathrm{Hz}}$
Noise Spectra Referred to Ground Displacement	$4 \cdot 10^{-13}\,\mathrm{m}/\sqrt{\mathrm{Hz}}$
Dynamic Range ($f < 5$ Hz)	170 dB

4910.1.1 Accelerometer test specifications

For each accelerometer a response curve is measured. This includes coupling from the two other axis. Vertical accelerometers need to be adjusted. A test bench with a driving mechanism and measurement station is foreseen.

4910.1.2 Construction

The components of the accelerometer prototypes have been satisfactorily produced by outside firms. It is foreseen to assemble the accelerometers in the Pisa workshops.

Table 2: Main characteristics of the LVDT.

Bandwidth	100 Hz
Sensitivity	100 kV/m
Noise Spectrum	10^{-9} m/$\sqrt{\text{Hz}}$

4910.1.3 Acceptance

The test of each accelerometer includes vacuum and heat qualifying for one day. Setup and measurement of characteristics for each accelerometer should be rather fast. If one accelerometer is tested at a time eleven weeks are needed for fiftyfour devices corresponding to one stage cooling. This time should be doubled if two stages have to be cooled. However it is easily thinkable to test for heat and vacuum two accelerometers. Depending on the rate of success the whole procedure could be speeded up.

4910.2 Linear Variable Differential Transformer

The position sensor we use is a Linear Differential Transformer. A sinusoidal wave is driven into a primary winding connected with the SA stage while the two secondary windings are connected with the grounded structure supporting the coils. The differential signal induced into the two secondary windings is proportional to the relative displacement. Its characteristics are listed in table 2

4910.3 Actuators

The actuators used in the SA control consist of a permanent magnet located on the SA stage and a coil located on the grounded structure. The coils are driven with a transconductance amplifier. The magnet-coil couple conversion factor between current and force is 0.2 N/A.

4910.4 Feedback loops

The structure of the feedback loop is shown in fig. 2.

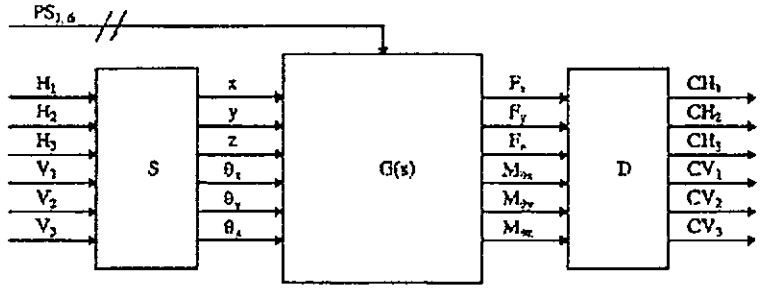

Figure 2: Damping system feedback.

The signals H1, H2 , H3, V1, V2 and V3 coming out from the three horizontal and the three vertical accelerometers are first of all combined with a "Sensing Matrix" S. The elements of this matrix

take into account the position of the acceleration sensors with respect to the SA seismic filter. Since this position is fixed, they don't depend on time. The sensing matrix produces six signals which represent the acceleration in a external reference frame. Once this acceleration has been obtained, the multivariate system denoted by G(s) produces three forces and three torques taking into account the signals coming out from the six position sensors (PS1, PS2, ... , PS6). The final step is the generation of the six signal (CHi, CVi , i=1..3) to be sent to the coils. These signals are the outputs of the "Driving Matrix" D, matrix whose elements are constants depending on the position of the magnets on the SA stage.

The described implementation allows to simplify the loop stability design. The six degrees of freedom system is divided into six one degree systems.

4910.5 Electronic implementation

The "heart" of the SA control system is a Digital Signal Processor, which is a general purpose microprocessor able to perform up to 60 millions floating point operation per second.

The main characteristics of the adopted DSP are summarized in table 3.

Table 3: SA DSP characteristics.

Company	Motorola
Product Name	DSP96002
Product Type	Gen. Purpose DSP
Arithmetic Format	Floating Point
Data Word-Length	32 (bits)
Address Word-Length	32 bits
Internal RAM	2048 (words)
Internal ROM	64 (words)
Clock Speed	40 (MHz)
Instruction Cycle Time	50 ns
MFlOPS	60

The processor implements the "Sensing Matrix" S, the "Driving Matrix" D and the control system G(s).

Signals coming from sensors are converted to digital signal to be processed by the DSP. The conversion is done by the board ADC416b (INFN-Pisa design), which is a 4 channels, 16 bits, 160 ksamples/s ADC VME board. The conversion from digital to analogue is performed by the board DAC820b (INFN-Pisa design), an 8 channels, 20 bits, 250 ksamples/s DAC VME board.

The control system acts under the supervision of a VME integrated CPU board based on a Motorola MC68040 processor. The main module of the software running on this system implements I.I.R. digital filters. The operator introduces transfer functions as series of poles, zeroes and gains in the Laplace domain; the program translates them into a z-domain represent-ation (by means of a bilinear transformation), builds and downloads the binary code for the DSP. In this way the operator do not have to write source code lines to let the system work. A second module, to date under development, performs data acquisition and analysis on time.

4910.6 Power Dissipation

Electronic devices inside the tower are critical concerning the power dissipation. It is necessary to calculate the power dissipation for each of them.

4910.6.1 Accelerometers

The only non negligible power dissipation is due to the driving signal used by the position sensor (about 2 W for each accelerometer). The primary sides of each transformer should be driven separately. The current is about 200 mA (r.m.s. value), the operation frequency is 50 kHz and the impedance of the primary side of the transformer is about 50 ohms.

4910.6.2 Position Sensor

The position sensor is about a factor 1000 less sensitive than the accelerometer position sensor. For this reason it is possible to drive al least 6 position sensor connected in series. The total power dissipation shouldn't be higher than $6 \cdot 0.2$ W. The current flowing in each primary side is about 30 mA.

4910.6.3 Feed-back Coils

The r.m.s. force to be applied on a stage of the SA is the equivalent seismic force on that stage, that is a force that produce on the SA stage the same displacement due to the seismic noise within the bandwidth of the control system. Some easy calculations demonstrate that the r.m.s. current flowing in a coil (0.2 N/A) depends on the control system bandwidth lower limit f_L:

$$I_{rms} = k/f_L^{3/2}\,\mathrm{A}$$

where k can be assumed equal to $10\,\mathrm{mA} \cdot \mathrm{Hz}^{3/2}$ for a seismic spectral density of $10^{-6}/f^2\,\mathrm{m}/\sqrt{\mathrm{Hz}}$ ($k = 1\,\mathrm{mA\,Hz}^(3/2)$ if the noise is $10^{-7}/f^2$). The foreseen f_L is about 20 mHz so the r.m.s. value of the current is about 350 mA. Assuming $I_{rms} = 500$ mA to be conservative the power turns out to be

$$W = I_{rms}^2 R = 1.25\,\mathrm{W}.$$

4920 Filter vertical working point control

The detailed design of SA length control system has been developed by an external firm (I.S.E.-Pisa) following the specifications described below.

A position sensor based on a linear variable differential transformer (LVDT) gives a signal proportional to the relative displacement between the frame and the mobile part of a seismic filter. This signal is used as a position feedback to control the equilibrium position of four (or two) metallic springs on the filter. This is achieved by driving a brushless motor which pumps water into the bellows mounted on the filter. The error signal given by the position sensor is sampled at 100 Hz with a 12-bit ADC. The digital signal is elaborated by a CPU board (Advantech PCA-6143DX2-66) having the following specifications:

- processor 80486 DX2 66Mhz
- 4 MB RAM

- ROM disk
- controller IDE
- serial, parallel port and keyboard input

The control signal is converted in an analogue signal by a 12-bit DAC and is fed to the servo-amplifier which drives the motor.

The CPU board is fully programmable through a serial link with an external terminal.

4930 Wiring and cabling

The seismic attenuation cascade requires a relevant amount of isolated wires (for steering coils) and single isolation coaxial cables (for signals).

Both wires and cables should be UHV compatible. Moreover, the signal cables and the wires arriving to the coils should be flexible enough to avoid coupling to seismic vibrations of the support structure and to be anchored in a few points along the seismic attenuation cascade to reduce seismic transmission.

The flexibility requirements rules out the coaxial cables with external insulation made of stainless steel or fiber glass. The options currently under evaluation for the coaxial cables are:

- Kapton isolated cables by AML, England;
- Kapton isolated cables by Caburn/MDC, England;
- alumina isolated cables by California Fine Wires, USA.

Some options are currently under evaluation for the coil winding wires:

- Kapton isolated wires by AML, England;
- Kapton isolated wires by Caburn/MDC, England;
- alumina isolated wires by Dipsol Chemicals, Japan.

4940 Transfer function measurement

The final stage of the suspension, including the transduction efficiency of the magnetic coils, has to be characterized. This is necessary for the design of the servo-loops used in the locking system and for continuous monitoring of the suspensions during VIRGO operation. Possible changes in the suspension behaviour have to be reflected into the servo-loop filters. The specifications for transfer function measurement are particularly stringent for displacement along the optical axis, while there is no need of very fast and sensitive measurement for angles since the related servo-loops will work only in very low frequency. The transfer function measurements should be performed from low frequency up to 100 Hz at least. In the hypothesis of applying to the marionetta a sinusoidal force of amplitude $F_0 \leq 1$ N the mirror displacement system should have a sensitivity of at least $10^{-12}\ m/\sqrt{Hz}$ at 100 Hz to keep the measurement time acceptable. This is due to the mechanical filtering of the last stage giving a factor proportional to ν^{-4} between force and mirror position.

This is a demanding task both in sensitivity and in bandwidth which cannot be taken in charge by the position monitoring CCD cameras. In addition the device used for TF measurement need some seismic isolation to reach the required sensitivity

The preliminary measurement to be performed on the prototype suspension in Pisa should be separated from the on-line, routine measurement for the final suspensions during VIRGO operation. For the first point two possible techniques have been proposed, a first one using quadrant photodiodes and a second one which uses an interferometric sensor. Preliminary tests have been performed in Rome on quadrant systems and using the 3 m Napoli suspended interferometer. A proposal shall be made by Napoli for one of the systems keeping in mind the opportunity of using commercially available interferometric sensors (Hewlett-Packard, Polytec, Aerotech , EG&G). Such a system will then be developed to be implemented on one tower to measure the transfer functions on a full scale suspension.

In view of monitoring the suspension response during data taking it has not yet been determined whether dedicated measurement systems are necessary around each tower. The Virgo signals themselves are indeed sensitive enough to measure the transfer functions even with a very small excitation of the marionetta. While the necessary room and openings are foreseen around each tower a first indication shall come after the measurement performed on the prototype suspension in Pisa. The decision to equip each tower with the necessary measurement devices shall be taken when having gained experience in the operation of the VIRGO 97 interferometer.

References

[1] *A Low Noise Wide Band Accelerometer Using an Inductive Displacement Sensor*, S. Braccini *et al.*, Rev. Sci. Instrum. 66 (1995) 2672.

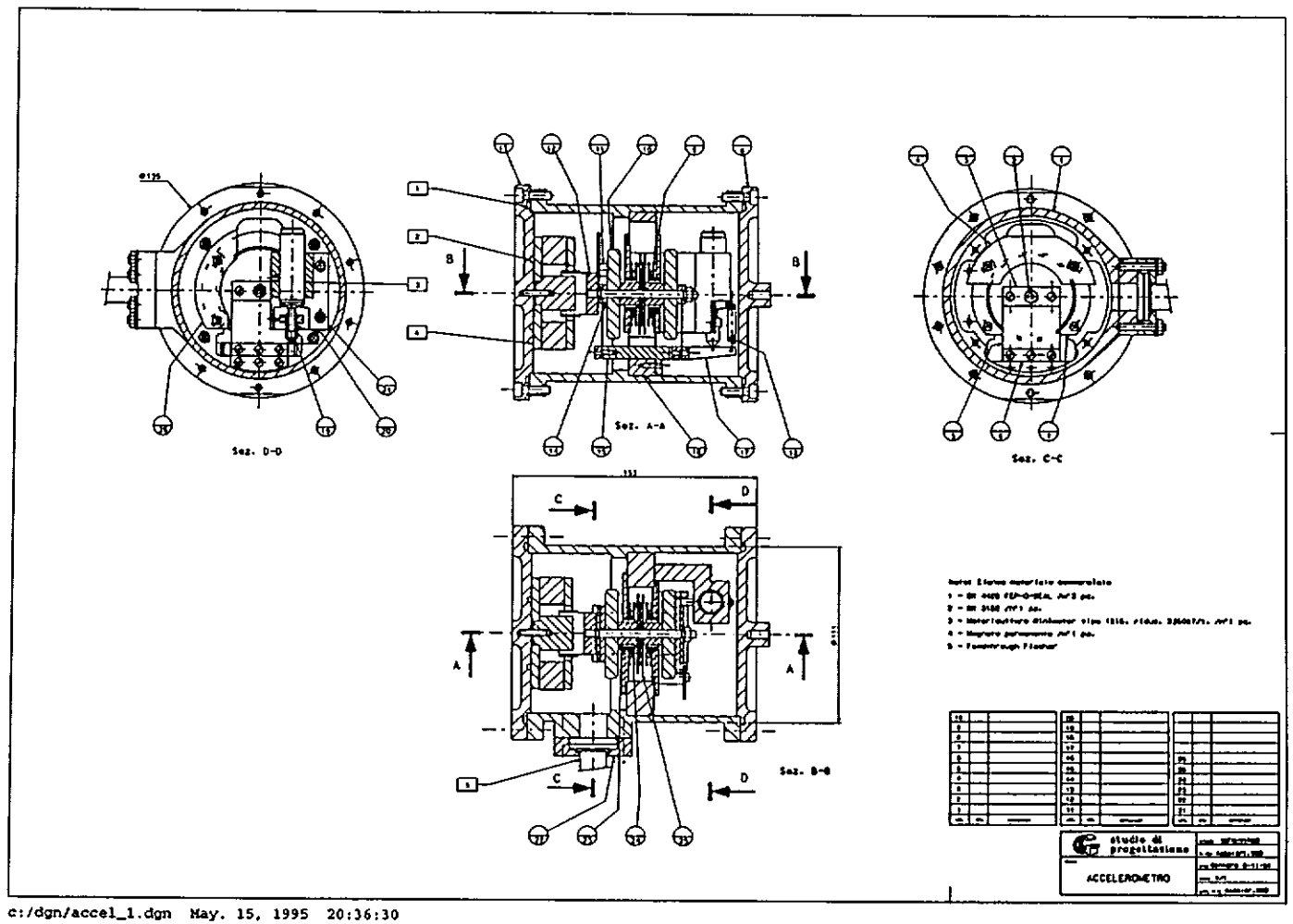

Figure 3: The linear accelerometer.

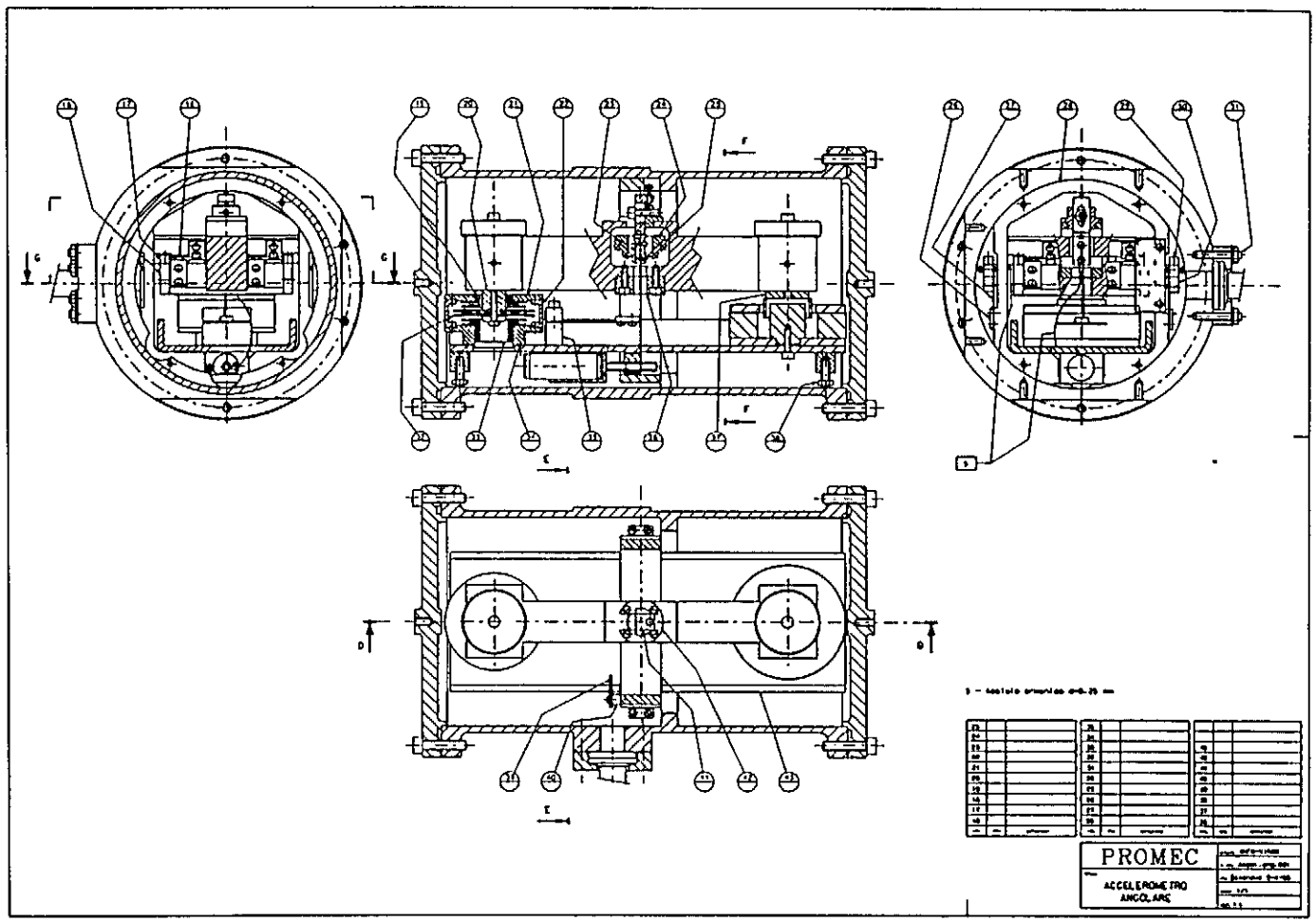

Figure 4: The angular accelerometer.

-5000-

Electronics

5000 ELECTRONICS AND SOFTWARE

Introduction

This chapter describes all the needed activities starting from the output of the local electronic up to the data ready to be analyses for Gravitational Waves search. It covers four fields:

- The online activity. It concerns the controls of the interferometer, the acquisition, online processing, and monitoring of the data produced by the various detectors or control process.
- The detector simulation activity. It concerns the generation of gravitational events like coalescent binaries, pulsars, supernovae and the simulation of the response of the interferometer to such signals and to all possible noises.
- The offline activity. It concerns the basic tools for the refined analysis of the large amount of collected data.
- The detector commissioning and calibration activity. It concerns the strategy to check parts or all of the system and the calculation of all calibration parameters.

A coherent view of all these activities will optimize the design, the commissioning, the running and the understanding of the first results produced by the interferometer. In addition to the discution of these four fields, the standardization and rules, the hardware implementation and the cost estimate will be also presented.

Most of the solutions presented here have already been described in the Virgo note PJT93-16 and in its updated version from September 94.

5000.1 The online Architecture

The various active parts of the detector which produce digitized information or 'data' are represented on figure 5000.1. Most of the signals produced by the different sensors are processed by a layer of local controls which compute and apply local corrections to keep the controlled elements (laser, mirror, vacuum pump,..) within a given set of tolerances. These controls produce data like status informations or feedback values. Several local controls may be supervised by a higher level control, the Global Control in charge of the locking or the alignment.

The data generated by these detectors and controls (the 'raw data') are collected by a local readout process, concentrated and structured by an Frame builder and written to tape (Data archiving). They are processed ('reconstructed') to convert ADC counts and feedback signals to an h value, and 'filtered' to reduce their amount to a level manageable by the offline analysis. The data quality is permanently monitored by surveying the noise level and a known signal produced by a calibration device stimulating permanently the interferometer as a gravitational wave would do it. Finally, the 'filtered' data are send to a storage and distribution system which is the experiments front end for the offline analysis. The system provides also tools for histogramming and data editing (including monitoring data).

All these controls are coordinated by a Supervisor and synchronized with a central Timing system.

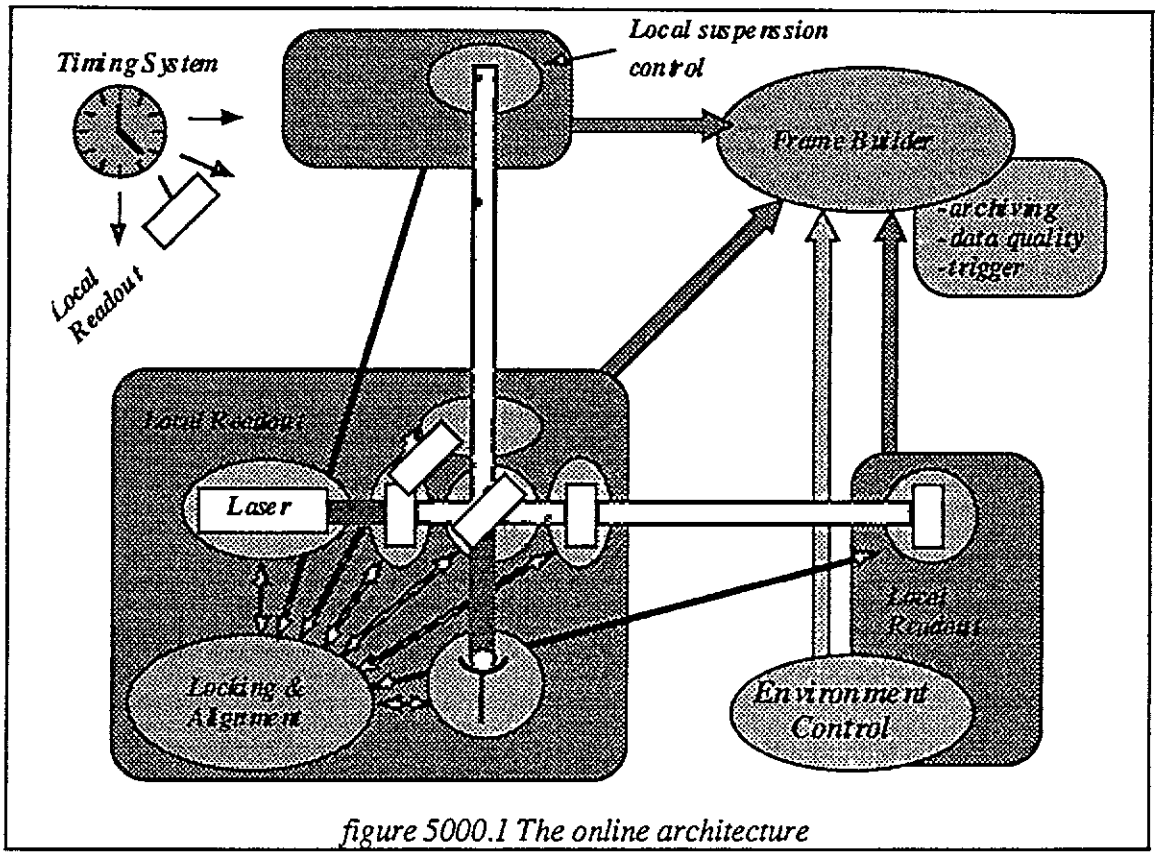

figure 5000.1 The online architecture

5000.1.1. Specifications:

The main specifications for the online system are:

- a real time control system with fast decision taking processes and correlation capability (up to 20 kHz) all over the site,
- a data acquisition system with a maximum sampling frequency of 20 kHz and a data rate up to 10 MBytes/sec,
- a dead time between the user interface and the real time process lower than one second,
- a system easy to reconfigure and to use on small test bench,
- test capability at all levels.

5000.1.2. The architecture

The interferometer is kept at its working point by a set of controls which process data provided by captors and adjust accordingly its main components: the laser, the two mirrors of each Fabry Perot cavity, the end mirror of the mode cleaner, the recycling mirror, the beam splitter, the injection and detection benches.

The architecture of the control and read out systems has to account for the large distances which may separate two components. To preserve flexibility in the interferometer setting up, the control systems are organized as much as possible into independent units in charge of the adjustment of a well defined component. They are run locally in standalone mode and accessed remotely by some high level control process. Similarly, the readout systems are implemented into independent units in charge of the concentration of the data produced near the components located in a same building: end mirror west and north, mode cleaner, and main buildings. A central data acquisition system, located in the control room, collects and assembles these data before writing them to tape.

The knowledge of the precise timing of the various measurements and actions performed around the interferometer is one of the key points of its operation as a gravitational wave detector. This is implemented with a central timing system, located in the control room, and set up to distribute a well defined clocking sequence all over the site.

5000.1.3. The hardware options

To achieve a few khz bandwidth on the interferometer sensitivity, one has to design its various servo loops with a much higher bandwidth in the range of 10 kHz. As a consequence, one has to implement the system with 'fast' captors, processors and actuators connected with 'fast' links. To execute the various feedback loops within a constant time the system has to be build with conflict free accesses.

Sensors, processors, and their actuators sampled at those high rates are thus implemented within the commercially available VME standard. High transfer rate digital servo loop are implemented with a dedicated bus. Conflictual bus accesses are avoided by housing only exclusive controls in the same crate. To keep proper track of all the measurements only digital informations can be exchanged. Higher level control process transfer their informations from building to building via a Digital Optical Link (DOL). Short distance transfers between different controls are performed through mirrored memories connected on a local vertical bus or using a DOL.

The environment status is generally measured with captors sampled at a low rate. They are thus implemented in VME or G64, depending on their availability and cost. They are read out by slow monitoring systems and the data are exchanged using a dedicated ETHERNET network (the slow monitoring network) extending all over the site.

The data sampled at high rates are collected by the local fast readout systems. Then they are transferred to the main control room by a digital optical link.

All the processors are networked via ETHERNET or FDDI and accessible for control and file exchange by all workstations. Figure 5000.2 shows the networking which has to be implemented between the main building, an end mirror building and the control room. The basic rule is that hardware links are used for any real time connections while computer networks are used for state control and for slow monitoring.

The use of standard hardware is mandatory since it allows easy reconfiguration and long term maintenance.

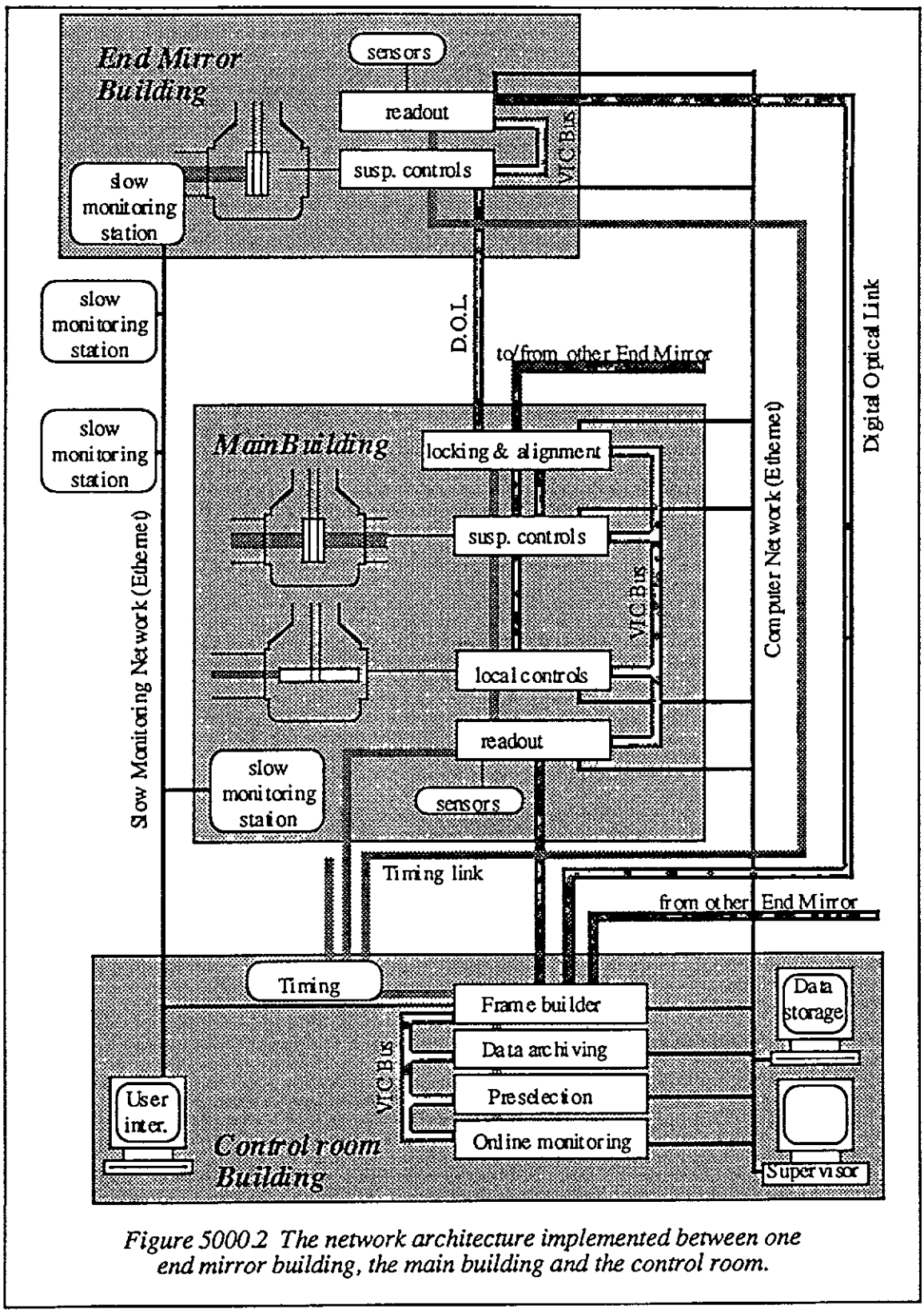

Figure 5000.2 The network architecture implemented between one end mirror building, the main building and the control room.

5000.1.4. The software options

The steady operation of the interferometer is implemented in the context of distributed processing synchronized by a 'central' timing system. The various control processes are designed as standalone tasks getting data from a dedicated local captor and/or from another control process. The different readout tasks are organized to operate under the mastership of a central DAQ task.

Each control process (fig. 5000.3) is a server built in the framework of the client-server model. It is a real time program usually running on a VME CPU. It has direct access to the hardware required by its functionality (typically ADC's, servoloop,...). It should be able to run and to deal with its possible error conditions, minimizing its access to the computer network. For fast control proccess, only data for test, configuration parameters and status information should be exchanges using the computer network.

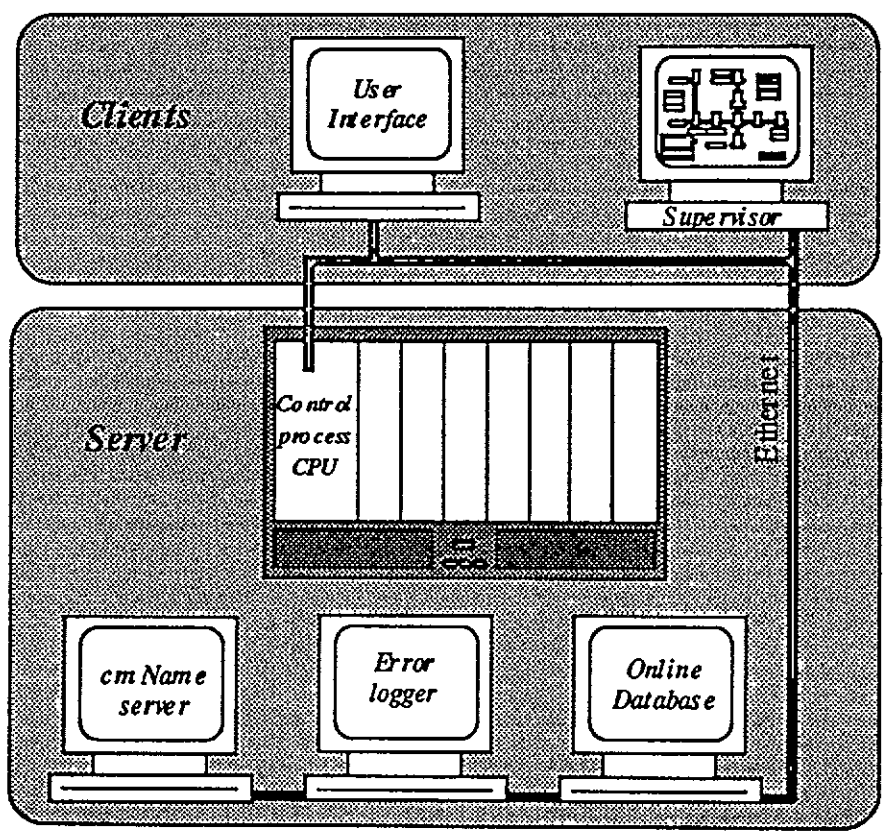

Figure 5000.3 client/server process organization

The user interface (a client of the control process) configure the server and/or monitor and display the data provided by the server. Several user interface clients can be simultaneously used to monitor its informations, but only one client at a time (the master client) has the privilege to configure a server. Possible conflicts are locally solved using standard rules and information provided by the online database. The user's interfaces are run on workstations and they don't need to be real time.

The cm library is used for ALL the communications between process on the computer network. This package provides platform independent communications tools and access to the process using logical name. The correspondence between logical names and physical addresses is provided by the cm name server. This server is needed for all applications using cm and therefore it should always be running. There is a unique cm name server for the experiment.

To provide an easy control of all the process by a single user interface (The supervisor) all the running servers are able to respond to a standard set of messages. These messages allow the supervisor to control the basic server operations and some monitoring facility. The list of the standard message is given in table 5000.1. Figure 5000.4 and 5000.5 gives additional information about the exchanges messages. In addition to this standard list, messages specific to a type of server are available. They should always start with the two key letters of the process type.

Request		Expected return information	
Message type	Data send	Message type	Data send
SuGetStatus	none	SuServerStatus	status (see note 1)
SuBecomeStatusUser	none	SuServerStatus	status (see note 1)
SuNoMoreStatusInfo	none	SuServerStatus	status (see note 1)
SuLoadConfigFromDisk	file name	SuServerStatus	status (see note 1)
SuLoadConfigFromDB	file name	SuServerStatus	status (see note 1)
SuPutConfig	none	SuServerStatus	status (see note 1)
SuGetConfig	none	SuSendConfig	config file
SuSaveConfigOnDisk	file name	SuSaveConfigStatus	success or failed
SuLoadConfig	none	SuServerStatus	status (see note 1)
SuCheckConfig	none	SuCheckStatus	success or failed
SuRunServer	none	SuServerStatus	status (see note 1)
SuGoToLevel	an integer	SuServerStatus	status (see note 1)
SuStopServer	none	SuServerStatus	status (see note 1)
SuKillServer	none	SuServerStatus	status (see note 1)
SuWhoIsMaster	none	SuMasterIs	master name
SuBecomeMaster	none	SuMasterIs	master name
SuDelegateMaster	client name	SuMasterIs	master name

note 1: The text given the server status should start with one of the following words:
• 8 character for the current status: `-stable-`, `runLvlnn` (where `nn` is a number), `configLd`, `configAv`, `noConfig` (see figure 2.4):
• 6 characters for the time with the format: hhmmss
• 4 characters for the config checksum (computed with a short)
Then additional text could describe the changes like: waiting for DataBase, trying to load,...

Table 5000.1

The stable state is reached when the server and its hardware are operated in a mode which allows stable data taking. Running is for the cases where the system try to reach the stable case like pumping down, trying to align, to lock,...Several running levels could be specified.

All the parameters needed to run a server are stored in configuration files which could be stored locally, by the server, or by the Online Data Base. These configuration files are just an ASCII text to allow easy understanding and debugging. In fact one of the main tasks of the user interface is to be a intelligent configuration editor. The Online Data Base store also all the information about privileges access to the server. This is done by using the machine name and the user account as selection parameters.

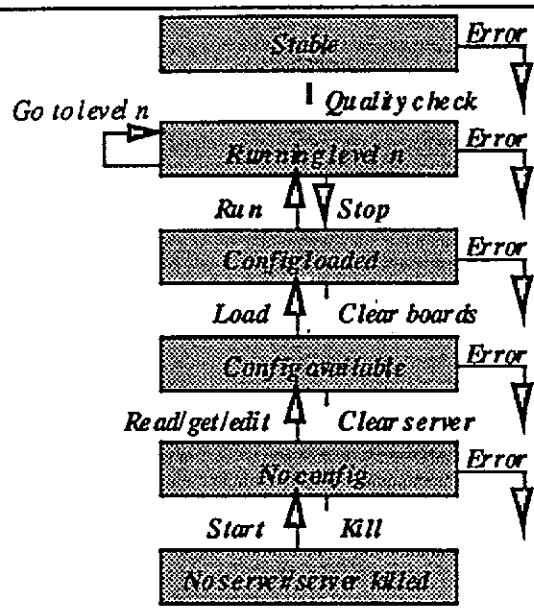

figure 5000.4 Server states. Changes from one state to an other is triggered by one of the messages given in table 2.1 except for the error and for running/stable which is done using some quality check.

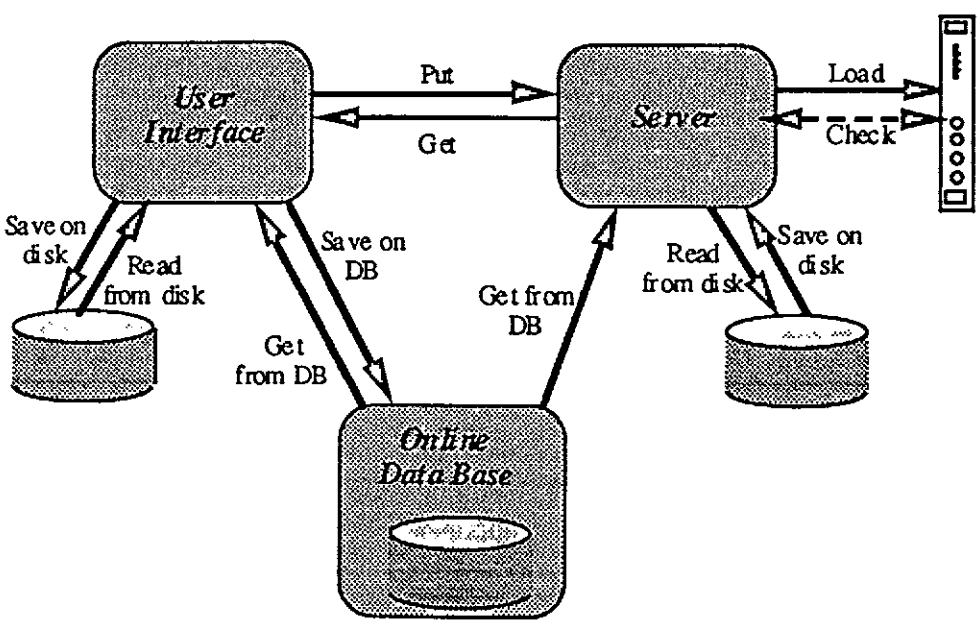

Figure 5000.5 The possible moves for the configuration files

The error logger is the last server which should always be running. It collects the information and error messages from all the process. The error display is the error logger client which provides the tools to select and display error messages collected by the error logger.

5000.1.5. Security

It is important to be able to protect the hardware against any kind of wrong action. We first have to remenber that the hardware is connected to a VME CPU which run the server. The first protection will be to limit the number of account on these processors.

Then the server is driven by a client which run on a different computer. Since all connections use Cm, the next protection will be the limitation (using domaine name for instance) of computers able to be connected to the name server. The Cm connection will also provide the user name for the client. Therfore we can restrict the connections to a limited number of account run on a limited number of workstations. The server will get these informations from the online data base. When two clients want to control the same server, the server will ask the online data base to know which one has the higgest priority. If the connection with the data base is not possible, the first connected client will have the priority.

5000.1.6. The timing system

A central timing system is required to synchronize perfectly the interferometers control, servo loops and readout systems. This is achieved with a master clock driving a bunch of timers which reduce the original frequency to the frequency specific to a given device (see figure 5000.6). Practically, the master clock is derived from a GPS system located in the control room building. Clocking signals are distributed by an optical fiber link to the different buildings where they are converted to TTL signals for local use.

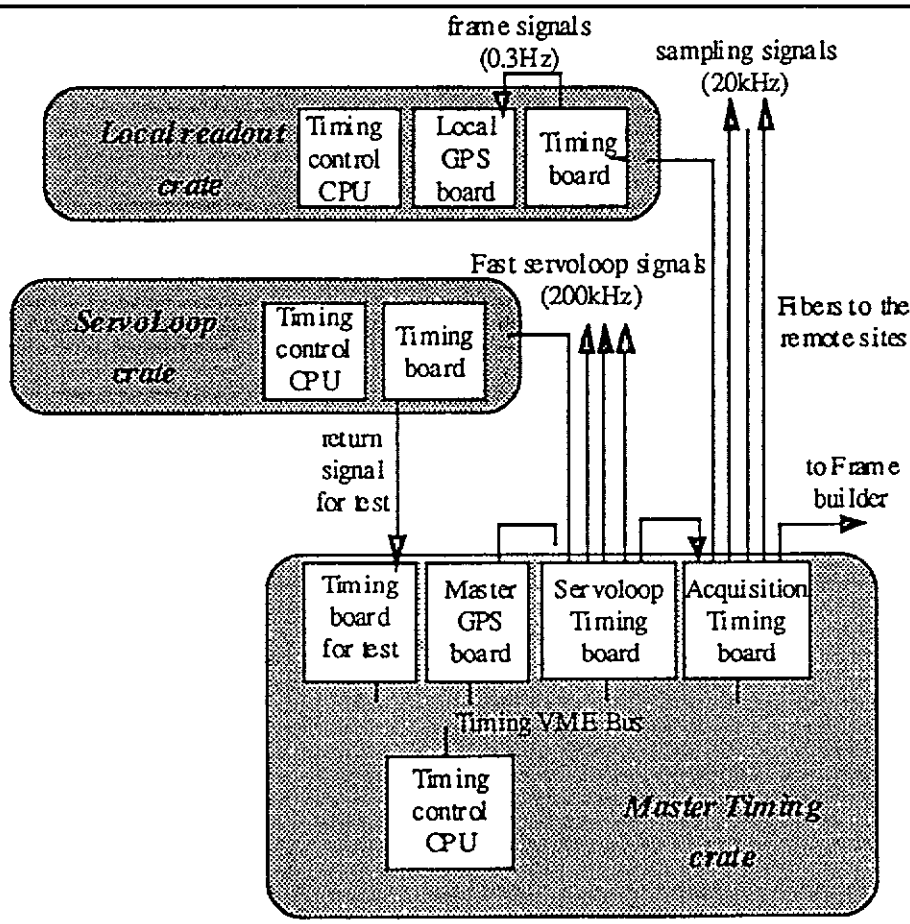

figure 5000.6 The timing system

Whereas the different captors and controls are sampled and operated at rates adapted to their sensitivities, the basic acquisition cycle is set to the sampling frequency of the dark fringe. The timing system produces the necessary interrupts (at 20 khz) to trigger the acquisitions with a 'sampling number' for their later identification. Depending on the required sensitivity, one may be lead to group together several acquisition cycles,

covering thus larger time intervals called frames. The timing system provides the frame number for their later identification. The frame starting time is given by the GPS system at reception of this interrupt. It is the time stamp of the data acquisition.

The different controls and feedbacks are operated on fractions or multiples (i.e 200khz) of the basic acquisition cycle. Their action is thus precisely known with respect to the acquisition time. The implementation of this clocking sequence is the corner stone of the safe operation of the detector.

For simplification, the number of clock will be minimized. We forseen three basic clocks:

- The fast servo loop clock (about 200 kHz). It will be use to oversample ADC used by the precise measurement (signal detection or suspension damping)
- The sampling frequency (10 to 20 kHz). It will be use for most of the digital servo loop (locking, suspension control) and for the main data acquisition
- The seismic frequency (100 Hz). It will be use to record monitoring accelerometer.

Each timing board is able to generate a frequency signal by its own in order to guarantee a clock signal to the ADC and DAC boards, even if the connection with the master source is lost. There is a timing server for each crate holding a timing board.

The full timing system could be tested and will be permanently monitored by measuring the sampling time in each local readout crate using independent GPS boards or by using a return signal for fast servo loop. This show the advantage to use this system instead of only a set of independant GPS boards where no cross-checks are possible and where the relative phases between clocks are much difficult to control.

5000.1.7. The Slow monitoring network organization:

The slow monitoring network is designed to control and collect data from Slow Monitoring Station (SMS). A SMS is a standalone system which controls some hardware and which provides a small amount of data with no precise timing information (the foreseen timing accuracy is 1 second). A typical SMS is a Tube control station which controls a pumping station.

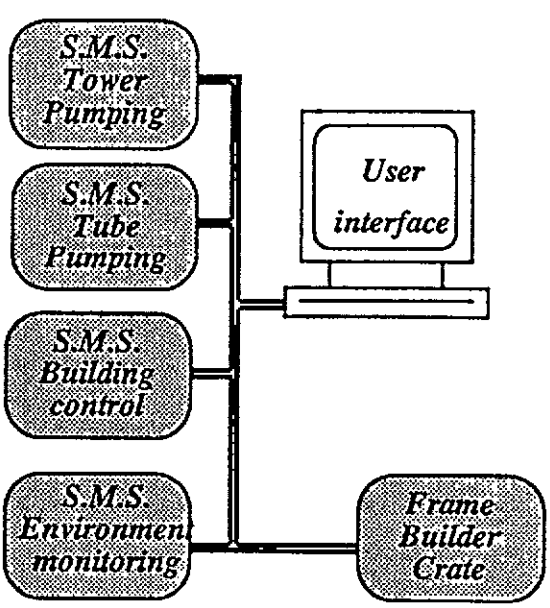

Figure 5000.7 Logical organization of the slow monitoring

A SMS follows the standard software rules. It is a server with user interface run on different machines(see figure 5000.7). The data read by the SMS are formated and

send to the frame builder on its request once per frame. The frame builder will send these data to the data distribution and the archiving system even if the fast data acquisition is not running. The history of the parameters can be displayed on a workstation using the Data display and the data distribution systems. For this data collection the SMS has to be able to answer to the following additional cm messages:

- message type: FbGetAllSmsData: the SMS should return all the data to be recorded
- message type: FbGetUpdSmsData: the SMS should return only the data which have changed since the last update request

The SMS answer to these requests is a message with message type: FbSmsData. The message data sent is an ASCII text where all SMS data are described. The format of this text is the following where all the words are separated by a space:

A header:
- SMS station name (4 characters) (see section on standardization)
- the day of the year (ddd)
- time with the format: hhmmss
- 'ALL' or 'UPD' according to the type of data send
- time interval since last update in second
- time interval between the request and the measurement (in second)

Data blocks with for each data:
- the data name
- the data value starting with 1 characters given the data type:
  - i for integer
  - e for exponent
  - f for float
  - s for a string (could be a quoted string)
  - v for a vector. in this case the vector size is given just after v and is followed by the values. Example: v3 i20 i23 i19
  - o for open (for a valve) or for on (a pump for instance)
  - c for close or for off

A end of data trailer:
- the 'EndOfData' string

The figure 5000.8 gives an example of on data block send by a SMS.

```
TOBS 123 084521 UPD 20 1
G31 e5.01e-8
G32 e2.34e-6
SamplInt i200
CPartCh1 i32222
EndOfData
```

figure 5000.8 example of SMS message data. The data comes from the slow monitoring station TWBS (tower control for the beam splitter). The data have been send the day 123 at 8h45m21s. It is a data update over a 20 s. interval.. Four data values are send. Unlike on this figure no newline character should be included in the message.

To preserve the network bandwith, a dedicated network is used for the slow monitoring. The only connected CPU on this network are the SMS, the needed workstations to run the user interfaces and the fame builder.

5000.2. The control of the interferometer.

The various optical and electrical components of the interferometer are driven by local, standalone, controls. Several components can be correlated by a higher level process (locking & alignment) acting through local controls. During setting up, any local control can be operated using the supervisor. The figure 5000.9 is a sketch of this general control architecture which will be detailed in the following sections.

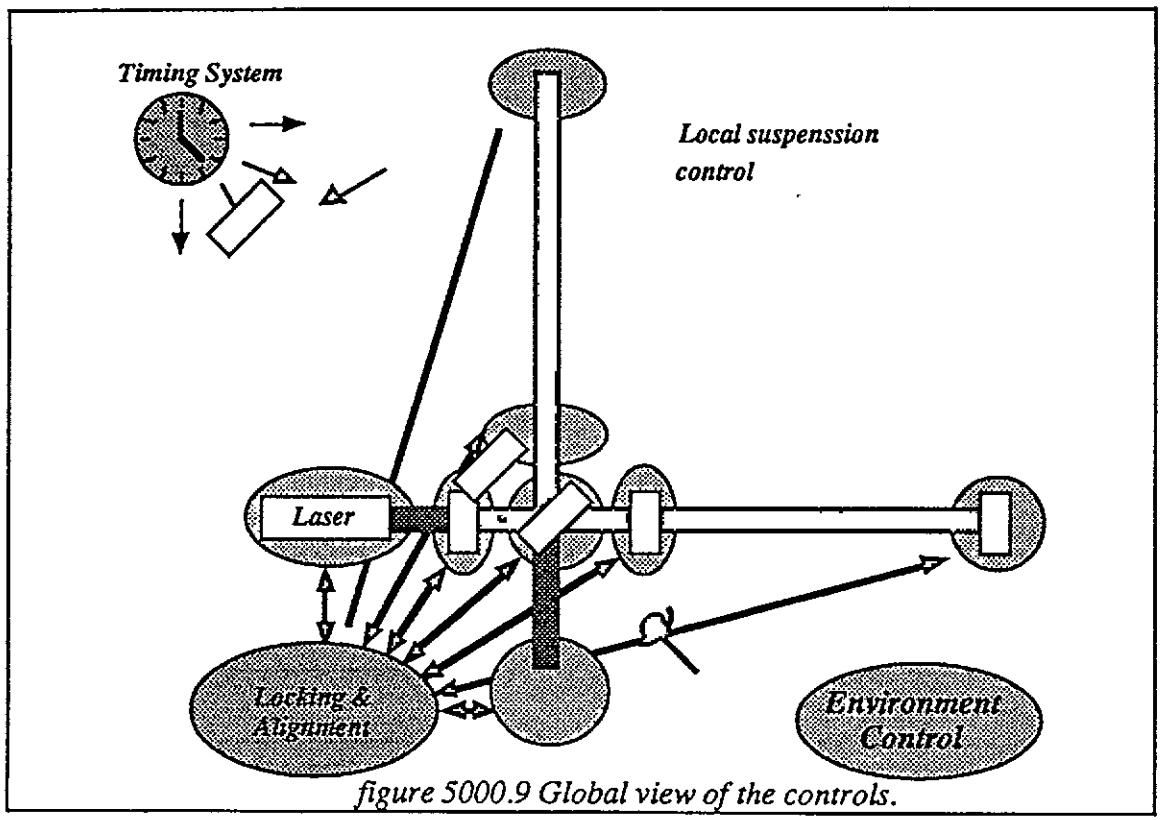

figure 5000.9 Global view of the controls.

Figure 5000.10 presents the chain of hardware component needed for the control implementation. It is a distributed digital servo loop running at a frequency around 10 kHz (this frequency is limited by the transfert time between the component, given their relative distances). The status of each component is control by the supervisor using the computer network, while the real time data are exchanges using hardware connection (DOL). The data exchanges in the links are:

- From signal detection: power seen by the various photodiodes in Watts (DC and demodulated signals)
- From the local position measurement: Three absolute positions and angles
- From the suspension control to the locking & alignement: the mirror absolute position from the local position, the force apply on the mirror and any relevent status information.
- From the locking to the suspension control: the position and angle error.

This scheme is basically the same for the longitudinal locking and for the alignment and strong connection between them will be possible, though we will try to disconnect as much as possible all the functions. The next sections will give more details on the box contents.

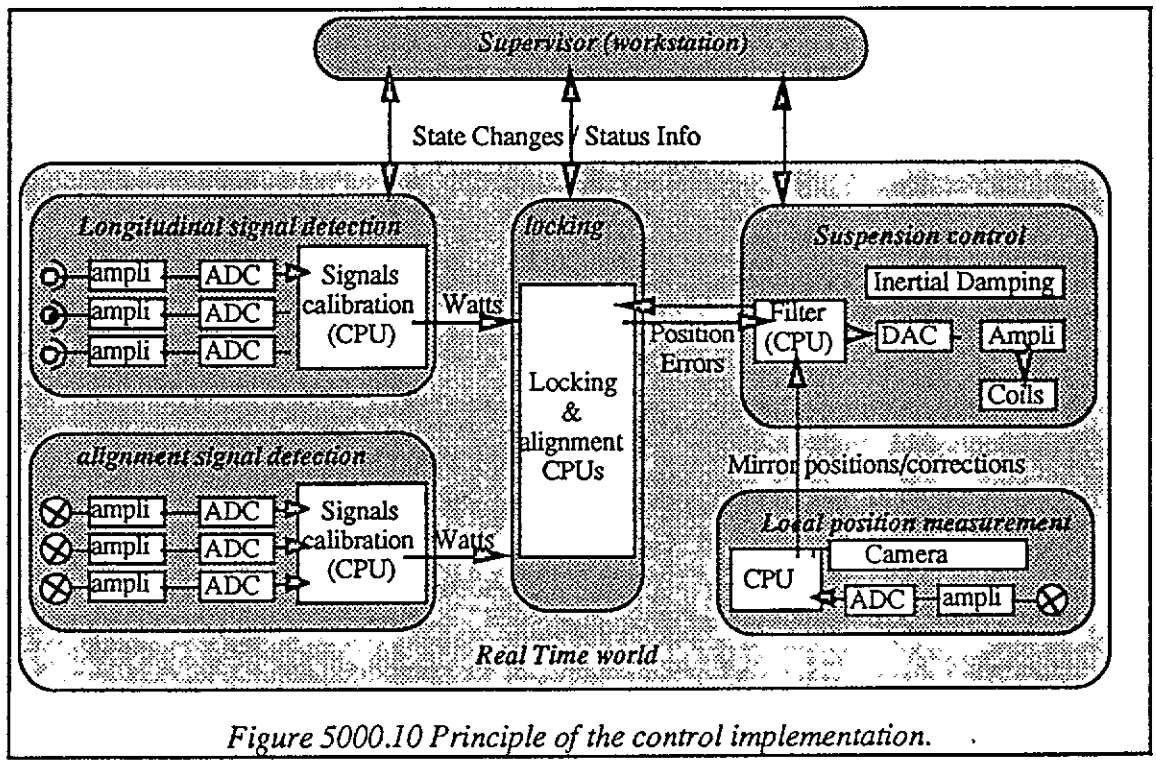

Figure 5000.10 Principle of the control implementation.

5000.2.1. The suspension control

Each optical component hangs on a suspension housed in a tower: the two pairs of Fabry Perot input and end mirrors, the beam splitter, the recycling mirror, the mode cleaner end mirror, the input and detection benches. They are put and kept in position with several mechanisms :

a) coils behind the mirror: for the fine setting of the mirror angles and position along the optical axis

b) marionetta: complements the action of the coils

c) second stage damping

d) upper mechanism: to set the vertical axis of the attenuator and a first approximation of the angle of the mirror with respect to the vertical axis

e) differential vacuum mechanism which separates upper and lower tower vacuum It has to be adjusted according to the mirror final alignment to set the vacuum conductance around the marionetta wire.

The digital hardware necessary for the implementation of such a system is shown on figure 5000.11. Given the large number of boards needed to control a suspension it may be necessary to set up the suspension control in a few VME crates tightly connected and controlled by a single CPU.

Under normal conditions mechanisms a), b) are controlled with feedback loops. The error signals are absolute reference positions measured locally (mainly a DC error signal) or correction signals provided by the locking system or by the linear alignment system trough the Digital Optical Links. A local VSB bus is used as private bus for these servoloops. The absolute reference positions are measured with the imaging system or with quadrant photodiodes or PSD looking at a reference laser beam. They can also be modified by the non-linear alignment system.

The damping of the second stage is run as an independent 'black box', but its parameters could be controled by the suspension control CPU as well as all the other feedack parameters.

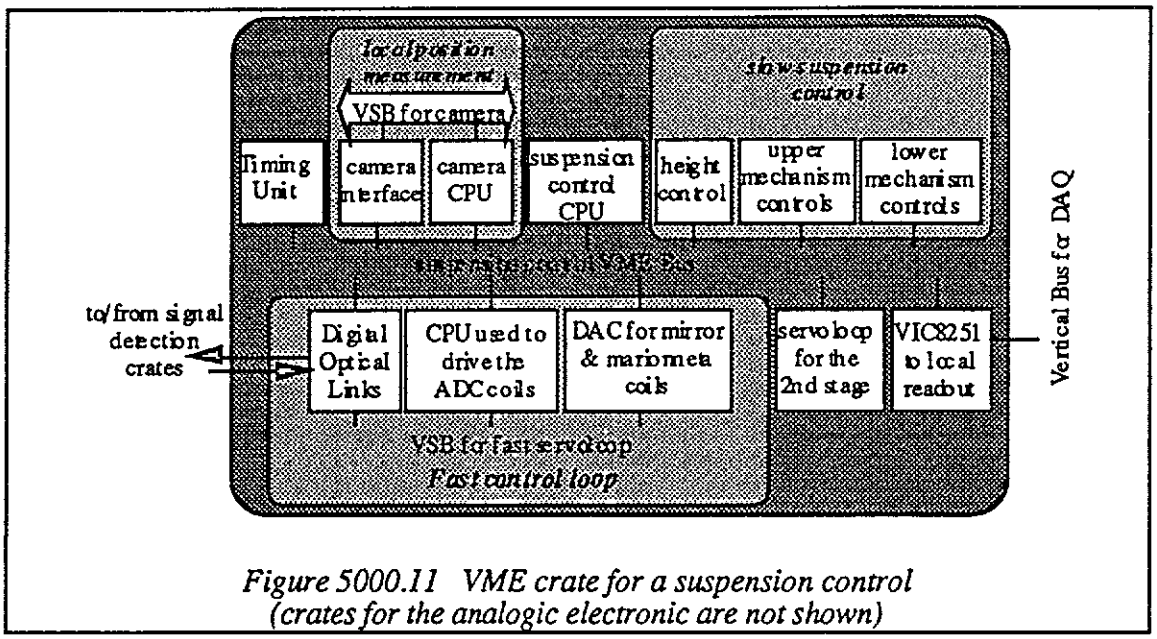

Figure 5000.11 VME crate for a suspension control (crates for the analogic electronic are not shown)

Mechanisms d) and e) are not used in normal operation but they are monitored to check if an action may be required. The absolute mirror position, the suspending wire position relative to the edge of the differential vacuum mechanism are measured with photodiodes, PSD or beam imaging system.

The component control should stay safe, even if error signals are produced by the locking system or if the linear alignment system is misleading. For test purposes the suspension control could be operated as a standalone system using only local data without any global positioning informations.

Each suspension control provides status informations and reference positions to the data acquisition system by putting these data in the mirror memory. It has the capability to send feedback information to the data acquisition when detailed studies are performed.

5000.2.2. Longitudinal signal detection

The signal detection crate is in charge to read the photodiodes and to calibrate the signals. The value computed by the Longitudinal signal detection (DC and AC values) are transmitted to the locking system using a D.O.L. or a VIC board. The figure 5000.12 gives a possible implementation for this crate which in fact has been split in two for noise reasons. This crate is located in the central building because the photodiodes are located in the detection bench or in the input bench. Twin systems are forseen in the end mirror building to measure the transmitted light. Given the expected light power on the dark fringe several photodiodes are foreseen for the main beam. We will have more ADC chanels than the four real signals. The photodiode ADC's are sampled at fast sampling rate (typically 200 kHz) and an inboard CPU reduce this sampling rate to about 20 kHz. Then the photodiode CPU reads the data trough the VSB and a local vertical bus connected to the ADC crate. This CPU sums the channels coming from the same beam. Since the photodiode have tw outputs with two different dynamic corresponding to the two type of signals (one for locking and one for the dark fringe signal), two CPU are used for readout. A low gain channel is also read in parallel to extend the signal dynamic during the start up procedure.

The errors signals and the status of the servo-loops are also written in the vertical bus memory to be recorded by the data acquisition.

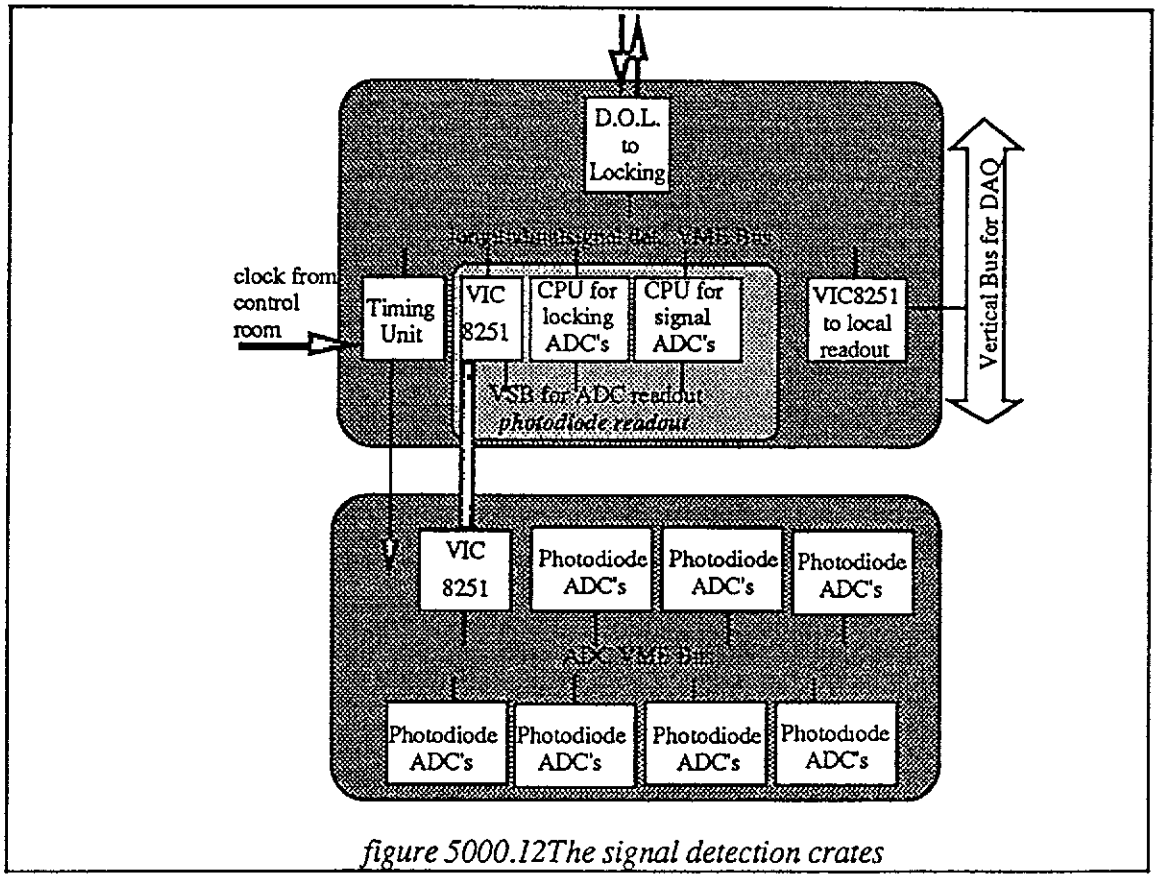

figure 5000.12The signal detection crates

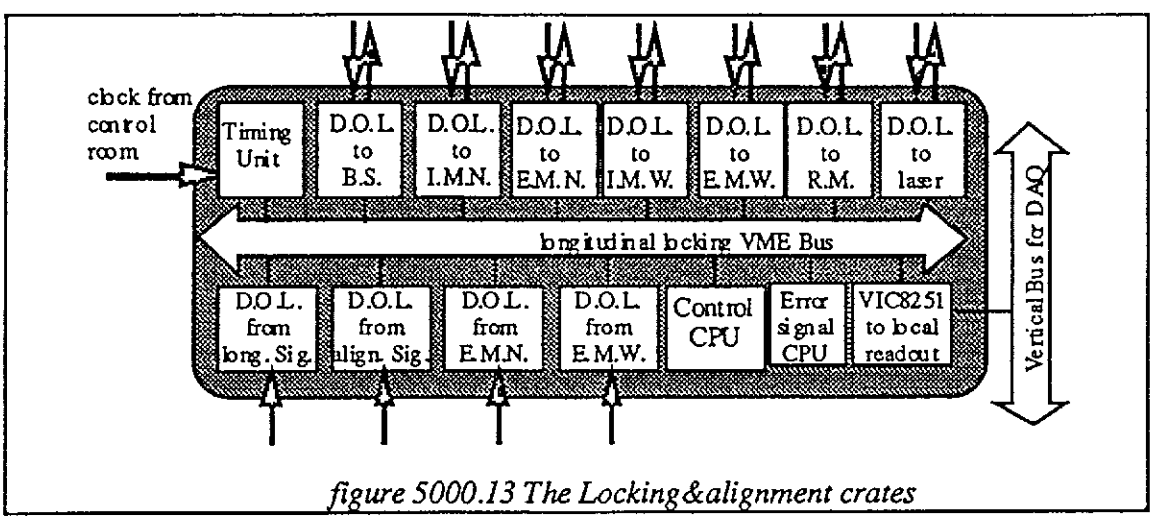

figure 5000.13 The Locking&alignment crates

5000.2.3. Global Control

This first component of the Global Control is located in the Locking and Alignment crate, in the main building: It is completed by the Global Control Survey (cf. online processing) in the Control Room building

The real time Global Control is in charge of the longitudinal locking and alignment of the interferometer. It is activated by the Supervisor once the interferometer has been brought close enough to the linear regime for the dedicated softwares to be able to lock it on the dark fringe. These Global Control softwares are flexible enough to accomodate different kinds of locking schemes, to handle longitudinal as well as alignment drifts, and to be able to guarantee smooth operation of the interferometer both in its linear and non-

linear regimes. A hierarchy of several layers of cpu's is foreseen. This hierarchy is based on the time response of the various cpu's; each using its own (more or less sophisticated and, hence, time consuming) model of the interferometer. During smooth operations, only the simplest and fastest of these models is to be used while the other cpu layers are working only in spy mode to check the validity of the responses of the fast model. When necessary, if the quality of models is no longer sufficient, a higher hierarchy layer can update the parameters of lower level models or, if needed, take care directly of the locking and alignment tasks.

This Global Control (fig. 5000.13) uses the error signal provided by the various signal detection systems to compute the time dependent parameters needed to describe the status of the interferometer. It is also kept informed of the relevant actions decided locally, for example, by the servo-loops in charge of the suspension chains. Its principal task is to compute the positions and the corrections to be applied on the current positions of the main optical elements. These correction requests are sent to the corresponding local controls which are in charge of implementing them. The corrections, together with the error signals and the status of Global Control and local servo-loops are sent to the DAQ, for monitoring and for the Global Control Survey.

5000.2.4 Non-linear Global Control

At setting up, an initialization operation is performed to bring the different components of the interferometer in positions close enough to the ideal ones to allow the software of Global Control to be activated. When this activation has been successfully performed - i.e when the interferometer is in its normal running mode - the non-linear alignment process is operated in spy mode, to check and update the various reference positions.

The non-linear alignement task is a high level task closely related to the linear aligment one. It also acts on the various component positions by sending requests to the local servo-loops. This task is achieved mostly by manual operations through a dedicated user interface, using general resources, among which the beam-imaging system.

5000.2.5. Laser control

It controls the laser running (power suply, prestabilization, ...). Fast information could be : exchanges with the input bench control and data sent to the data acquisition (local readout). Status informations are collected using the slow monitoring network.

5000.2.6. Input bench control

It controls the alignment of the laser in the input bench, the input bench and mode cleaner electronics. It keeps the mode cleaner locked by running servoloop exchanging data with the end mirror mode cleaner control. Monitoring signals are sent to the main building readout through the vertical bus.

5000.2.7. Detection bench control

It controls the electronics and the hardware located on the detection bench. It is connected to the signal detection crate. It runs the local bench alignment and provided status information using the slow monitoring network.

5000.3. The control and monitoring of the interferometer environment

This control is done using Slow Monitoring Station. The Building control station and the Environment Monitoring Station are described in section 5500.

5000.3.1. The Tube Control Station

It controls all the vacuum system for one pumping station. This includes the baking control, and therefore the temperature control and the power needed to heat the tube. A diffuse light monitoring could also be connected to the tube control station.

A G64 (or a VME) crate is foreseen for the each tube control station.The electronic is controlled by the local CPU. the slow monitoring network. It provides a timed set of vacuum measurements performed at regular time intervals. Summary informations are send on request to a global vacuum control and monitoring user interface and to the frame builder. A dedicated workstation for the vacuum control and monitoring is foreseen in the control room. Furthermore, mobile terminals which can be linked to any crate will allow to work close to the vacuum components (particularly in the pumping station).

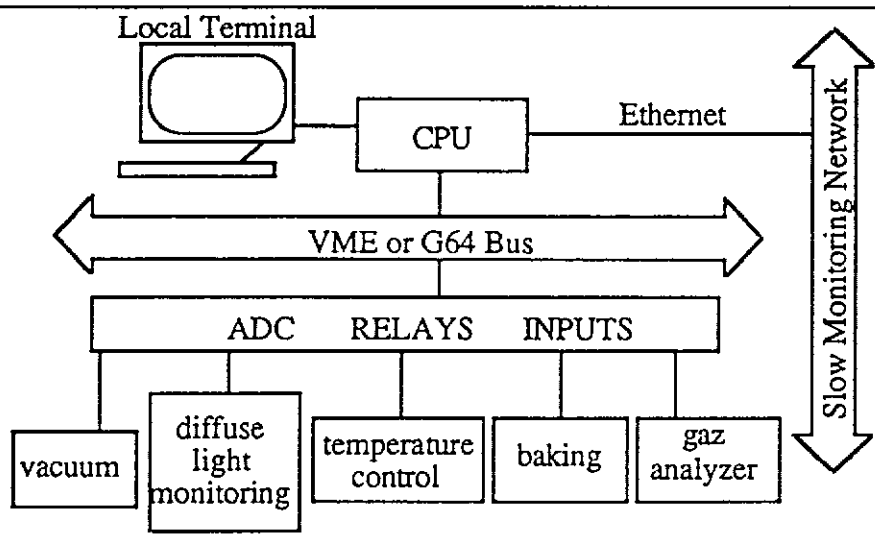

Figure 5000.14 A tube control station

5000.3.2. The Tower Control Station

Like the tube control station it drives all the pumping system and also the tower clean room installation. It controls the backing of the tower, the tower temperature and the gaz analyzer (see note from P. Roudier from 27/6/94 for more details about the components). It is connected to the slow monitoring network and provides a timed set of measurements performed at regular time intervals.

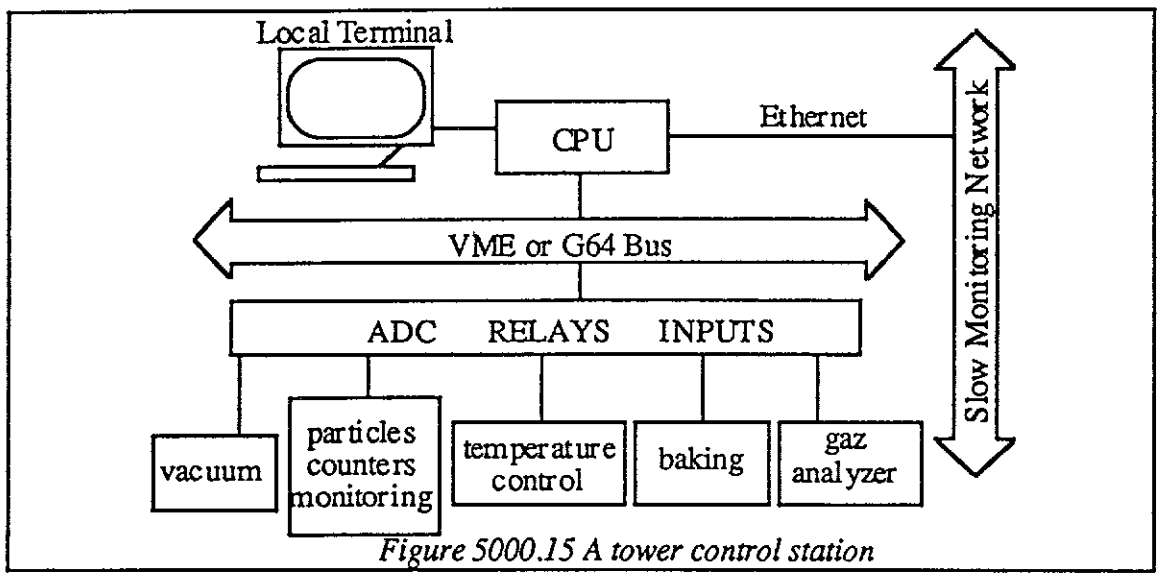

Figure 5000.15 A tower control station

5000.3.3. Imaging system

This is the front end for all the beam imaging systems (camera) which measure beam intensity or wavefront. It starts the various processes which control the cameras and provide images for all the interferometer. Graphical user's interface can be run on any workstation to display the beams. It provides information to the alignment system and sends beam profile to the data acquisition.

5000.3.4. Calibrators control

This controls the calibrators initialization and running (frequency signal, wavefront in the case of the laser calibration). It is a slow monitoring station. The current calibrator status is recorded and the generated signal is send to the local readout process.

5000.4. Offline

The major offline activity is the data analysis aiming at the extraction of a gravity wave signal. This activity where imagination is very important should stay widely open within the collaboration. But one needs a set of tools and rules which should be managed in common to provide basic software environment and to allow for comparisons of different works.

There will be a simple analysis framework to provide the basic functionality of analysis jobs like read/write frames, simple monitoring, run the online selection. Such programs could already be tested with SIESTA.

During data analysis we will need some generic tools, usually in the area of histogramming, plotting and fitting. For this need, we will use as much as possible the tools developed at CERN. This is especially true for the histogramming with HBOOK and interactive plotting with PAW .

The offline reconstruction program which converts the raw data to an h value has also to be standard and identical to the online reconstruction run for the frame selection. Improvements in the knowledge of the transfer functions or of the calibration constants may justify an offline re-run of the h reconstruction.

5000.5. Detector Commissioning and Calibration

It is mandatory to allow for a progressive and independent commissioning of the various components of the experiment. To that purpose, the readout has been organized in autonomous subsystems capable of local standard data acquisition. To exercise locally and independently the various controls, one has to provide the necessary excitations and measurements devices. Once everything is set up, i.e. once the interferometer is running its beams, then a calibration device is foreseen to monitor permanently its sensitivity.

5000.5.1. Data acquisition commissioning

The DAQ of the experiment is performed by a central system which assembles the frames whose details are collected trough optical links fed by the local readouts. Once the local readouts have been set up, one certifies their frame building capability with appropriate test procedures which do not need any special hardware. As an example, the local readouts can be programmed to deliver on output simulated data. This would allow for a test of the optical links and of all the procedures following the frame assembly.

5000.5.2. Controls commissioning

The suspension control is organized in independent system with local position measurement. This gives the capability to test all the actuators and the controls. For the global control, simulated data can be generated and sent in the data links. But we will have also the capability to illuminat the photodiodes with known signal and to test the effectiveness of the global controls.

5000.5.3. Calibration

A direct calibration of the interferometer is obtained by stimulating it as a gravitational wave would do it. This can be achieved by moving an end mirror in a known way , and recording the result in the standard acquisition stream.

This calibration has at least two different goals. The first one is a general study of the Virgo sensitivity and a help for the commissioning of the full antenna (global controls, reconstruction software,...). The other is to provide a continuous monitoring of the interferometer in order to study long term effects. For that purpose, one uses the periodic signal of well known amplitude and very stable frequency produced by a dedicated device. The clock used to stabilize the input signal is different from the one used by the data acquisition system in order to allow cross checks.

From the data management point of view, there will be a calibration control to operate the calibrators (set frequency and intensities). The status of the calibrators will be recorded by the VME data acquisition system. When the calibrator injects a signal with variable frequency, this signal has to be recorded with the standard data.

5100. Global controls (associated software)

5100.1. The Supervisor

The function of the Supervisor is to keep track of, to request, allow or inhibit modifications of the status of the various components of the interferometer. With respect to this functionality directed towards Organisation and Security, it is intended to provide the overall user interface (the master client) of VIRGO. The Supervisor, in particular, provides a graphic display of the status of all the VIRGO components. It will also use the output of the Data Monitoring programs and should later house the expert system in charge of the interferometer. A set of automatic sequences will be available for the interferometer start up for instance.

The Supervisor controls all the servers using the messages described in table 5000.1. It displays the status of all the available servers. When a special action is required for a given server it can start the corresponding client and delegate its privileges.

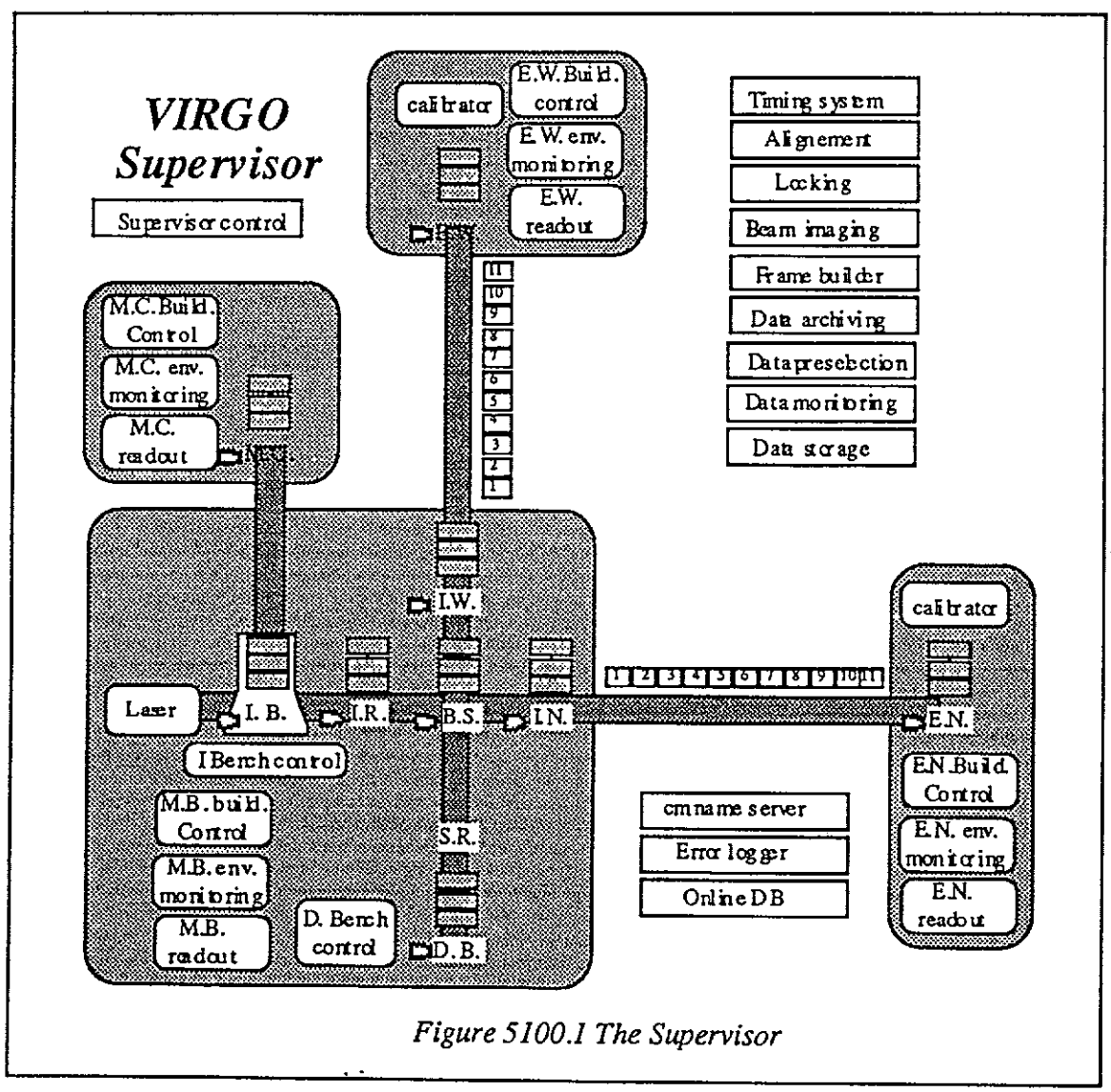

Figure 5100.1 The Supervisor

The list of servers controlled by the supervisor is called the partition. This partition which can be modified, is described in the supervisor configuration. The supervisor is in fact the 'front page' of Virgo as it provides a very short description of the status of all available tasks using a color code. The possible status are:

- Not in partition	grey
- In partition but not connected	black
- Connected and no configuration file	red
- Connected and config available	orange
- Connected and config loaded	yellow
- Connected and running	blue
- Connected and stable	green

In addition, the type of client can be specified (master which is the default, or ordinary client) and a message displayed. A changing status is indicated by a flashing color. The figure 5100.1 shows a possible supervisor.

By clicking within the Supervisor panel on a server icon, one may perform the following actions on a server with the help of a pop up menu:

- add or remove from the partition
- configure (set parameters like server name,...)
- start server (task)
- ask for connection
- read status
- read and load server configuration file
- run and stop the action performed by the server
- start the corresponding user interface.
- kill the server
- become master or slave user

& sub-supervisor

Under smooth conditions there is only one Supervisor running in the control room with all the privileges for the hardware access. It collects the status information from the servers and checks the error logger for warning or error messages. It asks periodically for status. A non answering server could be considered as an error message. Additional supervisors without privileges for the hardware access could be run in different places to monitor the interferometer.

5100.2. The communication tool: Cm

This package manages task to task communications by providing a wide range of mechanisms required to manipulate transparently the network layer (TCPIP) and uniformly across the various platforms. A complete description is available within the Cm distribution kit. However, one may summarize the basic features it implements as follows :

Cm is meant to manage the task to task communications (sending or receiving messages) running on heterogenous machines (with different architectures or operating systems) without limitations on the number of active connections apart from those induced by the operating systems.

The set of tasks or applications that may participate this network define a Cm domain managed by one special application - the NameServer - in charge of the physical addressing scheme, allowing several independant such domains to coexist.

An application with which a connection is requested is referenced by a name, that must be unique within one Cm domain and that does not need to mention anyhow the machine on which it runs, nor the transport charectiristics (such as TCPIP parameters).

The central manager application NameServer is in charge of every mechanism for name registration, port number allocation, and physical addressing operations transparently for the user application.

The Cm Message part handles the formatting issues, insuring that a structured information frame is transmitted across the network (reaching heterogenous architectures) without loosing its integrity.

Elements of security management are introduced by the internal protocole, by transmitting the host name and user name of the message senders.

5100.3. The ErrorLogger

The error logger collects the information and error messages from all the process. The messages are send using the El library which use Cm.
Each message contain a severity code and a text. The levels of severity are:

- info just information message
- warning their is some problem but the standard operation can continue
- severe some non standard procedure has to be follow to fix the problem. The server goes one state down for severe error.
- fatal the server is stop or going to kill. It goes more than one state down.

The error display is the error logger client which provides the tools to select and display error messages collected by the error logger.
Query operations can be requested by aplications giving selection criteria based on the date, the severity, the source, the message. The diagnostics and monitoring applications will be the normal users of the error logger.

5100.4. The Online DataBase

This package is meant to handle the online configuration database. It is based on one server (although several servers may coexist) responsible for the accesses to the stored objects (controling the protections, the selections and the manipulations) and of the effective storage medium for the objects. Access to the data base will be achieved from any application through the network. (DB is based on Cm)

Data items consist on named C objects and can be of most legal C type.

Management of items is centralized in a DB server (that also handles access control on objects)

Items (or objects) are accessed by their nam transparently over the network and selections of set-of-objects can be done with various criteria (name pattern, conditions on nvalue, ...)

An history of the contents evolution for every object is maintained by the system and recoveries of object values are possible on the basis of azbsolute or relative time and date specifications.

Objects are eventually stored into textual files (using a human readable format) that may even permit a non-network access to objects.

5200 Standardized components

5200.1. Standardization and Software rules

5200.1.1. Language

- Lynx OS for real time VME CPU (or OS9 for G64 crates)
- UNIX system for workstation
- Motif and X window for graphic
- C with C++ style for language

The software run on various processors will be written in C language as much as possible to be able to use it in the simulation program and analysis programs if needed. This is also true for monitoring task run on the front end workstations which are in charge of the control and monitoring of the real time processor.

5200.1.2. Coding rules

Here is a short list of the main suggest coding rules

• Use `double` instead of `float` (for 'scientific' calculations),
• Use `long` instead of `int` (to make sure we have 32 bits).
• Use a naming convention:
  - All function names, structure types and variables which are not local should start with the two key letters of the library. Example: `FrRawData`
  - Keep UPPER case for `define`.
  - Start local variables with lower case.
  - Start global variables with upper case.
  - To build composed words use upper case instead of underscore.
• Write `simple' C code
• Only one instruction per line (except for `for`, `while`)
• Use indentation for loops, if... (at least 2 spaces)
• No C++ keyword to allow a futur migration to C++. As a reminder here is the list of C++ keywords: `asm`, `catch`, `class`, `delete`, `friend`, `inline`, `new`, `operator`, `private`, `protected`, `public`, `template`, `try`, `this`, `throw`, `virtual`.
• Use comments, especially in the header file to describe each variable defined in a structure.

5200.1.3. File organization

The files organization is presented in figure 5200.1. The reference version for the Virgo software is stored in the machine LAPPSUN18.IN2P3.FR for the time being. Accounts on this machine are available on simple request. The virgoApp directory could be found in /virgoApp. The notes directory is a public space were general information could be install. All packages are stored in separated directory. A readme file should give some basic information like the person in charge of this package and who to contact in case of problem. The table 5200.1 gives the list of the current packages and their key words and manager. Each package as a single person in charge of the updates. The standard version of the software is found by using the 'pro' directory which contain logical links on the various packages. When several people are working on the same package, CVS is used as code manager.

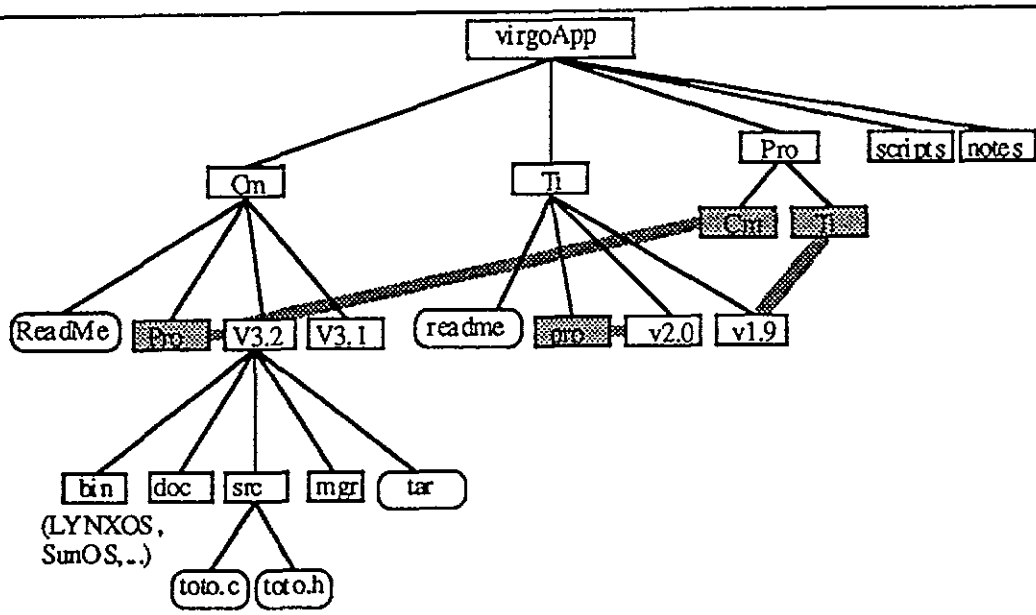

figure 5200.1 The file organization

Package	Key letter	Manager
Communication	Cm,Ci,Cset	C. Arnault
Digital servoloop	Ds	F. Barone
Online database	Db	C. Arnault
Data Display	Dy	X. Grave
Error logger	El	C. Arnault
Frame Builder	Fb	E. Delorme
Frame Lib	Fr	B. Mours (+UJ,UM,UH,UA,US)
Imaging system	GX	C. Drezen
Timing system	Ti	F. Bellachia
Tube control	Tu	
Tower control	To	Orsay
Environment monitoring	Em	F. Barone
Building control	Bc	F. Barone
Laser control	La	H.H.
Input bench-control	Ib	
Signal detection	Sd	
Detection bench-control	Db	
Non-linear alignment	Nl	
Linear alignment	Li	
Supervisor	Su	M. Delaunay ?
Local readout	Lr	F. Bellachia
Reconstruction	Re	
Online trigger	Tr	
Data archiving and distribution	Dd	F. Barone
Historical monitoring	Hm	F. Barone
Calibration	Ca	
Simulation	Siesta	F. Marion (+ME,GR,MI,OP,FR,EL,FO)

Table 5200.1 Packages list

5200.1.4. The list of Slow Monitoring Stations

Here is the list of the foreseen slow monitoring station with there name:

Tube control station:	TW01,TW02,...TW11,TN01,...TN11 (for west & north arm)
Tower control:	TOIB (input bench), TOMC (mode cleaner), TOPR (power recycling), TOBS (beam splitter), TOIN (input mirror north), TOEN (end mirror north) TOIW (input mirror west), TOEW (end mirror west) TOSR (signal recycling), TODB (detection bench)
Building control:	BCCE (for central building), BCMC(for mode cleaner) BCEW (for end west), BCEN(for end north)
Environment monit:	EMCE (for central building), EMMC(for mode cleaner) EMEW (for end west), EMEN(for end north)
Laser control:	LASR
Benchs:	IBEN (input), DBEN (detection), NBEN (north arm bench), WBEN (west arm bench)
Calibrator:	CALM

5200.1.5. Data format on tape:

Frame number and sampling number are limited to 65536. Frames collected with the same experimental condition are grouped in 'Run' identify with a run number.

A data file should start with a file header with the following data:

- 1 byte giving the format version (current version number is 0)
- 1 byte = sizeof(short)
- 1 byte = sizeof(int)
- 1 byte = sizeof(long)
- 1 byte = sizeof(float)
- 1 byte = sizeof(double)
- a 4 bytes word containing 0x01020304 (to check the bytes swaping)
- a float (4 bytes) containing PI
- a double(8 bytes) containing PI

The file is structured in records. One record contains one C struct. For each record there is a short header of three long words:

- the first is the number of bytes in the record including the header
- the second is the type the C struct. This number is dynamically generated by the write program. The correspondence with the structure name is given by the dictionnary which is included on tape.
- the third is the instance number (a unique number per structure of one type). This number is dynamically generated by the write program.

The content of the C struct follows this header. Data are written in binary IEEE format (68040 format) in the same order as in the structure. Character strings are preceded by their length coded as a long.

The file starts by the detector description (if any) which written in several records. Then follow the frames which are also written in several records. A Frame starts with the FRameH record and ends with the EndOfFrame record.

When frames are exchanges between client and server, we just send on binary file per frame with the same format as the one used to write on tape.

More informations and examples could be found in the Siesta directory in the file UJobL.h

5200.1.6. Information distribution

News could be broadcast to a list of Virgo people by send a mail to VIRGO-L@FRCPN11.IN2P3.FR. VIRGOS-L is for software people and VIRGO-F for Virgo 'Friends', To be include in this list, please send a mail to MOURS@FRCPN11. A WWW server is available (....). Documentation could be found also with the software storage.

5200.2. Summary of crate content

5200.2.1. Control Building:

C1: Timing
1 CPU (control), 1 GPS, 2 Timing (out), ≈ 5 Timing (in)
C2: Frame Builder:
3 CPU, 4 DOL, 1 VIC (to data distribution)
C3,4: Raw data archiving
1 VIC, n CPU
C5: Data quality
1 VIC, n CPU
C6: Trigger
1 VIC, n CPU
C7: Online monitoring
1 VIC, n CPU

5200.2.2. Main building:

C21: Laser control
1 CPU(control), 1 VIC (to DAQ), 1 Timing, ≈ 5 ADC/DAC (slow)
1 DOL -> input bench, 1 ADC (fast)
C22: Input bench control
1 CPU(control), 1 VIC (to DAQ), 1 Timing, ≈ 5 ADC/DAC (slow)
1DOL (to laser), 1 DOL (to mode cleaner), 1 DOL (to locking), 1 ADC (fast)
[3 Camera, 1 CPU](VSB)
C23: Detection bench control
1 CPU (control), 1 VIC (to DAQ), 1 Timing, ≈ 5 ADC/DAC (slow)
1DOL (to laser), 1 DOL (to mode cleaner), 1 DOL (to locking), 1 ADC (fast),
[1 CPU (signal processing), 1 VIC (to analog crate)](VSB),
[3 Camera, 1 CPU](VSB)
C24: Signal detection
1 VIC (to det. bench control), ≈ 8 ADC (fast) (about 32 channels)
C25: Signal detection
Analogic electronic
C26: Signal detection
Analogic electronic
C27: Alignment signals:
1 CPU (control &signal processing), 1 VIC (to DAQ), 1 Timing,
1DOL (to locking), ≈ 4 ADC (fast) (about 16 channels), ≈ 2 ADC/DAC (slow)
C28: Alignment:
Analogic electronic
C29: Locking
3 CPU (control &signal processing), 1 VIC (to DAQ), 1 Timing, 11 DOL
C30: Calibration
1 CPU (control &signal processing), 1 GPS, 2 ADC/DAC (fast)
C31: Environement & building control

1 CPU (control), dedicated network hardware
C32: Local readout
1 CPU (control &signal processing), 1 VIC (to collect DAQ), 1 Timing, 1 GPS,
1 DOL (to frame builder), ≈ 5 ADC (fast)
C33,35,37,39,41,43: Suspension control (21 b.)
1 CPU (control), 1 Timing, ≈ 5 ADC/DAC (slow)
[1 CPU (signal processing), 1DOL (to locking), 1 DAC (fast),
1 VIC (to DAQ),](VSB),
[2 Cameras, 1 CPU](VSB, local position measurement)
[1 DSP , 2 ADC, 1 DAC] (2nd stage dumping)
C44,46,48,40,42,44: Suspension control
Analogic electronic

5200.2.3. Mode cleaner:

C61: Local readout
1 CPU (control &signal processing), 1 VIC (to collect DAQ), 1 Timing, 1 GPS,
1 DOL (to frame builder), ≈ 2 ADC (fast)
1 CPU (control), 1 Timing, ≈ 5 ADC/DAC (slow)
C62: Suspension control (21 b.)
[1 CPU (signal processing), 1DOL (to input bench), 1 DAC (fast),
1 VIC (to DAQ),](VSB),
[2 Cameras, 1 CPU](VSB, local position measurement)
[1 DSP , 2 ADC, 1 DAC] (2nd stage dumping)
C63: Suspension control
Analogic electronic

5200.2.4. End building:

C71: End mirror bench control (long. signals & alignment)
1 CPU (control & signal processing), 1 VIC (to DAQ), 1 Timing,
1DOL (to locking), ≈ 3 ADC (fast) (about 12 channels)
≈ 2 ADC/DAC (slow)
[1 Camera, 1 CPU](VSB)
C72: Signal detection
Analogic electronic
C73: Calibration
1 CPU (control &signal processing), 1 GPS, 2 ADC/DAC (fast)
C74: Environement & building control
1 CPU (control), dedicated network hardware
C75: Local readout
1 CPU (control &signal processing), 1 VIC (to collect DAQ), 1 Timing, 1 GPS,
1 DOL (to frame builder), ≈ 2 ADC (fast)
C76: Suspension control (21 b.)
1 CPU (control), 1 Timing, ≈ 5 ADC/DAC (slow)
[1 CPU (signal processing), 1DOL (to locking), 1 DAC (fast),
1 VIC (to DAQ),](VSB),
[2 Cameras, 1 CPU](VSB, local position measurement)
[1 DSP , 2 ADC, 1 DAC] (2nd stage dumping)
C77: Suspension control
Analogic electronic

(crate number are given for the north arm. Add 10 to get crate numbers for the west arm)

5200.3. Workstations Implementation

5200.3.1. Control Room & Computer Room

The Control room will contain a set two clusters of identical workstations. Even though they will be able to run any user interface they will be dedicated to one or two specific type of control. Two clusters will be use instead of one in order to do system maintenance without stoping Virgo. Here is the list of the forseen workstations:

- W1: Tube control & Tower control (on slow mon. net.)
- W2: Building control & Environnement control (on slow mon. net.)
- W3: Laser & input bench control
- W4: Detection bench control & Signal detection
- W5: Suspenssion control
- W6: Locking & Linear alignement
- W7: Name Server, Supervisor & Timing control
- W8: Non Linear Alignement & Beam Imaging
- W9: Local Readout & Frame Builder
- W10: Data distribution control & Data archiving
- W11: Trigger control & Data Monitoring

- W12: Data distribution: This workstation is located inside the computer room. It is a more powerfull workstation with lot of disk space and special hardware.
- W13: Network analyseur

The rack content is the following:

- R1 Cabling arrival
- R2 Network Hardware
- R3 Master timing (1 c.) Frame Buidler(1.c) Reconstruction & Trigger (1c.) Data monitoring (1 c.)
- R4 Data archiving (1crate + space for tape drives and disks)
- R5 Free (could hold CPU monitors)

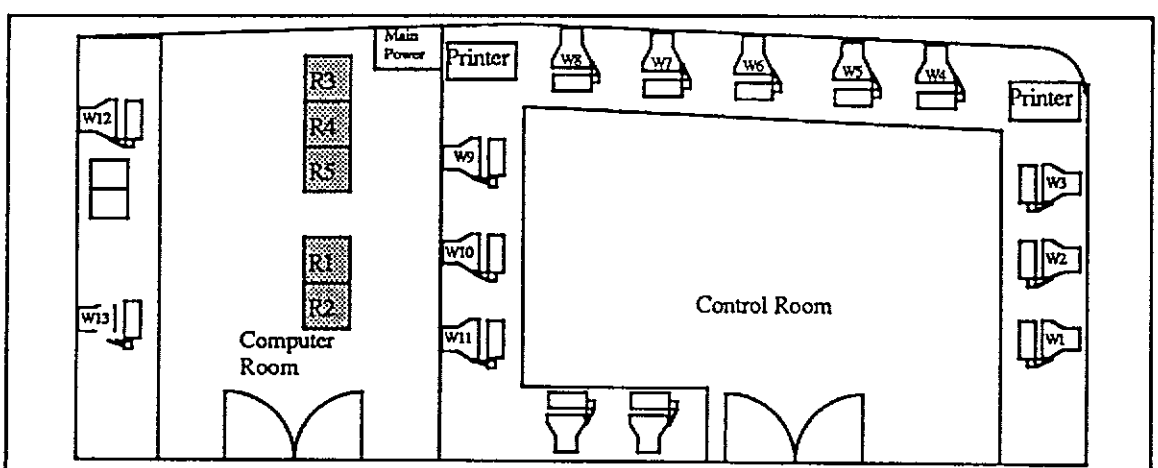

Figure 5200.2 Control Room and Computer room. Video monitor (for beam imaging or for room survey) will be install above the workstation

5200.3.2. Main Building

Few workstations (or X terminal) will be available in the Data acquisition room to locally work on the control. They will be on the same cluster as those in the Control Room.Here is the list:

- W21: Tower control & Tube control (on slow mon. net.)
- W22: (for W3,W6)
- W23: (for W4)
- W24: (for W6)
- W25: (for W8)

The rack content is the following:

- R11 Cabling arrival
- R12 Network Hardware
- R13 Detection Bench control (1.c) Signal detection (2 c.)
- R14 Detection Bench Suspension control (2 crates)
- R15 local readout(1c.), Calibration (1 c.), Env. monit & Build control (1c.)
- R16 Input North and Input West Suspension control (2x2 crates)

(These crates may need to be closer to these towers)

- R17 Recycling and Beam Split. Suspension control (2x2 crates)
- R18 Locking&alignment(1c.), alignement signals(1c.),
- R19 Detection Bench (2 crates)
- R20 Laser control (1 c.), Input bench control (1c.)

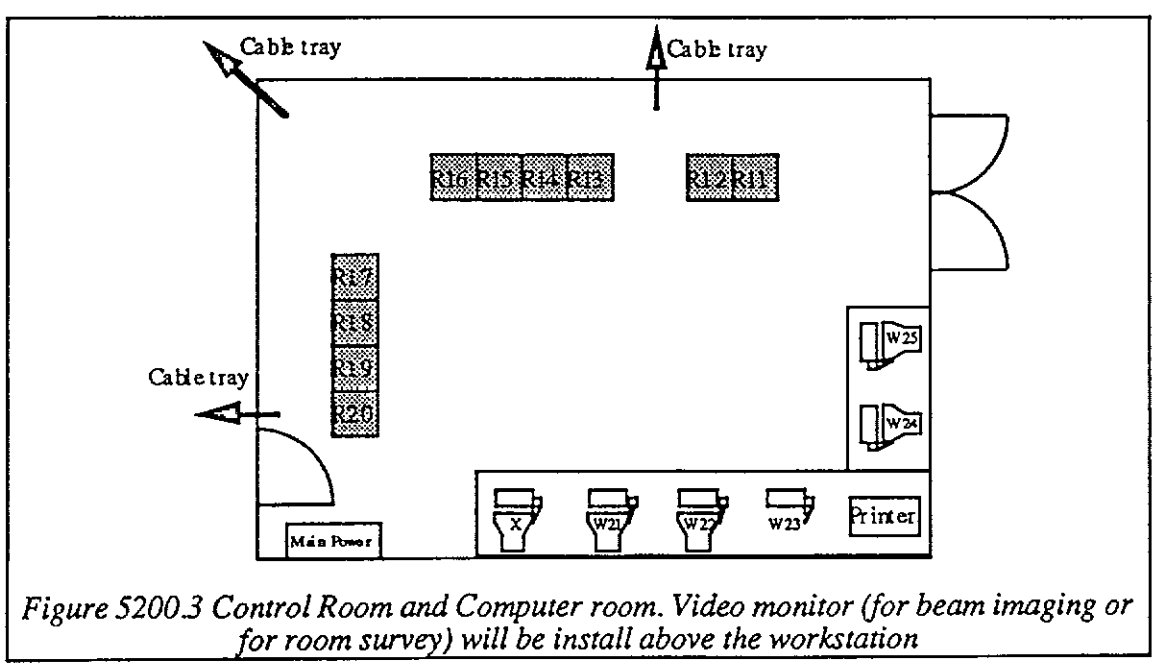

Figure 5200.3 Control Room and Computer room. Video monitor (for beam imaging or for room survey) will be install above the workstation

5200.3.3. Mode Cleaner or End Mirror Building

One general purpose workstation (W31, 32, 33) and one X Termnial will be available next to the tower. There will be also one rack with 2 crates for the suspension control and one for the local readout.

5200.4. Standardization: Hardware

For the hardware, we use as standard:

- the VME bus with A24D32 addressing mode for fast system
  or G64 for slow monitoring system like vacuum control
- an Ethernet network for the slow monitoring
- the VIC vertical bus between VME crate with the VIC8251 interface
- the same general purpose VME CPU
- Ethernet or FDDI for the general computer network.
- The Digital Optical link for fast crate to crate connections. These links are seen has a FIFO on each crate. The data rate on the 3 km optical fiber is 14 MBytes/s.

We will use the same type of VME crate and general purpose board (ADC,DAC,..)

BNC connector for cables.

The estimation of the overall number of standardized components is the following (including spears):

20 Worksations
40 VME crates
60 VME CPUs
40 DOL boards
.. fast ADC (> 20 kHz) + .. slow ADC (< 1 kHz/channel)
.. fast DAC (> 20 kHz) + .. slow DAC (< 1 kHz/channel)
30 Timing boards
8 GPS boards
32 Pumping stations

5300. Networks

The cabling necessary for the networks of VIRGO can be divided as follows:

• Optical Links for high speed transfers: This applies to the distribution of the time signal, to the servoloops control and to the acquisition.
• Slow Monitoring Network: This applies to the monitoring of all parameters collected from many crates in all buildings, towers, pumping stations, etc...
• Computer Network: This applies to the connection of all computers, workstations and some of the VME crates.
• Telephone: This applies to ordinary telephone lines in all rooms of all buildings.
• Video: This applies to video monitoring of remote places and of surroundings.

The cabling we propose conforms to the standard EIA/TIA 568 for cabling, and is generally referred to as "structured cabling". This means a hierarchical organization from a central point to peripheral points, with radial configuration of cables departing from each system and with a maximum length of 100 meters for each cable, reaching a "telematic outlet" placed wherever necessary.

Let us consider a schematic diagram of the VIRGO buildings, with the various relative distances.

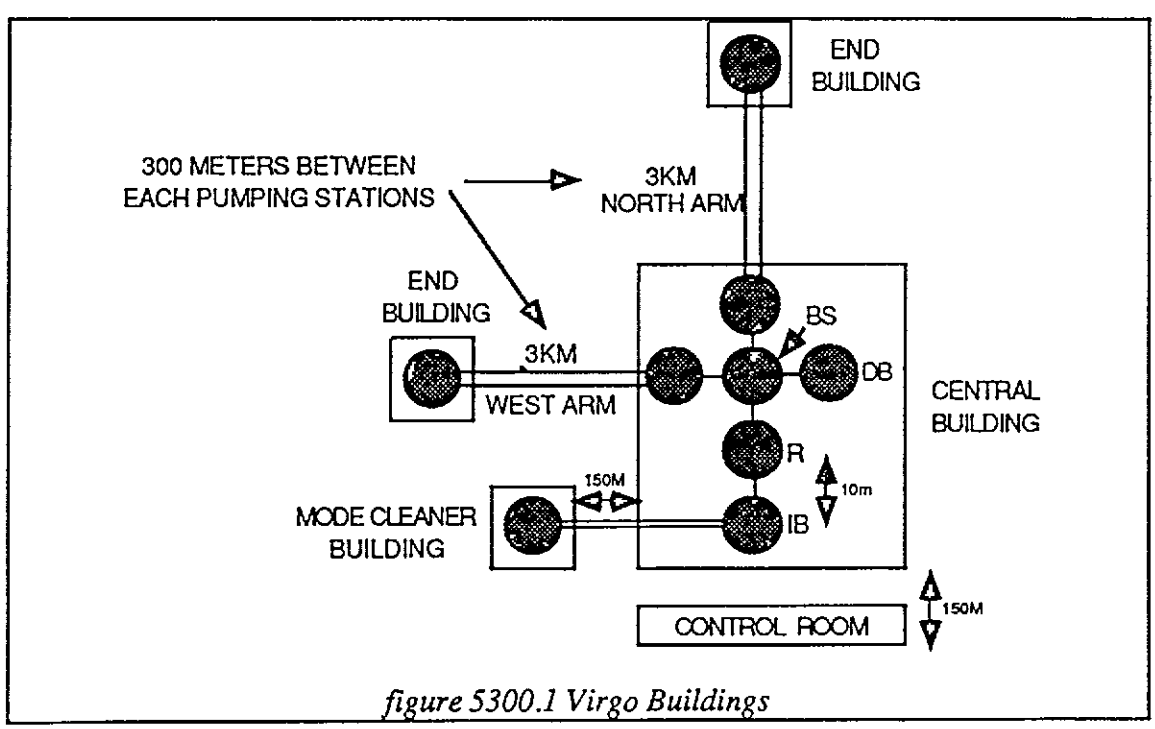

figure 5300.1 Virgo Buildings

It is necessary to use fibers from one building to another, and twisted pairs within the buildings, as far as possible; these latter can be STP (Shielded Twisted Pairs) or UTP (Unshielded Twisted Pairs). This kind of cabling accomodates both audio communications (telephone) and video (remote monitoring), as well as ETHERNET (10 base T) Serial (RS422) and FDDI (over copper).

Optical fibers will also be used to reach dedicated systems, e.g. for control of servoloops, timing and acquisition.

The central system will be placed in the Control room.

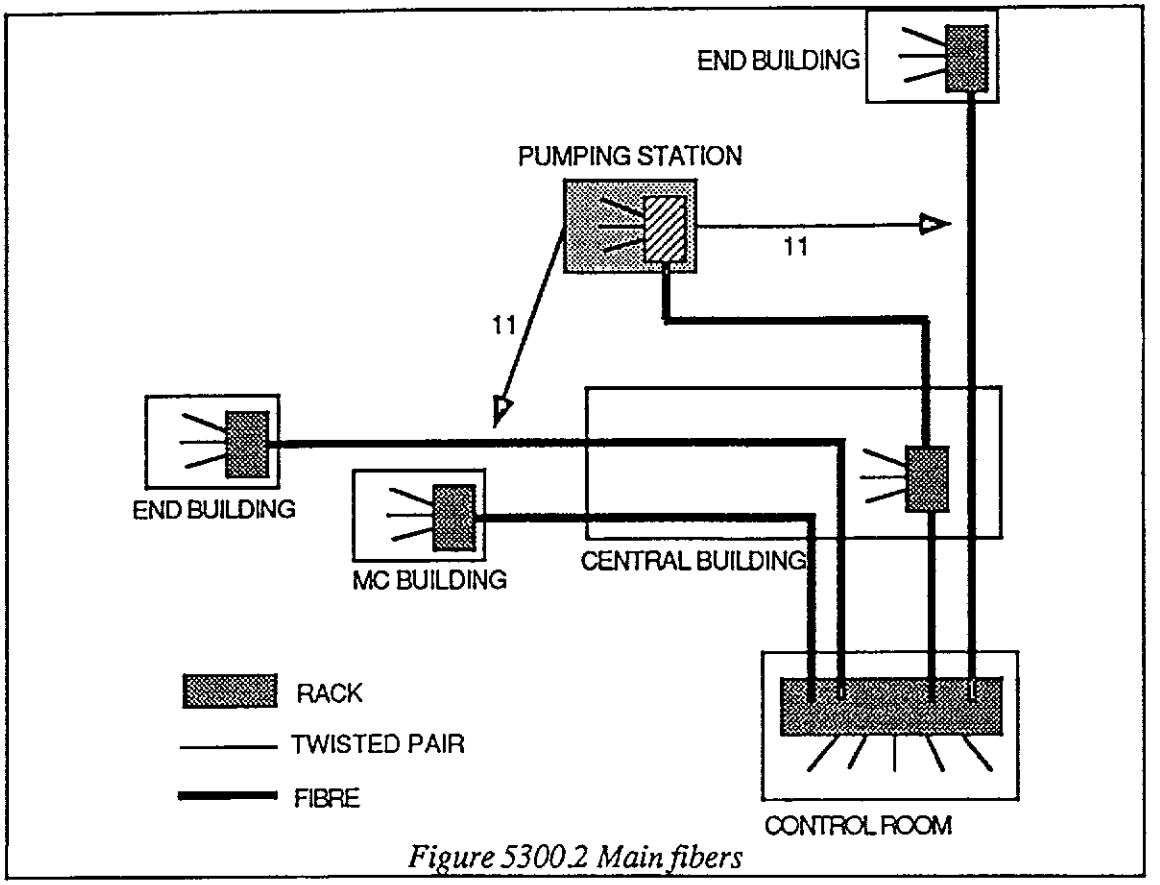

Figure 5300.2 Main fibers

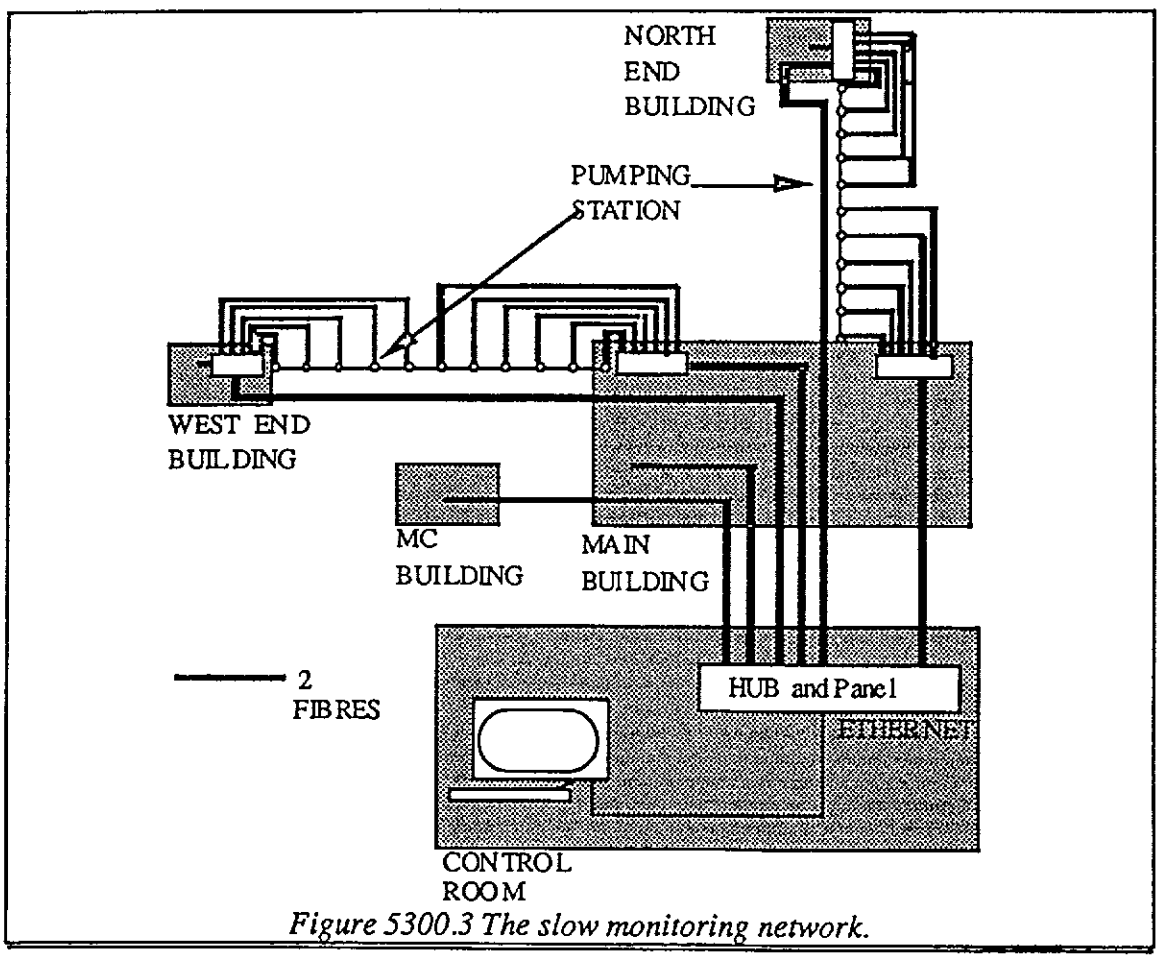

Figure 5300.3 The slow monitoring network.

We can give the number of fibres needed between the buildings:

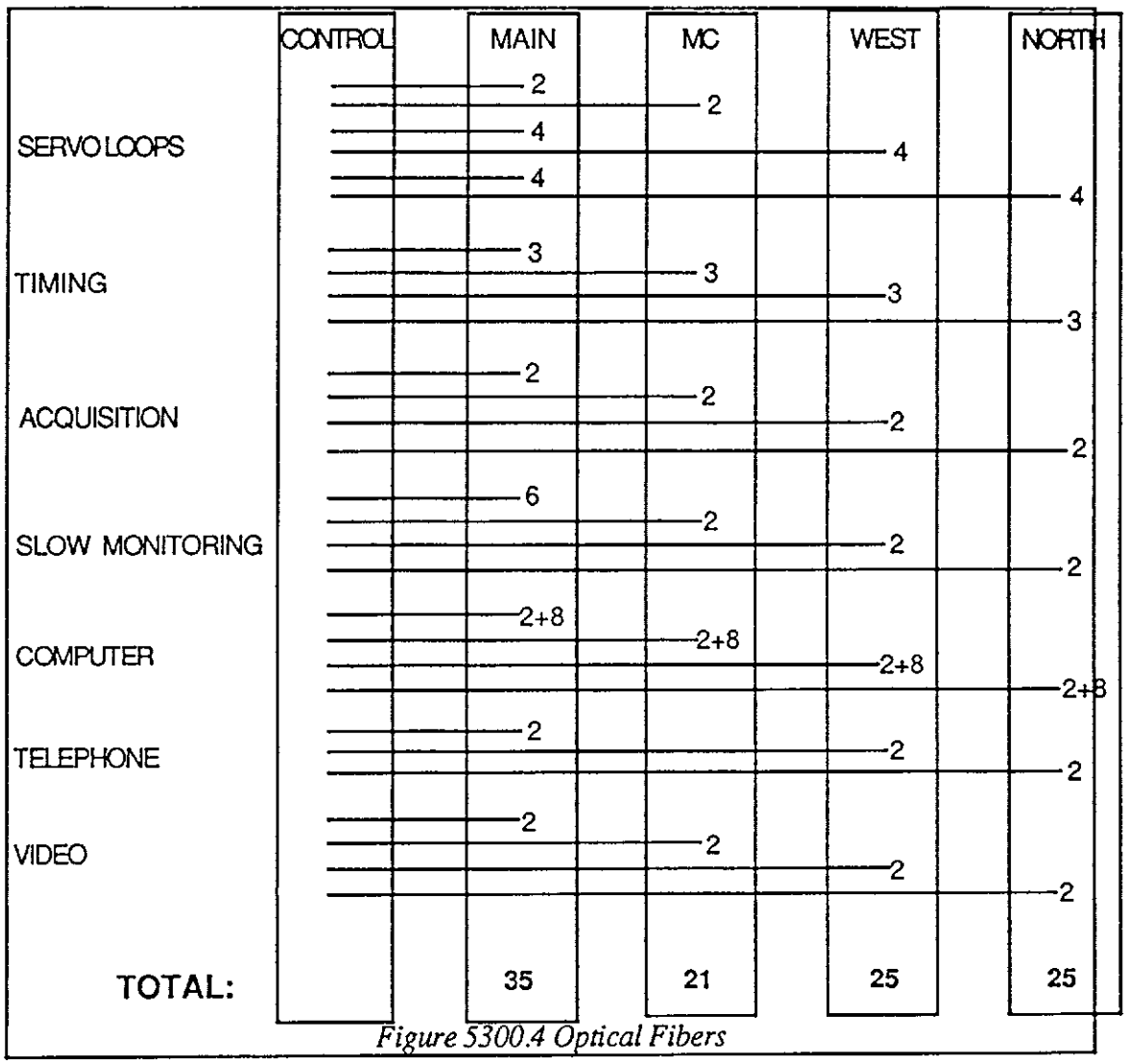

Figure 5300.4 Optical Fibers

We have 3 cables (one for reserve)with 18 fibres . The total length would be 21KM.

For the Slow Monitoring, we also need cable for the Pumping Stations. We would have cables with 4 Fibres (2 for reserve). A total of 15 KM will be necessary.

For Telephone, we will also need 15 KM of Twisted pairs cable to go into the Pumping Stations.

In the 5 buildings of VIRGO, we find a Fibre Distribution Panel which receives all the fibres and distributes them to the Hub for networking, or to the other systems as necessary. All this is done via a Patch Panel for both fibres and copper.

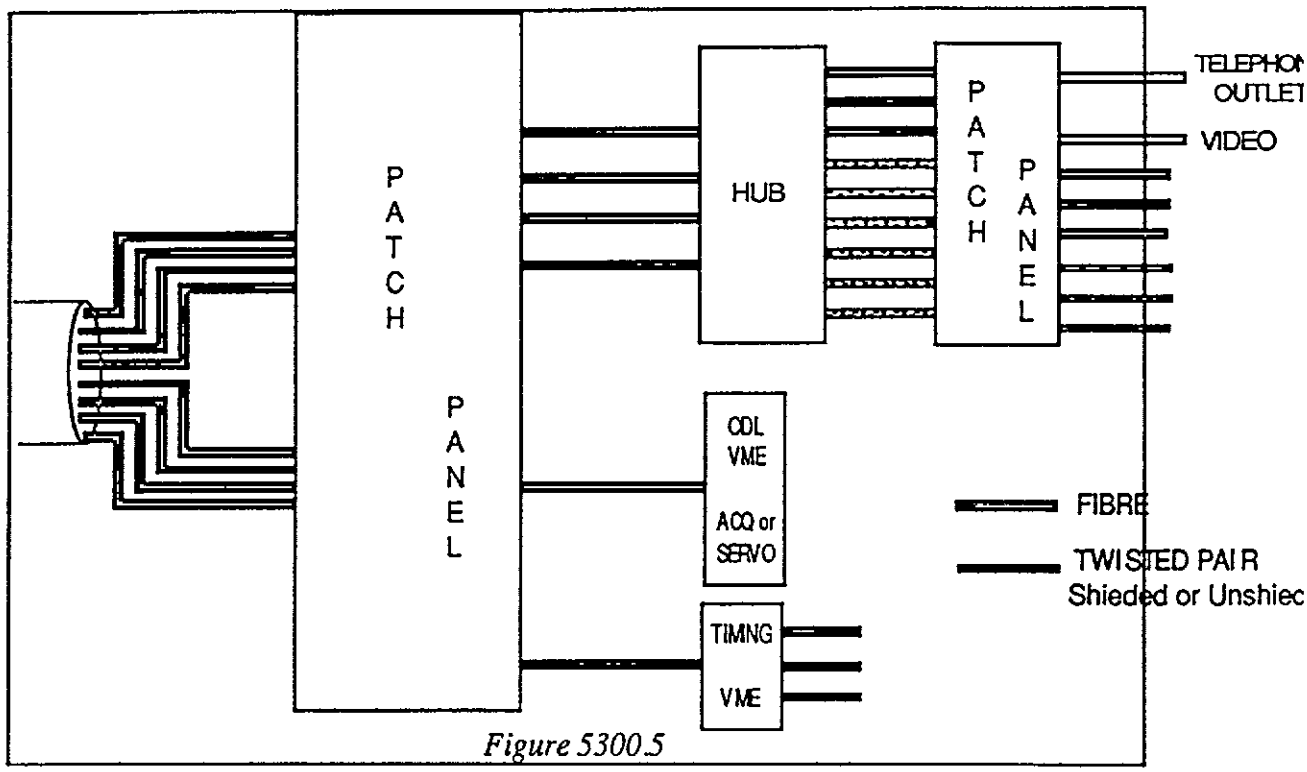

Figure 5300.5

In different buildings, each distribution system is a rack (Secondary); the number is dictated by the necessity to have only 100m cables from Sec to "outlets". Each rack accomodates a "patch panel" for configuring each outlet according to needs, and a "hub" with the intelligent part for computer network, or slow monitoring (repeaters, bridges, terminal servers...). The racks has to be powered via Uninterrupted Power Supplies, and uses about 1KW

The main system is also a rack, which contains a router for connections to INFNet, a module for connection to a telephone system (PBX) as well as a "hub" for communication via fibres with the secondary systems

Each "outlet" shall have 4 connectors of RJ45 type, all identical for phone, video, computers, and so on. The destination will be made on the patch panel in the SEC system, not in the outlets. The cable from the outlet to the equipment may change according to needs.

A PTT line for Telecommunications to the INFN in PISA or, better, to CNUCE in PISA (this latter is on the backbone of the Italian Network, which is 2 Mbit/s) is needed.

5400. Data acquisition and Online processing

The configuration of the interferometer requires the implementation of a distributed readout system (figure 5400.1). In each building, a local readout system collects the available data and sent them via a FIFO memory connected to a digital optical link. In the control room building, the central data acquisition task collects the data from the digital optical link. It structures the data into frames which are written to tape and distributed to the online processing. All these tasks are synchronized with the timing system. For safety, the frame builder checks the reference time of each local system against the global time reference.

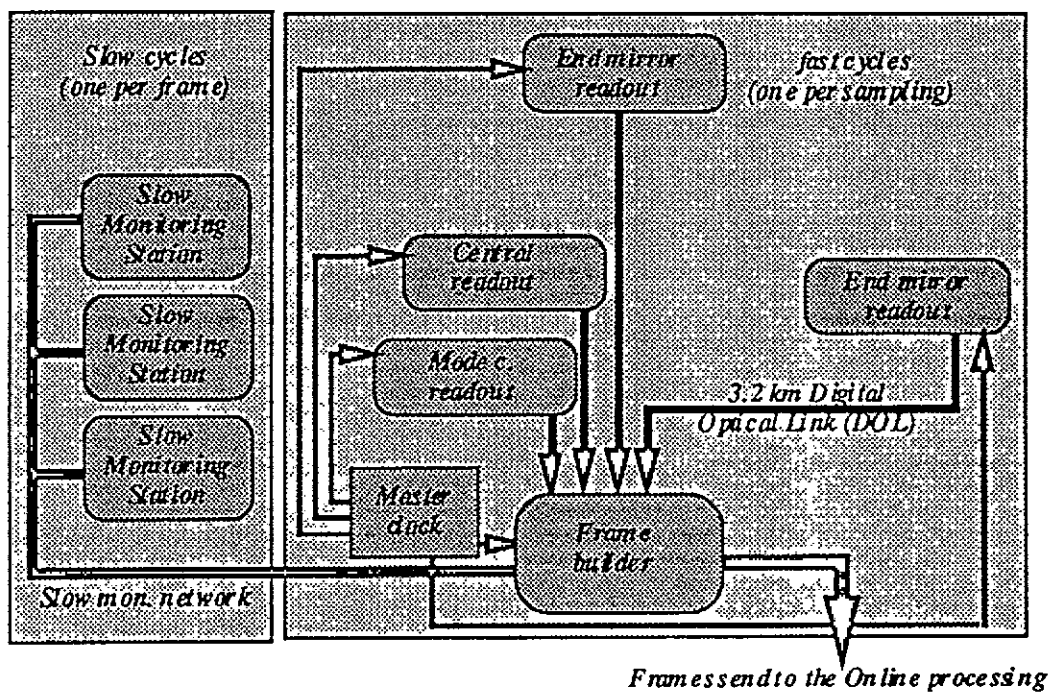

figure 5400.1 The distributed data acquisition system

5400.1. The local readout system.

On reception of the interrupts delivered by the central timing system (corresponding to one sampling of the dark fringe signal), the local readout system shown on figure 5400.2 reads the connected VME boards and builds a small data set. This data set, which is of fixed length, is made with the informations provided by the different captors, status registers, feedbacks and GPS timing module. Once assembled, it is written to a FIFO memory acting as an interface with the digital optical link connected to the central DAQ.

The figure 5400.3 gives a detailed description of the timing cycles performed on a local system after reception of the acquisition interrupt. While the expected sampling frequency is about 10kHz, the system is designed to run up to 20kHz in order to accommodate testing sequences with two times more data. The ADC readout frequency could be a fraction of the dark fringe sampling frequency for the signals which doesn't needed faster readout (alignment for instance). Some redundant control words are added to the data set to check the reliability of the transmission to the frame builder. A given measurement is identified by its position within the data set.

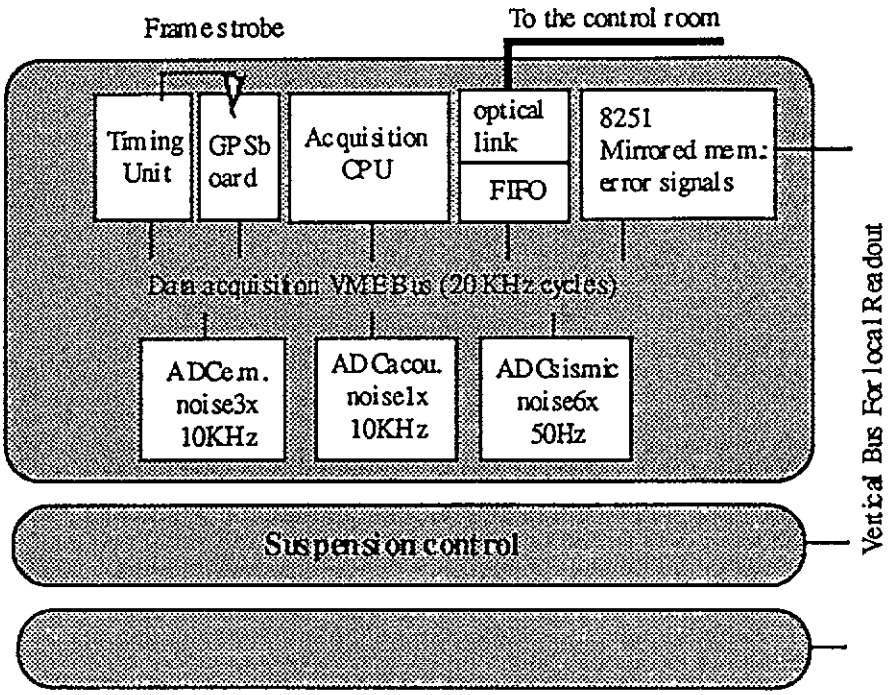

figure 5400.2 A local readout system

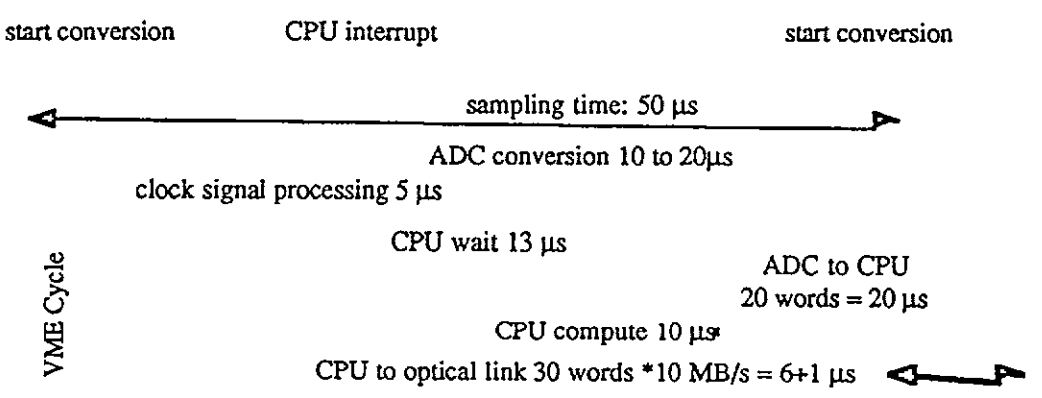

figure 5400.3 The timing sequence of a local readout cycle

5400.2. The frame builder

The architecture of the frame builder is shown on figure 5400.4 and its timing sequence on figure 5400.5. To accommodate for the readout time and the transmission time, there is one sampling cycle offset between the local readout timing and the frame builder timing.

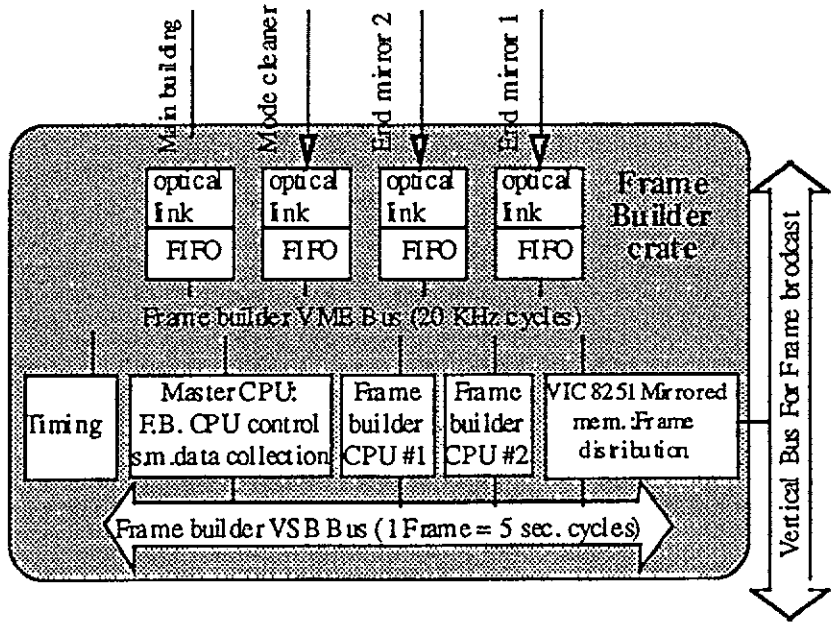

figure 5400.4 Block diagram for the Frame Builder.

Synchronized by the clocking sequence, one processor of the data acquisition system, frame builder 1, collects for one frame the data sets sitting in the different FIFO memories while another processor, frame builder 2, assembles together those from the previous frame to form and distribute 'frames' to the storage and online processing system through the VSB and vertical bus (see figure 5400.4). The slow monitoring data are collected in parallel by the master CPU and included in the frames even if the fast readout is not working.

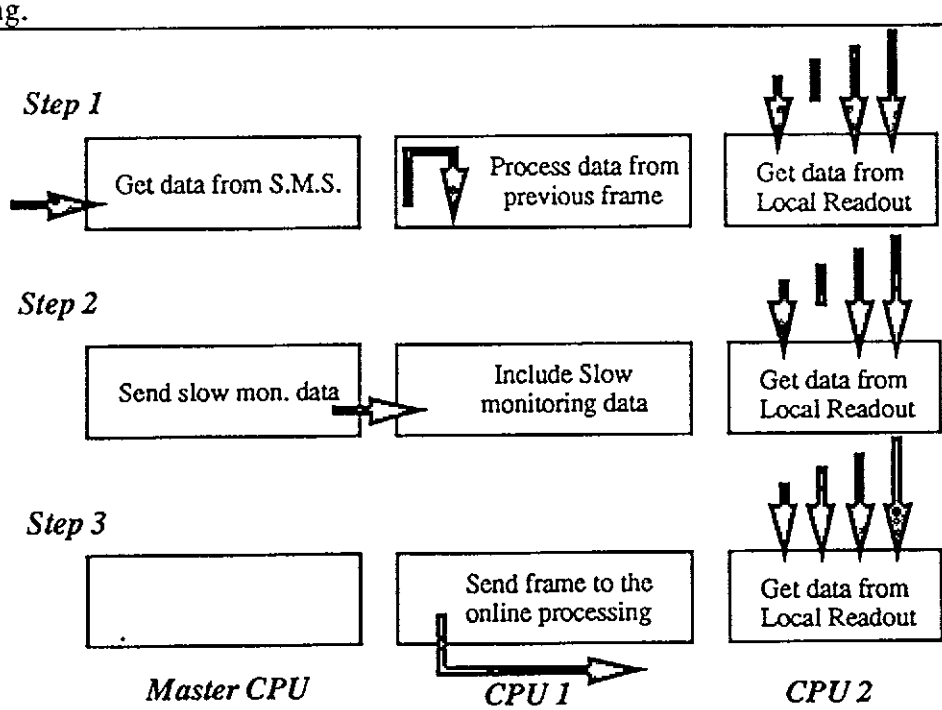

Figure 5400.5 The three steps performed by the frame builder for each frame. After these steps CPU 1 and CPU 2 switch their tasks.

The content of the various FIFO's read by frame builder 1 is a stream of data sets collected according to the clocking sequence. To speed up their further processing, these sets are compressed and structured by frame builder 2. Then frame builder 1 and 2 switch their task for the next frame. The two frame builders CPU's are synchronized by the master frame builder CPU.

The table below gives a first estimate of the amount of data to be recorded. Only the parameters recorded at high rate are quoted. The slow monitoring stations are expected to provide a much smaller amount of data (40 SMS station x 100 words x 10 bytes = 40kBytes/frame).One distinguishes three types of parameters: the ones used to compute the signal (feedback, dark fringe), the ones which may be used to improve the signal/noise (seismic noise for instance) and the ones used for quality check.

Signal	# of chanels	rate	bits
Longitudinal photo. signals(5 signalsx3)	15	20KHz	16
longitudinal feedback (5 mirrors+laser)	6	20KHz	16
Alignment signal (2x4 quadrant diodes)	16	1KHz	16
Alignment data (5mirrors x 2corrections)	10	1KHz	16
Laser power&frequency	2	20KHz	16
Mode cleaner locking (signal + correction)	2	20KHz	16
Mode cleaner alignment	8	1KHz	16
Seismic noise (6 per tower)	6x9	100Hz	16
Acoustic noise (one per building)	4	20KHz	8
elec. mag. noise (one per building)	4	20KHz	8
Line voltage (one per building)	4	20KHz	8

This list leads to a total average rate of the order of 1.5 MBytes/sec. This number is certainly not final and will evolve before the start of data taking. It gives however an order of magnitude to dimension the required online performances. Few MBytes/sec. have to be added to estimate the maximum data rate to take into account data recorded for debugging like internal data coming from the second stage damping of the suspension. This explain our specification of 10MBytes/sec.

5400.3. The frame structure.

An frame is a unit of information containing all the information necessary for the understanding of the interferometers behavior over a finite time interval which integrates several sampling. It contains thus not only the sampling performed during the integrated time interval, but also those performed at a frequency smaller than the frame frequency.

To simplify its manipulation, an frame is organized as a set of C structures described by a header holding pointers to additional structures and values of parameters expected to be stable over the integrated time interval: the starting time of the frame, its duration, values produced by the slow monitoring. This header is followed by an arbitrary number of additional structures, each holding the values of a rapidly varying parameter like the main signal, the seismic noise. Each active element producing data at a rate higher than the frame rate is thus accumulated in a dedicated structure.

This frame structure is a standard which has to be conserved over the various stages of the analysis. Frame history, detector geometry, trigger results, monitoring data, reconstructed data, simulation results lead thus just to additional structures. It is always possible to add new structures or to drop old ones.

The input and output routines used for their creation and the specifications of their format have to be unique and kept as stable as possible. Their format has to be saved on tape to allow for automatic processing. More technical aspects will be described later in the software rules section.

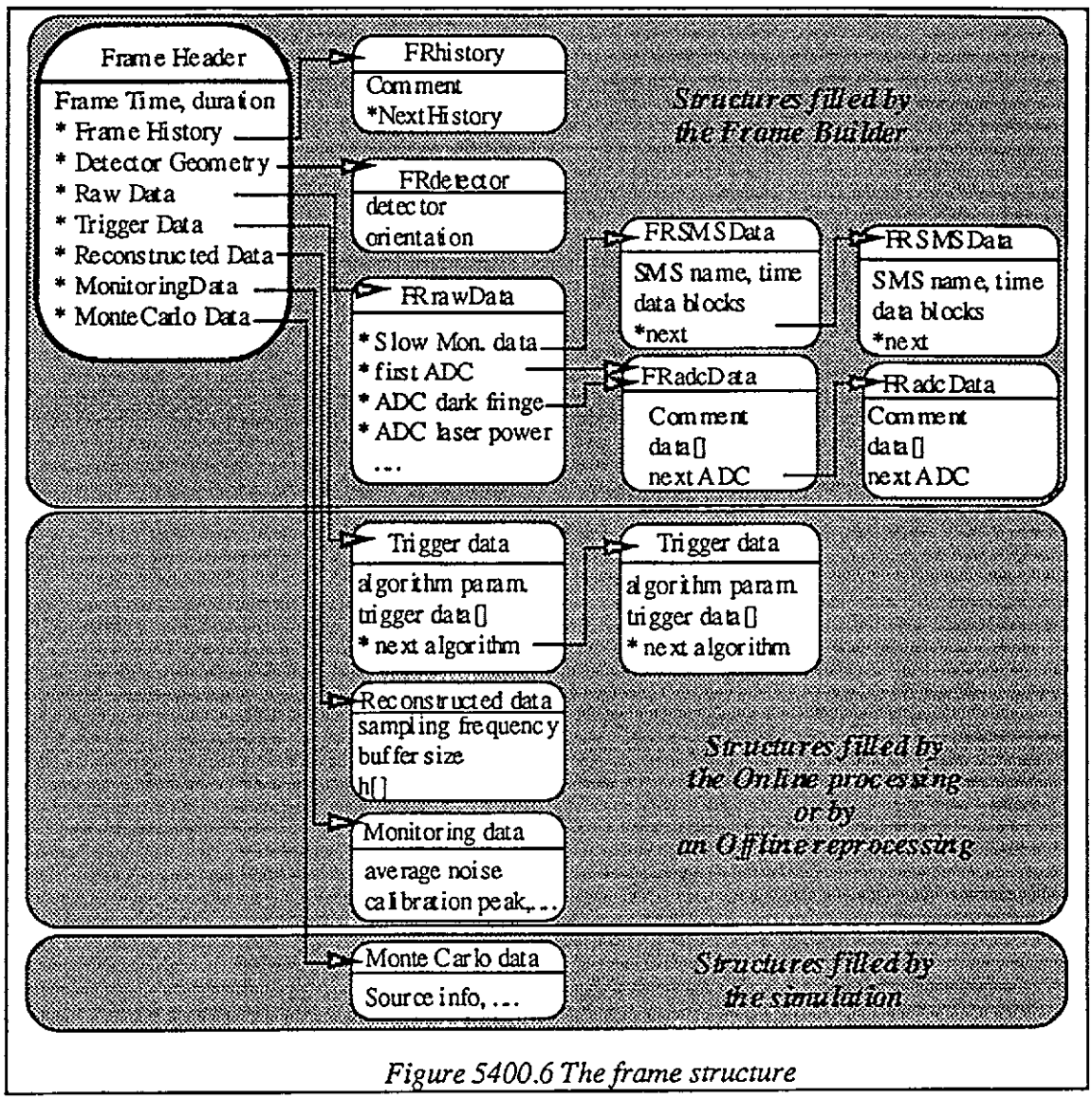

Figure 5400.6 The frame structure

5400.4. The Data Display.

This is a tools to look at the content of Frames (from disk files or from the Data Distribution) and provides tools to plot the data in various way. It could be used online to survey data or off line to play with simulated data or reconstructed data.

5400.5. Online processing

In parrallel to the raw data archiving, Tthe online processing has mainly three tasks (see figure 5400.7) described in the following sections. All these task are run in CPUs connected in parallel to the Frame builder vertical bus.

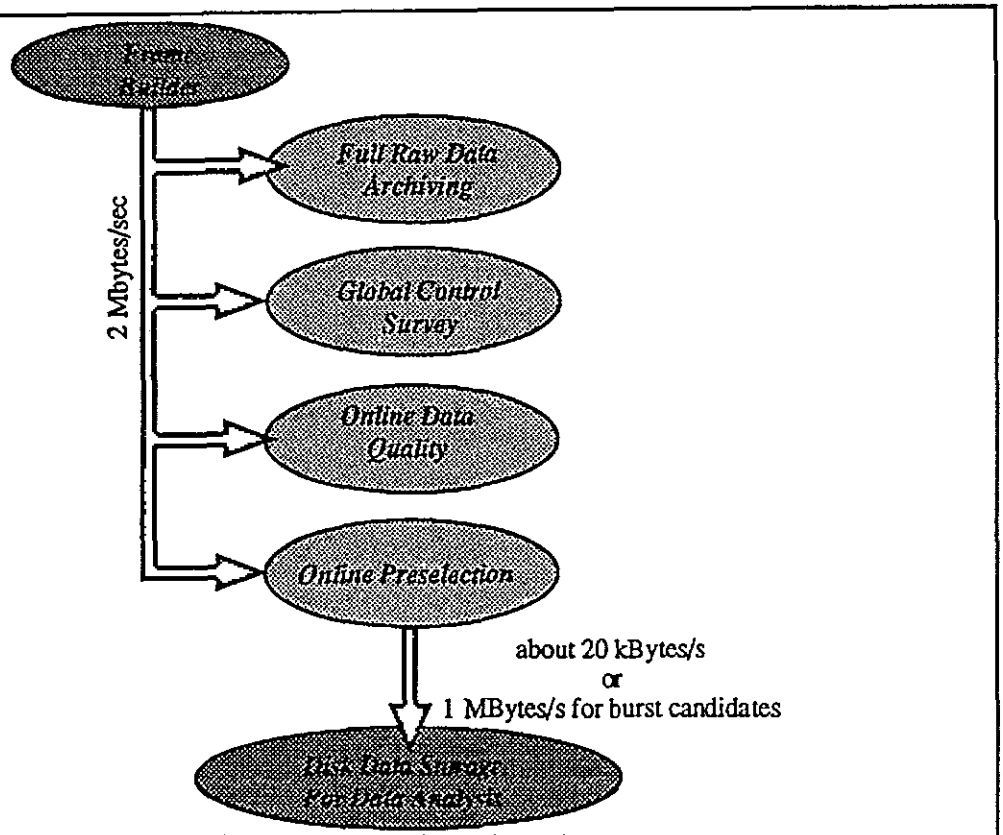

figure 5400.7The principle of the online processing

5400.5.1. Global Control Survey

The purpose of the Global Control Survey is to complement the real time component of the Real time Global Control.

Its main role is to detects unwanted trends in the various servo-loops and, more generally, to react on faulty behaviors thwarting the locking of the interferometer. It should be in a position to perform all correlations deemed necessary to fulfill its task. Its decisions are reached on the basis of the overall response of the interferometer, taking into account as much as possible, all the information available at this level. Its other function is to permit the development onlline of Global Control softwares.

5400.5.2. Data monitoring and quality

This online task will survey permanently the data quality produced by the interferometer. It uses the signal induced by the calibrators, the noise level and run data quality algorithms. It should provide a fast feedback in case of problems. It is a real time data quality check. The corresponding informations are stored in the Data storage system to allow further data selection according to the data quality requirements of the offline analysis. It may be run has part of the Trigger system.

5400.6.3. Data Filtering or frame trigger

Let's remember the data rate of 1MBytes/sec in continuous mode. This means about 1 DAT tape (4 GBytes) every hour and translates into about 9000 tapes/year. Such an amount of data is not a problem for the online writing or for the storage, but it may very quickly overflow any data analysis. Therefore it may be wise to reduce their amount for the detailed data analysis. A typical goal would be a reduction of more than one order of magnitude. The final reduction factor will in fact be driven by our data analysis

capability and by the data production rate. Remember that this rate is also function of our operational efficiency.

Prior to any kind of physics analysis one has to convert raw data (i.e. ADC counts provided by the main feedback and the remaining dark fringe signal) to physical quantities and to compute h values. This is the first task of the trigger. This computation requires the knowledge of the 'transfer functions' of the various controls and of the calibration constants. These quantities are available from a special database accessible from any Virgo laboratory. This reconstruction should be the same as the offline reconstruction.

Then trigger algorithms looking for burst events are run. Triggered frames are defined within 'time windows' during which binary coalescence or burst candidates may occur. These candidates will be selected using simple and robust search algorithms to minimize a possible bias in the further offline analysis: selection efficiency has to supersede rejection efficiency. Random triggers are recorded to monitor the trigger algorithm efficiency. To cover a large type of astrophysical events, several trigger algorithms will be run in parallel.

The informations kept after trigger selection are written to Data Summary Tapes (DST). They are the followings:

For each frame:

- reconstructed h value resampled at lower frequency (1 or 2 kHz) : This represents 4 to 8 kBytes per second. It allows long term pulsars searches.
- slow monitoring records (less than 5 kBytes per second) to follow permanently the interferometers environment.

For 'triggered frames':

- all the raw data required to perform a full analysis of the signal candidates.

The triggered frames are send to the data storage system using a standard network.

Of course, false signals will be selected. But this filtering is not the final data analysis and a lot of work is still needed to extract and proof the existence of the gravitational waves from the DST tapes. The achieved data reduction should provide the conditions for a fast analysis and a fast data dispatching over the collaboration. Most of the data analysis will thus be performed on this filtered sample. But remember that it will always be possible to start again from the original raw data sample.

The filtering algorithms will be designed and tuned using simulated and real data. They will certainly change and improve with some learning experience. This is why we are prepared to reprocess the original raw data. Dedicated computers will be installed on the site for this purpose.

5500. Data archiving storage and distribution

5500.1. The Building Control Station

It controls the parameters describing the status of the buildings, like temperature, pressure, humidity and similar parameters. It uses a distributed I/O acquisition protocol (ETN) which is interfaced to a standard VME environment. In case of need there is the possibility of commanding some actuators in the building. For each building it is foreseen a VME crate, controlled by a local CPU, running the operating system LynxOS (building control server) and linking each server to the slow monitoring network (Ethernet). A user interface running on one of the control room workstation will provide the possibility of managing the whole building control network, setting the configurations of each server and, if necessary, displaying the history of the single parameters.

5500.2. The Environment Monitoring Stations

It monitors all the environment parameters, that are the parameters not directly connected with the interferometer, but necessary for the correlation analysis. Typical parameters which must be monitored are:

- electromagnetic noise — sampled at 10 kHz or faster
- acoustic noise — sampled at 10 kHz or faster
- seismic noise — sampled at 1 kHz
- cosmic ray noise
- all power supplies
- weather — pressure, wind, temperature, etc.
- human activity — count number of people in or close to the buildings
- status information

Due to the fact that some of these variables have to be sampled at quite high frequency and due to the need of a precise timing (electromagnetic noise and acoustic noise) part of the environment monitoring system will be integrated within the fast VME data acquisition system (local readout). The other parameters are sent directly to the frame builder by a standard slow monitoring system, that consists of a dedicated VME crate, controlled by a local CPU, running the operating system LynxOS (environment monitoring server) and linking each server to the slow monitoring network (Ethernet). The sensors are defined and chosen within the environment monitoring structure with direct acquisition by the system or internal sampling and data transfer to the environment monitoring system via a standard RS232.

An user interface running on one of the control room workstations will provide the possibility of managing the whole environment monitoring network, setting the configuration of each server and of the sensors. Such user interface has one graphical page for each type of parameter. The history of each environment monitoring parameter can be displaied on this workstation using the Historical Monitoring software in connection with the Data Distribution System.

5500.3. Raw data archiving

The first task of the on line processing is that of archiving all the frames produced by the frame builder in order to have a complete archive containing all the information acquired by the interferometer, which allows a future full reprocessing of the original data if necessary. The raw data archiving gets the data from a VME CPU reading the vertical bus and writing them on tapes. For security reasons, two copies of the raw data are made and stored in two different locations.

The architecture of the raw data archiving will be defined at the latest possible time, because of the fast technological evolution which may render obsolete the present

time solution. Anyway, according to the frame data rate and the typical output on tape drives, the present time technical solution is that of a parallel staging of the data on disk before copying them on tapes. In this case several CPU are needed which work in parallel.

5500.4. Data Distribution

The data distribution system collects the data produced by the on line processing and by the frame builder and store them on disk. At the same time, acting as server, it distributes all the requested data to the authorized Virgo user interfaces. These operations have different priorities: the highest priority is assigned to the data collection from the frame builder and from the on-line processing, while the lowest is assigned to the requests of data from users.

To avoid any interference between these two different operations the system must use a dedicated Ethernet line for Data Collection and another Ethernet line for serving the Data Requests. Cm protocol is used for both the operations

The structure of the stored data is organized according to a tree structure, as shown in the figure 5500.1.

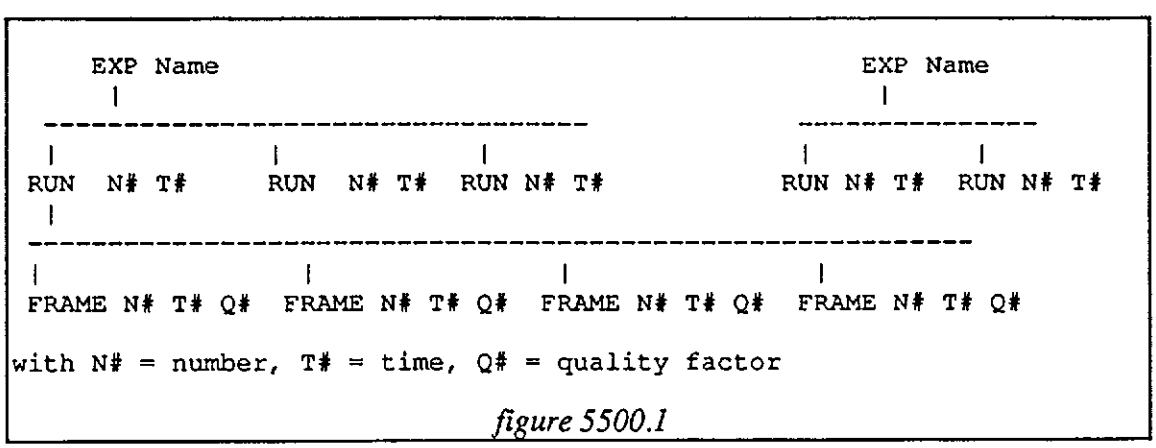

figure 5500.1

In this way, the stored data have the same structure defined by the frame builder and by the on line processing (frames). Therefore the user interface access the Data Distribution System getting blocks of data (frames) exactly as stored. In its requests it must specify the experiment name (EXP#), the run RUN#) (number or starting time) and the frames (FRAME#) (numbers or starting time/ending time).

On request the Data Distribution System will provide also specific parameters within specified intervals of time (or number of frames). Because this kind of request would mean a cross access to many frames with a considerable loss of time for some parameters, the Data Distribution System also stores some parameters contained in the frames according to a table structure (as in a classic database), which surely guarantees a faster and more efficient data access.

The access to the Data Distribution System is restricted only to Virgo labs and only for reading and getting data. The access to the stored data for changing their structure, for deleting and moving files and for all the relevant operations of management of the system itself, will be restricted to authorized people.

5500.5. Historical Monitoring

The historical monitoring is a user interface running on any workstation, which, acting as a client to the Data Distribution System, can retrieve and present the data stored in the Data Distribution System (i.e. making histograms, etc). The Historical Monitoring works with the parameters stored as function of time by the Data Distribution system, while the Data Display works with full frame.

5600. Simulation: SIESTA

With the increase in size and complexity of the gravitational wave experiment like the Virgo project, it becomes very important to be able to predict the behavior of the detector before its construction, in order to optimize all the components. Such predictions could be done in first approximation by analytical computations, but if one looks for a detailed description or for a study of a correlation between effects like mechanical motion, thermal noise and light propagation, the only realistic approach becomes the numerical approach. Therefore, the first goal of the simulation is to be a tool for the detailed design of the Virgo detector.

The natural next step is to use the simulation as a tool for the understanding of the behavior of Virgo as a detector by comparing its results to simulated data. This will be important when the detector starts working, and even before, when individual components are tested. Simulated data may also be used as inputs to exercise the data acquisition system.

Finally, the last task of the simulation is to allow the study of search algorithms on well known data . The level of description we are aiming at will allow us to study real and fake signals in a quantitative way, as it is done for big experiment in High Energy Physics. We think this will be a very important point when real data are analyzed.

To meet all this requirements one uses two complementary approaches. First one uses a set of small simulation programs, adapted to the study of well defined problems. Then one develops a general purpose program (SIESTA) which can ideally study all the problems related with correlations. Such a program is usually run with more emphasis on a specific issue. More informations about SIESTA could be found in the Siesta directory with documentation and examples